Space Plasma Physicsâ€"The Study of Solar-System Plasmas: Volume 2, Working Papers, Part 1, Solar-System Magnetohydrodynamics

Study Committee and Advocacy Panels, Space Science Board, Assembly of Mathematical and Physical Sciences, National Research Council

ISBN: 0-309-12339-9, 775 pages, 8 1/2 x 11, (1979)

Space Plasma Physics:

THE STUDY OF SOLAR-SYSTEM PLASMAS

VOLUME 2
WORKING PAPERS

Space Science Board
Assembly of Mathematical and Physical Sciences
National Research Council

PART I
Solar-System Magnetohydrodynamics

NATIONAL ACADEMY OF SCIENCES
Washington, D.C. 1979

NOTICE: The project that is the subject of this report was approved by the Governing Board of the National Research Council, whose members are drawn from the Councils of the National Academy of Sciences, the National Academy of Engineering, and the Institute of Medicine. The members of the Committee responsible for the report were chosen for their special competences and with regard for appropriate balance.

This report has been reviewed by a group other than the authors according to procedures approved by a Report Review Committee consisting of members of the National Academy of Sciences, the National Academy of Engineering, and the Institute of Medicine.

Available from
Space Science Board
2101 Constitution Avenue
Washington, D.C. 20418

FOREWORD

The space age began exactly 20 years ago with the launch of Sputnik I and Explorer I. The Explorer spacecraft discovered regions of trapped radiation around the earth--the van Allen belts. This was the beginning of the study of particles and fields in space, or space plasma physics. A large part of the effort in the early years of the space program was devoted to the mapping of the magnetosphere, the measurements of time variations in particles and fields, and the exploration of the solar wind.

From these studies a sophisticated empirical knowledge of phenomena in space plasma physics has emerged. With the attainment of this observational maturity in the field, NASA funding for space plasma physics has declined as priorities have shifted to other exploratory ventures. The present study of space plasma physics was therefore requested by NASA in order to obtain guidance for future directions in the subject.

The study has involved a major effort on the part of a great many people working in space plasma physics. The Space Science Board formed a panel chaired by Stirling Colgate, composed for the most part of physicists expert in plasma physics but not especially knowledgeable about the space aspects of plasmas; the report of this panel constitutes the first part of Volume 1 of the report. The Committee on Space Physics of the Board was charged with the responsibility for soliciting technical review papers on a large number of topics in space plasma physics. These reviews are Volume 2 of the report; they constitute a most valuable resource for those working in the field. From these reviews, two advocacy panels prepared overview position papers that served as resource information for the Colgate panel and appear as Chapters 7 and 8 of Volume 1.

The Colgate panel has recommended that future research in space plasma physics should involve a much closer integration between theory and observation as is appropriate to the maturity of the field and in order to bring the research into closer contact with the mainstream of plasma physics research. The panel also concurred in the unified recommendations of the advocacy panels.

The Space Science Board is most grateful to the many people who have devoted so much time and effort to carrying out this study.

A. G. W. Cameron, Chairman
Space Science Board

PREFACE

This study was undertaken by a specially created committee of the Space Science Board of the National Research Council, at the request of the National Aeronautics and Space Administration, in order to identify the future objectives of research in space plasma physics.

The Space Science Board divided its study of plasmas in the solar system into four parts. The Study Committee on Space Plasma Physics, chaired by Stirling A. Colgate, consisted of six experts drawn from laboratory plasma physics and plasma astrophysics and the chairmen of three advocacy panels. Its function was to give an overall evaluation of the current status of solar-system plasma physics. The Study Committee on Space Plasma Physics was aided by three "advocacy" panels, whose members were practicing solar-system plasma physicists: a Panel on Plasma Physics of the Sun, chaired by E. N. Parker; a Panel on Solar System Magnetohydrodynamics, chaired by C. F. Kennel; and a Panel on Solar System Plasma Processes, chaired by L. J. Lanzerotti. The Kennel and Lanzerotti panels dealt with plasma phenomena beyond the solar corona. Solar-system magnetohydrodynamics treated large-scale plasma phenomena in the solar wind and at the planets. Solar-system plasma processes considered those microscopic plasma problems that emerged from the study of the objects considered in solar-system magnetohydrodynamics and also considered the impacts of these processes on terrestrial science and technology. The solar-physics panel treated macroscopic and microscopic plasma processes occurring on the sun together and included many topics from what is conventionally called solar astronomy.

Each member of the advocacy panels on solar-system magnetohydrodynamics and solar-system plasma processes wrote a scientific review article on his specialty. Using these review articles as working papers, these two advocacy panels met to compose overview reports that summarized the salient points of the working papers and made recommendations. The Committee on Space Physics of the Space Science Board, chaired by R. A. Helliwell, appointed outside reviewers for each of the scientific review articles and supervised the reviewing process. These working papers are the subject of this volume.

PARTICIPANTS AND CONTRIBUTORS

Study Committee

Stirling A. Colgate, Los Alamos Scientific Laboratory, Chairman
Harold Furth, Princeton Plasma Physics Laboratory
Jack R. Jokipii, University of Arizona
Charles F. Kennel, University of California, Los Angeles
Louis J. Lanzerotti, Bell Telephone Laboratories
Eugene N. Parker, University of Chicago
David Pines, University of Illinois
Marshall Rosenbluth, Institute for Advanced Study
Malvin Ruderman, Columbia University

Panel on Solar System Magnetohydrodynamics

Charles F. Kennel, University of California, Los Angeles, Chairman
Peter M. Banks, Utah State University
Aaron Barnes, NASA, Ames Research Center
Len A. Fisk, NASA, Goddard Space Flight Center
Thomas E. Holzer, High Altitude Observatory
Juan G. Roederer, University of Denver
George L. Siscoe, Dartmouth College

Panel on Solar System Plasma Processes

Louis J. Lanzerotti, Bell Laboratories, Chairman
Donald T. Farley, Cornell University
William C. Feldman, Los Alamos Scientific Laboratory
Robert W. Fredericks, TRW Systems Group
Eugene Greenstadt, TRW Systems Group
Gehard Haerendel, Institute for Estraterrestrischphysik
Lawrence R. Lyons, NOAA, Space Environment Laboratory
Francis W. Perkins, Princeton University
Stanley Shawhan, University of Iowa
Bengt U. O. Sonnerup, Dartmouth College
Peter A. Sturrock, Stanford University

1975 SSB Study Panel on Solar Physics

Eugene N. Parker, University of Chicago, Chairman
Jacques M. Beckers, Sacramento Peak Observatory
Arthur J. Hundhausen, High Altitude Observatory
Mukul R. Kundu, University of Maryland
Cecil E. Leith, National Center for Atmospheric Research
Robert Lin, University of California, Berkeley
Jeffrey Linsky, Joint Institute for Laboratory Astrophysics
Frank B. MacDonald, NASA, Goddard Space Flight Center
Robert Noyes, Smithsonian Astrophysical Observatory
Frank Q. Orrall, University of Hawaii
Laurence E. Peterson, University of California, San Diego
David M. Rust, American Science and Engineering
Peter Sturrock, Stanford University
Arthur B. C. Walker, Jr., Stanford University
Adrienne F. Timothy, NASA, Headquarters
Kenneth A. Janes, Boston University, Study Director

Study Director

Richard C. Hart, National Research Council

Space Science Board

A. G. W. Cameron, Chairman
Francis P. Bretherton
Stirling A. Colgate
Robert A. Helliwell
Francis S. Johnson
Charles F. Kennel
Lynn Margulis
Peter Mazur
Peter Meyer
Robert A. Phinney
Vera C. Rubin
Richard B. Setlow
Gerald J. Wasserburg
Sheldon Wolff

George E. Solomon, Ex officio
Milton W. Rosen, Executive Secretary

CONTENTS

PART I
Solar-System Magnetohydrodynamics

I. Solar-System Magnetohydrodynamics

THE SOLAR WIND AND RELATED ASTROPHYSICAL PHENOMENA

Thomas E. Holzer

High Altitude Observatory
National Center for Atmospheric Research*
Boulder, Colorado 80307

*The National Center for Atmospheric Research is sponsored by the National Science Foundation.

1. INTRODUCTION

In this paper we shall review our current state of understanding of the large-scale dynamics of the solar wind and suggest some directions that research in this area is likely to follow in the future. We shall also consider the relationship between physical processes in the solar wind and in various astrophysical plasmas, with an emphasis being given to the study of stellar winds. The paper is concluded with a detailed summary and a tentative timetable for solar wind research over the next 25 years.

Most of the discussion of the solar wind will be presented in the context of the recent studies of coronal holes, which have been largely carried out in connection with the Skylab Coronal Hole Workshops and have produced a rapid evolution of our understanding in several areas of solar wind research. Many of the last two decades' theoretical predictions and observational inferences regarding the solar corona and solar wind must now be thoroughly reexamined in light of the picture of a magnetically controlled coronal expansion that is inferred from these recent studies. At the same time, it now seems possible to map out a course of action that is likely to bring all areas of solar wind research to a high degree of sophistication within the next two decades.

The emphasis throughout the paper will be placed on basic physical concepts, although a mathematical framework will be provided for those readers who might find it useful. The basic mathematical framework is developed in section 2, where both the microscopic and macroscopic descriptions of the solar wind plasma are briefly introduced. Throughout the paper we shall generally restrict ourselves to the macroscopic

magnetohydrodynamic (MHD) description, as it applies to large-scale dynamical processes. The description of small-scale-MHD and microscopic processes will be considered elsewhere in this volume[15,55]

2. BASIC EQUATIONS

In the corona and solar wind the number of particles in a Debye sphere is always large, so it is appropriate to describe the plasma behaviour by a series of kinetic equations written in terms of the single-particle distribution functions, f_j ($\underline{x}$, $\underline{v}$, t), of the various particle species:

$$\frac{\partial f_j}{\partial t} + \frac{\partial}{\partial \underline{r}} \cdot (\underline{v} f_j) + \frac{\partial}{\partial \underline{v}} \cdot (\underline{F}_j f_j) = C_j \qquad (1)$$

where the force per unit mass for the j^{th} particle species is

$$\underline{F}_j = Z_j \frac{e}{m_j} (\underline{E} + \frac{1}{c} \underline{v} \times \underline{B}) - \frac{GM_\odot}{r^2} \hat{e}_r \qquad (2)$$

Here, $\underline{E}$ and $\underline{B}$ are the 'smoothed' electric and magnetic fields, G is the gravitation constant, $M_\odot$ is the solar mass, and r is the heliocentric radial distance. (Gaussian units are used throughout.) Fluctuating 'microfields' and 'microforces' are included in the so-called collision term, C_j.

Equation (1), together with Maxwell's equations, potentially yields an accurate description of the plasma, provided a suitable form for C_j can be determined. In practice, however, the separation of smoothed fields from microfields and the specification of C_j represent a quite formidable problem. In the past, applications of (1) to the solar wind have generally either set $C_j = 0$ or assumed a highly simplified form for C_j. In the future, more careful studies of (1) are needed to provide a better understanding of the effects of wave-particle interactions on momentum and energy transfer and transport processes. Nevertheless,

our basic understanding of the dynamical properties of the solar wind has and will come from macroscopic, rather than microscopic, descriptions.

If we multiply (1) by 1, $m_j \underline{c}_j$, and $m_j c_j^2/2$ (where $\underline{c}_j = \underline{v} - \underline{u}_j$) and integrate over velocity space, we obtain the j^{th} species equations for the conservation of mass, momentum, and energy:

$$\frac{\partial n_j}{\partial t} + \underline{\nabla} \cdot n_j \underline{u}_j = Q_j^c \tag{3}$$

$$n_j m_j \left(\frac{\partial \underline{u}_j}{\partial t} + \underline{u}_j \cdot \underline{\nabla}\, \underline{u}_j\right) + \underline{\nabla} p_j + \underline{\nabla} \cdot \underline{\tau}_j$$

$$+ n_j m_j \frac{GM_\odot}{r^2} \hat{e}_r - n_j Z_j e\left(\underline{E} + \frac{1}{c}\, \underline{u}_j \times \underline{B}\right) = \underline{Q}_j^m \tag{4}$$

$$\frac{3}{2}\left(\frac{\partial p_j}{\partial t} + \underline{u}_j \cdot \underline{\nabla} p_j\right) + \frac{5}{2} p_j \left(\nabla \cdot \underline{u}_j\right)$$

$$+ \underline{\nabla} \cdot \underline{q}_j + \underline{\tau}_j : \underline{\nabla}\, \underline{u}_j = Q_j^e \tag{5}$$

where the number density n_j, bulk flow speed $\underline{u}_j$, scalar pressure p_j, stress tensor $\underline{\tau}_j$, and heat flow vector $\underline{q}_j$ are defined by

$$n_j = \int \underline{dv}\, f_j \tag{6a}$$

$$\underline{u}_j = \frac{1}{n_j} \int \underline{dv}\, \underline{v} f_j \tag{6b}$$

$$p_j = \frac{1}{3} \mathrm{Tr}\, \underline{P}_j \tag{6c}$$

$$\underline{\tau}_j = \underline{P}_j - p_j \underline{I} \tag{6d}$$

$$\underline{\underline{P}}_j = m_j \int \underline{dv}\, \underline{c}_j\, \underline{c}_j\, f_j \tag{6e}$$

$$\underline{q}_j = \frac{1}{2} m_j \int \underline{dv}\, \underline{c}_j\, c_j^2\, f_j \tag{6f}$$

and $\underline{\underline{I}}$ is the unit dyadic. Formally, Q_j^c, $\underline{Q}_j^m$, and Q_j^e are the 1, $m_j\underline{c}_j$, and $\frac{1}{2} m_j c_j^2$ moments of the collision term C_j, although they may be thought of simply as mass, momentum, and energy source terms. In fact, quite often the source terms are specified, at least in part, on the basis of heuristic derivations that largely ignore the fact that they are formally moments of the kinetic collision term.

Equations (3)-(5) for all plasma species, together with Maxwell's equations, provide a set of equations that are not closed owing to the presence of higher moments (viz., the stress tensor, $\underline{\underline{\tau}}_j$, and the heat flow vector, $\underline{q}_j$). This closure problem, which is inherent in any moment technique, can be solved by specifying the higher moments ($\underline{\underline{\tau}}_j$ and $\underline{q}_j$) in terms of lower moments (n_j, $\underline{u}_j$, and p_j) and their derivatives. However, such a specification is readily accomplished only when the plasma is collision-dominated, which the coronal plasma is not beyond a few solar radii. Thus, closure of the equations in the region that is not collision-dominated must be accomplished either by some heuristic method or by taking higher moments of (1) and attempting to effect closure at a higher level. The former method has usually been used in solar wind studies.

3. SOLAR WIND

The subject of the solar wind can be broken down into six distinct but related topics: the coronal expansion[151,153,154,41,22,88,98,13,14,92]; the developmment of solar wind structures[98,68,69,44,27]; chemical composition and ionization state[98,81]; the interaction of the solar wind with the interstellar medium[7]; and the history and evolution of the solar wind. The following discussion of these topics will be presented in the context of coronal holes[132,4,160,143], which are regions in the solar corona exhibiting low electron densities and rapidly diverging (open) magnetic fields. It has recently been determined that during at least part of the solar cycle high speed streams, if not most of the solar wind, originate in coronal holes[114,115,144,145,98,105], and it follows that much of the coronal expansion is subject to the control of the rapidly diverging coronal hole magnetic fields (see sections 3.1.4-3.1.6). This magnetic control modifies a number of inferences drawn from solar wind observations, and it requires a re-examination of many aspects of solar wind theory. Hence, contrary to some past suggestions that the essential and interesting work in the solar wind has already been completed, it is now quite clear that our fundamental view of the solar wind must be changed and that much essential and interesting work, both theoretical and observational, remains to be done before a satisfactory understanding of the solar wind can be achieved (viz., an understanding of the roles of all basic physical processes important to the large-scale dynamics and thermodynamics of the solar wind).

3.1. Coronal Expansion

In the present paper, we shall use the term coronal expansion to refer to that region of the solar wind in which the energy flux density is transformed from predominantly a thermal and fluctuation (convected and propagating) energy flux to predominantly a bulk flow energy flux. It is the coronal expansion problem toward which Parker's[149] original work, as well as much of the work in the first decade of solar wind research, was directed. For the past few years, however, the emphasis in solar wind research has shifted away from the coronal expansion problem, and it is just recently, in response to the realization of the significance of coronal holes, that this problem has again begun to receive more attention.

3.1.1 The necessity of coronal expansion

If the corona were free of the constraining solar magnetic field, and if it were in hydrostatic equilibrium, its high temperature ($>10^6$ ^oK near the sun) would extend far into space because of the dominance of thermal conduction over radiative loss processes[36]. Owing to this high temperature and its extension into space, the pressure of the static corona would, at great distance from the sun, approach a constant value that is much larger than the pressure of the local interstellar medium. We would thus conclude that the interstellar medium could not contain the static (non-magnetic) solar corona, so that the corona would have to expand[149,151]. The corona, however, is strongly controlled by the solar magnetic field, and only a small fraction of a hydrostatic corona could extend throughout interplanetary space. Nevertheless, the coronal pressure is so large that this small fraction would still lead to an asymptotic pressure much larger than the interstellar pressure, and

thus, even in the presence of the strong solar magnetic field, some part of the corona must expand.

3.1.2 A simple description of the expansion

To obtain a description of the coronal expansion, we shall use the system of equations (3)-(5), at first making a number of simplifying assumptions to render the system more tractable. Let us consider a flow that is steady and radial but not, in general, spherically symmetric. Then, if we assume that the corona is composed of a fully ionized proton-electron plasma, and if we neglect viscous momentum transport, momentum source terms (e.g., mechanical-wave acceleration, radiation pressure), and magnetic stresses, it follows from (3) and (4) that

$$\frac{d}{dr}(nuA) = 0 \tag{7}$$

$$u\frac{du}{dr} + \frac{1}{nm}\frac{dp}{dr} + \frac{GM_\odot}{r^2} = 0 \tag{8}$$

where $n = n_e = n_p$, $\underline{u} = u\hat{e}_r = (m_p\underline{u}_p + m_e\underline{u}_e)/m$, $m = m_e + m_p$, $p = p_e + p_p$, and A is the cross-sectional area of a flow tube (for spherical symmetry, $A \propto r^2$). For the time being (cf. section 3.1.5), we shall replace the energy equation (5) with a polytropic relation between the pressure and density

$$\frac{d}{dr}\left(\frac{p}{n^\alpha}\right) = 0 \tag{9}$$

where α is the polytrope index. If $\alpha = 5/3$, (9) is simply the adiabatic equation of state, and if $\alpha < 5/3$, some form of heating is implied (e.g., degradation of a thermal conduction flux, dissipation of waves). Defining the Mach number M by $M^2 = nmu^2/\alpha p$, (7)-(9) can be combined to yield

$$\frac{M^2-1}{2M}\frac{dM}{dr} = \frac{1}{2}\left(\frac{\alpha+1}{\alpha-1}\right)\left[1 + \left(\frac{\alpha-1}{2}\right)M^2\right]\frac{1}{g}\frac{dg}{dr} \qquad (10)$$

where

$$E = \frac{1}{2}u^2 + \frac{\alpha}{\alpha-1}\frac{p}{nm} - \frac{GM_\odot}{r} \qquad (11)$$

$$g = A^{2\left(\frac{\alpha-1}{\alpha+1}\right)}\left(E + GM_\odot/r\right) \qquad (12)$$

and E is a constant of the flow.

3.1.3. Spherically symmetric flow

To illustrate some basic characteristics of the coronal expansion, let us begin by ignoring the channelling effects of the solar magnetic field and assuming a spherically symmetric ($A \propto r^2$) expansion. In this case, (10) takes the form of the familiar polytropic solar wind equation for steady, radial, spherically symmetric flow[151]. The family of solutions of this equation, for $\alpha < 5/3$, has the general form shown in Figure 1, which is characterized by a single x-type (i.e., saddle-type) critical point (labelled A) that occurs where g reaches its minimum and $M^2 = 1$. The appropriate solution from this family can be chosen by requiring subsonic ($M^2 < 1$) flow near the solar surface and pressure balance at the boundary between the extended solar atmosphere and the interstellar medium. The latter requirement leads to the choice of the subsonic branch of one of the double-valued solution curves lying to the right of the critical point. The former requirement, however, leads to the choice of one of the solution curves that is subsonic to the left of the critical point. These two choices can be made compatible only by choosing the ascending critical solution, OAB, and connecting it to the subsonic solution CD with the standing shock BC. In reality, of course, the

location of the shock transition terminating the supersonic solar wind is not at twice the critical radius but instead at a much greater distance (cf. section 3.5). Figure 1 is intended to show topological properties only.

For coronal temperatures $\lesssim 2.5 \times 10^6$ °K, the basic characteristics of the solar wind predicted by the simple model outlined above are as follows: very low expansion speeds ($M^2 \ll 1$) in $r \lesssim 2\ R_\odot$; a transition from subsonic ($M^2 < 1$) to supersonic ($M^2 > 1$) flow between 3 $R_\odot$ and 10 $R_\odot$; a highly supersonic ($M^2 \gg 1$) expansion at 1 AU (orbit of earth); and a terminal shock in or beyond the outer solar system. Another prediction, which requires the additional restriction of the frozen-field condition (generally valid in the corona and solar wind), is that of a spiral interplanetary magnetic field, the equatorial projection of which is shown in Figure 2. All except the first of these predictions can be said to agree qualitatively with observations of the corona and solar wind, but a thoughtful study of the observations reveals the need to remove many of the restrictions that were imposed in developing the simplified description. Let us first consider the assumption of spherical symmetry.

3.1.4 Coronal holes and the mass flux problem

Coronal holes are regions in the solar corona that exhibit low emission in certain frequency ranges, especially in soft x-rays (cf. Figure 3a). These regions are characterized by low electron densities (giving rise to the low emission) and rapidly diverging, open magnetic fields (cf. Figure 3b).[4,133] It appears certain that, during at least part of the solar cycle, coronal holes are the solar source of high speed solar wind streams[114,115,144,145,98,105] (cf. section 3.2), and probably of most

lower-speed solar wind as well, in spite of the fact that holes cover less than 20% of the solar surface (at least during the 9-month 1973-1974 Skylab period). If the solar wind comes from less than one fifth of the solar surface, then it is clear that the assumption of spherical symmetry is not valid. This lack of spherical symmetry, which is closely linked to the structure of coronal magnetic fields, has a number of important implications for the coronal expansion problem. However, in the past, very little work has been done with coronal expansion models that are not spherically symmetric, so the recent coronal hole observations point the way for a number of fundamental theoretical investigations that need to be carried out in the future.

One outstanding problem than might be resolved, at least in part, by considering a non-spherically symmetric expansion relates to the solar wind mass flux. It is observed[52] that the particle flux density in high speed streams at 1 AU is $(nu)_E \gtrsim 3 \times 10^8$ cm^{-2}sec^{-1}. If the electron density in a coronal hole is known, then the continuity equation (7) allows us to determine the flow speed in the coronal hole that is necessary to provide the observed mass flux at 1 AU:

$$u_2 = \frac{(nu)_E}{n_2} \frac{A_E}{A_2} \gtrsim \frac{3 \times 10^8}{n_2} \left(\frac{215}{2}\right)^2 y \qquad (13)$$

where the subscripts 2 and E refer to 2 $R_\odot$ and 1 AU, and y (≥ 1) is a factor that takes account of a divergence greater than $A \propto r^2$ in $r \geq 2\ R_\odot$. Taking[133] $n_2 \gtrsim 3 \times 10^5$ cm^{-3}, it follows that $u_2 \gtrsim 115$ km sec^{-1} (corresponding to $M^2 \gtrsim 1$), which is a much larger flow speed than is predicted by the spherically symmetric expansion model discussed above (for coronal temperatures $\lesssim 2.5 \times 10^6$ $^\circ$K; cf. section 3.1.3). A possible explanation of the discrepancy is as follows.

A rapidly diverging flow geometry tends to decrease the density scale height of the expanding corona (cf. (7)) and thus to increase the outward-directed pressure gradient force, while the inward-directed gravitational force is left unaltered (cf. (8)). This effect, which enhances the acceleration of the flow in the region of rapid divergence, is manifested in the solution topologies of (10) for a rapidly diverging flow (cf. Figure 4) and in the corresponding velocity and density profiles (cf. Figure 5).[112] It is seen that sufficiently rapid divergences can produce the required high flow speeds and low densities in the lower and middle corona. The same general flow characteristics can also result from direct momentum addition[91] (e.g., associated with a mechanical wave flux), and it is possible that a combination of flow geometry and momentum addition effects actually produce the inferred high flow speeds low in the solar corona.

This example illustrates one important consequence of the rapidly diverging, magnetically controlled flow geometries characteristic of coronal holes. As is discussed below (cf. section 3.1.5), such geometries also have important consequences for the energy balance of the flow. Of course, the mass, momentum, and energy balance problems, as well as the problem of determining the magnetic structure of coronal holes (cf. section 3.1.6), are not independent and eventually must be solved in a self-consistent manner. Yet, before a fully self-consistent description can be obtained, there is much groundwork (both theoretical and observational) to be laid, especially for the energy balance and coronal magnetic field problems, and for this reason we shall consider these problems separately.

3.1.5 Energy balance in the coronal expansion

The problem of the energy source for the coronal expansion is closely related to the general problem of coronal heating. The latter problem arises from the existence of a hot (10^6 ^oK) corona overlying a cool (6×10^3 ^oK) photosphere (cf. Figure 6) and the consequent need for a mechanism that transports energy from (or through) the photosphere and deposits it in the corona. It is currently thought that this energy transport is effected by fluctuations that are generated in the solar convection zone and propagate or are convected to the corona where they give up their energy to the thermal and/or flow energy of the plasma. In the conventional picture[117] the energy is carried by a mechanical wave flux, but energy sources involving such phenomena as the annihilation of emerging magnetic flux loops or of magnetic structures twisted by differential rotation cannot be ruled out. In the following discussion, we shall assume that MHD waves carry the energy into the corona, since this is the hypothesis that is currently most amenable to observational and theoretical tests. Nevertheless, most of our general comments will apply equally well to other possible mechanisms that must be turned to if the MHD wave hypothesis fails to meet the tests. Hence, at present, it appears that the flow energy of the coronal expansion is directly supplied by two sources: (1) thermal conduction from the hot corona; and (2) that part of the MHD wave flux (responsible for heating the corona) that does not supply its energy directly to the thermal conduction flux. These two sources will be the focus of our attention throughout this subsection.

Energy balance in a steady coronal expansion can thus be described by

$$nmuA\left(\frac{1}{2}u^2 + 5\frac{kT}{m} - \frac{GM_\odot}{r}\right) + (q + w)A = \text{constant} \qquad (14)$$

where the MHD-wave energy flux density, w, is defined by $Q^e = \nabla\cdot\underline{w}$, $Q^e = Q_e^e + Q_p^e$, $\underline{q} = \underline{q}_e + \underline{q}_p$, and $T = (T_e + T_p)/2$. (14) can be derived directly from (5), along with (3) and (4), when the coronal expansion is assumed to be the steady, radial flow of a proton-electron plasma in which viscous effects (terms involving $\underline{\tau}$) are negligible. Evidently, (14) is just a statement that the total energy flux in the expansion (including the convected flux of bulk flow energy, enthalpy, and gravitational potential energy, as well as the thermal conduction flux and MHD wave flux) is constant, or that the total energy flux density along a flow line varies inversely as the cross-sectional area, A, of the flow tube. For a typical[52] high-speed-stream energy flux density of 1.1 erg cm^{-2} sec^{-1}, it follows that the outward energy flux density (carried by conduction and waves) at the base of a coronal hole has a value of $\sim 8 \times 10^5$ erg cm^{-2} sec^{-1} (assuming an areal divergence a factor of 7.5 greater than an r^2-divergence[133]). This value is comparable to or larger than that corresponding to thermal conduction from the corona to the chromosphere and is much larger than that associated with radiation from the corona (cf. Figure 6). Thus, contrary to widely accepted conclusions drawn from spherically symmetric models, it is clear that the solar wind plays a dominant role in the coronal energy balance in coronal hole regions, and probably in all other open-field-line regions. For this reason, a complete solar wind theory must take into account the entire height range of the corona (possibly the transition region as well)[111] and not just that range above the coronal temperature maximum, to which previous solar wind theories have generally been restricted.

The major unresolved problem relating to the coronal expansion lies in determining what processes effect the conversion of MHD wave energy to flow energy (which accounts for virtually all of the solar wind energy flux at 1 AU). The conversion could involve a two-step process, in which the wave flux is converted into a thermal conduction flux that in turn is converted into a bulk flow energy flux, or it could involve a one-step process, in which the plasma is directly accelerated and the thermal conduction flux is (everywhere above the temperature maximum) a small fraction of the total energy flux. (An alternative to the two-step process is the heating of the protons in the region well above the coronal base, where protons and electrons are not thermally coupled, and the subsequent conversion of convected thermal energy to flow energy.) Unfortunately, the real process probably lies somewhere between these two extremes, and it will be necessary to understand both thermal conduction and wave propagation and dissipation throughout the corona and inner solar wind. This will require major theoretical and observational advances in the future.

Fortunately, despite their inherent limitations, spherically symmetric models developed in the past have taught us much about the physical processes important to energy balance in the coronal expansion. Such models have been constructed both for a single fluid (i.e., a single energy equation for the proton-electron plasma; c.f. (14)) and for two fluids (i.e., separate energy equations for protons and electrons).[98] One-fluid descriptions are more tractable and are generally satisfactory unless the proton and electron temperatures are unequal and an accurate determination of one of these temperatures is needed (e.g., in the specification of electron thermal conduction). The spherically symmetric models that assume classical conduction and include no mechanical wave flux (i.e., $w = 0$) above their

lower boundaries (which always lie above the temperature maximum) predict flow speeds that are too low and conduction fluxes that are too high at 1 AU. These results indicate that thermal conduction is limited below its calssical value[96] and probably also that the coronal expansion is heated and/or accelerated by a mechanical wave flux beyond the temperature maximum[153,73]. (These conclusions probably will also hold in the non-spherically symmetric case.) Both the problems of conduction inhibition and of extended wave heating and acceleration have been studied in the past few years (in the context of spherically symmetric models), but neither has yet been resolved.

There are several ways in which the thermal conduction might be changed from its classical form, which in the nonmagnetic case is represented by $\underline{q} = -\kappa_o T^{5/2} \underline{\nabla T}$. In the presence of plasma turbulence (e.g., generated by an instability), the heat transport can be significantly modified. In particular, the skewing of the electron distribution function associated with the thermal conduction process itself can drive certain wave modes unstable, leading to turbulence that can produce the conduction modification[58]. Even in the absence of plasma turbulence, the fact that solar wind electrons are not collision-dominated beyond a few solar radii indicates that the classical conduction law is not valid, and in this case the heat flux density, $\underline{q}$, may take on a form quite different from that shown above[155,85]. Of course, since in the solar wind the electron gyrofrequency is much larger than the electron collision frequency, a non-radial component of the ambient magnetic field (cf. Figure 2) can reduce the radial conduction flux[48], as can long wavelength fluctuations of the magnetic field reduce the conduction flux along the field[82]. These latter two (magnetic) conduction inhibition

processes are reasonably well understood but do not appear to be very important for the coronal expansion problem, whereas the former two processes (micro-turbulence and collisionless effects) are probably important but are not well understood at present. It should be noted that, even for classical conduction, the problem of a conductive flow in a rapidly diverging geometry has not been fully studied. It is not clear, for example, whether the geometric effects of a coronal hole tend to increase or decrease the conductive energy supply (per unit mass) to the coronal expansion in the classical limit[91]. In addition, the diverging geometry modifies the conduction inhibition problem since it leads to a lower density plasma near the sun, as well as an enhanced skewing of the distribution function in the diverging region.

Studies of wave heating and acceleration in the coronal expansion have concentrated on the propagation and damping of MHD waves in the fast and Alfvén modes[13,14,84]. The slow mode wave, which has been presumed to be damped below the coronal temperature maximum, will have to be considered in the future, as a result of the newly appreciated importance of this lower atmospheric region (see above). There are still aspects of the wave propagation and damping in a spherically symmetric system (which is all that has been considered) that are not satisfactorily understood. Specifically, for the fast mode, momentum transfer effects (analagous to radiation pressure) have yet to be included in models; for the Alfvén mode, the non-linear damping process needs to be better understood; and for both modes, the problem of mode transfer in a curved field geometry has not been adequately considered. These problems should be soluble with currently available plasma physics techniques, in contrast to the problems which now arise with the need to

consider the rapidly accelerating flows in rapidly diverging magnetic geometries inside 2 $R_\odot$. In such rapidly diverging regions, the shortest scale length characteristic of the fluid-field system will not generally be large in comparison with the wavelength of the waves (as long as the wave period is greater than about one minute), and thus the problems of refraction, damping, and mode transfer become very difficult. Some theoretical basis currently exists for dealing with Alfvén waves in this sort of situation[84], and it would appear that the outstanding theoretical problems for all three wave modes can be solved in the next several years.

Throughout the above discussion we have ignored the effects of viscosity. It has been known for some time that viscous effects are unimportant in the overall energy balance of the coronal expansion[151], but it is possible that energetically unimportant parameters, such as the proton temperature at 1 AU, can be significantly modified by viscous effects[199]. However, the key to understanding the coronal expansion lies in the physical processes important to the overall energy balance of the system, and this is why we have emphasized the theoretical studies of energy transport by waves and thermal conduction in coronal holes and other open field line regions. In the same spirit, it should be emphasized that the observations that are critical to understanding the coronal expansion involve these energetically important processes, rather than processes like thermal conduction at 1 AU, which may be unrelated to the conduction process in the corona and inner solar wind[53].

3.1.6 The coronal magnetic field

It should be clear to the reader by now that the solar magnetic field plays a critical role in the coronal expansion, although this

point has not been fully appreciated by solar wind workers until the recent realization of the importance of coronal holes. Unfortunately, owing to both observational and theoretical difficulties, the magnetic field in the corona cannot at present be accurately determined. The resolution of this problem must be given a high priority in future solar wind research.

An especially simple description of the coronal magnetic field can be obtained by using the potential field approximation. In this approximation it is assumed that between the photosphere and a (spherical) source surface in the corona local currents do not significantly modify the magnetic field structure (i.e., $\nabla \times \underset{\sim}{B} \approx 0$). Then boundary conditions can be placed on the magnetic field from photospheric magnetic observations and from the assumption that the field is radial at the source surface, and Laplace's equation can be solved to yield the magnetic field everywhere between the photosphere and the source surface[167,3,1,119]. Potential field models can thus predict the magnetic field geometry in coronal holes and other open field line regions, but the validity of such predictions remains in doubt. Although the use of a source surface implicitly takes account of the fact that the coronal expansion severely distorts the solar field beyond the surface (i.e., beyond 2 $R_\odot$ or 3 $R_\odot$), it is likely that, at least in some regions, the plasma energy density is sufficiently large (in comparison with the magnetic field energy density) to distort the field significantly well inside the source surface[49]. This may be the reason why potential field representations with reasonable source surface locations predict open field line regions where coronal holes are observed but yield much smaller areas for the open field regions than are observed for the coronal holes[158].

If the potential field method cannot provide a satisfactory representation of the coronal magnetic field, and if observations of only the photospheric magnetic field are available, then it will be necessary to obtain a self-consistent solution of the flow equations (including

magnetic stresses) together with Ampere's law ($\nabla \times \underline{B} = 4\pi \underline{j}/c$) in order to determine the coronal field geometry. A simple example of such a self-consistent solution has been obtained [159] for an isothermal corona and a photospheric dipole field (cf. Figure 7). However, a full MHD solution with realistic photospheric boundary conditions is prohibitively difficult at the present time, and it is hoped that some compromise between the potential field and full MHD representations will prove adequate. One possibility is a description currently being developed[203], in which the field is assumed potential everywhere except near coronal streamers.

In the coronal magnetic field problem, as in the coronal expansion energy balance problem, theoretical progress will, in the near future, be severely limited by the lack of satisfactory observations, unless certain observational programs are aggressively pursued.

3.1.7 Future observations

Perhaps the most important observational information needed by the coronal expansion theorist is an identification of the waves transporting energy from the lower atmospheric layers to the corona and a measurement of the energy flux density carried by each type of wave (whether these be propagating MHD waves, as in the conventional coronal heating picture, or whether they be some other type of fluctuations, as mentioned at the beginning of section 3.1.5). At the present time, no observational technique has been shown to be capable of yielding this information, but there are hopeful avenues to follow. If the energy flux is transported in one of the three MHD modes discussed earlier, then evidence of these waves should be detectable in transition-region and coronal EUV lines that are observable with detectors borne above the earth's atmosphere by rocket, satellite, or space platform. Some appropriate observational

data is currently available, but the theoretical basis for its interpretation is not yet as firm as is necessary. Specifically, a nonlinear MHD description of waves propagating through the transition region and lower corona, coupled with appropriate atomic physics (but not radiative transfer) calculations, is needed to determine what should be looked for in the observational data. Another technique for observing these waves involves a ground-based K-coronameter or a space-borne coronagraph, either of which might allow the direct observations of wave motions in coronal density structures. It would appear that the most serious problem with this type of observation is the superposition of many structures along a given line of sight and the consequent masking of the motion of an individual structure. Other potentially useful indirect methods of observing wave motions in the corona include scintillation[200] and radar[65] techniques, but the viability of neither of these methods has yet been well established. In situ observations of waves beyond some 4 $R_\odot$ would be possible with a spacecraft such as the proposed Solar Probe, and such observations would be invaluable, even though they would not provide a complete picture of wave propagation and damping in the lower corona.

A critical check on any future coronal expansion theory is the observation of the radial profile of the coronal temperature in coronal hole regions. Probably the best chance of obtaining such a measurement rests with the Lyman-alpha scattering technique[60,16], which yields a value for the neutral hydrogen temperature from observations of resonant scattering of Lyman-alpha radiation in the corona. Presumably, at least in the lower corona, the neutral hydrogen temperature should be very nearly equal to the proton and electron temperatures. Again, in situ

observations of the coronal temperature beyond 4 $R_\odot$ could be obtained by the Solar Probe (on only a single trajectory of the spacecraft, of course), and course), and such measurements should be complementary to those obtained by the Lyman-alpha technique at lower levels. Finally, a method of estimating the temperature at various levels in the corona and, perhaps in the transition region is the observation of the ionization states of various atoms in the solar wind[94]. Unfortunately, owing to the uncertainty in the 'freezing-in' points for the various ionization states in coronal hole regions (cf. section 3.3), this method, by itself, does not give a complete picture of the coronal temperature profile and is thus useful but not entirely adequate. Of course, if the electron temperature is relatively constant over the freezing-in range, the usefulness of this method is increased.

Excellent clues to the coronal expansion energy balance problem could be obtained from measurements of the variation of the total escaping mass flux and energy flux densities across a coronal hole. Almost the only practicable means of making such measurements would be with an out-of-the-ecliptic space probe (equipped with standard solar wind plasma instrumentation) that passes over the solar pole (s) near solar minimum, when large solar polar coronal holes are known to exist. Such a space probe could also yield important information about the interplanetary magnetic field above a coronal hole and about the high-latitude photospheric magnetic field, if the probe were equipped with standard magnetometers and a magnetograph (not necessarily high-resolution). High latitude photospheric magnetic field data is, of course, not currently available, and this lack of data may produce significant flaws in potential field representations of the coronal magnetic field. It is

possible that within the next several years the coronal magnetic field problem can be resolved by direct observation, which would obviate the need for the cumbersome combination of photospheric observations and a theoretical magnetic field model. Polarimeters that might provide the necessary coronal observations are currently being developed. However, in the absence of direct observations of the coronal field, there is a need to improve the observations of the magnitude of the photospheric field, especially below coronal holes. Improved resolution in the photospheric measurements is not nearly so important to the coronal field problem.

3.2. Development of Solar Wind Structures

In the preceding discussion of the coronal expansion, we did not explicitly consider the effects of spatial and temporal variations of the coronal plasma and magnetic field boundary conditions. Yet it is just such spatial and/or temporal variations that can give rise to large-scale structures in the solar wind. Fortunately, the coronal-expansion and solar-wind-structure problems can usually be largely decoupled, with the solutions to the one-dimensional coronal expansion problem (for a representative set of flow tubes) providing the boundary and/or initial conditions for the multi-dimensional solar wind structure problem.

We shall consider here only large-scale structures, which are characterized[98] by length scales that are comparable to or larger than the distance over which a sound wave propagates (in a frame of reference moving with the plasma) during the time required for the plasma to move

through its primary scale size. Although small-scale MHD structures (such as Alfvén waves[18] and hydromagnetic discontinuities[171,26]) and microscale structures[14] will not be considered for their intrinsic interest, we shall continue to discuss their expected roles in the physics of the

larger-scale phenomena (cf. section 3.1.5). Unfortunately, without observational improvements our understanding of the smaller-scale processes will not progress rapidly beyond its current, rather primitive state. Such improvements include better time resolution in most observations and greater spatial coverage by the observing spacecraft (viz., missions like the Solar Probe and Out-of-the-Ecliptic). On the other hand, current observational techniques have been adequate for the development of a reasonably good understanding of large-scale solar wind structures.

In this section we shall discuss large-scale structures that fall into two categories: (1) corotating structures, which arise from spatially non-uniform boundary conditions that vary little in the time it takes a fluid element to be convected from the sun to the observer; and (2) transient structures, which arise from boundary conditions that vary significantly in a time short in comparison with the sun-observer transit time. The archetypal structures of these two categories are high-speed solar wind streams and interplanetary magnetic sectors for the former and flare-produced interplanetary disturbances for the latter. The nature of an intermediate type of structure, which is associated with spatially non-uniform boundary conditions that vary over a time comparable to or somewhat less than the sun-observer transit time, can be understood qualitatively once we understand the basic physics of the corotating and transient structures.

3.2.1 Corotating structures

Even a superficial examination of solar wind data reveals the almost continuous presence of various types of structure in the expanding

solar wind flow. One of the dominant structures is the high-speed solar wind stream, which was first identified in the Mariner 2 data of 1962[138]. The scale size and spatial location of high speed streams are also found to be characteristic of organized unipolar regions of the interplanetary magnetic field, which have been termed interplanetary magnetic sectors[197]. Both the streams and the sectors are frequently observed to reappear on successive solar rotations, so it would seem that they are long-lived spatial structures corotating with the sun.

Observations of high-speed solar wind streams. No two high-speed solar wind streams observed at 1 AU are quite the same, but all streams have certain common features that are illustrated in Figure 8. In this example, we see that: (1) the flow speed rises rapidly from the ambient, peaking after about one day, and declines more gradually, returning to the ambient level after about four more days; (2) the density peaks sharply while the speed is increasing and falls below the ambient into a broad minimum as the speed gradually declines; and (3) the variation of the proton temperature is much like that of the velocity (The electron temperature, however, varies little with flow speed, though it tends to be lowest in high-speed streams.). Another common stream feature (not shown in Figure 8) is the tendency for the flow to come from slightly east of the sun as the speed begins to rise and from a more westerly direction as the speed approaches its peak[172,137]. The azimuthal flow speed, however, generally remains small in comparison with the radial flow speed.

High-speed solar wind streams are often observed to recur with a 27-day period (the synodic solar rotation period), especially during the late declining phase and the minimum of the solar cycle[138,203]. This

recurrence implies that the streams are associated with long-lived, corotating coronal structures, and as was mentioned earlier (cf. section 3.1.4) these coronal structures have been shown to be coronal holes. Figure 9 provides an example of two recurrent streams and their associated coronal holes, as they evolve over three solar rotations. The relationship between streams and interplanetary magnetic sectors, which is evident in Figure 9, will be discussed later.

Basic physics of stream interactions. If the expanding coronal plasma corotates very near the sun but flows essentially radially outward beyond a few solar radii, then outside the corotation region the solar magnetic field is drawn into a spiral shape like that shown in Figure 2, provided the frozen field condition ($\nabla \times (\underline{E} + \underline{u} \times \underline{B}/c) = 0$) is met. In this case, a magnetic field line traces the plasma that has originated at the point where the field line intersects the coronal base (i.e., the magnetic field lines are the streaklines of the plasma). Thus, owing to solar rotation, the streaklines are not parallel to the streamlines of the flow, which are radial (in a stationary reference frame) outside the corotation region, and the plasma at different points along a given streamline has come from different regions of the corona. Accordingly, if one coronal region is a source of fast solar wind and the regions adjacent (in longitude) to it are sources of slow solar wind, then both fast and slow flows will appear on the same streamline.

The consequences of such a situation are illustrated in Figure 10. Here the fast plasma stream overtakes the slow flow ahead of it and leaves behind the slow flow at its rear. The plasma is compressed towards the front of the stream (where the radial velocity gradient is negative) and rarefied towards the rear of the stream (where the radial

velocity gradient is positive). As the flow progresses outward, the motion of fast material relative to slow causes a narrowing of the compression region (relative to the rarefaction region) and a steepening of the gradients in this region, which may eventually lead to the formation of a shock (or a shock pair: see below) at the front of the stream.

Reference to Figure 8 indicates that the observed characteristics of plasma density and velocity in streams are consistent with the qualitative description just presented. Furthermore, we see in Figure 10 that the pressure gradients associated with the compressed plasma at the stream front will tend to produce azimuthal flows that are consistent in direction with the observed stream-associated azimuthal flows mentioned earlier.

Hydrodynamic descriptions of stream interactions. As with models of the coronal expansion, theoretical descriptions of solar wind streams have usually, for simplicity, ignored the effects of magnetic stresses (although some MHD descriptions have been developed[45,136]). The resulting hydrodynamic models should be generally satisfactory since the magnetic field is dynamically unimportant throughout most of the solar wind. It is only in the compression fronts of streams that magnetic stresses may play a significant role, but their inclusion in these regions should not alter the basic conclusions drawn below.

The existence of spatially (viz., azimuthally) non-uniform boundary conditions in conjunction with solar rotation requires the use of (at least) two independent variables in stream descriptions. One of these is still the radial distance, r and the other can be either the azimuthal angle, ϕ, or time, t, provided the boundary conditions are time stationary in the reference frame rotating with the sun. The equivalence of ϕ

and t is expressed by $\phi = \phi_0 - \Omega t$, with Ω the solar rotation frequency, ϕ_0 a fixed longtiude in a stationary frame, and ϕ the longitude in the corotating frame. This equivalence leads to the view that the (periodic) time dependence at the point (r, ϕ_0) arises from the rotation of a spatial structure. Clearly, the introduction of a third dimension (colatitude, θ) is not as important as that of the second dimension because the strong effects of solar rotation only relate to the azimuthal dimension (ϕ).

The hydrodynamic equations that have been used in the past to describe the structured solar wind are

$$\frac{\partial n}{\partial t} + \underline{\nabla} \cdot n\underline{u} = 0 \tag{15}$$

$$nm\left(\frac{\partial}{\partial t} + \underline{u} \cdot \underline{\nabla}\right)\underline{u} = -\underline{\nabla} p - nm \frac{GM_\odot}{r^2} \tag{16}$$

$$\left(\frac{\partial}{\partial t} + \underline{u} \cdot \underline{\nabla}\right)\left(p/n^\alpha\right) = 0 \tag{17}$$

These equations are simpler than those used to describe the coronal expansion in that they do not explicitly contain source or transport terms, but they are more complex in that they are multi-dimensional, whereas the coronal expansion equations are one-dimensional (cf., however, section 3.1.6). Although the simplifications are necessary to maintain a reasonably tractable system in more than one dimension, they are probably also quite reasonable on physical grounds (except for the neglect of electron thermal conduction near strong compressions). This is because beyond several solar radii the solar wind is probably essentially an adiabatic ($\alpha \gtrsim 5/3$) expansion.

Various simplifications of (15)-(17) have been used in the study of solar wind streams. Most studies have been two-dimensional, although we shall mention some three-dimensional results later. These studies have included the analytic treatment of a linearized set of equations[28,173,120] and computational evaluations of the nonlinear equations[124,64,157], both classes involving the independent variables r and ϕ and the dependent variables n, p, u_r, and u_ϕ. However, one of the most fruitful approaches, and the one whose results we shall consider here, is a nonlinear two-dimensional radial flow model[100], which was originally developed to study transient phenomena[95]. The replacement of ϕ by t in this model is equivalent to treating the spatially nonuniform, time-independent boundary conditions that rotate beneath a given streamline as spatially uniform time-dependent boundary conditions (see above discussion of the equivalence of ϕ and t). The assumption that $u = u_r$ (i.e., the neglect of terms of order u_ϕ/u_r) appears to be reasonably well justified by observations and theoretical results. An additional benefit of considering this model is that the following results will also have direct application to our discussion of transient structures (cf. section 3.2.2).

Some theoretical predictions. Figures 11, 12, and 13 show some results of the nonlinear, two-dimensional, radial-flow stream model. For these results, as well as for those to be shown in Figures 14, 15, and 16, the inner boundary of the stream model was taken to be somewhere between 20 $R_\odot$ and 30 $R_\odot$, where the solar wind is already highly supersonic. The results presented would not vary substantially if the inner boundary were taken closer to the sun, but if it were taken inside the sonic point in the flow, there would be a significant increase in computational difficulty.[45]

Figure 11 shows radial profiles of u, n, p, and T (interpreted as T_p since it is recognized that T_e would be modified by thermal conduction) at six different times in the range $0 \leq t \leq 250$ hours. In $t < 0$ and $t > 100$ hours conditions at the inner boundary are held steady, while in $0 \leq t \leq 100$ hours the temperature is increased linearly for 50 hours and then decreased at the same rate for the second 50 hours (referred to as a 100 hour pure temperature pulse). The development of the resultant high speed stream is clearly a quantitative manifestation of the phenomena described qualitatively in connection with Figure 10. As the disturbance moves outward the plasma in the stream front is strongly compressed, forming a pressure ridge, and as the gradients steepen shocks are formed on either side of the pressure ridge. The shocks are both driven away from the pressure ridge (in opposite directions) in the sense of the respective pressure gradient forces. Although in a frame moving with the plasma the downstream (forward) shock is moving downstream and the upstream (reverse) shock is moving upstream, in a stationary frame both shocks are convected downstream at a speed much larger than their relative speed of separation. Since even an adiabatic shock is not isentropic (i.e., p/n^{α} is not constant across the shock), 'entropy structures', like those shown in the density and temperature, can develop. While the density peaks at the middle of the pressure ridge, the temperature peaks in the two strongly heated regions just inside the shock fronts. Such structures, which owe their existence to the shock formation, can survive even after the shocks are dissipated and pressure equilibrium is attained[175].

The development of solar wind structures depends strongly on the period of the perturbing signal (or, alternatively, on the scale size of the azimuthally varying inner boundary condition) as is illustrated in

Figure 12[102]. Here plots of u and n as functions of time (which represent what a spacecraft at 1 AU would observe) are shown for pure velocity pulses at the inner boundary with periods τ = 15, 50, and 150 hours and with identical peak amplitudes. Evidently, the 15 hour stream is the most highly evolved and the most strongly damped, whereas the 150 hour stream has just begun its evolution and has been damped relatively little. The pressure ridge in the 15 hour stream is fully developed and has sent a strong (shocked) disturbance running downstream and a weaker (unshocked) disturbance running upstream (in the rest frame of the plasma). In fact, the material originally contained in the 15 hour stream has approached the ambient speed and density, while the high velocity pulse and its associated compression have run into the material ahead and the deep rarefaction lies in the material behind. The compression in the 50 hour stream is nearly fully developed, but the 150 hour compression is not yet near its peak amplitude.

The tendency (just noted in Figure 12) of the interplanetary medium to act as a low-pass filter for solar wind disturbances is well illustrated in Figure 13[102]. Specifically, we see that structures with wavelengths comparable to or greater than the transit time to 1 AU (i.e., period, τ, comparable to or greater than transit time to 1 AU, which is $\sim$ 80 hours) are damped very little at 1 AU, whereas structures with much shorter wavelength are strongly damped at 1 AU. Similarly, an observer at 20 AU would observe a structure with a 1 AU wavelength ($\tau \sim$ 3 days) to be strongly damped, and a structure with a 10 AU wavelength ($\tau \sim$ 27 days) to be only weakly damped. Thus, the dominant scale of solar wind structure can be expected to increase with increasing distance from the sun.

This change in structure is manifested in Figure 14, which shows density contours from 1 to 20 AU that are calculated from the input of solar wind observations at 1 AU over one solar rotation[103]. Here the two-stream structure at 1 AU develops two shock pairs by 3 AU and evolves into a single structure with separating forward and reverse shocks by 10 AU. Some other alterations of solar wind character concomitant with this basic structural change are manifested in the histograms of Figure 15, which show the distributions of solar wind speeds, densities, and temperatures at 1 AU (observed) and 20 AU (predicted) for a rather typical three-stream (at 1 AU) rotation[103]. The distribution of speeds, which is broad at 1 AU, is drastically narrowed at 20 AU, owing to the strong damping of the large-amplitude shorter-period ($\sim$ 5-day) structures, which preludes the dominance of the smaller-amplitude 27-day wave. The density and temperature distributions show the opposite trend toward broadening at greater distances from the sun. Especially noteworthy is the tendency of the densities at 20 AU to cluster well away from the average density, with densities of less than half the average occurring more than 50% of the time and densities of more than twice the average occurring more than 15% of the time. Each of these density clusters (the very low and very high) tends to occur in a continuous time interval (a fact not inferable from Figure 15).

The conseqences of the changing nature of the solar wind throughout the solar system (in the ecliptic plane) for planetary magnetospheres is discussed in another paper in this collection[177].

Observational checks. As was noted earlier, our qualitative description of stream evolution seems to be consistent with observed properties of streams at 1 AU. A more quantitative comparison of

observation and theory is made in Figure 8, where the model stream of Figure 11 is compared directly with observational data. The agreement is seen to be remarkably good, even when it is realized that the period and amplitude of the temperature pulse at the inner boundary were adjusted to obtain a best fit. However, a better observational test of this model has been performed using satellite data at 1 AU as an inner boundary condition, predicting the solar wind behavior at 4.5 AU with the radial flow model, and comparing the predictions with satellite data obtained at 4.5 AU[71]. Figure 16 shows that the model was quite successful in predicting the evolution of all the observed large-scale features of the stream. We conclude that our current understanding of the development of large-scale corotating structures near the ecliptic plane (the region of applicability of the model considered) is in very good shape.

Recently, as is discussed in the following paragraph, several theoretical studies dealing with corotating structures out of the ecliptic plane and with the general problem of meridional flow of the solar wind have been initiated. Although interplanetary scintillation measurements[93] can give some information on solar wind structure out of the ecliptic plane, in situ measurements by an out-of-the-ecliptic space probe would prove invaluable in testing the results of and in stimulating the development of theoretical models. In addition, a conspicuous observational gap in the ecliptic plane lies in the region between the sun and the earth. A spacecraft like the Solar Probe would be very helpful in testing our understanding of the evolution of the smaller large-scale structures that are significantly damped by the time the solar wind reaches 1 AU (cf., Figure 13). Of course, further observations in the region beyond 1 AU that are capable of providing useful

density and temperature data (in addition to the presently available speed data) would be helpful in adding to our understanding of corotating structures in that region.

Extending the models. Currently there is a considerable effort going into the problems of the evolution of large-scale corotating structures out of the ecliptic plane[157,188,176] and of three-dimensional solar wind flow[157,186,187,189]. Since solar rotation plays such an important role in the development of solar wind structures, it is clear that the development at higher solar latitudes will be quite different from that in the ecliptic plane. Because of the decreased importance of solar rotation, meridional flows may play a more significant role in determining the nature of the solar wind at high latitudes. Of course, meridional and azimuthal components of the flow can modify the evolution of smaller-scale features of corotating structures even in the ecliptic plane (e.g., the formation of shocks near a stream front[186]).

In the same context, the inclusion of magnetic forces[182,45] and electron thermal conduction in stream models should be considered. Such details of the structure problem certainly must be worked out in the future, but they do not present any fundamental difficulties (in understanding corotating structures) comparable to those faced in the coronal expansion problem.

Interplanetary magnetic sectors. The interplanetary magnetic field exhibits a tendency (when observations are suitably averaged) to point toward or away from the sun (along the basic spiral orientation of Figure 2) for intervals of several days. These intervals of organized magnetic polarity tend to recur with a 27-day period, which implies the existence of a large-scale interplanetary magnetic sector structure that

corotates with the sun[197,198]. One might expect that magnetic sectors should be closely related to recurrent solar wind streams, and this suspicion is confirmed by observations (e.g., Figure 9). Streams tend to be characterized by a single magnetic polarity (again, when suitable averages are taken), but contiguous streams sometimes exhibit the same polarity, so there is not a one-to-one correspondence between sectors and streams. Rather the organized interplanetary magnetic polarity seems to reflect the magnetic polarity of the coronal region from which the solar wind has come, so if two contiguous streams originate in separate coronal holes with the same polarity, they will together give rise to a single two-stream magnetic sector.

Thus, it would seem that streams are the more basic interplanetary structure and that magnetic sectors provide a valuable solar-interplanetary tracer. For example, in Figure 9, where there is a good one-to-one correspondence between streams and sectors, the sector polarity gives a clear indication of which polar coronal hole has extended to low enough solar latitudes to give rise to a solar wind stream (note the dominant positive polarity of the northern hole and the dominant negative polarity of the southern hole). Of course, in periods other than the declining phase of the solar cycle the related coronal, interplanetary-sector, and solar-wind-stream structures are not usually so simple as that shown in Figure 9[101].

3.2.2 Transient structures

The most familiar solar wind transient structure is the solar-flare-produced interplanetary shock wave[63], an example of which is shown in Figure 17. However, it appears that flare-produced interplanetary

shocks are only the most energetic members of a broad class of coronal mass ejection events[123,67], which are associated with a subset of the long-observed coronal transient events. Whether the less energetic coronal transient events produce an observable disturbance at 1 AU is not clear at present, although there is some indication that very subtle large-scale solar wind features (termed non-compressive density enhancements) are the interplanetary manifestation of the ordinary coronal transients[69,70].

The general inferences that can be drawn about flare-produced interplanetary shock waves from observations are summarized in Figure 19[99]. The shape of the shock at the leading edge of the disturbance resembles that of a distorted sphere and is quite different from the shape of a shock that might be associated with a high-speed solar wind stream at 1 AU (cf. Figure 10). (It appears that almost all of the interplanetary shock waves observed at 1 AU have been produced by solar flares and thus that stream-produced shocks generally develop only beyond 1 AU (cf. 3.2.1).) The shock generally moves past the earth with a speed on the order of 500 km sec^{-1}, but its speed in the rest frame of the plasma is much less, so the shock is of intermediate strength and is largely convected through interplanetary space (beyond 1 AU). A reverse shock that might be expected to follow the observed forward shock (cf. section 3.2.1) is almost never seen[35]. However, the forward shock is followed by a 0.1 to 0.2 AU thick region of compressed ambient solar wind plasma, which is expected to be bounded (upstream) by a tangential discontinuity that marks the leading edge of the flare ejecta[79]. Sometimes a 0.01 to 0.1 AU thick shell of helium-rich material is associated with the flare ejecta[79,31]. Finally, a localized stream of high-speed, low-density

plasma generally follows the flare and lasts for at least two days. One interesting and important feature of the flare disturbance that has not been observationally determined is the magnetic topology in the region of the flare ejecta (i.e., whether the field lines in this region are open or closed)[66,130]. The same question arises for all coronal transients (and their interplanetary counterparts), and it is certainly an important point to be resolved by future observations.

Hydrodynamic descriptions. In developing theoretical descriptions of flare-produced shocks, solutions to (15)-(17) have generally been sought for the case of non-steady, radial, spherically symmetric flow. Early studies[150,170,43] made use of the classical theory of progressing (self-similar) waves[37]. However, with the development of the numerical model discussed at some length in section 3.2.1[95], the highly specialized solutions of similarity theory, which proved very valuable in the early studies, became outmoded[98]. Despite the differences in the geometrical shape of the structures involved, the same physical assumptions are required in applying this numerical model to solar wind streams and to flare-produced shocks, so the entire discussion relating to Figures 11-13 is also applicable here.

The two basic shock wave structures predicted by the similarity approach (viz., the blast wave and the driven wave) are found to be part of a broad spectrum of structures that are associated with the full set of solutions to (15)-(17) for radial, spherically symmetric flow. The blast wave corresponds to the short-period pulse limit ($\tau \ll 80$ hours in Figure 13), and the driven wave is associated with a longer period pulse at the inner boundary. The 15-hour wave shown in Figure 12 and the 100-hour wave shown in Figure 11 (at $t = 150$ hours) illustrate the basic

features characteristic of a blast wave and a driven wave, respectively, as observed at 1 AU. Of course, the perturbation producing these shocks would probably be better represented by a combined velocity, density, and temperature pulse at the inner boundary[46] rather than a pure temperature pulse (Figure 11) or a pure velocity pulse (Figure 13). It appears that the radial spherically symmetric numerical model can provide results that are in reasonable agreement with shock observations, if the conditions at the inner boundary of the model are properly chosen[98].

Nevertheless a more detailed description of the evolution and spatial configuration of flare-produced interplanetary shock waves will require modifications of the numerical model discussed above. Some steps have been taken in this direction with studies of non-spherically symmetric shock propagation through a spherically symmetric ambient[42] and of the effects on shock evolution of a structured ambient solar wind[176,56]. Of course, as with solar wind streams, the effects of the interplanetary magnetic field[182-184] and electron thermal conduction must eventually be included. Future theoretical advances could be greatly aided by observations like those that could be obtained on the Solar Probe and Out-of-the-Ecliptic spacecraft.

The detailed structure of collisionless interplanetary shock waves (flare- or stream-produced) is not critical to the discussion in this section but is certainly interesting in its own right. Unfortunately, without much better time resolution in space measurements, there will be no observational information available on the structure of these shocks. In the meantime, the earth's bow shock will have to serve as the one interplanetary shock whose structure can be studied[59].

Interplanetary magnetic bubbles. Finally, let us return our attention to the ordinary coronal transient events. Although it has not been observationally demonstrated, it appears likely that these events will produce closed magnetic field loops or magnetic bubbles (perhaps, flattened bubbles) moving through interplanetary space. Because of the relatively small amplitude and short duration of ordinary coronal transients, we expect, on the basis of Figure 13, that solar wind structures (in n, u, and T) should not be very significant in $r \gtrsim 1$ AU. However, the structure associated with the direction and topology of the interplanetary magnetic field should be quite significant: the direction for planetary magnetospheres[177] and the topology for cosmic ray modulation[57]. If coronal transient events increase in frequency with increasing sunspot number[78], then the magnetospheric and cosmic ray effects associated with these magnetic bubbles should exhibit a solar cycle dependence. A simple model of interplanetary magnetic bubbles (at solar minimum), based on the nonlinear, two-dimensional, radial flow model discussed at length in this section, is shown in Figure 20[142].

3.3. Chemical Composition and Ionization State

Like most astrophysical plasmas, the solar wind is composed of many different elements, each of which generally occurs in more than one state of ionization. Although hydrogen and (to a much lesser extent) helium dominate all the important physical processes in the coronal expansion, the heavier elements may carry with them a number of important clues to our understanding of dynamical and thermodynamical processes (microphysical processes, as well) in the corona and lower solar atmospheric

layers. In general, of course, a knowledge of the solar wind chemical composition can provide an important constraint on the composition of the lower solar atmosphere, which in turn may reflect the nature of certain processes in the solar interior.

3.3.1. Helium[98,81]

Hydrogen and helium are both essentially fully ionized as they flow out of the corona (see, however, section 3.3.3), so they appear in the solar wind as protons ($^1H^+$) and alpha particles ($^4He^{+2}$). Together, protons and alphas make up more than 99% of the solar wind ions, and for this reason they are the only two ions that are routinely observed in the solar wind.

Observations. Nearly all information regarding solar wind composition is based on determinations of the energy per charge spectra of the plasma constituents. Since the solar wind is highly supersonic, each constituent should produce a relatively sharp spectral peak, and if all constituents have essentially the same bulk flow speed, the peaks in an energy per charge spectrum should be separated according to the constituents' mass per charge (cf. Figure 21). The interpretation of such data is clearly not free of ambiguities. For example, if a heavy ion species were flowing at a speed different from the proton and alpha speed, its position in the energy per charge spectrum (Figure 21) would by shifted. On the other hand, if all constituents are flowing at the same speed, different elements with different ionization states will have their peaks superposed (cf. Figure 21). Nevertheless, a sufficient bulk of energy per charge data exists[98,81] and is consistent with the few mass per charge determinations[146] (and foil experiments[62]) that proton and alpha observations seem to have a fairly firm basis.

The abundance of helium in the solar wind has an average value that varied from He/H = 3.5% at solar minimum to 4.5% at solar maximum during the last solar cycle[81]. The only time He/H $\gtrsim$ 15% is in association with a major solar flare[80] (cf. section 3.2.2). Proton and alpha flow speeds at 1 AU generally are found to differ by no more than $\sim$ 10%, with the most probable value of u_α/u_p being very nearly unity[81]. The most common occurrence of $u_\alpha/u_p > 1$ is in high-speed solar wind streams. Finally, the alpha-proton temperature ratio varies over a rather wide range of $1 \lesssim T_\alpha/T_p \lesssim 10$, with a mean of about 4[163,140]. Although much more detailed helium observations than those cited here do exist[81], there is little point in reciting them here, because, as we shall see below, not even the very basic observations cited above have been given a satisfactory theoretical explanation.

The determination of helium abundance in the solar atmosphere is a difficult problem[98]. Indirect spectroscopic determinations yield values ranging from He/H = 6% to 9%. Values ranging from 5% to 9% have been estimated for the solar interior (not necessarily the atmosphere) on the basis of an upper limit to the solar neutrino flux and also on the basis of the mass-luminosity relationship of conventional stellar evolution theory. Taken at face value, these observations indicate that the photospheric and chromospheric helium abundance is at least 50% greater than the solar wind helium abundance, but the uncertainties in the solar observations may be comparable to this difference[98].

Theory. In our discussion of the coronal expansion (cf. section 3.1) a proton-electron plasma was assumed. The introduction of a third constituent (alpha particles) seriously complicates the problem and requires, in principle, three sets of equations (3)-(5) to be used (one

for each constituent). To make the three-constituent solar wind problem tractable, most workers have assumed that the alphas represent a minor species, so that the expansion of the proton-electron gas can be described independently of the alphas, and the alpha expansion can be described in terms of the predetermined proton results[152,61,83]. (One solution to the coupled continuity and momentum equations for the three constituents has been obtained[202], but in this study it was found necessary to ignore frictional coupling terms.) It now appears that not only is the frictional force on the alphas (due to the protons) important, but also the frictional force on the protons (due to the alphas) cannot be neglected near the sun[110]. Nevertheless, our current understanding of the behaviour of alpha particles in the solar wind is based primarily on models that ignore the effects of alphas on protons.

One result of these models seems to be that Coulomb collisions alone are not sufficent to overcome (through proton-alpha momentum transfer) the tendency for the heavier alphas to expand more slowly than the protons[140]. It appears, therefore, that some microscopic plasma process that produces an 'anomalous friction' may be necessary to explain the near equality of u_α and u_p at 1 AU[83,38]. However, an anomalous frictional force cannot explain observations of $u_\alpha/u_p > 1$, and if these observations cannot be attributed to some local process in high-speed streams then some other mechanism in the coronal expansion must be sought. Two such mechanisms for producing $u_\alpha/u_p > 1$ at 1 AU have been proposed (anomalous heating of alphas near the sun of an unspecified nature[166] and resonant interaction of Alfvén waves with alphas[86]), but it is not clear at present how either model can be tested observationally[139]. The problem of explaining large values of T_α/T_p at 1 AU is not in a very good state either. So far, investigations of this problem have been largely inconclusive[109,12,135].

Studies of the solar wind helium abundance are necessarily related to the velocity question since continuity of mass along a stream tube requires that $n_\alpha u_\alpha / n_p u_p$ = constant. Unfortunately, it is not clear just what the solar wind helium problem is from an observational standpoint, because the coronal helium abundance is unknown. If plasma in the chromosphere and transition region is well-mixed, then the corona should display the photospheric helium abundance; but if thermal diffusion (in the presence of the strong transition region temperature gradient) dominates mixing processes, then the upward diffusion of heavy ions (relative to protons) should produce a coronal helium abundance significantly enhanced over that of the photosphere. Currently existing models of diffusion and mixing in the transition region have not been able to resolve this difficult problem[108,39,134]. Thus the solar wind theorist cannot be certain what coronal-solar wind abundance variation must be explained, but in view of the current state of the velocity problem it is not clear that a well posed abundance problem could at present be solved.

3.3.2 Heavy ions

Owing to the relatively low abundance of elements heavier than ^{4}He, the observation of heavy ions in the solar wind is quite difficult and can only be accomplished with current space experiments when the solar wind flux is high and the temperature is low[98,11]. (However, certain isotopic abundances of heavy elements can be determined by foil experiments for any solar wind conditions[62].) From the few solar wind energy per charge spectra that do exist for heavy ions[81] (e.g., Figure 21), some information about abundance and ionization state can be determined, but little, if any, speed and temperature information for the individual species can be extracted.

The theoretical problem of describing the expansion of heavy ions in the corona and solar wind differs from the helium problem only in that the heavy ions can always be treated as minor constituents and their ionization state can change during the early part of the expansion (i.e., near the sun). The latter characteristic allows the use of heavy ion spectra to learn something of the temperature of the coronal region from which the observed solar wind flow originated. When the characteristic expansion time for a fluid element in the corona is long compared with all important collisional-ionization and recombination times, the coronal plasma can be considered to be in ionization equilibrium, and the ionization state of a given element is determined almost exclusively by the coronal temperature. However, when the expansion time becomes short in comparison with ionization and recombination times, the ionization state of that element becomes fixed or 'frozen-in'[94]. The freezing-in point will generally be different for each solar wind ion, and, as noted in section 3.1, the high flow speeds at low altitudes associated with coronal holes may cause some freezing-in points to occur as low as the transition region. If all relevant ionization states were to be frozen-in at nearly the same electron temperature, then solar wind energy per charge spectra could give an indication of that temperature. Unfortunately, since our new understanding of coronal holes has clouded the picture of freezing-in points, we can only say that these spectra contain some information about temperatures in the corona, but it is not at present clear just what that information is or how it can be used.

3.3.3. Interstellar modification of the ionization state.

Sometimes apparently anomalously high count rates appear in the solar wind energy per charge spectra. One such case is at an energy per charge of 4.0 in Figure 21. It has been suggested that this is due to the presence of singly ionized helium ($^4He^+$) in the solar wind. Since the corona is too hot to permit such a large amount of $^4He^+$ in the coronal expansion, it is possible that the $^4He^+$ reflects the penetration of interstellar helium into interplanetary space and its subsequent ionization[94,88]. Even if this is the case, it appears that no other ions produced from interstellar gas in this way would be detectable with current observational techniques[7]. In fact, subsequent attempts to detect $^4He^+$ in Vela spacecraft data have proved unsuccessful[54]. The general problem of the penetration of the interstellar neutral gas into interplanetary space is discussed in section 3.5.

3.3.4. Future developments

Evidently, the two most important steps to be taken in improving our understanding of the chemical composition and ionization state in the solar wind are the acquisition of heavy ion observations with an ion mass spectrometer and the development of an adequate model of the basic (proton-electron) coronal expansion (cf. section 3.1). It is for this reason that, at the present time, the solar wind composition and ionization state must be considered a second generation problem, which cannot be exhaustively studied for a few years hence. Meanwhile, there are some important avenues to follow in laying a sound basis for the detailed studies that can be undertaken when the coronal expansion problem is well in hand. For example, a self-consistent three-constituent model with full energy equations should be developed and used to study the new

physical processes that become important in rapidly accelerating, rapidly diverging (coronal hole) flow[110]. The source and transport terms in such a model can be treated in an arbitrary manner at this time, as the future studies of the coronal expansion necessarily must lead to a better understanding of these terms. It must be emphasized that an overriding observational need that differs from those of the coronal expansion problem is for the development of an instrument (viz., an ion mass spectrometer) that better measures the solar wind composition and ionization state under all solar wind conditions.

3.4. The Transport of Angular Momentum

Although the mass lost from the sun through the solar wind is negligible (mass loss time $\sim 5 \times 10^{13}$ years), the angular momentum loss may be quite significant from the standpoint of long-term solar evolution. Solar wind observations at 1 AU indicate an average value of the azimuthal velocity of $u_\phi \approx 8$ km sec^{-1}, although owing to possible experimental errors, this value is very uncertain[98]. Assuming, for the moment, that this value is correct, the corresponding rate of angular momentum loss associated with the solar wind plasma is

$$dL_\odot/dt \approx -\frac{1}{2} u_\phi \, r \, dM_\odot/dt \approx 2.4 \times 10^{38} \text{ gm cm}^2 \text{ sec}^{-1} \text{ yr}^{-1}.$$

Since the solar moment of inertia is $I \approx 6 \times 10^{53}$ gm cm^2 and the sideral angular rotation frequency is $\Omega \approx 3 \times 10^{-6}$ sec^{-1}, it follows that the angular momentum of the sun is

$$L_\odot \approx I\Omega \approx 2 \times 10^{48} \text{ gm cm}^2 \text{ sec}^{-1}.$$

If we increase $dL_\odot/dt$ for magnetic effects

$$(\tfrac{1}{2} B_r B_\phi r^3 \approx 7 \times 10^{37} \text{ gm cm}^2 \text{ sec}^{-1} \text{ yr}^{-1}),$$

we obtain a characteristic time for solar angular momentum depletion of $L_\odot/|dL_\odot/dt| \approx 7 \times 10^9$ years. This is comparable to the thermonuclear-evolution time scale for the sun and thus may have important conse-qeunces for solar evolution (cf. section 3.6).

The question still remains as to the average observed value of u_ϕ. From a simple theoretical argument[149], we might expect (to a first approximation) the solar wind to corotate with the sun as long as the magnetic energy density is greater than the plasma kinetic energy density (i.e., in $r < r_A$ = radius where Alfvén Mach number is unity) and to flow free of torque when the kinetic energy density is greater. If this were a correct description, then $dL_\odot/dt \approx -\frac{1}{2}\Omega r_A^2\, dM_\odot/dt$, which would yield essentially the result derived above. However, detailed theories of angular momentum loss through the solar wind give values for $dL_\odot/dt$ as much as a factor of five smaller than that estimated above[194,22,195,199]. It also has been pointed out that fast mode waves (but not Alfvén waves) may carry away a substantial amount of angular momentum from the sun[169]. At the present time, it is not clear whether the theoretical or observational estimates are more realistic. In any case, the characteristic time for loss of solar angular momentum is small enough to be of interest (cf. section 3.6).

3.5. Interaction with the Interstellar Medium[7]

As the solar wind flows away from the sun, it must eventually come under the influence of the particles and fields of the local interstellar medium. In the solar neighborhood, the interstellar medium is largely composed of four components: a magnetic field ($\sim$3.5 μG)[75]; a

thermal plasma (density and temperature uncertain, but perhaps $0.02 \lesssim n_{ge} \lesssim 0.07$ cm^{-3}, $10^3 \lesssim T_g \lesssim 10^4$ ^oK)[180]; a neutral gas ($0.06 \lesssim n_{gH} \lesssim 0.1$ cm^{-3}, $10^3 \lesssim T_g \lesssim 10^4$ ^oK)[180]; and cosmic rays ($\sim$ 1 eV cm^{-3})[57]. The magnetized thermal interstellar plasma will tend to interact with the magnetized solar wind plasma at a (somewhat diffuse) boundary separating the two plasmas, but the interstellar neutral gas and cosmic rays can readily penetrate deeply into the region of supersonic solar wind flow.

3.5.1. The magnetized thermal plasma

As mentioned in section 3.1.3., the condition of pressure balance at the boundary (called the heliosphere boundary) between the solar wind and interstellar plasmas requires subsonic solar wind flow inside the boundary and a shock transition somewhere upstream (in the steady state). The fact that the sun is moving relative to the interstellar gas ($V_g \gtrsim 20$ km sec^{-1}) leads to a turning of the subsonic flow into a comet-like tail, as is illustrated in Figure 22. The locations and shapes of the heliosphere boundary and the shock terminating supersonic solar wind flow have not been calculated, but it is possible to estimate the boundary locations along the stagnation flow line (running from the sun toward the direction from which the interstellar gas appears to be flowing).

In the absence of magnetic stresses and neutral gas effects it can be shown that the ram pressure of the solar wind (nmu^2) along the stagnation line, just inside the shock, is about a factor of 1.12 larger than the solar wind pressure at the stagnation point on the heliosphere boundary[7]. Thus the condition of pressure balance across the heliosphere boundary yields a relation between the solar wind ram pressure just upstream of the shock and the sum of the interstellar magnetic, ram, and thermal pressures:

$$n_o m u_o^2 \, r_o^2/r_s^2 \approx 1.12 \, (\beta B_g^2/8\pi + n_{ge} m V_g^2 + 2 n_{ge} k T_g) \qquad (18)$$

where r_s is the minimum shock distance (i.e., along the stagnation line), $r_o (< r_s)$ is some reference level, u is assumed constant in $r_o \leq r < r_s$, and β (>1) accounts for the enhancement of the interstellar field due to presence of the solar wind[7]. For $nmu^2 = 2.5 \times 10^{-8}$ dyne cm^{-2} at 1 AU, the interstellar parameters given above, and $\beta = 1.5$, the minimum shock distance is estimated from (18) to be $r_s \approx 130$ AU. Effects of the interstellar neutral gas and magnetic stresses (in the subsonic region) could very well decrease this value to $r_s \approx 100$ AU (cf. section 3.5.3)[90].

The turning of the subsonic solar wind flow into the heliospheric tail (cf. Figure 22) could be accomplished purely through the interaction of the two plasmas at the heliosphere boundary, but it appears likely that the dominant process in turning the flow is associated with the friction-like interaction with the neutral interstellar gas that penetrates into the subsonic flow region (cf. section 3.5.3). The characteristic (radial) scale over which the flow is turned by the neutrals is of the order $u/\nu \approx 50$ AU, where ν is the momentum transfer collision frequency for H^+-H resonant charge exchange. Thus, we expect the stagnation point on the heliosphere boundary to be about 150 AU from the sun.

The preceding steady-state description of the heliosphere provides a useful average picture, but, in reality, the structured nature of the solar wind (cf. section 3.2; in particular Figures 14 and 15) will modify this picture considerably. We recall that in an example discussed earlier, near 20 AU the solar wind was dominated by a deep rarefaction region (with density $\sim$ 25% of the average) about 5 AU in extent and a

strong compression region (with density $\sim$ 4 times the average) some 2 AU in extent; both regions were characterized by essentially the same flow speed. If we were to choose nmu^2 appropriate to the rarefaction and compression regions, (18) (modified for neutral gas and magnetic effects) would yield shock distances of 50 AU and 200 AU, respectively. Although a steady shock could not be established at either of these distances unless the average value of nmu^2 were changed, the region of supersonic solar wind should expand and contract in the general sense indicated. Over a period of a few months, the minimum extent of the supersonic region might vary by some 20 or 30 AU, say from 90 AU to 120 AU. It is unlikely that the heliosphere boundary suffers as large perturbations, because the solar wind structures should be strongly damped in the nearly constant-density subsonic region. Of course, long period ($\tau \gtrsim 2$ years) variations in the solar wind ram pressure should be felt at both the shock and the heliosphere boundary.

3.5.2. Galactic cosmic rays.

Galactic cosmic rays can have two effects on the solar wind expansion. (The effects of the solar wind on galactic cosmic rays are discussed in another paper in this collection[57].) The higher-energy (> 10 MeV) cosmic rays have sufficiently high speeds that they can move upstream in the supersonic solar wind through net magnetic-field-aligned motions alone, whereas the lower-energy (< 10 MeV) particles are convectively inhibited from penetrating the supersonic flow region, unless the perpendicular diffusion coefficient is unexpectedly large. For this reason, the lower-energy cosmic rays which can penetrate the region of subsonic flow, provide a net pressure (at the shock terminating the supersonic flow) that acts in the same sense as the interstellar magnetic and thermal plasma pressures, that is, to drive the shock inward. Little is known about the low energy portion of the galactic cosmic ray spectrum outside the heliosphere[57], so we cannot make a firm estimate of its effect on the shock distance. However, if the energy density (below 10 MeV) were as large as 1 eV cm^{-3} the mean minimum shock distance could be reduced to 70 AU.

As the higher energy cosmic rays make their way into the solar system they undergo scattering by interplanetary irregularities, and this scattering together with outward convection by the solar wind, serves to reduce their energy density in the inner solar system from that in interstellar space[57]. The reduction in energy density is equivalent to an outward-directed cosmic ray pressure gradient that enters the solar wind equations as a negative (decelerating) contribution to the momentum source term, $\underline{Q}^m$ (= $\underline{Q}_e^m + \underline{Q}_p^m$) (cf. equation 4). Although it is not possible to specify accurately the magnitude of this deceleration,

it is clear that the maximum possible effect is small, decreasing the minimum shock distance by less than 10%.

3.5.3. Interstellar neutral gas.

The interstellar neutral gas apparently has a chemical composition basically similar to that of the sun[180], and we shall consider here only the dominant atomic hydrogen component. The effects of other elements in the gas on the solar wind are relatively minor, though interesting (cf. section 3.3)[7,192]. Interstellar atomic hydrogen, which is flowing at a speed of $V_g \approx 20$ km sec^{-1} relative to the sun in the solar neighborhood[190], penetrates rather freely into the solar system. It interacts with the solar wind directly through charge exchange with solar wind protons and indirectly through photoionization (which adds electron-proton pairs to the solar wind).

The interstellar hydrogen gas flowing through the solar system behaves as a collection of individual particles, rather than as a fluid. The motion of a single hydrogen atom in the presence of the attractive solar gravitational field and the repulsive solar Lyman alpha radiation pressure (which produce a net force $(\mu - 1)\, GM_\odot m/r^2\, \hat{e}_r$) is illustrated in Figure 23 for a dominant gravitational force ($\mu<1$) and for a dominant radiation force ($\mu>1$). If all atoms were moving with the same velocity (i.e., if $T_g = 0$), it is clear that there would be a focussing of atoms at the downwind symmetry axis for $\mu < 1$ and an exclusion of atoms from a parabolic region for $\mu > 1$. The consequences of these focussing and exculsion effects are illustrated in Figure 24, where contours of constant hydrogen density are displayed (for $t_g = 0$). Calculations of these contours assume that a hydrogen atom is lost to the system when

photoionized or charge-exchanged, although the latter process actually just produces a slow (20 km sec^{-1}) proton and fast (500 km sec^{-1}) H atom in place of a slow H atom and a fast proton. The fast H atoms are considered a part of the solar wind. Observations[190] indicate that $\mu \gtrsim 1$ and that the downwind forbidden region is filled in significantly as a result of the high interstellar gas temperature.

The distribution of interstellar atomic hydrogen throughout interplanetary space serves to slow and heat the solar wind[90,193]. The photoionization of the atoms introduces source terms in the continuity momentum and energy equations, while the more important charge exchange process affects only the latter two equations. In the charge exchange process, a solar wind proton of speed u is lost and a new proton with essentially zero speed (20 km sec^{-1}) is produced. Owing to its interaction with the interplanetary magnetic field, which is aligned nearly normal to the solar wind flow beyond 5 AU (cf. Figure 2), the new proton is rapidly brought up to the solar wind speed, but in addition it has gained a random energy equal to its flow energy. (The random motion is a circular motion perpendicular to the magnetic field in the rest frame of the plasma.) Thus the charge exchange process (photoionization as well) leads to a transformation of solar wind bulk flow energy into random energy and to a consequent slowing and heating of the plasma. In the highly supersonic solar wind, this transformation of energy obviously has a much larger effect on the temperature than on the flow speed, as is demonstrated in Figure 25.

The interaction of the neutral gas with the solar wind is, then, a friction-like interaction that involves momentum transfer and heating. In the region of supersonic solar wind flow, the neutral gas acts as an

essentially stationary frictional medium through which the solar wind passes. In the subsonic region, the flow of the neutral gas is important, as it turns the solar wind flow and directs it into the tail of the heliosphere (cf. Figure 22). In principle, the neutral gas in interplanetary space can lead to a shock-free transonic deceleration of the solar wind[193,90], but in practice n_{gH} is too small in the solar neighborhood (however, see below).

3.5.4. Interstellar clouds

It has been suggested by several authors[125,17] that the solar system may, at one or more times in the past, have been immersed in a dense interstellar cloud. We can investigate the consequences of such an immersion for the solar wind by a simple extension of the preceding discussion. (Consequences for the planets and their magnetospheres are discussed in another paper in this collection[177].) As an example, let us consider an interstellar cloud composed of atomic hydrogen ($n_{gH} = 10^2$ cm^{-3}) and dust (mass density of dust/mass density of H = 10^{-2})[127].

Interplanetary penetration of dust. It is not clear that the dust in an interstellar cloud could penetrate deeply into interplanetary space, owing to the strong solar radiation flux. Let us parametrize the radiation pressure effect (as above) by μ_d, such that the effective gravitation constant is $G' = G\ (1 - \mu_d)$. If we define $\overline{Q}$ as the frequency-averaged extinction efficiency factor for a dust grain, we can write[2]

$$\mu_d = 0.6\ \overline{Q}/\eta a \qquad (19)$$

where η (gm cm^{-3}) is the grain mass density and a (microns) is the grain radius. On the basis of (19), it appears that $\mu_d \gtrsim 1$. We shall take

$\mu_d = 1$ in order to maximize the effect of the dust in interplanetary space. It is readily shown that the resulting interplanetary dust population displays much too small a total cross-section to have any significant direct effect on the solar wind. However, solar wind protons striking dust grains will be adsorbed and neutralized, and once a grain is saturated with H, for every proton adsorbed by the grain there will be an H atom desorbed. Thus the de-ionization of solar wind protons on dust grains can serve as the source of an atomic hydrogen density distribution in interplanetary space. The associated density, n_H^d, can be calculated in terms of the hydrogen density in the interstellar cloud as

$$n_H^d \approx (n_{gH}/\eta a) \times 10^{-7} \text{ cm}^{-3} \qquad (20)$$

Clearly, if η and a are chosen so that n_H^d is significant, then μ_d in (19) becomes so large that the dust would be excluded from interplanetary space. Thus we neglect dust.

Atomic hydrogen penetration. As was mentioned earlier, solar Lyman alpha radiation pressure gives rise to $\mu \gtrsim 1$ for atomic hydrogen in interplanetary space. (For a dense interstellar H cloud this value of μ will be appropriate only insofar as the assumptions for Ly-α photons of coherent scattering and no dust absorption profice a satisfactory approximation.) In order to make use of previous results, let us assume that $V_g = 20$ km sec^{-1} and $\mu = 1.2$. Then Figure 24d gives the interplanetary H distribution, assuming that $T_g = 0$ and that the solar wind extends throughout the solar system. However, since the scale over which the supersonic solar wind is slowed is $u/\nu \approx 30/n_H$ AU, and the turning scale

for the subsonic solar wind is somewhat less, the solar wind cannot extend beyond some 3 AU upstream in the interstellar neutral wind. Furthermore, n_H/n_{gH} will be substantially larger than indicated in Figure 24d. Hence it appears that the supersonic solar wind will be confined to a region of essentially the same shape as but of slightly larger dimensions than the forbidden region (cf. open dashed curve in Figure 24d). The transition to subsonic flow may be through a shock or a continuous transition[90,193], and the heliosphere boundary should lie a short distance beyond this transition. (Note that the inclusion of the effects of interstellar helium could, under some circumstances, lead to a significant slowing of the solar wind in the center of the forbidden region[54].)

The question now arises as to the effects of finite cloud temperature (viz., $T_g \gtrsim 10^2\ ^oK$[180]). First, we note that $V_g >> (kT_g/m)^{\frac{1}{2}}$, so that the filling of the forbidden region would ordinarily be sufficiently slow that the region would extend much farther downstream (with respect to $\underline{V}_g$) than upstream. However, there is the additional effect resulting from the optical thickness of the cloud for Lyman alpha radiation. The mean free path against scattering for a Lyman alpha photon is $\sim 17/n_H$ AU, so the cloud is optically thick and an intense, nearly isotropic Lyman alpha radiation field can be expected to fill the forbidden region and maintain its integrity (against filling due to finite gas temperature) for a greater distance downstream. For $\mu < 1$, the intense (nearly isotropic) Lyman alpha radiation field would exist, but it could not produce a forbidden region.

In conclusion, in the presence of a 100 cm^{-3}, 20 km sec^{-1} interstellar cloud and $\mu > 1$, the heliosphere should be a region shaped much

like the forbidden region of Figure 24d but slightly larger in scale. The heliosphere must close several tens of AU downstream with respect to $\underline{V}_g$) as it merges gradually into the interstellar cloud. The solar wind flow can remain supersonic only a short distance ($\lesssim$ 3 AU), except in the forbidden region. If the interstellar velocity vector lies nearly in the ecliptic plane, then all the planets will be exposed to the supersonic solar wind, at least over part of an orbit about the sun. However, if the velocity vector makes a substantial angle with the ecliptic, the outer planets may reside permanently outside the heliosphere. Nevertheless, all of the planets should be bathed in a relatively intense, nearly isotropic scattered solar Lyman alpha radiation field. The effect of larger n_{gH} or V_g would be to decrease the scale of the heliosphere without drastically altering its shape, so that the orbit of earth could extend, at least in part, outside the heliosphere.

3.6 History and Evolution

The subject of the history and evolution of the solar wind, though intriguing, is fraught with uncertainty owing to the lack of any firm observational base. However, in the past few years, more observations have become available, and an increased interest in the subject has ensued. Here, we shall indicate very briefly the general nature of the observations, current trends of thinking, and possibilities for future progress in this area.

Indirect observations relating to solar wind history include studies of the behaviour of the sunspot cycle and of geomagnetic data in the last few hundred years. The most interesting of these studies

relates to the Maunder Minimum, a period ($\sim$ 1645-1715 A.D.) when sunspots apparently disappeared completely from the face of the sun[50]. Since the nature of solar coronal holes depends strongly on solar magnetic activity, it is entirely possible that during the Maunder Minimum and other such periods (if they existed) the solar wind exhibited a character distinctly different from that observed today, although it is not clear what that character would have been. An understanding of the solar wind during such periods probably must await a better understanding of how processes in the solar convection zone might produce a Maunder Minimum[51] and of exactly how the convection zone supplies energy to the coronal expansion (cf. section 3.1).

Another (more direct) source of information about solar wind history is the study of gases trapped in the lattices of lunar rocks and meteorites[77]. The records in these rocks may span as much as the last 4.6×10^9 years; unfortunately, at present, the chronology is rather uncertain. Preliminary results from the studies of meteorites and lunar rocks appear to indicate: (1) that a solar-wind-like entity has been extant for the last 4×10^9 to 4.6×10^9 years, although its continuity in time cannot be determined; (2) that the elemental and isotopic composition of the solar wind has not changed significantly in the last $\sim 10^9$ years; and (3) that the average solar wind speed may have been considerably greater some 3×10^9 to 4×10^9 years ago. As these studies are carried out in the next several years, the reproducibility of results will determine the level of confidence we can give to them, and the potential for improved analysis techniques and improved understanding of current techniques opens the possibility of essentially new results.

If the inference of high solar wind speeds some 4×10^9 years ago stands up to future observational tests, it may lend some credence to the speculation that the sun experienced a T Tauri episode in its evolution[179]. (T Tauri stars have an age $\sim 10^5$ to 10^7 years, a relatively low mass (0.2-2 $M_\odot$), a strong stellar wind, and appear to represent the pre-main-sequence evolutionary phase of main-sequence spectral types G, K, and M.)[185] If the sun did at one time possess a much stronger solar wind, the consequences could be quite important for the evolution of the solar system[116]. However, until better observational data are available, this subject must remain in a speculative state. Less speculative is the suggestion that the sun had a much larger rotation rate (at least, for its outer layers), early in its lifetime on the main sequence[113]. Such an inference can be drawn from statistical studies of F and G type stars in galactic clusters. It is found that below-middle-F stars exhibit Ca II emission, characteristic of a stellar chromosphere (and, by implication, a corona and a coronal wind; cf. Figure 6), and on the average have much lower rotational velocities than stars that are above middle F on the main sequence, which do not exhibit Ca II emission. The conclusion[168] drawn from this result is that a star reaching the main sequence below middle F has a well-developed hydrogen convection zone and a consequent chromosphere, corona, and coronal wind, the last of which can transport angular momentum away from the star's outer layers, thus leading to the lower observed angular velocities. A higher F star, on the other hand, has no chromosphere, corona, or coronal wind and maintains its rotation rate during its main sequence life. Additional studies[196] of below-middle-F stars in galactic clusters of different ages indicate that young stars ($\sim 3 \times 10^7$ years) exhibit rotation

velocities some 20 times as large as those of the older stars ($\sim 5 \times 10^9$ years), like the sun, which is consistent with the lower-F and G stars having a significant slowing in the rotation of their outer layers during their lifetime on the main sequence. This conclusion is not in conflict with the present characteristic time for loss of solar angular momentum of $\sim 7 \times 10^9$ years (cf. section 3.4), since this time was probably somewhat shorter when the sun was younger (consistent with stronger Ca II lines (and probably stronger coronal winds) observed for the younger below-middle-F stars).

4. RELATED ASTROPHYSICAL PHENOMENA

There are many astrophysical phenomena that are closely related to large-scale solar wind processes discussed in section 3. Because of our ability to make direct observations of the interplanetary plasma and (indirect) detailed observations of the solar atmosphere, our understanding of several large-scale solar wind phenomena has reached a relatively high level. This understanding, together with necessarily indirect astronomical observations, should provide a basis for many astrophysical studies that is much sounder than that provided by the astronomical observations alone. In this section we shall examine briefly some of these solar-wind-related astrophysical problems, although no attempt will be made to present an exhaustive list of such problems. The question of microscopic processes in the solar wind that are important in an astrophysical context is dealt with in another paper in this collection[15].

4.1. Stellar Winds

The flow energy in the expanding atmosphere of a star can be derived from a number of sources: (1) from fluctuations that are generated in the star's hydrogen convection zone and propagate or are convected into the outer atmospheric layers (coronal winds, such as the solar wind); (2) from the electromagnetic flux passing through the outer atmospheric layers of the star (radiatively driven winds); (3) from the star's rotational energy (rotationally driven winds); or (4) from any combination of these three energy sources. As will be seen below (section 4.1.2), the descriptions of stellar winds associated with

these various sources of energy are all quite closely related, so that a thorough understanding of the solar wind should be a valuable aid in the studies of all types of stellar winds.

4.1.1. Some general observational considerations[129]

Stellar winds can be very massive (mass-loss rate $\sim 10^{-5}$ $M_\odot$/year) or very tenuous ($\sim 10^{-14}$ $M_\odot$/year for the solar wind). It is generally the very massive winds from early-type stars that are most readily observed. By combining line and continuum observations in various spectral ranges (ultraviolet, visible, infrared, radio), it is possible in many instances to deduce a radial velocity profile in the transonic and supersonic flow regimes for the massive winds. These winds are optically thick in spectral lines and appear to derive a significant fraction of their energy from the stellar radiation field (cf. section 4.4.4). Less massive winds of later-type stars, particularly Red Giants, can be observed with optical spectroscopy and infrared measurements of circumstellar dust[162]. The existence of tenuous stellar winds can only be inferred, either from the apparent presence of suitable physical conditions (e.g., a hot corona) or from the apparent consequences of the winds (e.g., loss of stellar angular momentum with increasing age). Such inferences (for stars later than about F5 on the main sequence) drawn from observations of Ca II lines and rotational velocities have already been discussed in section 3.6. Obviously, there may be a wide range of stellar winds whose existence can neither be detected nor be inferred using current observational techniques. In any event, it is quite clear that observations of stellar winds are (necessarily) in a state that is very primitive in comparison with that of solar wind observations.

4.1.2. Some general theoretical considerations[91]

A useful starting point in the development of any stellar wind theory is the one-fluid, radial-flow formulation of the conservation laws (3)-(5):

$$nmuA = f = \text{constant} \tag{21}$$

$$nmu \frac{du}{dr} + \frac{dp}{dr} + nm \frac{GM_*}{r^2} = nmD \tag{22}$$

$$3nuk \frac{dT}{dr} = 2ukT \frac{dn}{dr} + S \tag{23}$$

where A is the cross-sectional area of a (radial) flow tube, M_* is the stellar mass, $p = 2nkT$, and nmD and S are the volume rates at which momentum and heat, respectively, are added to the flow. D includes the effects of radiation pressure, mechanical-wave pressure, centrifugal force, magnetic stresses and frictional forces, while S includes the effects thermal conduction, radiative heating and cooling, mechanical-wave dissipation, and frictional heating. Clearly, if one considers the proper functional forms of D and S, (21)-(23) are not nearly so simple mathematically as they appear, and they do not generally form a closed set. However, from a physical standpoint, stellar wind flows are, to first order, just as simple as (21)-(23) would make them appear. In other words, these flows are retarded by stellar gravity and accelerated by the fluid pressure gradient and/or by one or more of the forces accounted for in D (cf. equation (22)). At the same time, the pressure gradient force is determined by the density gradient (given by mass continuity: (21)) and by temperature, which is fixed by the balance

among the expansive cooling process and the various heating and cooling processes accounted for in S.

An energy integral. An energy integral for the flow is readily derived from (21)-(23):

$$\frac{1}{2}u^2 + 5\frac{kT}{m} - \frac{GM_*}{r} - \int_{r_o}^{r} dr\,(D + SA/f) = \text{constant} \qquad (24)$$

E ($= u^2/2 + 5kT/m - GM_*/r$) is the energy per unit mass of the fluid and the integral term is the total energy added to a unit mass of the fluid as it moves from r_o to r. Normally, for a stellar wind, $E < 0$ near the star (because of the strong gravitational attraction) and $E > 0$ at large distances (reflecting the supersonic expansion). Thus the energy deficit, $E_\infty - E_o$ ($\approx u_\infty^2/2 + GM_*/r_o$), must be made up by the total energy supplied through heat and momentum addition between the atmospheric base ($r = r_o$) and the region of highly supersonic flow (including $r = r_\infty$).

Solution topologies. Let us, for the moment, ignore proper functional forms and assume that D and S are arbitrary functions of r. Then (21)-(23) can be combined to yield an equation of motion describing the Mach number, M ($= (3nmu^2/5p)^{1/2}$), as a function of r alone, in standard[88] solar wind form:

$$\frac{1}{M^2}\frac{dM^2}{dr} = \frac{4}{3}\frac{(M^2+3)}{rH}\left(\frac{E_o+\varepsilon}{M^2-1}\right) \qquad (25)$$

where

$$\varepsilon = \int_{r_o}^{r} dr\,(D + SA/f) + \frac{5}{12}(M^2+3)\,rD$$

$$- \frac{5}{12} \left(M^2 + \frac{3}{5}\right) rS \frac{A}{f} + \left(\frac{r}{2A} \frac{dA}{dr} - 1\right) H \qquad (26)$$

and H ($= E + GM_*/r$) is positive definite. Critical points (cf. section 3.1 and Figures 1 and 4) of (25) occur when $M^2 = 1$ and $E_o = -\varepsilon$, so if ε is a monotonically increasing function of r, there should be only a single critical point, as in the simple solar wind case (cf. Figure 1). In general, however, with rapidly diverging flow and/or localized heating and momentum addition, ε will not vary monotonically, and (25) may exhibit more than one critical point. The possible solution topologies of (25) for three critical points are shown in Figure 26 (cf. Figure 4). Obviously, one must be very careful to consider the full implications of the flow geometry and the heat and momentum addition functions appropriate to a particular stellar wind problem and to avoid assuming that the simplest of solar wind solutions (cf. Figure 1) can be directly extended to the stellar wind flow.

4.1.3. Coronal winds

According to our earlier definition, the energy for a coronal wind comes from fluctuations generated in the hydrogen convection zone of a star. These fluctuations can directly accelerate or dissipatively heat the outer layers of the star. Thus, a coronal wind can be driven by a mechanical-wave pressure gradient (nmD), by the usual thermal pressure gradient (-dp/dr), or by a combination of the two (cf. (22)). If the thermal pressure gradient is important, the dynamics of the coronal wind will depend strongly on the stellar coronal temperature, which is determined by the balance of expansive cooling, dissipative heating, and thermal conduction (cf. (23)), although conduction may not always be important.

Many studies of conductive, thermally driven coronal winds (i.e., mechanical-wave acceleration and heating negligible above the coronal temperature maximum) have been carried out in a very general way[153,164,47,165]. However, the temptation to draw any general conclusions about coronal winds from such studies[165] must be resisted, because of the neglect of the potentially important mechanical-wave-flux effects. Such effects in coronal winds (other than the solar wind) have been treated only in a very specialized study, in which thermal effects are regarded as negligible[19].

Actually, the first step that must be taken in studying coronal winds is to determine the mechanical energy flux entering the stellar corona[117,40,191,74]. Unfortunately, this problem is prohibitively difficult at the present time, for the following reasons: (1) theories predicting the outward energy flux from a stellar hydrogen convection zone are in a primitive state; (2) the energy flux entering the corona is only a small fraction of that leaving the convection zone (cf. Figure 6), so a very accurate description of dissipation of the mechanical flux in the lower atmospheric regions is required; (3) the nature (e.g., the mode of an MHD wave), as well as the magnitude, of the energy flux entering the corona must be known in order to determine what fraction of the energy is given to the coronal wind; and (4) the fraction of the corona that is free to expand (cf. the magnetic control problem of section 3) must be known in order to determine the total energy flux that can be given to a coronal wind. It is clear that coronal winds cannot be satisfactorily understood until we have a thorough understanding of the solar coronal expansion problem (cf. section 3.1), especially that part of the problem dealing with the transport of energy out of the solar convection zone, through the lower atmospheric layers, and into the solar corona.

4.1.4. Radiatively driven winds[129]

In radiatively driven stellar winds, the transonic acceleration is accomplished largely through the transfer of momentum from the stellar radiation field to the stellar atmosphere (i.e., D, arising from radiation pressure, dominates (22)). At the base of the atmosphere the momentum addition term (D) is small, but it increases rapidly as the flow accelerates until it dominates the gravitational term. This behaviour of D is consistent with the fact that the radiation force on the fluid (associated with its line spectrum) is increased as lines are shifted away from their rest frequency by the expanding flow, so that they are able to intercept continuum radiation from the lower atmosphere. (The continuum radiation at the lines' rest frequencies is strongly absorbed.)

Several models of radiatively driven winds have recently been developed in an attempt to explain the observations of massive winds of early-type supergiants and Of stars[122,29,31,30]. Of all stellar wind (excluding the solar wind) models, these for radiatively driven winds have, by far, reached the highest degree of sophistication[31,30]. The actual description of the transonic acceleration for a radiatively driven wind is, in some ways, more complex than for the solar wind, because in the former case the first two moments of the radiative transfer equation must be used along with the ordinary fluid equations in order to specify D and S properly. Of course, the radiative wind models do not deal with the difficult mechanical energy transport problem that faces solar wind workers.

A process which has been seen to be important for the solar coronal expansion and which should be considered in future radiatively driven

wind models is the magnetic control of the flow in the lower atmospheric levels. The magnetic control can, in some instances, lead to a rapid flow tube divergence, which in turn can drive the region of supersonic flow much lower in a stellar atmosphere than would be expected from spherically symmetric models (cf. sections 3.1.4, 4.1.2)[91]. This process should be especially effective for radiatively driven winds, because D depends on the velocity gradient (du/dr).

4.1.5. Rotationally driven winds

A rotationally driven stellar wind is accelerated essentially through a centrifugal force, as modified by the presence of a stellar magnetic field. In other words, for this type of wind the thermal pressure gradient in (22) is small in comparison with D (which contains centrifugal and magnetic terms). The description of a rotationally driven wind requires the use of Maxwell's equations and the azimuthal momentum equation, in conjunction with (21) and (22). Of course, the extreme latitudinal asymmetry that must be associated with the wind of a rapidly rotating star indicates the need for consideration of that dimension. At present, however, only axially symmetric models for the rotational plane have been developed[128,20], both of these models being direct extensions of the simplest description[194] of solar wind angular momentum transport (cf. section 3.4). One of these models[128] is relativistic and has been applied to the winds of rapidly rotating compact stars, in an attempt to explain the slowing of rotation inferred for pulsars. The other[20], which is non-relativistic, is intended to apply to the early main sequence lifetime of solar-type (later than F5) stars (cf. section 3.6). It is quite possible that the effects of rapid rotation are important, but not dominant, in accelerating certain coronal and radiatively driven winds.

4.1.6. Stellar breezes

In addition to the three classes of stellar winds mentioned above (and combinations thereof), there probably is another type of atmospheric expansion that occurs in some stars, and this is called a stellar breeze[33,34,164]. Originally discussed in relation to the expansion of the solar corona, a stellar breeze is simply the subsonic expansion of a stellar atmosphere (cf. single-valued subsonic solutions of Figure 1) and it may be appropriate to stars where all the physical processes contributing to D and S in (22) and (23) are relatively weak. A stellar breeze should be relatively difficult to observe, because its density profile closely resembles that of a static atmosphere and because it should have a negligible effect on the stellar mass, although it could have a significant effect on stellar angular momentum.

4.1.7 Mass and angular momentum loss

If we take the simple view (cf. section 3.4) that a stellar wind corotates out to the point where the flow speed equals the Alfvén speed (i.e., to $r = r_A$), then the rates of angular momentum loss and mass loss associated with the stellar wind are related by

$$\frac{dL_*}{dt} \approx \Omega_* r_A^2 \frac{dM_*}{dt}$$

and the characteristic time scales for loss of mass and angular momentum are related by

$$\tau_M \approx \frac{r_A^2}{r_*^2} \tau_L \gtrsim \tau_L$$

Thus we see that a stellar wind generally has a greater influence on a

star's angular momentum than on its mass. (This disparity is enhanced with increasing stellar magnetic field.) To determine whether either effect is significant in a given case, one must compare τ_L and τ_M with the characteristic evolutionary time scale for the star. For the very massive winds of early-type stars (cf. section 4.1.4), even τ_M is small and stellar wind mass loss may play a significant role in determining the evolutionary tracks of these stars. For main sequence stars later than F5 (including the sun), which apparently have tenuous coronal winds, the wind mass loss is probably insignificant, but the angular momentum loss is apparently sufficient to account for the observed sudden decrease in rotation speeds below F5 on the main sequence (cf. section 3.4). Of course, if these late-type-F and G stars have a pre-main-sequence T Tauri phase, then stellar wind mass loss may well play a role in determining their position on the main sequence.

4.1.8 Interaction with the interstellar medium

The interaction of solar-type stars (i.e., late-type-F and G stars) with the interstellar medium is likely to be reasonably well described by the discussion in section 3.5 of the interaction of the solar wind with the interstellar medium. In this case, the stellar wind reaches nearly complete equilibrium with the interstellar medium in a time short in comparison with the lifetime of the star. The situation is different in the case of the massive stellar winds ($u \sim 2000$ km sec^{-1}, $dM_*/dt \sim 10^{-6} M_\odot$ yr^{-1}) of early type stars[156,181,32]. Although the shock terminating the supersonic flow of these winds should reach an equilibrium position ($r_s \sim 10$pc) in a time ($t \sim 10^4$ years) that is short in comparison with the lifetime of the star, the region of subsonic flow does not equilibrate

nearly so rapidly. In the region just outside the subsonic stellar wind, a shell of dense, cold, swept-up interstellar gas is formed and survives for most of the lifetime of the star, before eventually dissipating into the ambient interstellar medium[32].

4.1.9. Binary stellar winds

Another example of stellar wind interactions is the interaction of two stellar winds from a binary star pair[174]. This problem can be approached using techniques quite similar to those employed in describing the multi-dimensional solar wind and the interaction of the solar wind with planetary magnetospheres[177]. The binary stellar wind problem can also involve outflow from one member of the pair (a normal star) and accretion by the other (a compact object). This problem is discussed below, in section 4.2.2.

4.2. Related Flows

Expanding and contracting flows of atmospheres of distributed or compact gravitating masses are all closely related to the basic solar wind problem[88]. In this section we shall consider briefly the expanding flows of galaxies and globular clusters and the general problem of spherically symmetric accretion.

4.2.1. Galactic and globular cluster winds

In the stellar wind problem we have a central gravitating mass surrounded by an atmosphere. A globular cluster, on the other hand, is characterized by a distributed gravitating mass pervaded by an atmosphere. A galaxy may possess both of these features: a large central gravitating mass surrounded by a distributed gravitating mass that is pervaded by

the galactic atmosphere (i.e., the interstellar medium). We thus restrict ourselves to the more general problem of galactic winds.

The galactic wind problem requires the use of mass, momentum, and energy source terms in the fluid equations (3)-(5)[107,25,126,201,106]. Mass addition arises from stellar winds and various energetic particle sources in the galaxy, including explosions (e.g., supernovae). The momentum and heat addition terms both may be associated with the addition of mass, as well as with processes such as heating and cooling through interaction with the ambient radiation field. (Cosmic rays can be treated either as an integral part of the expanding atmosphere[107] or as a separate fluid[106].) If the central gravitating mass is allowed to be either a source or a sink of mass (e.g., a Seyfert-type nucleus or a black hole), then the general galactic wind flow can include both an accretion region (cf. section 4.2.2, below) and an expansion region, with transonic flow in each (cf. Figure 27). Of course, the inner accretion region is not necessarily a general feature of galactic winds.

There are several threads of observational evidence, which, taken together, seem to support the suggestion that galactic winds exist and play an important role in the creation of certain radio and X-ray sources[106]. As we shall see below (cf. section 4.3.1) they may also play a significant role in galactic structure in much the way that the solar wind creates interplanetary structures.

4.2.2. Accretion

The theory of the spherically symmetric accretion of a polytropic gas onto a massive object[21] was fully developed several years before the virtually identical (except for flow direction) theory of the spherically

symmetric expansion of the polytropic atmosphere of a massive object (cf. sections 3.1.2, 3.1.3). The solution topologies appropriate to the spherically symmetric accretion problem are shown in Figure 1, where M is negative (it is positive in the stellar wind case) and the appropriate accretion solution is the critical solution that is subsonic at large radial distances. (Note that equation (10), which gives rise to Figure 1, yields solutions for M^2 that are independent of the sign of M.)

Despite the similarity in mathematical descriptions of the stellar wind and accretion problems, the two types of flow are quite different physically. For example, in the accretion problem the flow is accelerated by the gravitational force and is decelerated by the fluid pressure gradient, by the fluid's angular momentum, and by any radiative or mechanical energy flux emanating from the central body. Furthermore, the flow is compressive and tends to heat the atmosphere, as opposed to the cooling expansive flow of stellar winds. From an energetic standpoint, the flow of a stellar wind increases a fluid's gravitational potential energy, whereas in accreting flows the gravitational energy of the fluid is converted to kinetic energy and eventually to radiative energy.

The release of gravitational potential energy is the property of an accreting flow that makes it a viable candidate for the origin of high luminosities associated with certain objects. The outstanding example is the X-ray source, in particular, the binary X-ray source[72,24]. In a binary X-ray source, the stellar wind of one object (presumably a normal star) is accreted by the other object (presumably a neutron star or black hole), and the kinetic energy of the accreting gas is converted

to outflowing radiative energy near the compact object. The binary X-ray source illustrates a number of difficulties that arise in applying the simple steady, spherically symmetric accretion theory to a real problem. These difficulties include: (1) the inherent angular momentum of the accreting gas, which if too large, preculdes accretion[76]; (2) the luminosity of the compact object produced by accretion, which, if too large, also precludes accretion[148]; (3) the inherent asymmetry of a binary wind-accretion pair; and (4) the ever-present, rarely considered magnetic field of the accreting gas.

4.3. Development of Astrophysical Structures

In any flowing, non-uniform gas there will develop structures. The study of the development of various such structures has been carried out at close range, in some detail in the solar wind, which is a characteristic astrophysical plasma. The good understanding of solar wind structures that we have obtained in the past and shall obtain in the future (cf. section 3.2) should prove invaluable to workers studying many kinds of astrophysical structures. In this section, we shall mention briefly just two types of astrophysical structure where solar wind studies may prove useful.

4.3.1. Galactic structure.

Disk galaxies exhibit a spiral density structure that is quite similar to the interplanetary density structure that arises from solar wind stream interactions (cf. section 3.2.1 and Figure 15)[104]. One might reason by analogy that a galactic wind that is characterized by azimuthal non-uniformities near the galactic center could produce the

general type of galactic structure that is observed. In fact, radial velocities observed in our own galaxy appear to be generally consistent with such a proposition. Of course, there currently exists a rather well-accepted theory for spiral galactic structure (viz., the theory of spiral density waves in a rotating gas-star disk[121]), but it is possible that a galactic wind could play a role in establishing the density waves, or even that a galactic wind model would obviate the need for the density wave theory.

4.3.2 Blast waves.

Any explosive process, from a large stellar flare to a supernova, will produce a shocked disturbance that resembles somewhat the blast wave of similarity theory (cf. section 3.2.2). Such disturbances in astrophysical systems have been and still are modelled by using the classical blast wave theory for self-similar waves[178]. As was seen in section 3.2.2, the blast wave represents the limiting case of a wide range of structures that can be produced by time variations in plasma parameters, and it was found that similarity theory, which deals only with such limiting cases, has become outmoded in describing transient interplanetary structures. It is likely that descriptions of the evolution of many astrophysical transient structures would be improved by the use of techniques developed in studies of the solar wind structures (cf. section 3.2).

4.4. Elemental Abundances and Ionization State

The determination of the ionization state of many astrophysical plasmas is much more complex than the determination of the solar wind

ionization state. However, abundances in some astrophysical systems (in particular, the interstellar medium) may be related to the solar wind abundance problem. For example, much of the matter in the interstellar medium may have come from stellar winds, so that any change of abundance from the star to the stellar wind (cf. section 3.5) could be reflected as an abundance difference between stars and the interstellar medium.

5. SUMMARY

5.1. The Solar Wind

There are two fundamental problems, the solutions to which must form the basis for all studies of large-scale dynamical processes in the solar wind. The first of these is the coronal expansion problem, which relates to the transformation of an energy flux that is carried into the corona (from lower atmospheric layers) by fluctuations into an energy flux that is carried away from the sun by the bulk flow of the expanding corona. The second of these problems is the solar wind structure problem, which relates to the spatial and temporal evolution of large-scale density, velocity, and temperature structures in the interplanetary plasma. The basic physical processes important in the latter problem are currently reasonably well understood, and future theoretical and observational efforts in this area should serve primarily to provide the necessary refinement of this basic understanding. The coronal expansion problem, however, is not in nearly such good shape, owing primarily to limitations of the available observational data, and it is this problem toward which much of our effort must be directed in the next few years.

The development of our understanding of the solar wind over the past two decades has clearly illustrated the critical role of observational advances in directing theoretical progress. The recent observations of coronal holes have elucidated the important role of magnetic control in the coronal expansion and in this way have opened a new avenue which theoretical research can now follow. By making various assumptions about the mechanical energy flux entering the corona from

below, a solid theoretical framework for describing a magnetically controlled coronal expansion can be developed over the next several years. The development of this framework will require substantial theoretical efforts in the areas of large-scale-MHD, small-scale-MHD, and microscopic-plasma processes. However, this theoretical framework, though necessary, will not alone be sufficient to provide a satisfactory understanding of the coronal expansion.

There are two other areas of research that need substantial advancement before the coronal expansion problem can be adequately solved. These involve the determination of the coronal magnetic field and the description of the mechanical energy flux entering the corona from below. The coronal magnetic field problem can be solved in one of two ways: either by the direct observational determination of the coronal magnetic field (magnitude and direction) or by the improvement (in magnitude, not necessarily resolution) of observations of the line-of-sight photospheric field, together with the development of an accurate theoretical description (at least quasi-MHD) of the coronal field (based on photospheric observations). The solution of the mechanical energy flux problem is considerably more difficult. It requires, at the very least, an observational determination of the nature and magnitude of the energy flux as it passes through the transition region and enters the corona. This requirement, in itself, necessitates significant experimental and theoretical advances, in order to supply the appropriate data and provide a means of interpreting it. However, to develop an understanding of the coronal expansion that will be useful in studies of the long-term evolution of the solar wind and of stellar coronal winds, it is necessary to be able to describe the generation of fluctuations in

the solar convection zone and the transport and dissipation of these fluctuations through the lower atmospheric layers. Such a description will require major advances in convection zone theories and, of course, in observations relevant to those theories.

Once a detailed coronal expansion model is developed, it will be important to have adequate observations to test the model. Such observations could be obtained from a solar-minimum out-of-the-ecliptic spacecraft, a 'solar probe' spacecraft that passes very close to the sun, and space-borne solar Ly-α observations to determine the coronal temperature. These observations would obviously aid in the development of the detailed coronal expansion theory if they were obtained soon enough. They also should prove valuable in developing and refining theories of all other aspects of the solar wind, including solar wind structures and three-dimensional solar wind flow, chemical composition and ionization state, and angular momentum transport.

A comprehensive theory of solar wind chemical composition and ionization state must await the development of an adequate coronal expansion theory. In the meantime, a solid theoretical framework should be developed on the basis of various sets of assumptions about the coronal expansion, so that when the proper coronal expansion information becomes available, the chemical composition and ionization state problem can be rapidly solved. The solar wind angular momentum transport problem currently awaits better observations of the mean azimuthal velocity of the solar wind. Once firm observational evidence is available the angular momentum transport theories can be reconsidered to determine what physical processes are, indeed, important in the three-dimensional solar wind flow. It will be difficult to make any significant

advances in the theory of the evolution of the solar wind (over the lifetime of the sun) until the models of the generation of fluctuations in the solar convection zone (and the transport of these fluctuatuions through the solar atmosphere) are in much better shape.

5.2. Related Astrophysical Phenomena

It is clear that many physical processes in the solar wind are closely related to processes important in a number of astrophysical problems. Observations, and consequently theories, of these processes as they occur in the solar wind are necessarily much more advanced than the corresponding astronomical observations and astrophysical theories. Thus it should be helpful to supplement astronomical observations with our understanding of the solar wind in providing a basis for much astrophysical research.

Obviously, the solar wind is most closely related to stellar winds, particularly coronal winds. Although solar wind studies can currently be of some help in developing stellar wind theories, it will not be until we develop a detailed theory of the coronal expansion (including the role of the solar convection zone) that our understanding of stellar coronal winds can be significantly improved.

In order to implement the use of our understanding of the solar wind in developing theories describing related astrophysical phenomena, it is necessary to develop a strong line of communication between astrophysicists and solar wind physicists.

6. TIMETABLE FOR SOLAR WIND RESEARCH

In conclusion, let us suggest a possible timetable for carrying out the solar wind studies discussed in this paper. In the following list, t = 0 represents the present, and the numbering of items in each of the three groupings more or less represents a priority rating, although it is anticipated that all suggested studies can be carried out in the allotted time. Of course, it must be kept in mind that in any such list the time scale over which the character of the list changes is often much shorter than the time span of the list. For example, if this timetable had been constructed two years ago (prior to the Skylab Coronal Hole Workshops) it would have been quite different.

The reader should note that small-scale MHD and plasma microphysics studies are not specifically mentioned here (see references 152 and 191), although they are important to the ultimate understanding of the large-scale processes.

t = 0 to 5 years

1. Development of a theoretical description of the magnetically controlled coronal expansion for various types of energy flux input to the corona from lower layers.

2. Development of observational and theoretical capabilities for obtaining and interpreting observations of the mechanical energy flux passing through the transition region and entering the corona.

3. Refinement of the theories of large-scale solar wind structures and general three-dimensional solar wind flow.

4. Development of a theoretical framework to describe the solar wind chemical composition and ionization state in the context of a magnetically controlled coronal expansion, and acquisition of composition and ionization state for all solar wind conditions with a satellite-borne ion mass spectrometer.

5. Improvement in observations of the mean azimuthal component of the solar wind velocity at 1 AU.

6. Laying of the groundwork for future theoretical and observational progress in the modelling of the generation of fluctuations in the solar convection zone.

7. Application of knowledge gained from the solar wind to relevant astrophysical problems.

t = 5 to 15 years

1. Acquisition and interpretation of observations of the mechanical energy flux passing through the transition region and entering the corona.

2. Development of a definitive model for the magnetically controlled coronal expansion based on the observations in 1.

3. Testing and improvement of the coronal expansion model with observations from out-of-the-ecliptic and near solar (Solar Probe) spacecraft and with Lyman alpha observations of the coronal temperature in coronal holes.

4. Testing and improvement of solar-wind-structure and three-dimensional-flow models on the basis of the above spacecraft observations.

5. Development and refinement of a theoretical model of the solar wind chemical composition and ionization state, making use of the coronal

expansion model mentioned in 2 above and the observations mentioned in 1 and 3.

6. Refinement of observations and theoretical model of solar wind angular momentum transport.

7. Development of basic theoretical model of the convection zone generation of fluctuations and of the transport and dissipation of the fluctuations through the lower solar atmosphere, with the aid of observations mentioned in 1 and 3 above.

8. Refinement of historically relevant experiments with lunar rocks and meteorites.

9. Application of knowledge gained from the solar wind to relevant astrophysical problems.

t = 15 to 25 years

1. Refinement of theoretical model of the convection generation of fluctuations and of the transport and dissipation of the fluctuations through lower solar atmosphere, including relevant convection zone variations with solar evolution.

2. Development of theoretical description of solar wind evolution over the lifetime of the sun.

3. Development of theoretical models of coronal winds of various stars, especially those later than F5 on the main sequence.

4. Further refinements of the various theoretical solar wind models.

5. Application of knowledge gained from the solar wind to relevant astrophysical problems.

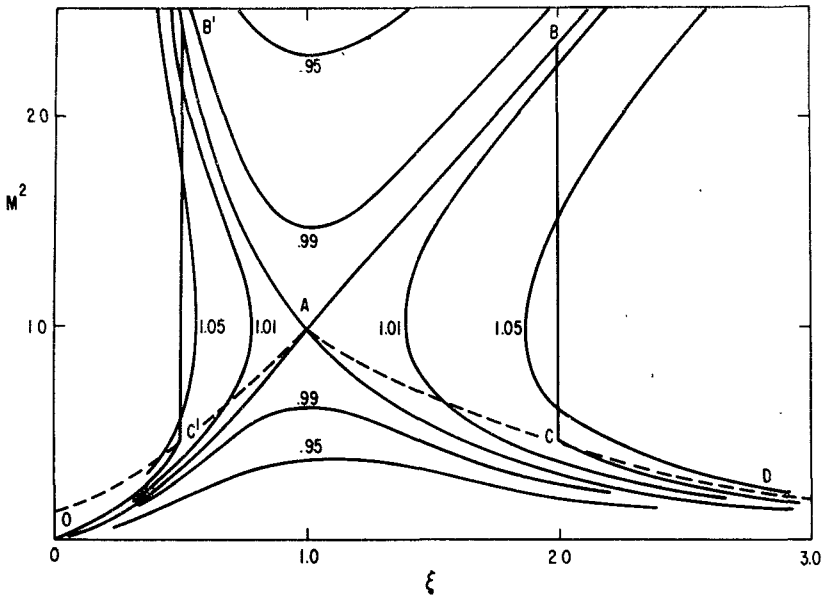

FIGURE 1 Mach number squared versus radial distance (in units of the critical point radius) for the stellar wind and accretion problems with $\alpha = 4/3$. Numbers labelling curves are values of δ ($\propto (p/n^{\alpha})^{2/(\alpha+1)}$). OABCD is the complete solution for a stellar wind expanding into the interstellar medium with $p_{\infty}/p_{*} = 5.61 \times 10^{-2}$ (p_{∞} is the interstellar pressure, and p_{*} is the pressure at the base of the stellar corona). DAB'C'O is the complete solution corresponding to accretion towards a star with $(p_o/p_{*})\,(r_o/r_{*})^4 = 0.1797$ (p_o is the pressure at r_o in $\xi > 1$). The dashed lines represent the square of the postshock Mach number as determined from the Rankine-Hugoniot relations applied to the supersonic branches of the critical solutions.[6]

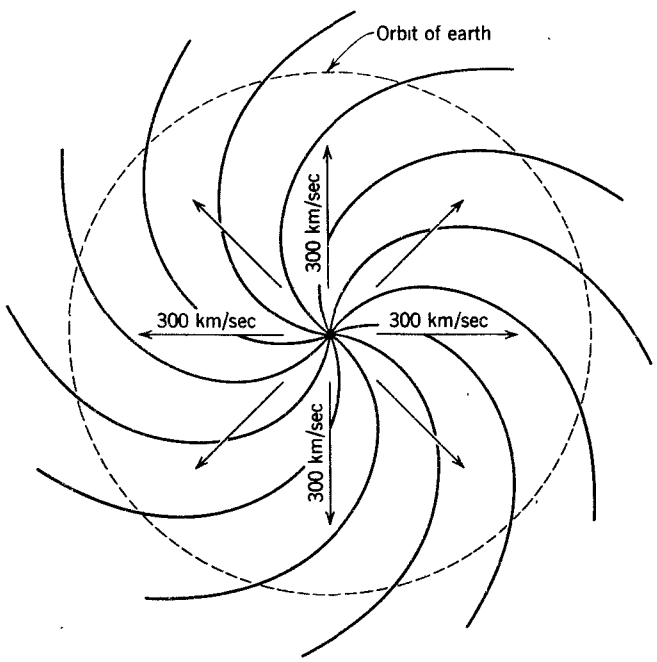

FIGURE 2 Interplanetary magnetic field lines (in the solar equatorial plane) resulting from the extension of the solar magnetic field by a 300 km sec^{-1} (constant speed) solar wind. Magnetic stresses in the extended solar field and angular momentum imparted to the solar wind by the angular velocity of the sun are neglected (see section 3.4).[151]

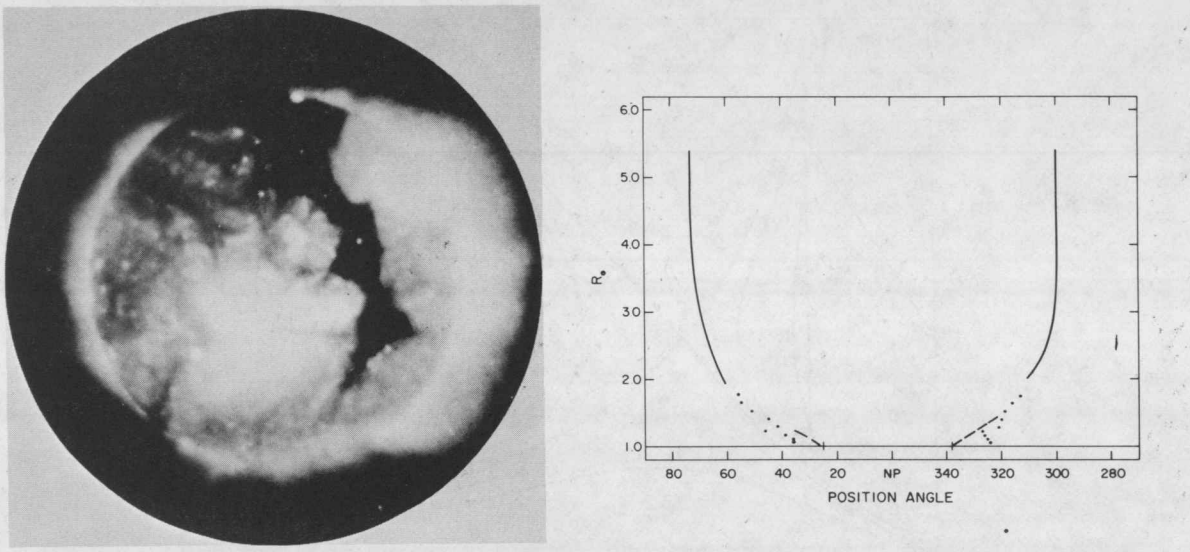

FIGURE 3 (a) AS&E X-ray photograph of the sun (courtesy A. Krieger). A large coronal hole (dark region) is shown extending from the northern polar cap (top of picture) across the equator and well into the southern hemisphere. Smaller holes can be seen on the disk in the northeast (top left) and on the limb in the southeast (bottom left). (b) Boundary of a polar coronal hole shown in the radial distance, position angle plane.[133] The solid lines represent hole boundaries derived from the HAO Skylab coronagraph, the dashed lines are deduced from AS&E Skylab X-ray photographs, and the dots are inferred from HAO ground-based K-coronameter data. Note that a radial boundary would appear as a vertical straight line in the figure.

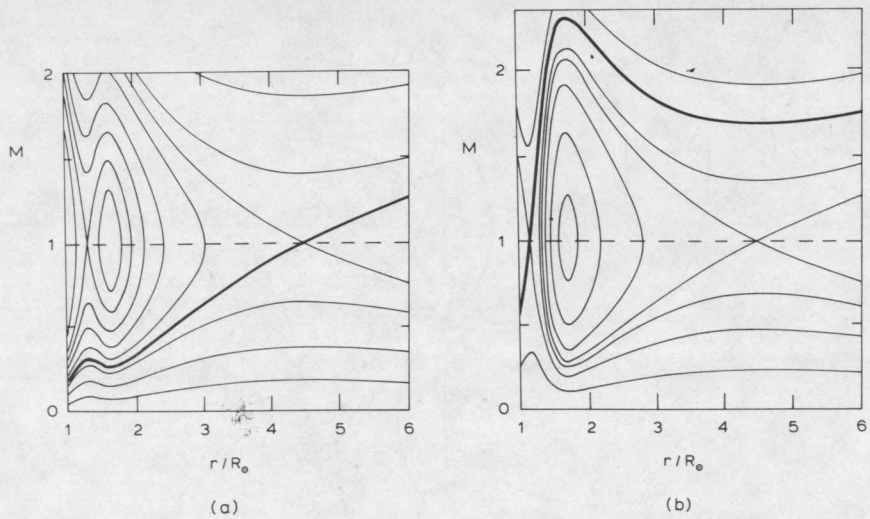

FIGURE 4 Solution topologies for polytropic ($\alpha = 1.1$) flow in rapidly diverging geometries (cf. Figure 1, where divergence is r^2). The divergence is more rapid than r^2 in $1\ R_\odot \lesssim r \lesssim 2\ R_\odot$, and two new critical points (one *saddle point* and one *center*) are added in this region. The net divergence is greater in (b) than it is in (a). The solar wind solution (heavy curve) is the only continuous solution that is subsonic at $r = 1\ R_\odot$ and is supersonic beyond the outermost critical point. In (a) the solution of interest passes through the usual (spherically symmetric case) critical point and exhibits low flow speeds near the solar surface (cf. Figure 1). In (b) the solar wind solution passes through the innermost critical point and exhibits high flow speeds near the solar surface.[112]

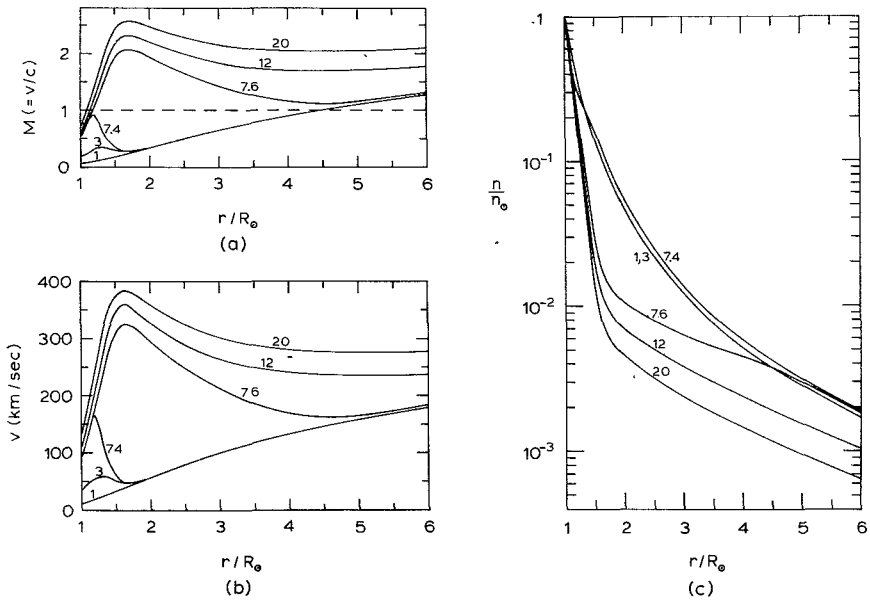

FIGURE 5 Radial distributions of (a) Mach number, (b) bulk flow speed, and (c) number density for various values of a parameter (Z_{max}) that measures the net increase in flow tube area over that characteristic of an r^2 divergence (i.e., 7.6 means the flow tube area at $r = 6\ R_\odot$ is 7.6 times as large as for a flow tube diverging as r^2). Note the high flow speeds and low densities in the inner and middle corona when $Z_{max} > 7.5$ ($Z_{max} = 1$ corresponds to $A \propto r^2$). The $Z_{max} = 3$ and $Z_{max} = 12$ solutions correspond to the heavy curves in Figures 4a and b, respectively. All solutions have $\alpha = 1.1$ and $E = 1.8 \times 10^{15}$ erg gm^{-1}, and thus they all asymptotically approach the same bulk flow speed.[112]

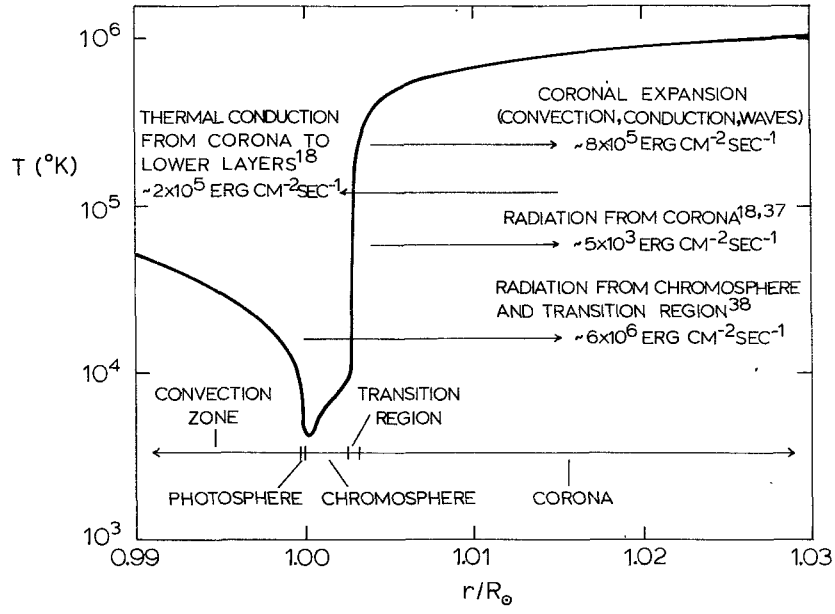

FIGURE 6 Radial temperature profile near the solar surface $(r = R_o)^2$, with the profile in the transition region and corona being characteristic of coronal holes.[132] The coronal temperature is uncertain and may well be much higher; the location of the coronal temperature maximum is unknown. The energy flux densities associated with the three major coronal energy loss processes[117,97] and the one major chromospheric and transition region loss process are shown; the coronal values are characteristic of coronal holes. The wave flux from the convection zone required to balance the energy losses from the atmosphere above the photosphere is $\sim 7 \times 10^6$ erg cm^{-2} sec^{-1}, but only 15% of this flux is required to supply the coronal energy.

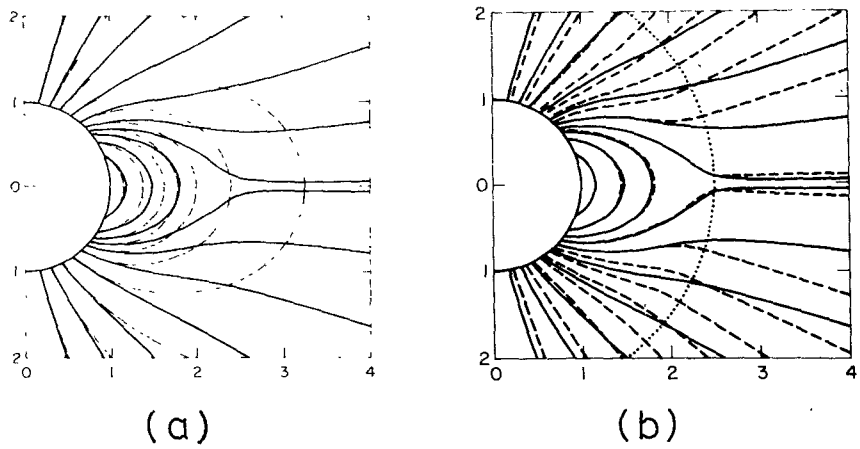

FIGURE 7 (a) A comparison of the self-consistent MHD representation of the magnetic field (solid lines) with a potential field (dashed lines) having the same normal (dipole) component at the photospheric reference level. The field lines for the two configurations are chosen so as to be coincident at this level. The source surface for the potential field is taken at $r = \infty$.[159] (b) A comparison of the same self-consistent MHD representation[159] (solid lines) with a potential field for which the source surface (dotted line) is taken at r 2.49 $R_\odot$.[141] The relatively good agreement results from the careful choice of the source surface location and from the isothermal assumption of the MHD representation. Without this assumption it is unlikely that very good agreement would be obtained.

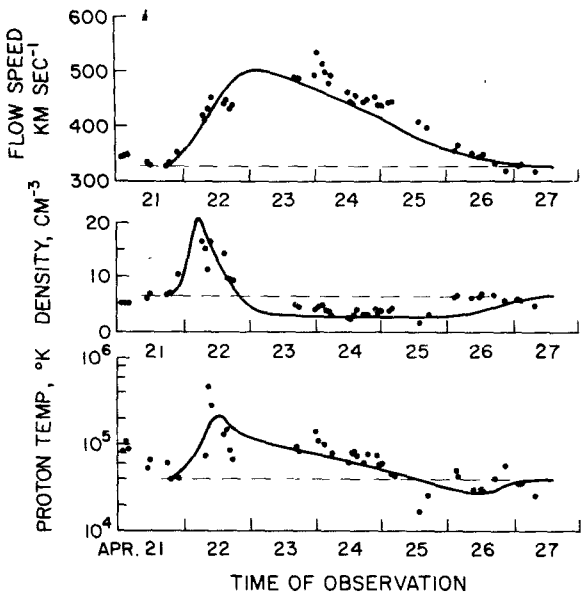

FIGURE 8 Seven-day time profiles of u, n, and T_p for a well-defined (isolated) high-speed solar wind stream. Observations (dots) were made by Vela 3 in April 1966.[10] The theoretical curves derive from the two-dimensional radial flow model[100] described in the text.

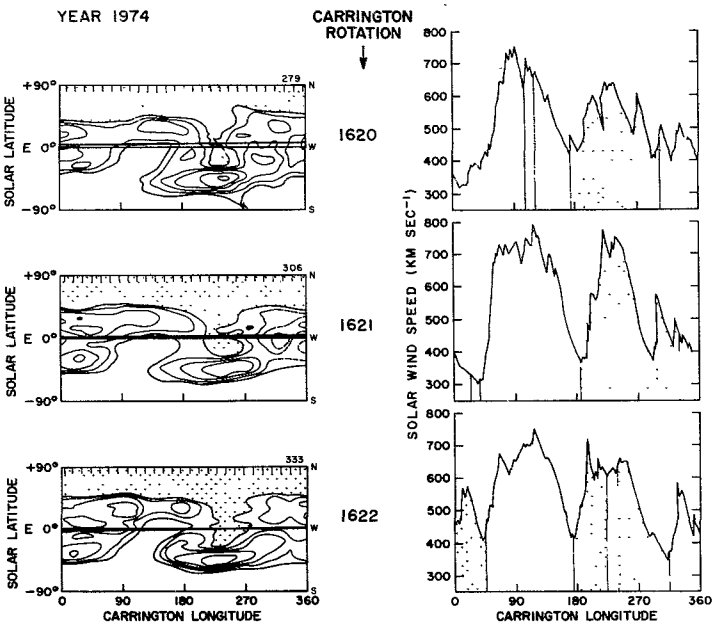

FIGURE 9 (a) Contours of constant polarization brightness (for three Carrington rotations) from limb observations by the HAO K-coronameter. The areas shaded with (+) are coronal holes with positive (outward) magnetic field and the areas shaded with (-) are coronal holes with negative (inward) magnetic field.[101] (b) Solar wind flow speed (observed at 1 AU) as a function of Carrington longitude (determined by a constant-speed mapping back to the sun) for the same Carrington rotations. The areas shaded with (+) are away (outward) magnetic sectors and the areas shaded with (-) are toward (inward) magnetic sectors.[101]

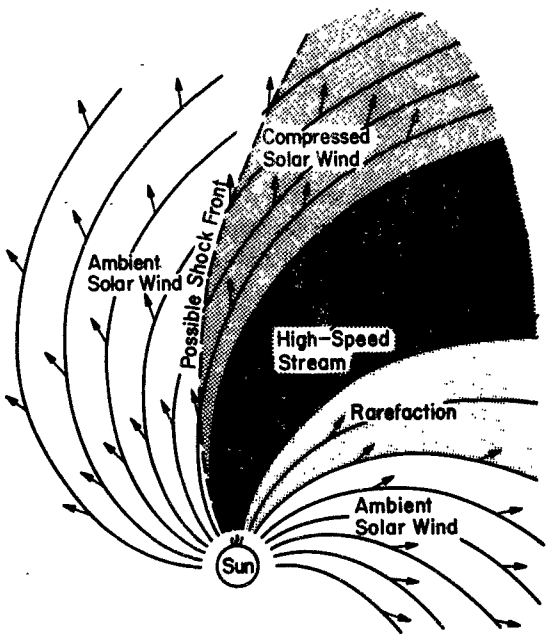

FIGURE 10 The interaction (in equatorial cross-section) of a steady, localized stream of high-speed plasma with the slower ambient solar wind, as viewed in a stationary frame of reference.[98]

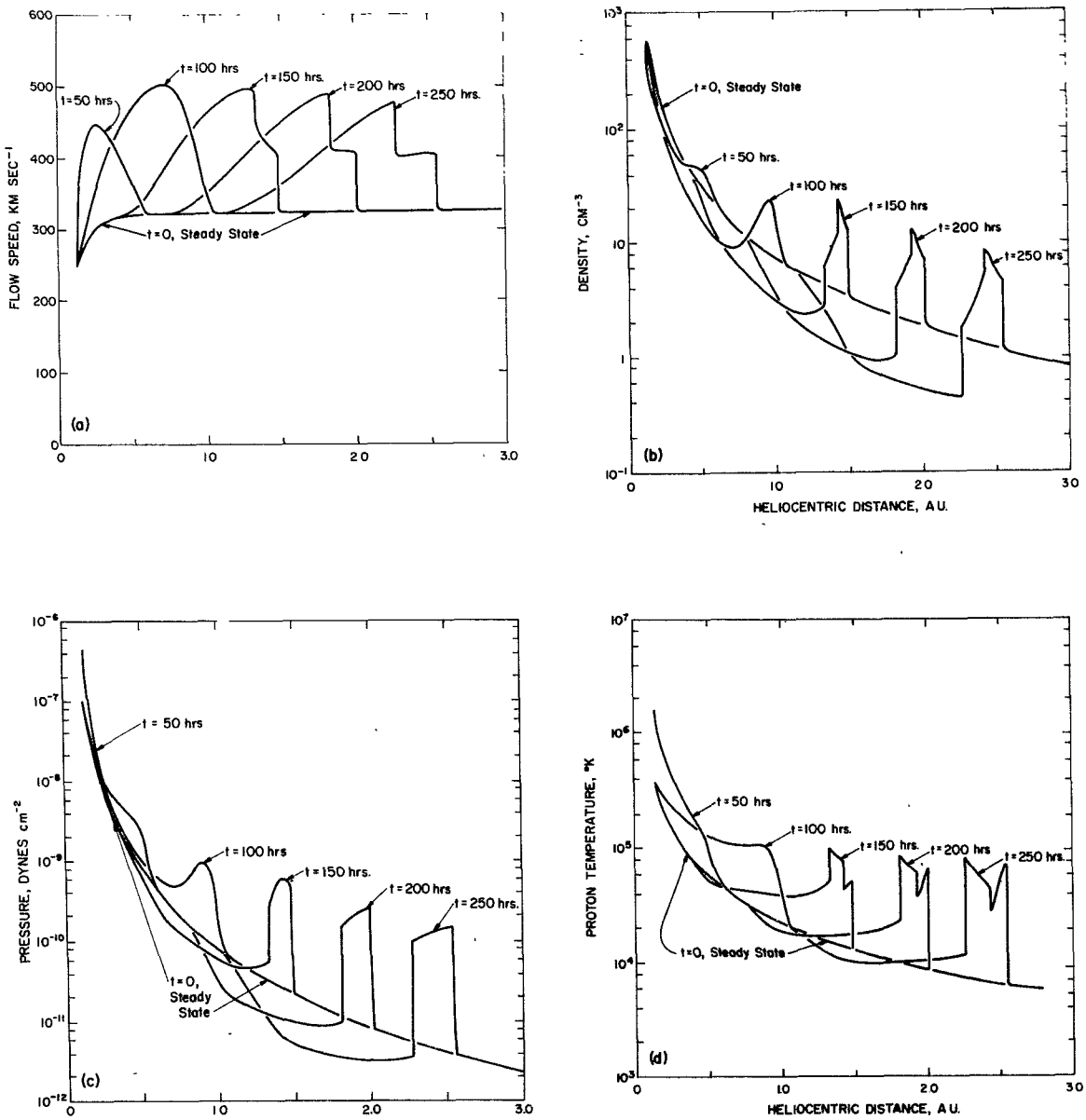

FIGURE 11 Radial profiles of u, n, p, and T at 1 AU for six different times at and following the start (t = 0) of a pure 100 hour temperature pulse at the inner boundary. Note the development (in $t \geqslant 150$ hours, at radial distances $r > 1$ AU) of the pressure ridge, the associated forward and reverse shocks, and the consequent 'entropy structures' in density and temperature.[100]

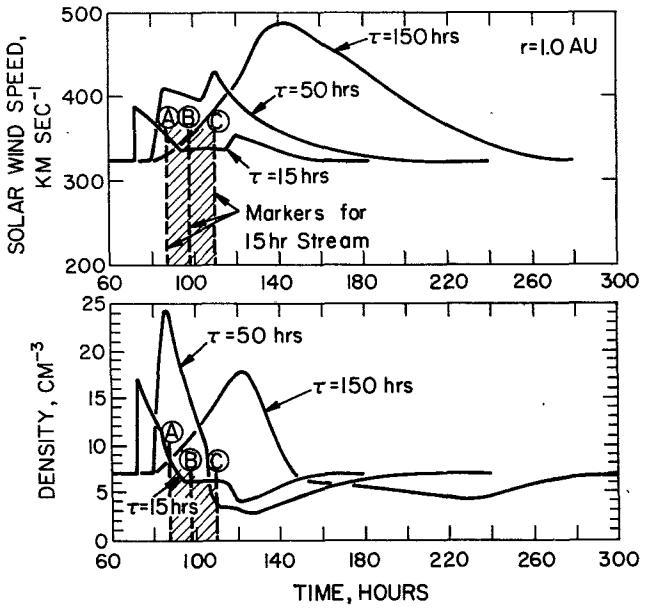

FIGURE 12 Time profiles of u and n, as they would be observed at 1 AU, for pure velocity pulses at the inner boundary (starting at t = 0) of duration 15, 50, and 150 hours.[102] The shading marks the extent of the plasma that was associated with the 15 hour pulse at the inner boundary and indicates that the disturbance has moved well into the leading and trailing ambient solar wind by the time it reaches 1 AU. Note carefully the difference in format between this time-profile presentation and the radial-profile presentation of Figure 11.

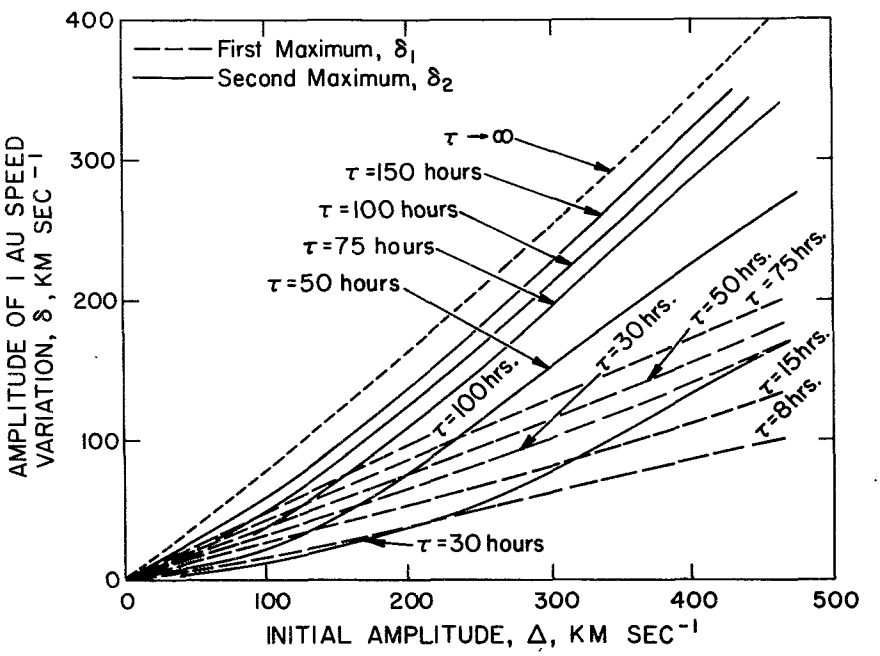

FIGURE 13 Plot of the amplitude of a velocity disturbance at 1 AU as a function of the amplitude of the pure velocity pulse generating the disturbance at the inner boundary, for several periods of the initial pulse.[102] The long dashed curves are for the first velocity peak to reach 1 AU (the left peak for the 15 and 50 hour pulses in Figure 12), and the solid curves are for the second peak (and for the only peak when there is just one, as in the case of the 150 hour pulse in Figure 12).

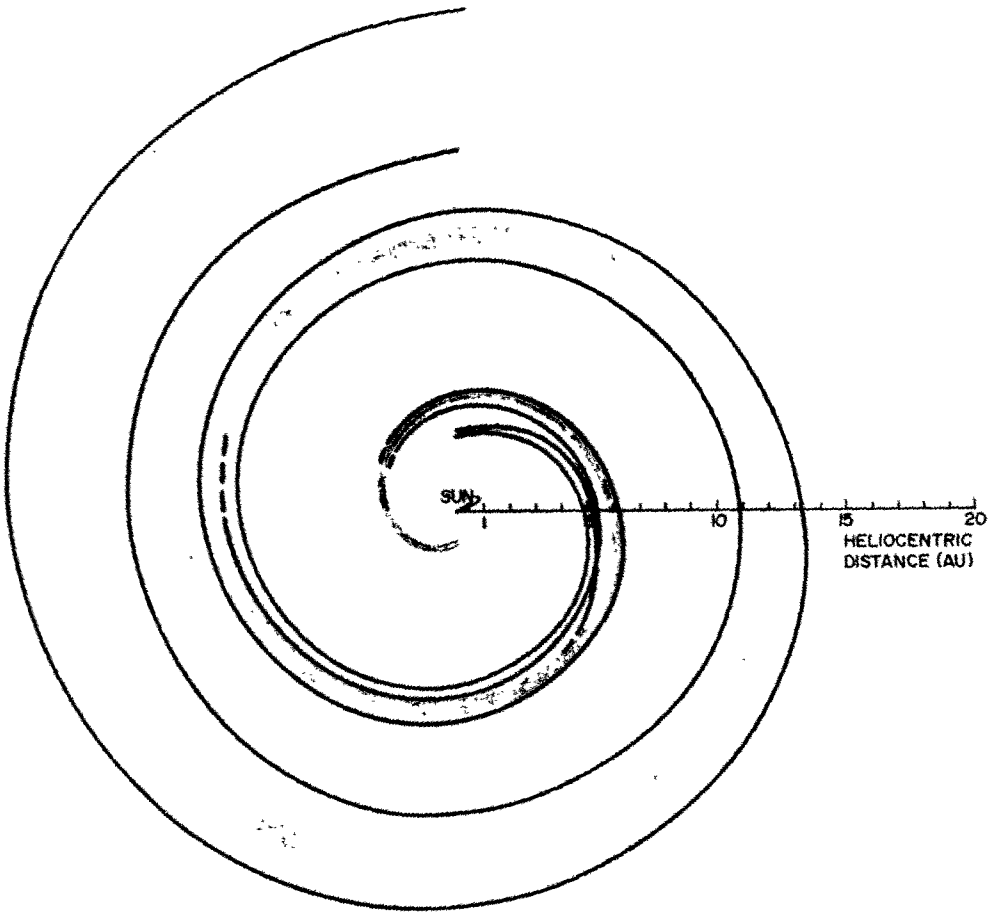

FIGURE 14 Contours of constant solar wind density for a two-stream (at 1 AU) solar rotation, from 1 AU to 20 AU.[103] Darker shading implies higher densities. The contour levels are separated by a factor of 4. Solid lines mark the locations of stream-associated shocks.

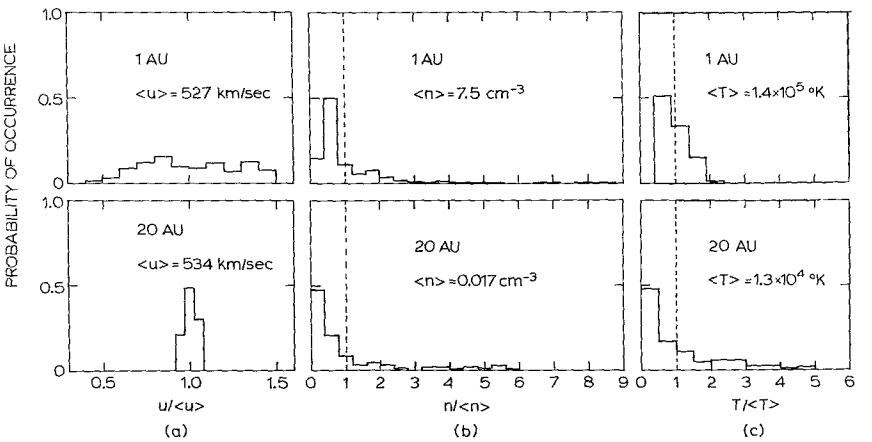

FIGURE 15 Histograms representing frequency of occurrence (for equally spaced time intervals) of u, n, and T at 1 AU and 20 AU for a three-stream (at 1 AU) rotation.[103] The mean values of u, n, and T are given (e.g., $\langle u \rangle$ = 527 km sec^{-1} at 1 AU) and the horizontal coordinate is normalized to these means.

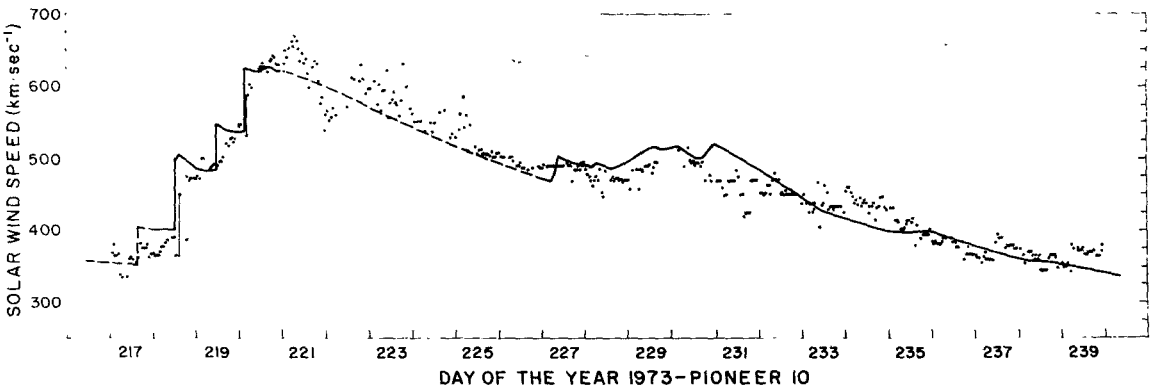

FIGURE 16 A comparison of predictions of the radial flow stream model (using observed boundary conditions at 1 AU) with Pioneer 10 observations (dots) at 4.5 AU.[71] The dashed line represents interpolated or extrapolated model predictions owing to IMP-7 data gaps (at 1 AU).

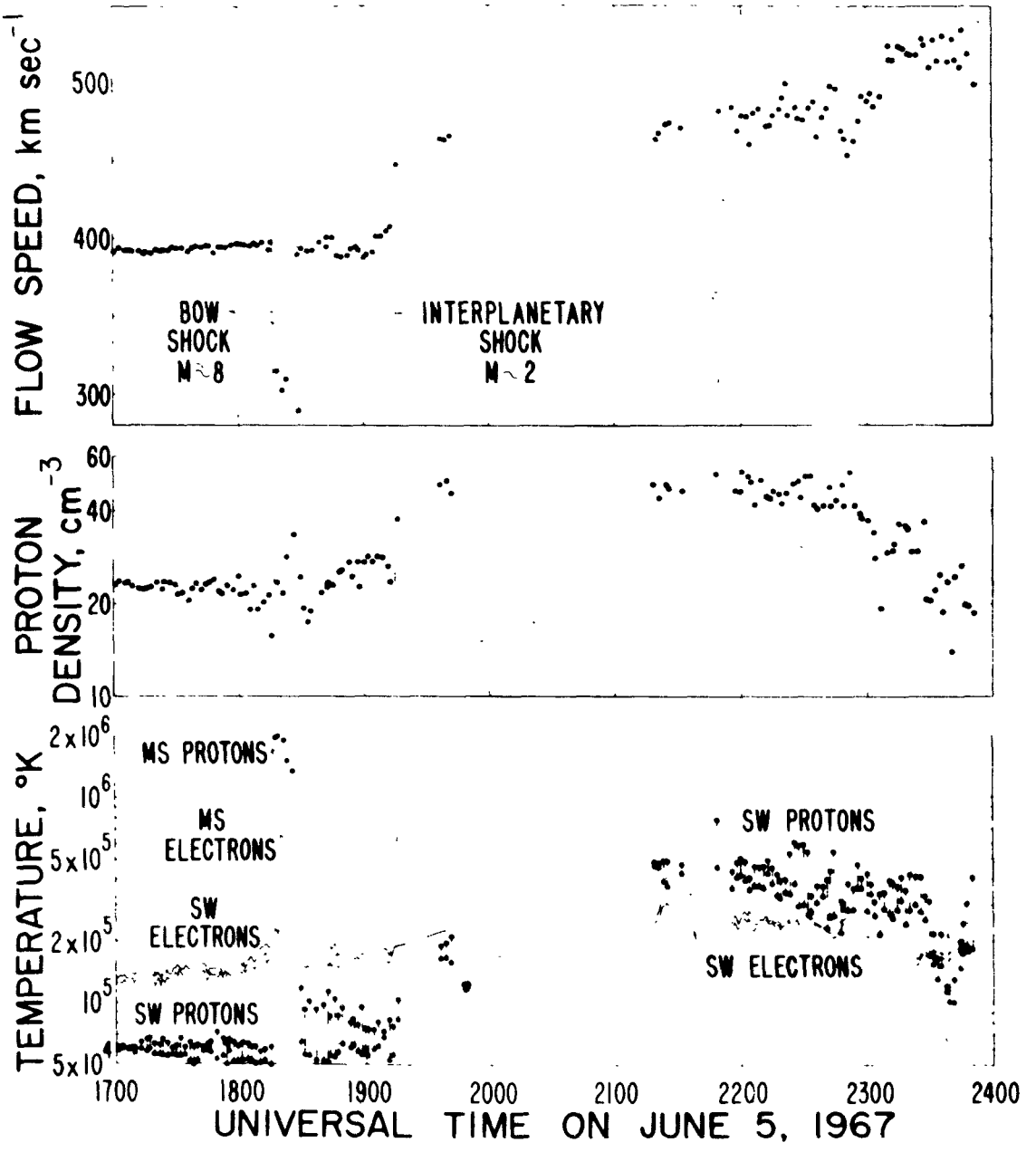

FIGURE 17 Solar wind properties observed by the Vela 4B spacecraft on June 5, 1967. The abrupt changes at 1915 UT signal the passage of an interplanetary shock.[98]

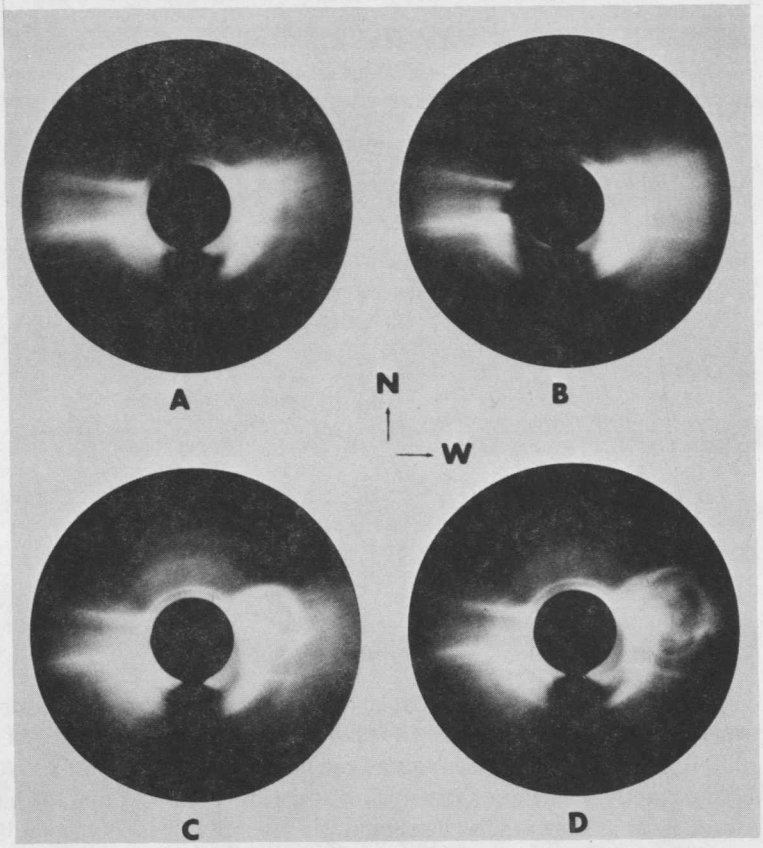

FIGURE 18 A mass ejection from the sun (coronal transient) photographed at 1332, 1343, 1424, and 1448 UT (frames A-D, respectively) on August 10, 1973.[67] The field of view of each frame is six solar diameters, and the sun is obscured by an occulting disk of effective radius 1.5 $R_{\odot}$, whose support pylon extends downward in the figure. The photographs are obtained by the HAO white light coronagraph on ATM.

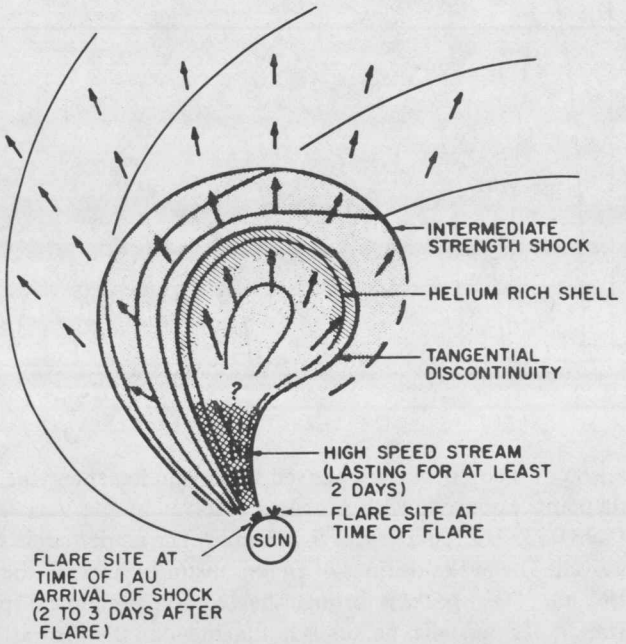

FIGURE 19 A sketch, in equatorial cross-section, of observed features of flare-produced interplanetary shock waves.[99]

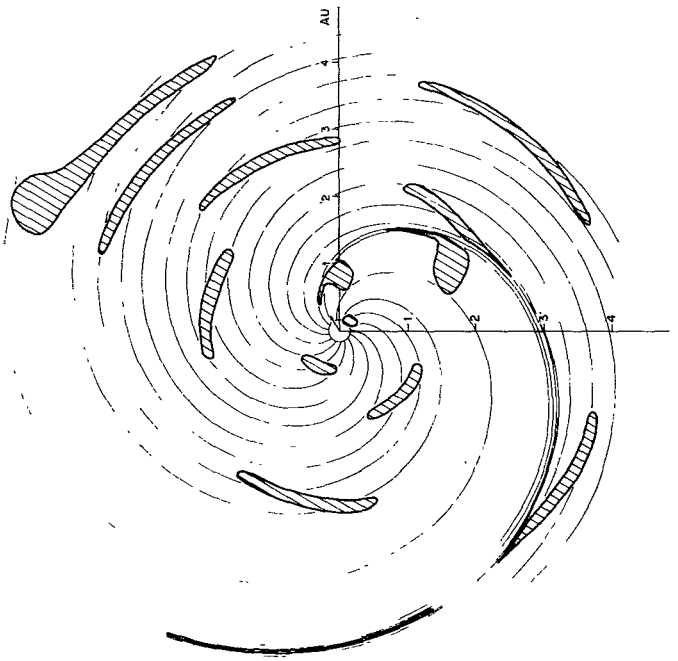

FIGURE 20 A schematic plan view of the interplanetary magnetic field in the ecliptic during sunspot minimum. The single fast solar wind stream has a maximum speed of 420 km sec^{-1} in an ambient flow of 280 km sec^{-1} at 30 $R_{\odot}$. The smooth spiral structure can be expected to be more convoluted during solar maximum owing to the non-recurrence of fast streams at that time. In addition, the bubble population should be some three times as large at solar maximum. No attempt is made to depict the distortion of the smooth spiral field produced by the bubble.[142]

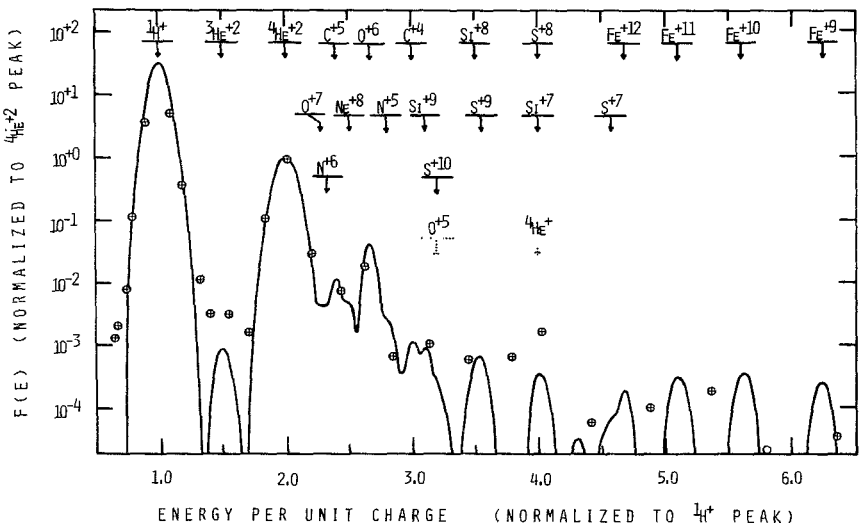

FIGURE 21 Comparison of theoretical and observed solar wind ion energy per charge spectra.[87] The circled crosses are data points associated with A counts observed by the Vela 3A electrostatic analyzer on October 8, 1965, at 0338-0335 UT (courtesy of S. J. Bame). The empty circle marks an energy at which no A counts were observed. The peak positions of all ions distinguishable in the theoretical spectrum are noted. Neither the $^4He^+$ nor $^{16}O^{+5}$ peaks is distinguishable in the theoretical spectrum. The contribution to $^4He^+$ through ionization of interstellar helium is not included in the theoretical calculations.

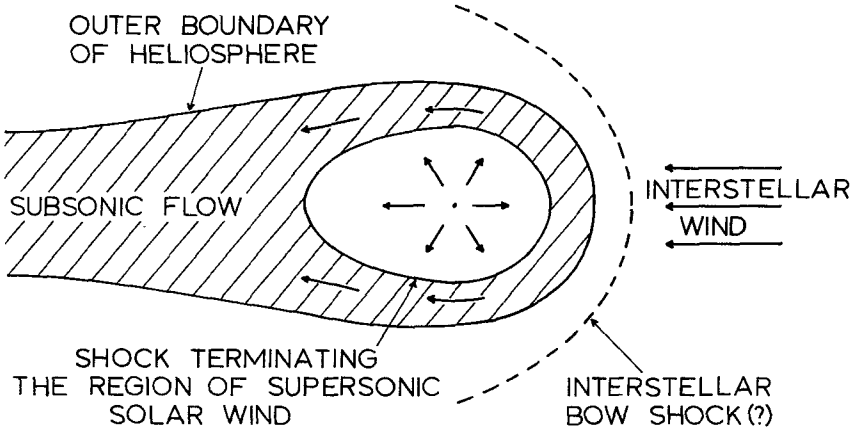

FIGURE 22 A schematic representation of the heliosphere in steady state.[8] The suggested interstellar bow shock probably does not exist because of the relatively large speed of fast-mode MHD waves in the local interstellar medium ($\sim$ 40 km sec^{-1} for the parameters listed in the text). However, such a shock may well exist in connection with other stellar winds. In the real heliosphere, none of the boundaries shown is likely to be either simple or fixed, owing to the structuring of the solar wind. The most structured and variable boundary is probably that which terminates the supersonic solar wind flow.

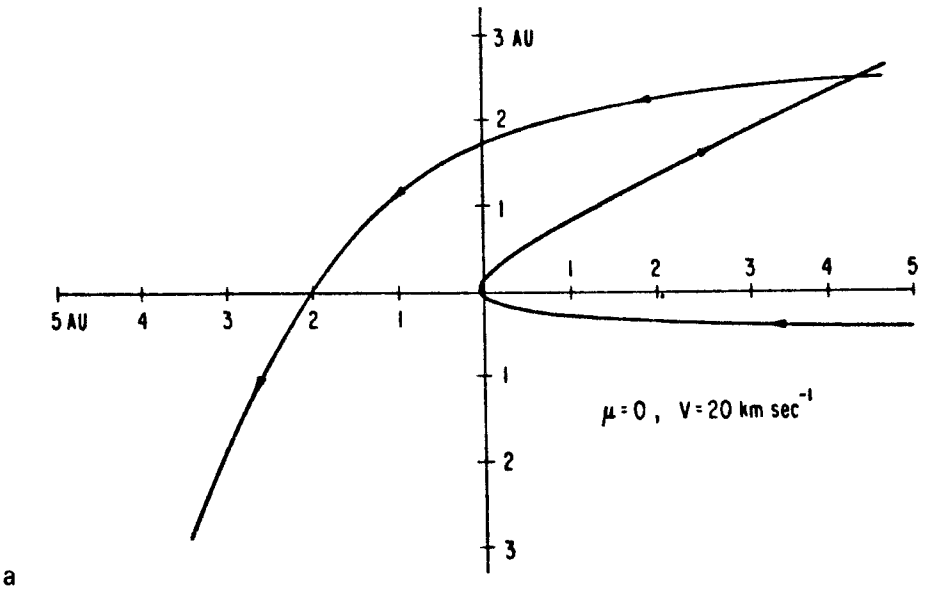

a

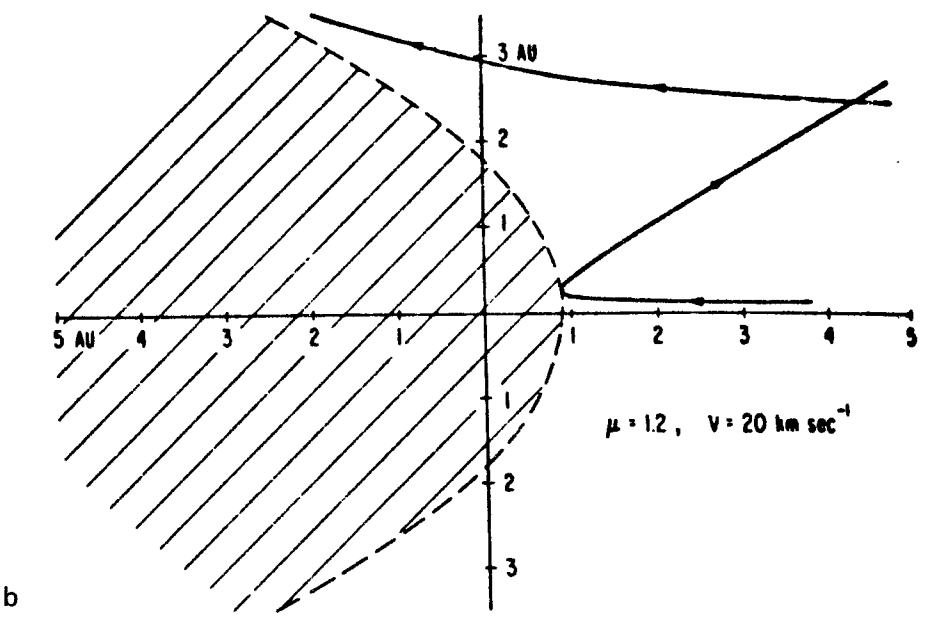

b

FIGURE 23 (a) Examples of intersecting particle trajectories for the case of a cold interstellar wind approaching the sun (at the origin) from the right of the diagram at 20 km sec^{-1}, with no radiation pressure ($\mu = 0$). Note that all trajectories cross the axis of symmetry on the downward side of the sun. (b) Same as (a), but with the effects of a radiation pressure exceeding gravity. A parabolic forbidden region (hatched) is produced with the sun at the focus.[7]

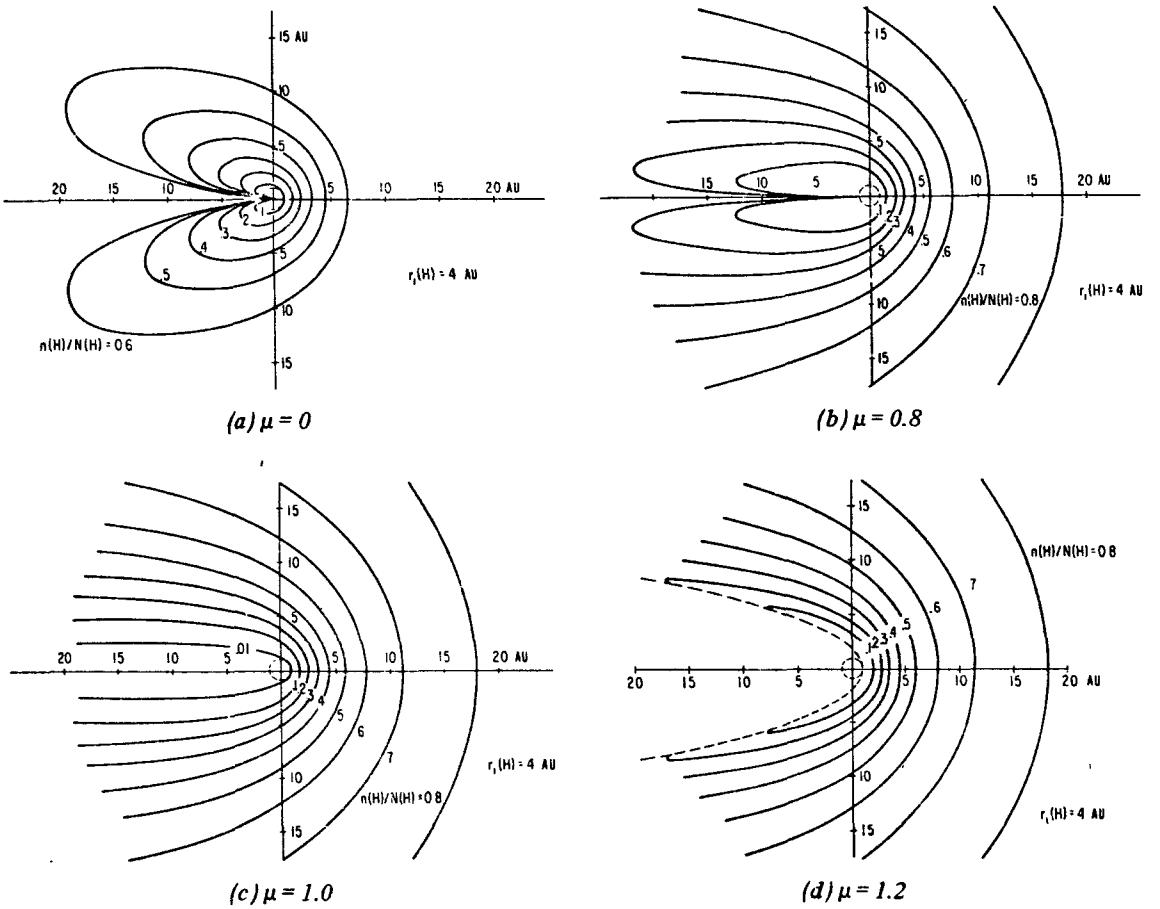

FIGURE 24 Contours of constant density (relative to the interstellar density) of neutral interstellar hydrogen. The sun is at the center of each diagram and the orbit of earth is shown as a dashed line. The plane of the diagram is the ecliptic plane, which fortuitously has been found to contain the velocity vector V_g. The three-dimensional contours are axisymmetric with respect to the horizontal axis. Note the infinite density along the axis of symmetry downwind of the sun for $\mu < 1$ and the parabolic void which appears for $\mu > 1$. Finite temperature effects eliminate the singularity and fill in the void to a certain extent.[7]

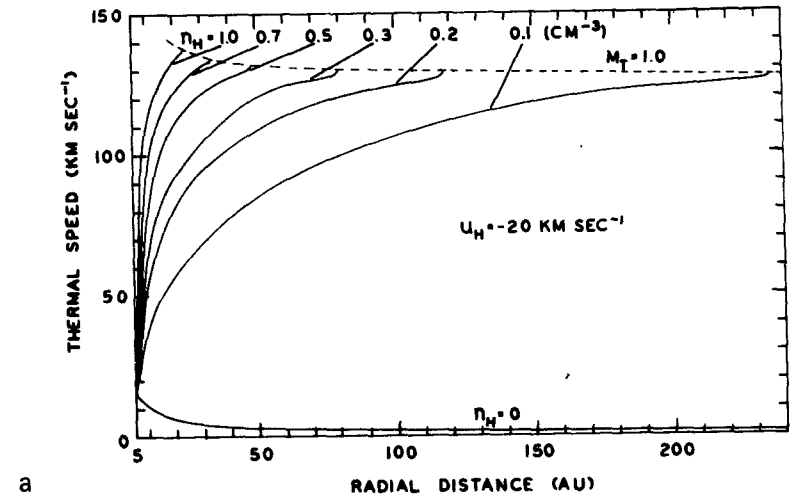

a

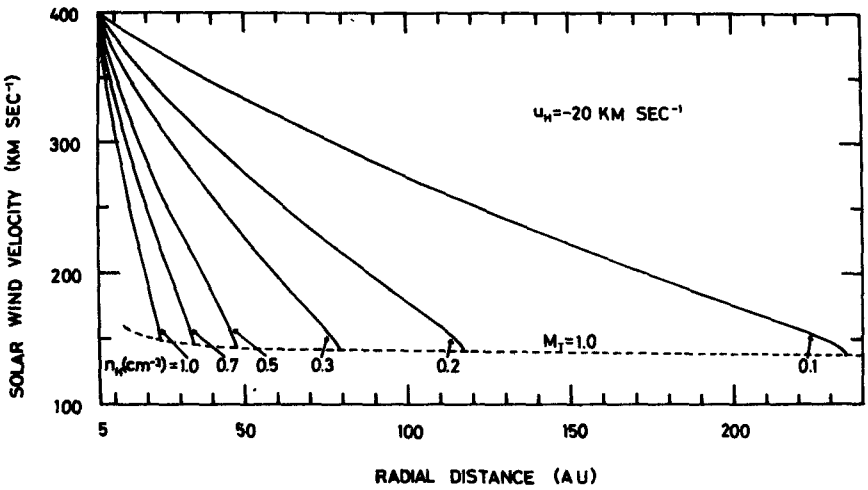

b

FIGURE 25 (a) Radial profiles of solar wind speed along the stagnation line for an interstellar gas of V_g (= u_H) = 20 km sec^{-1}, T_g = 0, and several values of N_{gH} (= N_H). The dashed line represents the locus of sonic points for the profiles. (b) Radial profiles of the solar wind sound speed, c_s = 5 kT/3m, for the same conditions as in (a).[90]

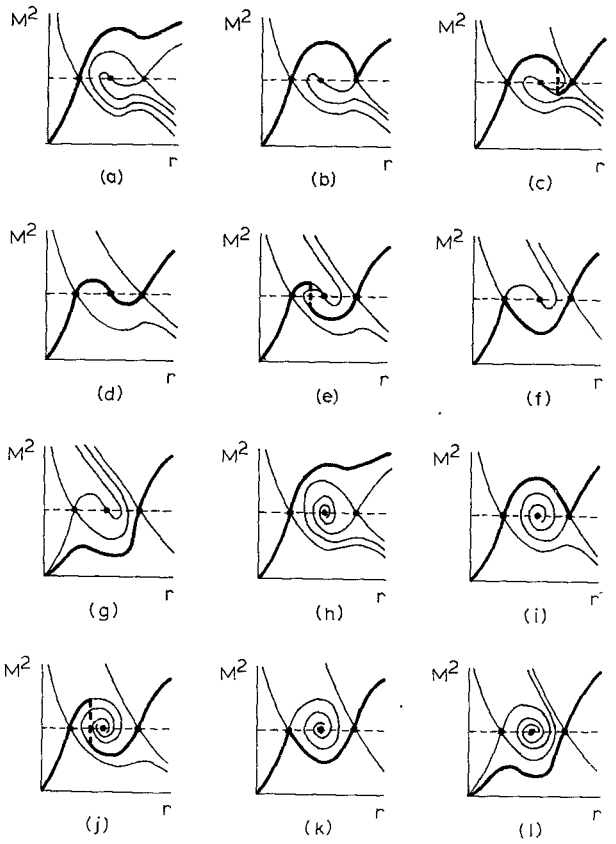

FIGURE 26 Schematic representation of solution topologies (M^2 versus r) for three critical points, the inner and outer being saddle points and the middle being a node (a-g) or a focus (h-l). Only the four saddle-point critical solutions are shown, as these completely determine the solution topologies. Topologies (b), (f), (i), and (k) are singular and are shown only for completeness. The heavy line marks the appropriate stellar wind solution for transonic flow. In some cases, the stellar wind solution, which is unique in all the topologies shown, requires a shock transition, which is represented by a vertical dashed line.[91]

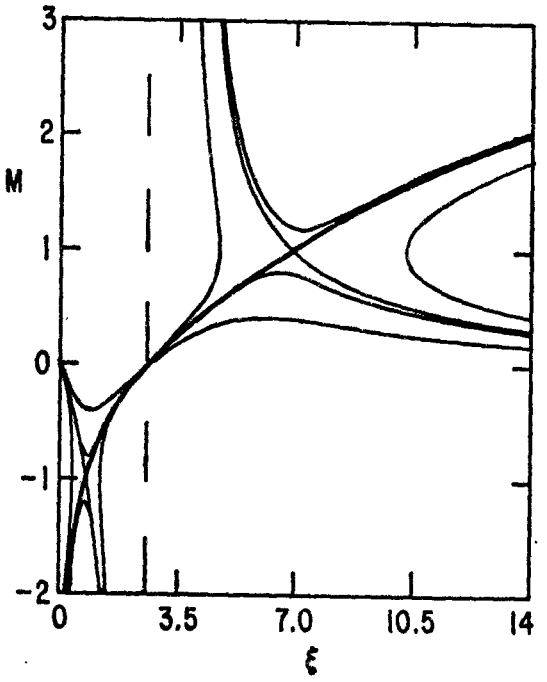

FIGURE 27 Mach number versus radial distance (in units of scale height of stellar mass density) for the case of a galactic wind allowing for an exponential mass production function. A stagnation point occurs at $\xi = \xi_o = 3$, with accreting flow ($M<1$) outside. A critical point exists in each of the regions $\xi > \xi_o$ and $\xi < \xi_o$, and one continuous solution intersects both critical points.[107]

ACKNOWLEDGMENTS

I wish to thank J. Hollweg, A. Hundhausen, D. Mihalas, and G. Siscoe for valuable discussions of material presented in this review. In addition, W. I. Axford, M. Dryer, W. Feldman, J. Hollweg, A. Hundhausen, and M. Montgomery have made several helpful suggestions after reading earlier drafts of the manuscript. I am especially grateful to B. Kirwin for an excellent job of typing the manuscript under less than ideal conditions.

REFERENCES

1. Adams, J., and G. W. Pneuman, A new technique for the determination of coronal magnetic fields: A fixed mesh solution to Laplace's equation using line-of-sight boundary conditions, Solar Phys., in press, 1976.

2. Allen, C. W., Astrophysical Quantities, Third Edition, Athlone Press, London, 1973.

3. Altschuler, M. D. and G. Newkirk, Jr., Magnetic fields and the structure of the corona, I: Methods of calculating coronal fields, Solar Phys., 9, 131, 1969.

4. Altschuler, M. D., D. E. Trotter, and F. Q. Orrall, Coronal holes, Solar Phys., 26, 354, 1972.

5. Athay, R. G., Theoretical line intensities, V. Solar UV emission lines of heavy elements, Astrophys. J., 145, 784, 1966.

6. Axford, W. I. and R. C. Newman, Viscous-transonic flow in the accretion and stellar wind problems, Cornell-Sydney Univ. Astron. Cent. Rep. 34, 1966.

7. Axford, W. I., The interaction of the solar wind with the interstellar medium, in The Solar Wind, NASA SP-308, ed. C. P. Sonett et al., p. 609, 1972.

8. Axford, W. I., Interaction of the interstellar medium with the solar wind, Space Sci. Rev., 14, 582.

9. Bame, S. J., J. R. Asbridge, A. J. Hundhausen, and M. D. Montgomery, Solar wind ions $^{56}Fe^{+8}$ to $^{56}Fe^{+12}$, $^{28}Si^{+8}$, $^{28}Si^{+9}$, and $^{16}O^{+6}$, J. Geophys. Res., 75, 6360, 1970.

10. Bame, S. J., J. R. Asbridge, H. E. Felthauser, H. E. Gilbert, A. J. Hundhausen, D. M. Smith, I. B. Strong, and S. J. Sydoriak, A Compilation of Vela 3 Observations, 1965-1967, Rep. LA-4536, vol. 1, Los Alamos Sci. Lab., 1971.

11. Bame, S. J., Spacecraft observations of the solar wind composition, in Solar Wind, edited by C. P. Sonett, P. J. Coleman, Jr., and J. M. Wilcox, NASA-SP308, p. 535, 1972.

12. Barnes, A. and R. J. Hung, On the kinetic temperature of He^{++} in the solar wind, Cosmic Electrodynamics, 3, 416, 1973.

13. Barnes, A., Theoretical studies of the large-scale behaviour of the solar wind, Advances in Electronics and Electron Physics, 36, 1, 1974.

14. Barnes, A., Plasma processes in the expansion of the solar wind and in the interplanetary medium, Rev. Geophys. Space Phys., 13, 1049, 1975.

15. Barnes, A., Turbulence and dissipation in the solar wind, in this volume.

16. Beckers, J. M. and E. Chipman, The profile and polarization of the coronal Ly-α line, Solar Phys., 34, 151, 1974.

17. Begelman, M. C. and M. J. Rees, Can cosmic clouds cause climatic catastrophes?, Nature, 261, 298, 1976.

18. Belcher, J. W. and L. Davis, Jr., Large amplitude Alfvén waves in the interplanetary medium: II, J. Geophys. Res., 76, 3534, 1971.

19. Belcher, J. W. and S. Olbert, Stellar winds driven by Alfvén waves, Astrophys. J., 200, 369, 1975.

20. Belcher, J. W. and K. B. MacGregor, Magnetic acceleration of winds from solar-type stars, submitted to Astrophys. J., 1976.

21. Bondi, H., On spherically symmetrical accretion, Mon. Not. Roy. Astron. Soc., 112, 195, 1952.

22. Brandt, J. C., C. L. Wolff, and J. P. Cassinelli, Interplanetary gas XVI. A calculation of the angular momentum of the solar wind, Astrophys. J., 156, 1117, 1969.

23. Brandt, J. C., Introduction to the Solar Wind, Freeman, San Francisco, 1970.

24. Buff, J. and R. McCray, Accretion flows in galactic X-ray sources. I. Optically thin spherically symmetric model, Astrophys. J., 189, 147, 1974.

25. Burke, J. A., Mass flow from stellar systems, Mon. Not. Roy. Astron. Soc., 140, 241, 1968.

26. Burlaga, L. F., Microscale structures in the interplanetary medium, Solar Phys., 4, 67, 1968.

27. Burlaga, L. F., Interplanetary streams and their interaction with the earth, Space Sci. Rev., 17, 327, 1975.

28. Carovillano, R. L. and G. L. Siscoe, Corotating structure in the solar wind, Solar Phys., 8, 401, 1969.

29. Cassinelli, J. P. and J. I. Castor, Optically thin stellar winds in early-type stars, Astrophys. J., 179, 189, 1973.

30. Cassinelli, J. P. and L. Hartmann, The subsonic structure of radiatively driven winds of early-type stars, Astrophys. J., 202, 718, 1975.

31. Castor, J. I., D. C. Abbott, and R. I. Klein, Radiation-driven winds in Of stars, Astrophys. J., 195, 157, 1975.

32. Castor, J., R. McCray, and R. Weaver, Interstellar bubbles, Astrophys. J., 200, L107, 1975.

33. Chamberlain, J. W., Interplanetary gas II. Expansion of a model solar corona, Astrophys. J., 131, 47, 1960.

34. Chamberlain, J. W., Interplanetary gas III. A hydrodynamic model of the corona, Astrophys. J., 133, 675, 1961.

35. Chao, J. K., V. Formisano, and P. C. Hedgecock, Shock pair formation, in Solar Wind, edited by C. P. Sonett, P. J. Coleman, Jr., and J. M. Wilcox, NASA-SP308, 435, 1972.

36. Chapman, S., Notes on the solar corona and the terrestrial ionosphere, Smithsonian Contrib. Astrophys., 2, 1, 1957.

37. Courant, R. and K. O. Friedrichs, Supersonic Flow and Shock Waves, Interscience, New York, 1948.

38. Cuperman, S. and N. Metzler, Solution of three-fluid model equations with anomalous transport coefficients for the quiet solar wind, Astrophys. J., 196, 205, 1975.

39. Delache, P., Contribution a l'etude de la zone transition chromosphere et couronne, Ann. Astrophys., 30, 827, 1967.

40. De Loore, C., Convection regions and coronas of sun and stars, Astrophys. Space Sci., 6, 60, 1970.

41. Dessler, A. J., Solar wind and interplanetary magnetic field, Rev. Geophys., 5, 1, 1967.

42. De Young, D. S. and A. J. Hundhausen, Non-spherical propagation of a flare-associated interplanetary blast wave, J. Geophys. Res., 76, 2245, 1971.

43. Dryer, M., Interplanetary double-shock ensembles with anomalous electrical conductivity, in Solar Wind, edited by C. P. Sonett, P. J. Coleman, Jr., and J. M. Wilcox, NASS-SP308, 453, 1972.

44. Dryer, M., Interplanetary shock waves generated by solar flares, Space Sci. Rev., 15, 403, 1974.

45. Dryer, M. and R. S. Steinolfson, MHD solution of interplanetary disturbances generated by simulated velocity perturbations, J. Geophys. Res., 81, 5413, 1976.

46. Dryer, M., Z. K. Smith, R. S. Steinolfsen, J. D. Mahalov, J. H. Wolfe, and J. K. Chao, Interplanetary disturbances caused by the August 1972 solar flares as observed by Pioneer 9, J. Geophys. Res., 81, 4651, 1976.

47. Durney, B. R. and P. H. Roberts, On the theory of stellar winds, Astrophys. J., 170, 319, 1971.

48. Durney, B. and A. J. Hundhausen, The expansion of a low density solar corona: A one-fluid model with magnetically modified thermal conductivity, J. Geophys. Res., 79, 3711, 1974.

49. Durney, B. R. and G. W. Pneuman, Solar-interplanetary modelling: 3-D solar wind solutions in prescribed non-radial magnetic field geometries, Solar Phys., 40, 461, 1975.

50. Eddy, J. A., The Maunder Minimum, Science, 192, 1189, 1976.

51. Eddy, J. A., P. A. Gilman, and D. E. Trotter, Solar rotation during the Maunder Minimum, Solar Phys., in press, 1976.

52. Feldman, W. C., J. R. Asbridge, S. J. Bame, and J. T. Gosling, Plasma and magnetic fields from the sun, in the Solar Output and Its Variation, ed. O. R. White et al., University of Colorado Press, 1976.

53. Feldman, W. C., J. R. Asbridge, S. J. Bame, M. D. Montgomery, and S. P. Gary, Solar wind electrons, J. Geophys. Res., 80, 4181, 1976.

54. W. C. Feldman, personal communication, 1976.

55. Feldman, W. C., Kinetic processes in the solar wind, in this volume.

56. Feynman, J. and V. Pizzo, work in progress, 1976.

57. Fisk, L. A., The interaction of energetic particles with the solar wind, in this volume.

58. Forslund, D. W., Instabilities associated with heat conduction in the solar wind and their consequences, J. Geophys. Res., 75, 17, 1970.

59. Fredricks, R. and E. Greenstadt, Collisionless shocks, in this volume.

60. Gabriel, A. H., Measurements of the Lyman alpha corona, Solar Phys., 21, 392, 1971.

61. Geiss, J., P. Hirt, and H. Leutwyler, On acceleration and motion of ions in corona and solar wind, Solar Phys., 12, 458, 1970.

62. Geiss, J., Elemental and isotopic abundances in the solar wind, in Solar Wind, edited by C. P. Sonett, P. J. Coleman, Jr., and J. M. Wilcox, NASA-SP308, 559, 1972.

64. Gold, T., in Gas Dynamics of Cosmic Clouds, edited by H. C. van de Hulst and J. M. Bergers, North Holland, Amsterdam, p. 103, 1955.

64. Goldstein, B., Nonlinear corotating solar wind structure, unpublished report, 1971.

65. Gordon, J. M., Plasma theory of radio echoes from the sun and its implication for the problem of the solar wind, Space Sci. Rev., 15, 157, 1973.

66. Gosling, J. T., V. Pizzo, and S. J. Bame, Anomalously low proton temperature in the solar wind following interplanetary shock waves - evidence for magnetic bottles, J. Geophys. Res., 78, 2001, 1973.

67. Gosling, J. T., E. Hildner, R. M. MacQueen, R. H. Munro, A. I. Poland, and C. L. Ross, Mass ejections from the sun: A view from Skylab, J. Geophys. Res., 79, 4581, 1974.

68. Gosling, J. T., Large-scale inhomogeneities in the solar wind of solar origin, Rev. Geophys. Space Phys., 13, 1053, 1975.

69. Gosling, J. T., Transient phenomena in the solar atmosphere and solar wind, to appear in Proceedings of the Internat. Symp. on Solar-Terr. Phys., Boulder, 1976.

70. Gosling, J. T. and E. Hildner, Transient phenomena in the solar wind, submitted to J. Geophys. Res., 1976.

71. Gosling, J. T., A. J. Hundhausen, and S. J. Bame, Solar wind stream evolution at large heliospheric distances: Experimental demonstration and the test of a model, J. Geophys. Res., 81, 2111, 1976.

72. Gursky, H., Observations of galactic X-ray sources, in Black Holes, p. 291, edited by C. DeWitt and B. S. DeWitt, Gordon and Breach, New York, 1973.

73. Hartle, R. E. and P. A. Sturrock, Two-fluid model of the solar wind, Astrophys. J., 151, 1155, 1970.

74. Hearn, A., Chromosphere heating of very hot stars by radiation driven sound waves. II., Astron. Astrophys., 14, 275, 1971.

75. Heiles, C., The interstellar magnetic field, Ann. Rev. Astron. Astrophys., 14, 1, 1976.

76. Henriksen, R. N. and K. C. Heaton, Accretion and effluxion of mass and angular momentum, Mon. Not. Roy. Astron. Soc., 171, 27, 1975.

77. Heymann, D., Particle output of the sun in the past, in The Solar Output and Its Variation, ed. O. R. White et al., University of Colorado Press, 1976.

78. Hildner, E., J. T. Gosling, R. M. MacQueen, R. H. Munro, A. I. Poland, and C. L. Ross, Frequency of coronal transients and solar activity, Solar Phys., in press, 1976.

79. Hirshberg, J., A. Alksne, D. S. Colburn, S. J. Bame, and A. J. Hundhausen, Observation of a solar-flare-induced interplanetary shock and helium-enriched driver gas, J. Geophys. Res., 75, 1, 1970.

80. Hirshberg, J., S. J. Bame, and D. E. Robbins, Solar flares and solar wind helium enrichments, July 1965 - July 1967, Solar Phys., 23, 467, 1972.

81. Hirshberg, J., Composition of the solar wind: Present and past, Rev. Geophys. Space Phys., 13, 1059, 1975.

82. Hollweg, J. V. and J. R. Jokipii, Heat conduction in a turbulent magnetic field with application to solar wind electrons, J. Geophys. Res., 77, 3311, 1972.

83. Hollweg, J. V., Alfvenic acceleration of solar wind helium and related phenomena, I. Theory, J. Geophys. Res., 79, 1357, 1974.

84. Hollweg, J. V., Waves and instabilities in the solar wind, Rev. Geophys. Space Phys., 13, 263, 1975.

85. Hollweg, J. V., Collisionless electron heat conduction in the solar wind, J. Geophys. Res., 81, 1649, 1976.

86. Hollweg, J. V. and J. M. Turner, Acceleration of solar wind He^{++}: 3. Inclusion of resonant interactions with transverse waves, submitted to J. Geophys. Res., 1976.

87. Holzer, T. E. and W. I. Axford, Solar wind ion composition, J. Geophys. Res., 75, 6345, 1970.

88. Holzer, T. E. and W. I. Axford, The theory of stellar winds and related flows, Ann. Rev. Astron. Astrophys., 8, 30, 1970.

89. Holzer, T. E. and W. I. Axford, Interaction between interstellar helium and the solar wind, J. Geophys. Res., 76, 6965, 1971.

90. Holzer, T. E., Interaction of the solar wind with the neutral component of the interstellar gas, J. Geophys. Res., 77, 5407, 1972.

91. Holzer, T. E., Effects of rapid flow tube divergence, heat addition, and momentum addition in the solar wind and stellar winds, to appear in J. Geophys. Res., 1976.

92. Holzer, T. E., Our quantitative understanding of the coronal expansion, to appear in Proceedings of the Internat. Symp. on Solar-Terr. Phys., Boulder, 1976.

93. Houminer, Z., Enhanced scintillation sectors outside the plane of the ecliptic, Planet. Space Sci., 21, 1617, 1973.

94. Hundhausen, A. J., H. E. Gilbert, and S. J. Bame, Ionization state of the interplanetary plasma, J. Geophys. Res., 73, 5485, 1968.

95. Hundhausen, A. J. and R. A. Gentry, Numerical simulation of flare-generated disturbances in the solar wind, J. Geophys. Res., 74, 2980, 1969.

96. Hundhausen, A. J., Non-thermal heating in the quiet solar wind, J. Geophys. Res., 74, 5810, 1969.

97. Hundhausen, A. J., Dynamics of the outer solar atmosphere, in Physics of the Solar System, ed. S. I. Rasool, NASA SP-300, 1972.

98. Hundhausen, A. J., Coronal Expansion and Solar Wind, Springer-Verlag, New York, 1972.

99. Hundhausen, A. J., Interplanetary shock waves and the structure of solar wind disturbances, in Solar Wind, edited by C. P. Sonett, P. J. Coleman, Jr., and J. M. Wilcox, NASA-SP308, 393, 1972.

100. Hundhausen, A. J., Nonlinear model of high-speed solar wind streams, J. Geophys. Res., 78, 1528, 1973.

101. Hundhausen, A. J., R. T. Hansen, S. F. Hansen, W. C. Feldman, J. R. Asbridge, and S. J. Bame, The evolution of coronal and solar wind structure in 1973 and 1974, submitted to J. Geophys. Res., 1976.

102. Hundhausen, A. J. and V. Pizzo, The dependence of solar wind stream structure on near-sun boundary conditions, submitted to J. Geophys. Res., 1976.

103. Hundhausen, A. J. and V. Pizzo, unpublished results, 1976.

104. Hundhausen, A. J., personal communication, 1976.

105. Hundhausen, A. J., An interplanetary view of coronal holes, to appear in Coronal Holes and High Speed Wind Streams, University of Colorado Press, 1977.

106. Ipavich, F., Galactic winds driven by cosmic rays, Astrophys. J., 196, 107, 1975.

107. Johnson, H. E. and W. I. Axford, Galactic winds, Astrophys. J., 165, 381, 1971.

108. Jokipii, J. R., Effects of diffusion on the composition of the solar corona and solar wind, in The Solar Wind, edited by R. J. Mackin and M. Neugebauer, p. 215, Pergamon Press, New York, 1966.

109. Jokipii, J. R. and L. Davis, Jr., Long-wavelength turbulence and heating of the solar wind, Astrophys. J., 156, 1101, 1969.

110. Joselyn, J. A., work in progress, 1976.

111. Kopp, R. A. and F. Q. Orrall, Temperature and desnity structure of the corona and inner solar wind, to appear in Astron. Astrophys., 1976.

112. Kopp, R. A. and T. E. Holzer, Dynamics of coronal hole regions, I. Steady polytropic flows with multiple critical points, to appear in Solar Phys., 1976.

113. Kraft, R. P., Evidence for changes in the angular velocity of the surface region of the sun and stars, in Solar Wind, edited by C. P. Sonett et al., NASA SP-308, p. 276, 1972.

114. Krieger, A. S., A. F. Timothy, and E. C. Roelof, A coronal hole and its identification as the source of a high velocity solar wind stream, Solar Phys., 29, 505, 1973.

115. Krieger, A. S., A. F. Timothy, G. S. Vaiana, A. J. Lazarus, and J. D. Sullivan, X-ray observations of coronal holes and their relation to high velocity solar wind streams, in Solar Wind Three, ed. C. T. Russell, UCLA, p. 132, 1974.

116. Kuiper, G. P., The Atmospheres of the Earth and Planets, University of Chicago Press, 1952.

117. Kuperus, M., The heating of the solar corona, Space Sci. Rev., 9, 713, 1969.

118. Lange, J. and F. Scherb, Ion abundances in the solar wind, J. Geophys. Res., 75, 6350, 1970.

119. Levine, R. H., M. D. Altschuler, B. V. Jackson, and J. W. Harvey, Open-magnetic structures on the sun, Solar Phys., in press, 1976.

120. Lewis, R. R. and G. L. Siscoe, Solar wind structure between 20 solar radii and the orbit of Mars, J. Geophys. Res., 78, 6443, 1973.

121. Lin, C. C. and F. H. Shu, On the spiral structure of disk galaxies, Astrophys. J., 140, 646, 1964.

122. Lucy, L. B. and P. M. Solomon, Mass loss by hot stars, Astrophys. J., 159, 879, 1970.

123. MacQueen, R. M., J. A. Eddy, J. T. Gosling, E. Hildner, R. H. Munro, G. A. Newkirk, Jr., A. I. Poland, and C. L. Ross, The outer solar corona as observed from Skylab: Preliminary results, Astrophys. J., 187, L85, 1974.

124. Matsuda, T. and T. Sakurai, Dynamics of the azimuthally dependent solar wind, Cosmic Electrodynamics, 3, 97, 1972.

125. McCrea, W. H., Ice Ages and the galaxy, Nature, 255, 607, 1975.

126. Mathews, W. G. and J. C. Baker, Galactic winds, Astrophys. J., 170, 241, 1971.

127. Mezger, P. G., Interstellar matter: An observer's view, in Interstellar Matter, edited by N. C. Wickramasinghe, F. D. Kahn, and P. G. Mezger, Geneva Observatory, p. 1, 1972.

128. Michel, F. C., Relativistic stellar-wind torques, Astrophys. J., 158, 727, 1969.

129. Mihalas, D., Stellar Atmospheres, 2nd edition, W. H. Freeman, New York, 1977.

130. Motgomery, M. D., J. R. Asbridge, S. J. Bame, and W. C. Feldman, Solar wind electron temperature depressions following some interplanetary shock waves: evidence for magnetic merging, J. Geophys. Res., 79, 3103, 1974.

131. Montgomery, M. D., Solar wind observations throughout the solar system, to appear in Proceedings of the Internat. Symp. on Solar-Terr. Phys., Boulder, 1976.

132. Munro, R. H. and G. L. Withbroe, Properties of a coronal "hole" derived from extreme-ultraviolet observations, Astrophys. J., 176, 511, 1972.

133. Munro, R. H. and B. V. Jackson, Geometry and density of a polar coronal hole, submitted to Solar Phys., 1976.

134. Nakada, M. P., A study of the composition of the lower solar corona, Solar Phys., 7, 302, 1969.

135. Nakada, M. P., Some effects of diffusion on the flow of ions in the solar wind, J. Geophys. Res., 79, 1364, 1974.

136. Nakagawa, Y. and R. E. Wellck, Numerical studies of azimuthal modulations of the solar wind with magnetic fields, Solar Phys., 32, 257, 1973.

137. Ness, N. F., A. J. Hundhausen, and S. J. Bame, Observations of the interplanetary medium: Vela 3 and Imp 3, 1965-1967, J. Geophys. Res., 76, 6643, 1971.

138. Neugebauer, M. and C. W. Snyder, Mariner 2 observations of the solar wind, 1, Average properties, J. Geophys. Res., 71, 4469, 1966.

139. Neugebauer, M., Relation of solar wind fluctuations to differential flow between protons and alphas, Solar Wind Three, C. T. Russell, editor, p. 33, 1974.

140. Neugebauer, M., The Role of Coulomb collisions in limiting differential flow and temperature differences in the solar wind, J. Geophys. Res., 81, 78, 1976.

141. Newkirk, G., Jr. Coronal magnetic fields and the solar wind, in The Solar Wind, NASA SP-308, ed. C. P. Sonett et al., p. 11, 1972.

142. Newkirk, G., Jr., A. J. Hundhausen, and V. Pizzo, Solar cycle modulation of galactic cosmic rays: The role of coronal transients, submitted to J. Geophys. Res., 1976.

143. Noci, N., Energy budget in coronal holes, Solar Phys., 28, 403, 1973.

144. Nolte, J. T. and E. C. Roelof, Large-scale structure of the interplanetary medium, I: High coronal source longitude of the quiet-time solar wind, Solar Phys., 33, 241, 1973.

145. Nolte, J. T. and E. C. Roelof, Large-scale structures of the interplanetary medium, II: Evolving magnetic configuration deduced from multi-spacecraft observations, Solar Phys., 33, 483, 1973.

146. Ogilvie, K. W., L. F. Burlaga, and T. D. Wilkerson, Plasma observations on Explorer 34, J. Geophys. Res., 73, 6809, 1968.

147. Orrall, F. Q. and J. B. Zirker, Heat conduction and the fine structure of solar prominences, I. Optically thin model prominences, Astrophys. J., 134, 72, 1961.

148. Ostriker, J. P., R. McCray, R. Weaver, and A. Yahil, A new luminosity limit for spherical accretion onto compact X-ray sources, Astrophys. J., 208, L61, 1976.

149. Parker, E. N., Dynamics of the interplanetary gas and magnetic fields, Astrophys. J., 128, 664, 1958.

150. Parker, E. N., Sudden expansion of the corona following a large solar flare and the attendant magnetic field and cosmic ray effects, Astrophys. J., 133, 1014, 1961.

151. Parker, E. N., Interplanetary Dynamical Processes, Interscience, New York, 1963.

152. Parker, E. N., Comments on coronal heating, in The Solar Corona, edited by J. W. Evans, p. 11, Academic Press, New York, 1963.

153. Parker, E. N., Dynamical theory of the solar wind, Space Sci. Rev., 4, 666, 1965.

154. Parker, E. N., Theoretical studies of the solar wind phenomena, Space Sci. Rev., 9, 325, 1969.

155. Perkins, F. W., Heat conductivity, plasma instabilities, and radio star scintillations in the solar wind, Astrophys. J., 179, 637, 1973.

156. Pikel'ner, S. B., Interaction of stellar wind with diffuse nebulae, Astrophys. Lett., 2, 97, 1968.

157. Pizzo, V., Ph.D. Thesis, University of Colorado, 1976.

158. Pneuman, G. W., personal communication, 1976.

159. Pneuman, G. W. and R. A. Kopp, Gas-magnetic field interactions in the solar corona, Solar Phys., 18, 258, 1971.

160. Pneuman, G. W., The solar wind and the temperature-density structure of the solar corona, Solar Phys., 28, 247, 1973.

161. Pneuman, G. W., Latitude dependence of the solar wind speed: Influence of the coronal magnetic field geometry, submitted to Solar Phys., 1976.

162. Reimers, D., Circumstellar envelopes and mass loss of Red Giant stars, in Problems of Stellar Hydrodynamics, Proceedings of 19th Liege Colloquium, p. 369, 1975.

163. Robbins, D. E., A. J. Hundhausen, and S. J. Bame, Helium in the solar wind, J. Geophys. Res., 75, 1178, 1970.

164. Roberts, P. H. and A. M. Soward, Stellar winds and breezes, Proc. Roy. Soc. Lond. A328, 185, 1972.

165. Roberts, P. H., Stellar winds, in Solar Wind Three, edited by C. T. Russell, UCLA, p. 231, 1974.

166. Ryan, J. M. and W. I. Axford, The behaviour of minor species in the solar wind, J. Geophys., 41, 221, 1975.

167. Schatten, K. N., J. M. Wilcox, and N. F. Ness, A model of interplanetary and coronal magnetic fields, Solar Phys., 6, 442, 1969.

168. Schatzman, E., A theory of the role of magnetic activity during star formation, Ann. d. Astrophys., 25, 18, 1962.

169. Schubert, G. and P. J. Coleman, Jr., The angular momentum of the solar wind, Astrophys. J., 153, 943, 1968.

170. Simon, M. and W. I. Axford, Shock waves in the interplanetary medium, Planet. Space Sci., 14, 901, 1966.

171. Siscoe, G. L., L. Davis, Jr., P. J. Coleman, Jr., E. J. Smith, and D. E. Jones, Power spectra and discontinuities of the interplanetary magnetic field: Mariner 4, J. Geophys. Res., 73, 61, 1968.

172. Siscoe, G. L., B. Goldstein, and A. J. Lazarus, An east-west asymmetry in the solar wind velocity, J. Geophys. Res., 74, 1759, 1969.

173. Siscoe, G. L. and L. T. Finley, Solar wind structure determined by corotating coronal inhomogeneities, 2, Arbitrary perturbations, J. Geophys. Res., 77, 35, 1972.

174. Siscoe, G. and M. A. Heinemann, Binary stellar winds, Astrophys. Space Sci., 31, 363, 1974.

175. Siscoe, G. L., personal communication, 1976.

176. Siscoe, G. L., Three dimensional aspects of interplanetary shock waves, J. Geophys. Res., 82, in press, 1977.

177. Siscoe, G. L., Comparative magnetospheres, in this volume.

178. Solinger, A., S. Rappaport, and J. Buff, Isothermal blast wave model of supernova remnants, Astrophys. J., 201, 381, 1975.

179. Sonett, C. P., Evidence of a primordial solar wind, in Solar Wind Three, edited by C. T. Russell, UCLA, p. 36, 1974.

180. Spitzer, L., Jr. and E. B. Jenkins, Ultraviolet studies of the interstellar gas, Ann. Rev. Astron. Astrophys., 13, 133, 1975.

181. Steigman, G., P. A. Strittmatter, and R. E. Williams, The Copernicus observations: Interstellar or circumstellar material?, Astrophys. J., 198, 575, 1975.

182. Steinolfson, R. S., M. Dryer, and Y. Nakagawa, Numerical simulation of interplanetary shock ensembles, in Solar Wind Three, edited by C. T. Russell, 175, 1974.

183. Steinolfson, R. S., M. Dryer, and Y. Nakagawa, Numerical MHD simulation of interplanetary shock pairs, J. Geophys. Res., 80, 1223, 1975.

184. Steinolfson, R. S., M. Dryer, and Y. Nakagawa, Interplanetary shock pair disturbances: comparison of theory with space-probe data, J. Geophys. Res., 80, 1989, 1975.

185. Strom, S. E., K. M. Strom, and G. L. Grasdalen, Young stellar objects and dark interstellar clouds, Ann. Rev. Astron. Astrophys., 13, 187, 1975.

186. Suess, S. T. and S. F. Nerney, Meridional flow and the validity of the two dimensional approximation in stellar wind modelling, Astrophys. J., 184, 17, 1973.

187. Suess, S. T., Three-dimensional modelling, in Solar Wind Three, edited by C. T. Russell, UCLA, 311, 1974.

188. Suess, S. T., A. J. Hundhausen, and V. Pizzo, Latitude dependent nonlinear high speed streams, J. Geophys. Res., 80, 2023, 1975.

189. Suess, S. T., Latitudinal variations in the solar wind, to appear in Proceedings of the Internat. Symp. on Solar-Terr. Phys., Boulder, 1976.

190. Thomas, G. E., Interplanetary gas of nonsolar origin, Rev. Geophys. Space Phys., 13, 1063, 1975.

191. Ulmschneider, P., On the propagation of a spectrum of acoustic waves in the solar atmosphere, Astron. Astrophys., 14, 275, 1971.

192. Vaslyliunas, V. M. and G. L. Siscoe, On the flux and spectra of interstellar ions, J. Geophys. Res., 81, 1247, 1976.

193. Wallis, M., Shock-free deceleration of the solar wind, Nature, 233, 23, 1971.

194. Weber, E. J. and L. J. Davis, Jr., The angular momentum of the solar wind, Astrophys. J., 148, 217, 1967.

195. Weber, E. J. and L. J. Davis, Jr., The effect of viscosity and anisotropy in the pressure on the azimuthal motion of the solar wind, J. Geophys. Res., 75, 2419, 1970.

196. Wilson, O. C., A probable correlation between chromospheric activity and age in main-sequence stars, Astrophys. J., 138, 832, 1963.

197. Wilcox, J. M. and N. F. Ness, Quasi-stationary corotating structure in the interplanetary medium, J. Geophys. Res., 70, 5793, 1965.

198. Wilcox, J. M. and N. F. Ness, The interplanetary magnetic field. Solar origin and terrestrial effects, Space Sci. Rev., 8, 258, 1968.

199. Wolff, C. L., J. C. Brandt, and R. G. Southwick, A two-component model of the quiet solar wind with viscosity, magnetic field and reduced heat conduction, Astrophys. J., 165, 181, 1971.

200. Woo, R., Multifrequency techniques for studying interplanetary scintillations, Astrophys. J., 201, 238, 1975.

201. Yahil, A. and J. P. Ostriker, Winds and X-rays from clusters of galaxies, Astrophys. J., 185, 787, 1973.

202. Yeh, T., A three-fluid model of solar winds, Planet. Space Sci., 18, 199-215, 1970.

203. Yeh, T. and G. W. Pneuman, A sheet-current approach in coronal-interplanetary modelling, submitted to Solar Phys., 1976.

The Interactions of Energetic Particles With the Solar Wind

L. A. Fisk
Laboratory for High Energy Astrophysics
NASA/Goddard Space Flight Center
Greenbelt, Maryland 20771

I. INTRODUCTION

Studies of the interaction of energetic particles with the solar wind have both an immediate application and a far-reaching implication. The application is to the interpretation of observations of solar and galactic cosmic rays. Knowledge of the interaction with the solar wind is required so that we can deduce from these observations the full information that they contain. The implication is for the behavior of energetic particles in other large-scale astrophysical plasmas. We have a unique opportunity in the solar wind to observe the propagation and acceleration of energetic particles in random magnetic fields. The theories that we develop to explain these observations should have broad implications for particle behavior in other astrophysical settings.

The spectra, and chemical and isotopic composition of galactic cosmic rays can reveal the nature of the sources of these particles (e.g., supernovae), the mechanisms by which they are accelerated, and their behavior as they propagate through the interstellar medium. At energies below $\sim$10 GeV/nucleon, however, galactic cosmic rays are effected by the magnetic fields which are being carried outward through the solar cavity by the solar wind--the continuous expansion of the solar atmosphere. The flow of the solar wind, which may extend over dimensions in excess of 50 AU, alters the spectra of the cosmic rays (or equivalently the composition as a function of energy), and may even exclude low-energy particles ($\lesssim$100 MeV/nucleon) from the inner solar system, near earth. Our observations of galactic cosmic rays are thus biased by this interaction with the solar wind, or, as we say, by the solar modulation

of the cosmic rays. Clearly, to derive the maximum information from our observations of cosmic rays, we must understand this modulation and take it into account.

An identical situation exists for solar cosmic rays. These particles provide us with a sample of the composition of the solar atmosphere, and they reveal information on the flare acceleration process. But again, the spectra of these particles are altered by propagation through the solar wind.

Knowledge of the interaction of energetic particles with the solar wind is also required so that we can use solar and galactic cosmic rays as probes of what conditions are like in regions of the heliosphere that are presently inaccessible to spacecraft. Galactic cosmic rays respond to, and therefore are a measure of conditions in the solar wind throughout the heliosphere, including regions far off of the solar equatorial plane where to date no spacecraft has ever ventured. For example, as we discuss in § II h, the recent anisotropy measurements from Pioneer 10 and 11 are consistent with the current belief that galactic cosmic rays have an easy access to the inner solar system over the solar poles, i.e. that in this region the field lines are nearly radial and there is less turbulence. Temporal variations in the cosmic-ray intensity, gradient and anisotropy (e.g., over the 11-year solar cycle or on even longer timescales) can also provide a measure of global variations in the heliosphere with time. Solar cosmic rays can serve as a probe of conditions in the solar corona.

The importance of studies of energetic particle behavior in the solar wind, however, transcends the information that this subject provides on the interpretation of cosmic-ray observations. Cosmic rays in the solar wind provide us with a unique opportunity to study the propagation of energetic particles in a large-scale magnetic field with a significant random component. The solar wind is our only accessible example of a large-scale astrophysical plasma in which we can study in situ and in detail both the behavior of the particles, and the properties of the magnetic field and its fluctuations.

The theories and techniques that we develop for propagation in the solar wind should be applicable to propagation in other astrophysical settings. Turbulence in the solar wind is similar to that which is expected in other astrophysical plasmas, such as the interstellar medium. For example, solar wind turbulence is believed to result from finite amplitude Alfvén and magnetosonic waves, and it has a power spectrum that is similar to what is expected for Kolomogorov turbulence. The energetic particles that we deal with in the solar wind have gyro-radii which span the full range from very large to very small in comparison with the scale length of the turbulence.

In fact, studies of propagation in the solar wind are expected to be particularly relevant for astrophysics in the coming years. As we shall discuss in § III, we have discovered that propagation theories in the solar wind, which are based on standard quasi-linear and nonlinear techniques and on standard assumptions about hydromagnetic waves, are inconsistent with observation, in that they

overestimate the amount of scattering at low rigidities. As we develop more reliable theories--by treating the finite amplitude turbulence more properly, by considering non-Markovian processes, or whatever--we will develop ideas and techniques which will have a direct influence on our understanding of how particles should behave in other astrophysical plasmas, or perhaps even on how to describe properly some aspects of particle behavior in laboratory plasmas.

Similarly, we have found and continue to find in the solar wind numerous examples of the acceleration of energetic particles. For example, as we shall discuss in § IV, low-energy particles ($\lesssim$ a few MeV/nucleon) have been observed recently to undergo a general acceleration in the solar wind, possibly by a statistical mechanism. Propagating shock waves in the solar wind produce energetic particles near the shock front. Both of these mechanisms are commonly invoked in explaining the acceleration of energetic particles elsewhere in the universe. Clearly, with our continuous and in situ observations in the solar wind we are in a position to provide detailed testimony as to what acceleration processes are possible in an astrophysical plasma, and how they work.

It is the purpose of this article to review the status of studies of the interaction of energetic particles with the solar wind, and to make recommendations on research which should be undertaken in the coming years. This subject has of course been very active during the last twenty years with the result that the amount of material which could be reviewed here is enormous, and far exceeds what could be contained in a reasonable-length article. In this review, then, we will concentrate on three topics which will give

the flavor of the work done in this area, and which will serve as the basis for the recommendations that we make. In § II we discuss the theory of the solar modulation of galactic cosmic rays, which has come under some criticism in recent years. In § III we review theories for the propagation of energetic particles in the solar wind and in § IV, theories for their acceleration. It should be noted that we make a distinction here between modulation and propagation theory. In modulation theory the details of the particle interaction with the solar wind are contained in phenomenological parameters such as diffusion coefficients, which can often be inferred directly from the particle observations. Propagation theory, as it is defined here, concerns itself with the calculation of these diffusion coefficients from the observed properties of the magnetic field, and with the justification for describing particle propagation as a diffusive process.

We do not review in detail studies of solar particle behavior in the solar wind, other than to cite the evidence that these studies provide on the inadequacies of current propagation theory. The theories for solar particle behavior and galactic cosmic ray modulation are effectively the same (at least above a few MeV/nucleon (See § III, d)) except that in the solar case the intensity varies rapidly in time (e.g., flare events).

Recommendations on directions that research in this area should take in the future are given in § V.

II. MODULATION THEORY

a) Introduction

Shown in Figure 1 are the spectra of galactic protons at energies <1 GeV/nucleon, which were observed near earth in the years 1965-72. The spectra turn over at energies ∿ a few hundred MeV/nucleon, and then decrease with decreasing energy. The intensity also varies from year to year. The intensity is lowest in 1969, which is a period of maximum solar activity, and highest in 1965 and 1972, when solar activity was reduced. This variation in the spectra of galactic cosmic rays with energy and time is what is known as the solar modulation of the cosmic rays.

It is the purpose of modulation theory to understand how this modulation occurs, and to treat it quantitatively. We attempt to determine how cosmic-ray spectra observed near earth are affected by modulation; in particular, how the spectra of different species (e.g., electrons, protons, heavier nuclei) are affected. We thus attempt to deduce from cosmic-ray observations near earth the maximum information that they contain about cosmic-ray spectra and composition in the interstellar medium. We also predict in this field where we need to fly spacecraft and make measurements which will reveal more about the modulation process, and what is the best direction to fly in order to find truly unmodulated spectra.

In this section we discuss first the basic idea on which modulation theory is founded. We next derive and discuss the equations which govern cosmic ray behavior in the interplanetary medium. In §II.e we consider how these equations can be solved, and in §II.f we

summarize the information which is available on the extent to which particles are modulated. We then discuss some of the successes of current modulation theory, and some of the challenges to this theory, which have come from recent spacecraft measurements, e. g. from Pioneer 10 and 11.

b) The Basic Idea

The outer atmosphere of the Sun undergoes a continuous expansion and produces a flow of plasma out through the interplanetary medium that is known as the solar wind (see the accompanying review by Holzer[1]). The speed of this flow is quite variable near the ecliptic plane, but generally averages about 400 km/sec, and the flow lies essentially always in the radial direction. To our knowledge, this flow occurs at all heliographic latitudes, with perhaps increasing speed toward the solar poles[2]. The ram pressure of the flow appears to be sufficient to sweep back the interstellar medium for distances in excess of 50 AU from the Sun[3].

The flow of the solar wind drags the solar magnetic field outward from the Sun. At distances beyond a few tens of solar radii, the kinetic energy in the flow of the wind dominates over the field energy, with the result that the field is pulled essentially radially outward. The field, however, remains attached to the rotating Sun, with the result that the large-scale field executes a spiral pattern. For example, with the simplifying assumption that the solar wind flows radially at constant speed V, the field pattern is that of an Archimedes spiral[4]. In a spherical coordinate system centered on the Sun, the components of the large-scale field are in this case

$$B_r(r,\theta,\phi) = B_r(r_o,\theta,\phi-r\Omega_\odot/V)(r_o/r)^2 \qquad (1)$$

$$B_\theta(r,\theta,\phi) = 0 \qquad (2)$$

$$B_\phi(r,\theta,\phi) = B_r(r_o,\theta,\phi-r\Omega_\odot/V)(r_o\Omega_\odot/V)(r_o\sin\theta/r) \qquad (3)$$

Here, r is heliocentric radial distance, and ϕ and θ are the azimuthal and polar angles, respectively, with the latter measured relative to the axis of rotation of the Sun. The angular velocity of the Sun is $\Omega_\theta (=2.7 \cdot 10^{-6}$ rad/sec); $B_r(r_o,\theta,\phi)$ is the radial component of the field at a distance $r_o (\simeq 0.1 AU)$, which lies just beyond where the field becomes a passive partner in the expansion of the solar wind. Other spiral patterns can result if variations in the flow speed are taken into account[5].

Superimposed on the large-scale field structure are numerous small-scale variations, which result from waves and discontinuities in the solar wind (see, for example, the review by Burlaga[6]). The field variations which result from this small-scale turbulence are generally quite large. For example, the mean square (ms) variation in a component B_x of the field, relative to the mean field strength B_o is typically $\langle(\delta B_x)^2\rangle/B_o^2 \simeq 0.1$-0.3 in the inner solar system near earth[7]. Shown in Figure 2 is a typical power spectrum for the field fluctuations, as was observed near earth[8]. Note that the characteristic size of the turbulence, the correlation length, is $\sim 2.10^{11}$cm (or $\sim$0.01AU). Further, the power density falls off relatively slowly with wave number k, with the result that there is considerable energy in the fluctuations at large k. Indeed, the shape of the spectrum is similar (for reasons that are not well understood) to what is expected for Kolomogorov turbulence in that it decreases as $k^{-5/3}$ for large k.

The small-scale fluctuations in the field scatter cosmic rays in pitch angle. In particular, particles should be effectively

scattered by fluctuations which have scale sizes comparable to the particles' gyro-radii[9]. Based on the power spectrum in Figure 2, we expect that near earth particles with gyro-radii less than or on the order of the correlation length of the turbulence (i.e. $\leq$ several hundredths of an AU) should be scattered (See §III). Since $B_o \sim 5 \cdot 10^{-5}$G, we thus expect that, e.g. nuclei at energies $\leq$ 10 GeV/nucleon are effectively scattered.

The small-scale field fluctuations, along with the large-scale field, thus produce a coupling between the solar wind and cosmic rays with energies $\leq$ 10 GeV/nucleon. It is from this coupling that the modulation is believed to result. As was noted by Parker[10], cosmic rays that wish to penetrate into the inner solar system must fight their way upstream against the outward flow of the solar wind, which is attempting to sweep them out of the solar cavity. At energies $\leq$ 10 GeV/nucleon only a fraction of the cosmic rays are able to make this trek successfully, with the result that at a given energy the number density in the inner solar system is reduced from what it is in the interstellar medium, or equivalently, the spectra are altered or modulated.

c) The Modulation Equations

We require, of course, a set of equations which describes the behavior of cosmic rays in the interplanetary medium. These equations can be readily derived if we assume that the interaction of the cosmic rays with the magnetic field irregularities in the solar wind is a diffusive process.

Let U denote the differential number density of the cosmic rays, per interval of kinetic energy T. Let $\underline{S}$ denote the differential current density or streaming--the net number of particles in a given energy interval which crosses a unit area normal to $\underline{S}$ in unit time. Both U and $\underline{S}$, and also T, are measured here in the frame fixed with respect to the Sun (as opposed to, e.g., the frame moving with the solar wind). The equation of continuity of number of particles is then[11,12]

$$\frac{\partial U}{\partial t} + \nabla\cdot\underline{S} = -\frac{\partial}{\partial T}\,(\underline{V}\cdot\nabla P) \tag{4}$$

Here t is time and V is again the solar wind speed. The differential pressure of the cosmic rays is denoted by P. Since galactic cosmic rays are observed to exhibit only small anisotropies in interplanetary space[13]

$$P = \frac{\alpha}{3}TU \tag{5}$$

where $\alpha=(T+2T_o)/(T+T_o)$ with T_o particle rest energy[14]. The term on the right side of (1) results from the work done on the cosmic rays by the solar wind, as it sweeps them out of the solar cavity. The solar wind does work against the pressure gradient of the cosmic rays, or equivalently it alters the cosmic ray energy and as a

result the differential number density[15,16].

As a result of our assumption that particle propagation is a diffusive process, we consider that cosmic rays stream relative to the solar wind because there are gradients in U, and that these gradients are directly proportional to the streaming. Hence,

$$-\underline{\underline{\kappa}}\cdot\nabla U = \underline{S}-\underline{S}_o \tag{6}$$

where $\underline{\underline{\kappa}}$ is the diffusion tensor and $\underline{S}_o$ is the streaming that is seen in the frame fixed with the Sun, when the cosmic-ray distribution is isotropic in the frame moving with the solar wind (i.e. when there is no streaming relative to the solar wind).

The term $\underline{S}_o$ must be treated with some care. Consider a particle with a given energy in the frame moving with the solar wind. If the particle is moving in the direction of the solar wind, it will be seen at a higher energy in the frame fixed with respect to the Sun; conversely, if it is moving opposite to the wind it is seen at a lower energy in the fixed frame. Thus, the streaming in the fixed frame which results from an isotropic distribution in the frame of the wind depends not only on $\underline{V}$ but also on the shape of the cosmic-ray spectrum. This last effect is known as the Compton-Getting effect[17]. It has been cast in its modern context by Gleeson and Axford[18], and by Forman[19], who find that

$$\underline{S}_o = \underline{V}U-\frac{V}{3}\frac{\partial}{\partial T}(\alpha TU) \equiv C\underline{V}U \tag{7}$$

where $C = 1-(1/3U)(\partial(\alpha TU)/\partial T)$ is the so-called Compton-Getting coefficient. It should be noted that, while the streaming in the frame

moving with the solar wind differs from that in the fixed frame, the differential number density in these two frames is the same to $0(V^2/v^2)$, where v is particle speed[15,18]

The diffusion approximation which is used in (6) has been invoked as a valid description of cosmic ray behavior for more than twenty years[20]. Indeed, in cases where we can think of particles scattering off of well-defined 'scattering centers' this approximation can be rigorously justified[21]. However, the validity of this approximation becomes less clear when we think of a cosmic ray spiraling about a mean magnetic field and slowly changing pitch angle as it interacts, resonately or otherwise, with a random field component. In fact, in propagation theory, which we consider in the next section, there is currently no defendable proof that low-energy particles diffuse. Of course, the ultimate justification for this approximation will come from how well it can explain particle observations. As we shall see, in this context it appears to do quite well.

Upon substituting (5), (6) and (7) into (4), we obtain a Fokker-Planck equation for U[22,11,23]

$$\frac{\partial U}{\partial t} = \nabla\cdot(\underline{\underline{\kappa}}\cdot\nabla U) - \nabla\cdot(\underline{V}U) + \frac{\nabla\cdot\underline{V}}{3}\frac{\partial}{\partial T}(\alpha T U) \qquad (8)$$

This is the basic equation which governs cosmic ray behavior in interplanetary space.

In studies of the modulation of galactic cosmic rays we will be concerned primarily with steady-state solutions to (8); i.e.,

$\partial U/\partial t=0$. In general, the average conditions in the solar wind change on time-scales long compared with the dwell time of cosmic rays in the solar cavity. Some caution, however, should be exercised in treating the modulation of low-energy particles which can have relatively long dwell times[24,25,26]. Also, we will not be concerned with azimuthal variations in U because we will be dealing with times long compared with a solar rotation period (~27 days). Thus, it is convenient to express (8) in the spherical coordinate system which was used in (1)-(3), or as

$$\frac{1}{r^2}\frac{\partial}{\partial r}\left(r^2\kappa_{rr}\frac{\partial U}{\partial r}\right)+\frac{1}{r^2\sin\theta}\frac{\partial}{\partial\theta}\left(\sin\theta\,\kappa_{\theta\theta}\frac{\partial U}{\partial\theta}\right)+\frac{1}{r\sin\theta}\frac{\partial}{\partial\theta}\left(\sin\theta\kappa_{\theta r}\frac{\partial U}{\partial r}\right)$$

$$+\frac{1}{r^2}\frac{\partial}{\partial r}\left(r\kappa_{r\theta}\frac{\partial U}{\partial\theta}\right)-\frac{1}{r^2}\frac{\partial}{\partial r}\left(r^2VU\right)+\frac{1}{3r^2}\frac{\partial}{\partial r}\left(r^2V\right)\frac{\partial}{\partial T}\left(\alpha TU\right)=0 \qquad (9)$$

where the solar wind has been assumed here to flow only in the heliocentric radial direction.

The radial component of the diffusion tensor κ_{rr} can also be expressed as[27]

$$\kappa_{rr}=\kappa_{\parallel}\cos^2\psi+\kappa_{\perp}\sin^2\psi \qquad (10)$$

where $\kappa_{\parallel}$ is the diffusion coefficient for propagation parallel to the mean field direction, and $\kappa_{\perp}$, for propagation normal to this direction, along cones of constant θ. The angle between the mean field direction and the radial direction is ψ. If the mean field lies along cones of constant θ, as it does, for example, if it executes

the Archimedes spiral pattern given in (1)-(3), then $\kappa_{\theta\theta}$ results from cross-field diffusion and in most circumstances is equal to $\kappa_{\perp}$. The off-diagonal elements of the diffusion tensor, $\kappa_{\theta r}$ and $\kappa_{r\theta}$, describe the effects of particle drift motions in the large-scale magnetic field and can be expressed as[23]

$$\kappa_{\theta r} = - \kappa_{r\theta} = - \frac{1}{3} v r_g \sin\psi \qquad (11)$$

Here v is particle speed and r_g is the gyro-radius of the particle, which is assumed to have a positive charge. If the charge or the mean field change sign, $\kappa_{\theta r}$ (and $\kappa_{r\theta}$) also reverses sign. The effects of these drift terms have been considered in detail in the recent work of Jokipii *et al*[135].

d) Energy Loss

It is interesting to note that in the final equations, (8) and (9), the term which describes the effects of cosmic-ray energy changes has the form

$$-\frac{\partial}{\partial T}\left(\frac{dT}{dt}U\right) \tag{12}$$

where

$$\frac{dT}{dt} = -\frac{1}{3r^2}\frac{\partial}{\partial r}(r^2V)\alpha T \tag{13}$$

is the rate at which particles are adiabatically cooled due to the expansion of the solar wind. The expression $(1/r^2)(\partial(r^2V)/\partial r)$ is just the rate at which a volume in the solar wind expands as it moves radially outward. Indeed, Parker[22] first derived (8) by assuming simply that the principal energy change suffered by the cosmic rays results from this adiabatic cooling.

We have here, however, a slight puzzle. We derived (8) and (9) under the assumption that the solar wind does work against the cosmic rays. The cosmic-ray intensity in the inner solar system is lower than it is in the interstellar medium, or equivalently $\underline{V}\cdot\nabla P = V dP/dr > 0$. Yet in the final analysis the cosmic rays are losing energy. To understand this apparent paradox we must consider in detail who does work on what, and where.

It is instructive for this explanation of cosmic-ray energy changes to consider the following simplified model, which was discussed by Fisk[12]. Imagine a series of infinitely thin concentric spherical shells as are depicted in Figure 3. At a given time these

shells are all expanding with radial speed V, and particles are trapped between any two shells. The density is taken to be uniform over the narrow distance between contiguous shells, but it is assumed that the density between successive shells increases with radial distance.

Consider now the work done by a given shell at radius r_1. Particles that strike the shell from radial distances $r>r_1$ gain energy since the particles make 'head-on' collisions with the outward moving wall. Particles striking the surface from $r<r_1$ lose energy in 'overtaking' collisions. Since the density of particles increases with r, there are more particles striking from $r>r_1$ than from $r<r_1$ and the moving shell does work on the particles.

Consider, however, the particles trapped between two successive shells. The particles gain energy by striking the inner shell (at r_1) and lose energy by striking the outer shell (at r_2, $r_2>r_1$). However, the surface area of the outer shell exceeds that of the inner shell. Thus, overtaking collisions outnumber head-on collisions and the particles are cooled. Indeed since the differential number density is the same in the frame moving with the shells as it is in the frame when the shells are moving (to $0(V^2/v^2)$), this cooling occurs at the adiabatic cooling rate given in (13).

The cooling, however, must stop at the outermost shell which we place at r=R. Particles in r>R can only make head-on collisions; i.e., they can only gain energy.

The analogy between the solar wind and this simple model is straightforward. The solar wind does work against the cosmic-ray

gradient everywhere in the interplanetary medium, as do the shells. However, the work which is done on the cosmic rays through head-on collisions at one radial distance is immediately undone, and more so, by the more numerous overtaking collisions which occur at slightly larger radial distances. Thus, cosmic rays in the solar wind, as with the particles trapped between shells, are adiabatically cooled continuously. Particles, however, which penetrate only ~one mean free path into the solar wind and depart (strike only the outermost shell) do gain energy.

Of course, energy must be conserved in the modulation process. The energy which is carried off by particles making only ~one collision with the solar wind must equal the work done on all the cosmic rays by the wind, throughout the solar cavity. Indeed, as has been shown by Jokipii and Parker[15], (8) can be integrated to prove that energy is properly conserved.

For observations made deep within the solar wind (e.g., for observations made near earth) only the energy loss process is important. The particles that we see have been continuously cooled in the solar wind at the rate given in (13).

It should be noted also that the energy loss results directly from our assumption that the solar wind tends to sweep the cosmic rays out of the solar cavity. If there is convection by the solar wind, there will also be energy loss. The two processes cannot be decoupled.

e) Solving the Modulation Equations

To discuss the behavior of cosmic rays in actual interplanetary conditions it is necessary to solve (9) by numerical techniques. This equation is a sufficiently complicated partial differential equation so that analytic solutions exist only for special and unrealistic forms of $\underline{\underline{\kappa}}$ and of the unmodulated, interstellar spectrum[28,29,30,31]. Approximate solutions to (9) are also available. The most useful of these is the 'force-field' approximation of Gleeson and Axford[32]; however, this approximation holds only when variations in the modulation with heliocentric latitude can be ignored, and only at energies above a few hundred MeV/nucleon.

In a paper by Fisk[33] a numerical method is outlined for solving (9) in spherically-symmetric models of the interplanetary medium, i.e. in models where diffusion is restricted to occur only in the radial direction. In a subsequent paper[34] this method has been extended by Fisk to solve (9) with all the latitude-dependent terms included. The numerical methods of Fisk have been refined and expanded upon by Urch and Gleeson[35] and by Moraal and Gleeson[36]. Similar numerical methods have been developed independently by, e.g., Quenby and his co-workers[37].

f) Techniques of Modulation Theory

We have here, of course, a somewhat difficult problem. What we wish to determine are galactic cosmic-ray spectra in the local interstellar medium, i.e. unmodulated spectra. To determine these spectra by use of (9), however, we need to know the solar wind speed and the elements of the diffusion tensor throughout the solar cavity. That is, we need to be fully informed about interplanetary conditions in regions of the solar cavity which are presently inaccessible to spacecraft observations. The intractability of our problem is brought home in particular when we realize, as we discuss below, that modulation may depend sensitively on interplanetary conditions at mid- and high-heliographic latitudes, where no spacecraft has ever ventured. Clearly, the best we can hope for is a consistent solution. Namely, we assemble all the pertinent facts about cosmic rays in the interstellar medium and about acceptable forms for $\underline{V}$ and $\underline{\underline{\kappa}}$, and then we find solutions to (9) consistent with these assumptions. When we draw conclusions based on these solutions, however, we must be aware of the limitations of our assumptions.

The most important restrictions on acceptable solutions to (9) come from studies of electrons, positrons, and to some extent low-energy protons. We can estimate the interstellar spectra of each of these particles without resorting to arguments concerned with modulation. By comparing each of these predicted interstellar spectra with the corresponding observed spectra in the inner solar system, we then obtain a measure of the total modulation experienced

by each of these test species, as a function of energy. The estimates of the modulation of the test species can then be scaled to yield constraints on the modulation suffered by other species, i.e. by all nuclei.

Energetic electrons propagating in the interstellar magnetic field synchrotron radiate, and are believed to produce the observed nonthermal radio background[38]. Upon making reasonable assumptions concerning interstellar conditions such as density, temperature, and magnetic field strength, we can then predict, from the radio observations, the interstellar electron spectrum in the energy range from $\sim$200 MeV through several GeV[39,40]. Similarly, higher energy protons ($\gtrsim$1 GeV) interacting with the interstellar gas produce pions which in turn decay to produce positrons. Since these higher energy protons do not suffer much modulation, the observed proton intensity at these energies is representative of the interstellar value and can be used to yield a prediction of the interstellar positron spectrum above a few MeV in energy[41]. The interaction of these higher energy protons with the interstellar gas will also produce knock-on protons, which provide a lower limit on the density of protons that must be present in the interstellar medium at energies $\sim$50 MeV[42].

Of the three measures of the modulation, the one which results from electron studies is the most useful. Not only is the interstellar electron spectrum predicted in detail, but also substantial electron observations at 1 AU are available for comparison, e.g. more reliable observations than for the positrons. Shown in Figure 4 is the interstellar electron spectrum which is predicted by using the observed nonthermal radio background. This interstellar intensity

is the lowest that is found to be acceptable by Cummings et al.[40]; i.e., by using this spectrum we underestimate the electron modulation. Shown also in Figure 4 are the electron spectra observed at Earth in 1970, 1971, and 1972, by Fulks et al.[43]. Clearly, during all these years electrons with energies $\lesssim$1 GeV experience significant modulation. The measures of the modulation provided by studies of positrons and low-energy protons, which are essentially independent measures, can be shown to be consistent with the modulation seen in Figure 4.

The principal objection to the use of these predicted interstellar spectra to measure the modulation is the fact that this technique makes no allowance for any spatial inhomogeneities present in the galactic cosmic-ray flux. In the case of electrons, for example, the observed radio noise data comes from a volume that is several kpc in dimension. The predicted electron spectrum is then an average interstellar spectrum, and may differ from the spectrum directly outside the solar cavity. The latter is of course the one needed for measuring the modulation. In defense of this technique, however, note in Figure 4 that the radio noise data can be used to predict an interstellar electron spectrum at energies $\gtrsim$1 GeV, which agrees well with the observed spectra. Since at these energies there is little modulation, the observed spectrum represents the local interstellar spectrum, and thus here the average and local interstellar spectra coincide. In the interstellar medium the propagation of electrons with energies $\sim$200 MeV, which is the lowest energy at which we can predict the interstellar electron spectrum,

should not be drastically different from the propagation of 1-GeV electrons. Thus, over its entire energy range, the predicted average spectrum in Figure 4 may be a good measure of the local interstellar electron spectrum.

To use the predicted interstellar electron spectrum to place constraints on the modulation of other particle species, we need to note that under most circumstances the elements of the diffusion tensor $\underline{\underline{\kappa}}$ must have the form $vg(P,\underline{r})$, where v is particle speed and $g(P,\underline{r})$ is a function of particle rigidity P and position $\underline{r}$. Cosmic rays view the interplanetary magnetic field and its irregularities as static since v is so much larger than the Alfvén speed and the solar wind speed. The form $vg(P,\underline{r})$ is simply a statement that the mean free path of a particle in a static magnetic field is independent of its speed.

The technique for estimating the modulation of different species of cosmic rays is then as follows. We first determine a combination of $\underline{V}$, $\underline{\underline{\kappa}}$, and a size for the modulating region, which when used in (9), with the predicted interstellar electron spectrum as a boundary condition, can account for the electron observations at earth. In choosing our parameters we require, of course, that $\underline{V}$ and $\underline{\underline{\kappa}}$ be compatible with what is measured directly, or inferred from observations in the inner solar system. We then use these same parameters, with the elements of $\underline{\underline{\kappa}}$ expressed as $vg(P,\underline{r})$, to predict the modulation of other species, or equivalently to estimate the unmodulated interstellar spectra of these species. Note that since

the interstellar electron spectrum is determined down to energies ∿200 MeV, the chosen $\underline{\underline{\kappa}}$ will be valid down to rigidities ∿200 MV; i.e., it will be valid for protons with energies as low as 25 MeV. Thus we can use the electron modulation to estimate the modulation of nuclei at all energies of interest.

The technique outlined here has been used in numerous studies of the modulation[44,45,136]. It should be emphasized, however, that this technique does not yield unique predictions of the modulation or of the interstellar spectra of cosmic-ray nuclei. There are, for example, assumptions and uncertainties in the prediction of the interstellar electron spectrum. The range of acceptable forms of $\underline{\underline{\kappa}}$ is large, particularly in models where the modulation varies with heliographic latitude. There are also, as we discuss below, inherent limitations in our ability to use this technique to predict the interstellar spectra of low-energy galactic nuclei ($\lesssim$100 MeV/nucleon). Nonetheless, this technique provides some useful general guidelines on the extent to which particles are modulated--guidelines which we will exploit in the coming sections.

g) Successes of Modulation Theory

The estimates of the total modulation of cosmic-ray electrons can be used to predict the extent to which particles are adiabatically cooled in the solar cavity, due to the expansion of the solar wind. As we shall see, this energy loss is appreciable and is of particular importance for low-energy ions. We predict that ions which are observed at energies $\lesssim$100 MeV/nucleon all originate at energies above $\sim$100 MeV/nucleon in the interstellar medium. Low-energy galactic cosmic rays do not appear to penetrate into the inner solar system near earth. This prediction of modulation theory must be considered as one of its major successes. The exclusion of low-energy ions from the inner solar system provides a natural explanation for several different features in cosmic-ray observations.

The best illustrations of the extent and influence of the energy loss can be found in the work of Goldstein et al.[46] and of Gleeson and Urch[47]. Goldstein et al., for example, use the predicted electron modulation in 1965 and a spherically symmetric model for the interplanetary medium to compute a likely form for the interstellar proton spectrum. They then divide this proton spectrum into a series of essentially monoenergetic spectra, and recompute the modulation that each of these subspectra experiences. With this technique we can see how a particle which enters the interplanetary medium at a given energy is likely to behave.

The results of the calculations of Goldstein et al.[45] are reproduced in Figure 5. The essentially monoenergetic interstellar

spectra are shown in the solid curves and the resulting modulated spectra at 1 AU (each labeled with the same number as its interstellar input spectrum), in the light dashed curves. (The heavy dashed curve represents the sum of all the light dashed curves.) Note that at high energies (spectra 8-10) the effects of the modulation are rather small. There is only a slight reduction in the intensity at 1 AU as compared with the interstellar intensity, and only a slight shift in the mean energy of the particles as they are modulated. At intermediate energies (spectra 4-7) the reduction and shift are more pronounced. There is also a considerable spread in energy here. Since the particles diffuse, there is a distribution in the time which particles spend in the solar cavity, and thus also a distribution in the energy loss. At low energies the reduction in intensity and shift in energy is extreme. In fact, the intensity of protons that enter the interplanetary medium at energies below $\sim$100 MeV is so reduced at 1 AU that the probability of observing these particles is quite small. As can be seen in Figure 5, at energies below $\sim$100 MeV we are more likely to see particles from spectra 4 and 5, which entered the interplanetary medium at energies above 100 MeV and were cooled down.

These calculations were repeated by Goldstein *et al.*[45] for helium, with essentially the same results. At the same energy per nucleon, helium and heavier ions have a rigidity twice that of the protons, and thus experience somewhat less modulation (cf. Figure 4). The true exclusion of helium and heavier ions from the inner solar system near earth then occurs at a slightly lower energy of 60-80 MeV/nucleon.

From observations near earth we are thus unable to sample directly cosmic rays which have low energies in the interstellar medium. For example, we cannot measure the composition of these particles and infer whatever information is contained in this composition about the nature of cosmic-ray sources. Similarly, our observations near earth are insensitive to the shape of low-energy interstellar spectra. We could, for example, raise spectrum 2 in Figure 5 by two orders of magnitude and yet produce no appreciable effect on the total spectrum at 1 AU (the heavy dashed curve). Thus, we cannot infer from our observations at earth whether there is sufficient energy density in low-energy galactic cosmic rays to affect the pressure or ionization state of the interstellar medium.

This exclusion of low-energy ions, however, does have the positive feature of providing explanations for what would otherwise be puzzling observations. For example, in Figure 6 we have plotted the ratio of the intensity of He to that of CNO, vs. kinetic energy, for data which was collected during the last solar cycle[48]. We note that this ratio is essentially invariant with energy despite the fact that low-energy CNO should suffer substantially more ionization loss in the interstellar medium than does He. For example, if we assume that cosmic rays in the interstellar medium traverse sufficient material to produce, by spallation, the observed Li, Be, and B (which is the normal mechanism for producing these light elements in cosmic rays), we find that at energies $\lesssim$100 MeV/nucleon

the ratio of He/CNO in the interstellar medium is noticeably above the observed ratio[49]. This puzzle is resolved, however, by noting that the He and CNO that we observe at energies $\lesssim$100 MeV/nucleon originated in the interstellar medium at energies above this value, where ionization loss is negligible.

Similarly, it is interesting to note in Figure 1 that the shape of the modulated proton spectrum at low energies ($\lesssim$100 MeV) is roughly the same in each year despite the fact that the level of modulation changes substantially. In fact, Rygg and Earl[50], who have studied this effect, find that the slope of the low-energy proton spectrum is always near unity throughout the solar cycle; i.e., the differential intensity j ($=vU/4\pi$) is proportional to kinetic energy T.

We note also that particles which should have substantially different interstellar spectra at low energies, from that of the protons, also have low-energy modulated spectra with slopes near unity. For example, the measured intensities of H^2 and He^3 are seen in Figure 7 to be well fit by such a spectrum[51]. Both H^2 and He^3, however, are secondary particles which are produced mainly by the interaction of cosmic-ray protons and He^4 with the interstellar gas. At low energies, the interstellar spectra of H^2 and He^3 should differ markedly from the proton spectrum because of the strong energy dependence of the production cross sections. In fact, in some cases the primary and secondary spectra are simply unrelated at low energies since the secondaries are produced by higher energy primaries[52,53].

This slope of unity also finds its explanation in the energy-loss process. We note first that it is not surprising that there is a common slope for low-energy particles. These particles are being cooled down in interplanetary space. The spectral shape is thus determined here, and is essentially independent of the spectral shape in interstellar space. To see that this common slope is unity requires that we reexamine (9), which for this purpose we rewrite in terms of the differential intensity j, or as

$$\frac{1}{3r^2}\frac{\partial}{\partial r}(r^2V)\left(2j-\alpha T\frac{\partial j}{\partial T}\right) = \frac{1}{r^2}\frac{\partial}{\partial r}(r^2\kappa_{rr}\frac{\partial j}{\partial r}) + \frac{1}{r^2\sin\theta}\frac{\partial}{\partial\theta}(\sin\theta\,\kappa_{\theta\theta}\frac{\partial j}{\partial\theta})$$
$$+ \frac{1}{r\sin\theta}\frac{\partial}{\partial\theta}(\sin\theta\,\kappa_{\theta r}\frac{\partial j}{\partial r}) + \frac{1}{r^2}\frac{\partial}{\partial r}(r\,\kappa_{r\theta}\frac{\partial j}{\partial\theta})$$
$$- V\frac{\partial j}{\partial r} \qquad (14)$$

We note here that the radial gradient $(\partial j/\partial r)$ of particles which are cooled down should not be large. The source of the cooled particles is higher energy particles which are not heavily modulated, and which are thus distributed more or less uniformly with radial distance. In fact, the measured radial gradient of low-energy particles as seen from Pionner 10 and 11 are quite small[54,55]. Let us also suppose that the polar gradients $(\partial j/\partial\theta)$ are small. Then, upon noting that the elements of $\underline{\underline{\kappa}}$ should decrease with decreasing energy (at least down to $\sim$25 MeV/nucleon), we conclude that the right side of (14) can be near zero for low-energy ions. Hence, (14) becomes

$$2j - \alpha T\frac{\partial j}{\partial T} \simeq 0 \qquad (15)$$

or since $\alpha \approx 2$ for $T \ll T_o$, we find that $j \propto T$.

It should be emphasized that the result $j \propto T$ is only an approximation and that there are forms of $\underline{\underline{\kappa}}$ for which it does not hold. Nonetheless, there is a wide range of $\underline{\underline{\kappa}}$ for which this spectral form is a direct consequence of the energy-loss process[56]. It should also be emphasized that this result is wholly compatible with the small gradients seen from Pioneers 10 and 11.

We note finally that because of the exclusion of low-energy ions from near earth our only choice for measuring these particles is to fly spacecraft into regions where the modulation is less. It was hoped that this function would be performed by Pioneer 10, which is currently at 10 AU from the Sun, near the ecliptic plane. Regrettably, the spectra from Pioneer show no marked deviations from those seen at earth, and thus it appears that Pioneer is still well embedded in the region where there is extensive modulation[57]. As we shall discuss, a more promising region for finding low-energy ions may be the region over the solar poles.

h) Challenges to Current Modulation Theory

In addition to the observations which current modulation theory explains well, there are also observations which present a challenge to the theory. In some cases the challenge is not serious. For example, the radial gradients of the intensity which have been seen from Pioneers 10 and 11 are much smaller than were predicted prior to the Pioneer launch. However, as we shall discuss, the gradient observations can be understood either by a simple reevaluation of the parameters used in modulation theory, or by taking into account variations in the modulation with heliographic latitude, which certainly must occur. The gradient observations do not in themselves require that we abandon any of the basic tenets of the theory. A more serious challenge to the theory comes from the observations of the so-called anomalous cosmic-ray component, which as we shall see cannot be readily explained by current modulation theory. Fortunately, there are other explanations for the origin of this component.

Solar-cycle variations. One of the persisting challenges to current modulation theory is to explain the 11-year solar-cycle variation in the cosmic-ray flux. As we noted in Figure 1, the cosmic-ray intensity varies roughly inversely with solar activity. From observations near earth, however, it is not clear what conditions in the interplanetary medium are changing over the solar cycle, to cause these cosmic-ray variations. For example, the average solar wind speed is relatively constant over the solar cycle[58]. In fact, there may be more pronounced and persistent high-speed streams in periods of minimum solar activity[59].

The recent work of Morfill et al.[68], however, does offer a possible explanation for the solar-cycle variations in the cosmic ray flux. As we discuss in more detail in §III, Morfill et al.[68] point out that Alfven waves propagating outward from the sun should, from geometric considerations, have their wavevectors directed into the heliocentric radial direction. Since the mean magnetic field, in contrast, is being wound into a tight spiral, the wavevectors and the field direction thus tend to become orthogonal to each other -- an effect which will reduce the scattering (i.e. increase $\kappa_{\parallel}$). Competing against this reduction is the tendency of the long wavelength waves to alter the local mean field direction. In cases, then, where there is significant power in long wavelength fluctuations, Morfill et al.[68] argue that the scattering will be systematically greater than when this power is reduced. In fact, Hedgecock[60] does find that the power density in low-frequency (long-wavelength) fluctuations ($<10^{-4}$Hz) varies directly with solar activity. It is not clear, however, whether the variations in this power density are sufficient to explain the cosmic ray variations.

It may be also that the observed cosmic ray intensity is not sensitive to local interplanetary conditions. We observe in situ only a small part of the solar cavity (from ~0.4 - 10 AU near the ecliptic plane). The cosmic rays in contrast respond to interplanetary conditions over a much larger region. Thus, the changes in interplanetary conditions which give rise to cosmic-ray changes may occur in regions not currently sampled by spacecraft.

In particular, cosmic rays may be sensitive to conditions out of the equatorial plane of the Sun, which is a region which has yet to be explored by spacecraft. (All spacecraft to date have been confined to fly within $\sim 15^{\circ}$ of the equatorial plane.) For example, it may well be that cosmic rays have a much easier access to the inner solar system over the solar poles than they do in the equatorial plane. After all, the magnetic field in the equatorial plane is wound in a tight spiral by solar rotation. Thus, cosmic rays which attempt to come from the interstellar medium to the inner solar system must follow a highly circuitous path along the equatorial field, or diffuse across the field over long distances (e.g. 10's of AU). In contrast, the polar field is nearly radial (cf. (1)-(3)) and may give easy access to the cosmic rays. Moreover, there may be less turbulence and hence less cosmic-ray scattering over the solar poles. Because of solar rotation, high- and low-speed streams in the solar wind can be injected at the same heliographic longitude (ϕ) in the equatorial plane, and thus pronounced stream-stream interactions result here. Over the poles such interactions should be essentially absent. It may well be, then, that the cosmic rays that we observe near earth have in fact entered the inner solar system over the solar poles and then diffused across the fields (a distance $\lesssim 1$ AU) to the equatorial plane.

The possibility that the cosmic-ray flux near earth may depend sensitively on conditions off of the solar equatorial plane has been illustrated recently by Fisk[34] with some numerical solutions to (9). In this model the variation in modulating conditions with latitude is caused solely by the latitude variation in the direction and magnitude of the interplanetary magnetic field which is

given in (1) - (3). The parallel diffusion coefficient $\kappa_{\parallel}$, which depends on the field magnitude through the particle gyro-radius, is taken to be the one given by Jokipii[61]. Diffusion perpendicular to the mean magnetic field is assumed to result only from particle scattering, i.e. diffusion due to field-line random walk[62] is ignored. With this choice the cross-field diffusion coefficient is very small at low energies and is consistent with observations of solar particle events (see §III.f).

The effects of gradiant and curvature drifts of particles in the large-scale field (i.e. $\kappa_{r\theta}$ and $\kappa_{\theta r}$) have been ignored in these calculations, and, as Jokipii et al.[35] have argued recently, would have to be included in any realistic model. The cross-field diffusion used in these calculations, then, should be considered as a lower limit on the actual transport of particles in the polar direction.

The particles in these calculations are assumed to be protons, and the unmodulated proton spectrum is taken to be a power law in total energy for the number density. This unmodulated spectrum has been found to be compatible with the predicted electron modulated in studies which use the spherically symmetric form of (9)[45]. The size of the modulating region and the radial dependence of $\kappa_{\perp}$ are chosen so that the calculated intensity at 1 AU near the equatorial plane agrees with the observed low-energy proton spectrum in 1972. This calculated intensity together with the 1972 data is shown in Figure 8.

Shown in Figure 9 is the calculated intensity at 1 AU, plotted here as a function of polar angle θ, for two different energies. The curves marked $\kappa_{\theta\theta}\neq 0$ result from the full solution to (9) which

gives the intensity shown in Figure 8 (i.e. at $\theta=90^{\circ}$ the intensities in Figures 8 and 9 are the same). For the curves marked $\kappa_{\theta\theta}=0$ the model is the same but the effects of polar diffusion are ignored.

As is evident in Figure 9, the intensity of low-energy particles can be substantially larger over the solar poles than it is in the equatorial plane. Moreover, a large fraction of the low-energy particles near the equatorial plane at 1 AU entered the solar cavity at higher heliographic latitudes. As can be seen by comparing the $\kappa_{\theta\theta}=0$ and the $\kappa_{\theta\theta}\neq 0$ curves, some 80% of the 25 MeV particles appear near earth as a result of polar diffusion.

It is important to realize, however, that at low energies the effects of adiabatic deceleration are as important in these calculations as they were in the spherically symmetric model discussed in the previous section. At low energies $\kappa_{\theta\theta}$ is taken to be very small here, with the result that very few particles can diffuse in the polar direction. The bulk of the particles seen at low energies near earth diffused across the fields at higher energies, and then were cooled down near the equatorial plane yielding again a slope near unity (cf. Figure 8). In models in which only radial variations are included, the particles diffuse radially into the inner solar system and then are cooled down here. In models which include latitude variations, the particles, by diffusing radially, easily penetrate into the inner solar system over the solar poles. They then diffuse across the fields to the equatorial plane and are cooled down.

Of course, if these arguments on latitude variations in the modulation are correct, it follows that the region over the solar

poles is an appropriate place in which to look for cosmic rays that have low energies in the interstellar medium. Indeed, such particles may penetrate to within 1 AU of the Sun over the poles, whereas in the equatorial plane, as has been suggested by the Pioneer 10 observations, the exclusion of low-energy particles may hold out to distances in excess of 10 AU.

Gradient observations. One of the most publicized challenges to current modulation theory has come from the Pioneer 10 and 11 observations of the integral radial gradient. The integral gradient is typically the average gradient of protons with energies above ∿60 MeV. For the observed spectral shapes, the mean response energy of the integral gradient is ∿1 GeV, or equivalently the integral gradient is roughly equal to the gradient of 1 GeV protons.

Prior to the Pioneer launch several predictions were made as to what the integral gradient would be[45]. In general, these predictions were based on two simple assumptions. First, the interplanetary medium was taken to be spherically symmetric. With this assumption the streaming $\underline{S}$ can be shown to be negligible in (6) at high energies (e.g. at 1 GeV), and thus the radial gradient is given simply by[32,30,63]

$$\frac{1}{U}\frac{\partial U}{\partial r} \simeq \frac{CV}{\kappa_{rr}} \qquad (16)$$

Second, the radial diffusion coefficient κ_{rr} was assumed to be related to the observed properties of the interplanetary magnetic field according to the formulae of Jokipii[61]. For 1-GeV protons these formulae yield $\kappa_{rr} \sim 2.5 \cdot 10^{21}$ cm^2/sec. The Compton-Getting coefficient at these energies is C∿1. The solar wind speed is

$V \sim 4 \cdot 10^7$ cm/sec. And hence the predicted gradients from (16) were ~20%/AU.

However, the gradients which have been observed by comparing Pioneer 10 and 11 data with near-earth data from, e.g., IMP 7 and 8, have been much smaller than this value. For example, Teegarden et al.[54] and McKibben et al.[55] find an integral proton gradient of only ~4%/AU between 1 and 3 AU. Van Allen[64,65] reports a gradient which is consistent with zero over this distance. McKibben et al.[66] have found subsequently that the integral gradient remains at 4%/AU out to at least 5 AU. McDonald et al.[67], however, have argued recently that the corrections for Jovian electrons in their previous analysis, as well as in the analyses of other experiments, were inadequate. With these corrections taken into proper account, McDonald et al.[67] suggest that all previous gradient measurements could be reduced.

There are of course two obvious possibilities for why the predicted gradients were in error. The value of κ_{rr} which was used in these predictions could be unrealistically low, or the assumption of spherical-symmetry (i.e. that latitude-dependent effects can be ignored) could be untrue. Indeed, as we shall discuss in § III, the small gradient measurements have caused a reexamination of the theory which determines κ_{rr} from the observed field properties. Recent calculations by Morfill et al.[68], for example, now find values of κ_{rr} that yield integral gradients of 4%/AU, i.e. gradients which are in agreement with the observations of McKibben et al.[66]

Deviations from spherical symmetry could also have a major effect on the predicted gradient. For example, Jokipii et al.[135] have emphasized recently that the large-scale pattern of the interplanetary magnetic field can produce gradient and curvature drifts of high energy particles (1GeV/nucleon), which are comparable in speed to the solar wind. These drifts, which will vary in direction and magnitude with position in the solar cavity, will result in deviations from spherical symmetry, and have the potential for introducing major corrections to the predicted integral gradient. Numerical models for the modulation, which include drifts in realistic field configurations, are currently under development.

We also saw above in the calculations of Fisk[34] that a large fraction of the particles we observe in the inner solar system may have arrived here by diffusing in the polar direction from higher heliographic latitudes. In this particular model the radial dependence of $\kappa_{\theta\theta}$ is such that the polar diffusion occurs primarily at small radial distances. Polar diffusion, then, results in an effective source of particles in the inner solar system, and will tend to reduce the radial gradient seen near the equatorial plane. In these calculations κ_{rr}, which is taken to be the value predicted by Jokipii[61], yields an integral gradient of ~20%/AU in spherically symmetric models. As can be seen in Figure 8, however,

with latitude-dependent effects included the predicted gradient is now much smaller. Shown in this figure is the differential radial gradient determined between 1 and 5 AU in the equatorial plane. The integral gradient (for protons above 60 MeV) which corresponds to this differential gradient is only 0.6%/AU. Such a value is in good agreement with the observations of Van Allen[64,65] and of McDonald et al.[67]

There is in fact some additional evidence which suggests that latitude-dependent effects are contributing to the small gradients seen from Pioneer 10 and 11. An effective 'source' of particles in inner solar system near the equatorial plane, which results from polar diffusion, will, in addition to producing small gradients, also produce an outward radial streaming. Such a streaming is difficult to observe directly from Pioneer since the particle detectors here spin essentially orthogonal to the radial direction. This radial streaming, however, will have an effect on the azimuthal streaming, which Pioneer can see.

Let us suppose, as is the case in the calculations of Fisk[34], that $\kappa_\perp = \kappa_{\theta\theta} << \kappa_\parallel$. Also, we assume that conditions are symmetric above and below the equatorial plane, so that near the plane the polar gradients are small. The radial streaming then can be shown from (6) to be[27]

$$S_r = CVU - \kappa_\parallel \cos^2\psi \frac{\partial U}{\partial r} \tag{17}$$

and the azimuthal streaming

$$S_\phi = -\kappa_\parallel \sin\psi \cos\psi \frac{\partial U}{\partial r} \tag{18}$$

If we define an anisotropy $\xi \equiv 3S/vU$,[11] then from (17) and (18) the

radial anisotropy ξ_r can be determined from the azimuthal anisotropy according to the formula

$$\xi_r = (3CV/v) - \xi_\phi/\tan\psi \qquad (19)$$

Axford et al.[69] report that the azimuthal anisotropy seen from Pioneer 10 and 11 for particles with energies $\gtrsim$480 MeV/nucleon is $\xi_\phi = 0.46\pm.11\%$. We consider that this value is characteristic of the streaming at r=3AU, and we suppose that the mean response energy of these observations is again $\sim$1 GeV. Hence, $\tan\psi\simeq 3$ and $C\simeq 1$. With V=400 km/sec (19) then yields a radial anisotropy of $\xi_r = 0.3\%$.

Shown in Figure 8 is the radial anisotropy at 3 AU in equatorial plane, which is calculated in the latitude-dependent modulation model of Fisk[34]. At 1-GeV, the predicted ξ_r is also $\sim$0.3%. Thus, the observed azimuthal anisotropy from Pioneer 10 and 11 is wholly compatible with an influx of particles into the equatorial plane by polar diffusion, and a subsequent outward radial streaming of sufficient magnitude to substantially reduce the radial gradient (e.g. down to 0.6%/AU[34]). We note that if there was no radial anisotropy, which would be the case at these energies in a spherically-symmetric modulation model, that according to (19) the observed azimuthal anisotropy should have been 1.4%.

The observed gradients from Pioneer 10 and 11 are thus not a serious challenge to current modulation theory. These observations, however, have had the positive feature of causing us to reexamine our calculations of diffusion coefficients from the observed magnetic field properties (see § III), and they have made us give more serious consideration to latitude-dependent modulation models.

It should be emphasized that in its simplest interpretation the observation of a small integral gradient, together with the estimates of the total modulation from studies of galactic electrons, require a large modulating region, at least near the equatorial plane. If the change in the integral intensity with distance throughout the region near the equatorial plane is similar to the small change we have observed from Pioneer, then to produce the required overall change in the intensity in the solar cavity the distance over which modulation occurs must be large. For example, in the model of Fisk[34], where the small gradients were attributed to the effects of latitude-dependent modulation, the solar modulation was assumed to extend to a distance of 25 AU from the Sun. In models where latitude-dependent effects are unimportant and where the small gradients result from large diffusion coefficients, the size of the modulating region is ∿50 AU.

The requirement of a large modulating region, however, must also be considered as one of the positive features of the small gradient observations. In the past, when the gradient was predicted to be ∿20%/AU, it was necessary to terminate the modulation region at ∿10 AU, in order to remain compatible with the predicted electron modulation[137]. There is, however, no a priori reason why the modulation should be terminated at this point. The solar wind is predicted to flow to distances ∿50 AU [3], and could remain sufficiently turbulent to produce cosmic-ray scattering over this entire distance. With the small gradient measurements, however, our predictions of the size of the modulating region and the size of the region over which the solar wind flows are now comparable with each other.

The prediction of a large modulating region again suggests that the region near the equatorial plane may be an inappropriate one in which to search for cosmic rays that have low energies in the interstellar medium. As is discussed in § IIg, such particles do not appear to penetrate to the region of the equatorial plane near earth. With a modulating region several 10's of AU in dimension, we should not expect this situation to change rapidly with heliocentric radial distance, i.e. we may have to fly a spacecraft many 10's of AU into the equatorial plane to overcome this exclusion of low-energy particles. It may be better to search for low-energy cosmic rays in the region over the solar poles, where, as we discussed above, these particles may penetrate to within 1 AU of the Sun.

The anomalous component

The most serious challenge to current modulation theory has come from observations of the so-called anomalous component in low-energy cosmic rays. As we discussed in § IIg, the spectra of many species of cosmic rays (e.g. protons, deuterium and He^3) have slopes near unity at low energies, which is exactly what is expected if these particles are undergoing extensive adiabatic cooling in the solar wind. In recent years, however, four species, viz. helium, nitrogen, oxygen, and neon, have shown marked deviations from this expected behavior. It appears as if at low energies there is a separate component, which is composed only of He, N, O, and Ne, superimposed on the normal modulated intensity. The existence of this anomalous component was totally unexpected and its origin is now one of the most hotly debated subjects in low-energy

cosmic-ray physics. As we shall discuss, if these particles are galactic cosmic rays (i.e. there is a component of energetic particles with this composition in the interstellar medium), then much of the framework and many of the conclusions of modulation theory that are outlined above will have to be revised. There is, however, an alternative origin which requires no such revision. It will remain for new observations to decide which of the possible origins (if either) is correct.

Shown in Figure 10 is the low-energy spectra of oxygen and nitrogen that were observed by McDonald et al[70] and Hovestedt et al[71] for times of minimum solar activity in 1972-1973. As can be seen here, the intensities of O and N decrease from energies ∿150 MeV/nucleon consistent with what is expected for modulated galactic O and N. However, at energies ∿30 MeV/nucleon, both spectra undergo dramatic turnups, as if an entirely new component (the anomalous component) were being superimposed on this galactic flux. The intensity of, for example, O increases by several orders of magnitude between 30 and 6 MeV/nucleon, where the spectrum becomes level. Shown also in this figure is the spectrum of helium, which was measured by Garcia-Munoz et al[72] in the same time interval as the O and N. The anomalous behavior sets in for He at a higher energy of ∿50 MeV/nucleon, where the spectrum becomes essentially flat. Figure 10 also includes the observations of Von Rosenvinge and McDonald[73] of what are believed to be a turnup in the neon spectrum.

These anomalous spectral features appear to be restricted to He, N, O, and Ne. For example, the carbon spectrum, which is also shown in Figure 10, shows no evidence for a turnup. The carbon

data points below 10 MeV/nucleon are only upper limits. Also the measurements by Chan and Price[74], for example, show the oxygen enhancement at low energies with no corresponding enhancements in elements such as lithium through boron, magnesium and silicon, or elements with nucleon charge greater than 20. Mewaldt et al[138] place even lower limits on any lithium, beryllium or boron enhancements. The different spectral behavior for the various elements of course leads to a highly unusual composition at low energies. For example, as can be seen in Figure 10, the O/He ratio is near unity at ∿5 MeV/nucleon, whereas the O/C ratio at 10 MeV/nucleon can exceed 20.

These spectral features were first observed starting in about mid-1972, and have been present continuously since then[75]. During this time the galactic cosmic-ray flux was near its maximum value, i.e. the anomalous component occurs near solar minimum conditions. It is difficult to say, however, whether the anomalous component was present during the last solar minimum (in about 1965). Detailed compositional measurements of low-energy particles ($\lesssim$30 MeV/nucleon) were not available at this time. An examination of the helium spectrum in 1965, which was measured in detail[76], does appear to suggest that a flattening of this spectrum did occur at low energies. By no means, however, was this flattening as pronounced as it is in the current epoch.

The origin of the anomalous component is of course extraterrestrial. These particles are observed by Pioneer 10 and 11 in transit to Jupiter and beyond. The likely possibilities, then, are that the anomalous particles (i) originate on the Sun, (ii) come from Jupiter, (iii) have a galactic origin (i.e. are a galactic cosmic-ray component), or (iv) are accelerated in the interplanetary medium.

The first two possibilities here can be eliminated rather handily. The radial gradient of the intensity of the helium and oxygen, as measured by McDonald et al.[70] with Pioneer 10 and IMP-7 spacecraft, is positive; the intensity increases with increasing heliocentric distance. As McDonald et al.[70] note, this positive gradient, together with the unusual composition, suggests that a solar origin is unlikely. Similarly, a Jovian origin does not seem to be a good possibility. Although the gradient is positive, it remains small (<30%/AU) during the transit of Pioneer to Jupiter and shows no marked enhancement as the spacecraft approaches the planet. In contrast, the low-energy electrons from Jupiter which are responsible for the 'quiet-time electron increases' seen at earth[77] are observed to increase in intensity by a factor of ∿500 as Pioneer approaches Jupiter[78].

A galactic origin for the anomalous component, in which these particles are a component of the galactic cosmic-ray flux, would of course be most interesting. Low-energy cosmic rays can suffer substantial ionization loss in the interstellar medium, and hence must have originated in nearby cosmic-ray sources. If the composition of low-energy cosmic rays in the interstellar medium is then mainly He, N, O, and Ne, it would suggest that these nearby sources are rather exotic objects[79]. However, it is this explanation for the anomalous component which runs afoul of and creates difficul-

ties for current modulation theory, as has been discussed in detail by Fisk[80].

The difficulty here is that current modulation theory predicts, from quite general considerations, that an unrealistically large intensity of cosmic rays, by many orders of magnitude, would be required in the interstellar medium to account for the observed fluxes of the anomalous component. We can illustrate this problem by considering a simple model. We first ignore the effects of adiabatic deceleration and latitude-dependent effects, and then calculate the modulation according to the standard techniques of current modulation theory. We then argue that neither the deceleration nor nonspherical effects will tend to reduce our estimates of the modulation.

With adiabatic deceleration and latitude-dependent effects ignored, (14) (or (9)) reduces to the simple form

$$Vj = \kappa_{rr} \frac{\partial j}{\partial r} \tag{20}$$

Suppose, then, that we consider the modulation of anomalous oxygen and we define a 'modulation factor' M_o as the ratio of the observed oxygen intensity to the unmodulated intensity in the interstellar medium. According to (20),

$$M_o = \exp - \int_r^\infty \frac{V dr}{\kappa_{rr}} \tag{21}$$

We recall, as is discussed in § IIf, that to estimate the modulation of a given species in current modulation theory, e.g. to estimate M_o, we calibrate on the predicted modulation of galactic electrons. We recall also, again as is discussed in § IIf, that under

most reasonable circumstances κ_{rr} must have the specific form of particle speed v times some function $g(P,\underline{r})$ of particle rigidity P and position $\underline{r}$. Hence, we rewrite (21) as

$$M_o = \exp\left(- \frac{v_e}{v_o} \int_r^\infty \frac{V dr}{v_e g(P,r)} \right)$$

$$= \left(M_e\right)^{v_e/v_o} \qquad (22$$

where M_e is the modulation factor of electrons with rigidities identical to that of the anomalous oxygen, and v_e/v_o is the ratio of the speed of the electrons to that of the oxygen.

Anomalous oxygen particles, which originated as energetic particles in the interstellar medium, will surely be nearly or fully stripped of their electrons[80]. Thus, in the observed energy range from 5-30 MeV/nucleon, anomalous oxygen has a rigidity in the range 200-400 MV, or equivalently, it has rigidity equal to that of electrons in the energy range 200-400 MeV.

The predicted electron modulation in 1972, which is when the anomalous oxygen reported in Figure 10 was observed is shown in Figure 4. As can be seen in this figure, electrons with energies $\sim$200-400 MeV are predicted to be modulated by a factor $M_e \sim 25$. The ratio of the speed of the relativistic electrons to that of the low-energy oxygen is $v_e/v_o \sim 8$. Hence, for the simple model described in (20)-(22), we conclude that for the anomalous oxygen to be of galactic origin it would have to be modulated by $M_o \sim (25)^8 \sim 10$ Equivalently, to account for the observed flux, an interstellar intensity $\sim 10^{11}$ times more intense is required. Such a modulation factor is of course absurdly large and greatly exceeds any reason-

able limit on the allowed modulation. For example, if $M_o \gtrsim 10^4$ the energy density in the interstellar medium in anomalous oxygen alone would exceed 1 ev/cm^3, which is the expected average energy density of all cosmic rays[80].

This estimate of the modulation of anomalous oxygen of galactic origin was done, of course, in a simplisitic and unrealistic model. However, if we use the complete theory, which includes the effects of adiabatic deceleration and latitude-dependent modulation, our estimates of the modulation unfortunately do not decrease. In fact, with adiabatic deceleration included we predict that the required modulation of the anomalous oxygen is larger.

Consider, for example, anomalous oxygen at energies $\gtrsim$6 MeV/nucleon, in the region of the observed spectrum where the intensity is decreasing with increasing energy. As can be seen in Figure 4, modulation tends to become more pronounced with decreasing energy. To account for this observed oxygen spectrum, then, a spectrum in the interstellar medium at least as steep as the observed slope is required. Now, we note that the energy-loss process tends to bring particles into a given energy interval from a higher energy range. However, because of the steep slope of the spectrum, fewer particles are available in this higher energy range. Thus the deceleration increases the modulation seen at a given energy. Of course, energy loss has the opposite effect on a spectrum that decreases with decreasing energy. For example, for modulated galactic protons at energies $\lesssim$100 MeV, which were discussed in § IIg, the observed particles are primarily those which have cooled down from higher energies, and the level of modulation is substantially less than it would be without the energy loss.

Similarly, use of an interplanetary model in which the modulation conditions vary with heliographic latitude does not lead to an acceptable estimate for the expected modulation of anomalous oxygen. In nonspherical models, the modulation is still the result of a competition between the inward radial diffusion of the particles and their outward convection by the solar wind, just as it is in the simple model described by (23). However, in these more complicated models, where the intensity at different latitudes is coupled by cross-field diffusion, or by drift effects the balance between radial diffusion and convection is not necessarily a local balance. The inward diffusion in one latitude range can be balanced by the outward convection in some other range.

It would appear, therefore, that an explanation for the anomalous component in which these particles are galactic cosmic rays is incompatible with our current understanding of solar modulation. Of course, it is possible to imagine how current modulation theory could be modified so as to be consistent with a galactic origin for the anomalous component. Indeed, Fisk[80] has suggested one such modification, although, as is pointed out by Fisk, for this modification to work some extreme assumptions are required.

Fortunately, there is an alternative explanation for the anomalous component. Fisk, Kozlovsky, and Ramaty[81] and Fisk[82] have argued that the anomalous component results from interstellar neutral particles which were ionized and accelerated in the solar wind. The main virtues of this explanation are two-fold. It provides a natural explanation for the anomalous composition, and it requires

no modifications to current modulation theory. Indeed, standard modulation theory is an integral part of the explanation.

The neutral component of interstellar gas should consist mainly of hydrogen, helium, nitrogen, oxygen and neon. We in fact observe neutral interstellar hydrogen and helium in the solar system from the UV backscatter of solar radiation[3]. Neutral nitrogen, oxygen, and neon also are present because the first ionization potential of these elements is higher than that of hydrogen.

These neutral elements are swept into the solar cavity by the motion of the Sun through the interstellar medium. Once here they are ionized by photoionization from solar UV and by charge exchange with the solar wind. The particles are then picked up by the solar wind, obtaining energies $\sim$1 keV/nucleon in the process, and are convected outward. According to Fisk[62] the particles can then be accelerated in the solar wind, so that by the time they have reached heliocentric distances $\sim$50 AU they have energies $\sim$10 MeV/nucleon (see discussion in §IV.e).

Interstellar neutrals can be ionized only once during the time that they spend in the solar cavity; hence they will be singly charged. At 10 MeV/nucleon, singly charged helium, nitrogen, oxygen, and neon have a relatively high rigidity and thus do not undergo appreciable modulation (e.g., singly charged oxygen at 10 MeV/nucleon has a rigidity $\sim$2 GV). With current estimates of the modulation, these particles can then penetrate back into the inner solar system and produce the observed anomalous component. The

modulation, however, will exclude from the inner solar system accelerated interstellar hydrogen or any accelerated solar and galactic cosmic rays (which should be fully stripped of their electrons). These latter particles remain at low rigidities at 10 MeV/nucleon.

Clearly, the principal observation which is needed here is to determine the charge state of the anomalous component. If these particles are found to be singly charged, the explanation of Fisk et al[81] and Fisk[82] would appear to be correct, and no revisions to current modulation theory are required. On the other hand, if the particles prove to be fully stripped of their electrons, a galactic origin is a better possibility and major modifications to our current understanding of solar modulation will have to be considered. Unfortunately, direct measurements of the charge states of these particles are not possible from instruments which are currently being flown. However, some indirect indications of the charge state are available from the temporal behavior of the anomalous particles, and although certainly not conclusive, they appear to favor a single charge for anomalous oxygen and helium[73].

We note finally, as was pointed out by Mewaldt et al.[138] that if the anomalous component indeed has its origin as interstellar neutrals, these particles will provide us with a direct sample of the isotopic composition of the interstellar medium. This possibility should be a subject of future investigations.

i) Concluding Remarks

Modulation theory, then, is in a state of wary optimism. The theory is able to provide a reasonable explanation for many different features of the cosmic-ray observations. For example, it provides a natural explanation for the spectral shapes of modulated particles at low energies, and it is compatible with the recent gradient measurements. The theory, however, is challenged by the recent observations of the so-called anomalous component. This challenge can be met in that there is a plausible explanation which is compatible with the current theory. However, we need to be wary in that the principal experimental test of this explanation, viz. to determine the charge state of the particles, has yet to be made.

We should emphasize that, even if we have a theory that is compatible with available data, we are still far from the end of the problem. It is the aim of modulation theory to deduce from cosmic-ray observations the maximum information that they contain about the sources of these particles, their acceleration, and their behavior in the interstellar medium and the remote solar wind. There is a limit, however, as to what we can deduce from available observations. There is simply too much uncertainty at present in the parameters that we can use in the theory and the conclusions that we can draw. We need, as a result, to broaden our observational base. We need to have measurements in different regions of the heliosphere, which we can use to provide more definitive tests of our theory, and on which we can base more accurate

predictions of the implications of the cosmic-ray observations. In this regard, measurements at different heliographic latitudes of conditions in the solar wind and the cosmic-ray behavior would be particularly useful. As we discussed above, the bulk of the cosmic rays that we see near earth may have entered the inner solar system over the solar poles, with the result that temporal variations in the cosmic-ray intensity may be caused by solar wind variations at the higher latitudes. Indeed, it may be that the optimum location in which to look for essentially unmodulated cosmic-ray spectra is the region over the solar poles.

In § V we will make specific recommendations on research into the modulation process which should be undertaken in the coming years.

III. PROPAGATION THEORY

a) Introduction

In propagation theory we attempt to understand in detail how energetic particles interact with the magnetic fields in the solar wind. This theory of course has immediate application to modulation theory. We attempt with propagation theory to justify the diffusion approximation which is used in the derivation of the modulation equations (or to replace these equations with some alternate form), and to determine the elements of the diffusion tensor from the observed properties of the interplanetary magnetic field. Clearly, in justifying our equations we make modulation theory more rigorous. In determining the diffusion tensor we of course reduce the uncertainty in our choice of the parameters for use in these equations. We should be aware, however, in this latter regard that we cannot completely specify our parameters by this method. Cosmic rays respond to conditions in regions of the heliosphere which are presently inaccessible to spacecraft, i.e. regions for which we have no direct knowledge of the field conditions from which to determine the diffusion tensor.

Propagation theory, however, has a much broader application than simply providing input for modulation theory. The propagation of energetic particles in interplanetary space should occur by processes which are closely analogous to those which govern particle propagation in other astrophysical plasmas. The solar wind is, after all, a large-scale plasma in which, as in other astrophysical plasmas, propagation is determined by the interaction of particles

with the magnetic field, as opposed to by particle-particle interactions. The fluctuations in the interplanetary magnetic field are comparable to the mean field strength, again as should be the case in other astrophysical settings. For low-rigidity particles in interplanetary space, the gyro-radii are much smaller than the correlation length of the turbulence, as should be the case for the bulk of the cosmic rays in the interstellar medium. Studies of energetic-particle propagation in interplanetary space can thus serve as the basis for our understanding of particle behavior in other astrophysical plasmas. Equivalently, we can use the solar wind as a testing ground for propagation theories that we wish to apply elsewhere in the universe.

Because of its challenge and its importance, propagation theory has occupied the attention of a number of theorists, over approximately the last ten years. This extensive effort in fact has led to many advances in our understanding of particle propagation. As we shall document here, however, there are still important aspects of the problem which remain unsolved. We shall first review briefly the current theory for the calculation of diffusion coefficients. We shall then compare the results of these calculations with the observed behavior of energetic particles in interplanetary space, and we shall show that the calculated diffusion coefficients, particularly at low energies, are systematically low. We will then consider possible corrections to the current theory.

It is important to emphasize that the current difficulties of the interplanetary propagation problem should be a concern to a

wider portion of the astrophysical community than simply those concerned with interplanetary physics. The interplanetary theory has as its basis the same principles as, and tends to be more sophisticated than plasma theories which are used elsewhere in astrophysics, e.g. theories for cosmic-ray-generated instabilities in the interstellar medium[83,84]. And yet some of the predictions of the interplanetary theory appear to be inconsistent with particle observations. Indeed, the astrophysics community should also be concerned about the validity of some of its theories and it should watch with interest and encourage the extensive efforts which are currently being made by interplanetary physicists to reconcile theory and observation.

b) Quasi-linear Theory

To determine energetic-particle diffusion coefficients from quasi-linear theory (i.e. to calculate the elements of the diffusion tensor), we have two choices. We can either assume that a Fokker-Planck equation is the correct description of the particle behavior and then calculate the appropriate coefficients, as has been done by, e.g., Jokipii[85,86] and by Hasselmann and Wibberenz[87] Or we can start directly from the Vlasov equation and then derive Fokker-Planck equation, including the appropriate coefficients[88,8] Both procedures yield essentially the same results; however, the latter is more fundamental and is more likely to reveal any failings in the quasi-linear approach[90,91]. We shall use the latter procedure here; in particular we shall follow closely the derivation of the pitch angle scattering diffusion rate from quasi-linea theory which is given in a recent paper by Jones et al.[92]

The energetic particles are assumed to interact only with the electromagnetic fields in interplanetary space, and not with each other. These fields, in turn, are assumed to be unaffected b the particles since the particle energy density is much less than that of the field. The fields are also taken to be known quantiti which can be specified at least in a statistical sense. The only equation that is required here is then the Vlasov equation, which governs the behavior of the particle one-dimensional distribution function $f(\underline{r}, \underline{p}, t)$:

$$\left(\frac{\partial}{\partial t} + \frac{\underline{p}}{\gamma m} \cdot \nabla + \underline{F} \cdot \frac{\partial}{\partial \underline{p}}\right) f = 0 \qquad (23$$

Here, $\underline{r}$ is position and $\underline{p}$, particle momentum. The particle rest mass is m and the Lorentz factor is $\gamma = (1+p^2/m^2c^2)^{\frac{1}{2}}$, where c is the speed of light. The electromagnetic force is

$$\underline{F} = q(\underline{E} + \underline{p} \times \underline{B}/\gamma mc) \tag{24}$$

where $\underline{E}$ and $\underline{B}$ are the electric and magnetic fields respectively, and q is charge.

We are not interested, of course, in the detailed behavior of f, but rather in its average behavior on time scales long compared to the time during which the particles are scattered by interactions with the field. This coarse-grained behavior is what we require for our diffusion equation. To obtain this behavior we invoke the usual ergodic hypothesis in which averages of f over time are equated to averages of f over ensembles of $\underline{F}$.

By denoting ensemble averages by brackets <>, and by assuming that f and $\underline{F}$ have an average and fluctuating part (e.g. $f=\langle f\rangle+\delta f$), we can rewrite (23) as two equations:

$$\left(\frac{\partial}{\partial t} + \frac{\underline{p}}{\gamma m} \cdot \nabla + \langle \underline{F} \rangle \cdot \frac{\partial}{\partial \underline{p}}\right) \langle f \rangle = - \frac{\partial}{\partial \underline{p}} \cdot \langle \delta \underline{F}\, \delta f \rangle \tag{25}$$

and

$$\left(\frac{\partial}{\partial t} + \frac{\underline{p}}{\gamma m} \cdot \nabla + \langle \underline{F} \rangle \cdot \frac{\partial}{\partial \underline{p}}\right) \delta f + \delta \underline{F} \cdot \frac{\partial}{\partial \underline{p}} \delta f - \langle \delta \underline{F} \cdot \frac{\partial}{\partial \underline{p}} \delta f \rangle$$

$$= - \delta \underline{F} \cdot \frac{\partial \langle f \rangle}{\partial \underline{p}} \tag{26}$$

We then approximate (26) in such a manner that we can solve it exactly for δf in terms of its initial value $\delta f(\underline{r},\underline{p},t_o)$, and $\langle f \rangle$.

Upon substituting this result into (25) we obtain a single equation for the required ensemble averaged <f>.

The most basic of the approximations to (26) is the quasi-linear approximation, in which terms that are second order in the fluctuating components δf and δF are ignored, or (26) becomes

$$\left(\frac{\partial}{\partial t} + \frac{\underline{p}}{\gamma m} \cdot \nabla + \langle \underline{F} \rangle \cdot \frac{\partial}{\partial \underline{p}}\right) \delta f = -\delta \underline{F} \cdot \frac{\partial \langle f \rangle}{\partial \underline{p}} \tag{27}$$

This equation can be readily solved for δf, and the result substituted into (25) to yield

$$\left(\frac{\partial}{\partial t} + \frac{\underline{p}}{\gamma m} \cdot \nabla + \langle \underline{F} \rangle \cdot \frac{\partial}{\partial \underline{p}}\right) \langle f \rangle = -\frac{\partial}{\partial \underline{p}} \cdot \langle \delta F \left(U_o(t,t_o) \delta f(r,p,to) \right) \rangle$$

$$+ \frac{\partial}{\partial \underline{p}} \cdot \langle \delta F \int_{t_o}^{t} d\tau U_o(t,\tau) \delta \underline{F}(\underline{r},\underline{p},t) \rangle \cdot \frac{\partial}{\partial \underline{p}} \langle f \rangle (\underline{r},\underline{p},\tau) \tag{28}$$

Here, $U_o(t,t')$ is an operator which propagates the $\underline{r}$ and $\underline{p}$ dependence of all functions to the right of it backwards in time from t to t' along trajectories in the force field <F>. Since there are no mean electric fields in interplanetary space (<E>=0), this operator then causes the functions to the right of it to be evaluated along the trajectory of a particle as it moves backwards in time, spiralling about the mean magnetic field $\langle \underline{B} \rangle \equiv \underline{B}_o$.

Equation (28), however, is not yet in the form of a diffusion equation, and some additional approximations must be made. The first and probably most reasonable is that the initial value term in (28) can be ignored. We assume that correlations between $\delta \underline{F}$ and $U_o(t,t_o)\delta f(\underline{r},\underline{p},t_o)$ decrease sufficiently rapidly so that after a reasonable time the ensemble average of these quantities is zero.

We also assume for simplicity that <f> is gyrotropic about $\underline{B}_o$. Time variations in <f> on the scale of the gyroperiod are thus not considered here. This assumption, however, precludes consideration of cross-field diffusion (see §III.f for a discussion of cross-field diffusion).

We assume further that a change in a particle's orbit (i.e. a scattering of a particle) occurs on time scales that are long compared with the time over which the particle makes a correlated interaction with the fluctuating fields, i.e. long compared with the time $(t-t_o)$ that is required for the integral in (28) to saturate and to obtain essentially the full value that it will reach as $t-t_o \to \infty$. This latter assumption is of course consistent with the quasi-linear approximation. We assumed in deriving (28) that the interaction of the particles with the fields could be calculated by knowing only the particle's unperturbed trajectory along the mean magnetic field. As a consequence of this and the previous assumption, however, we can assume that <f> does not evolve on the time scales required for the integral in (28) to saturate, i.e. that $U_o(t,\tau)\langle f\rangle(\underline{r},p,\tau) \approx \langle f\rangle(\underline{r},p,t)$ and that <f> can be removed from under the integral. This last approximation is known as the adiabatic approximation.

Clearly, both the quasi-linear and the adiabatic approximation will have difficulties in dealing with particles that have pitch angles near 90^o. With a small change in pitch angle such particles can reverse direction and thus hardly maintain the unperturbed orbit that is assumed in quasi-linear theory. Moreover, these particles move slowly along the mean field, and thus for them there is no clear separation of the scattering time scale and the time required

for the integral in (28) to saturate[90]. In the next section we wil consider nonlinear corrections to quasi-linear/adiabatic theory which provide for a more accurate description of the behavior of near 90^{o} pitch-angle particles.

With the quasi-linear and adiabatic approximations, however, and with some manipulation, (28) can be written in the form of a Fokker-Planck equation, or as:

$$\left(\frac{\partial}{\partial t} + \frac{\underline{p}}{\gamma m} \cdot \nabla + \langle \underline{F} \rangle \cdot \frac{\partial}{\partial \underline{p}}\right) \langle f \rangle = \frac{\partial}{\partial \underline{p}} \cdot \underline{\underline{D}} \cdot \frac{\partial \langle f \rangle}{\partial \underline{p}} \qquad (29$$

where the diffusion tensor $\underline{\underline{D}}$ has components

$$D_{ij} = \hat{e}_i \cdot \underline{\underline{D}} \cdot \hat{e}_j = \hat{e}_i \cdot \int_0^{\infty} d\tau \langle \delta \underline{F}(\underline{r},\underline{p},t) U_o(t,t-\tau) \delta \underline{F}(\underline{r},\underline{p},t-\tau) \rangle \cdot \hat{e}_j \qquad (30$$

Here, $\hat{e}_i$ is a unit vector which projects $\underline{p}$ onto the axes of an orth gonal coordinate system. We have considered only diffusion in mome tum space under the assumption that to lowest order the spatial gra dients in $\langle f \rangle$ can be ignored in the calculation of particle inter- actions with the field. Note also that U_o acts on $\hat{e}_j$ and that the limits of the integral have been extended from $(0,t-t_o)$ to $(0,\infty)$. This last simplification is possible because we are dealing by assu tion with times $(t-t_o)$ long compared with the time required for the integral to saturate.

For the propagation problem we are concerned with directional changes in $\underline{p}$ as opposed to magnitude changes. Moreover, we are concerned here only with pitch-angle changes since cross-field diffusion was explicitly eliminated from consideration by our assumption of gyrotropy. Consider, then, that we express $\underline{p}$ in a spherical coordinate system with the polar angle θ measured relative to the mean magnetic field $\underline{B}_o$ (i.e. θ is the pitch

angle). Equation (29), then, for propagation parallel to $\underline{B}_o$ only, reduces to

$$\left(\frac{\partial}{\partial t} + \frac{\underline{p}}{\gamma m} \cdot \nabla + \langle F \rangle \cdot \frac{\partial}{\partial \underline{p}}\right) \langle f \rangle = \frac{\partial}{\partial \mu} D_{\mu\mu} \frac{\partial \langle f \rangle}{\partial \mu} \tag{31}$$

where we have followed the usual convention and described the pitch-angle scattering in terms of $\mu = \cos\theta$. Here

$$D_{\mu\mu} = (1-\mu^2)\ D_{\theta\theta}/p^2 \tag{32}$$

where $D_{\theta\theta}$ is determined from (30). We defer to §IV discussion of statistical acceleration processes, which are governed by the D_{pp} component of (30).

In evaluating (32) we must of course specify the fluctuating force $\delta\underline{F}$ or equivalently the fluctuating magnetic ($\delta\underline{B}$) and electric ($\delta\underline{E}$) field (cf. (24)). For the propagation problem we need concern ourselves only with $\delta\underline{B}$. In the solar wind, the fluctuations which affect energetic particles should arise from waves that are hydromagnetic in nature. For these waves the ratio of the force that is due to the electric field to that from the magnetic field is $\sim \omega/kv$, where ω/k is the phase speed of the waves and v, the particle speed. Since ω/k is $\sim$ the Alfvén speed which is typically $\sim$50 km/sec and thus small compared with v, the fluctuating magnetic field dominates in producing the scattering. Our problem then reduces in effect to a magnetostatic problem.

The knowledge of $\delta\underline{B}$ that we require for (30) and (32) is the behavior of its two-point correlation tensor $\underline{\underline{C}}(\underline{r}') = \langle\delta\underline{B}(\underline{r})\delta\underline{B}(\underline{r}+\underline{r}')\rangle$, where it is assumed here that the turbulence is homogeneous. Our present knowledge of this tensor, however, is incomplete. Spacecraft measure the interplanetary magnetic field as it is convected past by the solar wind. The correlations then can be measured only along a line which lies in the heliocentric radial direction, a procedure that is not sufficient to specify the full tensor without additional assumptions (e.g., that the tensor is isotropic).

The measured correlations of the field are often expressed in terms of their Fourier transforms, i.e. as one-dimensional power spectra. As the field is convected past the spacecraft, what is measured, of course, is a time series, which can then be converted into a power spectrum as a function of observed frequency ω'. This power spectrum, in turn, can be expressed in terms of k_r, the component of the wave vector $\underline{k}$ in the heliocentric radial direction. The wave speeds are much smaller than the solar wind speed, with the result that $\omega' \simeq k_r V$.

Suppose then that we take the Fourier transform or $\underline{\underline{C}}(r')$ which for homogeneous turbulence is

$$\hat{\underline{\underline{C}}}(\underline{k}) = \hat{\underline{\delta B}}\ (\underline{k})\ \hat{\underline{\delta B}}\ (-\underline{k}) \tag{33}$$

where

$$\hat{\underline{\delta B}}(\underline{k}) = \int_{-\infty}^{\infty} e^{i\underline{k}\cdot\underline{r}}\ \underline{\delta B}(\underline{r}) \tag{34}$$

Note that we have ignored time variations in $\underline{\delta B}$ under the assumption that scattering is, in effect, a magnetostatic problem. The measured power spectra then provide us only with $\underline{\underline{P}}(k_r)$ where

$$\underline{\underline{P}}(k_r) = \int \underline{\underline{\hat{C}}}(\underline{k}) d^2k \tag{35}$$

is the integration of $\underline{\underline{\hat{C}}}(\underline{k})$ over the components of $\underline{k}$ normal to k_r[93]. A typical example of an observed power spectrum is shown in Figure 2.

Since we cannot specify $\underline{\underline{\hat{C}}}(\underline{k})$ in detail, we must thus make assumptions about this tensor. The usual procedure here is to assume that the fluctuations are due only to normal mode oscillations in the solar wind, which in our case restricts us to transverse Alfvén waves, and fast and slow mode magnetosonic waves[93]. We then construct from these waves acceptable forms of $\underline{\underline{\hat{C}}}$.

For example, suppose that we assume that the waves are Alfvén waves, which have the property that $\underline{\delta B}$ must lie in the direction which is normal to the plane defined by $\underline{k}$ and $\underline{B}_o$. We thus assume that

$$\underline{\delta \hat{B}}(k) = \frac{A(\underline{k})}{k_\perp B_o} \underline{k} \times \underline{B}_o \tag{36}$$

where $k_\perp$ is the component of $\underline{k}$ normal to $\underline{B}_o$. The weighting function in $A(\underline{k})$ must be normalized such that

$$\int d^3k \; A(\underline{k}) \; A(-\underline{k}) = \langle (\delta B)^2 \rangle \tag{37}$$

and it is chosen such that (35) yields a power spectrum $\underline{\underline{P}}(k_r)$ which resembles the observations. If the waves are magnetosonic then

$$\delta\underline{\hat{B}}(k) = \frac{A(\underline{k})}{k\, k_\perp\, B_o}\, \underline{k} \times (\underline{k} \times \underline{B}_o) \qquad (38)$$

We can also consider correlation tensors which are the result of a combination of Alfvén and magnetosonic waves[93].

Upon substituting our assumed form for the correlation tensor into (30) we can then evaluate $D_{\theta\theta}$, and in turn through (32) obtain the pitch-angle diffusion coefficient $D_{\mu\mu}$. This procedure will yield the usual result that particles respond only to waves which satisfy the resonance condition

$$\mu\, k_\parallel\, v = \pm\, n\, \Omega \qquad (39)$$

where $k_\parallel$ is the components of $\underline{k}$ parallel to $\underline{B}_o$; Ω is the particle gyrofrequency in the mean field and n is an integer denoting the harmonic. The result in general will involve an infinite sum over these harmonics[93].

In most cases the infinite sum in $D_{\mu\mu}$ needs to be evaluated numerically. There are, however, two exceptions which illustrate in a simple form the scattering that is predicted by quasi-linear theory. As has been pointed out by Jokipii[86], if we assume that the turbulence is the result of Alfvén waves which propagate only along the mean magnetic field direction, then

$$D_{\mu\mu} = \frac{2\pi(1-\mu^2)v}{r_g^{\,2}\,|\mu|\,B_o^{\,2}}\, P_\perp\,(k_\parallel = k = 1/|\mu| r_g) \qquad (40)$$

Here r_g is the particle gyroradius and $P_\perp(k)$ is the one-dimensional power spectrum for fluctuations in the field component perpendicular to $\underline{B}_o$. We can of course evaluate (40) by equating $P_\perp(k_\parallel)$ with

observed power spectra; however, such a procedure yields only an approximation since what is observed is $P_\perp(k_r)$ and $k_r \neq k_\parallel$ in general.

Further, if we assume that the turbulence is isotropic, which requires the superpositron of both Alfvén and magnetosonic waves, then in cases where r_g is small compared with the correlation length of the turbulence,

$$D_{\mu\mu} = \frac{2\pi(1-\mu^2)v}{r_g^{\,2}\, B_o^{\,2}} P_\perp \quad (k=1/|\mu|r_g) \tag{41}$$

to a good approximation[94]. Note the similarities between (40) and (41); essentially $D_{\mu\mu}$ in (41) is a factor of $|\mu|$ greater than $D_{\mu\mu}$ in (40). The isotropic case, however, has a pathological behavior at $\mu=0$ in that at this point $D_{\mu\mu}$ becomes a delta function in μ[94]. In quasi-linear theory particles with $\mu=0$ have an unperturbed orbit that remains stationary. These particles then experience a force from magnitude variations in the magnetic field (the same force that would give rise to mirroring), which builds up indefinitely with time[95]. Such behavior is physically unrealistic; however, there is some truth in it, as we shall see in the next section when we consider in more detail the behavior of near 90° pitch-angle particles.

c) Nonlinear Corrections

Since $P_\perp$ decreases with k roughly as $k^{-5/3}$ (cf. Figure 2), the two predictions of $D_{\mu\mu}$ in (39) and (40) both yield that $D_{\mu\mu}\to 0$ as $\mu\to 0$ (excluding the delta function in μ at $\mu=0$ in (41)). Quasi-linear/adiabatic theory suggests then that particles have some difficulty in scattering through 90° in pitch-angle, or equivalently in executing collisions that reverse their direction. This prediction, however, must be considered highly suspect since quasi-linear/adiabatic theory is known to have difficulty in dealing with small μ particles (cf. previous section). Indeed, as we shall now discuss, this prediction is false.

Over the last few years several different nonlinear theories have been developed to treat the behavior of near 90° pitch-angle particles. For example, Völk[95,93] has considered some resonance-broadening modifications to quasi-linear theory, which are patterned after the work of Dupree[97] and of Weinstock[98]. In quasi-linear theory, particles are assumed to spiral unperturbed along $\underline{B}_o$ and thus have a well-defined pitch angle. As a consequence, the particles can resonate only with a narrow band of waves which satisfy (39). In actual fact, however, the perturbing fields will cause the pitch angle to wobble (i.e. there will be a spread $\Delta\mu$ in μ), and thus will broaden the range of waves with which the particles interact. For pitch angles with $\mu >> \Delta\mu$ this effect should be small and quasi-linear theory remains roughly correct. At small μ, however, where $\mu \lesssim \Delta\mu$ the broadening of the resonance has a major effect. In contrast to the quasi-linear result that small μ particles can

interact only with very high wave-number fluctuations (i.e. from (39) that $k_{\parallel}=1/\mu r_g$), for which there is little power and therefore little scattering, in resonance-broadening theory small μ particles see a finite range of waves, some of which have non-negligible power. Equivalently, $D_{\mu\mu}$ in resonance-broadening theory is nonzero at $\mu=0$. Moreover, in cases where the fluctuations result in variations in the magnetic field (i.e. magnetosonic waves), resonance-broadening theory predicts significant scattering for small μ particles. Such variations can of course cause particles to mirror and result in easy scattering through 90°. In quasi-linear theory this mirroring manifests itself in $D_{\mu\mu}$ as a physically unrealistic delta function in μ. In resonance-broadening theory the effects of the mirroring are spread over a finite range in μ around $\mu=0$.

Jones et al.[91,92] have also attempted to include perturbations in the particle orbit in the calculation of $D_{\mu\mu}$. Their approach, which is referred to as a partially averaged field approach, is more heuristic than that of, for example, Völk[96], and therefore somewhat easier to execute. Jones et al. replace the quasi-linear operator U_o, which is defined in terms of the mean field $\underline{B}_o$ (cf. (28)), with an operator U_p which propagates particles in a field which is averaged over only part of the ensemble and therefore which still contains information on the field fluctuations. The interactions are computed in terms of U_p and then the various results averaged over the full ensemble.

The recent work of Goldstein[101,102] treats the nonlinear problem in a more formal and presumably more complete manner than is done by either Völk[93,96] or by Jones et al.[99,92] Instead of using a simple extension of the electrostatic theory of Dupree[97] and Weinstock[98], as is done by Völk[93], Goldstein starts from the electromagnetic generalization of Weinstock's work as was developed by Ben Israel et al.[103]. It is found in this approach that perturbations in particle momentum, which are unimportant in the electrostatic theories, have a significant effect in the magnetic turbulence problem, as might be expected since the magnetic force involves particle momentum.

Remarkably, all of these approaches yield results which are quantitatively very similar. In general, it is found that there is more scattering at small μ than is predicted by quasi-linear theory, whereas for larger μ, non-linear and quasi-linear theory arein rough agreement.

These results can also be compared with the Monte Carlo calculations of $D_{\mu\mu}$ as done by Kaiser et al.[100] In general, the agreement here is quite good. It should be emphasized, however, that these numerical simulations of the scattering have not been performed for very low rigidity particles. Rather, in these simulations the ratio of the particle gyroradius to the correlation length of the turbulence is ≥ 0.25.

d) Comparison with the Observations

The principal tests of our predictions of $D_{\mu\mu}$ come from observations of the behavior of solar particles during flare events. Solar flares accelerate particles over a wide range of energy (up to ∿1 GeV/nucleon in some cases) and then inject them into the interplanetary medium. By examining the behavior of these particles as they tend to approach isotropy, we have in effect a 'controlled' experiment from which we infer the extent to which particles are scattered in the solar wind.

Measurements of particle behavior during flare events do not generally yield $D_{\mu\mu}$ directly, but rather yield $\kappa_{\parallel}$, the diffusion coefficient for propagation along $\underline{B}_o$, which is an average of $D_{\mu\mu}$ over μ. We expect that the particles will behave according to the time-varying form of (4) and (6) or equivalently by fitting solutions to (4) and (6) to data we can infer, or at least put limits on $\kappa_{\parallel}$. Of course, (4) and (6) can be derived by properly averaging (29) over μ and by adding the effects of the adiabatic deceleration in the expanding solar wind (or by including these effects formally through the coefficients of $\underline{D}$). According to Earl,[104] who has studied this aspect of the propagation problem in detail, the proper averaging scheme relates $\kappa_{\parallel}$ to $D_{\mu\mu}$ according to the formula

$$\kappa_{\parallel} = \frac{v^2}{4}\int_{-1}^{1} \frac{d\mu\,(1-\mu^2)^2}{D_{\mu\mu}} \qquad (42)$$

We should remark immediately that (4) and (6) are expected to be valid only when the anisotropy is not large, which in most circumstances requires that $\xi<30\%$ (See § II.h for the formal definition

of the anisotropy[21]). It was assumed in deriving (6), for example, that particles diffuse and thus 'inertial' terms, which can be important when the anisotropy is large, were neglected. We should not expect, then, that our description of flare events will be valid early in the event, when particles first begin to arrive from the Sun, or, as we shall see, at very low energies ($\lesssim$1 MeV/nucleon).

One of the most thorough studies of flare propagation in recent years has been the work of Zwickl and Webber,[105] who have analyzed the behavior of 3-30 MeV protons in some 15 flare events, as seen by the Pioneer 10 and 11 spacecraft over heliocentric distances from 1 to 5 AU. Zwickl and Webber find that there is no evidence for cross-field diffusion in these events (cf. § IV,f), and thus the data provides a direct measure of $\kappa_{\parallel}$. They fit numerical solutions to (8) to each of the observed events, and then determine the value of $\kappa_{\parallel}$ that provides the best fit to the five different parameters which are depicted in Figure 11. The curve in this figure is a typical profile of the behavior of the intensity with time. The parameters to be fit are (i) t_{max}, the time duration between the flare event and when the observed intensity is a maximum, (ii) the intensity at t_{max}, (iii) the anisotropy at t_{max}, (iv) τ, the characteristic decay time for the intensity, and (v) Δt_5, the width in time of the intensity profile, which is measured here between the points where the intensity is one fifth of its maximum value.

In Figure 12 the values of $\kappa_{\parallel}$ determined by Zwickl and Webber[105]

are expressed as a mean free path $\lambda_{\parallel}$ (i.e. $\lambda_{\parallel} = 3\kappa_{\parallel}/v$) and plotted as a function of particle rigidity. Also shown in this figure are some additional measures of $\lambda_{\parallel}$, which were inferred from particle observations. The points attributed to Ma Sung were inferred from flare observations, but here the model includes the focusing effects of the diverging interplanetary magentic, which were discussed recently by Earl[142] The points attributed to Palmer et al[106] and to Roelof and Gold[105] are also inferred from flare observations. The points attributed to McKibben et al[65] were determined from Pioneer 10 and 11 measurements of galactic cosmic-ray gradients, by use of (16). The point at the highest rigidity, which is determined from measurements of the integral proton gradient, may be somewhat high. In (16) it is assumed that variations in the modulation with heliographic latitude are unimportant. However, as we saw in § II.h, such variations can result in small gradients, or equivalently can cause us to overestimate $\kappa_{\parallel}$.

It should be noted that there are also estimates of the scattering from flare observations which yield somewhat smaller values of $\lambda_{\parallel}$ at low rigidities. For example, in the work of Lupton and Stone[139] $\lambda_{\parallel}$ is found to be $\sim$0.06 AU for .05 GV particles, which is roughly a factor of 3 smaller than the value shown in Figure 12. As a rule, however, studies which yield smaller values of $\lambda_{\parallel}$ do not require that the model fit observations of the anisotropy, which are often not available. It appears as if the anisotropy places some of the most severe constraints on acceptable values of $\lambda_{\parallel}$.

It should also be noted in Figure 12 that the observations imply that at low rigidities $\lambda_{\parallel}$ can approach 1 AU. With this value we would not expect that the anisotropy in flare events, as seen at earth, can readily decay, or equivalently that the diffusion approximation is appropriate. For the modulation of galactic cosmic rays, however, where we should compare $\lambda_{\parallel}$ with the size of the heliosphere, diffusion should still work even at these low rigidities.

To compare our predictions of $D_{\mu\mu}$ with the observed particle behavior, we must of course evaluate (42). For our purposes here an accurate evaluation is not necessary, or equivalently, we do not require a full specification of the behavior of $D_{\mu\mu}$ with μ, as obtained from the nonlinear theory. Rather, the point that needs to be made here requires only a meaningful upper limit on $\kappa_{\parallel}$ for representative examples of possible field fluctuations. This upper limit can be obtained from quasi-linear theory alone. The nonlinear theories discussed in the previous section all predict more scattering than quasi-linear theory at small values of μ, and roughly comparable scattering at the larger μ. Thus, $D_{\mu\mu}$ from quasi-linear theory is comparable to or smaller than the $D_{\mu\mu}$ from nonlinear theory, with the result that the quasi-linear $\kappa_{\parallel}$ is inherently larger.

In particular we consider the $\kappa_{\parallel}$ which is determined from (42) by using the quasi-linear $D_{\mu\mu}$ that is given in (40), with $P_{\perp}$ taken from Figure 2 (i.e. $P_{\perp}(k) \propto k^{-5/3}$ for large k). The fluctuations in this case result from Alfvén waves propagating along the mean field. In addition to providing an upper limit to the $\kappa_{\parallel}$ that this form of turbulence will yield with nonlinear corrections included, the re-

sult should also yield an upper limit for the nonlinear version of the isotropic turbulence case, which was used in (41). Isotropic turbulence includes magnitude fluctuations in the magnetic field which are more effective in scattering particles through 90° in pitch-angle, than are Alfvén waves alone. Equivalently, the nonlinear $D_{\mu\mu}$ for isotropic turbulence is larger at small μ than it is for the Alfvén wave case. At larger μ, however, where quasi-linear and nonlinear theories agree, the $D_{\mu\mu}$ in these two cases are comparable, as can be seen by comparing (40) and (41). Hence, $\kappa_{\parallel}$ as determined from $D_{\mu\mu}$ in (40) is a meaningful upper limit because the $D_{\mu\mu}$ here is smaller than or comparable to the nonlinear $D_{\mu\mu}$ for parallel propagating Alfven waves, which in turn is smaller than or comparable to the nonlinear $D_{\mu\mu}$ for isotropic turbulence.

In Figure 12 this upper limit on the predicted $\kappa_{\parallel}$ is also expressed as a mean free path $\lambda_{\parallel}$ and plotted as a function of rigidity. As is evident here, the upper limit on $\lambda_{\parallel}$ lies systematically below the data points. There is no evidence in the theoretical curve for the flattening or increasing at low rigidities which appears to be required by the data. Indeed, at low rigidities there is roughly a one order of magnitude difference between theory and observation.

e) Further Considerations

The obvious question to ask at this point is why does the theoretical curve in Figure 12 differ from the observations? We developed a quasi-linear theory for the propagation by using standard techniques. We recognized that this quasi-linear theory has some inherent difficulties in dealing with near 90^{o} pitch-angle particles. We then corrected the quasi-linear theory with presumably more accurate nonlinear theories. We even checked the accuracy of the nonlinear theories against computer simulations of the propagation and found reasonable agreement at least for the higher rigidity particles. Yet when we compare theory with particle observations in interplanetary space, we find systematic differences.

One distinct possibility for the discrepancy is that we have used the wrong form for the correlation tensor of the turbulence. The upper limit on $\lambda_{\parallel}$ in Figure 12 is derived for two specific cases of field fluctuations: Alfvén waves propagating along $\underline{B}_o$ and isotropic turbulence. In both of these cases, there is ample power in waves that are oriented such that their k-vectors have an appreciable component parallel to $\underline{B}_o$, i.e. there is ample power in waves with which the particles can resonate, through (39). If, however, the waves were oriented more normal to $\underline{B}_o$, then the scattering would be reduced, and $\lambda_{\parallel}$ in Figure 12 increased. This point has been made in particular by Völk and his co-workers[93]. They note that Alfvén waves propagating outward from the Sun should be channeled to have their k-vectors point in the heliocentric radial direction. This effect arises simply from geometric considerations. It is the same effect

which causes water waves originating from a point source to tend to a circular wave front far from the source. As the k-vectors of the Alfven waves are channeled to point radially, they will be oriented more normal to the interplanetary magnetic field, which is being wound into a tight spiral ((1)-(3)). This effect will increase $\lambda_{\perp}$ and bring theory and observation into better agreement.

Indeed, Völk and his coworkers[68,93] have developed this approach to a high degree of sophistication. They include not only the effects which result when the k-vectors of the waves are oriented more normal to the average spiral direction of $\underline{B}_o$, but also the influence of the longer wavelength fluctuations on the local direction of $\underline{B}_o$. Clearly, in computing the scattering it is the local orientation of $\underline{k}$ relative to $\underline{B}_o$ that is important. When long wavelength fluctuations cause deviations in $\underline{B}_o$ from the spiral direction, this will mitigate the extent to which $\underline{k}$ and $\underline{B}_o$ become orthojonel to each other. With this approach they find integral gradients that are comparable to the observed values, they predict a total modulation of at least high rigidity particles that is compatible with the estimates of the modulation from electron studies (See §II.f), and, as we discussed in §II.h, they even have an explanation for solar cycle variations in the cosmic-ray intensity.

It is unlikely, however, that the propagation model of Völk and his co-workers can by itself account for all of the discrepency in Figure 12. There is no obvious reason why effects associated with the channeling of the k-vectors into the radial direction should lead to $\lambda_{\perp}$ relatively independent of rigidity at low rigidities, as is required by the observations in Figure 12. Hence, even if

this explanation brings theory and observation into better agreement at high rigidities, which it can, the theoretical predictions of λ_{μ} will still lie systematically below the date at low rigidities.

It is also disquieting to note that there is currently no positive evidence for a preferred direction for the k-vectors of Alfven waves in the solar wind. Admittedly, it is difficult to determine the orientation of the k-vectors from current magnetic field observations. However, during a limited time interval, in which simultaneous observations from two closely spaced spacecraft were available, Densket and Burlaga[107] found no evidence that the k-vectors of Alfven waves tended to be oriented in the heliocentric radial direction.

It should also be noted that we have made the tacit assumption in our derivation that the waves causing the scattering have infinitesimal amplitude (cf. (36) and (38)). In actual fact, however, interplanetary field fluctuations have quite finite amplitudes, e.g. the fluctuation in a component of the field, B_x, is $\delta B_x/B_o \sim 1/3$. It may be, then, that we are not specifying correctly the properties of these finite amplitude waves, or their effect on the particles. For example, it may not be an appropriate procedure, as is done above, to Fourier decompose the turbulence into plane waves for which there is no mode coupling.[108] It may be also that particles, particularly at low rigidities, are experiencing 'trapping' effects in the finite amplitude fluctuations, which could in principle reduce the scattering.

It may also be that we still do not have our time scales properly separated. To have a Markovian process, or a Fokker-Planck equation, the essential assumption is that the time scale over

which the distribution function changes τ_d is long compared with the time scale τ_c during which a particle experiences a correlated interaction with the fields. This requirement, which leads to the adiabatic approximation, is not satisfied in quasi-linear theory by particles with pitch angles near 90^o. Such particles move very slowly as they execute unperturbed orbits along $\underline{B}_o$, with the result that τ_c can be large. Nonlinear theory presumes to improve the description of near 90^o pitch-angle particles by including orbit perturbations, which will lead to smaller τ_c. It is not transparent, however, whether the resulting τ_c is small compared to τ_d. It is somewhat difficult to imagine, however, how time-scale effects could be the source of our problems. The long mean free paths which are observed at low rigidities (Figure 12) suggest that τ_d, for whatever reason, is large compared with any reasonable time for a particle to transverse a correlated segment of the turbulence.

There is of course a continuing effort underway to develop more reliable propagation theories. For example, Klimas and his co-workers are currently developing theories which can deal with arbitrary amplitude turbulence, and for which a separation of time scales ($\tau_d >> \tau_c$) is not essential.[109] Because the time scales are not a concern, this theory is inherently non-Markovian. It is too early to tell whether the approach of Klimas and his co-workers will lead to an improvement of the agreement between theory and observation. It should be remarked, however, that the techniques under development here are novel and offer potentially powerful solutions to any plasma physics problem, including laboratory plasma problems, in which there is no clear separation of the time scales involved.

f) Cross-field Diffusion

The principal theory for cross-field diffusion is that due to Jokipii and Parker[62], who argue that $\kappa_\perp$ in interplanetary space results mainly from particles following random-walking magnetic-field lines. Supposedly, field lines in interplanetary space are mixed and intertwined by turbulence in the solar wind, or by the motions of the foot points of the field lines on the photosphere of the Sun. An individual field line then will stochastically wander in a direction normal to the mean field $\underline{B}_o$, as is shown in Figure 13. Equivalently, a particle propagating along this and other field lines will diffuse normal to $\underline{B}_o$.

The rate at which two field lines separate from each other, as a function of distance along $\underline{B}_o$, depends in general on how close together the field lines are. If the field lines are spaced by a distance that is more than the two-point correlation length of the turbulence, then Jokipii and Parker[62] find that the separation rate is determined by the power density of fluctuations at zero wave number. If, in contrast, the spacing is less than the correlation length, then according to Jokipii[110] the separation rate is determined by the power at the higher wave numbers. For power spectra similar to those in Figure 2, however, the two separation rates are nearly equal and provide that particles propagating from the Sun should, upon reaching 1 AU, have an rms spread in position normal to $\underline{B}_o$ $\sim$0.1 AU.

As we indicated above, Zwickl and Webber[105] find that they can interpret their solar-flare data by assuming that there is little or no cross-field diffusion. This conclusion, however, does not place severe contraints of $\kappa_\perp$. It requires only that $\kappa_\perp << \kappa_\parallel$. As we saw in Figure 12, however, the inferred $\kappa_\parallel$ (or $\lambda_\parallel$) are large, and thus there is a wide range of allowable values of $\kappa_\perp$, including ones that are consistent with the predictions of Jokipii and Parker[62] and Jokipii[110].

The predicted values of $\kappa_\perp$ do appear, however, to be incompatible with the observations of Krimigis et al.,[111] who has studied numerous flare events, and events where there is near steady emission of solar particles, by using data from three spacecraft widely separated in radial distance ($\sim$0.6-1.4 AU). As is evident from the data of Krimigis et al.,[111] there are pronounced gradients in the intensity normal to $\underline{B}_o$ in these events, on scales of a few hundredths of an AU and upward, which do not appear to dissipate with increasing heliocentric distance. There is no evidence, then, of the smoothing of the intensity variations that might be expected from the predicted rms spread in particle position normal to $\underline{B}_o$, over 1 AU, of $\sim$0.1 AU.

The discrepancy between the prediction and the observations could result simply from our inability to determine accurately the extent to which field lines random walk in interplanetary space. The power density at zero wave number that is used as a measure of the random walk is normally determined by extrapolating the

observed low wave-number power down in wave number, under the assumption that the power spectrum in this region is flat (cf. Figure 2). As has been pointed out by Fisk and Sari,[112] however, the observed low-frequency power may result principally from tangential discontinuities in the interplanetary magnetic field, and may as a result provide little direct evidence of the random walk.

Some of the discrepancy could result because field lines that are separated by less than a correlation length may tend to remain together, contrary to the prediction above that they separate at a rate similar to field lines spaced by more than a correlation length. As is pointed out by Jokipii,[110] calculation of the separation rate for closely spaced field lines requires knowledge of the correlations of the fluctuations normal to $\underline{B}_o$, at the higher wave numbers, as is sampled by moving along $\underline{B}_o$. However, since we can sample the field only in the heliocentric radial direction, there is clearly some uncertainty in the measured correlations, and hence some latitude in the predicted separation. If closely spaced field lines do not readily separate, the interplanetary field should to some degree behave as coherent flux tubes, each roughly a correlation length ($\sim$0.01 AU) in diameter. Even in this case, however, we should expect that gradients normal to $\underline{B}_o$ with scale length larger than several hundredths of an AU would dissipate with increasing heliocentric distance--a situation which does not appear to be confirmed in the observations of Krimigis *et al.*[111]

It may be also that the predictions by Jokipii and Parker[52] and by Jokipii[110] of the random walk of the field lines are correct,

but that the particles, particularly at low rigidities, do not participate in this process. As we discussed above, there is some effect prohibiting the scattering of particles in pitch angle at low rigidities, which we do not at present understand. It is not inconceivable that this same effect could restrict cross-field diffusion.

Whatever the cause of the discrepancy between prediction and observation, we should give a warning to workers in other fields. Cross-field diffusion by means of field-line random walk is invoked to explain, for example, the leakage of galactic cosmic rays from the galaxy.[113] However, when the same concepts are applied in interplanetary space, they do not appear to work as expected.

g) Concluding remarks

Propagation theory, then, is in a state of some dissatisfaction. A number of theories have been developed to calculate the pitch-angle scattering suffered by energetic particles in the interplanetary magnetic field. A straightforward application of these theories, however, yields scattering in excess of what is actually experienced by the particles. At the higher rigidities ($\gtrsim$1 GeV), the discrepency is not serious and can be eliminated by a judicious assumption about the nature of interplanetary turbulence. At lower rigidities, the discrepancy is more significant, and there is no preferred remedy. A similar situation exists for the cross-field diffusion rate, which from arguments based on the concept of field-line random walk is predicted to be larger than is observed. Clearly, much work should and will be done in this area in the future.

We emphasize again that the conditions that we deal with in the solar wind are similar to the conditions expected in other astrophysical plasmas. We have finite amplitude turbulence, with a power spectrum that has a near-Kolomogorov, or universal shape. We have energetic particles with gyro-radii that span the range from very large to very small in comparison with the scale lengths of the turbulence. The problems that we currently have in interplanetary propagation theory should thus be a concern to other astrophysical plasma theorists, and the cures to these problems that we develop should be of interest to them.

In § V we shall make specific recommendations on research which should be undertaken in this area in the coming years.

IV. ACCELERATION THEORY

a) Introduction

The ease with which nature can accelerate particles to high energies was emphasized for us recently with the discovery by McDonald et al.[114] that the solar wind is capable of accelerating protons to energies ~ a few MeV in large-scale regions. This discovery, of course, presents us with an enormous opportunity. As we discussed above, conditions in the solar wind are expected to be similar to conditions in other astrophysical plasmas. The mechanisms that we invoke for acceleration in the solar wind are also the mechanisms that are commonly invoked for acceleration in other astrophysical plasmas, e.g. statistical acceleration or acceleration by shock waves. With our in situ and in detail observations in the solar wind, we can thus provide insight into acceleration processes in an astrophysical plasma, which, as with our propagation studies, should have broad implications for particle behavior in other astrophysical settings.

It should be emphasized immediately that current theories for the acceleration of energetic particles are rather primitive in that they are based only on, for example, the quasi-linear approach. In the solar wind, however, this approach is unlikely to be adequate. We need to apply the theories at low-rigidities (to ~ 1 MeV protons), where, as we saw in § III.d, quasi-linear theory is unable to account for the propagation. Indeed, it may be that current theories are inadequate for other astrophysical plasmas as well. The essential feature of a low-rigidity particle in the solar wind is that its gyro-radius is much smaller than the correlation length of the turbulence. Such a situation should also prevail for cosmic rays

in the interstellar medium and in supernova remnants.

In this section we will review some of the explanations for the recent observations (1976) of McDonald et al.[114], but with the understanding that as these and other observations are worked over in more detail, more reliable theories may be required.

b) The Observations

For many years earth-orbiting spacecraft have observed that the intensity of low-energy particles (~ a few MeV/nucleon) can remain roughly constant in a region of interplanetary space over several solar rotations[115]. It was assumed that these 'co-rotating' events were the result of particles being steadily emitted from a region on the Sun, and then propagating out along the interplanetary magnetic field to earth and beyond. It was also assumed that the intensity in these events would decrease with distance from the Sun. Afterall, the cross-section of the co-rotating region increases with distance from the Sun. Moreover, since the spectrum in these events declines with increasing energy, adiabatic deceleration (cf II.d) should cause a decrease in the intensity seen at a given energy[126]

It therefore came as a surprise when McDonald et al.[114] reported that the observations from Pioneer 10 and 11 show that the intensity in co-rotating events, on the average, increases with increasing heliocentric distance, rather than decreasing. The intensity at 3 AU from the Sun is frequently more than an order of magnitude larger than the 1 AU intensity. As McDonald et al.[114] argue, the most likely explanation here is that particles are being accelerated in interplanetary space at a sufficient rate to overcome the intensity decreasing effects of the volume expansion and the adiabatic deceleration.

McDonald et al.[114] note that there is a coincidence between these co-rotating particle events and regions in the solar wind where high and low speed steam collide. In fact, Barnes and Simpson[117] have shown, as is depicted in Figure 14, that these events occur near the forward and reverse shock waves which are generated by the

stream-stream interactions. We have then two likely sources for the acceleration. It may be that the particles are accelerated by the turbulence generated by the stream-stream interaction or it may be that the particles are accelerated directly at the shock fronts. Indeed, both mechanisms may be operative. We note in Figure 14 that there is an abrupt increase in the intensity roughly coincident with the shock passage, which may be the result of the shock acceleration. The bulk of the increase, which is more broadly spread around the shock passage, could then result from acceleration in the enhanced turbulence present. In the following sections we will consider first statistical acceleration in solar wind turbulence, and then shock acceleration.

c) Statistical Acceleration

Turbulence in the solar wind is presumably the result of the superposition of Alfven and magnetosonic waves, with the former dominating since the latter can be readily damped[118,119,120,121]. Particles can then be statistically accelerated in solar wind turbulence by two possible interactions. As the particles are scattered in pitch angle by the Alfven waves, they will experience a change in energy that results in a statistical acceleration. Equivalently, the particles cyclotron damp the Alfven waves. A change in energy or a statistical acceleration will also result from particles interacting with the change in the magnitude of the magnetic field which accompanies magnetosonic waves. In this case the particles transit-time damp the magnetosonic waves.

Despite their reduced amplitude, it is the magnetosonic waves that are more likely to produce the acceleration than are the Alfven waves. Particles reasonate with Alfven waves principally at the first harmonic (See (39)), which requires that the field fluctuations have a scale size comparable to the particle gyro-radius. Such fluctuations are effective in pitch-angle scattering the particles, much more so than they are in producing energy changes. To yield the required acceleration rate, then, the pitch-angle scattering rate must be very high, and indeed, as we shall see, too high to be compatible with the observed particle behavior. On the other hand, particles can reasonate with magnetosonic waves at the Landau reasonance, or with waves that have a phase velocity parallel to the mean field $\underline{B}_o$ equal to the velocity of the particle parallel to $\underline{B}_o$ ($v_\parallel$). Such waves will have wavelengths large compared to the particles gyro-radius, with the result that the particle magnetic

moment is a constant of the motion. The changes in pitch-angle and energy during the interaction will then be comparable, and thus, as we shall see, the acceleration rate can be achieved without violating the observed constraints on the pitch-angle scattering.

Statistical acceleration can of course be described as a diffusion in momentum space, with a mean square (ms) change in momentum per unit time D_{pp}. The coefficient D_{pp} is related to the ms change in energy per unit time D_{TT} by $D_{TT} = v^2 D_{pp}$, where v is particle speed. The mean change in energy is in turn related to D_{pp} by $dT/dt = D_{TT}/2T$[82,122].

According to Fisk[122] a value of $D_{pp}/p^2 \simeq 1.5 \cdot 10^{-7} sec^{-1}$ for 1 MeV protons is required to produce the factor of ten increase in the intensity between 1 and 3 AU that is observed by McDonald et al.[11] This value is determined from numerical solutions to (9) with a term which describes the statistical acceleration included. This acceleration rate then is sufficient to overcome the intensity decrease that results from the volume expansion of the solar wind, and the accompanying adiabatic deceleration. The acceleration rate in energy D_{TT}/T^2, is $D_{TT}/T^2 = 4\ D_{pp}/p^2 \simeq 6 \cdot 10^{-7} sec^{-1}$.

Consider then the interaction of particles with Alfven waves. As the result of the interaction with any wave, a non-relativsitic particle will experience a change in energy by an amount

$$\Delta T \simeq m u_{\parallel}\ \Delta v_{\parallel} \qquad (43)$$

where m is particle mass, $u_{\parallel}$ is the phase speed of the wave parallel to B_o; and $\Delta v_{\parallel}$ is the change in $v_{\parallel}$ as the result of the interaction, as viewed in the frame moving with $u_{\parallel}$. For Alfven waves, $u_{\parallel} = V_A$, the Alfven speed. For a full collision with the waves, in which the particle reverses its direction, $\Delta v_{\parallel} \simeq 2v_{\parallel}$.

We can then estimate that for Alfven waves D_{TT} is

$$\frac{D_{TT}}{T^2} \simeq \frac{(\Delta T)^2}{T^2} \frac{v_{\parallel}}{\lambda_{\parallel}} \simeq \frac{16}{3\sqrt{3}} \frac{V_A^2}{v\lambda_{\parallel}} \tag{44}$$

where $\lambda_{\parallel}$ is the mean free path along $\underline{B}_o$ and $v_{\parallel} \simeq v/\sqrt{3}$.

The Alfven speed in the solar wind between 1 and 3 AU is $V_A \simeq 50$ km/sec. The speed of a 1 MeV proton is $v \simeq 1.4 \cdot 10^9$ cm/sec. Hence to produce the required acceleration rate of $D_{TT}/T^2 \simeq 6 \cdot 10^{-7} \text{sec}^{-1}$, $\lambda_{\parallel}$ must have the extremely small value of $\sim 6 \cdot 10^{-3}$ AU, or equivalently the pitch-angle scattering rate must be very high.

A value of $\lambda_{\parallel}$ this small is in fact quite unlikely. The required mean free path is a factor ~ 50 smaller than the low energy values shown in Figure 12, which are inferred from flare observations. (The rigidity of a 1 MeV proton is 0,046 GV). Moreover, with a mean free path this small, particles would be effectively 'frozen into' the solar wind and could have an anisotropy that pointed only in the direction of the solar wind flow -- the heliocentric radial direction[122]. In actual fact, however, Marshall and Stone[123] observe field alligned anisotropies in co-rotating events that are sufficiently large to preclude an extremely small mean free path.

For magnetosonic waves, we can calculate the acceleration rate by considering the interaction of the particles with a characteristic wave, which we assume has scale-lengths λ_z' and $\lambda_\perp'$ in a direction along and normal to $\underline{B}_o$, respectively. These scale-lengths are assumed to be long compared with the particle gyro-radius r_g. We note first that $u_{\parallel}$ in (43) is $\sim u\, \lambda_z'/\lambda_\perp'$, where u is the phase speed of the wave. Since the Alfven and sound speeds are comparable

in the solar wind, $u \sim \sqrt{2}\, V_A$. We next find $\Delta v_\parallel$ by noting that in the frame moving with $u_\parallel$ there is no electric field and thus the change in $v_\parallel$ is caused by $\partial B/\partial z$, the gradient in the magnitude of the magnetic field along $\underline{B}_o$, which is produced by the characteristic wave. Hence $v_\parallel$ should satisfy

$$\frac{dv_\parallel}{dt} \simeq -\frac{v_\perp^2}{B_o}\frac{\partial B}{\partial z} \tag{45}$$

or

$$|\Delta v_\parallel| \simeq \frac{v_\perp^2}{\lambda_z}\left|\frac{\delta B}{B_o}\right| \Delta t \tag{46}$$

Here, $v_\perp$ is the component of the particle's velocity normal to $\underline{B}_o$, $|\delta B|$ is the amplitude of the magnitude flucutation in the field, and Δt is the time during which the particle makes a coherent interaction with the wave. If the correlation length for the turbulence along $\underline{B}_o$ is λ_z, then $\Delta t \sim \lambda_z/v_\parallel$. Upon substituting for $u_\parallel$, $\Delta v_\parallel$, and Δt in (44) and (46), we then estimate that the acceleration rate for magnetosonic waves is

$$\frac{D_{TT}}{T^2} \simeq \frac{32}{3\sqrt{3}}\frac{V_A^2}{v}\left(\frac{\delta B}{B_o}\right)^2 \frac{\lambda_z}{\lambda_\perp'^2} \tag{47}$$

To evaluate (47) we must determine the ratio $(\delta B/B_o)^2/\lambda_\perp'^2$ for the characteristic wave, i.e. we must determine this ratio for the waves which have the strongest effect on the particles. As was noted by Fisk[82], it is in fact the smaller wavelength fluctuations that are dominant here. The observed power spectra of the fluctuations fall off rather slowly with increasing k, so that the largest gradients in the field magnitude are produced by waves with the higher values of k. For a power spectrum that decreases as $k^{-3/2}$, and for which the three orthogonal correlation lengths are equal, Fisk[82] finds that

$$\left(\frac{\delta B}{B_o}\right)^2 \frac{\lambda_z}{\lambda_\perp'^2} \simeq \left(\frac{\overline{\delta B}}{B_o}\right)^2 \frac{2}{(r_g\lambda_z)^{1/2}} \tag{48}$$

where $(\overline{\delta B})^2/B_o$ is now the ms fluctuation in the field magnitude.

It can be seen by comparing (47) with (46) that to yield the required acceleration rate of $D_{TT}/T^2 \sim 6 \cdot 10^{-7} sec^{-1}$, the ratio in (48) must have a value $\sim 10^2$ AU^{-1}. Such a value is in fact possible. In stream-stream interaction regions the turbulence is presumably locally generated with the result that the correlation lengths are smaller, and the amplitude of the waves larger than in average interplanetary conditions. Suppose, for example, that we take $\lambda_z \sim 10^{-3}$ AU. This value agrees well with the correlation length for small-scale field fluctuations found by Fisk and Sari[112] but is smaller than the traditional correlation length of $\sim 10^{-2}$ AU given by Jokipii and Coleman[8]. Suppose also that we use the observed value for $(\overline{\delta B})^2/B_o^2$ of ~ 0.01-0.03.[7] With, in addition, $B_o \sim 5 \cdot 10^{-5}$G or r_g for a 1 MeV proton $\sim 2 \cdot 10^{-4}$ AU, (48) is $\sim 10^2$ AU^{-1}.

Fisk[82] has calculated more formally the acceleration rate that results from the transit-time damping of magnetosonic waves, by using standard quasi-linear/adiabatic theory and realistic forms for the power spectrum. The results, expressed as D_{pp}/p^2, are shown in Figure 15. As can be seen in this figure D_{pp}/p^2 has the required value of ~ 1.5 $10^{-7} sec^{-1}$ at 1 MeV (Recall $D_{TT}/T^2 = 4\ D_{pp}/p^2$). Shown here also is the pitch-angle scattering mean free path which results from these interactions. As expected, acceleration by transit-time damping does not require or imply extensive pitch-angle scattering. It should be noted, however, that these calculations consider only the magnetosonic waves. The Alfven waves, which are not included, should be of primary importance in determining the actual pitch-angle scattering rate at these low energies (by mechanisms that are not well understood, however (See § III)).

It appears, therefore, that transit-time damping of the observed low-level of magnetosonic waves in the solar wind can result in a sufficient acceleration rate to account for the observations of McDonald et al.[114] In fact, this mechanism is more efficient than might have been expected. It does not appear to be well-known that in cases where the power spectrum falls off slowly with k, the relevant scale length for this acceleration is not the correlation length of the turbulence. Rather, the relevant scale length, which varies inversely as the acceleration rate, is a smaller value which is determined by the higher-k fluctuations[82]. Indeed, it is interesting to note that the power spectrum in the interstellar medium might have the Kolomogorov shape of interplanetary turbulence[124], with the result that the statistical acceleration of galactic cosmic rays might be more important than previously thought.

d) Acceleration at Shock Fronts

The essential feature in most current theories for the acceleration of particles at shock fronts is that the shock front, as it propagates relative to the upstream plasma, will reflect energetic particles and in the process impart energy to them. Consider, for example, the situation shown in Figure 16, where we assume that we are in the frame S that moves with the shock front such that the shock is a normal shock (i.e. the direction of the incoming flow is normal to the shock front). In analogy with (43) the energy gained by reflected particles in this frame is then

$$\Delta T' = mu_t \Delta v_t . \tag{49}$$

Here u_t is the speed that we must move along the shock front so that there is no electric field or equivalently, that the energy of the particle is conserved during reflection. The quantity Δv_t is the change in the reflected particle's speed parallel to the shock front, as seen in the frame moving with u_t.

We assume here that the electric fields in the shock front result only from the motion of the shock relative to the interplanetary magnetic field. As can be seen in Figure 16, then, to have the magnetic field appear stationary, u_t must equal $V' \tan \chi$, where V' is the speed of the incoming solar wind, and χ is the angle between the magnetic field direction and the shock normal.

The change in speed Δv_t is more difficult to determine, and will in general depend on the details of the reflection. A reasonable estimate of this quantity, however, can be obtained by assuming that the particles magnetic moment is a constant of the motion in the frame moving with u_t. The particle then will retain the same pitch

angle after reflection, as it had before, with the result that

$$\Delta v_t = 2v_t = 2(v'_{\parallel} \sin\chi + u_t) \tag{50}$$

where $v'_{\parallel}$ is the speed of the particle parallel to the magnetic field in the S frame, prior to reflection. The expression in (50) should be a reasonable approximation in cases where χ is near 90° or when the change in field magnitude across the shock is small[126]. We note also that by using (50) we will overestimate Δv_t by at most a factor of two i.e. the worse case is that v_t is near zero after reflection.

The relative change in energy $\Delta T'/T'$ in the S frame is then found from (49) and (50) to be

$$\frac{\Delta T'}{T'} \simeq \frac{4V'}{v^2} (v_{\parallel}' \sin\chi + V' \tan\chi) \tan\chi \tag{51}$$

in agreement with the results of Sarris and Van Allen[126]. To find the energy change in the frame fixed with respect to the Sun we must include in our calculations the motion of the shock, i.e. we must add to (51) a term $\sim V_s/v$ where V_s is the shock speed. It should be noted here also that not all particles will be reflected by the shock. In general, it is the larger pitch angle particles that are most easily reflected.

As is evident from (51), perpendicular shocks, i.e. shocks for which χ is near 90° or $\tan\chi$ large, are the most efficient accelerator of particles. Indeed, as is discussed in detail by, for example, Sarris and Van Allen[126], for such shocks $\Delta T'/T'$ can exceed unity. Further, in perpendicular shocks the field lines can be expected to encounter the shock front at several different locations due to the ever-present large scale fluctuations in the direction of the interplanetary field. Particles moving along the

field lines thus have several opportunities in which to gain energy, or, equivalently, the particles can be expected to undergo an appreciable acceleration, with an accompanying increase in the differential intensity. This increase will be confined to occur near the shock front, and thus the mechanism provides a satisfactory explanation for the spike-like increases in intensity which occur at some propagating shock fronts[126,127,128,129]. Indeed, it may be that this mechanism can explain the sharp intensity increases which occur near the shock fronts for the events shown in Figure 14.

We note, however, that the magnetic field need not intersect the shock at several points for the particles to make repeated collisions with the front. As was discussed by Fisk[130], and by Scholer and Morfill[140], particles can also be reflected back to the shock by being scattered from irregularities in the magnetic field upstream from the shock. If the particles are reflected back to the shock many times, they can of course gain considerable energy.

The intensity increase in this latter mechanism can be considered to result from the particles being compressed between the shock front and the upstream irregularities. Limiting the compression, of course, is the ability of the particles to diffuse through the irregularities, or to be transmitted through the shock. In cases where the spectrum falls steeply with increasing energy, the increase in the differential intensity that results from the compression can overwhelm the decrease from particles being lost to diffusion or passage through the shock, and large intensity increases near the shock front can occur[130,140].

With diffusion coefficients similar to those given in Figure 12, we might expect a rather broad increase in the intensity associated

with particles trapped between the shock and the upstream irregularities. Indeed, it is possible that this mechanism, in addition to or instead of statistical acceleration, could account for the broad intensity increases ahead of the shocks for the events shown in Figure 16. The intensity increases which follow the shock passage would in this explanation be due to particles which after some acceleration have passed through the shock.

e) Acceleration of Interstellar Ions

As is discussed in § II.h, the explanation for the anomalous cosmic-ray component of Fisk et al.[81] and Fisk[82] requires that interstellar neutral particles, which are ionized in the solar cavity, can be accelerated in the solar wind from energies ~ 1 keV/nucleon to energies in excess of 10 MeV/nucleon. According to Fisk[82], the statistical transit-time damping mechanism, which is outlined in § IV.c, can accomplish the needed acceleration. Here, the particles do not interact with small-scale magnitude fluctuations in the magnetic field, as in the case of acceleration in co-rotating regions, but rather with the large-scale fluctuations in the outer solar system, which may be the remnants of stream-stream interaction regions.

It is essential that the field fluctuations which are responsible for the acceleration of the interstellar ions have a large spatial scale. The acceleration presumably takes place throughout the outer solar system. Afterall, the acceleration of particles over four decades in energy will require considerable time, e.g. the full time from when particles are first ionized to when they are convected out of the solar cavity by the solar wind at, say, 50 AU from the Sun. Moreover, the particles in this mechanism must obtain energies ~ 10 MeV/nucleon sufficiently far out in the solar cavity so that between this region and the inner solar system there is adequate solar modulation to exclude from near earth any accelerated interstellar hydrogen, or accelerated solar and galactic particles (§ II.h). In the outer solar system, however, the magnetic field is weak with the result that the gyro-radii of the singly charged interstellar particles are large (e.g. ~ 0.5 AU for singly charged

oxygen at 50 AU). Since the efficiency of the acceleration drops drastically when the gyro-radius exceeds the scale size of the fluctuations[82], it is only the large-scale fluctuations then, which can perform the needed acceleration.

The dependence of the efficiency of the acceleration on the ratio of the gyro-radius to the scale-size of the fluctuations provides a natural explanation for why the helium in the anomalous component occurs at a higher energy than does the oxygen (See Figure 10). Singly charged interstellar helium has a smaller gyro-radius than does singly charged oxygen, and hence the helium remains efficiently accelerated to higher energies.

Large-scale fluctuations in the field magnitude in the outer solar system may in fact be very efficient accelerators. We note in (47) that the transit-time damping acceleration rate varies directly as the correlation length along the mean field $\underline{B}_o$ (λ_z), and inversely as the square of the scale-length of the fluctuations normal to $\underline{B}_o$ (i.e. as $1/\lambda_\perp'^2$ or more formally as $1/\lambda_x'^2 + 1/\lambda_y'^2$, where λ_x' and λ_y' are the two orthogonal scale lengths normal to $\underline{B}_o$). In the outer solar system, $\underline{B}_o$ and thus λ_z should lie mainly in the azimuthal direction about the Sun. The normal expansion of the solar wind, then, will cause λ_z to increase with heliocentric distance. The solar wind, however, does not expand in the radial direction, and thus $1/\lambda_\perp'^2$ is roughly constant with distance, or equivalently $\lambda_z/\lambda_\perp'^2$ can become quite large in the outer solar system.

Indeed, with reasonable choices for the magnitude and scale-sizes of the fluctuations in the outer solar system, Fisk[82] finds that transit-time damping can raise the interstellar ions to energies

sufficent to account for the observed anomalous component. We must emphasize, however, that it is clearly necessary in this explanation to speculate on conditions in the outer solar system where we currently have no direct spacecraft observations. Thus, this acceleration mechanism for the interstellar ions should be viewed as only one of perhaps several possible mechanisms.

f) Concluding Remarks

Interplanetary acceleration theory, then, is in a state of expectant naivete. We have high expectations for this work. The conditions that we deal with in the solar wind are similar to conditions that should exist in other astrophysical plasmas. We thus have a unique opportunity here to develop and test reliable theories for the acceleration of energetic particles, which should have broad implication for acceleration in other astrophysical settings. However, we are aware also that our current theories are probably too simpleminded. At first glance, many of the acceleration theories appear to provide an adequate explanation for the observed particle behavior. However, we generally apply these theories at low rigidities where propagation theory, which is based on some of the same principles as the acceleration work, has its difficulties. We are pessimistic then that our current concepts of interplanetary acceleration will prove to be inadequate when subjected to closer scrutiny.

In § V we will make specific recommendations on research into acceleration processes which should be undertaken in the coming years

V. RESEARCH IN THE COMING YEARS

In this section we suggest directions that research into the interactions of energetic particles with the solar wind should take in the coming years. We comment first on immediate efforts -- projects which are clearly called for at present and which can be accomplished using existing data. We next comment on the long range prospects for this field, including new experimental efforts that will be required.

Immediate Efforts

In modulation work, a serious effort should be made to use existing data to infer the charge state of particles in the so-called anomalous cosmic ray component. As we discussed in § II.h, if these particles are found to be single-charged, their origin is compatible with our current understanding of solar modulation. If they are fully-stripped, revisions to current modulation theory will have to be considered. Existing data cannot yield the charge-state directly. However, it may be possible to find convincing, albeit circumstantial evidence in favor of one charge state or the other by observing how the anomalous particles behave, i.e. by observing their gradients, time-variations, etc. Singly-charged oxygen, for example, has a rigidity eight times that of fully-stripped oxygen, which may result in a measurably different behavior. Of course, if the anomalous cosmic rays prove to be fully stripped, efforts should be made to develop a modulation theory that is compatible with this result.

Existing data on cosmic ray behavior in the solar wind should be thoroughly and systematically analyzed to provide information on and additional tests of modulation theory. We recognize that we have at present an extensive network of spacecraft spread over large distances in the ecliptic plane. Helios attains distances ∿0.3 AU from the Sun. There are IMP spacecraft in orbit about the earth. Pioneer 11 is in transit from Jupiter to Saturn. Pioneer 10, which is currently at ∿10 AU from the Sun, is in transit out of the solar system. The ISEE spacecraft, which will be launched in 1977 and 1978, will provide additional baseline measurements at earth. The Voyager spacecraft will be launched in 1977 and will provide deep space measurements while in transit to Jupiter, Saturn, and perhaps Uranus. We also recognize that this network exists at an interesting time in the solar cycle. We are currently in solar minimum conditions. Hence, this network can be used to study the evolution of the cosmic ray intensity, and of the gradients and in some cases anisotropies, during the declining and rising portion of the solar cycle, as seen in widely separated regions of the ecliptic plane. Such information, if exploited to the fullest, will provide invaluable information on the modulation process.

A word of caution is appropriate here. Pioneer 10, which is flying to ever further distance from the Sun, is an essential part of this network of spacecraft. Pioneer 10, however, is currently in an extended mission phase, and therefore is always in danger of being 'turned-off'. It is to be hoped that this spacecraft will be tracked to the furthest distance from which useful data is available -- ∿30 AU from the Sun.

We should also undertake a study of correlations between changes in the cosmic ray flux and changes in solar and solar

wind conditions. This last solar cycle has been an unusual one in that the cosmic ray flux returned to solar minimum levels several years earlier than expected. We note in Figure 1, for example, that the 1972 flux is comparable to the 1965 solar minimum level. The solar cycle is usually ∿11 years in length, i.e. we might have expected that the recent data would not return to 1965 levels until ∿1976. In the period from 1972 on, there were also large-scale coronal holes on the Sun, some of which were extensively studied by the Skylab mission. These coronal holes extend over large latitude ranges on the Sun, and give rise to high speed solar wind streams, and other phenomena, which can effect cosmic rays. Clearly, a study of correlations between changes in the cosmic ray flux and the evolution and behavior of coronal holes and solar wind structures might provide valuable information on modulation, and perhaps even on changes in the modulation out of the ecliptic plane.

In propagation work, a dedicated effort should be undertaken to develop reliable theories for the propagation of low-rigidity particles, which, as we discussed in § III, is the region where current theory is most inaccurate. This effort should involve the development of new analytic theories, and the extensive use of computer simulation studies. This effort should also be done in close cooperation with the ongoing experimental program. In the development of propagation theories it is frequently necessary to make a choice between various possible procedures. The choice of these procedures, which is seldom obvious, could be made considerably simpler, and indeed correctly, by the availability of detailed information on the behavior of the particles and the turbulence. Some of this information currently exists -- unfortunately, it

has not always been fully exploited. Recent spacecraft, for example, have made high time resolution anisotropy measurements which can provide detailed information on the behavior of the particles as they are scattered. Information on power spectra and other properties of the turbulence are also, in principle, available.

It should be emphasized, however, that much of the information needed for the propagation problem is not currently available. Current observations are generally made only from one spacecraft, whereas, as we discuss below, reliable and detailed measurements of the fields and particles require multi-spacecraft measurements.

In acceleration work an effort should be made to use existing data to determine the reliability of current acceleration theories. As we discussed in § IV, we are suspicious that current theories may not be adequate because they are frequently based on the same principles, and applied in the same regions as low-rigidity propagation theories, which are known to have their problems. Data from Pioneers 10 and 11, which include plasma, energetic particles, and magnetic field measurements, will be particularly useful for studying the adequacy of current acceleration theories, as will data from upcoming deep space missions such as Voyager. Of course, if current acceleration theories prove to be inadequate, as we may reasonably assume they will, a theoretical effort identical to that required for the solution of the propagation problem will have to be mounted.

Long-Range Efforts

We should recognize that a complete understanding of the solar modulation of galactic cosmic rays will not be possible with current observations, which have been made only near the ecliptic. As we discussed in § II.h cosmic rays should respond to conditions at the higher heliographic latitudes. Equivalently to understand the modulation we must study the solar wind and the cosmic ray behavior at all latitudes on an out-of-the-ecliptic mission. Such a mission or series of missions is essential for understanding the solar cycle variations in the modulation, and for observing the cosmic rays with low energies in the interstellar medium, which appear to be excluded from any accessible region near the ecliptic.

We should recognize also that the problem of the propagation and acceleration of energetic particles in magnetic fields is one of the more fundamental and difficult problems in astrophysics. Thus, we should not expect that a detailed understanding of propagation and acceleration in the solar wind, sufficient so that it can be scale for application in other astrophysical plasmas, will come easily. Rather, we should expect that a concerted theoretical effort in this field will be required in the foreseeable future.

It is of course necessary for this theoretical effort that there be a continuous input of new and better observations. Out-of-the-ecliptic measurements will be particularly useful in this regard, since they will allow us to study propagation and acceleration under substantially different conditions than are available for study near

the ecliptic. The properties of interplanetary turbulence are expected to vary markedly with heliographic latitude. We also require more detailed measurements near earth of interplanetary turbulence and of the behavior of low energy particles. In particular, multi-spacecraft observation are required. A case in point is our current need to determine the orientation of the wavevectors of Alfven waves in the solar wind, which if oriented towards the heliocentric radial direction would reduce the scattering of particles and, as we discussed in §III.e, bring theory and observation into better agreement. A meaningful determination of the orientation of the wave planes, as well as other properties of the turbulence, requires simultaneous observations from at least two spacecraft. Other required measurements are discussed in the recent report of Interplanetary Physics Subcommittee of the National Academy of Sciences Committee on Space Astronomy and Astrophysics[131].

Finally, we comment that in this field, in the past, there has not always been an adequate collaboration between the experimental and theoretical efforts. Too often theories, in certain areas, have been developed without regard to whether they would explain or contribute to the explanation of data. Too often the detailed and systematic analyses of data that will provide needed information for and meaningful tests of current theories are not done, often for the lack of funding. We have in this field an enormous potential for providing information on the Sun, the heliosphere, the interstellar medium, and the behavior of energetic particles in astrophysical plasmas, in general. It is hoped that in the coming years all reasonable efforts will be made to realize this potential.

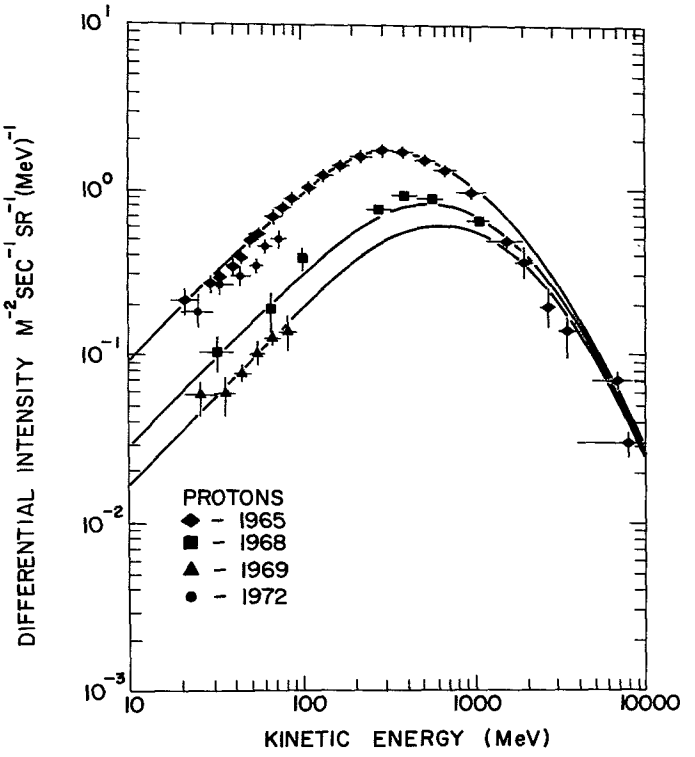

FIGURE 1 The observed differential proton intensity observed near earth in 1965, 1968, 1969 and 1972.

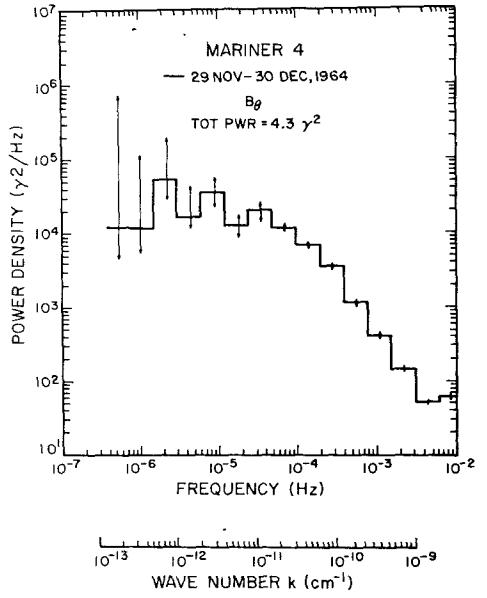

FIGURE 2 A typical power spectrum of the component of the interplanetary magnetic field normal to the solar equatorial plane, observed on Mariner 4. The wavenumber is calculated from the observed frequency by assuming that the waves are being convected past the spacecraft at a solar wind speed of 350 km/sec. The correlation length of the turbulence is roughly the inverse of the wavenumber where the power spectrum breaks from being constant in k to declining as $k^{-5/3}$, i.e. at $k \sim 5 \cdot 10^{-12}\,cm^{-1}$.

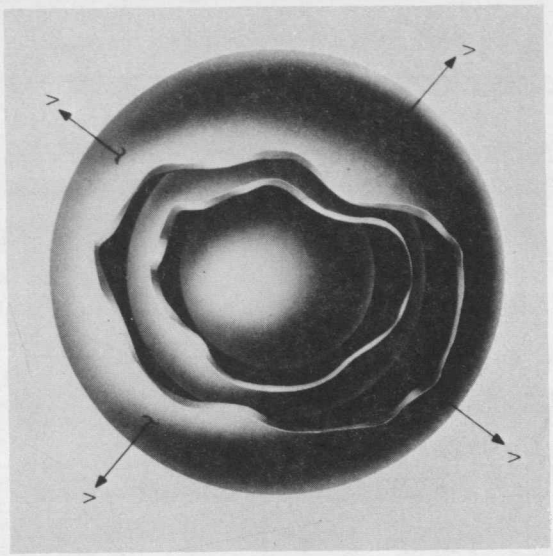

FIGURE 3 A series of infinitely thin concentric spherical shells, all expanding uniformly in radius at a rate V.

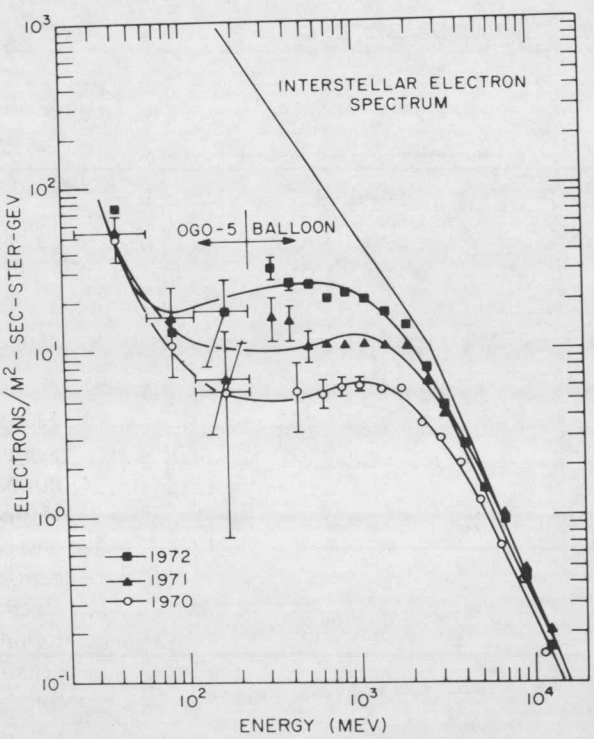

FIGURE 4 The observed electron spectrum in 1970-1972, and the interstellar electron spectrum that is predicted by using the observed nonthermal radio background. The electron data are taken directly from a paper by Fulks *et al.*[43] The predicted interstellar intensity is the lowest found to be acceptable by Cummings *et al.*[40]

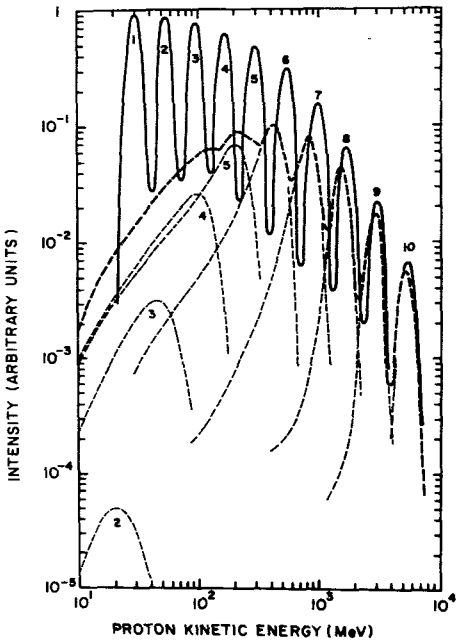

FIGURE 5 A series of essentially monoenergetic proton spectra in interstellar space (solid) and their resulting modulated spectra at earth (dashed).

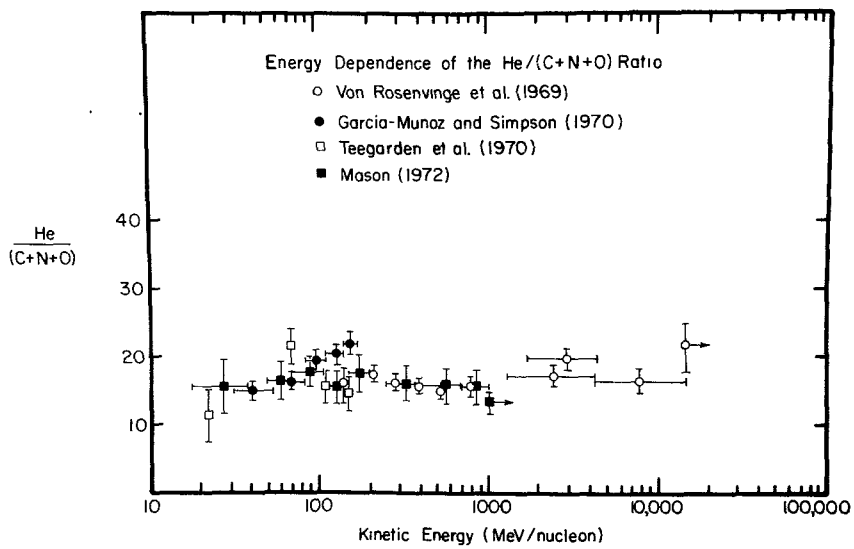

FIGURE 6 Measurements of the energy dependence of the ratio of He/(C+N+O), obtained in the years prior to 1970 (from the rapporteur paper of Garcia-Munoz[48]). The data is taken from papers by von Rosenvinge *et al.*,[132] Garcia-Munoz and Simpson,[133] Teegarden *et al.*,[134] and Mason.[49]

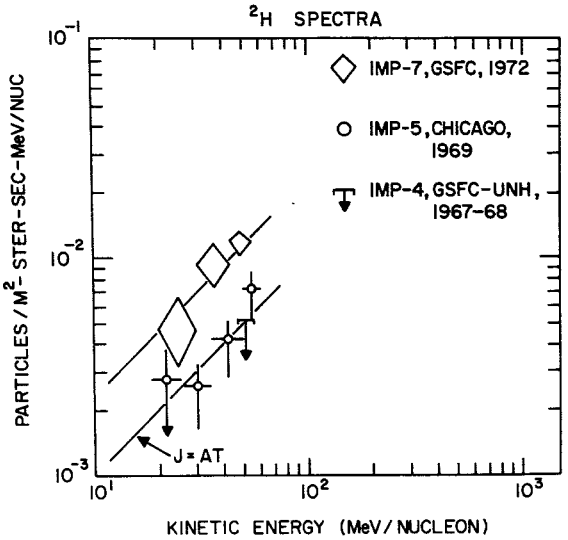

FIGURE 7a The deuterium spectrum at different times during the last solar cycle. The data shown here have been proposed by Teegarden *et al.*[51] as a self-consistent set of data. The solid lines show that the data is consistent with $j \propto T$.

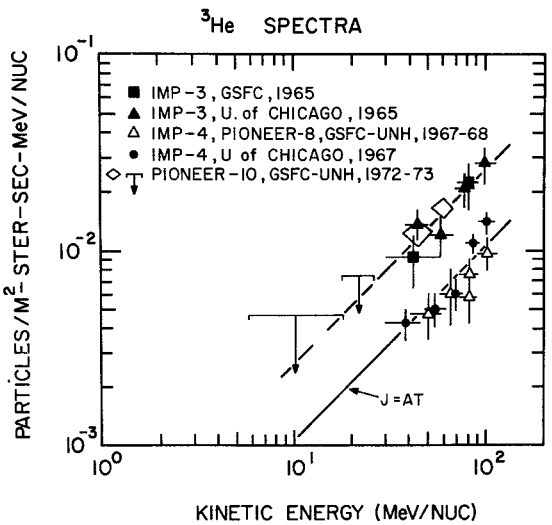

FIGURE 7b Same as Figure 7a for ^{3}He.

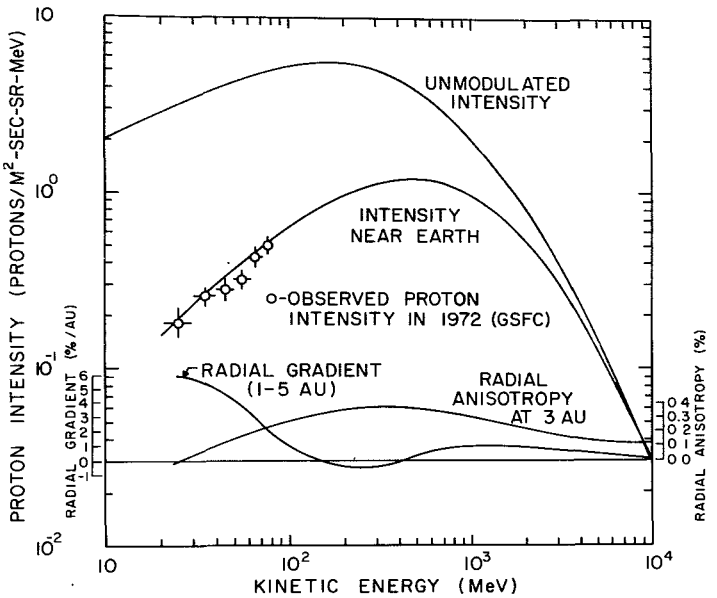

FIGURE 8 The differential intensity near earth, the differential radial gradient in the equatorial plane between 1 and 5 AU, and the differential radial anisotropy in the equatorial plane at 3 AU, plotted vs kinetic energy for the numerical model of Fisk.[34] The data points are the observed proton intensity during quiet-times in 1972, as were obtained from the GSFC experiment on IMP 5. Also shown is the unmodulated interstellar spectrum that was used in the numerical example.

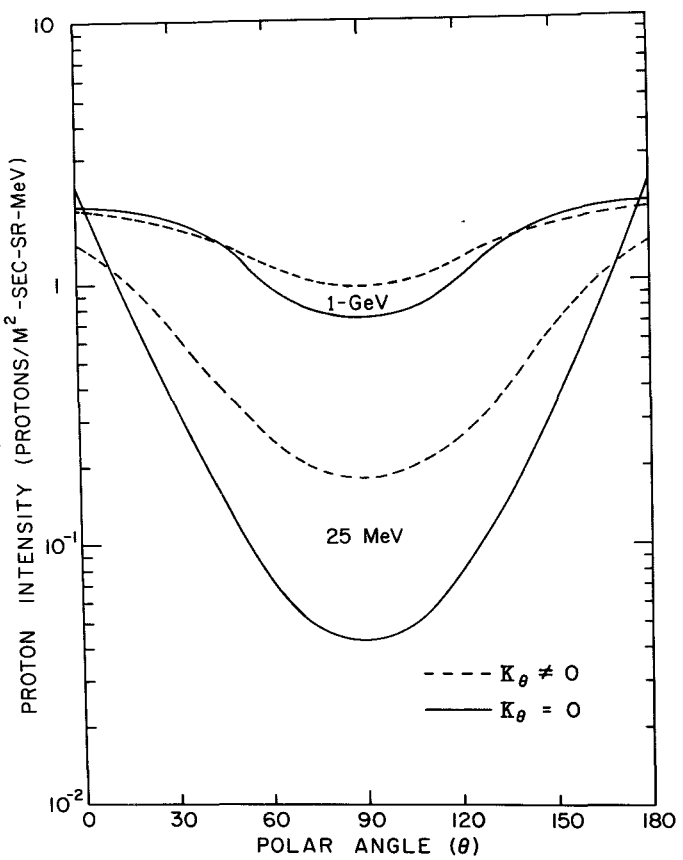

FIGURE 9 The differential intensity at 1 AU in the numerical model of Fisk,[34] plotted versus polar angle θ for two different energies: T = 1 GeV and 25 MeV. For the curves marked $\kappa_\theta \neq 0$, the effects of polar diffusion are included (at 1 AU, $\kappa_\theta = 7 \cdot 10^{20}$ cm^{2}s^{-1} and $7.5 \cdot 10^{18}$ cm^{2}s^{-1} for T = 1 GeV and 25 MeV, respectively). With $\kappa_\theta = 0$, these effects are ignored.

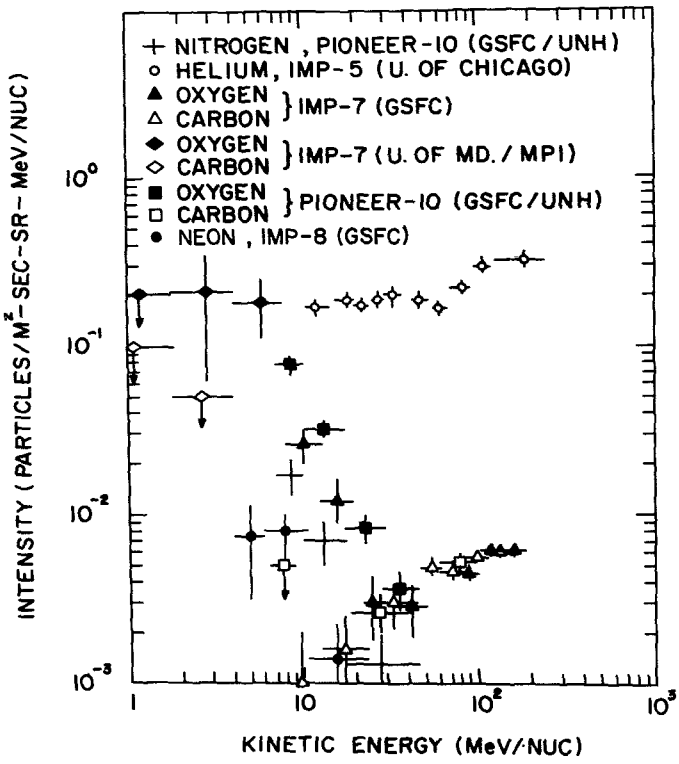

FIGURE 10 The observed spectra of low-energy helium, carbon, nitrogen, and neon during quiet-times in 1972-73. The data are taken from papers by McDonald *et al.*,[70] Hovestadt *et al.*,[71] Garcia-Munoz *et al.*,[72] and von Rosenvinge and McDonald.[73]

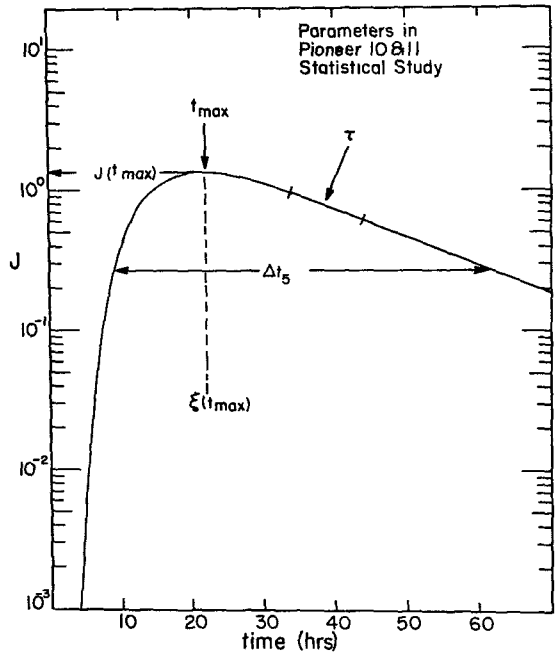

FIGURE 11 A illustration of the five parameters that were fit by Zwickl and Webber[105] in their statistical study of solar flare events seen from Pioneer 10 and 11.

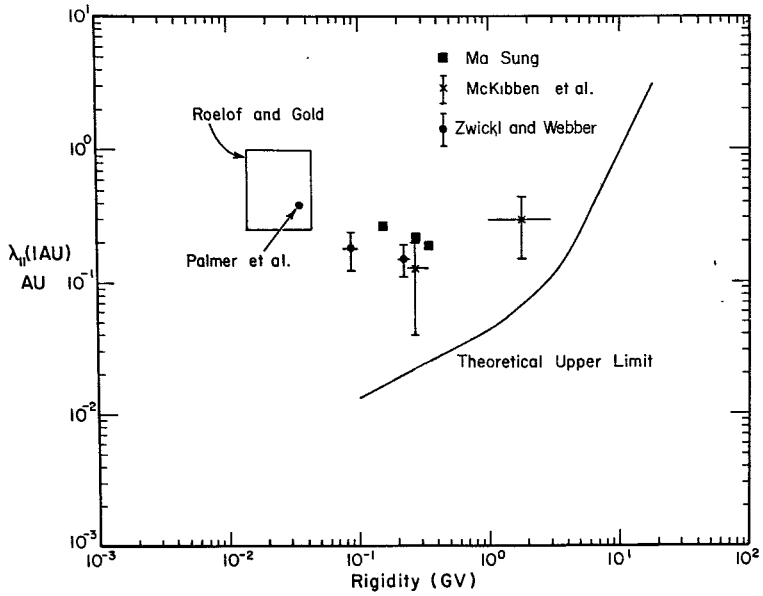

FIGURE 12 A comparison between the mean free path parallel to the mean magnetic field ($\lambda_{\parallel}$) as inferred from particle observations, and the upper limit for $\lambda_{\parallel}$ which is yielded by current theories by using representative forms for interplanetary turbulence (from paper by Zwickl and Webber[105]).

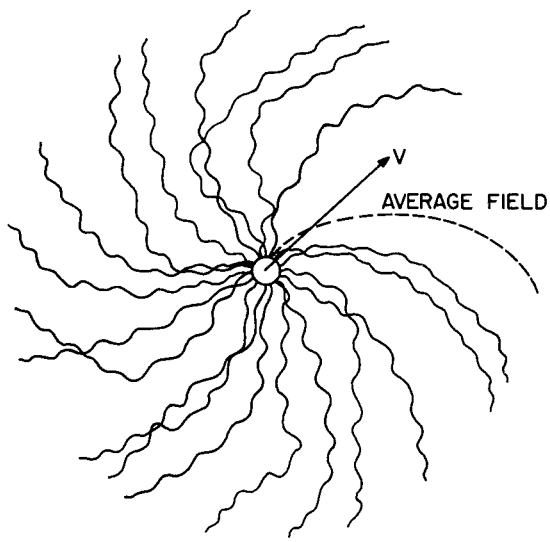

FIGURE 13 An illustration of the stochastic wandering of the interplanetary magnetic field lines relative to the mean field direction (from the review article by Jokipii[61]).

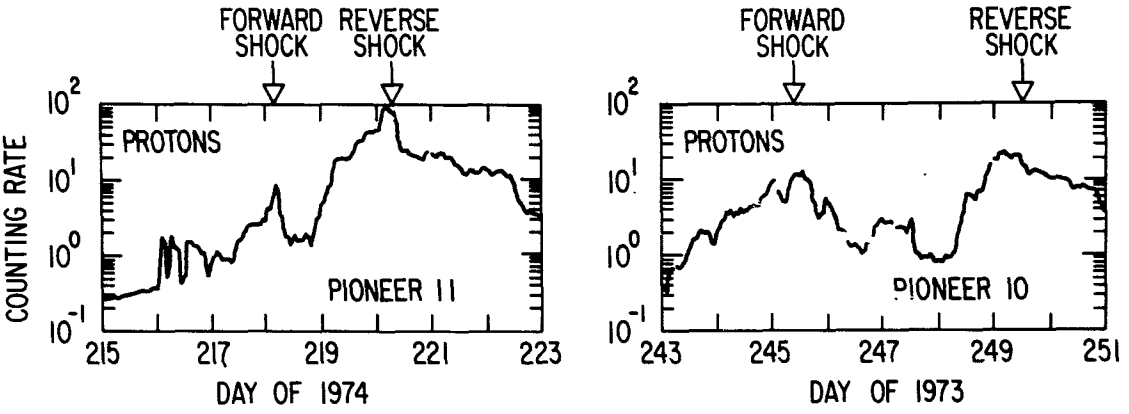

FIGURE 14 The counting rates of 0.5-1.8 MeV protons in typical stream-stream interaction regions, as seen from Pioneer 10 and 11 by Barnes and Simpson.[117]

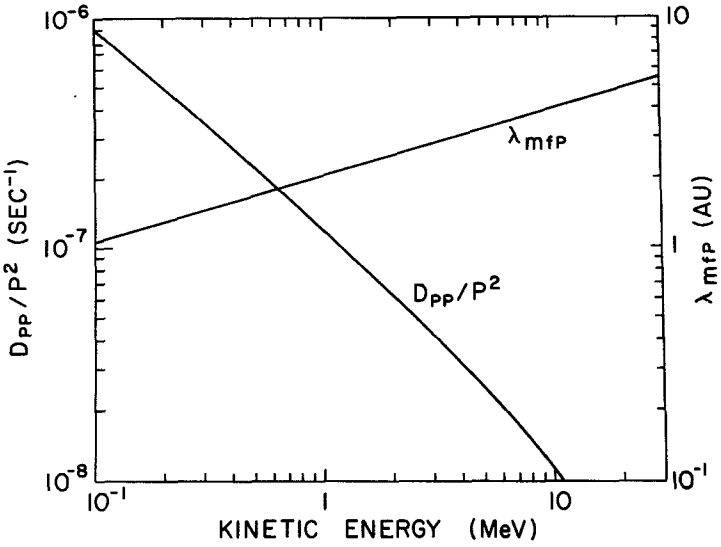

FIGURE 15 The acceleration rate D_{pp}/p^2 that results from protons transit time damping the observed low-level of magnitude fluctuations in the interplanetary magnetic field, plotted versus kinetic energy. Also shown is the characteristic mean free path for pitch angle scattering which results from the magnitude fluctuations that are used in calculating D_{pp}/p^2 (from the paper by Fisk[82]).

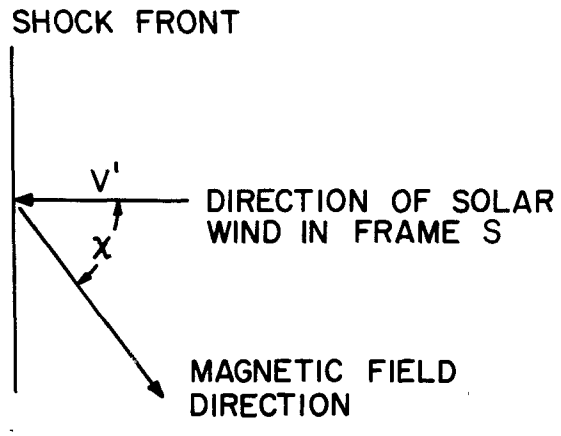

FIGURE 16 The geometry of the magnetic field and shock front in frame S, where the shock is a normal shock.

Acknowledgements

The author is grateful for the advice and council during the preparation of the review article of Drs. M. A. Forman, M. L. Goldstein, F. C. Jones, and A. J. Klimas.

Much of the work on the article was done while the author was on leave at the University of New Hampshire (UNH). The hospitality of the Department of Physics at UNH, in particular of Drs. R. Arnoldy, R. E. Houston, J. A. Lockwood, and W. R. Webber, is gratefully acknowledged.

References

1. Holzer, T. E., The solar wind and related astrophysical phenomena, Report of the NAS Subpanel on Heliosphere Hydrodynamics, to be published, 1977.

2. Coles, W. A., and S. Maagoe, Solar-wind velocity from IPS observations, J. Geophys. Res., 77, 5622, 1972.

3. Axford, W. I., The interaction of the solar wind with the interstellar medium, Solar Wind, ed. by C. P. Sonett, P. J. Coleman, Jr., and J. M. Wilcox, NASA Spec. Pub. 308, p. 609, 1972.

4. Parker, E. N., Dynamics of the interplanetary gas and magnetic field, Astrophys. J., 128, 664, 1958.

5. Jokipii, J. R., Fluctuations and the radial variation of the interplanetary magnetic field, Geophys. Res. Letters, 2, 473, 1975.

6. Burlaga, L. F., Microstructure of the interplanetary medium, Solar Wind, ed. by C. P. Sonett, P. J. Coleman, Jr., and J. M. Wilcox, NASA Spec. Publ. 308, p. 309, 1972.

7. Smith, E. J., Radial gradients in the interplanetary magnetic field between 1.0 and 4.3 AU: Pioneer 10, in Solar Wind Three, edited by C. T. Russell, p. 257, University of California Press, Los Angeles, 1974.

8. Jokipii, J. R., and P. J. Coleman, Jr., Cosmic ray diffusion tensor and its variation observed with Mariner 4, J. Geophys. Res., 73, 5495, 1968.

9. Parker, E. N., The scattering of charged particles by magnetic irregularities, J. Geophys. Res., 69, 1755, 1974.

10. Parker, E. N., Cosmic-ray modulation by solar wind, Phy. Rev., 110, 1445, 1958.

11. Gleeson, L. J., and W. I. Axford, Cosmic rays in the interplanetary medium, Astrophys. J. (Letters), 149, L115, 1967.

12. Fisk, L. A., Solar modulation, in High Energy Particles and Quanta in Astrophysics, p. 170, ed. by F. B. McDonald and C. E. Fichtel, MIT Press, Cambridge, Mass., 1974.

13. Lezniak, J. A. and W. R. Webber, Measurements of gradients and anisotropies of cosmic rays in interplanetary space: Pioneer 8, Proc. inter Conf. Cosmic Rays, Budapest, Acta Phys. (Suppl.) 2, 111, 1970.

14. Parker, E. N., The kinetic properties of the galactic cosmic ray gas, Astrophys. J. 144, 916, 1966.

15. Jokipii, J. R., and E. N. Parker, Energy changes of cosmic rays in the solar system, Planet. Space Sci., 15, 1375, 1967.

16. Jokipii, J. R., and E. N. Parker, On the physical interpretation of the cosmic-ray transport equations, Astrophys. J., 208, 220, 1976.

17. Compton, A. H., and I. A. Getting, An apparent effect of galactic rotation on the intensity of cosmic rays, Phys. Rev., 47, 817, 1935.

18. Gleeson, L. J., and W. I. Axford, Solar modulation of galactic cosmic rays, Astrophys. J., 154, 1011, 1968.

19. Forman, M. A., The Compton-Getting effect for cosmic-ray particles and photons and the Lorentz-invariance of distribution functions, Planet. Space Sci., 18, 25, 1970.

20. Cocconi, G., On the origin of the cosmic radiation, Phys. Rev., 83, 1193, 1951.

21. Fisk, L. A., and W. I. Axford, Anisotropies of solar cosmic rays, Solar Phys., 7, 486, 1969.

22. Parker, E. N., The passage of energetic charged particles through interplanetary space, Planet. Space Sci., 13, 9, 1965.

23. Jokipii, J. R., and E. N. Parker, On the convection, diffuson, and adiabatic deceleration of cosmic rays in the solar wind, Astrophys. J., 160, 735, 1970.

24. O'Gallagher, J. J., Cosmic ray hysteresis as evidence for time-dependent diffusive processes in the long term solar modulation, Proc. 13th Inter. Cosmic Ray Conf., 2, 1135, 1973.

25. O'Gallagher, J. J., A time-dependent diffusion-convection model for the long term modulation of cosmic rays, Astrophys. J., 197, 495, 1975.

26. O'Gallagher, J. J., and G. A. Maslyar III, A dynamic model for the time evolution of the modulated cosmic ray spectrum, J. Geophys. Res., 81, 1319, 1976.

27. Parker, E. N., Cosmic ray diffusion, energy loss, and the diurnal variation, Planet. Space Sci., 15, 1723, 1967.

28. Parker, E. N., The effect of adiabatic deceleration on the cosmic ray spectrum in the solar system, Planet. Space Sci., 14, 371, 1966.

29. Jokipii, J. R., Cosmic-ray propagation, 2, Diffusion in the interplanetary magnetic field, Astrophys. J., 149, 405, 1967.

30. Fisk, L. A., and W. I. Axford, Solar modulation of galactic cosmic rays, 1, J. Geophys. Res., 74, 4973, 1968.

31. Webb, G. M., Steady-state cosmic-ray propagation in interplanetary space, Ph.D. thesis, Monash University, Melbourne, Australia, 1976.

32. Gleeson, L. J., and W. I. Axford, Solar modulation of galactic cosmic rays, Astrophys. J., 154, 1011, 1968.

33. Fisk. L. A., Solar modulation of galactic cosmic rays, 2, J. Geophys. Res., 76, 221, 1971.

34. Fisk, L. A., Solar modulation of galactic cosmic rays 4, Latitude-dependent modulation, J. Geophys. Res., 81, 4646, 1976.

35. Gleeson, L. J., and I. H. Urch, Solar sources and the cosmic ray transport equation, J. Geophys. Res., 76, 2510, 1971.

36. Moraal, H., and L. J. Gleeson, Three-dimensional models of the galactic cosmic-ray modulation, Proc. 14th Inter. Cosmic Ray Conf., 12, 4189, 1975.

37. Cecchini S., and J. J. Quenby, Three-dimensional models of galactic cosmic ray modulation, Proc. 14th Inter. Cosmic Ray Conf., 3, 911, 1975.

38. Alexander, J. K., L. W. Brown, T. A. clark, R. G. Stone, and R. R. Weber, The spectrum of the cosmic radio background between 0.4 and 6.5 MHz, Astrophys. J. (Letters), 157, L163, 1969.

39. Goldstein, M. L., R. Ramaty, and L. A. Fisk, Interstellar cosmic ray spectra from the nonthermal radio background from 0.4 to 400 MHz, Phys. Rev. Letters, 24, 1193, 1970.

40. Cummings, A. C., E. C. Stone, and R. E. Vogt, Interstellar electron spectrum from the galactic non-thermal radio emission, Proc. 13th Inter. Conf. Cosmic Rays, 1, 335, 1973.

41. Ramaty, R., Cosmic electrons, in High Energy Particles and Quanta in Astrophysics, p. 122, ed. by F. B. McDonald and C. E. Fichtel, MIT Press, Cambridge, 1974.

42. Wang, H. T., Low-energy cosmic ray protons from nuclear interactions of cosmic rays with the interstellar medium, J. Geophys. Res., 78, 5693, 1973.

43. Fulks, G., P. Meyer, and J. L'Hereux, The cosmic ray electron spectrum and its modulation from 1968 through 1972, Proc. 13th Inter. Conf. Cosmic Rays, 2, 753, 1973.

44. Lezniak, J. A., and W. R. Webber, Solar modulation of cosmic ray protons, helium nuclei, and electrons: A comparison of experiment with theory, J. Geophys. Res., 76, 1605, 1971.

45. Urch, I. H., and L. J. Gleeson, Galactic cosmic-ray modulation from 1965 to 1970, Astrophys. Space Sci., 17, 426, 1972.

46. Goldstein, M. L., L. A. Fisk, and R. Ramaty, Energy loss of cosmic rays in the interplanetary medium, Phys. Rev. Letters, 25, 832, 1970.

47. Gleeson, L. J., and I. H. Urch, Energy loss and modulation of galactic cosmic rays, Astrophys. Space Sci., 11, 288, 1971.

48. Garcia-Munoz, M., Cosmic ray charge composition ($Z \leq 28$), Proc. 13th Inter. Conf. Cosmic Rays, 5, 3513, 1973.

49. Mason, G. M., Interstellar propagation of galactic cosmic-ray nuclei $2 \leq Z \leq 8$ in the energy range 10-1000 MeV per nucleon, Astrophys. J., 171, 139, 1972.

50. Rygg, T. A., and J. A. Earl, Balloon measurements of cosmic-ray protons and helium over half a solar cycle, 1965-1969, J. Geophys. Res., 76, 7445, 1971.

51. Teegarden, B. J., T. T. von Rosenvinge, F. B. McDonald, J. H. Trainor, and W. R. Webber, Measurements of the fluxes of galactic cosmic-ray ^{2}H and ^{3}He in 1972-1973, Astrophys. J., 202, 815, 1975.

52. Meyer, J. P., Galactic cosmic ray deuterons and energy spectra of sources, Astrophys. Letters, 7, 61, 1970.

53. Meyer, J. P., Deuterons and ^{3}He formation and destruction in proton induced spallation of light nuclei ($Z<8$), Astron. and Astrophys. Suppl., 7, 417, 1972.

54. Teegarden, B. J., F. B. McDonald, J. H. Trainor, E. C. Roeloff, and W. R. Webber, Pioneer-10 measurements of the differential and integral cosmic-ray gradient between 1 and 3 astronomical units, Astrophys. J. (Letters), 185, L155, 1973.

55. McKibben, R. B., J. J. O'Gallagher, J. A. Simpson, and A. J. Tuzzolino, Preliminary Pioneer-10 intensity gradient of galactic cosmic rays, Astrophys. J. (Letters) 181, L9, 1973.

56. Fisk, L. A., M. A. Forman, and W. I. Axford, Solar modulation of galactic cosmic rays, 3, Implications of the Compton-Getting coefficient, J. Geophys. Res., 78, 995, 1973.

57. Webber, W. R., private communication, 1976.

58. Gosling, J. T., R. T. Hansen, and S. J. Bame, Solar wind speed distributon: 1962-1970, J. Geophys. Res., 76, 1811, 1971.

59. Gosling, J. R., J. R. Asbridge, S. J. Bame, and W. C. Feldman, Solar wind speed variations: 1962-1974, J. Geophys. Res., 81, 5061, 1976.

60. Hedgecock, P. C., Measurements of the interplanetary magnetic field in relation to the modulation of cosmic rays, Solar Phys., 42, 497, 1975.

61. Jokipii, J. R., Propagation of cosmic rays in the solar wind, Rev. Geophys., Space Phys., 9, 27, 1971.

62. Jokipii, J. R., and E. N. Parker, Stochastic aspects of magnetic lines of force with applications to cosmic ray propagation, Astrophys. J., 155, 777, 1969.

63. Fisk. L. A., and W. I. Axford, Radial gradients and anisotropies of cosmic rays in the interplanetary medium, Solar Phys., 12, 304, 1970.

64. Van Allen, J. A., Observations of galactic cosmic-ray intensity at heliocentric distances of 1.0 to 2.0 astronomica units, Astrophys. J. (Letters), 177, L49, 1972.

65. Van Allen, J. A., Heliocentric radial dependence of galactic cosmic ray intensity from 1.0 to 3.0 AU (abstract), EOS Trans. AGU, 53, 1083, 1972.

66. McKibben, R. B., K. R. Pyle, J. A. Simpson, A. J. Tuzzolino, and J. J. O'Gallagher, Cosmic ray intensity gradients measured by Pioneer 10 and 11, Proc. 14th Inter. Conf. Cosmic Rays, 4, 1512, 1975.

67. McDonald, F. B., N. Lal, B. J. Teegarden, J. H. Trainor, and W. R. Webber, The radial gradient of galactic cosmic rays, Proc. 14th Inter. Conf. Cosmic Rays, 4, 1511, 1975.

68. Morfill, G. E., H. J. Völk and M. A. Lee, On the effect of directional medium scale interplanetary variations on the diffusion of galactic cosmic rays and their solar cycle variation, J. Geophys. Res., 81, 5841, 1976.

69. Axford, W. I., W. Fillius, L. J. Gleeson, W-H lp, and A. Mogro Campero, Measurements of cosmic ray anisotropies from Pioneer 10 and 11, Proc. 14th Inter. Conf. Cosmic Rays, 4, 1519, 1975.

70. McDonald, F. B., B. J. Teegarden, J. H. Trainor, and W. R. Webber, The anomalous abundance of cosmic ray nitrogen and oxygen nuclei at low energies, Astrophys. J. (Letters) 185, L105, 1974.

71. Hovestadt, D., O. Vollmer, G. Gloeckler, and C. Y. Fan, Differential energy spectra of low-energy (<8.5 MeV per nucleon) heavy cosmic rays during solar quiet times, Phys. Rev. Letters, 31, 650, 1973.

72. Garcia-Munoz, M., G. M. Mason, and J. A. Simpson, A new test for solar modulation theory: The 1972 May-July low-energy galactic cosmic ray proton and helium spectra, Astrophys. J. (Letters), 182, L81, 1973.

73. von Rosenvinge, T. T., and F. B. McDonald, IMP-6, 7, and 8 observations of the composition and time variations of low energy cosmic rays, Proc. 14th Inter. Conf. Cosmic Rays, 2, 792, 1975.

74. Chan, J. H., and P. B. Price, Anomalies in the composition of interplanetary heavy ions with 0.01<E<40 MeV per amu, Astrophys. J. (Letters), 190, L39, 1974.

75. Webber, W. R., private communication, 1976.

76. Gloeckler, G., and J. R. Jokipii, Low-energy cosmic-ray modulation related to observed interplanetary magnetic field fluctuations, Phys. Rev. Letter 17, 203, 1966.

77. Teegarden, B. J., F. B. McDonald, J. H. Trainor, W. R. Webber, and E. C. Roelof, Interplanetary MeV electrons of Jovian origin, J. Geophys. Res., 79, 3615, 1974.

78. Teegarden, B. J., private communication, 1975.

79. Hoyle, F., and D. D. clayton, Nucleosynthesis in white-dwarf atmospheres, Astrophys. J. 191, 705, 1974.

80. Fisk, L. A., Solar modulation and a galactic origin for the anomalous component observed in low-energy cosmic rays, Astrophys. J., 206, 333, 19

81. Fisk, L. A., B. Kozlovsky, and R. Ramaty, An interpretation of the observed oxygen and nitrogen enhancements in low-energy cosmic rays, Astrophys. J.

(Letters), 190, L35, 1974.

82. Fisk, L. A., The acceleration of energetic particles in the interplanetary medium by transit time damping, J. Geophys. Res., 81, 4633, 1976.

83. Wenzel, D. G., The propagation and anisotropy of csomic rays, I, Astrophys. J., 156, 303, 1969.

84. Kulsrad, R., and W. P. Pierce, The effect of wave-particle interactions of the propagation of cosmic rays, Astrophys. J., 156, 445, 1969.

85. Jokipii, J. R., Cosmic-ray propagation, 1, Charged particles in a random magnetic field, Astrophys. J., 146, 480, 1966.

86. Jokipii, J. R., Fokker-Planck equations for charged-particle transport in random fields, Astrophys. J., 172, 319, 1972.

87. Hasselman, K., and G. Wibberentz, Scattering of charged Particles by random electromagnetic field, Zeitschrift fur Geophys., 34, 353, 1968.

88. Hall, D. E., and P. A. Sturrock, Diffusion, scattering, and acceleration of particles by stochastic electromagnetic fields, Phys. Fluids, 10, 2620, 1967.

89. Roelof, E. C., Statistical theory of charged particle transport in distorted magnetic fields, Ph.D. thesis, Univ. of California, Berkeley, 1966.

90. Klimas, A. J., and G. Sandri, Foundation of the theory of cosmic-ray transport in random magnetic fields, Astrophys. J., 169, 41, 1971.

91. Klimas, A. J., and G. Sandri, A rigorous cosmic ray transport equation with no restrictions on particle energy, Astrophys. J., 180, 937, 1973.

92. Jones, F. C., T. J. Birmingham, and T. B.Kaiser, The partially averaged field approach to cosmic ray diffusion, GSFC preprint #X-602-76-175, 1976.

93. Völk, H. J., Cosmic ray propagation in interplanetary space, Rev. Geophys. Space Phys., 13, 547, 1975.

94. Fisk, L. A., M. L. Goldstein, A. J. Klimas, and G. Sandri, The Fokker-Planck coefficient for pitch-angle scattering of cosmic rays. Astrophys. J., 190, 417, 1974.

95. Goldstein, M. L., A. J. Klimas, and G. Sandri, Mirroring within the Fokker-Planck formulation of cosmic ray pitch angle scattering in homogeneous magnetic turbulence, Astrophys. J., 195, 787, 1975.

96. Völk, H. J., Non-linear perturbation theory for cosmic ray propagation in random magnetic fields, Astrophys. Space Sci., 25, 471, 1973.

97. Dupree, T. H., A perturbation theory for strong plasma turbulence, Phys. Fluids, 9, 1773, 1966.

98. Weinstock, J., Formulation of a statistical theory of strong plasma turbulence, Phys. Fluids, 12, 1045, 1969.

99. Jones, F. C., T. B. Kaiser, and T. J. Birmingham, New approach to cosmic ray diffusion theory, Phys. Rev. Letters, 31, 485, 1973.

100. Kaiser, T. B., T. J. Birmingham, and F. C. Jones, in preparation, 1977.

101. Goldstein, M. L., A non-linear theory of cosmic-ray pitch-angle diffusion in homogeneous magnetostatic turbulence, Astrophys. J., 204, 900, 1976.

102. Goldstein, M. L., Consequences of using non linear particle trajectories to compute spatial diffusion coefficients, J. Geophys. Res., in press, 1977.

103. Ben-Israel, I., T. Piran, A. Eviatar, and J. Weinstock, A statistical theory of electromagnetic waves in turbulent plasmas, Astrophys. Space Sci., 38, 125, 1975.

104. Earl, J. A., The diffusive idealization of charged-particle transport in random magnetic fields, Astrophys. J., 193, 231, 1974.

105. Zwickl, R. D., and W. R. Webber, Solar particle propagation from 1 to 5 AU, Solar Phys., in press, 1977.

106. Palmer, I. D., R. D. Zwickl, W. R. Webber, and F. B. McDonald, Spectra of mean free paths near earth in the solar cosmic ray event of 29 April 1973, preprint, 1976.

107. Denskat, K. U., and L. F. Burlaga, Multi-spacecraft observation of microscale fluctuations in the solar wind, GSFC preprint, 1977.

108. Goldstein, M. L., A. J. Klimas, and F. D. Barish, On the theory of large amplitude Alfvén waves, in Solar Wind Three, p. 385, ed. by C. T. Russell, Inst. of Geophys and Planetary Physics, UCLA, 1974.

109. Klimas, A. J., G. Sandri, J. D. Scudder, and D. R. Howell, Test particle propagation in magnetostatic turbulence I, Failure of the diffusion approximation, GSFC preprint, X-692-76-207, 1976; Test particle propagation in magnetostatic turbulence II, The local approximation method, GSFC preprint, X-692-76-252, 1976.

110. Jokipii, J. R., The rate of separation of magnetic lines of force in a random magnetic field, Astrophys. J., 183, 1029, 1973.

111. Krimigis, S. M., E. C. Roelof, T. P. Armstrong, and J. A. Van Allen, Low energy (≥ 0.3 MeV) solar-particle observations at widely separated points (> 0.1 AU) during 1967, J. Geophys. Res., 76, 5921, 1971.

112. Fisk, L. A., and J. W. Sari, Correlation length for interplanetary magnetic field fluctuations, J. Geophys. Res., 78, 6729, 1973.

113. Jokipii, J. R., and E. N. Parker, Cosmic-ray life and the stochastic nature of the galactic magnetic field, Astrophys. J., 155, 799, 1968.

114. McDonald, F. B., B. J. Teegarden, J. H. Trainor, T. T. von Rosenvinge, and W. R. Webber, The interplanetary acceleration of energetic nucleons, Astrophys. J. (Letters), 203, L149, 1976.

115. McCracken, K. G., and U. R. Rao, Solar comsic ray phenomena, Space Sci. Rev., 11, 155, 1970.

116. Gleeson, L. J., Convective transport of low energy cosmic rays in the interplanetary region, Astrophys. Space Sci., 10, 471, 1971.

117. Barnes, C. W., and J. A. Simpson, Evidence for interplanetary acceleration of nucleons in corotating interaction regions, Astrophys. J. (Letters), 210, L91, 1976.

118. Barnes, A., Collisionless damping of hydromagnetic waves, Phys. Fluids, 9, 1483, 1966.

119. Barnes, A., Quasi-linear theory of hydromagnetic waves in collisionless plasma, Phys. Fluids, 11, 2644, 1968.

120. Barnes, A., Collisionless heatingof the solar wind plasma, 1, Theory of the heating of collisionless plasma by hydromagnetic waves, Astrophys. J., 154, 751, 1968.

121. Barnes, A., Collisionless heating of solar wind plasma, 2, Application of the theory of plasma heating by hydromagnetic waves, Astrophys. J., 155, 311, 1969.

122. Fisk, L. A., On the acceleration of energetic particles in the interplanetary medium, J. Geophys. Res., 81, 4641, 1976.

123. Marshall, F. E., and E. C. Stone, Persistent sunward flow of ∿1.6 MeV protons at 1 AU, Geophys. Res. Letters, 4, 57, 1977.

124. Lee, L. C., and J. R. Jokipii, The irregularity spectrum in interstellar space, Astrophys. J. 206, 735, 1976.

125. Hudson, P. D., Reflection of charged particles by plasma shocks, Mon. Notic. Ray. Astron. Soc., 131, 23, 1965.

126. Sarris, E. T., and J. A. Van Allen, Effects of interplanetary shock waves on energetic charged particles, J. Geophys. Res., 79, 4157, 1974.

127. Armstrong, T. P., S. M. Krimigis, and K. W. Behannon, Proton fluxes at 300 keV associated with propagating interplanetary shock waves, J. Geophys. Res., 75, 5980, 1970.

128. Ogilvie, K. W., and J. F. Arens, Acceleration of protons by interplanetary shocks, J. Geophys. Res., 76, 13, 1971.

129. Singer, S., and M. D. Montgomery, Detailed directional and temporal properties of solar energetic particles associated with propagating interplanetary shock waves, J. Geophys. Res., 76, 6628, 1971.

130. Fisk, L. A., Increases in the low-energy cosmic ray intensity at the front of propagating interplanetary shock waves, J. Geophys. Res., 76, 1662, 1971.

131. Anderson, K. A., L. A. Fisk, and G. Gloeckler, Studies of the sun and astrophysical phenomean based on particle observations in interplanetary space, to be published in the Report of the Committee on Space Astronomy and Astrophysics of the National Academy of Sciences, 1977.

132. von Rosenvinge, T. T., W. R. Webber, and J. F. Ormes, The relative energy spectra of carbon and oxygen nuclei in the primary cosmic radiation, Astrophys. Space Sci., 3, 4, 1969.

133. Garcia-Munoz, M., and J. A. Simpson, Galactic abundances and spectra of cosmic rays measured on the IMP-4 satellite, I, Helium and medium, and the very heavy nuclei, Proc. 11th Inter. Conf. Cosmic Rays, Acta. Phys. Acad. Sci. Hung. 29, Suppl. 1, 317, 1970.

134. Teegarden, B. J., F. B. McDonald, and V. K. Balasubrahmanyan, Spectra and charge composition of the low energy galactic cosmic radiation from Z = 2 to 14, Proc. 11th Inter. Conf. Cosmic Rays, Acta. Phys. Acad. Sci. Hung. 29, Suppl. 1, 345, 1970.

135. Jokipii, J. R., E. H. Levy, and W. B. Hubbard, Effects of particle drift on cosmic-ray transport. I. General properties, application to solar modulation, Univ. of Arizona, preprint, 1977.

136. Cummings, A. C., E. C. Stone, and R. E. Vogt, Interplanetary diffusion coefficients for cosmic rays, Proc. 13th Inter. Conf. Cosmic Rays, 2, 772, 1973.

137. Garrard, T. L., E. C. Stone, and R. E. Vogt, Relation of the radial gradient of cosmic-ray protons to the size of the solar modulation region, Proc. 13th Inter. Conf. Cosmic Rays, 2, 1336, 1973.

138. Mewaldt, R. A., E. C. Stone, S. B. Vidor, and R. E. Vogt, Isotopic and elemental composition of the anomalous low-energy cosmic-ray fluxes, Astrophys. J., 205, 931, 1976.

139. Lupton, J. E. and E. C. Stone, Solar flare particle propagation: Comparison of a new analytic solution with spacecraft measurements, J. Geophys. Res., 78, 1007, 1973.

140. Scholer, M., and G. Morfill, Simulation of solar flare particle interaction with interplanetary shock waves, Solar Phys., 45, 227, 1975.

141. Ma Sung, L. S., A study of the propagation and intrinsic characteristics of flare-associated particle events, Ph. D. thesis, Univ. of Maryland, 1977.

142. Earl J. A., The effect of adiabetic focusing upon charged-particle propagation in random magnetic fields, Astrophys. J., 205, 900, 1976.

HYDROMAGNETIC WAVES AND TURBULENCE IN THE SOLAR WIND

Aaron Barnes

Theoretical and Planetary Studies Branch

Ames Research Center, NASA

Moffett Field, California 94035

1. INTRODUCTION

The earliest plasma and magnetic observations of the solar wind showed sizable fluctuations on all observed time scales. It was immediately realized that these fluctuations are to a large extent random in appearance and therefore apparently turbulent.* However, occasional examples of fairly pure wave modes of magnetohydrodynamic theory also appeared in the data. It was eventually discovered that much, but not all, of the interplanetary turbulence could be identified as transverse Alfvén waves propagating outward from the sun.

Thus, the solar wind is an excellent laboratory for the study of large-amplitude hydromagnetic waves and turbulence, a topic of fundamental importance in both basic plasma physics and in astrophysics. Moreover, hydromagnetic waves and discontinuities provide clues about the dynamics of the solar wind and perhaps about the sun itself. Finally, hydrogmagnetic waves themselves carry energy and momentum and therefore may actively influence the acceleration and heating of the solar wind.

In this paper I review the current state of knowledge of interplanetary fluctuations, their origins and their effects on the wind, and suggest directions for future inquiry. In addition, I discuss some astrophysical problems for which solar-wind hydromagnetic-wave studies have relevance.

Section 2 gives typical values of parameters relevant to waves and turbulence in the solar wind. In sections 3 and 4 detailed reviews of the local magnetohydrodynamic and kinetic theories of hydromagnetic waves are given. I review the classification of large-amplitude waves, discuss when description by the MHD theory is qualitatively correct and when it can be misleading, and attempt to state rigorously the essential points of hydrogmagnetic-wave theory

*In this review, we use the term "turbulent" loosely to describe any apparently disordered motion.

and to identify areas in which theoretical research needs to be extended. Readers already familiar with these topics may wish to skip these sections, as may readers who have no need to know the details of the theory. However, I feel it is important to present this material because it is basic to the subject of this review and has not previously been reviewed in detail in a unified way.

In section 5, I review in detail observed hydromagnetic fluctuations, their interpretation in terms of current theory, and the degree of closure between observation and theory. In sections 6 and 7, the spatial distribution and origins of waves in the solar wind are discussed; here theory and observations are still in a primitive state. In section 8, I review what is known about how hydromagnetic waves can heat and exert pressure on a plasma and, very briefly, how these notions have been applied in theories of solar-wind dynamics. Some of the ways in which hydromagnetic waves may participate in astrophysical processes are discussed in section 9. In the final section, I summarize my main conclusions and attempt to identify the most important areas of future research.

This review was easier to write because of earlier reviews of interplanetary microstructure,[17,48,52,116,121,192,228] which are recommended to the reader. Three reviews[21,121,128] consider solar-wind heating and acceleration and the possible role of waves in these processes in more detail than this paper. The most up-to-date reviews on large-scale, solar-wind dynamics, interplanetary effects on cosmic rays, and kinetic processes in the solar wind are companion papers in the present series.[95,96,123]

2. SOLAR-WIND PLASMA PARAMETERS

The solar-wind plasma has been sampled by spacecraft-borne instruments over the range 0.3-11 astronomical units in the ecliptic plane. This plasma

is completely ionized and electrically neutral, its composition is typically 96% hydrogen and 4% helium by number, and its flow speed (300-800 km/sec) usually exceeds characteristic speeds of hydromagnetic waves by a factor of order 10. Parameters of the solar wind typically measured by plasma analyzers and magnetometers are listed in Table I.

TABLE I

PROPERTIES OF THE INTERPLANETARY MEDIUM IN THE ECLIPTIC PLANE

Measured parameter	Typical value in the ecliptic at 1 AU	High-speed streams	Variation with heliocentric radius r*
Composition of ion component	~96% H+, 4% He++	?	Constant
Flow velocity (v)	~400 km/sec, radially directed	~750 km/sec radial	Constant
Density (n)	~6 protons cm^{-3}	~4 protons cm^{-3}	$\propto r^{-2}$
Magnetic field ($\underset{\sim}{B}$)	$\sim 5\times10^{-5}$ gauss, oriented in ecliptic plane at about 45° to radial direction	?	radial component $\propto r^{-2}$ azimuthal component $\propto r^{-1}$
Proton temperature (T_p)	$\sim 4\text{-}10\times10^4$ K	$\sim 2\times10^5$ K	$\propto r^{-a}$, $2/7 \leq a \leq 4/3$
Electron temperature (T_e)	$\sim 10\text{-}20\times10^4$ K	$\sim 10^5$ K	$\propto r^{-b}$, $2/7 < b \leq 4/3$
Helium temperature (T_{He})	~4×proton temperature	?	?

*These parameters exhibit large temporal variations, due in part to solar rotation and the solar cycle, so that their radial profiles are not yet well determined by observation. Heliocentric profiles indicated here come from simple theoretical arguments (e.g., see Ref. 21, Sec. V.A.) and should not be considered reliable for more than order-of-magnitude estimates.

The values of velocity, etc., listed in Table I are only averages, and these quantities fluctuate greatly on a time scale of days, sometimes hours, or even faster. A second column gives some of the same parameters for high-speed streams;[93] these were observed in the ecliptic mainly during 1973-1974, and may represent normal conditions in the solar wind away from equatorial latitudes.[123] In this review I am mainly concerned with fluctuations (great or small) whose characteristic length scale L is much smaller than the length scale for variation of the average properties of the plasma, say $L \lesssim 0.01$ AU. Because the solar-wind speed is much higher than hydromagnetic-wave speeds, most fluctuations are convected at nearly the speed of the solar wind so the time scale of interest is $T = L/V \lesssim 1$ hr. Thus, we focus our attention on "microscale" fluctuations in the terminology of Burlaga and Ness[42] or fluctuations in classes 5-7 in the classification scheme of Hundhausen[128] (II.2).

In the lowest approximation, fluctuations of $L \lesssim 0.01$ AU may be idealized as fluctuations in an infinite background plasma that is spatially uniform on the average. These fluctuations may be waves, structures that are static in the plasma frame, or some complicated mixture of the two. They may be of large or small amplitude, and their characteristic length (wavelength in the case of waves) may range from around the Debye length (~6 m) to much longer than the proton gyroradius (~100 km = 6.7×10^{-7} AU). One requires the natural length and time scales for plasma dynamics to analyze solar-wind fluctuations; these scales, along with characteristic speeds, are given in Table II. Table II shows that Coulomb collisions have at most a weak effect on the solar-wind flow near 1 AU. This fact is reflected in the inequality and anisotropy of proton and electron temperatures; moreover, directly measured velocity distributions are generally non-Maxwellian. Clearly,

TABLE II

CHARACTERISTIC LENGTHS, TIME SCALES, AND SPEEDS OF THE INTERPLANETARY PLASMA

Lengths			
Characteristic length	Typical value at 1 AU	Time for convection past spacecraft at 1 AU, sec	Variation of characteristic length with heliocentric distance*
Proton gyroradius $r_{Lp} = (m_p c/eB)(2kT_p/m_p)^{1/2}$	~50-100 km	~0.1	$r^{1-a/2}(1+r^{-2})^{-1/2}$ (r in AU)
Electron gyroradius $r_{Le} = (m_e c/eB)(2kT_e/m_e)^{1/2}$	~1-2 km	$\sim 10^{-2}$	$r^{1-b/2}(1+r^{-2})^{-1/2}$ (r in AU)
Inertial length $\lambda_i = c/\omega_{pe}$	~2 km	$\sim 10^{-2}$	r
Debye length $\lambda_D = (kT_e/8\pi ne^2)^{1/2}$	~6 m	$\sim 10^{-5}$	$r^{1-b/2}$
Distance traveled by protons between Coulomb collisions (solar-wind speed × collision time)**	4×10^{13} cm ~3 AU	$\sim 10^{6}$	$r^{2-3a/2}$
Electron mean free path for Coulomb collisions	$\sim 10^{13}$ cm ~0.7 AU	$\sim 10^{5}$	r^{-2b+2}

*See footnote page 7.

**See footnote page 7.

TABLE II (Continued)

Times			
Characteristic time	Typical value at 1 AU, sec	Corresponding frequency, Hz	Variation of characteristic time with heliocentric distance*
Proton gyroperiod $2\pi/\Omega_p = 2\pi m_p c/eB$	~10	~0.08	$r(1+r^{-2})^{-1/2}$ (r in AU)
Electron gyroperiod $2\pi/\Omega_e = 2\pi m_e c/eB$	$\sim 10^{-2}$	~150	$r(1+r^{-2})^{-1/2}$ (r in AU)
Plasma period $2\pi/\omega_{pe} = 2\pi(m_e/4\pi ne^2)^{1/2}$	$\sim 4\times10^{-5}$	$\sim 2\times10^{4}$	r
Electron-electron Coulomb collision time $\tau_{ee} = \frac{3m_e^{1/2}(kT_e)^{3/2}}{4(2\pi)^{1/2}e^4 n \ln \Lambda}$	$\sim 5\times10^{4}$	$\sim 2\times10^{-5}$	$r^{2-3b/2}$
Proton-proton Coulomb collision time $\tau_{pp} = \frac{3m_p^{1/2}(kT_p)^{3/2}}{4\pi^{1/2}e^4 n \ln \Lambda}$	$\sim 10^{6}$	$\sim 10^{-6}$	$r^{2-3a/2}$

*See footnote page 7.

TABLE II (Continued)

Speeds		
Characteristic speed	Typical value at 1 AU, km/sec	Variation with heliocentric distance*
Alfvén speed $C_A = B/(4\pi m_p n)^{1/2}$	~50	$(1 + r^{-2})^{1/2}$ (r in AU)
Ion sound speed $C_s = [(5/3)k(T_e + T_p)/m_p]^{1/2}$	~50	$(r^{-b} + \lambda r^{-a})^{1/2}$ ($\lambda = T_p/T_e$ at 1 AU)
Proton thermal speed $V_{thp} = (3kT_p/m_p)^{1/2}$	~50	$r^{-a/2}$
Electron thermal speed $V_{the} = (3kT_e/m_e)^{1/2}$	~2000	$r^{-b/2}$

*See footnote of Table I.

** Since the solar-wind speed is much larger than the proton thermal speed, this length is not the same as the mean free path.

microfluctuations near 1 AU are unaffected by Coulomb collisions. As the number of particles in a Debye sphere is large ($n\lambda_D^3 \sim 10^9$ at 1 AU), the microfluctuations must be described by the Vlasov-Maxwell equations.

3. LOCAL MHD THEORY OF HYDROMAGNETIC FLUCTUATIONS

Large-amplitude fluctuations in magnetic field and plasma density and velocity are commonly observed in the interplanetary medium. Fluctuations are found at all time scales that magnetometers can resolve, but tend to have larger amplitude for longer periods. As shown in Table II, variations slower than about 0.1 sec correspond to spatial variations larger than the proton gyroradius, so that the most commonly observed fluctuations are often thought of as *hydromagnetic* fluctuations. We shall adopt this name for these fluctuations, but the name does not imply that they may necessarily be described by magnetohydrodynamic (MHD) theory. On the contrary, as mentioned previously, the Vlasov-Maxwell equations are the correct mode of description. Nevertheless, the MHD formulation of the problem provides a useful set of concepts and definitions that help to order the complexities of the collisionless theory. Therefore we first review the theory of MHD fluctuations, and then consider how this theory must be modified in the collisionless situation.

The usual MHD model of fluctuations starts with the MHD equations for an inviscid ideal gas of infinite electrical conductivity. The relevant equations are

$$\underset{\sim}{E} + \frac{\underset{\sim}{V}}{C} \times \underset{\sim}{B} = 0 \tag{3-1a}$$

$$\frac{\partial \rho}{\partial t} + \underset{\sim}{\nabla} \cdot (\rho \underset{\sim}{V}) = 0 \tag{3-1b}$$

$$\rho\left(\frac{\partial}{\partial t} + \underset{\sim}{V} \cdot \underset{\sim}{\nabla}\right)\underset{\sim}{V} + \underset{\sim}{\nabla}\left(p + \frac{B^2}{8\pi}\right) - \underset{\sim}{B} \cdot \underset{\sim}{\nabla} \frac{\underset{\sim}{B}}{4\pi} = 0 \tag{3-1c}$$

$$\left(\frac{\partial}{\partial t} + \underset{\sim}{V} \cdot \underset{\sim}{\nabla}\right)\underset{\sim}{B} + \underset{\sim}{B}\, \underset{\sim}{\nabla} \cdot \underset{\sim}{V} - \underset{\sim}{B} \cdot \underset{\sim}{\nabla}\, \underset{\sim}{V} = 0 \tag{3-1d}$$

$$\left(\frac{\partial}{\partial t} + \underset{\sim}{V} \cdot \underset{\sim}{\nabla}\right)(p\rho^{-\gamma}) = -(\gamma - 1)\rho^{-\gamma}\underset{\sim}{\nabla} \cdot \underset{\sim}{q} \tag{3-1e}$$

Here we use cgs units; $\underset{\sim}{E}$ is the electric field, $\underset{\sim}{B}$ the magnetic field, $\underset{\sim}{V}$ the fluid velocity, p the pressure, ρ the mass density, $\underset{\sim}{q}$ the heat flux, γ the ratio of specific heats, and c the speed of light *in vacuo*. In the important special case in which spatial variation occurs only in (say) the z direction, and $\underset{\sim}{\nabla} \cdot \underset{\sim}{q} = 0$, Eqs. (3-1) may be solved by the method of characteristics.[4,135,140] The solutions obtained in this way are classified into three propagating waves and two kinds of variation that do not propagate with respect to the fluid.

The simplest approach to this classification scheme is to assume that all dynamical variables depend on a single function $\psi(z,t)$, so that $\rho = \rho(\psi)$, $\underset{\sim}{V} = \underset{\sim}{V}(\psi)$, etc. For nontrivial solutions, $\psi_z \equiv \partial\psi/\partial z \neq 0$, so that $\underset{\sim}{\nabla} \cdot \underset{\sim}{B} = 0$ requires $B_z = B_{zo} = \text{const}$. Let $\underset{\sim}{e}_z$ be the unit vector in the z direction and define $V_z = \underset{\sim}{V} \cdot \underset{\sim}{e}_z$, $\underset{\sim}{V}_\perp = \underset{\sim}{V} - V_z\underset{\sim}{e}_z$, $\underset{\sim}{B}_\perp = \underset{\sim}{B} - B_{zo}\underset{\sim}{e}_z$. Then, for $\underset{\sim}{\nabla} \cdot \underset{\sim}{q} = 0$, Eqs. (3-1b)-(3-1e) become[22]

$$(\psi_t + V_z\psi_z)\rho' + \psi_z\rho V_z' = 0 \tag{3-2a}$$

$$(\psi_t + V_z\psi_z)\rho\underset{\sim}{V}_\perp' - \frac{\psi_z B_{zo}\underset{\sim}{B}_\perp'}{4\pi} = 0 \tag{3-2b}$$

$$(\psi_t + V_z\psi_z)\rho V_z' + \psi_z[p' + (\underset{\sim}{B}^2)'/8\pi] = 0 \tag{3-2c}$$

$$(\psi_t + V_z\psi_z)\underset{\sim}{B}_\perp' + \underset{\sim}{B}_\perp\psi_z V_z' - B_{zo}\psi_z\underset{\sim}{V}_\perp' = 0 \tag{3-2d}$$

$$(\psi_t + V_z\psi_z)(p\rho^{-\gamma})' = 0 \tag{3-2e}$$

where $f'(\psi) \equiv df/d\psi$.

Nonpropagating Structures ($\psi_t + V_z\psi_z = 0$). For nonpropagating structures Eqs. (3-2) imply

$$V_z = V_{zo} = \text{const} \tag{3-3a}$$

$$p + \frac{B^2}{8\pi} = \text{const} \tag{3-3b}$$

The system (3-2) is then self-consistent if and only if one of the two following conditions exists:

(i) Tangential pressure balance ($B_{zo} = 0$): In this case, $\underset{\sim}{B}_\perp$ and $\underset{\sim}{V}_\perp$ are arbitrary functions of ψ so long as Eq. (3-3b) is satisfied. In the limit of zero thickness, this structure is called a tangential discontinuity.

(ii) Entropy "wave" ($\underset{\sim}{B}_\perp$, $\underset{\sim}{V}_\perp$, p constant): In the limit of zero thickness, this structure is called a contact discontinuity.

For both kinds of nonpropagating structures, the varying quantities are functions only of $z - V_{zo}t$.

Transverse Alfvén Wave (or Intermediate Wave). If $p + B^2/8\pi$ is constant but $\psi_t + V_z\psi_z \neq 0$, then self-consistency of Eqs. (3-2) requires that

$$\left.\begin{aligned} V_z &= V_{zo} = \text{const} \\ \rho &= \rho_o = \text{const} \\ p &= p_o = \text{const} \\ \underset{\sim}{B}_\perp^{\,2} &= \text{const} \end{aligned}\right\} \tag{3-4a}$$

that

$$\psi_t + (V_{zo} \pm C_{Az})\psi_z = 0 \tag{3-4b}$$

where

$$C_{Az} \equiv \frac{B_{zo}}{(4\pi\rho_o)^{1/2}} \tag{3-4c}$$

and that

$$\underset{\sim}{V}_\perp = \mp \frac{C_{Az}\underset{\sim}{B}_\perp}{B_{zo}} + \text{const} \tag{3-4d}$$

This mode, the transverse Alfvén mode, is noncompressive with constant magnitude (but not direction) of magnetic field. The fluctuating velocity and magnetic field are functions of $z - (V_{zo} \pm C_{Az})t$ and are related by Eq. (3-4d). The wave does not steepen as it propagates and, in the limit of zero thickness, it is called rotational discontinuity.

Magnetoacoustic Waves. If a fluctuation does not fall into the three previous classes, then both $\psi_t + V_z\psi_z \neq 0$ and $p' + (\underset{\sim}{B}^2)'/8\pi \neq 0$. Self-consistency of Eqs. (3-2) then implies that

$$p' = \left(\frac{\gamma p}{\rho}\right)\rho' \equiv C_s^2(\psi)\rho' \tag{3-5a}$$

$$\underset{\sim}{B}_\perp \text{ and } \underset{\sim}{B}_\perp' \text{ are parallel} \tag{3-5b}$$

and either

$$\psi_t + (V_z \pm \underset{-}{V}_f)\psi_z = 0 \tag{3-5c}$$

or

$$\psi_t + (V_z \pm \underset{-}{V}_s)\psi_z = 0 \tag{3-5d}$$

where

$$\underset{-}{V}^2_{(f,s)} = \frac{1}{2}\left\{C_A^2 + C_s^2 \pm [(C_A^2 + C_s^2)^2 - 4C_s^2C_{Az}^2]^{1/2}\right\} \tag{3-5e}$$

and

$$C_A^2 = \frac{B^2}{4\pi\rho} \tag{3-5f}$$

These two modes, the fast and slow magnetoacoustic modes, are compressive and their magnetic fluctuations are linearly polarized (Eq. (3-5b)). The solution $\psi(z,t)$ of Eqs. (3-5c, 3-5d) determine the characteristic curves ψ = const, whose differential equations are

$$\frac{dz}{dt} = -\frac{\psi_t}{\psi_z} = V_z(\psi) \pm \underset{-}{V}_{(f,s)}(\psi) \tag{3-6}$$

Since ψ is constant along a characteristic curve, the solutions of Eq. (3-6) are straight lines in the z-t plane. If all quantities are specified as functions of z at t = 0, the characteristics z(t) may be labeled by $\zeta = z(0)$. The solution of (3-6) is

$$z(t,\zeta) = \zeta + [V_z(\zeta) \pm \underline{V}_{(f,s)}(\zeta)]t \tag{3-7}$$

Then, for arbitrary $f(\zeta)$,

$$\frac{\partial f}{\partial z} = \frac{df/d\zeta}{1 + t\{d[V_z \pm \underline{V}_{(f,s)}]/d\zeta\}} \tag{3-8}$$

Thus, this derivative will be infinite when $t = -\{d[V_z \pm \underline{V}_{(f,s)}]/d\zeta\}^{-1} \equiv T(\zeta)$. Thus, the fast and slow magnetoacoustic waves exhibit the familiar phenomenon of steepening and rarefaction. In particular, a steepening wave will begin to form a fast or slow shock after the time $T(\zeta_c)$ where

$$\frac{\partial^2}{\partial z^2}\,[V_z(z,0) \pm \underline{V}_{(f,s)}(z,0)]\Big|_{z=\zeta_c} = 0$$

Small-amplitude limit. The nonlinear characteristic modes, in the limit of small amplitude, become the well-known modes of linearized MHD theory.[133,147,216] In this limit, the fast and slow wave speeds are independent of space and time, and steepening and rarefaction do not occur. Furthermore, in the linearized theory, a field of MHD turbulence can be regarded as a superposition of the fundamental modes, which is not permissible when large-amplitude waves are present. Polar diagrams of phase velocity as a function of (phase) propagation direction are given in Fig. 1. One can construct Friedrichs diagrams to analyze the shape of nonplanar wave fronts.[135] The group velocity is used in analysis of energy propagation; in particular, in

the plasma frame, the group velocity of the Alfvén (intermediate) mode is directed along the magnetic field.

According to nonlinear theory, the magnetic fluctuations in magnetoacoustic modes are linearly polarized and, of course, this conclusion applies in the small-amplitude limit as well. On the other hand, according to nonlinear theory, the transverse Alfvén mode must have $\underset{\sim}{B}^2 = \text{const}$. Thus the tip of the magnetic vector must move along a circle. The wave may actually be circularly polarized or the magnetic vector may merely oscillate back and forth along a segment of the circle. In either case, linear polarization is strictly prohibited. It is therefore somewhat surprising that the polarization becomes linear in the small-amplitude limit. This comes about because the requirement $(\langle\underset{\sim}{B}\rangle + \underset{\sim}{\delta B})^2 = \text{const}$ means that $\langle\underset{\sim}{B}\rangle \cdot \underset{\sim}{\delta B}$ is of order $\underset{\sim}{\delta B}^2$ and therefore vanishes in linear theory.

The fast and slow magnetoacoustic modes are quite different from the Alfvén modes. Unfortunately, the two kinds of waves have sometimes been confused when small-amplitude theory has been used, since the Alfvén mode is degenerate with one of the magnetoacoustic modes in the linearized theory for propagation along the average magnetic field (cf. Fig. 1). This degeneracy is removed if second-order terms in the wave amplitude are retained in the theory. Barnes and Hollweg[22] give the fast-mode speed for propagation nearly parallel to the mean magnetic field as

$$V_f^2 \cong C_{Az}^2 \left[1 + \frac{(\underset{\sim}{\delta B}_\perp)^2 + \langle(\underset{\sim}{\delta B}_\perp)^2\rangle}{2(B_{zo}^2 - 4\pi\gamma p_o)} \right] \tag{3-9}$$

for $C_A > C_s$, where the angle brackets denote a temporal average and $\underset{\sim}{\delta B} = \underset{\sim}{B} - \langle\underset{\sim}{B}\rangle$. Thus, for propagation along the average magnetic field, the magnetoacoustic wave is exactly linearly polarized and slightly compressive, and its phase speed slightly exceeds the Alfvén speed; the transverse Alfvén

wave is nearly linearly polarized, is exactly noncompressive, and travels at the Alfvén speed. The degeneracy between magnetoacoustic and Alfvén modes is also removed in the linearized kinetic theory if corrections due to nonzero frequency are retained.

Nonplanar Alfvén Waves. The analysis of MHD fluctuations in terms of characteristic modes is based on the assumption that the disturbances are planar. This assumption may or may not be realistic for interplanetary fluctuations. Certainly it is plausible that propagating disturbances far from their source can be approximated at least locally as plane waves. However, disturbances may conceivably be generated nearby, and even those originating far away may be distorted from planar form by inhomogeneities or by dynamical processes in the solar wind. Therefore it is appropriate to ask how nonplanar disturbances behave.

This question is essentially unanswered for magnetoacoustic waves and the convected stationary structures. Some progress has been made for Alfvénic disturbances. Goldstein *et al.*[106] have shown that there exist self-consistent nonplanar solutions of the full nonlinear MHD equations which give constant density, pressure, and magnetic-field strength but allow fluctuations in the magnetic-field direction. Velocity and magnetic fluctuations are related by

$$\Delta \underset{\sim}{V} = \mp \frac{\Delta \underset{\sim}{B}}{(4\pi\rho)^{1/2}} \tag{3-10}$$

and, in the plasma frame, the magnetic fluctuations satisfy the equation

$$\frac{\partial^2}{\partial t^2} \Delta \underset{\sim}{B} = \frac{1}{4\pi\rho} \left(\langle \underset{\sim}{B}_o \rangle \langle \underset{\sim}{B}_o \rangle \; : \; \underset{\sim}{\underset{\sim}{\nabla\nabla}} \right) \Delta \underset{\sim}{B} \tag{3-11}$$

Solutions of Eq. (3-1) thus have all the properties of the transverse Alfvén wave previously discussed (Eqs. (3-4)) without being restricted to plane

waves. Thus, in Alfvénic fluctuations the tip of the magnetic vector moves on a sphere and is not necessarily restricted to a circle. Apparently, no non-trivial solutions of Eq. (3-11) have yet been given; however, it has been shown that there are no solutions in which $\underset{\sim}{B}$ is restricted to a plane containing $\underset{\sim}{B}_o$.[25]

4. LOCAL KINETIC THEORY OF HYDROMAGNETIC FLUCTUATIONS

There is special interest in microscale fluctuations whose temporal variations in a spacecraft reference frame are slow on the time scale 0.1 sec, as the corresponding spatial variations are longer than a proton gyroradius. As mentioned previously, these hydromagnetic fluctuations must in principle be described by a kinetic theory, as the Coulomb collision times are much larger than the wave period. Nevertheless, the MHD theory discussed in the previous section provides a number of concepts that are useful in classifying hydromagnetic fluctuations.

MHD Analogy. The relevance of the MHD theory is due to the fact that there is a strong formal analogy between the MHD Eqs. (3-1) and the equations that describe a collisionless plasma. If the average properties of the plasma and fields vary slowly in space and time on the scales of gyroradii and gyroperiods, then to a good approximation $\underset{\sim}{E} \cdot \underset{\sim}{B} = 0$ and the fluid velocity in the direction transverse to the magnetic field is approximately the $\underset{\sim}{E} \times \underset{\sim}{B}$ drift, in which case Eq. (3-1a) is approximately satisfied.[208]

Equation (3-1d) is a consequence of Eq. (3-1a) and Faraday's law. Continuity and momentum equations analogous to Eqs. (3-1b,c) are easily derived from moments of the Vlasov equation

$$\left[\frac{\partial}{\partial t} + \underset{\sim}{v} \cdot \frac{\partial}{\partial \underset{\sim}{x}} + \frac{q_\alpha}{m_\alpha}\left(\underset{\sim}{E} + \frac{\underset{\sim}{v}}{c} \times \underset{\sim}{B}\right) \cdot \frac{\partial}{\partial \underset{\sim}{v}}\right] f_\alpha = 0 \qquad (4\text{-}1)$$

(here $f_\alpha(\underset{\sim}{v}, \underset{\sim}{x}, t)$ is the velocity distribution of the αth charged species; q_α and m_α are the charge and mass of each particle of the αth species). The zeroth, first, and second moments of f_α are

$$n_\alpha(\underset{\sim}{x},t) = \int f_\alpha \, d^3v \tag{4-2a}$$

$$n_\alpha \underset{\sim}{V}_\alpha = \int \underset{\sim}{v} f_\alpha \, d^3v \tag{4-2b}$$

$$\underset{\approx}{p}_\alpha = m_\alpha \int (\underset{\sim}{v} - \underset{\sim}{V}_\alpha)(\underset{\sim}{v} - \underset{\sim}{V}_\alpha) f_\alpha \, d^3v \tag{4-2c}$$

where n_α is the particle density, $\underset{\sim}{V}_\alpha$ the bulk velocity, and $\underset{\approx}{p}_\alpha$ the stress tensor of the αth species. The mass density $\rho = \sum_\alpha m_\alpha n_\alpha$, the fluid velocity $\underset{\sim}{V} = (1/\rho)\sum_\alpha m_\alpha n_\alpha \underset{\sim}{V}_\alpha$, the total stress $\underset{\approx}{P} = \sum_\alpha \underset{\approx}{p}_\alpha$, the electric charge density $\rho_Q = \sum_\alpha q_\alpha n_\alpha$, and the electric current density $\underset{\sim}{J} = \sum_\alpha q_\alpha n_\alpha \underset{\sim}{V}_\alpha$. The zeroth moment of Eq. (4-1) is

$$\frac{\partial n_\alpha}{\partial t} + \underset{\sim}{\nabla} \cdot (n_\alpha \underset{\sim}{V}_\alpha) = 0 \tag{4-3}$$

(It is assumed that $f_\alpha \to 0$ for large $|\underset{\sim}{v}|$ fast enough that all moments of interest are finite.) Equation (4-3) states that the number of particles of each species is conserved, and multiplying (4-3) by m_α and summing over species gives (3-1b). Taking the first moment of (4-1), multiplying by m_α, and summing over species yield the momentum equation

$$\frac{\partial}{\partial t}(\rho \underset{\sim}{V}) + \sum_\alpha m_\alpha \underset{\sim}{\nabla} \cdot (n_\alpha \underset{\sim}{V}_\alpha \underset{\sim}{V}_\alpha) + \underset{\sim}{\nabla} \cdot \underset{\approx}{P} = \rho_Q \underset{\sim}{E} + \frac{1}{c} \underset{\sim}{J} \times \underset{\sim}{B} \tag{4-4}$$

If the plasma consists of one heavy ion species and electrons, the second term of Eq. (4-4) is approximately $\underset{\sim}{\nabla} \cdot (\rho \underset{\sim}{V}\underset{\sim}{V})$. If the plasma is quasineutral, $\rho_Q V \ll J$, so that Eq. (3-1a) implies that the first term of the right-hand side of (4-4) is negligible in comparison with the second term. Using Ampère's law and neglecting displacement current, and using the equation of

continuity, we finally obtain

$$\rho\left(\frac{\partial}{\partial t} + \underset{\sim}{V} \cdot \underset{\sim}{\nabla}\right)\underset{\sim}{V} + \underset{\sim}{\nabla} \cdot \underset{\approx}{P} = \frac{1}{4\pi}\left(\underset{\sim}{B} \cdot \underset{\sim}{\nabla}\underset{\sim}{B} - \frac{1}{2}\underset{\sim}{\nabla}B^2\right) \tag{4-5}$$

Thus, Eq. (4-5) is almost identical with (3-1c), the only difference being that $\underset{\approx}{P}$ is no longer required to be isotropic. Thus, the kinetic theory of hydromagnetic waves gives four equations analogous to the first four of Eqs. (3-1). The analogy between MHD and the moment equations can be extended. The second moment of (4-1) gives an equation that involves a third-rank heat-flow tensor:

$$\underset{\approx}{Q}_\alpha = \frac{1}{2} m_\alpha \int (\underset{\sim}{v} - \underset{\sim}{V}_\alpha)(\underset{\sim}{v} - \underset{\sim}{V}_\alpha)(\underset{\sim}{v} - \underset{\sim}{V}_\alpha) f_\alpha \, d^3v \tag{4-6}$$

The heat-flow vector is $(q_\alpha)_i = \sum_j (Q_\alpha)_{jji}$ and the heat equation analogous to Eq. (3-1e) is

$$\frac{\partial}{\partial t}\mathscr{T}r\underset{\approx}{p}_\alpha + \underset{\sim}{\nabla} \cdot (\underset{\sim}{V}_\alpha \mathscr{T}r\underset{\approx}{p}_\alpha + 2\underset{\sim}{q}_\alpha) + 2\underset{\approx}{p}_\alpha : (\underset{\sim}{\nabla}\underset{\sim}{V}_\alpha) = 0 \tag{4-7}$$

If $\underset{\approx}{p}$ were isotropic and $\underset{\sim}{V}_\alpha$ approximately the same for all species, Eq. (4-7) would yield Eq. (3-1e) with $\gamma = 5/3$.

In fact, $\underset{\approx}{p}$ is not generally isotropic. For hydromagnetic scales, the velocity distribution is, to a good approximation, independent of the direction of $\underset{\sim}{v}_\perp \times \underset{\sim}{B}$. Thus the stress tensor must have the form[64]

$$\underset{\approx}{p}_\alpha = \frac{p_{\parallel\alpha}\underset{\sim}{B}\underset{\sim}{B}}{B^2} + p_{\perp\alpha}\left(\underset{\approx}{1} - \frac{\underset{\sim}{B}\underset{\sim}{B}}{B^2}\right) \tag{4-8}$$

for all possible forms of the velocity distribution. This structure of the stress tensor has been confirmed by direct measurements of solar-wind protons.[127,191] If one attempts to construct a fluid theory of collisionless hydromagnetic waves, one must replace the pressure of MHD theory by two new variables $P_{\parallel}$ and $P_{\perp}$. The MHD equations are closed by setting $\underset{\sim}{\nabla} \cdot \underset{\sim}{q} = 0$

in Eq. (3-1e); the analogous collisionless theory would require two closure assumptions. The assumptions suggested by Chew, Goldberger, and Low[64] are

$$\left(\frac{\partial}{\partial t} + \underset{\sim}{v}_\alpha \cdot \underset{\sim}{\nabla}\right)\left(\frac{p_{\perp\alpha}}{n_\alpha B}\right) = 0 \tag{4-9a}$$

$$\left(\frac{\partial}{\partial t} + \underset{\sim}{v}_\alpha \cdot \underset{\sim}{\nabla}\right)\left(\frac{p_{\parallel\alpha} B^2}{n_\alpha^3}\right) = 0 \tag{4-9b}$$

The first equation corresponds to conservation of the first adiabatic invariant (or magnetic moment) $\mu_\alpha = (1/2)m_\alpha v_\perp^2/B$ and therefore should be valid for phenomena of hydromagnetic scale.[168] The physical interpretation of Eq. (4-9b) is not so straightforward. In fact, it turns out that generally, the use of Eq. (4-9b) in the theory of hydromagnetic waves give results that conflict with predictions of the full kinetic theory. The one advantage of using this double-adiabatic fluid theory (Eqs. (4-9)) in the theory of hydromagnetic waves is that it admits a relatively simple qualitative description of the effects of pressure anisotropy on wave propagation and plasma stability. These matters have been explored in some detail.[1,2,141] However, this theory does not significantly change the MHD classification scheme. We will not discuss the double-adiabatic theory further, but proceed directly to the full kinetic theory of hydromagnetic waves.

Kinetic Theory of Transverse Alfvén Waves. There is a self-consistent solution of the Vlasov-Maxwell equations with properties nearly identical with those of the MHD transverse Alfvén wave (Eqs. (3-4)). Specifically, the wave is noncompressive, its magnetic field varies in direction but not magnitude, and it propagates with constant phase velocity. Thus, there is a frame of reference in which the plasma and fields are in a steady state.

The proof of these assertions[16] starts with the assumption that such a plane wave and the corresponding wave frame exist. The Vlasov and Maxwell

equations are expanded in $\varepsilon = R_L/L$, where R_L is the gyroradius and L the characteristic scale (minimum wavelength) of the wave; $|\underset{\sim}{B}|$ is assumed constant, and spherical coordinates in momentum space, with their axis along the local magnetic-field direction, are used. The Vlasov and Maxwell equations may then be solved self-consistently through first order in ε, provided that the zeroth-order momentum distributions $f_o(p,\theta)$ are related to the magnetic-field strength by[16]

$$\frac{B^2}{4\pi} = \pi \sum_{\alpha} \int_0^{\infty} p^2 \, dp \int_0^{\pi} d\theta \, \sin\theta \, \frac{p^2(2\cos^2\theta - \sin^2\theta)}{[m_\alpha{}^2 + (p^2/c^2)]^{1/2}} \, f_o^{(\alpha)}(p,\theta) \qquad (4\text{-}10)$$

This expression is relativistically correct. Equation (4-10) gives the speed of propagation of the wave relative to the plasma. This wave propagates as a plane electromagnetic wave of arbitrary amplitude, associated with fluctuations in the direction but not the magnitude of $\underset{\sim}{B}$; the pressure and density fluctuations of the plasma are zero in the first approximation; and the electric field of the wave in the laboratory frame is $-\underset{\sim}{V} \times \underset{\sim}{B}/c$ plus a small $[0(\varepsilon^2)]$ electrostatic field parallel to $\underset{\sim}{B}$.

Discussion of Eq. (4-10) in its full relativistic form would go far beyond the scope of the present review. If in lowest order the particles have no relative streaming and if the zeroth-order heat flow vanishes, Eq. (4-10) reduces to

$$\left(\frac{V_{ph}}{c\cos\theta}\right)^2 = \frac{(B^2/4\pi) + P_\perp - P_{||}}{(B^2/4\pi) + P_\perp + \mathscr{E}} \qquad (4\text{-}11)$$

where V_{ph} is phase velocity in the (average) plasma rest frame, θ is the (constant) angle between $\underset{\sim}{B}$ and the propagation direction, and $\mathscr{E}$ is the energy density (including rest energy) of the plasma; B, $P_\perp$, $P_{||}$, and $\mathscr{E}$ are all evaluated in the local plasma rest frame. Equation (4-11) is true independently of wave amplitude; this relation had been found earlier in the

small-amplitude limit.[152,167] Note also that Eq. (4-11) can be satisfied only if

$$P_{||} < P_{\perp} + \frac{B^2}{4\pi} \tag{4-12}$$

If inequality (4-12) is violated, the plasma is unstable to the firehose instability.

Now consider the nonrelativistic limit, the case appropriate to the solar wind. Let $\Delta\underset{\sim}{V}_\alpha$ be the difference between $\underset{\sim}{V}_\alpha$ and the average plasma velocity. Rewrite the nonrelativistic limit of Eq. (4-10) as

$$\left(\frac{V_{ph}}{\cos\theta}\right)^2 = \frac{B^2}{4\pi\rho}\left[1 + \frac{4\pi}{B^2}(P_{\perp} - P_{||})\right] - \frac{1}{\rho}\sum_\alpha m_\alpha n_\alpha (\Delta\underset{\sim}{V}_\alpha)^2 \tag{4-13}$$

If $\Delta\underset{\sim}{V}_\alpha = 0$, Eq. (4-13) is just the nonrelativistic limit of (4-11). Equation (4-13) can be satisfied only if

$$P_{||} + \sum_\alpha m_\alpha n_\alpha (\Delta\underset{\sim}{V}_\alpha)^2 < P_{\perp} + \frac{B^2}{4\pi} \tag{4-14}$$

If (4-14) is violated, the plasma is firehose unstable. The stability criterion (4-14) was first discussed for the limit $\Delta\underset{\sim}{V}_\alpha = 0$[58,174] and generalized to interstreaming plasmas by Parker.[176]

In the wave frame, the plasma velocity is parallel to the magnetic field. Therefore the fluctuating part of the velocity $\Delta\underset{\sim}{V}_\perp$ is related to the fluctuating magnetic field $\Delta\underset{\sim}{B}_\perp$ by

$$\begin{aligned}\Delta\underset{\sim}{V}_\perp &= -\frac{V_{ph}}{|\cos\theta|}\frac{\Delta\underset{\sim}{B}_\perp}{B}\,\mathrm{sgn}\,B_z \\ &= \mp\frac{\Delta\underset{\sim}{B}_\perp}{(4\pi\rho)^{1/2}}\left[1 + \frac{4\pi}{B^2}(P_{\perp} - P_{||}) - \frac{4\pi}{B^2}\sum_\alpha m_\alpha n_\alpha (\Delta\underset{\sim}{V}_\alpha)^2\right]^{1/2}\end{aligned} \tag{4-15}$$

The upper sign is used if $\underset{\sim}{B}$ is more nearly parallel than antiparallel to the propagation direction, and the lower sign is used in the opposite case. Equation (4-15) is thus the appropriate generalization of Eq. (3-4d).

Thus, the large-amplitude transverse Alfvén wave appears in collisionless kinetic theory as well as in MHD theory. The reader should be cautioned that the theory of that wave is based explicitly on the assumption that cyclotron (or synchrotron) resonances are negligible, i.e., that a negligible number of particles are moving so fast that the wave period is Doppler-shifted to near the cyclotron frequency in the particle frame. Moveover, the nonlinear stability of the collisionless transverse Alfvén wave seems not to have been studied explicitly, although related MHD studies[186] may be a useful guide. Lastly, radiation of the plasma has been neglected, and this factor must be considered when the relativistic theory is applied.

Kinetic Theory of Stationary Structures. The MHD theory of plane fluctuations admits two solutions, the tangential pressure balance and the "entropy wave," which are stationary in the plasma rest frame. It turns out that the tangential pressure balance is essentially the same in collisionless as in collisional plasma. It can be shown from the guiding-center theory (or by expanding the Vlasov-Maxwell equations in ε) that equilibrium is possible for plane variations transverse to the magnetic field if[59]

$$\nabla\left(P_{\perp} + \frac{B^2}{8\pi}\right) = 0 \tag{4-16}$$

Components of flow velocity and pressure $P_{||}$ along the magnetic-field direction are unrestricted, although the values of these and other quantities can affect the stability of the equilibrium.[169]

On the other hand, the MHD notion of the entropy wave is essentially irrelevant to collisionless plasmas. This is fairly obvious physically because an entropy wave would have a component of magnetic field parallel to its density gradient, permitting particles to diffuse along the gradient.[69]

Thus an entropy wave would disappear in a time of order $L \cos \theta / v_{th}$, where v_{th} is the proton thermal velocity, and entropy waves in the solar-wind microstructure would be eradicated in a time short compared with the characteristic expansion time of the wind.

This conjecture can be checked formally in the limit of small amplitudes. For example, it can be shown that no small-amplitude stationary structure (apart from the tangential pressure balance) whose characteristic length L is long compared with the Debye length can exist in a collisionless plasma.[14] However, the dispersion relation of small-amplitude hydromagnetic fluctuations in collisionless plasmas admits solutions of purely imaginary frequency that may be identified as rapidly decaying entropy waves; these fluctuations are discussed further in the next section.

Kinetic Theory of Small-Amplitude Hydromagnetic Waves. We have seen that the large-amplitude transverse Alfvén wave and transverse pressure balance occur in kinetic theory as well as MHD theory. One expects intuitively that magnetoacoustic waves of large amplitude can exist in collisionless plasma. However, except for the special case of the fast mode propagating exactly transverse to the magnetic field, the analysis of large-amplitude modes analogous to the MHD fast and slow modes has not been carried out in the framework of kinetic theory. Therefore, at present, rigorous analysis of magnetoacoustic waves in collisionless plasma is limited to the small-amplitude theory.

The small-amplitude analysis is based on the linearized Vlasov-Maxwell equations:

$$\left(\frac{\partial}{\partial t} + \underset{\sim}{v} \cdot \underset{\sim}{\nabla}\right) \delta f_\alpha + \frac{q_\alpha}{m_\alpha} \left(\frac{\underset{\sim}{v}}{c} \times \underset{\sim}{B}_o\right) \cdot \frac{\partial}{\partial \underset{\sim}{v}} \delta f_\alpha = - \frac{q_\alpha}{m_\alpha} \left(\underset{\sim\sim}{\delta E} + \frac{\underset{\sim}{v}}{c} \times \underset{\sim\sim}{\delta B}\right) \cdot \frac{\partial}{\partial \underset{\sim}{v}} f_\alpha^{(0)} \qquad (4\text{-}17a)$$

$$\nabla \times \delta\underset{\sim}{\underset{\sim}{B}} - \frac{1}{c}\frac{\partial}{\partial t}\delta\underset{\sim}{\underset{\sim}{E}} = \frac{4\pi}{c}\sum_{\alpha} q_\alpha \int \underset{\sim}{v}\delta f_\alpha \, d^3v \tag{4-17b}$$

$$\nabla \cdot \delta\underset{\sim}{\underset{\sim}{E}} = 4\pi\sum_{\alpha} q_\alpha \int \delta f_\alpha \, d^3v \tag{4-17c}$$

$$\nabla \times \delta\underset{\sim}{\underset{\sim}{E}} + \frac{1}{c}\frac{\partial}{\partial t}\delta\underset{\sim}{\underset{\sim}{B}} = 0 \tag{4-17d}$$

$$\nabla \cdot \delta\underset{\sim}{\underset{\sim}{B}} = 0 \tag{4-17e}$$

Here $f_\alpha^{(0)}$ and $\underset{\sim}{B}_o$ are the unperturbed spatially uniform background velocity distribution and magnetic field. These equations are solved self-consistently under the assumption that $\varepsilon_\alpha \sim kR_L^{(\alpha)} \ll 1$, $|\omega/\Omega_\alpha| \ll 1$ (k is a typical wave number and ω, a typical frequency). One may either solve the general problem[3,4,160,210] and then take the limit $\varepsilon \ll 1$, or approximate Eqs. (4-17) for small ε_α and then solve the approximate equations.[57,58,91] The standard method of solution is to Fourier analyze the equations spatially and then solve the resulting temporal differential equations either by Laplace analysis[146] or by integration over the unperturbed particle orbits.[210] The result is that, long after the initial disturbance, the Fourier components of the perturbed fields and moments of the perturbed velocity distributions (but *not* the velocity distributions themselves) oscillate in proportion to $\exp(-i\omega_{\underset{\sim}{k}}t)$ where the complex frequency $\omega_{\underset{\sim}{k}}$ is related to the wave vector $\underset{\sim}{k}$ by a dispersion relation

$$D(\underset{\sim}{k}, \omega_{\underset{\sim}{k}}) = 0 \tag{4-18}$$

The mathematical basis of this calculation is discussed in detail in textbooks.[3,4,160,210]

For our purposes, it is sufficient to consider the fluctuations as a superposition of plane waves varying as $\exp(i\underset{\sim}{k} \cdot \underset{\sim}{x} - i\omega_{\underset{\sim}{k}}t)$. Then solution

of Vlasov's equation, using Faraday's law (4-17d) to express magnetic fluctuations in terms of electric fluctuations, yields a linear relationship between the fluctuating electric fields and bulk velocities:

$$\delta V^{(\alpha)}_{\underset{\sim}{k},\omega} = \frac{c}{B_o} \underset{\approx}{M}_\alpha(\underset{\sim}{k},\omega) \cdot \underset{\sim}{\delta E}_{\underset{\sim}{k},\omega} \tag{4-19}$$

$\underset{\approx}{M}_\alpha$ is known as the effective mobility tensor and depends on the unperturbed properties of the plasma and magnetic field. The current density is thus (if $\underset{\sim}{V}^0_\alpha = 0$)

$$\underset{\sim}{\delta J}_{\underset{\sim}{k},\omega} = \left[\sum_\alpha \frac{q_\alpha n_0^{(\alpha)} c}{B_o} \underset{\approx}{M}_\alpha\right] \cdot \underset{\sim}{\delta E}_{\underset{\sim}{k},\omega} \equiv \frac{\omega}{4\pi i}\left[\underset{\approx}{K}(\underset{\sim}{k},\omega) - \underset{\approx}{1}\right] \cdot \underset{\sim}{\delta E}_{\underset{\sim}{k},\omega} \tag{4-20}$$

where $\underset{\approx}{K}$ is the effective dielectric tensor. Equation (4-20) gives the currents due to particle motions in the fluctuating electric fields. However, these currents and their associated charge densities are also the sources of the fluctuating fields. Substituting Eq. (4-20) in (4-17b) yields

$$\frac{c^2}{\omega^2}(k^2\underset{\approx}{1} - \underset{\sim}{k}\underset{\sim}{k}) \cdot \underset{\sim}{\delta E}_{\underset{\sim}{k},\omega} = \underset{\approx}{K}(\underset{\sim}{k},\omega) \cdot \underset{\sim}{\delta E}_{\underset{\sim}{k},\omega} \tag{4-21}$$

Equation (4-17d) was used to relate the magnetic fluctuations to electric fluctuation; if (4-17b) is satisfied, conservation of charge guarantees that (4-17c) is also satisfied. Equation (4-21) has nontrivial solutions if and only if

$$\det\left[\frac{c^2}{\omega^2}(\underset{\sim}{k}\underset{\sim}{k} - k^2\underset{\approx}{1}) + \underset{\approx}{K}(\underset{\sim}{k},\omega)\right] = 0 \tag{4-22}$$

The dispersion relation (4-22), of course, agrees with relations (4-18) obtained by a fully rigorous approach.

Equation (4-22) is valid for all frequencies and wave numbers. However, $\underset{\approx}{K}$ and the related $\underset{\approx}{M}_\alpha$ are complicated functionals of the unperturbed

velocity distributions; they are tabulated in many books.[3,4,160,210] For example, if $V_{||\alpha}^{(0)} = 0$,

$$M_{yz}^{(\alpha)} = -M_{zy}^{(\alpha)}$$
$$= \frac{2\pi|\Omega_\alpha|}{n_\alpha\omega} \sum_{m=-\infty}^{\infty} \int_0^\infty dv_\perp \int_{-\infty}^{\infty} dv_{||} \frac{v_\perp v_{||} J_m J_m'}{m|\Omega_\alpha| - \omega + k_{||}v_{||}} \left[(\omega - k_{||}v_{||}) \frac{\partial f_\alpha^{(0)}}{\partial v_\perp} + k_{||} v_\perp \frac{\partial f_\alpha^{(0)}}{\partial v_{||}} \right] \tag{4-23}$$

in a coordinate system in which $\underset{\sim}{B}_o$ lies along the z axis and $\underset{\sim}{k}$ lies in the x-z plane.[3] Here $J_m = J_m(k_\perp v_\perp/|\Omega_\alpha|)$ is the Bessel function of order m, $J_m'(x) = dJ_m/dx$, $v_{||} = v_z$, $v_\perp = |\underset{\sim}{v} - v_{||}\underset{\sim}{B}_o/B_o|$. Equation (4-23) applies for $\text{Im}\ \omega > 0$; if $\text{Im}\ \omega < 0$, $\underset{\approx}{M}$ is obtained by analytic continuation into the lower half ω plane. Note that the integrand of Equation (4-23) produces resonance for

$$k_{||}v_{||} \simeq \omega_{\underset{\sim}{k}} \pm n|\Omega_\alpha| \qquad (n = 0, 1, 2, \ldots) \tag{4-24}$$

i.e., when the wave frequency in the particle frame is Doppler-shifted to either near zero or near an integral multiple of the gyrofrequency. The first kind of resonance ($n = 0$) is called a Landau (or Cerenkov) resonance, and the second kind ($n = \pm1, \pm2, \ldots$) is called a cyclotron resonance or gyroresonance. If $\omega_{\underset{\sim}{k}} = \nu_{\underset{\sim}{k}} + i\gamma_{\underset{\sim}{k}}$, where $\nu_{\underset{\sim}{k}}$ and $\gamma_{\underset{\sim}{k}}$ are real and $|\gamma_{\underset{\sim}{k}}| \ll |\nu_{\underset{\sim}{k}}|$, then

$$\frac{1}{i(k_{||}v_{||} - \omega_{\underset{\sim}{k}} \pm n\Omega_\alpha)} \simeq P \frac{1}{i(k_{||}v_{||} - \nu_{\underset{\sim}{k}} \pm n\Omega_\alpha)} + \pi\delta(k_{||}v_{||} - \nu_{\underset{\sim}{k}} \pm n\Omega_\alpha) \tag{4-25}$$

in Eq. (4-23). Thus resonance has a special role in relating real and imaginary parts of components of $\underset{\approx}{K}$, and thus by Eq. (4-22), in relating real and imaginary parts of $\omega_{\underset{\sim}{k}}$. But $\gamma_{\underset{\sim}{k}} = \text{Im}\ \omega_{\underset{\sim}{k}}$ is just the growth ($\gamma_{\underset{\sim}{k}} > 0$) or damping ($\gamma_{\underset{\sim}{k}} < 0$) rate of the kth wave. Therefore, resonant particles are of central importance in determining the growth or damping of a wave. This fact can be understood on physical grounds for the Landau and first cyclotron resonances

by noting that resonant particles see electric fields of the wave as either static (Landau resonance) or oscillating at the gyrofrequency (first cyclotron resonance).

For hydromagnetic waves, $|\omega_{\underset{\sim}{k}}| << |\Omega_\alpha|$ and, for thermal particles, $|k_{||} v_{||}| << |\Omega_\alpha|$, $|k_\perp v_\perp| << |\Omega_\alpha|$ for conditions typical of the solar wind. Thus, *if there is a negligible number of suprathermal particles at the cyclotron resonances*, growth or damping of small-amplitude hydromagnetic waves is affected only by the Landau resonance. Under these assumptions, the mobility and dielectric tensors are appreciably simplified, e.g., Eq. (4-23) becomes

$$M_{yz}^{(\alpha)} = -M_{zy}^{(\alpha)} = -\frac{\pi k_\perp}{n_\alpha} \int_{-\infty}^{\infty} dv_{||} \int_0^{\infty} dv_\perp \frac{v_\perp^3 \, \partial f_\alpha^{(0)}/\partial v_{||}}{k_{||} v_{||} - \omega} \qquad (4\text{-}26)$$

It is readily shown that, in a coordinate system in which $\underset{\sim}{B}_o$ lies along the z axis and $\underset{\sim}{k}$ lies in the x-z plane, the order of magnitude of the dielectric tensor is

$$\underset{\approx}{K} \sim \left(\frac{c}{C_A}\right)^2 \begin{pmatrix} \varepsilon & \varepsilon^2 & \varepsilon \\ \varepsilon^2 & \varepsilon & 1 \\ \varepsilon & 1 & \varepsilon^{-1} \end{pmatrix} \qquad (4\text{-}27)$$

so that the dispersion relation (4-22) becomes

$$\left[K_{xx} - \left(\frac{k_{||} c}{\omega}\right)\right]^2 \left\{\left[K_{yy} - \left(\frac{kc}{\omega}\right)^2\right] K_{zz} - K_{zy}^2\right\} = \left(\frac{kc}{\omega}\right)^6 \cdot O(\varepsilon^2) \qquad (4\text{-}28)$$

This equation can readily be generalized to include relative drifts between the plasma species. This dispersion relation was first analyzed in various special limits by Stepanov,[209] Kitsenko and Stepanov,[144] and Stix.[210] The simplest root of Eq. (4-28) comes from

$$K_{xx} = \left(\frac{k_{||} c}{\omega}\right)^2 \qquad (4\text{-}29)$$

Since the hydromagnetic limit $K_{xx} = (c/C_A)^2[1 + (4\pi k_{||}{}^2 C_A{}^2/\omega^2)\,(P_{||} - P_\perp)/B_o{}^2]$ (neglecting terms or order $C_A{}^2/c^2$), Eq. (4-29) implies that

$$\left(\frac{\omega}{k_{||} C_A}\right)^2 = 1 + \frac{4\pi}{B_o{}^2}\,(P_\perp - P_{||}) \tag{4-30}$$

This equation is the familiar dispersion relation for the transverse Alfvén mode (in the absence of interparticle streaming). As we have seen in the previous section, this result is a special case of the theory of the large-amplitude Alfvén wave and so gives us no new information. We remark that in the small-amplitude limit the magnetic fluctuations of this wave are linearly polarized, but that this linear polarization is simply the limit of the finite-amplitude condition $B^2 = \text{const}$, just as in MHD theory. The other roots of Eq. (4-28) are roots of

$$\left[K_{yy} - \left(\frac{kc}{\omega}\right)^2\right] K_{zz} - K_{yz}^2 = 0 \tag{4-31}$$

Equation (4-31) may be expressed as a relation between $u = \omega/(|k_{||}|C_A)$ and $\theta = [\measuredangle(\underset{\sim}{k}, \underset{\sim}{B}_o)]$ of the form

$$\cot^2\theta = \frac{S(u)}{\alpha - u^2} \tag{4-32}$$

where $\alpha = 1 + 4\pi(P_\perp - P_{||})/B_o{}^2$ and $S(u)$ is an analytic function of the complex variable u. For the special case where $f_\alpha^{(0)}$ is bi-Maxwellian, i.e.,

$$f_\alpha^{(0)} = n_\alpha \left(\frac{m_\alpha}{2\pi k_B T_{||\alpha}}\right)^{1/2}\left(\frac{m_\alpha}{2\pi k_\perp T_{\perp\alpha}}\right) \exp\left(-\frac{m_\alpha v_{||}{}^2}{2k_B T_{||\alpha}} - \frac{m_\alpha v_\perp{}^2}{2k_B T_{\perp\alpha}}\right) \tag{4-33}$$

we have, for a hydrogen plasma,[10]

$$-S(u) = 1 + \beta_\perp + \frac{1}{4}\left[\frac{\beta_{\perp+}^2}{\beta_{||+}}\,Z'(y_+) + \frac{\beta_{\perp-}^2}{\beta_{||-}}\,Z'(y_-)\right] + \frac{\beta_\perp{}^2}{4}\,\frac{Z'(y_+)Z'(y_-)}{\beta_{||-}Z'(y_+) + \beta_{||+}Z'(y_-)} \tag{4-34}$$

where

$$\beta_{||,\perp} = \frac{8\pi P_{||,\perp}}{B^2} , \qquad \beta_{||,\perp\alpha} = \frac{8\pi P_{||,\perp\alpha}}{B^2} ,$$

$$y_{\pm} = \left(\frac{m_{\pm}}{2k_B T_{||\pm}}\right)^{1/2}\left(\frac{\omega}{|k_{||}|}\right) = \left(\frac{m_{\pm}}{m_{+}}\right)^{1/2} \frac{u}{\beta_{||\pm}^{1/2}} , \tag{4-35}$$

the subscripts $\pm$ refer to protons and electrons, and $Z'(y) = dZ/dy$ where Z is the Fried-Conte plasma dispersion function.[99]

In general, Eq. (4-32) must be solved numerically, although some special limits and asymptotic approximations are available.[144,209,210] For example, Eq. (4-32) reduces to the familiar cold-plasma dispersion relation for the fast hydromagnetic wave

$$\omega^2 = k^2 C_A^2 \tag{4-36}$$

in the limit $T_{||,\perp\pm} \to 0$. In the limit $\theta \to \pi/2 (\underset{\sim}{k} \cdot \underset{\sim}{B}_o \to 0)$, if $\omega/k \neq 0$, then $u \to \infty$ and $-S(u) \simeq 1 + \beta_{\perp}$, so that asymptotically Eq. (4-32) becomes $\cot^2 \theta \simeq (1 + \beta_{\perp})/u^2$, i.e.,

$$\frac{\omega^2}{k^2} \simeq C_A^2 + \frac{2P_{\perp}}{\rho} \tag{4-37}$$

Thus, the collisionless fast magnetoacoustic mode propagates across the magnetic field like the corresponding MHD mode for $\gamma = 2$. In the limit $\theta \to 0$, Eq. (4-32) is satisfied if either $u^2 = \alpha$, i.e.,

$$\frac{\omega^2}{k^2 C_A^2} = 1 + \frac{4\pi(P_{\perp} - P_{||})}{B^2} \tag{4-38a}$$

or $S(u) \to \infty$, e.g., if

$$\beta_{||-} Z'(y_+) + \beta_{||+} Z'(y_-) = 0 \tag{4-38b}$$

Equation (4-38a) is the dispersion relation for the small-amplitude magnetoacoustic wave propagating along $\underset{\sim}{B}_o$ and is the same as the Alfvén wave

dispersion relation, just as in the MHD theory of small-amplitude waves. Equation (4-38b) is the long-wavelength form of the dispersion relation for ion sound waves propagating along $\underset{\sim}{B}_o$. This wave is quite different from the corresponding MHD wave, as the collisionless ion sound wave is known both from theory and laboratory experiment to be strongly damped unless $T_{||-} >> T_{||+}$.[100,234] $T_{||-}$ is typically only two to three times larger than $T_{||+}$ in the solar wind at 1 AU so that normally interplanetary ion sound waves should be strongly Landau damped.

Equation (4-32) is in a convenient form for numerical integration. The solutions of Eq. (4-32) all lie on contours Γ in the complex plane such that $\mathrm{Im}[S(u)/(\alpha - u^2)] = 0$. Those sections of the Γ contours such that $\mathrm{Re}[S(u)/(\alpha - u^2)] \geq 0$ are then the entire set of solutions of Eq. (4-32). For each solution u there is a corresponding propagation direction $\theta(u)$. It has been shown[10] that unstable solutions ($\mathrm{Im}\, u > 0$) must be purely imaginary,† so that the stability or instability of a bi-Maxwellian plasma to hydromagnetic modes is determined by the dispersion relation at $u = 0$. The plasma is thus unstable if $S(0)/\alpha > 0$, i.e., if either

$$\alpha < 0 \tag{4-39a}$$

or

$$Q \equiv 1 + \beta_\perp\left(1 - \frac{\beta_\perp}{\beta_{||}}\right) - \frac{1}{2\beta_{||}}\,\frac{(\beta_{||+}\beta_{\perp-} - \beta_{||-}\beta_{\perp+})^2}{\beta_{||-}\beta_{||+}} < 0 \tag{4-39b}$$

The instability criterion (4-39a) is the same as that for the Alfvén firehose instability. However, the magnetoacoustic waves grow slower than Alfvén waves for $\theta \neq 0$ and are stable for $\theta > \theta_o$ (or $\pi - \theta < \pi - \theta_o$) where θ_o

---

†Chandrasekhar, Kaufman, and Watson[58] presented a proof, due to Rosenbluth, of this fact for cylindrical geometry.

is a critical angle given by $\cot^2 \theta_o = -Q/\alpha$. By contrast, the firehose unstable Alfvén wave grows for all angles, with a growth rate proportional to $|\cos \theta|$. The instability criterion (4-39b) applies to the so-called mirror instability ($P_\perp > P_\parallel$). If this criterion is satisfied, magneto-acoustic waves are unstable for $|\pi/2 - \theta| < |\pi/2 - \theta_o|$.

If the plasma is stable under criteria (4-39), there is still an infinite set of pure imaginary solutions $u = iw$ where $w \leq w_o < 0$.[10,214] These fluctuations are nonpropagating, rapidly damped structures that may be identified as the analog of the MHD entropy wave. The fact that these fluctuations are strongly damped supports the assertion of the previous section, made on physical grounds, that entropy waves should not exist in the interplanetary medium.

We have already seen that in certain limits (cf. Eqs. (4-36, 37, 38a)) the collisionless dispersion relation gives undamped waves much like their MHD analog. Thus, one expects that near these limits weakly damped solutions exist. Assume that u_o is real and $\mathrm{Re}[S(u_o)/(\alpha - u_o^2)] \geq 0$. Then if $|\mathrm{Im}\ S(u_o)| \ll |\mathrm{Re}\ S(u_o)|$, $u = u_o + iV$ with

$$V = -\left[\frac{\mathrm{Im}\ S(u_o)}{\alpha - u_o^2}\right] \Bigg/ \frac{d}{du_o}\left[\frac{\mathrm{Re}\ S(u_o)}{\alpha - u_o^2}\right] \tag{4-40}$$

is an approximate solution of Eq. (4-32).

Although some useful information can be extracted from Eq. (4-40), direct numerical integration of Eq. (4-32) gives a much more complete picture of the damped-wave solutions.[10,214] Figure 2 gives solution contours Γ in a portion of the complex u plane for an isotropic plasma of $\beta_{\parallel +} = \beta_{\perp +} = \beta_{\parallel -} = \beta_{\perp -} = 1/2$ Because the plot is logarithmic, it is not possible to show the segment of the imaginary axis which is also a solution contour (the "entropy-wave"-like solution); this segment consists of all imaginary numbers $u = iw$ where $w < -0.45$.

In the region of the u plane shown, there are four distinct trajectories. The main one begins at $u = 1$ and runs through two minima before going asymptotically to the real axis; this trajectory corresponds to the fast magnetoacoustic wave. The strongly damped "island" trajectory corresponds to the ion sound wave (or slow magnetoacoustic wave). In addition, there are many other very strongly damped branches, two of which are shown in Fig. 2.

We focus on the two least damped modes. These are analogous to the fast and slow magnetoacoustic waves of the MHD theory. Figure 3 shows the real parts of their phase velocities as functions of propagation direction, for two different plasmas. The phase velocities predicted by the double-adiabatic fluid model are also shown for comparison; the phase velocities predicted by the two theories are qualitatively similar but quantitatively different. The results of the full kinetic theory should, of course, be the more reliable.

The damping rates for these modes in the same plasmas are shown in Fig. 4. For the $\beta = 1$ plasma, the slow mode is very strongly damped ($|\text{Im } \alpha| \sim |\text{Re } \omega|$) for all propagation directions. The fast mode is less strongly, but not negligibly, damped ($|\text{Im } \omega| \lesssim 0.05 \ |\text{Re } \omega|$), and the damping curve has two peaks. The peak at smaller propagation angle ($\theta \sim 25°$) corresponds to maximum proton resonance and the other peak ($\theta \sim 87°$) corresponds to maximum electron resonance. The electron damping peak lies near 90° because at electron resonance $V_{th}^{(e)} \sim |\omega/k_{||}| = |\omega/k \cos \theta| >> |\omega/k|$. For the $\beta = 5$ plasma, the electron damping peak is similar to that for $\beta = 1$ (but somewhat stronger), and ion resonant damping is much stronger. Just as in MHD theory, at high β the slow mode is degenerate with the Alfvén mode and the fast mode is degenerate with the sound wave at $\theta = 0$. Thus the slow mode propagates undamped at the Alfvén speed at $\theta = 0$ but is strongly damped

for θ greater than a few degrees; the fast mode is undamped at $\theta = 90°$ but is strongly damped at other angles.

Equation (4-32) depends on only four plasma parameters, $\beta_{\perp\pm}$ and $\beta_{\parallel\pm}$. Barnes[10] solved this dispersion relation over a fairly broad range of these parameters. He found that, unless $T_{\parallel e} \gg T_{\parallel p}$, the sound-like mode is so strongly damped ($|\text{Im } \omega| \sim |\text{Re } \omega|$) that it can scarcely be said to propagate. The least-damped magnetoacoustic wave exhibits a fairly strong electron damping peak unless $\beta_- \ll 1$, but this damping occurs only for a relatively small range of propagation directions ($\theta \gtrsim 75°$). Proton damping occurs over a broader range of θ but is quite sensitive to $\beta_{\parallel +}$. For an isotropic plasma it turns out that $\exp(-1/\beta_p)$ is a good order-of-magnitude estimate of the maximum value of $|\text{Im } \omega/\omega|$ for proton damping unless $\beta_+ \ll 1$. Burlaga, Ogilvie, and Fairfield[45] reported that measured values of β_+ in the solar-wind range from less than 0.1 to more than 5. If we take $\beta_+ \sim 0.3$-0.5 as typical at 1 AU, compressive waves would be damped out in 10-100 wave periods. Therefore, any magnetoacoustic waves of (spacecraft frame) period $\lesssim 1$ hr in the interplanetary medium near 1 AU would be expected to be of local origin.

Physical Mechanism of Magnetoacoustic Wave Dissipation. It is important to have an intuitive picture of the collisionless damping process. Such a picture increases one's confidence in the rather abstract calculations discussed above. Furthermore, theoretical studies of large-amplitude collisionless magnetoacoustic waves have been heuristic and require a sound intuitive basis. It is fairly obvious that the collisionless damping of magnetoacoustic waves is associated with the Landau resonance between waves and particles and thus is usually called Landau damping. However, Landau damping requires not only a substantial number of particles moving at the resonant velocity

$v_{||} \simeq \omega/k_{||}$, but also the existence of a suitable accelerating force. In the usual heuristic pictures of the Landau damping of electrostatic plasma oscillations,[82,132,236] the accelerating force is provided by the electrostatic field of the wave. Such an electrostatic field presumably also accounts for the Landau damping of the sound-like magnetoacoustic wave.

However, the damping mechanism for the least-damped magnetoacoustic wave (= the fast wave for $\beta < 1$) is a little more complicated. Stix[210] pointed out that as guiding-center theory[168] is appropriate for particles in hydromagnetic waves, the guiding center of such a particle will be accelerated along the magnetic-field direction according to

$$m \frac{dv_{||}}{dt} = qE_{||} - \mu \frac{\partial |\underset{\sim}{B}|}{\partial s} \tag{4-41}$$

where $\mu = (1/2)mv_{\perp}^2/B$ is the effective magnetic moment of the particle and $\partial/\partial s$ is the gradient along the local magnetic field. Stix argued that even if $E_{||}$ were zero in a magnetoacoustic wave (it is not) the magnetic mirroring force $-\mu(\partial B/\partial s)$ would accelerate resonant particles in the same way as $qE_{||}$ accelerates resonant particles in an electrostatic wave. The magnetic acceleration process has been dubbed "transit time heating" and is analogous to the Fermi cosmic-ray acceleration mechanism. On the average, the wave tends to bring the velocities of resonant particles toward $\omega/k_{||}$ and results in a net exchange of energy between the wave and the resonant particles; thus, e.g., if $\partial f/\partial v_{||}\big|_{v_{||}=\omega/k_{||}(>0)} < 0$, there is a net transfer of energy to the particles and the wave is damped. Stix showed that equating the rate of particle energy gain with the rate of wave energy loss gives a reasonable estimate of the damping rate if $|\text{Im } \omega| \ll |\text{Re } \omega|$.

In fact, the complete picture of the damping process is still more complicated. Barnes[11] analyzed the weak limit of the electron damping process

in detail. He showed that the mirror force $-\mu(\partial B/\partial s)$ by itself would produce charge separation and that an electrostatic field $E_{||}(\sim\varepsilon E_{\perp})$ must be set up to maintain quasineutrality in the plasma. If the zeroth-order electron velocity distribution factors into $F(v_{||})G(v_{\perp})$, this electrostatic field for waves near electron resonance is given by

$$E_{||} = -\frac{\bar{\mu}}{|e|}\frac{\partial B}{\partial s} \tag{4-42}$$

where $\bar{\mu}$ is the mean magnetic moment of all electrons in the plasma. Thus, Eq. (4-41) becomes

$$m_e \frac{dv_{||}}{dt} = (\bar{\mu} - \mu)\frac{\partial B}{\partial s} \tag{4-43}$$

Barnes analyzed acceleration of test electrons, according to the force law (4-43), in a stochastic field of hydromagnetic waves, generalizing the stochastic acceleration theory that Sturrock[213] developed for electrostatic fluctuations. Sturrock showed that the electrostatic Landau damping rate could be recovered from his theory. Barnes made the analogous argument for magnetoacoustic waves, equating the energy gain of the test particles to the energy loss of the waves. The energy lost per unit volume per unit time is 2 Im $\omega\mathscr{W}$ where $\mathscr{W}$ is the wave energy density. The resulting expression for Im ω is

$$\text{Im }\omega = \frac{2\pi^2 n_e}{m_e}\frac{}{(\mu - \bar{\mu})^2}\frac{C_A^2 \sin^2\theta}{V_{ph}^2}\frac{(\text{Re }\omega)k_{||}}{|k_{||}|}\mathscr{F}'\left(\frac{\omega}{k_{||}}\right) \tag{4-44}$$

where the bar denotes averaging over all electrons, $V_{ph} = \text{Re }\omega/k$, and

$$\mathscr{F}(V_{||}) = \frac{1}{n_e\left(v_{\perp}^2 - \overline{v_{\perp}^2}\right)^2}\int d^2v_{\perp}\left(v_{\perp}^2 - \overline{v_{\perp}^2}\right)^2 f_e(\underset{\sim}{v}) \tag{4-45}$$

Equation (4-44) is consistent with (4-40) for bi-Maxwellian electrons.

To summarize, in fast-mode damping the resonant acceleration is due both to the mirror force $-\mu(\partial B/\partial s)$ and electrostatic force $-eE_{||}$, and $E_{||}$ must

exist because the mirror force by itself would produce charge separation. The preceding picture was developed for resonant electron acceleration, but can be generalized to include ion acceleration. Barnes[12] worked out the general expression for the resonant heating rate $\partial \mathscr{E}_{res}^{(\alpha)}/\partial t$ in the quasi-linear approximation. We only state the result:

$$\frac{4\pi}{|\underset{\sim}{\delta B}_{\underset{\sim}{k}}|^2}\frac{\partial \mathscr{E}_{res}^{(\alpha)}(\underset{\sim}{k})}{\partial t} = -\frac{\pi n_\alpha k_{||} k_\perp^2 \omega}{|k_{||}| m_\alpha k^2}\sin^2\theta\left\{\overline{\mu_\alpha^2}\, F'_{3,\alpha}\left(\frac{\omega}{k_{||}}\right)\right.$$

$$\left. -(\bar{\mu}_\alpha)^2\left[2\mathrm{Re}(\xi_\alpha)F'_{2,\alpha}\left(\frac{\omega}{k_{||}}\right) - |\xi_\alpha|^2 F'_{1,\alpha}\left(\frac{\omega}{k_{||}}\right)\right]\right\} \qquad (4\text{-}46)$$

where $\underset{\sim}{\delta B}_{\underset{\sim}{k}}$ is the kth Fourier component of the fluctuating magnetic field, $\bar{\mu}_\alpha$ and $\overline{\mu_\alpha^2}$ are, respectively, the mean and mean-square magnetic moments of the αth charge species, $\xi_\alpha = q_\alpha \delta E_{||_{\underset{\sim}{k}}}/(ik_{||}\bar{\mu}_\alpha \delta B_{||_{\underset{\sim}{k}}}) = q_\alpha \delta E_{||_{\underset{\sim}{k}}}/[\bar{\mu}_\alpha \partial(\delta|\underset{\sim}{B}_{\underset{\sim}{k}}|)/\partial s]$, and

$$F_{n,\alpha}(v_{||}) = \left\{\overline{\left[v_{\perp\alpha}^{2(n-1)}\right]}\right\}^{-1}\int d^2 v_\perp \cdot v_\perp^{2(n-1)} f_\alpha^{(0)}(\underset{\sim}{v}) \qquad (4\text{-}47)$$

If $f_0(\underset{\sim}{v}) = F(v_{||})G(v_\perp)$, then $F_1 = F_2 = F_3 = F$; $|\underset{\sim}{\delta B}_{\underset{\sim}{k}}|^2/4\pi$ is an order-of-magnitude estimate of the wave-energy density, so that Eq. (4-46) summed over α is a good estimate of $2\,\mathrm{Im}\,\omega_k$. An accurate calculation (to $O(\mathrm{Im}\,\omega_k/\omega_k)$) may be made by obtaining the wave-energy density $\mathscr{W}$, multiplying Eq. (4-46) by $4\pi|\underset{\sim}{\delta B}_{\underset{\sim}{k}}|^2$, and summing over α. The resulting expression is exactly analogous to the hydromagnetic limit of the Kennel-Wong expansion[142] of general $\mathrm{Im}\,\omega$. The result is useful but, as both $\mathscr{W}$ and f_α are determined by the dispersion relation, exact solution of the dispersion relation is still required if accurate numerical results are desired. For order-of-magnitude estimates, $\mathscr{W} \sim |\underset{\sim}{\delta B}_{\underset{\sim}{k}}|^2/4\pi$ and $|\xi_\alpha| \sim O(1)$ are sufficient. It is clear from Eq. (4-46) or (4-44) that some non-Maxwellian velocity

distributions may admit resonant growth of magnetoacoustic waves for certain propagation directions. In particular, streaming may produce unstable situations.[210]

Large-Amplitude Collisionless Magnetoacoustic Waves and Related Topics of Nonlinear Theory. There is apparently no rigorous unified theory of large-amplitude magnetoacoustic waves that would be appropriate for interplanetary conditions. Theoretical work on this topic is typically based on MHD theory plus *ad hoc* notions borrowed from collisionless theory. Nevertheless, work done so far probably has some validity and can be tested against interplanetary observations.

The interplanetary medium is a fairly high β plasma in which the electron temperature is rarely more than three to four times higher than the proton temperature. As we have seen, small-amplitude theory predicts that, under these plasma conditions, all magnetoacoustic waves are strongly damped for most directions of propagation. This fast suggests that magnetoacoustic waves ought to be rare in the interplanetary medium; as we shall discuss later, this appears to be the case. On the other hand, MHD theory predicts that magnetoacoustic waves steepen and form shocks. One expects analogous processes in a collisionless plasma; in fact, it has been shown that steepening can occur for certain kinds of collisionless waves, although anomalous exchange of the roles of steepening and rarefaction in discontinuity formation is possible under certain conditions.[5]

One process that may limit the nonlinear steepening of magnetoacoustic waves is Landau damping of the higher-k Fourier components generated as the wave steepens. The characteristic time of nonlinear steepening of the least-damped mode may be estimated very crudely as

$$T_s \sim \frac{\tau_{wave}}{2\pi}\left(\frac{B}{\Delta B}\right) \tag{4-48}$$

where τ_{wave} is the wave period and ΔB is the (magnetic) wave amplitude.[22] As mentioned previously, a good order-of-magnitude estimate of the (proton) Landau damping rate for most propagation directions is

$$|\mathrm{Im}\ \omega| \sim |\omega| \exp\left(-\frac{1}{\beta_{||+}}\right) \tag{4-49}$$

Landau damping competes with steepening for Fourier components whose frequency ω satisfies

$$|\omega| T_s \exp\left(-\frac{1}{\beta_{||+}}\right) \sim |\mathrm{Im}\ \omega| T_s \sim 1 \tag{4-50}$$

so that, from Eq. (4-48),

$$|\omega| \tau_{wave} \sim 2\pi \frac{\Delta B}{B} \exp\left(\frac{1}{\beta_{||+}}\right) \tag{4-51}$$

This frequency ω thus corresponds to a length δ that is related to the initial wavelength L by[26]

$$\frac{\delta}{L} \sim \frac{B}{\Delta B} \exp\left(-\frac{1}{\beta_{||+}}\right) \tag{4-52}$$

If δ calculated by Eq. (4-52) exceeds the characteristic shock thickness (e.g., the proton Larmor radius), then Landau damping might interfere with the formation of the shock. Unfortunately, there is at present no rigorous theory to support or deny this idea. Some observational support for this notion is provided by the study of Chao and Lepping,[63] which showed that 30% of the observed interplanetary "shocks" were much thicker than the expected shock thicknesses.

For waves of sufficiently small amplitude, Landau damping may dominate over steepening for all wave numbers and no steepening would occur. This

situation arises if the Landau damping time is short compared with the steepening time, i.e., if[22]

$$\frac{T_d}{T_s} \sim 2\pi \frac{\Delta B}{B} \exp\left(\frac{1}{\beta_{||+}}\right) \ll 1 \qquad (4\text{-}53)$$

If, on the other hand, $T_d/T_s \gg 1$, the wave will steepen, but the steepening may be limited by the Landau damping of higher-k Fourier components as discussed previously. For β_p in the range 0.2 to 1, $T_d/T_s \sim 10\text{-}10^3\ \Delta B/B$ for most propagation directions. For a narrow range of propagation directions nearly transverse to $\langle \underset{\sim}{B} \rangle$, electron Landau damping is significant; this damping is not sensitive to $\beta_{||+}$, and $T_d/\tau_{wave} \sim 10$ for typical interplanetary conditions. Thus, for θ near $\pi/2$, Landau damping may inhibit steepening of fast mode waves if $\Delta B/B \lesssim 0.1$. But, for most propagation directions, the strength of this inhibition is sensitive to β_p. Finally, the very strong Landau damping of the sound-like magnetoacoustic wave will prevent formation of shocks from that wave mode under most, if not all, situations of interest for the solar wind.

The physical mechanism of Landau damping of hydromagnetic waves, as mentioned previously, is the combined effect of the mirror force $-\mu\nabla_{||}B$ and the electrostatic force acting along the magnetic-field direction on resonant particles. This process in a sinusoidal wave would trap the resonant particles in a time of order

$$T_t \sim 2\pi[m/(\mu|\Delta B \sin\theta|)]^{1/2}/|k_{||}| \qquad (4\text{-}54)$$

if the wave is undamped. By analogy with the nonlinear theory of electrostatic plasma oscillations,[8,88,170] we expect that if the Landau damping time $T_d \ll T_t$, the wave should damp out before trapping effects can be significant, but if $T_d \gg T_t$ trapping should eventually stop Landau damping. The

details of this nonlinear process have not been worked out for the resonant acceleration associated with hydromagnetic wave damping. Toptygin[218] made a preliminary study of this problem. For ion-damped waves,

$$\frac{T_d}{T_t} \sim \frac{\cos\theta \exp(1/\beta_p)}{V_{ph}} \left(\frac{m}{\mu|\Delta B \sin\theta|}\right)^{-1/2} \sim \left|\frac{\Delta B \sin\theta}{B}\right|^{1/2} \frac{V_{\perp,th}}{V_{ph}} \cos\theta \exp\left(\frac{1}{\beta_p}\right) \tag{4-55}$$

where V_{ph} is the wave phase velocity and $V_{\perp,th}$ is the thermal velocity transverse to the magnetic field. Clearly, trapping could be an important effect for a wide range of wave amplitudes. Recently, Matsumoto (private communication) has numerically simulated the trapping of electrons in a *sinusoidal* large-amplitude magnetoacoustic wave and found that trapping does, in fact, limit resonant wave-particle energy exchange. Note, however, that in a field of magnetoacoustic turbulence the importance of trapping may not be as great as in a plane wave of comparable energy density. This is so because the kth wave can trap a particle only if it is approximately resonant with the particle over the trapping time. Since $\omega/k_{||}$ depends on the direction of $\underset{\sim}{k}$, a given particle can be resonant with waves from only a limited set of propagation directions. This set of propagation directions corresponds in turn to only a fraction of the fluctuation energy, so that the trapping time is correspondingly longer than would be the case if all the fluctuation energy were in a single plane wave. Hartle, Barnes, and Bredekamp[108] used these notions to make a crude quantitative estimate of the importance of trapping in a magnetoacoustic wave field. An analogous reduction of electrostatic trapping time for waves of limited spatial extent has been discussed by Davidson.[79]

Nonlinear theory of magnetoacoustic waves has not been worked out on a level that rigorously includes trapping effects. Such a theory would broaden

considerably our base for understanding the microstructure of the solar wind. It is possible that success in this topic will require numerical simulation studies.

One example of nonlinear Landau damping of magnetoacoustic waves has been worked out in detail. In the limit of small amplitude, the least-damped mode propagating exactly parallel to $\langle \underset{\sim}{B} \rangle$ is degenerate with the Alfvén mode, is noncompressive, and is therefore not damped. In second order, however, the magnetoacoustic mode, being linearly polarized, exhibits fluctuations in $|\underset{\sim}{B}|$ and therefore exerts a mirror force on resonant particles. Hollweg[110] modeled the resulting nonlinear Landau damping with a mixed fluid-kinetic theory, and Lee and Völk[149] worked out an accurate damping rate from kinetic theory. As one would anticipate, the associated resonant heating affects the proton component.

One point of semantic confusion has arisen both in connection with this work and elsewhere. When hydromagnetic wave modes are classified according to linear theory, a transverse linearly polarized wave propagating along the magnetic field can always be described as an Alfvén wave. However, in second order, a transverse Alfvén wave is *strictly noncompressive* and not exactly linearly polarized. Therefore, the calculations of nonlinear Landau damping apply to magnetoacoustic waves, which, of course, are linearly polarized. The transverse Alfvén wave is not subject to nonlinear Landau damping, as may be seen from the fact that it is an exact propagating solution of the Vlasov-Maxwell equations for arbitrary amplitude.[16] Physically, Landau damping does not occur because $|\underset{\sim}{B}|$ is constant in the transverse Alfvén wave, so that there can be no mirror force $-\mu \nabla_{||} |\underset{\sim}{B}|$.

Barnes and Hollweg[22] studied what happens to a linearly polarized MHD disturbance when terms of second order in the wave amplitude are retained.

They considered a linearly polarized source set up so that in the small-amplitude limit it would generate the small-amplitude Alfvén wave of linearized theory. The small-amplitude wave would be linearly polarized, the magnetic fluctuation $\underset{\sim}{\delta B}$ being perpendicular to $\underset{\sim}{k}$ and $\underset{\sim}{B}_o$. When second-order effects are included, the fluctuations are no longer a simple transverse Alfvén wave. Barnes and Hollweg showed that if $B_o \sin\theta >> |\underset{\sim}{\delta B}|$, then, to second order, the fluctuation is exactly a superposition of the transverse Alfvén wave and a magnetoacoustic wave. The magnetoacoustic contribution to the amplitude $\underset{\sim}{\delta B}_M$ is smaller than the Alfvénic contribution $\underset{\sim}{\delta B}_A$, $|\underset{\sim}{\delta B}_M|/|\underset{\sim}{\delta B}_A| \sim |\underset{\sim}{\delta B}_A|/B_o$. On the other hand, if $B_o \sin\theta \lesssim |\underset{\sim}{\delta B}|$, the fluctuation propagates at the Alfvén speed. It may be regarded as a superposition of two circularly polarized Alfvén waves and a magnetoacoustic wave, but can also be loosely described as a "linearly polarized Alfvén wave." It may be anticipated that this fluctuation, being slightly compressive, would dissipate by nonlinear Landau damping. However, bear in mind that this fluctuation exists only if third-order terms in the wave amplitude may be neglected.

Apparently, wave-particle interactions do not damp transverse Alfvénic fluctuations (unless an appreciable number of suprathermal particles is available for cyclotron resonance). On the other hand, MHD theory predicts the Alfvén wave to be subject to nonlinear decay instability.[5,65,186] The prototype of this mechanism is a circularly polarized Alfvén wave propagating along the magnetic field; this wave decays into a sound wave and a backward-propagating Alfvén wave. The growth rate of this instability[186] is

$$\gamma \simeq kC_A \left(\frac{C_A}{C_s}\right)^{1/2} \frac{|\underset{\sim}{\delta B}|}{B_o} \tag{4-56}$$

where $\underset{\sim}{k}$ is the wave vector of the parent wave. Equation (4-56) is appropriate for the decay of a single Alfvén wave. For Alfvénic turbulence, the

random-phase approximation is required;[219] then decay rates are characteristically proportional to $|\underset{\sim}{\delta B}_k|^2$ rather than $|\underset{\sim}{\delta B}_k|$.

It may be anticipated that the MHD theories of nonlinear wave decay are not directly applicable to collisionless plasmas because the sound wave, which is linearly damped in collisionless plasmas and undamped in collisional plasmas, plays a central role in the theory.[66,149,153] Livshits and Tsytovich[153] developed a theory of the spectra of hydromagnetic turbulence in collisionless plasma and concluded that hydromagnetic turbulence power spectrum proportional to k^{-N} is stable for $N \geq 1$, at least when the Alfvén speed is large in comparison with the electron and ion thermal speeds. Cohen and Dewar[66] reached the same conclusion for Alfvénic turbulence using a fluid model with the added assumption of strong damping of sound waves.

As the solar wind varies on all observed scales, it is also germane to study the propagation of hydromagnetic waves through a randomly fluctuating medium. Valley[225] studied the scattering of small-amplitude hydromagnetic waves in a stochastic magnetic field, and later[226] the scattering of Alfvén waves by density fluctuations. His results suggest that waves may undergo appreciable scattering in the solar wind over the distance of 1 AU. In particular, scattering may convert Alfvén waves into magnetoacoustic waves that can Landau damp, thus providing a mechanism for dissipation of Alfvén waves.

Another nonlinear process that may be relevant to the solar-wind microstructure has been analyzed by Cohen and Kulsrud[67] and by Wray.[235] Cohen and Kulsrud showed that non-Alfvénic ($B^2 \neq$ const) MHD fluctuations propagating along the mean magnetic field steepen into shocks and subsequently evolve into purely Alfvénic fluctuations of lower energy density. They show that the characteristic time scale of this process in the solar wind is comparable to

the expansion time scale. They also show that linearly polarized fluctuations (among others) will evolve into rotational discontinuities.

The preceding topics in nonlinear hydromagnetic wave theory are those that, in my opinion, have so far had the most impact in understanding hydromagnetic turbulence in the interplanetary plasma. Clearly, there is much room for further progress. It is probable that the application of existing tools of nonlinear theory has not reached its limit. For example, hydromagnetic waves in a warm plasma may be studied by means of the Korteweg-de Vries equation;[143] possibly, this fact is a clue for further progress. Examples of work that may prove relevant to large-amplitude hydromagnetic waves in the solar wind are that of Sakai,[188] Elsässer and Schamel,[89] Patterson,[179] Rogister,[184] Taniuti and Washimi,[215] and Demchenko and Hussein.[83] It is also likely that numerical simulation of large-amplitude waves will play a significant role in the future development of the subject.

5. OBSERVED HYDROMAGNETIC FLUCTUATIONS AND THEIR INTERPRETATION

The basic instruments used to monitor the solar-wind plasma are the magnetometer and the plasma analyzer. These instruments provide most of the direct data about the hydromagnetic microstructure of the wind. From the earliest sustained direct observations of the interplanetary medium, from instruments aboard Mariner 2, it became apparent that there are fluctuations on all time scales.[81,165] The first attempt to interpret interplanetary fluctuations in terms of hydromagnetic waves was due to Coleman.[71,73] He studied power spectra and cross-spectra of plasma velocity and magnetic field from Mariner 2 measurements, and compared these spectra with those expected on the basis of linearized MHD wave theory. He found significant coherences between all pairs of components of magnetic field and radial flow velocity;

these pairs exhibited phase differences and power densities that were roughly independent of frequency. From the details of these correlations, Coleman concluded that the fluctuations are consistent with a superposition of Alfvén and fast magnetoacoustic waves. The phase relation between velocity and magnetic-field direction corresponded to outwardly propagating waves (cf. Eq. (4-15)), i.e., to propagation *away from the solar direction* in a reference frame at rest with respect to the plasma.

Coleman's study was unable to determine the relative importance of Alfvén and fast magnetoacoustic waves (slow waves would not have been detected because of their comparatively weak magnetic fluctuations). However, Coleman noted that magnetic variations along the mean field direction were sizable, and arguing from small-amplitude MHD theory, interpreted this fact as indicating that the fluctuations could not be purely Alfvénic. This conclusion could be questioned in the light of large-amplitude theory (although we do not claim that the fluctuations were in fact purely Alfvénic). The essential magnetic feature of the transverse Alfvén wave is that $B^2 = \text{const}$, and such a finite-amplitude wave does in general have a nonzero fluctuating component along the mean field direction. In fact, his power spectra show appreciably more power in components B_i^2 than in the magnitude $\sum_i B_i^2$,[72] so that the data possibly could be interpreted as a field of primarily Alfvénic turbulence (although this interpretation would not be the only possible one). Coleman[74] also found the magnetic power spectra to be roughly of the power-law form, k^{-N}, where N lies between 1 and 2; the theories of Livshits and Tsytovich[153] and Cohen and Dewar[66] indicate stability for such a spectrum.

Unti and Neugebauer[221] made the first positive identification of an Alfvén wave train in the solar wind. They found a 2-hr set of Mariner 2 plasma and magnetic data that showed an oscillatory structure (period ~10-20 min) for

which the velocity and magnetic fluctuations satisfied Eq. (4-15) and which had nearly constant density. Burlaga[41] reported magnetic data that showed oscillations in the magnitude but not the direction of $\underset{\sim}{B}$, which would be consistent with a fast magnetoacoustic wave propagating transverse to $\langle\underset{\sim}{B}\rangle$ (recall that there is no Landau damping for this particular direction of propagation). Plasma density and velocity measurements were not sensitive enough to confirm or deny the interpretation of this structure as a fast wave.

Belcher, Davis, and Smith[30] used Mariner 5 plasma and magnetic data to attempt to identify hydromagnetic waves predicted by linearized MHD theory. They inferred from the correlation between velocity and magnetic-field fluctuations that at least 30% of the time the fluctuations were dominated by large-amplitude aperiodic Alfvén waves. They found no occasions when they could identify inward propagating waves. They found no evidence for magnetoacoustic waves.

This study was later expanded greatly by Belcher and Davis.[32] They used the correlation coefficient between the radial components of $\underset{\sim}{V}$ and $\underset{\sim}{B}$ as a quantitative measure of the contribution of Alfvénic fluctuations to interplanetary turbulence. They concluded again that Alfvén waves occur quite frequently in the solar wind (Fig. 5), and in fact "dominate" the microstructure over the wavelength range from 10^3 to 5×10^6 km more than 50% of the time. These waves propagate outward from the sun (in the plasma frame). The purest examples of Alfvén waves (i.e., those segments of data with the least admixture of non-Alfvénic noise) occurred in high-velocity streams and on their trailing edges. The largest amplitude Alfvénic fluctuations were found in the leading edges of high-velocity streams. However, the latter regions also contain a significant non-Alfvénic component, and *possibly*

backward-propagating Alfvén waves (contrary to statements in some later theoretical papers, definitive measurements of backward-propagating Alfvén waves were not made). They found the power in field magnitude fluctuations to be 10% of that in components on the average; these fluctuations could be due either to magnetoacoustic waves or to convected stationary structures. The magnetoacoustic component of the interplanetary turbulence was thus estimated to be 10% *or less* of the Alfvénic component, and appreciable contributions to the spectra due to convected stationary fluctuations are likely. Belcher and Davis found power spectra of the magnetic field to have spacecraft frequency (i.e., essentially wave number) dependences ranging from $f^{-1.5}$ to $f^{-2.2}$ (stable according to the theoretical criteria mentioned earlier). They reported that on the average the magnetic fluctuations have a 5:4:1 power anisotropy in an othogonal coordinate system whose axes are $(\underset{\sim}{e}_B \times \underset{\sim}{e}_R, \underset{\sim}{e}_B \times (\underset{\sim}{e}_B \times \underset{\sim}{e}_R), \underset{\sim}{e}_B)$, where $\underset{\sim}{e}_B$ is a unit vector in the average field direction and $\underset{\sim}{e}_R$ is a unit vector radially away from the sun.

The Belcher-Davis paper is a landmark in the relationship between space physics and plasma physics in that it achieved at least a partial closure between plasma kinetic theory and interplanetary plasma observations. Theory predicts strong damping of all wave modes but the Alfvén mode, so that far from strongly disturbed regions it is reasonable to expect interplanetary turbulence to consist of the Alfvén wave, the stationary transverse pressure balance, and possible fluctuations due to their nonlinear interactions and/or decays. The existence of Alfvén waves has been established beyond doubt, and the work of Belcher and Davis provides compelling evidence that in some regions the interplanetary turbulence is more than 90% Alfvénic. This fact means that, unless there is some unknown mechanism that preferentially generates Alfvén waves, magnetoacoustic waves are effectively dissipated in the

solar wind. This interpretation is consistent with the result of Belcher and Davis that non-Alfvénic turbulence is associated with the compression regions associated with the overtaking of slow streams by faster ones, where one would intuitively expect large-scale turbulence to be generated.

Another fascinating aspect of the work of Belcher and Davis is its confirmation of earlier findings that Alfvénic fluctuations are propagating outward in the plasma frame. Thus, either the waves are generated by some mechanism that favors the outward direction or else they must be generated in the region of sub-Alfvénic flow (nearer the sun than about 0.1 AU). The latter possibility would mean that interplanetary Alfvén waves are remnants of the turbulence field in the outer solar corona. The question of the source of interplanetary Alfvén waves is discussed in more detail later.

Daily[76] and Change and Nishida[56] studied Alfvénic fluctuations from Pioneer 6 and from Explorer 33-35 data, respectively. Their results were generally consistent with those of Belcher and Davis and showed further that the directions of minimum variance of $\underset{\sim}{B}$ tended to be roughly parallel to $\langle\underset{\sim}{B}\rangle$. If the fluctuations are plane waves, the directions of minimum variance are normal to the planes of constant phase. This interpretation would then imply that the phases of the Alfvén waves are propagating along the mean magnetic field on the average; however, the scatter in the directions of minimum variance is large. Saka and Kitamura[187] found Alfvén waves in fast streams from Explorer 34 data; their power spectra are similar to those of Belcher and Davis.

Burlaga and Turner[53] obtained similar results in a recent study based on Explorer 43 plasma and magnetic data. They stressed the fact that $\Delta|\underset{\sim}{B}|/|\underset{\sim}{B}| \sim 0.06$ $|\Delta\underset{\sim}{B}|/|\underset{\sim}{B}| \neq 0$, even in relatively pure Alfvénic turbulence. They also point out that the presence of Alfvén waves has no simple relation to solar-wind stream structure. The results of Belcher and Davis[32] are

generally consistent with these conclusions. However, Belcher and Davis stressed that, although the *presence* of waves is not strongly correlated to stream structure, the *amplitude* of the waves is related to stream structure. Burlaga and Turner[53] did not state whether their data showed a relationship between amplitude and stream structure.

At present there is no clear interpretation of the small (but real) fluctuations in $|\underset{\sim}{B}|$ associated with the observed Alfvén waves. Burlaga and Turner suggested several possibilities in this regard. One is that the apparently Alfvénic fluctuations may have been misinterpreted as transverse Alfvén waves and might instead by magnetoacoustic waves. This alternative is difficult to reconcile with the theory of hydromagnetic waves. Magnetoacoustic waves are linearly polarized, whereas the observed fluctuations are not. One might imagine a superposition of two (or more) simple waves; however, the fluctuations are generally of large amplitude ($|\Delta\underset{\sim}{B}|/|\underset{\sim}{B}| \sim 0.4$), so that strong nonlinear interactions between superposed waves would occur. It would be very fortuitous for such a nonlinear superposition to produce a fluctuation that resembles the transverse-Alfvén simple wave so closely.

From the point of view of hydromagnetic wave theory, it is more useful to view the apparently Alfvénic fluctuations as being transverse Alfvén waves contaminated by other fluctuations. Burlaga and Turner examined the possibilities that the contaminant fluctuations are magnetoacoustic waves and/or structures that are static in the plasma frame. If they were purely static, $|\underset{\sim}{B}|$ should be anticorrelated with the plasma pressure; density and temperature measurements were not precise enough to confirm or deny this hypothesis. Similarly, if the fluctuations in $\underset{\sim}{B}$ are due to coupling to the magnetoacoustic wave, $|\underset{\sim}{B}|$ and density should be coupled; again plasma data were not

precise enough to decide the issue. Clearly, more observational and theoretical work is required.

At this point, we return to the question of the directions of propagation of Alfvén waves. The tendency of the directions of minimum variance is to lie along $\langle \underset{\sim}{B} \rangle$.[56,76] If the waves are plane waves, the directions of minimum variance coincide with the directions of phase propagation, which therefore also are peaked in the magnetic-field direction. This interpretation, and the further assumption that the waves originate near the sun, are in conflict with the predictions of the WKB calculation of rays and wave vectors propagating and being convected from the sun in a spherically symmetric radially flowing solar wind. Such calculations[13,227] predict radially directed wave vectors near 1 AU. Daily[76] suggested that the discrepancy might be associated with scattering of the Alfvén waves by interplanetary inhomogeneities. Daily presented some observational evidence consistent with this notion, but the statistics are not good enough to draw any firm conclusions. Hollweg[120] and Richter[183] argued theoretically that refraction in the inhomogeneous high-speed streams in which the Alfvén waves are found would orient $\underset{\sim}{k}$ parallel to $\langle \underset{\sim}{B} \rangle$. Burlaga and Turner[53] found that the detailed predictions of these models were not consistent with their observed distributions of minimum variance directions. A recent study by Solodyna and Belcher[207] arrived at similar conclusions.

It is yet to be established whether the constant-phase surfaces of the Alfvénic fluctuations are truly normal to the minimum variance directions, i.e., whether the Alfvén waves are planar on the scale of their wavelength. This question is difficult to answer because in principle the determination of the phase normal requires simultaneous measurements from four spacecraft. A preliminary step in this direction has been taken by Denskat and Burlaga,[84]

who obtained limited information on the phase normals using *two* spacecraft (Explorers 33 and 35). Although projection effects precluded unique definition of the phase normals, they were able to test for consistency with propagation along the magnetic field and along the antisolar direction. They found that of 17 Alfvén waves, 5 were consistent with propagation along $\langle \underset{\sim}{B} \rangle$, 2 were consistent with radial propagation, and 10 were propagating in other directions. They also compared their inferred phase normals with the directions of minimum variance and found very poor correlation. If these results are confirmed by subsequent studies, it would appear that Alfvén waves are decidedly nonplanar at 1 AU. The question can only be resolved by extensive comparison of data from multiple spacecraft.

It has been remarked many times that clearly non-Alfvénic fluctuations are also found in the solar wind, and that these may be at least partly magnetoacoustic waves. However, unambiguous identifications of magnetoacoustic waves have been rare. The case reported by Burlaga[41] is probably a fast magnetoacoustic wave propagating across the magnetic field. Linear theory predicts that, except for very special propagation directions, magnetoacoustic waves of solar origin should not normally reach 1 AU. Thus, magnetoacoustic turbulence in the vicinity of earth should be of relatively local origin (with a few exceptions due, e.g., to very large disturbances produced by solar flares). The relatively large contribution of non-Alfvénic fluctuations in the compression region of fast streams is consistent with this general view.

Chao[62] reported two interesting examples of structures that seemed to be large-amplitude magnetoacoustic waves. Two structures observed by Mariner 5 were consistent with the variations in magnetic field and plasma parameters expected for an MHD shock, but were considerably thicker than the shock (thickness $\geq$ 1000 proton Larmor radii). These same events were seen later by

earth-orbiting Explorer satellites, but the thicknesses of the fluctuations had been reduced by a factor 30-100 in the transit between Mariner and the Explorers. Chao suggested that the reduction in thickness was due to nonlinear wave steepening and showed that the time of transit was comparable to the steepening time predicted by MHD theory. Barnes and Chao[26] pointed out that the linear Landau damping time for these waves was long in comparison with the steepening time, so that steepening is consistent with collisionless theory. Chao and Lepping[63] pointed out that many structures previously interpreted as interplanetary shocks are considerably thicker than a proton gyroradius; presumably these structures are large-amplitude magnetoacoustic waves.

Sari and Valley[190] recently studied cross-spectra and power spectra from Pioneer 6 magnetic data, for periods in which the mean interplanetary field was either directed along the radial direction or transverse to that direction. At these times, planar fluctuations would be detected only if their propagation vectors had nonzero components respectively parallel or transverse to the mean field. Consequently, no stationary fluctuations (viz. transverse pressure balance) would appear in the radial periods. In fact, Sari and Valley found significant fluctuations in $|\underset{\sim}{B}|$ during the radial periods; the cross-spectra exhibited coherencies consistent with magnetoacoustic waves. It was concluded that as much as a quarter of the power in the fluctuations could be due to magnetoacoustic waves, although stationary fluctuations may have contributed to the transverse-field periods. Their data set was rather limited and does not admit a firm conclusion as to whether the presence of a magnetoacoustic component is typical of interplanetary turbulence. If magnetoacoustic waves are normally present,

considerations of Landau damping require that the magnetoacoustic waves be of local rather than solar origin.

Turbulence Spectra. An alternative to interpreting the interplanetary microstructure in terms of waves and analogous stationary features is to consider the solar wind as a turbulent medium (the two viewpoints are not mutually exclusive). Coleman[74] presented extended power spectra of variations in $\underset{\sim}{B}$ and in the radial component of $\underset{\sim}{v}$ and argued that they could be interpreted in terms of MHD turbulence. He assumed that the two characteristic lengths of the turbulence spectrum were the size of the turbulence region itself and, at the other extreme, the proton gyroradius (which might be the characteristic length for dissipative processes). Coleman found the power spectra to be relatively flat at periods longer than ~1 day. He used Kraichnan's[145] theory of the inertial range of MHD turbulence to interpret the spectra. Coleman estimated that the inertial range lay somewhere in the (spacecraft frame) frequency range 10^{-4} to 10^{-1} Hz. Kraichnan's incompressible MHD turbulence consists of a superposition of Alfvén waves, and the theory predicts a spectrum proportional to $k^{-3/2}$ in the inertial range of wave numbers. Coleman found the fluctuations in the frequency range 10^{-4} to 10^{-2} Hz to be approximately Alfvénic; however, the wave-number dependence of the power spectra was $k^{-1.2}$, apparently in conflict with the theory.

It is not clear how to interpret this apparent discrepancy. Saka and Kitamura[187] found from Explorer 34 data that fluctuations in slow streams gave power spectra k^{-N} with N in the general Kraichnan-Kolmogorov range (3/2 to 5/3), but that fast stream fluctuations did not give power spectra of this kind. Sari and Ness,[189] using Pioneer 6 data, reported microstructure power spectra proportional to k^{-2} under both quiet and disturbed conditions. Goldstein and Siscoe[104] found that cross-spectra and power spectra from

Mariner 5 velocity measurements tend to flatten out at periods longer than about 1 day, consistent with Coleman's[74] findings, and argue that two distinct types of physical processes must dominate above and below this dividing period. Cohen[68] suggested that such flattening of the spectra would imply significant degradation of the Alfvénic component for periods longer than 1 day. Goldstein and Siscoe found their various cross-spectra to be consistent with domination of the microstructure by Alfvénic fluctuations about 50% of the time, and provide evidence for the presence of convected stationary structures at other times.

No clear picture of the turbulence spectra of the solar wind has yet emerged. The spectra vary with solar-wind conditions and apparently are primarily Alfvénic in the center of fast streams and at their trailing edges. No unique interpretation of the (apparently variable) slopes of the power spectra has emerged. In particular, the 3/2 slope of Kraichnan's turbulence theory is not generally found. This is not surprising, as Kraichnan's theory applies to an incompressible medium, and therefore does not admit coupling of Alfvénic to compressive "eddies." Theories aimed at describing Alfvénic turbulence in a collisionless medium do not prescribe the slope of the turbulence spectrum, except to require $N \geq 1$ for stability.[66,153] Observed spectra seem to be consistent with this stability condition.

The level of density fluctuations is low in Alfvénic turbulence, but not in other turbulence modes. Power spectra of density fluctuations have been reported.[130,131] These spectra appear consistent with long wavelength extrapolation of the spectrum of density fluctuations that cause scintillation of signals from compact radio sources. However, the relation of interplanetary scintillations to the solar-wind density structure is complicated and beyond

the scope of the present review; reviews of the subject have been given by Coles, Rickett, and Rumsey,[70] Hewish,[109] and Jokipii.[138] The spacecraft plasma flux (not density) spectra have been extended up to ~10 Hz.[166,222,224]

A small but apparently significant enhancement of the power at scale lengths corresponding to the proton gyroradius is found. Unti and Russell[224] correlated plasma and magnetic data and concluded that the sharp spectral peaks occasionally observed lie at longer scale lengths than the proton gyroradius, but a subtler enhancement of power at the proton gyroradius appears when a large number of power spectra are superposed.

Discontinuities. There has been much interest in abrupt changes observed in interplanetary magnetic and plasma data. This interest is due in large part to the fact that such "discontinuities" may correspond to well-defined entities of plasma theory, such as shocks or rotational or tangential discontinuities. They are studied also because they may provide clues about the larger-scale structure of the solar wind and because, once operationally defined, they are readily identified in the data (at least in principle). Various criteria have been used to define "discontinuties." The variety of definitions has unfortunately led to confusion and probably contributed to the origin of several heated disputes.

Surveys of the operational criteria used in defining discontinuities have been given by Burlaga[52] and Siscoe.[203] Various observers find discontinuities occurring at frequencies ranging from about one per hour to one per two days, depending in part on their definition of discontinuity.[34,36,44,154,155,161,182,198,205,206,220] One expects that these discontinuities should be identifiable as hydromagnetic fluctuations (propagating or stationary) whose characteristic lengths have been compressed to small values. Except for the contact discontinuity, which would be rapidly

eradicated in a collisionless plasma, all classes of MHD discontinuities (possibly modified by pressure anisotropy) are allowed and have been observed.[203] As discussed above, Landau damping may inhibit shock formation, and in fact most discontinuities are not shocks.[52] In particular, very strong Landau damping of the sound-like magnetoacoustic wave should essentially prohibit the formation of slow shocks by steepening. Nevertheless, the slow shock has occasionally been observed.[50,60,159,194,223] Neubauer[162,163] studied the nonlinear interaction of MHD discontinuities and concluded that slow shocks can be generated by the interaction of fast shocks with rotational or tangential discontinuities. Slow shocks are probably generated only in exceptional circumstances, but the question of slow-shock formation is nevertheless of considerable interest and should be studied further.

The most common discontinuities are either tangential discontinuities (zero-thickness tangential pressure balance) or rotational discontinuities (zero-thickness transverse Alfvén wave). It is generally agreed that both types of discontinuities are commonly present, although there seems to be some disagreement about the relative frequency of occurrence.‡ Rotational discontinuities seems to be propagating outward in the plasma frame like other Alfvén waves. Their origin is obscure, as Alfvén waves cannot steepen (at least in a homogeneous background) to form discontinuities. The nonlinear

---

‡The question is somewhat complicated by limitations in existing theory. MHD criteria are normally used to identify discontinuities. In collisionless plasmas, the jump conditions for a given kind of discontinuity do not completely determine the changes in plasma parameters across the shock.[61,124,125,126,151,203]

evolution of magnetoacoustic waves into rotational discontinuities as discussed by Cohen and Kulsrud[67] is one possible mechanism; there may be others. Certainly, the problem of the origin of rotational discontinuities requires further investigation.

Tangential discontinuities are especially interesting, as they represent sharp boundaries, stationary in the plasma frame, that separate different states of the solar wind. Such boundaries may extend over large regions of the solar wind. Attempts to determine the geometry of these regions have lead to the pasta metaphors: the twisted spaghetti model (round intertwined plasma filaments bounded by tangential discontinuities) of McCracken and Ness[156] and the flat-noodles-on-a-plate model of Burlaga.[43] The difference between the two pictures is reflected in the distributions of normals to the discontinuities. A relatively isotropic distribution of normals favors the "spaghetti" picture, and one with the normals primarily normal to the ecliptic plane favors the "noodles." Observational distributions favoring both the former and the latter have been found.[52,203] Burlaga[43,52] emphasized that filaments generally cannot be identified unambiguously from data, and suggested that it may be more useful to think of the microstructure of the wind as simply being "discontinuous."

Michel[158] argued that motions on the solar surface would modulate the solar wind into cells whose characteristic dimension $\lesssim 0.01$ AU and which are somewhat flattened in the radial direction. Jokipii and Parker[137] developed a kinematic theory of the random walk of magnetic-field lines in the solar wind; they suggested that interplanetary filaments (or shear surfaces) are produced by supergranular motion at the sun. Ideas such as these are very likely relevant to the formation of tangential discontinuities in the interplanetary medium. However, extended observations made simultaneously by two

or more spacecraft will be required to clarify these issues. It is also clear that tangential discontinuities must make some contribution to observed power and cross-spectra and may play some role in cosmic-ray scattering and diffusion (see the companion review of Fisk[96]).

There is no obvious reason why stationary structures should be primarily discontinuous. In fact, the tangential discontinuities may simply be easily identifiable extreme examples of a family of continuous tangential pressure balances. Burlaga and Ogilvie[47] inferred from six months of Explorer 34 data that the total plasma and magnetic pressures were anticorrelated on the scale 0.01 AU and suggested that the microstructure of the solar wind tends to be in pressure equilibrium. Denskat and Burlaga[84] found one example of a continuously varying structure whose phase plane, as determined from two spacecraft, was parallel to $\underset{\sim}{B}$. Density and temperature appeared to be anti-correlated in the way required for a tangential pressure balance, but the uncertainties in the plasma data were large enough that the identification could not be made with certainty.

Although interplanetary discontinuities are sometimes resolvable by high-time-resolution magnetometers, no detailed studies of the structure of the discontinuities have been reported. The MHD theory of the stability of tangential structures has been given by Northrop and Birmingham.[169]

6. CONVECTION AND PROPAGATION OF WAVES IN THE SOLAR WIND

For obvious reasons, most of our observations of interplanetary micro-structure have been made in the ecliptic plane near the orbit of earth. These observations have made considerable progress possible in defining and classi-fying the interplanetary microfluctuations. However, in order to understand the origins of the microstructure and its effect on the large-scale properties

of the wind, it will be necessary to observe the spatial variation of the microstructure. Some very preliminary observational information on the variation of fluctuations with heliocentric distance has been obtained. Essentially nothing is known about the variation of the microstructure with latitude outside a narrow band about the ecliptic plane.

Before discussing the observations that have been reported, we review briefly the theoretical tools available for their interpretation. The fundamental concept in most work on fluctuations in a spatially varying background is the eikonal or WKB approximation. In its usual version, the theory assumes that the waves are monochromatic with circular frequency ω, are of small amplitude, and propagate in a stationary background. A fluctuating quantity (e.g., the fluctuating part $\underset{\sim}{\delta B}$ of the magnetic field) is taken to be of the form:

$$\underset{\sim}{\delta B}(\underset{\sim}{x},t) = [\underset{\sim}{\delta B}_1(\underset{\sim}{x}) + \underset{\sim}{\delta B}_2(\underset{\sim}{x}) + \ldots]\exp[iS(\underset{\sim}{x}) - i\omega t] \qquad (6\text{-}1)$$

The dynamical equations (MHD or Vlasov-Maxwell) are linearized in the fluctuating variables (but not in the unperturbed background variables). The phase $S(\underset{\sim}{x})$ is assumed to vary on a length scale λ that is short compared with the scale L of large-scale variations in the unperturbed background; $\underset{\sim}{k}(\underset{\sim}{x}) = \text{grad } S$ is assumed to vary only on the long scale L, and $|\underset{\sim}{\delta B}_2|/|\underset{\sim}{\delta B}_1| \sim \lambda/L << 1$. The independent variables are expanded in powers of λ/L, and the dynamical equations are similarly expanded. The resulting equations, in first order, are self-consistent only if $\underset{\sim}{k}(\underset{\sim}{x}) = (\text{grad } S)$ and ω are related by the usual dispersion relation, i.e., if the dispersion relation

$$D(\underset{\sim}{k},\omega) = 0 \qquad (6\text{-}2)$$

derived from the theory of waves in a spatially homogeneous background is *locally* satisfied. Thus, e.g., the MHD Alfvén wave satisfies

$$\omega = (\text{grad } S) \cdot \left[\underset{\sim}{V}_o(x) \pm \frac{\underset{\sim}{B}_o(\underset{\sim}{x})}{4\pi\rho_o(\underset{\sim}{x})^{1/2}} \right] \tag{6-3}$$

In addition, in the first-order WKB approximation, Eq. (4-15) is locally satisfied (for the Alfvén-wave case). Equation (6-2) is a first-order, partial-differential equation for S and may be solved by the method of characteristics or, equivalently, by the Hamilton-Jacobi theory.[103] The Hamilton-Jacobi approach, and the fact that Eq. (6-2) implies that $\omega(k,x)$ is a constant of the motion, suggest a quantum analogy in which the waves are viewed as quanta of energy ω and momentum $\underset{\sim}{k}$. Hamilton's equations are

$$\frac{d\underset{\sim}{x}}{dt} = \left.\frac{\partial\omega}{\partial\underset{\sim}{k}}\right|_{\underset{\sim}{x}} \tag{6-4a}$$

$$\frac{d\underset{\sim}{k}}{dt} = -\left.\frac{\partial\omega}{\partial\underset{\sim}{x}}\right|_{\underset{\sim}{k}} \tag{6-4b}$$

Equation (6-4a) determines the rays along which the waves move; the parameter t is related to the distance s along a ray by $ds = |\partial\omega/\partial\underset{\sim}{k}|dt$. Once (6-4) are integrated, the phase $S(t)$ along each ray is easily found.

The self-consistency condition in the second-order WKB approximation turns out to be a differential equation for the amplitude of the wave. For MHD Alfvén waves, this condition turns out to be[135]

$$\frac{d}{dt}\,\ell n\left(\frac{|\underset{\sim}{\delta B}|^2}{\rho_o^{1/2}}\right) = -\underset{\sim}{\nabla}\cdot\underset{\sim}{V}_o \tag{6-5}$$

The operator $d/dt = (\partial\omega/\partial\underset{\sim}{k})\cdot\underset{\sim}{\nabla}$ as before. The WKB approximation in MHD has been discussed in great detail by Bazer and Hurley[9] and by Weinberg.[229] The theory was first discussed in the context of solar-wind theory by Parker.[177]

It should be reemphasized that calculations of this kind are based on linearized theory. In one instance, the WKB approach has been generalized to include waves of arbitrary amplitude. Barnes and Hollweg[22] showed that large-amplitude transverse MHD Alfvén waves satisfy Eqs. (6-3) and (6-5). Hollweg[119] later gave a simpler heuristic version of the proof and extended the result to a rotating system.

The WKB approximation for small-amplitude plasma waves of any mode can be succinctly summarized in terms of the effective dielectric tensor $\underset{\approx}{K}(\underset{\sim}{k},\omega)$. This approach is powerful and simple and is familiar to most plasma physicists, but has not been exploited in the studies of interplanetary fluctuations in some cases where it might have been useful. The dielectric tensor is rederived, allowing a slow spatial dependence due to spatial variation of the background plasma. The spatial variation of $\underset{\approx}{K}$ introduces new wave modes (drift waves), but we will not consider these here and will concentrate on the spatial variation of modes that can exist in homogeneous plasmas. We define the quantity

$$\mathscr{W}(\underset{\sim}{k},\omega,\underset{\sim}{x}) = \frac{1}{16\pi}\left\{\underset{\sim}{\delta E}^* \cdot \frac{\partial}{\partial\omega}\left[\omega\underset{\approx}{K}^{(h)}\right] \cdot \underset{\sim}{\delta E} + |\underset{\sim}{\delta B}|^2\right\} \tag{6-6}$$

where $\underset{\approx}{K}^{(h)}$ is the Hermitian part of the dielectric tensor evaluated at $\mathrm{Im}\ \omega = 0$.[29,139,210] It can be shown for waves such that $|\mathrm{Im}\ \omega| \ll |\mathrm{Re}\ \omega|$ that

$$\left(\frac{\partial}{\partial t} + \frac{\partial\omega}{\partial\underset{\sim}{k}} \cdot \frac{\partial}{\partial\underset{\sim}{x}} - \frac{\partial\omega}{\partial\underset{\sim}{x}} \cdot \frac{\partial}{\partial\underset{\sim}{k}}\right)\mathscr{W} = 2\gamma_{\underset{\sim}{k}}\mathscr{W} \tag{6-7}$$

where $\omega(\underset{\sim}{k},\underset{\sim}{x})$ is not the real part of the solution of the local dispersion relation and $\gamma_{\underset{\sim}{k}}$ is the growth or damping rate of the wave. Equation (6-7) is a form of the *kinetic equation of waves*, and $N_{\underset{\sim}{k}} = \mathscr{W}/\omega_{\underset{\sim}{k}}$ may be regarded as the distribution function for wave quanta in the $\underset{\sim}{k} - \underset{\sim}{x}$ phase space.

Equations (6-7) can be generalized to include nonlinear wave-wave interactions.[5,79,139] It is sometimes convenient to regard $\mathscr{W}$ as the phase-space energy density for quanta of energy ω and momentum $\underset{\sim}{k}$. However, as we shall stress later, this analogy can be misleading if it is applied literally to plasma acceleration and heating.

Because $\mathscr{W}$ is a quadratic form in the wave amplitudes, and because the relative phases of the components of $\underset{\sim}{\delta E}$ and $\underset{\sim}{\delta B}$ are uniquely determined by local conditions (cf. Eq. (4-21)), solution of Eq. (6-7) gives the spatial variation of wave amplitudes. If we assume $\partial\mathscr{W}/\partial t = 0$, then use the ray Equations (6-4), we find from (6-7) that the variation of $\mathscr{W}[\underset{\sim}{k}(s),\underset{\sim}{x}(s)]$ along a ray is given by

$$\frac{d\mathscr{W}}{ds} = \frac{2\gamma_{\underset{\sim}{k}}(s)}{|\partial\omega/\partial\underset{\sim}{k}|}\,\mathscr{W} \tag{6-8}$$

whose solution is

$$\mathscr{W}[\underset{\sim}{k}(s),\underset{\sim}{x}(s)] = \mathscr{W}[\underset{\sim}{k}(s_o),\underset{\sim}{x}(s_o)]\exp\int_{s_o}^{s}\frac{2\gamma_{\underset{\sim}{k}}}{|\partial\omega/\partial\underset{\sim}{k}|}\,ds' \tag{6-9}$$

Since the quanta satisfy Hamilton's Eq. (6-4), the phase-space volume element $d^3k d^3x$ is invariant. Hence, for a narrow bundle of rays of cross section $\delta A(s)$, the quantity $d^3k\delta A ds$ is constant. Suppose that this phase-space volume element is associated with quanta that pass through a reference surface of areas δA_o during time dt and that these quanta occupy the small volume (d^3k) of k-space. If the wave field is steady, it follows that $d^3k\delta A(s)\left|\partial\omega/\partial\underset{\sim}{k}\right|\Big|_s$ is conserved along the bundle of rays. Let $\mathscr{U}$ be the (x-space) energy density of the quanta, i.e., $\mathscr{U} = \mathscr{W}d^3k$. Thus, by Eq. (6-9),

$$\mathscr{U}\exp\left(-\int_{s_o}^{s}\frac{2\gamma_{\underset{\sim}{k}}}{|\partial\omega/\partial\underset{\sim}{k}|}\,ds'\right)\left|\frac{\partial\omega}{\partial\underset{\sim}{k}}\right|\Big|_s\,\delta A(s) = \text{const} \tag{6-10}$$

gives the spatial variation of $\mathscr{W}$.

Equation (6-10) is very useful, as it applies to any wave mode, and gives the spatial variation of the wave amplitude explicitly, provided that the solutions of the dispersion relation and of the ray equations are available. A particularly simple application is the Alfvén wave, for which $\gamma_{\underset{\sim}{k}} = 0$. In the usual coordinate system where $\underset{\sim}{B}_o$ lies in the z direction and $\underset{\sim}{k}$ lies in the x-z plane, the Alfvén wave is characterized by the dispersion relation (4-30) and the polarization $\underset{\sim}{\delta E} = \delta E_x \underset{\sim}{e}_x$, $\underset{\sim}{\delta B} = (k_{||} c/\omega)\delta E_x \underset{\sim}{e}_y$. Since

$$\frac{\partial}{\partial\omega}(\omega K_{xx}) \simeq \left(\frac{c}{C_A}\right)^2 \left[1 + \left(\frac{k_{||} C_A}{\omega}\right)^2 \frac{4\pi(P_\perp - P_{||})}{B_o^2}\right]$$

(cf. Eqs. (4-29, 4-30)), it follows from Eq. (6-6) that

$$\mathscr{W}_{\text{Alfvén}}(\underset{\sim}{k},\omega,\underset{\sim}{x}) = \frac{|\underset{\sim}{\delta B}_k|^2}{16\pi}\left[\left(\frac{\omega}{k_{||} C_A}\right)^2 + 1 + \frac{4\pi(P_\perp - P_{||})}{B^2}\right]$$

$$= \frac{|\underset{\sim}{\delta B}_k|^2}{8\pi}\left[1 + \frac{4\pi(P_\perp - P_{||})}{B^2}\right] \qquad (6\text{-}11)$$

Note that this formal energy density is negative if the plasma is firehose unstable. Equation (6-11) was derived for the plasma rest frame. It may be shown that, in a new frame moving with velocity $\underset{\sim}{V}_o$,

$$\mathscr{W} = \frac{\omega_o - \underset{\sim}{k} \cdot \underset{\sim}{V}_o}{\omega_o} \mathscr{W}_o \qquad (6\text{-}12)$$

where subscript o refers to the plasma frame; this equation holds for magnetoacoustic wave modes as well.[108] Finally, the mean-square amplitude associated with Fourier components is $|\underset{\sim}{\Delta B}|^2 = |\underset{\sim}{\delta B}_k|^2 \, d^3k$, so that from Eq. (6-10)

$$\frac{\omega}{\omega - \underset{\sim}{k} \cdot \underset{\sim}{V}} \left|\frac{\partial\omega}{\partial\underset{\sim}{k}}\right|_s |\underset{\sim}{\Delta B}|^2 \left[1 + \frac{4\pi(P_\perp - P_{||})}{B^2}\right] \delta A(s) = \text{const} \qquad (6\text{-}13)$$

where ω is the (constant) frequency in the inertial frame in which the flow is stationary and $\underset{\sim}{V}$ is the plasma flow velocity. From Eq. (4-30),

$$\omega - \underset{\sim}{k} \cdot \underset{\sim}{V} = \pm \frac{\Theta^{1/2} \underset{\sim}{k} \cdot \underset{\sim}{B}}{(4\pi\rho)^{1/2}} \tag{6-14a}$$

$$\frac{\partial \omega}{\partial \underset{\sim}{k}} = \underset{\sim}{V} \pm \frac{\Theta^{1/2} \underset{\sim}{B}}{(4\pi\rho)^{1/2}} \equiv \underset{\sim}{V}_g \tag{6-14b}$$

where $\Theta \equiv 1 + (4\pi/B^2)(P_\perp - P_{||})$. If we define $\underset{\sim}{w} = \Theta^{1/2}\underset{\sim}{B}/(4\pi\rho)^{1/2}$, then, using Eq. (6-4b) we have

$$\frac{d}{dt}(\omega - \underset{\sim}{k} \cdot \underset{\sim}{V}) = \pm \frac{d}{dt}(\underset{\sim}{k} \cdot \underset{\sim}{w}) = \pm \underset{\sim}{k} \cdot (\underset{\sim}{V} \cdot \underset{\sim}{\nabla}\underset{\sim}{w} - \underset{\sim}{w} \cdot \underset{\sim}{\nabla}\underset{\sim}{V}) \tag{6-15}$$

But, for a steady flow curl $(v \times B) = 0$, so that

$$\underset{\sim}{V} \cdot \underset{\sim}{\nabla}\underset{\sim}{w} - \underset{\sim}{w} \cdot \underset{\sim}{\nabla}\underset{\sim}{V} = -\underset{\sim}{w}\left\{\underset{\sim}{\nabla} \cdot \underset{\sim}{v} - \underset{\sim}{V} \cdot \underset{\sim}{\nabla} \ln\left[\frac{\Theta^{1/2}}{(4\pi\rho)^{1/2}}\right]\right\} \tag{6-16}$$

Combining Eqs. (6-15) and (6-16) yields

$$\frac{d}{dt} \ln |\underset{\sim}{k} \cdot \underset{\sim}{w}| = \underset{\sim}{V} \cdot \underset{\sim}{\nabla} \ln(\Theta^{1/2}\rho^{1/2}) \tag{6-17}$$

since $\underset{\sim}{\nabla} \cdot (\rho\underset{\sim}{V}) = 0$. Also

$$\underset{\sim}{\nabla} \cdot \underset{\sim}{V}_g = \underset{\sim}{\nabla} \cdot \underset{\sim}{V} \pm \underset{\sim}{\nabla} \cdot \underset{\sim}{w} = \frac{d}{dt} \ln\left(\frac{\Theta^{1/2}}{\rho^{1/2}}\right) - \underset{\sim}{V} \cdot \underset{\sim}{\nabla} \ln(\rho^{1/2}\Theta^{1/2}) \tag{6-18}$$

But $\underset{\sim}{\nabla} \cdot \underset{\sim}{V}_g = (d/dt)\ln(V_g \delta A)$ so that from Eq. (6-18) we have

$$\frac{d}{dt} \ln \delta A = \frac{d}{dt} \ln(\Theta^{1/2}\rho^{-1/2}V_g^{-1}) - \underset{\sim}{V} \cdot \underset{\sim}{\nabla} \ln(\rho^{1/2}\Theta^{1/2}) \tag{6-19}$$

Finally, by differentiating Eq. (6-13) and using Eqs. (6-17) and (6-19), we find that

$$\frac{d}{dt} \ln\left(\Theta^{3/2} \frac{|\Delta \underset{\sim}{B}|^2}{\rho^{1/2}}\right) = \underset{\sim}{V} \cdot \underset{\sim}{\nabla} \ln(\Theta\rho) \tag{6-20}$$

If $P_\perp = P_{||}$, $\Theta = 1$, and (6-20) reduces to the MHD result (6-5).

Clearly, Eqs. (6-13) and (6-20) are equivalent. Equation (6-13) has the advantage of being integrated, but requires more detailed knowledge of the rays than the differential Equation (6-20). However, Eq. (6-13) can be solved explicitly if $\underset{\sim}{B}$ is parallel to $\underset{\sim}{V}$. In that case, $\delta A \propto B^{-1} \propto (\rho V)^{-1}$ and

$$|\Delta \underset{\sim}{B}^2| = \text{const} \frac{\rho^{1/2}}{(\mathcal{M}_A \pm 1)^2[1 + 4\pi(P_\perp - P_{||})/B^2]^{3/2}} \tag{6-21}$$

where $\mathcal{M}_A = (4\pi\rho/\theta)^{1/2}V/B$. Hollweg[119] showed that Eq. (6-21) is also valid, if $P_{||} = P_\perp$, for a rotating frame in which the flow is steady; note that, in such a frame, the component of velocity due to rotation must be included in the computation of $\mathcal{M}_A$.

Equation (6-21) describes the spatial variation of the amplitude of an Alfvén wave along a ray whenever the flow velocity is parallel to the magnetic field. In particular, this equation should be valid in the solar corona, and is independent of the details of the field geometry. In the solar wind far beyond 1 AU, we expect a different situation: the magnetic field should be nearly transverse to the flow direction. In this region $\mathcal{M}_A >> 1$ so that $\underset{\sim}{k} \cdot \underset{\sim}{V} \simeq \omega$. In a symmetric radial solar-wind model, $\underset{\sim}{k}$ tends to be radially oriented far from the sun,[13,227] so that $\underset{\sim}{k} \cdot \underset{\sim}{B}/(4\pi\rho)^{1/2} \propto r^{-1} (r \to \infty)$. Since $\delta A \propto r^{-2}$, it follows from Eq. (6-13) that

$$|\Delta \underset{\sim}{B}^2| \propto r^{-3}\left[1 + \frac{4\pi(P_\perp - P_{||})}{B^2}\right]^{-1/2} \tag{6-22}$$

Since for $r >> 1$, $n \propto B^2 \propto r^{-2}$, we expect the anisotropy term to be small so that in symmetric radial flow $|\Delta \underset{\sim}{B}^2| \propto r^{-3}$ far from the sun. Note that the same result can be obtained by using Eq. (6-21) in the corotating frame ($\mathcal{M}_A \propto r\Omega$).

The simple picture of symmetric radial flow leads to the conclusion that $\underset{\sim}{k}$ is radially directed far from the sun. As discussed previously,

this prediction conflicts with observations.[53,76] One possible resolution of the discrepancy is that the background solar wind is not symmetric. Hollweg[120] and Richter[183] investigated this possibility and concluded that $\underset{\sim}{k}$ is refracted away from the mean field direction in the compression regions of streams and toward the mean field direction in the rarefaction regions. Observational studies[53,207] show that the directions of minimum variance tend to point in the mean field direction in both compression and rarefaction regions. The finding of Denskat and Burlaga[84] that minimum variance directions do not correlate well with phase propagation directions is not consistent with Hollweg's theoretical prediction that waves should be planar beyond 0.5 AU. Thus, we tentatively conclude that the WKB approach does not provide a good description of the distribution of Alfvén-wave propagation directions in solar-wind streams; however, more extended observational studies are required to resolve this issue firmly.

According to Burlaga,[48] the autocorrelation length of the interplanetary magnetic field is comparable to 0.01 AU. This statement should not be construed to mean that the interplanetary field is not ordered on a larger scale; indeed, it follows the Parker[175] spiral over many AU of heliocentric distance[178,185,204] (except possibly for compression regions[185]) and the field is organized into large (longitudinal) sectors of opposite polarity.[232,233] Burlaga interprets the short correlation length as indicating appreciable curvature in surfaces of constant phase over the scale 0.01 AU. This interpretation once again calls into question the application of the WKB approximation to large-scale variations of interplanetary turbulence.

At present the WKB approximation is our only theoretical tool for predicting the large-scale spatial variation of the interplanetary microstructure. This approximation has therefore been used as a guide in interpreting observed

gradients in the microstructure, and we adopt this spirit in reviewing the observations. However, it should be kept in mind that, for the reasons mentioned above, it is not clear that the WKB approximation is applicable over distances large compared with 0.01 AU, and its use may be misleading. Hollweg[112,115] has carried out preliminary investigations of some situations in which the WKB approximation breaks down.

If the WKB approximation is valid and if the plasma density falls off as r^{-2}, the mean-square magnetic fluctuations associated with Alfvén waves should vary roughly as r^{-3} is the absence of generation or damping of the waves (cf. Eq. (6-21)). Coleman *et al.*[75] made the earliest study of the radial variation of the interplanetary magnetic field from Mariner 4 data and found that the field fluctuations were dominated by transverse fluctuations whose mean-square amplitude decreased approximately as $r^{-2.5}$ for spacecraft-frame periods longer than about 3 hr. Belcher and Burchsted[33] later investigated the radial dependence of specifically Alfvénic fluctuations seen in Mariners 4 and 5 magnetic and plasma data, over the range $0.7 < r < 1.6$ AU. They found $|\underset{\sim}{\Delta B}|^2 \propto r^{-3.1\pm0.3}$ for Mariner 4 and $|\underset{\sim}{\Delta B}|^2 \propto r^{-3.3\pm0.3}$ for Mariner 5.

The radial variation of fluctuations has recently been studied for distances out to 3.3 AU by Rosenberg *et al.*,[185] using magnetic data from Pioneer 10. They found that the transverse fluctuations dominate the spectrum at frequencies greater than 1 cycle/day, as would be anticipated from measurements near 1 AU. Excluding data taken in or near compressional interaction regions (where local wave generation might occur), they found the sum of variances of field components to vary as $r^{-3.00\pm0.17}$. These results, like those from Mariners 4 and 5, are consistent with the presence of a field of Alfvénic turbulence being convected by the solar wind with little or no local generation or dissipation of waves.

Coleman *et al.*[75] found in their Mariner 4 study that fluctuations in the magnitude of $|\underset{\sim}{B}|$, though small, fell off less rapidly with increasing r than did fluctuations in the vector components. If confirmed by subsequent observations, this effect may be an important clue to understanding interplanetary turbulence.

Blake and Belcher[37] calculated power spectra of the interplanetary field measured by Mariners 4 and 5. They found that "except for a general decrease in the over-all power level. . . the spectra show no striking dependence on radius in the range between 0.7 and 1.6 AU."

The level of shocks and other discontinuities has also been the subject of a few investigations. These studies and others related to the spatial variation of the mean and fluctuating part of the interplanetary magnetic field have been reviewed in detail by Behannon.[27]

The Helios A plasma experiment detected very strong fluctuations in velocity direction in a high-speed stream near perihelion (0.3 AU). The density was very quiet at the same time, which suggests at least the occasional presence at 0.3 AU of Alfvén waves much more intense than those observed at 1 AU (H. Rosenbauer, private communication). These fluctuations have not yet been completely analyzed and, of course, the spacecraft spends little time near perihelion, so that no general conclusions about the properties of Alfvén waves so near the sun can be drawn at this point.

There is also some observational information on the radial profiles of the levels of higher frequency waves. Power spectra for the frequency range 0.01-12 Hz have been calculated from Mariner 10 magnetic data by Behannon.[28] These show a general increase of power with decreasing radial distance at all frequencies up to several Hertz, with a steepening of the spectrum at higher

frequencies. Behannon also found evidence for coherent sinusoidal fluctuations at all places traversed by Mariner 10. These waves are observed at frequencies near 1 Hz in the spacecraft frame; typical frequencies increase with decreasing heliocentric distance. These waves are relatively large amplitude ($|\Delta\underset{\sim}{B}|/B \sim 0.1$) and the direction of maximum fluctuation is approximately transverse to the mean field. Behannon suggests that these fluctuations may be ion cyclotron waves.

Scarf and Siscoe[193] found an appreciable radial gradient in VLF electric field noise during the passage of Pioneer 9 from 1 to 0.75 AU.

Altogether, observations of the spatial variation of the level of interplanetary microfluctuations are too scanty to permit even provisional closure of theory and observation. The problem may become clarified somewhat as studies of data from recent far-ranging spacecraft are extended. All fluctuations studied so far have the general property of decreasing in intensity as heliocentric distance increases. Studies of the spatial variations of hydromagnetic waves are roughly consistent with WKB theory; however, the applicability of WKB theory to large-scale fluctuation gradients has not yet been firmly established.

7. ORIGINS OF INTERPLANETARY FLUCTUATIONS

It should be stated at the outset that little progress in determining the origin of truly interplanetary fluctuations has been made. This subject has been rich in speculation, but observational tests of the theories have necessarily been very limited in scope. The problem of wave generation upstream of planetary bow shocks has proved somewhat more tractable, as the relevant observations come from a limited region of space that, at least for the earth, has been fairly extensively surveyed.

The firmest statement that can be made about the origin of truly interplanetary fluctuations is that there is strong evidence that the Alfvénic component is generated inside the Alfvénic surface (the surface bounding the region of sub-Alfvénic flow, $r \lesssim 20R_\odot$). The argument for this statement is based on the fact that the correlation between magnetic and velocity fluctuations in all regions of predominantly Alfvénic turbulence indicates that the waves are propagating outward from the sun (in the plasma frame).[30,32,53,73] If the waves were generated in the super-Alfvénic region, either they were produced by a mechanism that preferentially generates outward-propagating waves or backward-propagating waves were produced but dissipated or refracted (or scattered) into the forward direction. These alternatives cannot be absolutely rejected, but all mechanisms considered so far seem unlikely.

For example, since interplanetary ion velocity distributions are often elongated asymmetrically along the interplanetary magnetic field,[92] it is conceivable that resonant microinstabilities sometimes generate waves that propagate predominantly in either the solar or antisolar direction. However, resonant instabilities can generate Alfvén waves only by cyclotron resonance (as for damping, the Landau or Cerenkov resonance does not affect the Alfvén mode). Cyclotron resonance by suprathermal particles normally selects a relatively small band of wave numbers; in contrast, the Alfvénic turbulence encompasses a very wide range of wave numbers.[32] One could argue that initial seed fluctuations in a narrow range of wave numbers are nonlinearly cascaded to the observed spectrum; however, if this process occurs, why are no backward-propagating waves also nonlinearly generated?

On the other hand, the model of Alfvén waves being generated in the sub-Alfvénic region very simply accounts for the observations and has no obvious difficulties. Any backward-propagating waves generated will simply

propagate back toward the sun and not be seen beyond the Alfvénic surface. Other hydromagnetic modes generated by the same process would probably disappear by Landau damping long before reaching 1 AU. Theoretical studies based on weak-turbulence theory suggest that the observed Alfvénic spectrum is stable to nonlinear decay.[66,68,153] One possibly worrisome aspect of this picture is that certain recent observational studies cast doubt on the applicability of the WKB theory to the description of wave normals.[84,207] These results suggest that the observed waves have experienced considerable scattering during the passage from the Alfvénic surface to 1 AU; if so, why no backward-propagating waves are produced by scattering requires explanation.

Alfvén waves could be generated by the firehose instability, although their outward propagation implies that they would have to be generated in the sub-Alfvénic region, where one does not expect a large enough thermal anisotropy for instability. In any case, Patterson[180] has shown that radial expansion in the presence of small-amplitude Alfvén waves never reaches the condition of firehose instability. This work suggests that the presence of Alfvén waves in the solar wind prohibits the firehose instability. Altogether, this instability is not an attractive explanation of the interplanetary Alfvénic turbulence. Hollweg[121] reviewed other possible interplanetary generation mechanisms, none of which appears satisfactory. The most plausible source is the motion associated with photospheric and/or chromospheric convection. In this connection we note that the Alfvénic turbulence is a small fraction of the solar wind's energy efflux, all of which is ultimately derived from solar convection, so that there is no shortage of energy for the generation of interplanetary turbulence.

Coleman[73] proposed early on that solar granulation or supergranulation could be the source of interplanetary waves. The only model of a specific

solar source of the Alfvén waves is due to Hollweg,[111] who suggested horizontal motions in the solar supergranulation pattern. He argued that these motions can generate a wave flux of $\sim 4\times10^3$ erg cm^{-2} sec^{-1} with periods from 20 to 40 hr. This model gives an energy flux that, if extrapolated to 1 AU, would be much larger than can be associated with the observed Alfvénic turbulence; however, if the solar wind comes from only part of the solar surface, this difficulty may disappear. Moreover, the predicted wave periods are much longer than those characteristic of the observed Alfvénic turbulence, although Hollweg's mechanism might produce a much broader spectrum than his simple idealized model predicts. Thus, the connection between the proposed source and the observed turbulence is obscure. Hollweg suggested that this energy might cascade in wave number (cf. the model of Coleman[74]) to give the interplanetary turbulence; this notion, coupled with nonradial expansion and/or nonlinear dissipation of wave energy, could conceivably reconcile the theory with interplanetary observations.

As already discussed, it is plausible that stationary structures and, in particular, the tangential discontinuities, originate in plasma motions near the solar surface that twist or shear magnetic-field lines.[55,137,158,199-202] Burlaga[49] found that tangential discontinuities did not vary greatly between 0.8 and 1 AU. Later studies over a wider range of heliocentric distance indicate a decrease in the occurrence rate of discontinuities with increasing heliocentric distance,[27,154] although the possibility that the observed trends were due to variations in latitude rather than distance cannot be excluded. There seems to be no strong correlation between the occurrence frequency of discontinuities and stream structure.[49]

These various observations are generally consistent with the notion of solar origin of the discontinuities, but there is as yet no strong case against more local origins.

Reference to Table II shows that both proton and electron velocity distributions may be expected to be distorted from Maxwellian forms as the solar wind expands. The observed velocity distributions near 1 AU are in fact nonthermal. The proton distributions are anisotropic, often with extended (sometimes double-humped) "tails" of suprathermal particles. The electron velocity distribution has been described as a low-energy bi-Maxwellian "core" superposed on a high-energy bi-Maxwellian "halo" (see the companion review of Feldman[95] for detailed discussion of these matters). Parker[174] suggested that the expansion of the solar wind would generate thermal anisotropies and associated firehose and mirror instabilities. As already mentioned, Patterson's[180] calculations indicate that expansion in the presence of small-amplitude Alfvén waves cannot reach the point of firehose instability. Nevertheless, other higher-frequency instabilities driven by thermal anisotropy might occur. It has often been stated that some microinstability limits solar-wind anisotropy, and that it is important to determine which instability is responsible. In fact, it has not been established that there is any need to invoke microinstabilities; e.g., Coulomb collisions, though rare, may occur frequently enough to limit proton anisotropy to observed values,[107,150] and have a similar effect on the temperature ratios of He^{++} and H^{+}.[94,164]

Because it is not clear that anisotropy-driven instabilities are significant in the solar wind, we do not review their theory here. A very large class of instabilities due to thermal anisotropy can be discussed in the context of the solar wind, but none of these has been shown to have any direct connection with observations. These instabilities have been reviewed in considerable detail by Hollweg;[121] the interested reader is referred to his summary.

Eviatar and Schulz[90] carried the study of possible microinstabilities further by analyzing the stability of spherically symmetric exospheric flow of protons. They constructed a kinetic equation of the protons that included wave-particle scattering due to instability, in addition to Coulomb collisions. They suggested that the ion flow out to 1 AU is characterized by three different regions: (1) the collision-dominated outer corona, (2) a spherical shell of laminar exospheric expansion, and (3) an outer region in which instabilities govern the expansion.

Forslund[97] pointed out that beyond about $10R_{\odot}$ the electron velocity distribution would be highly skewed due to heat conduction. He showed that this collisional skewing can excite collisionless ion-acoustic, electrostatic ion cyclotron, magnetoacoustic, and ion cyclotron waves. These processes might influence the energy budget of the solar wind by inhibiting thermal conduction and heating the proton component, but would occur much too near the sun to have been detected by *in situ* observations so far made. Generation of various wave modes by instability due to collisionless distortion of the electron velocity distribution has also been discussed.[101,181,197]

8. INTERACTION OF WAVES WITH THE SOLAR WIND

One emphasis so far has been on the waves and how they are influenced by the solar wind, the latter being regarded as a passive background medium. However, the waves carry energy and momentum (and possibly angular momentum[115,196]) and can exert force on the background plasma, or heat it. The simplest example is the stress exerted on the plasma by transverse Alfvén waves. The existence of this force was first pointed out by Parker[177] and first incorporated into solar-wind models by Belcher[31] and by Alazraki and Couturier.[6] It is elementary to derive this stress from the WKB theory if the magnetic-field lines and flow streamlines coincide. In that case we have,

from Eq. (6-21), that[§]

$$|\Delta \underset{\sim}{B}|^2 = \text{const} \frac{\rho^{1/2}}{(\mathcal{M}_A \pm 1)^2[1 + 4\pi(P_\perp - P_{||})/B^2]^{3/2}} \tag{8-1}$$

It is readily shown from Eqs. (3-1a, 4-5, 4-7, and 4-8) that the energy flux (neglecting gravity) of the plasma and fields is

$$\underset{\sim}{F} = \underset{\sim}{V}\left(\frac{B^2}{4\pi} + \frac{1}{2}\rho V^2 + 2P_\perp + \frac{1}{2}P_{||}\right) + \frac{\underset{\sim}{B}\underset{\sim}{B} \cdot \underset{\sim}{V}}{4\pi}\left[\frac{4\pi(P_{||} - P_\perp)}{B^2} - 1\right] + \underset{\sim}{q} \tag{8-2}$$

Equation (8-2) is completely general. We now specialize to the case of steady flow with superposed Alfvénic fluctuations. Thus, ρ, $P_\perp$, $P_{||}$, and $|\underset{\sim}{B}|$ are time-independent and $\underset{\sim}{B}$ and $\underset{\sim}{V}$ fluctuate. Let angular brackets denote temporal averaging, $\underset{\sim}{B} = \langle\underset{\sim}{B}\rangle + \underset{\sim}{\delta B}$. Clearly, $B^2 = \langle|\underset{\sim}{B}|^2\rangle = \langle\underset{\sim}{B}\rangle^2 + \langle|\underset{\sim}{\delta B}|^2\rangle$ and $2\langle\underset{\sim}{B}\rangle \cdot \underset{\sim}{\delta B} + (\underset{\sim}{\delta B})^2 = \langle|\underset{\sim}{\delta B}|^2\rangle$. If we now assume that $\langle\underset{\sim}{V}\rangle$ and $\langle\underset{\sim}{B}\rangle$ are parallel, $\langle\underset{\sim}{B}\rangle \cdot \underset{\sim}{\delta B}$ and $\langle\underset{\sim}{V}\rangle \cdot \underset{\sim}{dV}$ are second-order in the fluctuation amplitude. To second order in amplitude, Eq. (8-2) implies that

$$\begin{aligned}
\langle\underset{\sim}{F}\rangle = {} & \langle\underset{\sim}{V}\rangle\left(\frac{\langle\underset{\sim}{B}\rangle^2}{4\pi} + \frac{1}{2}\rho\langle\underset{\sim}{V}\rangle^2 + 2P_\perp + \frac{1}{2}P_{||}\right) \\
& + \frac{\langle\underset{\sim}{B}\rangle\langle\underset{\sim}{B}\rangle \cdot \langle\underset{\sim}{V}\rangle}{4\pi}\left[\frac{4\pi(P_{||} - P_\perp)}{\langle\underset{\sim}{B}\rangle^2} - 1\right] + \langle\underset{\sim}{q}\rangle \\
& + \langle\underset{\sim}{V}\rangle\left\langle\frac{(\underset{\sim}{\delta B})^2}{4\pi} + \frac{1}{2}\rho(\underset{\sim}{\delta V})^2\right\rangle + \frac{\langle\underset{\sim}{B}\rangle}{4\pi}\left[\frac{4\pi(P_{||} - P_\perp)}{\langle\underset{\sim}{B}\rangle^2} - 1\right]\langle\underset{\sim}{\delta B} \cdot \underset{\sim}{\delta V}\rangle \\
& + \frac{\langle\underset{\sim}{B}\rangle}{4\pi}\frac{\langle\underset{\sim}{B}\rangle \cdot \langle\underset{\sim}{V}\rangle}{\langle\underset{\sim}{B}\rangle^2}\left[\frac{4\pi(P_\perp - P_{||})}{\langle\underset{\sim}{B}\rangle^2}\right]\langle(\underset{\sim}{\delta B})^2\rangle
\end{aligned} \tag{8-3}$$

[§]This formula was derived to order $(\Delta\underset{\sim}{B})^2$, but is known to be valid in MHD theory ($P_\perp = P_{||}$) for waves of arbitrary amplitude.[22]

Using Eq. (4-15) in (8-3), we obtain for the contribution to $\langle \underset{\sim}{F} \rangle$ due to Alfvén waves:

$$\langle \underset{\sim}{F}_A \rangle = \left(\frac{3}{2} \langle \underset{\sim}{V} \rangle \pm \frac{\langle \underset{\sim}{B} \rangle}{(4\pi\rho)^{1/2}} \Theta^{1/2} \right) \Theta \frac{\langle (\delta \underset{\sim}{B})^2 \rangle}{4\pi} \tag{8-4}$$

where $\Theta = 1 + 4\pi(P_\perp - P_{||})/\langle \underset{\sim}{B} \rangle^2$. Clearly, $\langle \underset{\sim}{F}_A \rangle$ is directed along the rays; from Eqs. (8-1) and (8-4), we have immediately that $\langle \underset{\sim}{F}_A \rangle = F_A(\partial\omega/\partial \underset{\sim}{k})/|\partial\omega/\partial \underset{\sim}{k}|$ and

$$F_A = \text{const} |\langle \underset{\sim}{B} \rangle| \frac{(3/2)\mathcal{M}_A \pm 1}{(\mathcal{M}_A \pm 1)^2} \tag{8-5}$$

where $\mathcal{M}_A = |\langle \underset{\sim}{V} \rangle| (4\pi\rho)^{1/2}/(|\langle \underset{\sim}{B} \rangle| \Theta^{1/2})$. Since Alfvén waves are not dissipated, the divergence of $\langle \underset{\sim}{F}_A \rangle$ is the negative of the work done on the plasma by the Alfvén waves. Thus, the component of force (per unit volume) along a ray due to Alfvén waves is

$$\begin{aligned} f_A &= - \frac{|\langle \underset{\sim}{B} \rangle|}{|\langle \underset{\sim}{V} \rangle|} \frac{d}{ds} \left(\frac{F_A}{|\langle \underset{\sim}{B} \rangle|} \right) \\ &= - \frac{F_{A_o}}{|\langle \underset{\sim}{V} \rangle|} \frac{(\mathcal{M}_{A_o} \pm 1)^2}{(3/2)\mathcal{M}_{A_o} \pm 1} \frac{|\langle \underset{\sim}{B} \rangle|}{|\langle \underset{\sim}{B}_o \rangle|} \frac{d}{ds} \left[\frac{(3/2)\mathcal{M}_A \pm 1}{(\mathcal{M}_A \pm 1)^2} \right] \end{aligned} \tag{8-6}$$

where subscript o indicates some reference point on the ray. In a region of highly sub-Alfvénic flow, $\mathcal{M}_A << 1$, and one finds from Eq. (8-6) that in order of magnitude

$$|f_A| \sim \left| \frac{F_{A_o}}{\rho_o V_o} \mathcal{M}_A \frac{d\rho}{ds} \right| \sim \left| \frac{F_{A_o}}{F_o} \mathcal{M}_A \frac{dp}{ds} \right|_{(\mathcal{M}_A << 1)} \tag{8-7a}$$

where F_o is the total nonwave energy flux. Clearly, if $F_{A_o} \lesssim F_o$, the Alfvénic pressure is normally weak compared to the gas pressure in regions of highly sub-Alfvénic flow. In the opposite case, $\mathcal{M}_A >> 1$,

$$|f_A| \sim \left|\frac{F_{A_o}}{\rho_o V_o}\frac{1}{\mathcal{M}_A}\frac{d\rho}{ds}\right| \sim \left|\frac{F_{A_o}}{F_o}\frac{\mathcal{M}_s^2}{\mathcal{M}_A}\frac{dp}{ds}\right|_{(\mathcal{M}_A>>1)} \tag{8-7b}$$

Here $\mathcal{M}_s$ is the normal Mach number; in typical solar-wind models, $\mathcal{M}_s \gtrsim \mathcal{M}_A$, so that if $F_{A_o} \sim F_o$ Alfvén waves can provide an important force in regions of super-Alfvénic flow.

Another useful form of Eq. (8-6) may be derived by noting that $\mathcal{M}_A \propto (\rho\theta)^{-1/2}$, so that $|\langle\underset{\sim}{B}\rangle|/|\langle\underset{\sim}{V}\rangle| \propto (\mathcal{M}_A^2\Theta)^{-1}$ and Eq. (8-6) becomes

$$f_A = \text{const}\,\frac{1}{\Theta\mathcal{M}_A^2}\frac{d}{ds}\frac{(3/2)\mathcal{M}_A \pm 1}{(\mathcal{M}_A \pm 1)^2}$$

$$= \frac{\text{const}}{2\Theta}\frac{d}{ds}\frac{1}{\mathcal{M}_A(\mathcal{M}_A \pm 1)^2} \propto \frac{1}{\Theta}\frac{d}{ds}\left(\Theta^2\langle|\underset{\sim}{\delta B}|^2\rangle\right)$$

Upon evaluation of the constant of proportionality, this expression becomes

$$f_A = -\frac{1}{\Theta}\frac{d}{ds}\left(\frac{1}{8\pi}\langle\Theta^2|\underset{\sim}{\delta B}|^2\rangle\right) \tag{8-8}$$

An alternative derivation of this formula has been given in the limit $\Theta = 1$ by Hollweg.[114]

Simple models of the solar wind including Alfvén wave pressure show that such waves can in principle accelerate the wind to much higher velocities than the same models without waves would predict.[6,31] The relativistic generalization of this theory and its relevance for stellar winds has been explored by Belcher and Olbert.[35] The notion that Alfvén waves participate in acceleration of the observed solar wind is consistent with the presence of outwardly propagating waves and their apparent association with high-speed streams. On the other hand, note that, according to Eq. (8-5), the ratio of the Alfvén-wave flux to total energy flux scales as $[(3/2)\mathcal{M}_A \pm 1)]/(\mathcal{M}_A \pm 1)^2$, *independently of the geometry of the flux tube*. Thus, the ratio of Alfvén-wave to total energy flux should be larger by the factor $2\mathcal{M}_A(1\text{ AU})/3 \simeq 5$

at the sun than at 1 AU. An upper limit to the Alfvén wave flux may be obtained by assuming that all microfluctuations are Alfvén waves; taking $\Delta B \sim 2\times10^{-5}$ gauss and flow parameters from Table I we compute 6×10^{-3} as the ratio of wave to total energy at 1 AU, and 0.03 for this ratio at the sun. Thus, according to the simplest theory of acceleration by Alfvén waves, observed waves at 1 AU are the remnant of coronal Alfvén waves that carry only a tiny fraction of the solar-wind energy and that therefore cannot appreciably accelerate the wind.

The above argument does not necessarily imply that Alfvén waves are unimportant in solar-wind acceleration. For example, a coronal wave flux powerful enough to modify solar-wind flow would consist of large-amplitude waves that might be subject to nonlinear decay.[31] Hollweg[114] attempted to simulate such dissipation by assuming that Alfvén waves damp if $\Delta B/B > 2^{-1/2}$, and obtained reasonable numerical models of Alfvén-wave-driven winds. Another difficulty with our extrapolation that estimated the coronal Alfvénic power is that it was based on the WKB approximation. The longest wavelength Alfvén waves found at 1 AU would have wavelengths larger than local macroscopic scale lengths when extrapolated back to the sun,[31] and thus are not consistent with the WKB approximation. Furthermore, there is a serious question whether the waves satisfy the WKB approximation even at 1 AU, as discussed previously.

If in fact there is a strong coronal source of Alfvén waves, there is no obvious reason why it should exclusively generate Alfvén waves. Waves of other modes would be dissipated long before they were convected to regions accessible to present spacecraft. The sound-like magnetoacoustic wave would be strongly dissipated in a thin region where the wavelength and proton mean free path are comparable.[77,78,129] Fast-mode waves, being more weakly damped, would dissipate over a region 10-20 $R_\odot$ in extent,[15] and could possibly

account for the apparent randomness of the solar-wind speed in this region inferred from scintillation observations.[87] Both modes could heat the proton component of the plasma appreciably by Landau damping. Heating by ion sound waves would occur in a thin region in the lower corona[77,78] and could raise the proton temperature well above the electron temperature. Heating by fast-mode waves would occur over a much larger region and profoundly influence the large-scale expansion of the wind.[15,108]

The detailed models of magnetoacoustic-wave-driven winds[15,108] share with the Alfvén-wave-driven models the limitations of small wave amplitude and the WKB approximation. Even allowing these assumptions, the computation of heating and momentum deposition due to wave damping has not yet been put on a completely satisfactory basis. A rigorous analysis of the rates of heating and momentum transfer has so far been possible only for a spatially homogeneous plasma.[18] In that case, magnetoacoustic wave dissipation heats the plasma at the rate predicted by resonant quasilinear theory,[12] and the heating goes entirely into random motion parallel to the magnetic field, i.e., increases $T_{||}$ but not $T_{\perp}$. Thus, the heating rate is $2\gamma \mathscr{W}_o$, where $\mathscr{W}_o$ is the wave energy density *in the plasma frame* (cf. Eqs. (6-6, 6-7)); in particular, the quantum analogy of quanta of energy ω being absorbed at a rate measured by γ is valid. Reasoning by analogy would lead to the conclusion that the quantum analogy and/or resonant quasilinear theory should give the correct momentum transfer rate between wave and particles. This inference is not correct, as Barnes and Hung[18] showed by calculating the rigorous momentum transfer rate. Thus, the quantum analogy and resonant quasilinear can be misleading in calculations of energy and momentum transfer and should be used with caution.

Moreover, the heating and acceleration rates in a homogeneous plasma are not directly applicable to calculations of wave-driven astrophysical systems;

one needs rather the rates for steady inhomogeneous systems. The modification of the wave field by the changing background can be handled in the WKB approximation, but the feedback of the waves on the background has not yet been properly calculated (except for the special case of Alfvén waves discussed previously). Calculation of these rates is nontrivial because of the vexing problem of separating the average wave energy, e.g., from the background energy.¶[212] The key to this problem may be Whitham's method[231] of using the local average Lagrangian density, which has been applied successfully in a number of contexts.[38-40,85,86] In particular, this technique has permitted a systematic formulation of wave pressure in (fluid) MHD theory.[40,85] Jacques[134] incorporated this formulation in simple, illustrative wave-driven solar-wind models. Unfortunately, the MHD theory of magnetoacoustic waves gives no information about heating and acceleration due to Landau damping. An average Lagrangian theory of collisionless hydromagnetic waves would be a welcome addition to the mathematical resources of plasma astrophysics.

Solar-wind models that include heating by Landau damping assume, in the absence of rigorous proof, that the homogeneous-plasma heating rate correctly gives the heating rate in the inhomogeneous solar wind. This assumption is plausible on physical grounds and certainly is correct in order of magnitude. Hartle *et al.*[108] argue on physical grounds that the force per unit volume associated with Landau damping is of order $2\gamma \mathcal{W}_0/(w + v)$, where w is the phase speed in the plasma frame and v is the flow speed; this quantity is of order $\nabla(\delta B^2/8\pi)$ as one would intuitively expect. Hartle *et al.* argue from

---

¶An analogous problem of separating fluctuations and background complicates the interpretation of measured large-scale spatial variations of solar-wind parameters.[178]

this estimate that wave pressure due to Landau damping is less important than the corresponding heating in influencing solar-wind dynamics in regions of sub-Alfvénic flow and is therefore neglected in their models.

Altogether, Alfvén waves of solar origin would influence solar-wind expansion both by wave pressure and heating from nonlinear dissipation, whereas magnetoacoustic waves would affect the wind primarily by heating its inner core, below the Alfvénic point. The power required in the form of waves to affect the wind significantly is of order 10^{27} erg/sec, about 10% of that required to heat the inner corona; a leakage of this much wave energy to the outer corona and inner solar wind is thus not unreasonable. Both wave mechanisms have been incorporated in spherically symmetric models of the wind[15,108,114] and predict reasonable values of flow parameters at 1 AU. In particular, they predict the observed correlation between flow speed and proton temperature at 1 AU.[46] It has not yet been established unambiguously whether hydromagnetic waves in fact play a major active role in solar-wind dynamics. It would take us far beyond the scope of this article to review the pros and cons of this question. These points have been discussed in detail and from various viewpoints by Hundhausen,[128] Hollweg,[121] and Barnes.[21,23] Auer and Rosenbauer[7] recently found relations among the observed adiabatic invariants at 1 AU that are consistent with the magnetoacoustic-wave-driven picture, although alternative explanations of their results may emerge. The heating problem has not yet been placed in the context of the apparent origin of the solar wind from coronal holes (see companion review of Holzer[123]).

A variety of other plasma mechanisms has been suggested for heating the plasma in the outer corona[98,173] and in interplanetary space.[19,105,136,172,181,217] These possibilities are all more or less plausible. Unfortunately, relevant

observational studies are very difficult to make; one useful study of heating in stream interaction regions was made by Burlaga *et al.*,[51] but the study was limited to three streams. Much work remains to be done in this area.

Fluctuations in the wind can also affect the large-scale flow by modifying transport properties. Attention has been primarily focussed on the effects of collisionless plasma processes on thermal conduction, the most important of the transport processes in the solar-wind problem.[123] Forslund[97] was the first to point out that the heat flux associated with thermal conduction can drive plasma instabilities in the solar wind. Hollweg and Jokipii[113] showed that the random walk of magnetic-field lines can reduce thermal conduction significantly. Nearly collisionless electrons trapped between an inner magnetic mirroring point and an outer electrostatic reflection point will exhibit reduced thermal conduction in the neoclassical sense.[181] Hollweg[118] argued, on the other hand, that the more energetic untrapped electrons would carry most of the heat flux and would not experience the neoclassical effect. The most thorough recent summary of theory in these and related theoretical ideas has been given by Hollweg,[122] and the observations of heat flow are reviewed by Feldman.[95]

9. HYDROMAGNETIC WAVES IN ASTROPHYSICS

A large fraction of the matter in the universe is in the plasma state. Large-scale motions in cosmic plasmas generate hydromagnetic waves, just as motions of air generate sound waves. Hydromagnetic waves can transfer energy and momentum over large distances and may participate in heating and acceleration of cosmic plasmas. It is conceivable that stellar winds, winds from globular clusters, and galactic winds are wave-driven. Hydromagnetic waves are very likely important in determining the behavior of suprathermal charged particles, including galactic cosmic rays. It is common in astrophysics to

describe disordered motions as "turbulent;" presumably much of this turbulence is due to hydromagnetic waves. The solar wind is the only laboratory in which fully developed hydromagnetic turbulence can now be studied, and solar-wind studies are therefore a resource of knowledge of fundamental physical processes in celestial objects.

In most problems of astrophysical interest the plasma is collisionless with respect to wave propagation. The theoretical tools discussed in previous sections are thus applicable, although they must sometimes be generalized to allow for special relativity. The relativistic extensions of the theory are generally straightforward, but some have not yet been made. Relativistic hydromagnetic wave modes are classified into magnetoacoustic and transverse Alfvén modes, as in the nonrelativistic theory. We have already discussed the relativistic transverse Alfvén mode, whose dispersion relation is Eq. (4-11). The linearized kinetic theory of small-amplitude relativistic magnetoacoustic waves has been worked out in detail.[20] The simplest case is the fast mode propagating transverse to the ambient magnetic field, for which the dispersion relation analogous to Eq. (4-37) is

$$\frac{\omega^2}{k^2} = \frac{1 + (2\pi P_\perp/B^2)(4 - \zeta)}{1 + (4\pi/B^2)(\mathscr{E} + P_\perp)} \tag{9-1}$$

where $\mathscr{E}$ is the energy density (including rest energy) of the plasma and ζ is a numerical factor between 0 and 1.

It is commonly supposed that hydromagnetic turbulence is found in a wide variety of astrophysical plasmas. Indeed, it is difficult to imagine that this is not the case. Nevertheless, hydromagnetic turbulence is, for the most part, not directly observable and can only be inferred from its effects. There is only one object outside the heliosphere, to my knowledge,

for which a strong case can be made that hydromagnetic waves are directly observed. Quasi-periodic disturbances (period ~10^6 sec) are seen in synchrotron emission and appear to be generated near the pulsar in the Crab Nebula.[195] The motion of these "wisps" has been studied from plates taken over many years. Their behavior is consistent with that expected for compressive waves propagating across the magnetic field with speed given by Eq. (9-1). In addition, "kinks" in magnetic-field direction appear to be Alfvén waves propagating along the field.

Synchrotron x-rays produced throughout a large part of the nebula require the existence of electrons whose radiation lifetimes are short in comparison with the light travel time between the pulsar and the source of the x-rays. Hence, it appears that energy must be deposited into electrons throughout the nebula, at a rate of about 10^{38} erg sec^{-1} (~10^5 solar luminosities). The energy efflux due to the wisps (compressive waves?) may be adequate to replenish the radiated energy.[157,195]

As in the nonrelativistic case, relativistic magnetoacoustic waves are subject to Landau damping.[20] Waves for which $|\omega/k_{||}| > c$ have no Landau-resonant particles, however, so that waves propagating more nearly perpendicular to $\underset{\sim}{B}_o$ than the critical angle given by $\cos\theta_o = V_{ph}/c$ are undamped. In the central region of the Crab, the phase speed of the waves is not small compared to c, so that the window of undamped propagation directions is not small. It has been suggested that electrons in the Crab are heated by compressive waves outside the zero-damping window.[20] As the wisps propagate out into regions of lower phase speed, the opening angle of this window narrows; the waves may or may not be refracted out of the window, depending on the detailed structure of the nebula. In the former case, waves would heat electrons in the far reaches of the nebula by Landau damping; in

the latter case, some other heating mechanisms such as synchrotron damping would have to be invoked. When Landau damping occurs, it primarily heats the most energetic (and thus most radiative) electrons if the electron energy spectrum is flatter than E^{-2}, and thus could balance radiative losses.

The preceding discussion is not meant to provide a definitive model of the Crab, but to illustrate one case in which hydromagnetic wave phenomena may bear on astrophysical phenomena. Hydromagnetic waves that cannot be observed are expected to be present in a variety of astrophysical processes. Galactic cosmic rays probably both generate and are scattered by hydromagnetic waves.[230] *In situ* acceleration of particles whose radiation lifetimes are short is often explained by hydromagnetic turbulence, though often not in the language of plasma physics. A recent example is the possible acceleration of particles in radio tail galaxies by "second-order Fermi acceleration, with the turbulent vortices acting as magnetic scattering centers."[171] It is clear that this process could also be discussed in terms of Landau-resonant acceleration of particles by hydromagnetic turbulence.

An especially fascinating aspect of the study of cosmic hydromagnetic waves is that it provides the opportunity to test the validity of applying Maxwell's electrodynamics on cosmic scales. Maxwell's theory is, of course, not the only electrodynamics consistent with terrestrial laboratory experiments; more general theories admit, e.g., a finite range to electromagnetic forces or, equivalently, a nonzero photon rest mass.[102] Various experiments have given upper bounds on the inverse Compton wavelength μ of the photon (or equivalently on its rest mass). The best limits correspond to very great length scales, so that further improvements require studies on cosmic scales. For example, becuase Jupiter's magnetic field is so extensive, it has been

possible to use Pioneer 10 measurements of the field to put an upper limit of 8×10^{-49} g on the photon mass, over a factor of 10 lower than the best upper limit derived from terrestrial experiment.[80]

Nonzero photon mass would imply limiting frequencies below which electromagnetic waves cannot propagate. Since the lowest frequency electromagnetic waves are in fact hydromagnetic waves, detection of a hydromagnetic wave of given frequency implies an upper limit on the photon mass. The dispersion relation (4-22) is changed by nonzero μ to[24]

$$\det\left\{\frac{c^2}{\omega^2}\left(\underset{\sim}{k}\underset{\sim}{k} - k^2\underset{\approx}{1}\right) + \underset{\approx}{K}(\underset{\sim}{k},\omega) + \frac{\mu^2c^2}{\omega^2}\left[\frac{\underset{\sim}{k}\underset{\sim}{k}}{k^2 - (\omega/c)^2} - \underset{\approx}{1}\right]\right\} = 0 \qquad (9\text{-}2)$$

Equation (9-2) implies limiting frequency $\omega_o(\mu)$ such that $\omega < \omega_o(\mu)$ is forbidden for a given kind of wave. Observed hydromagnetic waves in the solar wind and in the earth's magnetosphere give upper limits on the photon mass in the range $m_{ph} \sim 10^{-48} - 10^{-49}$ g.[117,148] Similar arguments have been applied to the wisps in the Crab.[24] The dispersion relation (9-1) is changed to

$$\left(\frac{\omega}{kc}\right)^2\left[1 + \frac{4\pi}{B^2}(\mathscr{E} + P_\perp)\right] = 1 + \frac{2\pi P_\perp}{B^2}(4 - \zeta) + \frac{\mu^2}{k^2} \qquad (9\text{-}3)$$

so that waves cannot propagate unless

$$\omega > \omega_o(\mu) = \mu c\left[1 + \frac{4\pi}{B^2}(\mathscr{E} + P_\perp)\right]^{-1/2} \qquad (9\text{-}4)$$

In practice, frequency is not well known for the wisps, so that equivalent expressions in terms of wavelength and propagation speed are used. It turns out that interpretation of the wisps as hydromagnetic waves gives $m_{ph} < 10^{-53}$ g; the uncertainties in the estimate are at most a factor of 100. Thus, the interpretation of the wisps as waves implies the lowest current upper limit on the photon mass. Consideration of the galactic magnetic

field may lead to still lower limits,[54] but no completely convincing argument of this kind has yet been made.

10. SUMMARY AND RECOMMENDATIONS

The most important class of fluctuations found in the solar wind is that of hydromagnetic fluctuations, which exist over the entire range of frequencies below the ion gyrofrequency (~0.08 Hz near earth orbit). The solar-wind plasma is collisionless with respect to these fluctuations and, when viewed on the scale 0.01 AU or less, appears as a relatively uniform background with large-amplitude magnetic and plasma variations superposed. Magnetohydrodynamic theory provides a number of concepts that are useful for classifying these fluctuations. In particular, they can be classified into fast, transverse Alfvén (or intermediate) and slow propagating modes plus two nonpropagating structures. MHD theory does not properly describe the dissipation of these waves, which has to be dealt with by plasma kinetic theory. Transverse Alfvén waves are observed to dominate the solar-wind microstructure roughly half the time. Magnetoacoustic waves are rarely present in the solar wind, consistent with theoretical predictions of their strong damping. Abrupt changes in magnetic-field and plasma parameters are regularly observed; these are a mixture of nonpropagating tangential discontinuities and sharply crested nonlinear transverse Alfvén waves. Fast and slow hydromagnetic shocks have also been identified. The amplitude of the interplanetary hydromagnetic waves is usually large, making waves in the solar wind a motivation for and a test of nonlinear turbulence and wave theory. The intensity of Alfvén waves is related to solar-wind stream structure; the turbulence in compression regions associated with fast streams is highly non-Alfvénic and not well understood. Power spectra and cross-spectra of interplanetary fluctuations are typically

power laws over several decades of wave number, perhaps analogous to the inertial range of fully developed turbulence. The power-law index varies with solar-wind conditions for reasons not understood at present.

Studies of correlations between plasma velocity and magnetic-field fluctuations indicate that the Alfvén waves propagate away from the sun; this fact provides a strong argument that they originate near the sun. If so, their intensity should decrease with heliocentric distance. Preliminary measurements indicate that the energy density of all classes of hydromagnetic fluctuations does in fact decrease with distance from the sun. However, except for this general intensity decrease, and some relations of wave properties to stream structure, little is known about the spatial distribution of interplanetary turbulence. This is true even on the local level, since it is questionable whether the WKB approximation can account for the distribution of wave normals in solar-wind streams. This difficulty plus the evidence from multiple-satellite observations that wave normals and phase propagation directions do not coincide suggest that interplanetary fluctuations are not planar even on the scale of 0.01 AU. If the surfaces of constant phase are indeed highly curved, theoretical techniques of calculating wave propagation and nonlinear interactions would have to be revised radically.

The observed power in Alfvén waves, extrapolated back to the sun, is inadequate to influence solar-wind dynamics strongly unless appreciable dissipation occurs inside 1 AU. Models of the solar wind driven by pressure and (dissipative) heating by various hydromagnetic wave modes of solar origin agree reasonably well with interplanetary observations. However, all such models make assumptions about the input of waves into the solar corona that can be neither confirmed nor denied by existing solar or interplanetary data.

Resolution of this issue is intimately bound to progress in studies of coronal heating and the origin of the solar wind.[123] In addition, the theory of heating and acceleration of collisionless plasma by nonlinear hydromagnetic waves is not yet adequate for more than order-of-magnitude calculations.

Fluctuations of shorter than hydromagnetic wavelengths have been detected in electric and magnetic fields in the interplanetary medium. These are for the most part not well understood, and no doubt are associated with interesting plasma physical processes. They are of such low intensity that they cannot directly influence solar-wind dynamics, although they might conceivably play some role in determining transport properties of the plasma. Considerable theoretical effort has been aimed at understanding how microinstabilities may participate in the regulation of thermal anisotropy and heat flux. The only observational studies directed at this general problem are based on data from near 1 AU (cf. Ref. 95), where wave-particle interactions are not expected to affect the large-scale properties of the solar wind in an important way.

The study of interplanetary hydromagnetic waves is an essential foundation for understanding turbulent processes in astrophysical plasmas. There is good evidence that certain moving structures in the Crab Nebula are hydromagnetic waves that may play an essential role in the energy budget of the Crab. Hydromagnetic waves carry energy and momentum and may therefore accelerate and heat astrophysical plasmas. Such waves are reasonable candidates to explain the *in situ* acceleration that seems to be required by the short radiative lifetimes of energetic synchrotron electrons in certain objects. Hydromagnetic waves may control the diffusion of galactic cosmic rays. The existence of hydromagnetic waves of low frequencies can be used as a

fundamental test of the validity of applying electrodynamics to cosmic scales by implying upper limits to the photon rest mass.

Two important problems stand out above all others in research on interplanetary hydromagnetic waves. First is the determination of the spatial distribution and, subsequently, the origins of interplanetary hydromagnetic fluctuations. Progress in this direction will require further exploration away from the orbit of earth and out of the ecliptic plane. Secondly, the turbulent wave spectrum and its variation with solar-wind conditions are poorly understood. Systematic studies of existing data may yield some progress in this area and should continue. However, some of the most fundamental questions about the turbulence spectrum can be resolved only by extensive simultaneous observations from multiple (ideally four) satellites. Observations of this kind would provide fundamental inputs to new developments in nonlinear wave and turbulence that are required; in this connection, we note that detailed theoretical understanding of the interplanetary turbulence may ultimately be based on numerical simulation.

To be more concrete, I have selected eight problem areas discussed in this review as especially important topics for future investigation. Any list of this kind is necessarily somewhat subjective and the omission of any one topic does not necessarily imply that I consider it unimportant. In any case, the selections that one would make would evolve as more becomes known. Some of the problems listed will be solved faster or more easily than others. A unifying theme is the need for close coordination of theory and observation. A common requirement of many of the problems listed is extended simultaneous observations from several spacecraft.

(1) The local three-dimensional hydromagnetic turbulence spectrum can be determined only by an extended set of *simultaneous* plasma and magnetic

observations from multiple spacecraft. An obvious fundamental question to be addressed is the validity of the widely used assumption that directions of minimum magnetic variance coincide with normals to surfaces of constant phase. If that assumption proves not to be reliable, i.e., if the surfaces of constant phase are highly curved, new theoretical techniques of calculating wave propagation and nonlinear interactions will have to be developed.

(2) The detailed character of local interplanetary turbulence and its relation to solar-wind morphology (e.g., to stream structure or magnetic sector structure) is not yet well understood; in this question, as in (1), extended multiple-satellite data would lead to great advances. Interpretation of non-Alfvénic turbulence will require the development of new theoretical tools. A reasonable starting point would be to investigate the compressive "noise" that appears in regions of otherwise Alfvénic turbulence, as it may be possible to treat the compressive component as a perturbation on a well-defined background state.

(3) Variations of interplanetary turbulence with heliocentric distance, heliographic latitude, and time in the solar cycle have only begun to be explored. The answers to these fundamental questions should be among the main scientific objectives for all deep-space missions in the next decades, not only for their intrinsic scientific interest, but also because they bear directly on the origin of solar-wind turbulence, its role in driving the solar wind, and the modulation of galactic cosmic rays. The proposed out-of-ecliptic mission would provide an opportunity for enormous advances in these areas.

(4) Extensive studies of the orientation, evolution, and dissipation of compressive waves and shocks are needed. Past studies have necessarily been

event-oriented, and, in most cases, could not provide an adequate statistical basis for general conclusions. The relative scarcity of compressive waves and shocks means that extended simultaneous, coordinated observations from two or more satellites will be required for an adequate understanding of these phenomena.

(5) The problem of the orientation, morphology, and origin of directional magnetic discontinuities is still not solved. As in the previous items, extended monitoring by multiple satellites would yield great progress.

(6) The rigorous theory of transport and dissipation of energy and momentum by collisionless magnetoacoustic waves is not yet complete.

(7) Theoretical capabilities must be developed to deal with propagation, convection, and dissipation of waves and turbulence in inhomogeneous plasma when the WKB approximation is not valid. Such a theoretical tool may be necessary both for understanding the spatial distribution of interplanetary turbulence and for understanding coronal heating in real coronal geometries.

(8) The kinetic theory of large-amplitude magnetoacoustic waves needs further development if we are to understand the roles and interplay of nonlinear steepening, collisionless damping, and particle trapping. It may be expected that the nonlinear behavior of single waves will be quite different from that of a turbulent system. Progress in these topics, which may have to be based on numerical simulation studies, would greatly strengthen our basis for understanding the plasma dynamics of the solar wind and other astrophysical systems.

The solar wind provides an excellent, and so far the primary, laboratory in which the generation and propagation of nonlinear hydromagnetic turbulence has been studied *in situ*. Understanding the observed regular wavelength spectrum would therefore be an important scientific achievement of general

interest. In addition, hydromagnetic waves may significantly accelerate or heat the solar wind or other astrophysical plasmas and may ultimately be important for heating plasma in some fusion machines.[211] Finally, hydromagnetic fluctuations scatter cosmic rays, certainly in the solar wind and probably throughout the galaxy.

ACKNOWLEDGMENTS

The efforts of a number of colleagues have been of great value to me in writing this review. In particular, I thank J. Belcher, L. Burlaga, P. Coleman, and J. Hollweg for extended, thoughtful written comments on the subject of this paper. I thank H. Rosenbauer for providing unpublished data from the Helios mission, and T. Holzer, H. Matsumoto, S. Nerney, and H. Völk for carefully and critically reading the first draft of this rather long paper. I am grateful to D. Higgins, D. Vierra, and P. Wilcox for their assistance in the lengthy jobs of typing and editing.

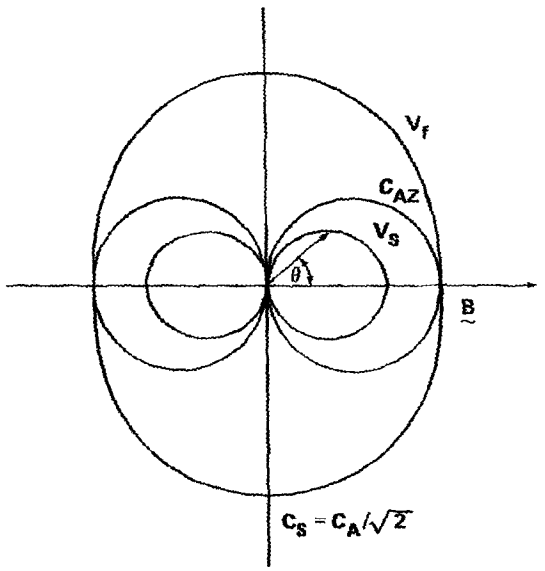

FIGURE 1 Polar plot of the phase speeds of small-amplitude fast, (transverse) Alfvén, and slow waves for $C_A > C_s$.

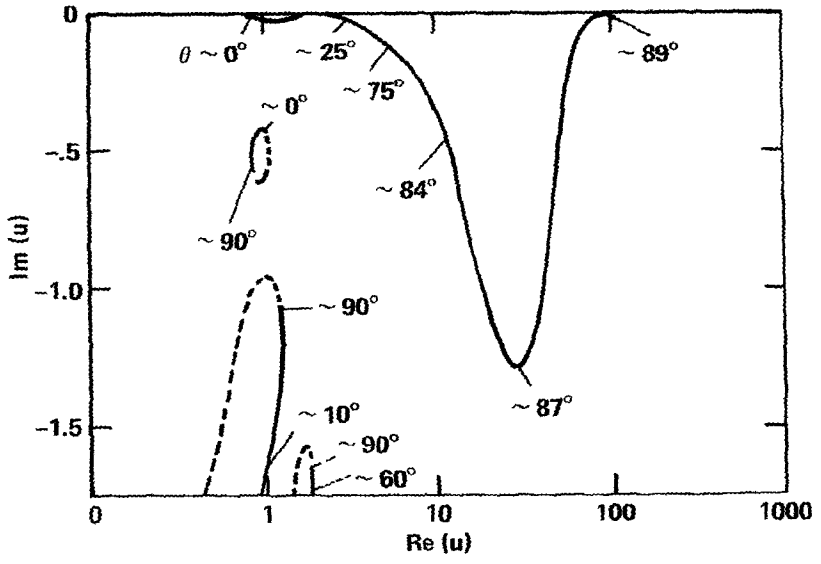

FIGURE 2 Solution trajectories in u plane for sample plasma (after Ref. 10).

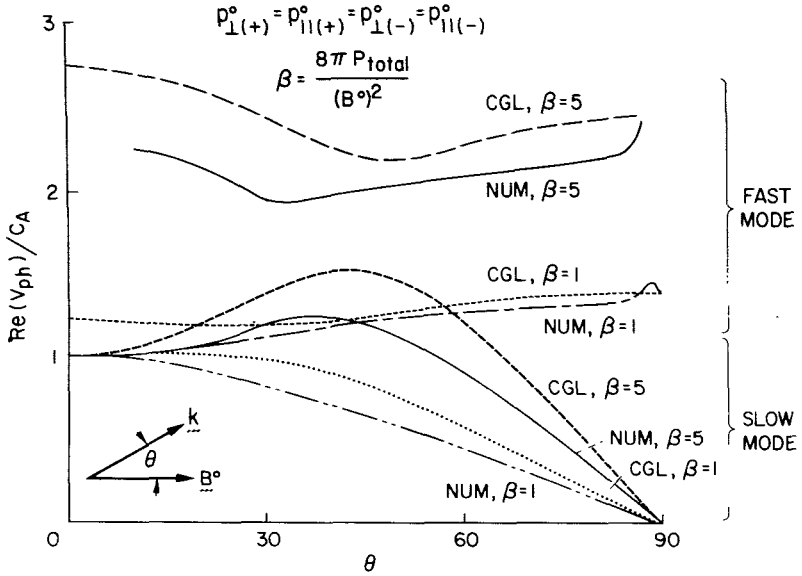

FIGURE 3 Phase speed vs. propagation direction for collisionless hydromagnetic waves. NUM denotes solutions from exact kinetic theory, CGL denotes solutions from Chew-Goldberger-Low double adiabatic theory (after Ref. 10).

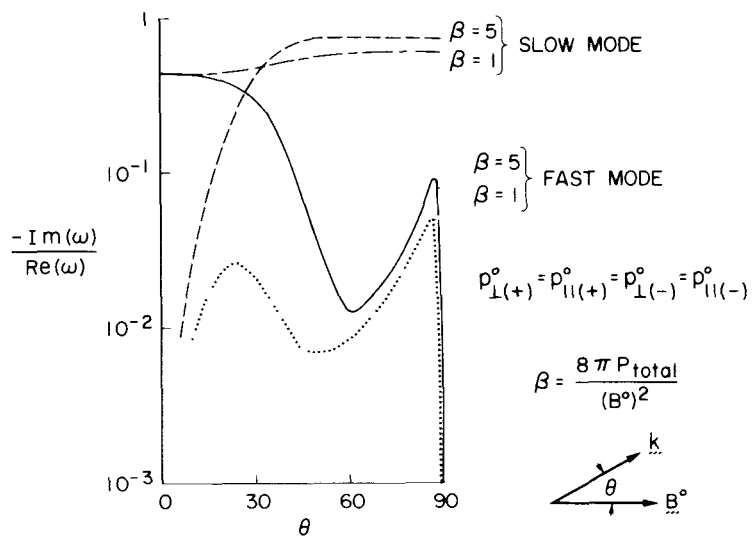

FIGURE 4 Landau damping rate vs. propagation direction for collisionless magnetoacoustic waves (after Ref. 10).

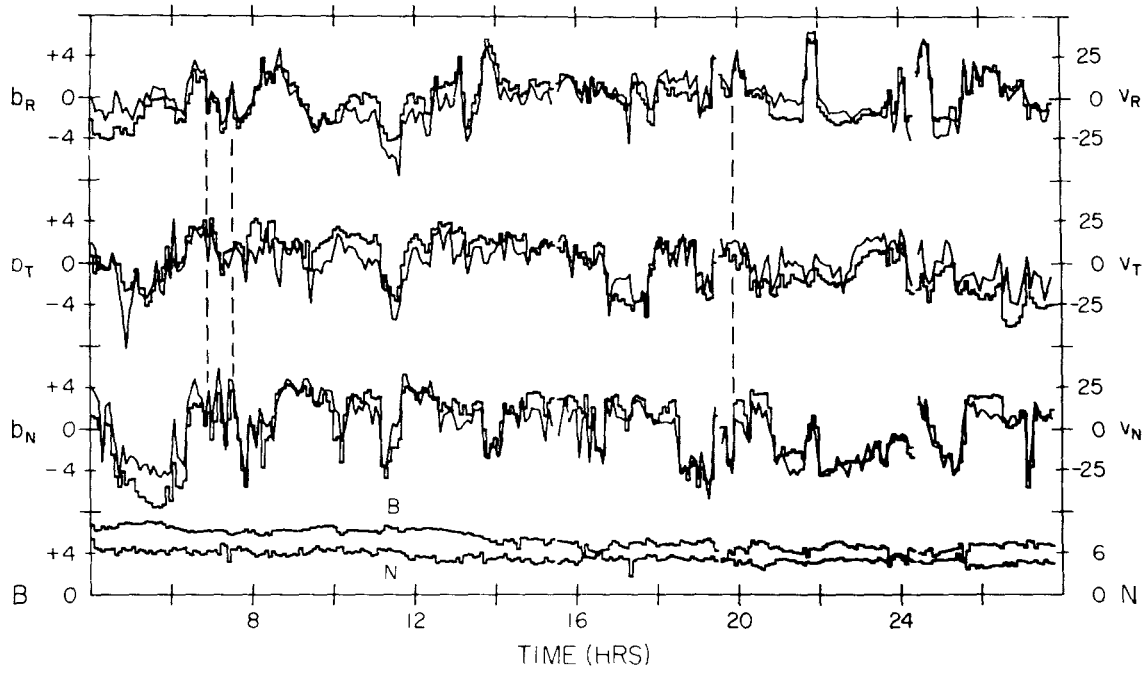

FIGURE 5 Twenty-four hours of magnetic-field and plasma data showing the presence of nearly pure Alfvén waves. The upper six curves are 5-min averages of velocity components (km/sec) and magnetic-field components averaged over the plasma probe sampling period (units of 10^{-5} gauss). The lower two curves are magnetic-field strength and proton number density.[32]

REFERENCES

1. Abraham-Shrauner, B., Propagation of hydromagnetic waves through an anisotropic plasma, *J. Plasma Phys.*, 1, 361, 1967.

2. Abraham-Shrauner, B., Double-adiabatic, hydromagnetic equations for electrons with pressure gradients, *Phys. Fluids*, 11, 2768, 1968.

3. Akhiezer, A. I., Akhiezer, I. A., Polovin, R. V., Sitenko, A. G., and Stepanov, K. N., *Collective Oscillations in a Plasma*, Ch. I-II, M.I.T. Press, Cambridge, Mass., 1967.

4. Akhiezer, A. I., Akhiezer, I. A., Polovin, R. V., Sitenko, A. G., and Stepanov, K. N., *Plasma Electrodynamics. 1. Linear Theory*, Pergamon, New York, 1975.

5. Akhiezer, A. I., Akhiezer, I. A., Polovin, R. V., Sitenko, A. G., and Stepanov, K. N., *Plasma Electrodynamics. 2. Non-Linear Theory and Fluctuations*, Ch. 8 and 10, Pergamon, New York, 1975.

6. Alazraki, G., and P. Couturier, Solar wind acceleration caused by the gradient of Alfvén wave pressure, *Astron. Astrophys.*, 13, 380, 1971.

7. Auer, R. D., and Rosenbauer, H., Evidence for extended solar wind heating by fast hydromagnetic waves, *J. Geophys. Res.*, 82, 1503, 1977.

8. Bailey, V. L., Jr., and Denavit, J., Nonlinear oscillations in collisionless plasma, *Phys. Fluids*, 13, 451, 1970.

9. Bazer, J., and Hurley, J., Geometrical hydromagnetics, *J. Geophys. Res.*, 68, 147, 1963.

10. Barnes, A., Collisionless damping of hydromagnetic waves, *Phys. Fluids*, 9, 1483, 1966.

11. Barnes, A., Stochastic electron heating and hydromagnetic wave damping, *Phys. Fluids*, 10, 2427, 1967.

12. Barnes, A., Quasilinear theory of hydromagnetic waves in collisionless plasma, *Phys. Fluids*, 11, 2644, 1968.

13. Barnes, A., Collisionless heating of the solar wind plasma. 2. Application of the theory of plasma heating by hydromagnetic waves, *Astrophys. J.*, 155, 311, 1969.

14. Barnes, A., Theoretical constraints on the microscale fluctuations in the interplanetary medium, *J. Geophys. Res.*, 76, 7522, 1971.

15. Barnes, A., Hartle, R. E., and Bredekamp, J. H., On the energy transport in stellar winds, *Astrophys. J.*, 166, L53, 1971.

16. Barnes, A., and Suffolk, G. C. J., Relativistic kinetic theory of the large-amplitude transverse Alfvén wave, *J. Plasma Phys.*, 5, 315, 1971.

17. Barnes, A., Microscale fluctuations in the solar wind, NASA SP-308, 333, 1972.

18. Barnes, A., and Hung, R. J., Plasma heating and acceleration due to Landau damping of hydromagnetic waves, *J. Plasma Phys.*, 8, 197, 1972.

19. Barnes, A., and Hung, R. J., On the kinetic temperature of He++ in the solar wind, *Cosmic Elec.*, 3, 416, 1973.

20. Barnes, A., and Scargle, J. D., Collisionless damping of hydromagnetic waves in relativistic plasma. I. Weak Landau damping; heating of the Crab nebula, *Astrophys. J.*, 184, 251, 1973.

21. Barnes, A., Theoretical studies of the large-scale behavior of the solar wind, *Advan. Electron. Electron Phys.*, 36, 1, 1974.

22. Barnes, A., and Hollweg, J. V., Large-amplitude hydromagnetic waves, *J. Geophys. Res.*, 79, 2302, 1974.

23. Barnes, A., Plasma processes in the expansion of the solar wind and in the interplanetary medium, *Rev. Geophys. Space Phys.*, 13, 1049, 1975.

24. Barnes, A., and Scargle, J. D., Improved upper limit on the photon rest mass, *Phys. Rev. Lett.*, 35, 1117, 1975.

25. Barnes, A., On the nonexistence of plane-polarized large-amplitude Alfvén waves, *J. Geophys. Res.*, 81, 281, 1976.

26. Barnes, A., and Chao, J. K., Landau damping and steepening of interplanetary nonlinear hydromagnetic waves, *J. Geophys. Res.*, 1977, in press.

27. Behannon, K. W., Variation of the interplanetary magnetic field with heliocentric distance, NASA-X-692-75-143, GSFC, Greenbelt, Maryland, 1975.

28. Behannon, K. W., Observations of the interplanetary magnetic field between 0.46 and 1 AU by the Mariner 10 Spacecraft, NASA-X-692-2, GSFC, Greenbelt, Maryland, 1976.

29. Bekefi, G., *Radiation Processes in Plasmas*, Ch. 1, Wiley, New York, 1966.

30. Belcher, J. W., Davis, L., Jr., and Smith, E. J., Large-amplitude Alfvén waves in the interplanetary medium: Mariner 5, *J. Geophys. Res.*, 74, 2302, 1969.

31. Belcher, J. W., Alfvénic wave pressures and the solar wind, *Astrophys. J.*, 168, 509, 1971.

32. Belcher, J. W., and Davis, L., Jr., Large-amplitude Alfvén waves in the interplanetary medium, 2, *J. Geophys. Res.*, 76, 3534, 1971.

33. Belcher, J. W., and Burchsted, R., Energy densities of the Alfvén waves between 0.7 and 1.6 AU, *J. Geophys. Res.*, 79, 4765, 1974.

34. Belcher, J. W., Statistical properties of the interplanetary microscale fluctuations, *J. Geophys. Res.*, 80, 4713, 1975.

35. Belcher, J. W., and Olbert S., Stellar winds driven by Alfvén waves, *Astrophys. J.*, 200, 369, 1975.

36. Belcher, J. W., and Solodyna, C. V., Alfvén waves and directional discontinuities in the interplanetary medium, *J. Geophys. Res.*, 80, 181, 1975.

37. Blake, D. H., and Belcher, J. W., Power spectra of the interplanetary magnetic field, 0.7-1.6 AU, *J. Geophys. Res.*, 79, 2891, 1974.

38. Bretherton, F. P., On the mean motion induced by internal gravity waves, *J. Fluid Mech.*, 36, 50, 1969.

39. Bretherton, F. P., and Garrett, C. J. R., Wavetrains in inhomogeneous moving media, *Proc. Roy. Soc., Ser. A*, 302, 529, 1969.

40. Bretherton, F. P., in *Math. Probs. Geophys. Sci.* (Am. Math. Soc.), 61, 1970.

41. Burlaga, L. F., Micro-scale structures in the interplanetary medium, *Solar Phys.*, 4, 67, 1968.

42. Burlaga, L. F., and Ness, N. F., Macro- and micro-structure of the interplanetary magnetic field, *Can. J. Phys.*, 46, S962, 1968.

43. Burlaga, L. F., Directional discontinuities in the interplanetary magnetic field, *Solar Phys.*, 7, 57, 1969.

44. Burlaga, L. F., and Ness, N. F., Tangential discontinuities in the solar wind, *Solar Phys.*, 9, 467, 1969.

45. Burlaga, L. F., Ogilvie, K. W., and Fairfield, D. H., Microscale fluctuations in the interplanetary magnetic field, *Astrophys. J.*, 155, L171, 1969.

46. Burlaga, L. F., and Ogilvie, K. W., Heating of the solar wind, *Astrophys. J.*, 159, 659, 1970.

47. Burlaga, L. F., and Ogilvie, K. W., Magnetic and thermal pressures in the solar wind, *Solar Phys.*, 15, 61, 1970.

48. Burlaga, L. F., Hydromagnetic waves and discontinuities in the solar wind, *Space Sci. Rev.*, 12, 600, 1971.

49. Burlaga, L. F., On the nature and origin of directional discontinuities, *J. Geophys. Res.*, 76, 4360, 1971.

50. Burlaga, L. F., and Chao, J. K., Reverse and forward slow shocks in the solar wind, *J. Geophys. Res.*, 76, 7516, 1971.

51. Burlaga, L. F., Ogilvie, K. W., Fairfield, D. H., Montgomery, M. D., and Bame, S. J., Energy transfer at colliding streams in the solar wind, *Astrophys. J.*, 164, 137, 1971.

52. Burlaga, L. F., Microstructure of the interplanetary medium, NASA SP-308, 309, 1972.

53. Burlaga, L. F., and Turner, J. B., Microscale 'Alfvén Waves' in the solar wind at 1 AU, *J. Geophys. Res.*, 81, 73, 1976.

54. Byrne, J. C., and Burman, R. R., A photon rest mass and electric currents in the galaxy, *J. Phys. A.: Math., Nucl. Gen.*, 6, L12, 1973.

55. Carovillano, R. L., and Siscoe, G. L., Corotating structure in the solar wind, *Solar Phys.*, 8, 401, 1969.

56. Chang, S. C., and Nishida, A., Spatial structure of transverse oscillations in the interplanetary magnetic field, *Astrophys. Space Sci.*, 23, 301, 1973.

57. Chandrasekhar, S., Kaufman, A. N., and Watson, K. M., Properties of an ionized gas of low density in a magnetic field. III, *Ann. Phys.*, 2, 435, 1957.

58. Chandrasekhar, S., Kaufman, A. N., and Watson, K. M., The stability of the pinch, *Proc. Roy. Soc., Ser. A.*, 245, 435, 1958.

59. Chandrasekhar, S., *Plasma Physics*, Sec. 23, Phoenix, Chicago, 1960.

60. Chao, J. K., and Olbert, S., Observation of slow shocks in the interplanetary space, *J. Geophys. Res.*, 75, 6394, 1970.

61. Chao, J. K., and Goldstein, B., Modification of the Rankine-Hugoniot relations for shocks in space, *J. Geophys. Res.*, 77, 5455, 1972.

62. Chao, J. K., Steepening of nonlinear waves in the solar wind, *J. Geophys. Res.*, 79, 1799, 1973.

63. Chao, J. K., and Lepping, R. P., A correlative study of SSC's, interplanetary shocks, and solar activity, *J. Geophys. Res.*, 79, 5411, 1973.

64. Chew, G. F., Goldberger, M. L., and Low, F. E., The Boltzmann equation and the one-fluid hydromagnetic equations in the absence of particle collisions, *Proc. Roy. Soc. London, Ser. A.*, 236, 112, 1956.

65. Chin, Y. C., and Wentzel, D. G., Nonlinear dissipation of Alfvén waves, *Astrophys. Space Sci.*, 16, 465, 1972.

66. Cohen, R. H., and Dewar, R. L., On the backscatter instability of solar wind Alfvén waves, *J. Geophys. Res.*, 79, 4174, 1974.

67. Cohen, R. H., and Kulsrud, R. R., Nonlinear evolution of parallel-propagating hydromagnetic waves, *Phys. Fluids*, 17, 2215, 1974.

68. Cohen, R. H., Mode decay and evolution of the solar wind Alfvén wave spectrum, *J. Geophys. Res.*, 80, 3678, 1975.

69. Colburn, D. S., and Sonett, C. P., Discontinuities in the solar wind, *Space Sci. Rev.*, 5, 439, 1966.

70. Coles, W. A., Rickett, B. J., and Rumsey, V. H., Interplanetary scintillations, in *Solar Wind Three* (C. T. Russell, ed.), Univ. Calif. Press, Los Angeles, 1974, p. 351.

71. Coleman, P. J., Jr., Hydromagnetic waves in the interplanetary plasma, *Phys. Rev. Lett.*, 17, 207, 1966.

72. Coleman, P. J., Jr., Variations in the interplanetary magnetic field: Mariner 2, 1, Observed properties, *J. Geophys. Res.*, 71, 5509, 1966.

73. Coleman, P. J., Jr., Wave-like phenomena in the interplanetary plasma: Mariner 2, *Planet. Space Sci.*, 15, 953, 1967.

74. Coleman, P. J., Jr., Turbulence, viscosity, and dissipation in the solar wind plasma, *Astrophys. J.*, 153, 371, 1968.

75. Coleman, P. J., Jr., Smith, E. J., Davis, L., Jr., and Jones, D. E., The radial dependence of the interplanetary magnetic field: 1.0-1.5 AU, *J. Geophys. Res.*, 74, 2826, 1969.

76. Daily, W. D., Alfvén wave refraction by interplanetary inhomogeneities, *J. Geophys. Res.*, 78, 2043, 1973.

77. D'Angelo, N., Heating of the solar corona, *Astrophys. J.*, 154, 401, 1968.

78. D'Angelo, N., Heating of the solar corona, *Solar Phys.*, 7, 321, 1969.

79. Davidson, R. C., *Methods in Nonlinear Plasma Theory*, Chs. 4.2.4, 13, Academic, New York, 1972.

80. Davis, L., Jr., Goldhaber, A. S., and Nieto, M. M., Limit on the photon mass deduced from Pioneer-10 observations of Jupiter's magnetic field, *Phys. Rev. Lett.*, 35, 1402, 1975.

81. Davis, L., Jr., Smith, E. J., Coleman, P. J., Jr., and Sonett, C. P., Interplanetary magnetic measurements, in *The Solar Wind* (R. J. Mackin, Jr., and M. Neugebauer, eds.), Pergamon, New York, 1966, p. 35.

82. Dawson, J., On Landau damping, *Phys. Fluids*, 4, 869, 1961.

83. Demchenko, V. V., and Hussein, A. M., On the stability of nonlinear magneto-sonic waves in a collisionless plasma, *J. Plasma Phys.*, 10, 459, 1973.

84. Denskat, K. U., and Burlaga, L. F., preprint, 1977.

85. Dewar, R. L., Interaction between hydromagnetic waves and a time-dependent, inhomogeneous medium, *Phys. Fluids*, 13, 2710, 1970.

86. Dewar, R. L., A Lagrangian theory for nonlinear wave packets in a collisionless plasma, *J. Plasma Phys.*, 7, 267, 1972.

87. Ekers, R. D., and Little, L. F., The motion of the solar wind close to the sun, *Astron. Astrophys.*, 10, 310, 1971.

88. Eldridge, O., Nonlinear Landau damping - the spectrum, *Phys. Fluids*, 13, 738, 1970.

89. Elsässer, K., and Schamel, H., Nonlinear evolution of firehose-unstable Alfvén waves, *J. Plasma Phys.*, 7, 475, 1972.

90. Eviatar, A., and Schulz, M., Ion-temperature anisotropies and the structure of the solar wind, *Planet. Space Sci.*, 18, 321, 1970.

91. Fejer, J. A., and Kan, J. R., A guiding centre Vlasov equation and its application to Alfvén waves, *J. Plasma Phys.*, 3, 331, 1969.

92. Feldman, W. C., Asbridge, J. R., Bame, S. J., and Montgomery, M. D., Interpenetrating solar wind streams, *Rev. Geophys. Space Phys.*, 12, 715, 1974.

93. Feldman, W. C., Asbridge, J. R., Bame, S. J., and Gosling, J. T., High-speed solar wind flow parameters at 1 AU, *J. Geophys. Res.*, 81, 5054, 1976.

94. Feldman, W. C., Asbridge, J. R., and Bame, S. J., The solar wind He^{2+} to H^{+} temperature ratio, *J. Geophys. Res.*, 79, 2319, 1974.

95. Feldman, W. C., Kinetic processes in the solar wind (this volume).

96. Fisk, L. A., (this volume).

97. Forslund, D. W., Instabilities associated with heat conduction in the solar wind and their consequences, *J. Geophys. Res.*, 75, 17, 1970.

98. Fredricks, R. W., Electrostatic heating of solar wind ions beyond 0.1 AU, *J. Geophys. Res.*, 74, 2919, 1969.

99. Fried, B. D., and Conte, S. D., *The Plasma Dispersion Function*, Academic, New York, 1961.

100. Fried, B. D., and Gould, R. W., Longitudinal ion oscillations in a hot plasma, *Phys. Fluids*, 4, 139, 1961.

101. Gary, S. P., Feldman, W. C., Forslund, D. W., and Montgomery, M. D., Heat flux instabilities in the solar wind, *J. Geophys. Res.*, 80, 4197, 1975.

102. Goldhaber, A. S., and Nieto, M. M., Terrestrial and extraterrestrial limits on the photon mass, *Rev. Mod. Phys.*, 43, 277, 1971.

103. Goldstein, H., *Classical Mechanics*, Ch. 9, Addison-Wesley, Reading, Mass., 1959.

104. Goldstein, B., and Siscoe, G. L., Spectra and cross-spectra of solar wind parameters from Mariner 5, NASA SP-308, 506, 1972.

105. Goldstein, M. L., and Eviatar, A., Turbulent heating of colliding streams in the solar wind, *Astrophys. J.*, 179, 627, 1973.

106. Goldstein, M. L., Klimas, A. J., and Barish, F. D., On the theory of large-amplitude Alfvén waves, in *Solar Wind Three* (C. T. Russell, ed.), Univ. Calif. Press, Los Angeles, 1974, p. 385.

107. Griffel, D. H., and Davis, L., Jr., The anisotropy of the solar wind, *Planet. Space Sci.*, 17, 1009, 1969.

108. Hartle, R. E., Barnes, A., and Bredekamp, J. H., Solar wind models with heating by magneto-acoustic wave damping and inhibition of thermal conduction, submitted for publication, 1977.

109. Hewish, A., Observations of the solar plasma using radio scattering and scintillation methods, NASA SP-308, 477, 1972.

110. Hollweg, J. V., Nonlinear Landau damping of Alfvén waves, *Phys. Rev. Lett.*, 27, 1349, 1971.

111. Hollweg, J. V., Supergranulation-driven Alfvén waves in the solar chromosphere and related phenomena, *Cosmic Elec.*, 2, 423, 1972.

112. Hollweg, J. V., Alfvénic motions in the solar atmosphere, *Astrophys. J.*, 177, 255, 1972.

113. Hollweg, J. V., and Jokipii, J. R., Heat conduction in a turbulent magnetic field, with application to solar-wind electrons, *J. Geophys. Res.*, 77, 3311, 1972.

114. Hollweg, J. V., Alfvén waves in a two-fluid model of the solar wind, *Astrophys. J.*, 181, 547, 1973.

115. Hollweg, J. V., Alfvén waves in the solar wind: wave pressure, Poynting flux, and angular momentum, *J. Geophys. Res.*, 78, 3643, 1973.

116. Hollweg, J. V., Hydromagnetic waves in interplanetary space, *Publ. Astron. Soc. Pac.*, 86, 561, 1974.

117. Hollweg, J. V., Improved limit on photon rest mass, *Phys. Rev. Lett.*, 32, 961, 1974.

118. Hollweg, J. V., On electron heat conduction in the solar wind, *J. Geophys. Res.*, 79, 3845, 1974.

119. Hollweg, J. V., Transverse Alfvén waves in the solar wind: Arbitrary $\underset{\sim}{k}$, $\underset{\sim}{v}_o$, $\underset{\sim}{B}_o$, and $|\underset{\sim}{\delta B}|$, *J. Geophys. Res.*, 79, 1539, 1974.

120. Hollweg, J. V., Alfvén wave refraction in high-speed solar wind streams, *J. Geophys. Res.*, 80, 908, 1975.

121. Hollweg, J. V., Waves and instabilities in the solar wind, *Rev. Geophys. Space Phys.*, 13, 263, 1975.

122. Hollweg, J. V., Collisionless electron heat conduction in the solar wind, *J. Geophys. Res.*, 81, 1649, 1976.

123. Holzer, T. E., The solar wind and related astrophysical phenomena (this volume).

124. Hudson, P. D., Discontinuities in an anisotropic plasma and their identification in the solar wind, *Planet. Space Sci.*, 18, 1611, 1970.

125. Hudson, P. D., Rotational discontinuities in an anisotropic plasma. *Planet. Space Sci.*, 19, 1993, 1971.

126. Hudson, P. D., Rotational discontinuities in an anisotropic plasma, II, *Planet. Space Sci.*, 21, 475, 1973.

127. Hundhausen, A. J., Bame, S. J., and Ness, N. F., Solar wind thermal anisotropies: Vela 3 and IMP 3, *J. Geophys. Res.*, 72, 5265, 1967.

128. Hundhausen, A. J., *Coronal Expansion and Solar Wind*, Ch. 2, 3, and 5, Springer, New York, 1972.

129. Hung, R. J., and Barnes, A., Dissipation of hydromagnetic waves with application to the outer solar corona. III. Transition from Collisional to collisionless protons, *Astrophys. J.*, 181, 183, 1973.

130. Intriligator, D. S., The power associated with density fluctuations in the solar wind, in *Solar Wind Three* (C. T. Russell, ed.), Univ. Calif. Press, Los Angeles, 1974, p. 368.

131. Intriligator, D. S., and Wolfe, J. H., Preliminary power spectra of the interplanetary plasma, *Astrophys. J.*, 162, L187, 1970.

132. Jackson, J. D., Longitudinal plasma oscillations, *J. Nucl. Energy*, C1, 190, 1960.

133. Jackson, J. D., *Classical Electrodynamics*, Sec. 10.8, Wiley, New York, 1962.

134. Jacques, S. A., Momentum and energy transport by waves in the solar atmosphere and solar wind, preprint, 1977.

135. Jeffrey, A., and Taniuti, T., *Nonlinear Wave Propagation*, Academic, New York, 1964.

136. Jokipii, J. R., and Davis, L., Jr., Long-wavelength turbulence and the heating of the solar wind, *Astrophys. J.*, 156, 1101, 1969.

137. Jokipii, J. R., and Parker, E. N., Stochastic aspects of magnetic lines of force with application to cosmic-ray propagation, *Astrophys. J.*, 155, 777, 1969.

138. Jokipii, J. R., Turbulence and scintillations in the interplanetary plasma, *Ann. Rev. Astron. Astrophys.*, 11, 1, 1973.

139. Kadomtsev, B. B., *Plasma Turbulence*, Academic, New York, 1965, I-II.

140. Kantrowitz, A., and Petschek, H. E., MHD characteristics and shock waves, in *Plasma Physics in Theory and Application* (W. B. Kunkel, ed.), McGraw-Hill, New York, 1966, p. 148.

141. Kato, Y., Tajiri, M., and Taniuti, T., Propagation of hydromagnetic waves in collisionless plasma. I., *J. Phys. Soc. Japan*, 21, 765, 1966.

142. Kennel, C. F., and Wong, H. V., Resonantly unstable off-angle hydromagnetic waves, *J. Plasma Phys.*, 1, 81, 1967.

143. Kever, H., and Morikawa, G. K., Korteweg-de Vries equation for nonlinear hydromagnetic waves in a warm collision-free plasma, *Phys. Fluids*, 12, 2090, 1969.

144. Kitsenko, A. B., and Stepanov, K. N., Instability of plasma with anisotropic distribution of ion and electron velocities, *Sov. Phys. JETP*, 11, 1323, 1960.

145. Kraichnan, R. H., Inertial-range spectrum of hydromagnetic turbulence, *Phys. Fluids*, 8, 1385, 1965.

146. Landau, L., On the vibrations of the electronic plasma, *J. Phys. USSR*, 10, 25, 1946.

147. Landau, L. D., and Lifshitz, E. H., *Electrodynamics of Continuous Media*, Sec. 52, Addison-Wesley, Reading, Mass., 1960.

148. Lanzerotti, L. J., Magnetohydrodynamic waves in the magnetosphere and the photon rest mass, *Geophys. Res. Lett.*, 1, 229, 1974.

149. Lee, M. A., and Völk, H. J., Damping and nonlinear wave-particle interactions of Alfvén waves in the solar wind, *Astrophys. Space Sci.*, 24, 31, 1973.

150. Leer, E., and Axford, W. I., A two-fluid solar wind model with anisotropic proton temperature, *Solar Phys.*, 23, 238, 1972.

151. Lepping, R. P., Influence of thermal anisotropy on best-fit estimates of shock normals, *J. Geophys. Res.*, 77, 2957, 1972.

152. Lerche, I., The relativistic gardenhose instability, *Astrophys. J.*, 145, 806, 1966.

153. Livshits, M. A., and Tsytovich, V. N., The spectra of magnetohydrodynamic turbulence in collisionless plasma, *Nucl. Fus.*, 10, 241, 1970.

154. Mariani, F., Bavassano, B., Villante, U., and Ness, N. F., Variations of the occurrence rate of discontinuities in the interplanetary magnetic field, *J. Geophys. Res.*, 78, 9011, 1973.

155. Martin, R. N., Belcher, J. W., and Lazarus, A. J., Observation and analysis of abrupt changes in the interplanetary plasma velocity and magnetic field, *J. Geophys. Res.*, 78, 3653, 1973.

156. McCracken, K. G., and Ness, N. F., The collimation of cosmic rays by the interplanetary magnetic field, *J. Geophys. Res.*, 71, 3315, 1966.

157. Melrose, D. B., Acceleration of ultrarelativistic electrons in the Crab nebula, *Astrophys. Space Sci.*, 4, 165, 1969.

158. Michel, F. C., Model of solar wind structure, *J. Geophys. Res.*, 72, 1917, 1967.

159. Mihalov, J. D., Colburn, D. S., Collard, H. R., Smith, B. F., Sonett, C. P., and Wolfe, J. H., Pioneer solar plasma and magnetic field measurements in interplanetary space during August 2-17, 1972, *Correlated Interplanetary and Magnetospheric Observations* (D. E. Page, ed.), Reidel, Dordrecht-Holland, 1974, p. 545.

160. Montgomery, D. C., and Tidman, D. A., *Plasma Kinetic Theory*, Ch. 10, McGraw-Hill, New York, 1964.

161. Ness, N. F., Scearce, C. S., and Cantanaro, S., Preliminary results from the Pioneer 6 magnetic field experiment, *J. Geophys. Res.*, 71, 3305, 1966.

162. Neubauer, F. M., Nonlinear oblique interaction of interplanetary tangential discontinuities with magnetogasdynamic shocks, *J. Geophys. Res.*, 80, 1213, 1975.

163. Neubauer, F. M., Nonlinear interaction of discontinuities in the solar wind and the origin of slow shocks, *J. Geophys. Res.*, 81, 2248, 1976.

164. Neugebauer, M., The role of Coulomb collisions in limiting differential flow and temperature differences in the solar wind, *J. Geophys. Res.*, 81, 78, 1976.

165. Neugebauer, M., and Snyder, C. W., Mariner-2 measurements of the solar wind, in *The Solar Wind* (R. J. Mackin, Jr., and M. Neugebauer, eds.), Pergamon, New York, 1966, p. 3.

166. Neugebauer, M., The enhancement of solar wind fluctuations at the proton thermal gyroradius, *J. Geophys. Res.*, 80, 998, 1975.

167. Noerdlinger, P. D., Relativistic effects on plasma stability, *Phys. Fluids*, 9, 140, 1966.

168. Northrop, T. G., *The Adiabatic Motion of Charged Particles*, Interscience, New York, 1963.

169. Northrop, T. G., and Birmingham, F. J., Stability of tangential discontinuities, *Solar Phys.*, 14, 226, 1970.

170. O'Neil, T., Collisionless damping of nonlinear plasma oscillations, *Phys. Fluids*, 8, 2255, 1965.

171. Pacholczyk, A. G., and Scott, J. S., *In situ* particle acceleration and physical conditions in radio tail galaxies, *Astrophys. J.*, 203, 313, 1976.

172. Papadopoulos, K., Electrostatic turbulence at colliding plasma streams as a source of ion heating in the solar wind, *Astrophys. J.*, 179, 931, 1973.

173. Papadopoulos, K., Nonthermal turbulent heating in the solar envelope, *Astrophys. J.*, 179, 939, 1973.

174. Parker, E. N., Dynamical instability of an anisotropic gas of low density, *Phys. Rev.*, 109, 1874, 1958.

175. Parker, E. N., Dynamics of the interplanetary gas and magnetic fields, *Astrophys. J.*, 128, 664, 1958.

176. Parker, E. N., A quasi-linear model of plasma shock structure in a longitudinal magnetic field, *J. Nucl. Energy*, C2, 146, 1961.

177. Parker, E. N., Dynamical theory of the solar wind, *Space Sci. Rev.*, 4, 666, 1965.

178. Parker, G. D., and Jokipii, J. R., The spiral structure of the interplanetary magnetic field, *Geophys. Res. Lett.*, 3, 561, 1976.

179. Patterson, B., Exact nonlinear evolution of Alfvén modes in the guiding-center model, *Phys. Fluids*, 14, 1127, 1971.

180. Patterson, B. R., The convective evolution of large amplitude Alfvén waves in the solar wind, Lawrence Berkeley Lab. Rept. LBL-45, 1971.

181. Perkins, F., Heat conductivity, plasma instabilities, and radio star scintillations in the solar wind, *Astrophys. J.*, 179, 637, 1973.

182. Quenby, J. F., and Sear, S. F., Interplanetary magnetic field irregularities and the solar proton diffusion mean free path during the February 25, 1969 event, *Planet. Space Sci.*, 19, 95, 1971.

183. Richter, A. K., Wave-trains in the solar wind. III: Alfvén waves in the azimuthally-dependent interplanetary medium, *Astrophys. Space Sci.*, 36, 383, 1975.

184. Rogister, A., Propagation of Alfvén waves in ion-sound turbulent plasma, *J. Plasma Phys.*, 6, 309, 1971.

185. Rosenberg, R. L., Kivelson, M. G., Coleman, P. J., Jr., and Smith, E. J., The radial dependences of the interplanetary magnetic field between 1 and 5 AU: Pioneer 10, submitted to *J. Geophys. Res.*, 1977.

186. Sagdeev, R. Z., and Galeev, A. A., *Nonlinear Plasma Theory*, Benjamin, New York, 1969, I-2.

187. Saka, O., and Kitamura, T., Turbulent spectra of the transverse Alfvén waves in the corotating solar wind structure, *Rep. Ionosp. Space Res. Jap.*, 29, 127, 1975.

188. Sakai, J. I., Nonlinear magnetosonic waves in a plasma with a finite conductivity, *Cosmic Electrodyn.*, 3, 260, 1972.

189. Sari, J. W., and Ness, N. F., Power spectra of the interplanetary magnetic field, *Solar Phys.*, 8, 155, 1969.

190. Sari, J. W., and Valley, G. C., Interplanetary magnetic field power spectra: mean field radial or perpendicular to radial, *J. Geophys. Res.*, 81, 5489, 1976.

191. Scarf, F. L., Wolfe, J. H., and Silva, R. W., A plasma instability associated with thermal anisotropies in the solar wind, *J. Geophys. Res.*, 72, 993, 1967.

192. Scarf, F. L., Microscopic structure of the solar wind, *Space Sci. Rev.*, 11, 234, 1970.

193. Scarf, F. L., and Siscoe, G. L., The Pioneer 9 electric field experiment, 2, observations between 0.75 and 1.0 AU, *Cosmic Elec.*, 2, 44, 1971.

194. Scarf, F. L., Greenstadt, E. W., Wolfe, J. H., and Colburn, D. S., An analysis of Pioneer 9 low-frequency wave observations near interplanetary discontinuities, *J. Geophys. Res.*, 77, 3317, 1972.

195. Scargle, J. D., Activity in the Crab nebula, *Astrophys. J.*, 156, 401, 1969.

196. Schubert, G., and Coleman, P. J., Jr., The angular momentum of the solar wind, *Astrophys. J.*, 153, 943, 1968.

197. Schulz, M., and Eviatar, A., Electron temperature asymmetry and the structure of the solar wind, *Cosmic Elec.*, 2, 402, 1972.

198. Siscoe, G. L., Davis, L., Jr., Coleman, P. J., Jr., Smith, E. J., and Jones, D. E., Power spectra and discontinuities of the interplanetary magnetic field: Mariner 4, *J. Geophys. Res.*, 73, 61, 1968.

199. Siscoe, G. L., and Finley, L. T., Meridional (north-south) motions of the solar wind, *Solar Phys.*, 9, 452, 1969.

200. Siscoe, G. L., The solar wind problem with fluctuations, *Cosmic Elec.*, 1, 51, 1970.

201. Siscoe, G. L., and Finley, L. T., Solar wind structure determined by corotating coronal inhomogeneities, 1, velocity-driven perturbations, *J. Geophys. Res.*, 75, 1817, 1970.

202. Siscoe, G. L., and Finley, L. T., Solar-wind structure determined by corotating coronal inhomogeneities, 2, arbitrary perturbations, *J. Geophys. Res.*, 77, 35, 1972.

203. Siscoe, G. L., Discontinuities in the solar wind, in *Solar Wind Three* (C. T. Russell, ed.), Univ. Calif. Press, Los Angeles, 1974, p. 151.

204. Smith, E. J., Radial gradients in the interplanetary magnetic field between 1.0 and 4.3 AU: Pioneer 10, in *Solar Wind Three* (C. T. Russell, ed.), Univ. Calif. Press, Los Angeles, 1964.

205. Smith, E. J., Identification of interplanetary tangential and rotational discontinuities, *J. Geophys. Res.*, 78, 2054, 1973.

206. Smith, E. J., Observed properties of interplanetary rotational discontinuities, *J. Geophys. Res.*, 78, 2088, 1973.

207. Solodyna, C. V., and Belcher, J. W., On the minimum variance direction of magnetic field fluctuations in the azimuthal velocity structure of the solar wind, *Geophys. Res. Lett.*, 3, 565, 1976.

208. Spitzer, L., Jr., *Physics of Fully Ionized Gases*, Interscience, New York, 1962.

209. Stepanov, K. N., Kinetic theory of magnetohydrodynamic waves, *Sov. Phys. JETP*, 7, 892, 1958.

210. Stix, T. H., *The Theory of Plasma Waves*, Ch. 3, 8, and 9, McGraw-Hill, New York, 1962.

211. Stix, T. H., Fast-wave heating of a reactor plasma, consideration of two frequency regions, *Bull. Am. Phys. Soc.*, 21, 1134, 1976.

212. Sturrock, P. A., In what sense do slow waves carry negative energy? *J. Appl. Phys.*, 31, 2052, 1960.

213. Sturrock, P. A., Stochastic acceleration, *Phys. Rev.*, 141, 186, 1966.

214. Tajiri, M., Propagation of hydromagnetic waves in collisionless plasma, 2, kinetic approach, *J. Phys. Soc. Japan*, 22, 1482, 1967.

215. Taniuti, T., and Washimi, H., Self-trapping and instability of hydromagnetic waves along the magnetic field in a cold plasma, *Phys. Rev. Lett.*, 21, 209, 1968.

216. Thompson, W. B., *An Introduction to Plasma Physics*, Ch. 5, Addison-Wesley, Reading, Mass., 1962.

217. Toichi, T., Thermal properties of the solar wind plasma, *Solar Phys.*, 18, 159, 1971.

218. Toptygin, I. N., Magnetohydrodynamic waves in the plasma of the solar wind, *Radiophys. Quant. Electron.*, 16, 745, 1973.

219. Tsytovich, V. N., *Nonlinear Effects in Plasma*, Plenum, New York, 1970.

220. Turner, J. M., and Siscoe, G. L., Orientations of 'rotational' and 'tangential' discontinuities in the solar wind, *J. Geophys. Res.*, 76, 1816, 1971.

221. Unti, T. W. J., and Neugebauer, M., Alfvén waves in the solar wind, *Phys. Fluids*, 11, 563, 1968.

222. Unti, T. W. J., Neugebauer, M., and Goldstein, B. E., Direct measurements of solar-wind fluctuations between 0.0048 and 13.3 Hz, *Astrophys. J.*, 180, 591, 1973.

223. Unti, T., Neugebauer, M., and Wu, C. S., Shock system of February 2, 1969, *J. Geophys. Res.*, 78, 7237, 1973.

224. Unti, T., and Russell, C. T., On the causes of spectral enhancements in solar wind power spectra, *J. Geophys. Res.*, 81, 469, 1976.

225. Valley, G. C., Propagation of hydromagnetic waves in a stochastic magnetic field, *Astrophys. J.*, 168, 251, 1971.

226. Valley, G. C., Scattering of Alfvén waves by random density fluctuations, *Astrophys. J.*, 188, 181, 1974.

227. Völk, H. J., and Alpers, W., The propagation of Alfvén waves and their directional anisotropy in the solar wind, *Astrophys. Space Sci.*, 20, 267, 1973.

228. Völk, H. J., Microstructure of the solar wind, *Space Sci. Rev.*, 17, 255, 1975.

229. Weinberg, S., Eikonal method in magnetohydrodynamics, *Phys. Rev.*, 126, 1899, 1962.

230. Wentzel, D. G., Cosmic-ray propagation in the galaxy: collective effects, *Ann. Rev. Astron. Astrophys.*, 12, 71, 1974.

231. Whitham, G. B., A general approach to linear and non-linear dispersive waves using a Lagrangian, *J. Fluid Mech.*, 22, 273, 1965.

232. Wilcox, J. M., and Ness, N. F., Quasi-stationary corotating structure in the interplanetary medium, *J. Geophys. Res.*, 70, 5793, 1965.

233. Wilcox, J. M., The interplanetary magnetic field: solar origin and terrestrial effects, *Space Sci. Rev.*, 8, 258, 1968.

234. Wong, A. Y., Motley, R. W., and D'Angelo, N., Landau damping of ion acoustic waves in highly ionized plasmas, *Phys. Rev.*, 133, A436, 1964.

235. Wray, A., Nonlinear magnetohydrodynamic phenomena, Ph.D. thesis, Calif. Inst. Technol., 1973.

236. Wu, C. S., Landau damping and resonant energy absorption, *Phys. Rev.*, 127, 1419, 1962.

EARTH'S MAGNETOSPHERE:
GLOBAL PROBLEMS
IN MAGNETOSPHERIC PLASMA PHYSICS

Juan G. Roederer
Department of Physics and Astronomy
University of Denver
Denver, Colorado 80208

May 1977

EARTH'S MAGNETOSPHERE: GLOBAL PROBLEMS IN MAGNETOSPHERIC PLASMA PHYSICS

Abstract

Selected problems of magnetospheric plasma physics are critically reviewed. The discussion is restricted to questions that are "global" in nature, i.e., involve the magnetosphere as a whole, and that are beyond the stage of systematic survey or isolated study requirements. Only low-energy plasma particle aspects are discussed. The article focuses on the following subjects: (i) General characteristics of magnetospheric field configuration; (ii) Effect of the interplanetary magnetic field on topography, topology and stability of the magnetospheric boundary; (iii) The mechanisms for the entry of solar wind plasma into the magnetosphere; (iv) Plasma storage, acceleration and release mechanisms in the magnetospheric tail; (v) Magnetic-field-aligned currents and magnetosphere-ionosphere interactions. A brief discussion of the prospects for the solution of these problems during the coming years is given.

1. Introduction

A magnetosphere arises from the interaction of a continuously streaming, hot, collisionless plasma with a magnetized body. In this interaction a cavity--the magnetosphere proper--is carved out in the flow by the magnetic field of the central body. This magnetic field also physically ties the points of the magnetosphere together, guiding charged particles, plasma waves and electric currents; trapping thermal plasma and energetic particles; and transmitting hydromagnetic stresses between the exterior flow and the resistive central body. Presently known magnetospheres scale from a few thousand kilometers in transverse dimension (Mercury) to over ten million light years (Radiogalaxy NGC 1265--Fig. 1). The principal energy source for magnetospheric processes may be the external plasma flow ("earth-like magnetospheres) or the rotating magnetized body ("pulsar-like" magnetospheres). The plasma itself may come from the external flow (Mercury, earth), from the central body (perhaps pulsars) or its ionosphere (the planets), or from satellites of the central body (Jupiter's satellite Io and Saturn's Titan), or all three. All known magnetospheres are highly time variable, exhibiting different variations upon a common theme: wherever nature creates a magnetosphere, she arranges that the magnetic energy stored in it be suddenly released, accelerating a small subset of charged particles to high energy.

During the past 20 years the study of the earth's magnetosphere has undergone a highly successful stage of discovery and exploration. Investigators have obtained a morphological description of the magnetic field and its time variations, the particle population embedded in it, and the interface with the solar wind. Many of the physical processes involved have been identified and are beginning to be understood; a fairly complete quantitative description of the energetic particles trapped in the earth's magnetic field exists.

Magnetospheric physics is now in a transition from the exploratory stage to one in which satellite missions and ground-based observations are planned with the specific objective of achieving a global understanding and

self-consistent quantitative description of the cause-and-effect relationships among the principal dynamical processes involved. Measurements turn to lower and lower energies as well as to higher ion mass species in order to encompass the entire particle population, and to a broader range of the frequency spectrum of magnetic and electric field variations. Today, the terrestrial magnetosphere may be considered as our private "backyard universe" where we can study in situ, systematically and quantitatively many fundamental plasma processes at work. This new stage of research has led to some fundamental advances in recent years, such as: (i) The discovery of layers of streaming or flowing plasma in the magnetosphere beneath its boundary surface (viz., the boundary layer, the mantle, and the entry layer); (ii) The identification of the terrestrial magnetosphere as a celestial source of kilometric radiation and relativistic particles; (iii) The identification of parallel electric field regions within the magnetosphere and their role in auroral particle acceleration; (iv) The discovery of large fluxes of energetic heavy ions trapped in the magnetosphere.

A vigorous development of new experimental techniques has also taken place. Among these we should point out the increased use of active experiments, in which man-made perturbations with well-defined initial conditions are introduced in the earth's plasma environment in order to break into the complex chains of cause-and-effect relationships and study the ensiung reactions.

The above developments represent only a small portion of the overall accomplishments of magnetospheric physicists in the last half decade, and demonstrate a continued active interest in this field. With the new advances, many new questions have emerged, mainly concerning the dynamical processes governing particle, momentum, and energy transfer between the solar wind, magnetosphere, and upper atmosphere, and involve the magnetosphere as a single, integral dynamic system (International Magnetospheric Study: Progress Report, SCOSTEP Secretariat, c/o National Academy of Sciences, Washington, D. C., 1977). The questions include:

(1) The effect of the interplanetary magnetic field on the topology, structure, and stability of the magnetospheric boundary.

(2) The mechanisms for the entry of solar wind plasma into the magnetosphere.

(3) The storage and release of energy in the magnetosphere and the processes by which particles are accelerated.

(4) Magnetosphere-ionosphere interactions.

These four global problems are sufficiently general that they may serve as organizing principles for future experimental and theoretical research in magnetospheric physics.

In the past decade, it also has become increasingly clear that processes stemming from solar-terrestrial interaction exert a subtle but significant influence in several domains that directly affect man and his interaction with the environment. Three major areas of relevance have been identified (International Magnetospheric Study: Progress Report, 1977):

(1) Magnetospheric perturbation effects on communications and power transmission: short-wave propagation; VLF signal propagation; underground telephone and telegraph transmission; and electric power transmission.

Relevant scientific research that needs to be carried out in connection with these topics includes magnetospheric storm and substorm prediction; particle precipitation effects on the ionosphere; study of ionospheric irregularities; and the study of geomagnetic induction effects.

(2) Magnetospheric effects on orbiting spacecraft: spacecraft charging; radiation damage; and atmospheric drag.

Relevant scientific research requires the study of magnetospheric plasma-spacecraft interaction; radiation belt dynamics; and magnetosphere-generated atmospheric heating by electric currents and precipitated particles.

(3) Magnetospheric effects on climate and weather: long-term and short-term effects.

It is believed that the magnetosphere may transmit solar or interplanetary perturbations to the atmosphere and thus influence in a subtle way the delicate balance of stratospheric and tropospheric dynamics. The implication is that long-term changes in the sun's hydromagnetic properties affecting the magnetosphere may therefore have an effect on terrestrial climate; short-term variations may affect weather. A total unknown in this process is how the magnetosphere, the ionosphere, and the upper atmosphere might be able to communicate these perturbations down to levels necessary to influence the atmospheric forces that then lead to changes in climate and weather patterns.

Abundant comprehensive literature exists on the progress of magnetospheric research during the past decade (e.g., McCormac, 1968-1976; Dyer, 1972; Williams, 1976) as well as on those aspects of magnetospheric physics which are presently well understood such as the radiation belts (e.g., Hess, 1968; Roederer, 1970; Cladis et al., 1974; Schulz and Lanzerotti, 1974 many fundamental processes are discussed elsewhere in this book. The main purpose of this chapter, rather than reviewing past developments, is to focus on current plasmaphysical problems that are of truly "global" nature, i.e., involve the magnetosphere as a whole, and that are beyond the stage of systematic survey or isolated study requirements. The picture presented and the research work quoted are far from complete; no original data will be shown; emphasis will be placed on controversial or mutually contradictory results. Because of the severe restriction in scope, there are four capital omissions, referring to fundamentally important problems of magnetospheric research. One omitted subject is energetic trapped particles, the ring current, and wave-particle interactions. Another is transient parallel electric fields and auroral particle acceleration; the third is the study of the composition of magnetospheric plasma; and the fourth, physics of the plasmasphere.

2. General Characteristics of Magnetospheric Field Configuration

Figure 2 (after Morfill and Quenby, 1971) qualitatively shows a possible steady-state magnetic field topology of a planetary magnetosphere, drawn in the plane defined by the magnetic axis of the planet and the bulk velocity vector of the solar wind. Four regions may arise, as defined by the topological features of their magnetic field lines. Region I comprises the family of field lines which emerge from the solar surface and return to it at another point.*) They enclose source currents flowing in the interior of the sun that are external to the plasma under consideration. Region II is defined by the field lines which link the sun with the planetary body. Region III contains the field lines which intersect the planetary surface at two points; they encircle source currents flowing in the interior of the magnetized body which are independent of the plasma elsewhere. Region IV is one in which the field lines are totally embedded in plasma; they do not contact the sun or the planetary body and do not encircle external source currents. Under certain conditions region II could shrink to zero (the case of a "closed" magnetosphere); region IV may exist only as a transient feature; it is conceivable that two or more such regions could exist simultaneously or that it could flatten to form an extended "neutral sheet."

These "field-topological" regions are cut across by plasma boundaries that define distinct "plasma-topological" regions (Fig. 2). Region A represents the unperturbed supersonic solar wind plasma whose "lower" boundary lies at the base of the corona. This lower boundary represents the acceleration region of the solar wind where the solar atmosphere is heated by local dissipation of hydromagnetic wave energy emitted from the photosphere. The local configuration of magnetic field and ambient gas determines the characteristics of the generated solar wind. For all practical purposes, the magnetic field and other plasma parameters of region A can be assumed to be

---

*) Or eventually are connected to the interstellar medium.

uniform in the vicinity of the magnetosphere during steady-state conditions.*) The standing bow shock represents the boundary with the magnetosheath, region B, containing initially compressed, subsonic and sometimes turbulent plasma that subsequently expands again to superalfvénic speed as it flows along the magnetospheric boundary. This boundary, the magnetopause, delimits the magnetospheric domain proper, region C. The bow shock and the magnetopause involve discontinuities of the magnetic field and of other plasma parameters. The lower ionosphere, or, in the case of planetary bodies devoid of an atmosphere, the planetary surface, represents the "lower" boundary of region C.

The electric conductivity along magnetic field lines appears to be extremely high so that the MHD approximation (V: plasma bulk velocity)

$$\underline{E} + \underline{V} \times \underline{B} = 0 \qquad (1)$$

is assumed to hold everywhere in the system of Fig. 2, with the following exceptions: (i) near the solar surface, i.e., for all practical effects, at the base of the corona; (ii) near the magnetized body in the lower ionosphere or on the planetary surface; (iii) on and near the bow shock; (iv) on and near the magnetopause; (v) in the vicinity of those points where the magnetic field vanishes (N_1, N_2, N_3 in Fig. 2). In addition to the above, there may be spatially and/or temporally limited regions (e.g., field lines which guide auroral particles) where an anomalous conductivity (turbulence along field lines) and/or parallel electric fields sustained by pitch angle anisotropies invalidate the MHD approximation.

Note again that region IV (Fig. 2) would be the only one in which magnetic field lines are totally embedded in the plasma of the system; all other regions contain field lines along which plasma is allowed to spread "freely" (without resistance) only within certain boundaries. Within such boundaries and wherever the MHD relation (1) holds, the magnetic field lines will be

---

*) This certainly does not apply to Jupiter's magnetosphere, whose impressive size (over 0.1 AU transverse dimension) compares with the scale-size of major solar wind inhomogeneities.

electric equipotentials in a steady-state configuration (one that changes on a time-scale long compared to the time it takes to short out any electric field component parallel to the magnetic field).

In this article we shall concentrate on region C (Fig. 2) and its boundaries, i.e., the magnetosphere proper. On occasion, we shall have to deal with the characteristics of the magnetosheath, region B. The perhaps most fundamental problem of magnetospheric physics is to determine the field- and plasma-topological features of Fig. 2 that are permanent characteristics of the interaction of a supersonic plasma flow against a magnetized, resistive central body, to identify all transient properties, and to establish a self-consistent, quantitative theoretical description of the cause-and-effect relationships between the intervening parameters. Unless otherwise stated, we shall refer to the terrestrial magnetosphere only and break up the abovementioned fundamental problem into several global "subproblems," each one focusing on certain chains of interaction mechanisms that involve the magnetosphere as a whole. In this discussion, the "external" boundary conditions of relevance to the magnetosphere proper will be represented by the given values of magnetic field, bulk velocity, density and temperature of the solar wind immediately in front of the bow shock, and by the values of similar parameters plus the local resistivity in the ionosphere.

3. Effect of the Interplanetary Magnetic Field on Topography, Topology and Stability of the Magnetospheric Boundary

Let us envisage a cylindrical magnetic flux tube of small cross section totally contained in region I-A (Fig. 2). As the solar wind plasma contained in this tube at any given time t moves with bulk velocity $\underline{V}$, it will remain in a thin flux tube at any later time $t + \Delta t$, due to the validity of relation (1) ("line-preservation," Newcomb, 1958) in the region occupied by this plasma. This is customarily interpreted by saying that the interplanetary field lines "move with velocity $\underline{V}_\perp$"*), where $\underline{V}_\perp$ is the component of $\underline{V}$ perpendicular to the local interplanetary magnetic field $\underline{B}_i$ (IMF). A less picturesque but perhaps more mature description (Alfvén, 1976a) is to state that the solar wind plasma tube is drifting transversely to the interplanetary field with a velocity $\underline{V}_\perp = \underline{E}_i \times \underline{B}_i / B_i^2$ due to the presence of a convective electric field $\underline{E}_i$. The physical sources of $\underline{E}_i$ are polarization charges due to the impressed forces acting at the base of the corona (and, possibly, due to equivalent electric charg associated with moving diamagnetic currents and with vortices or discontinuitie in the flow). On a global scale, $\underline{V}$ is to be considered the "cause," $\underline{E}_i$ the "effect" in relation (1) for the solar wind (Stern, 1976).

---

*) There is an infinite family of vectors which are "line preserving" and which could be used with equal legitimacy to define a field line velocity (Vasyliunas, 1972). What most investigators use (mostly without saying so) is a phenomenological definition of local field line velocity given by the electric drift velocity c a probe charge injected with vanishing kinetic energy in absence of non-electromagnetic forces (Roederer, 1970), or, which is the same, by the instantaneous velocity of a charged particle for which the Lorentz force exactly balances the electric force (Stern, 1976). Note that the component of the bulk velocity paral to the magnetic field does not appear in the moving field line picture at all. No also that the moving field line picture loses its "intuitive simplicity"--and as a matter of fact may become a serious conceptual trap (Alfvén, 1976b)--for all those field lines on which the validity of the MHD approximation (1) is limited t a finite portion (as it happens with field lines in all topological regions of Fig. except region IV!). See also footnote on p. 398.

When the plasma flux tube impinges on the bow shock wave, it is kinked in the rotational discontinuity; as it crosses the shock, the plasma is heated. The bulk motion of the flux tube in the magnetosheath will be governed by the particular interaction mechanism between the streaming plasma and the magnetosphere. Since the earth's magnetosphere is a small obstacle with respect to the macroscopic inhomogeneities of solar wind flow, on the local scale of this interaction it is the convective electric field $\underline{E}_i$, mapped down along equipotential magnetic field lines from the unperturbed regions of the solar wind, which is to be considered the externally impressed quantity in the MHD relation (1).

Two extreme cases can be envisaged, between which the real situation of solar wind-magnetosphere interaction may lie.

(1) One extreme situation would be that of a purely gasdynamic flow around a "closed magnetosphere," with the magnetopause acting as a two-way magnetic shield [tangential discontinuity only; perpendicular component of the magnetic field on the magnetopause $\underline{B}_\perp = 0$ everywhere; no field line connection (no region II in Fig. 2)]. In this case all incoming plasma tubes would swing around the magnetopause, and only an infinitesimally thin slab of plasma would maintain a tangential apposition on the latter at the stagnation point, from there gliding downstream. Diamagnetic currents and electric polarization in the magnetosheath would ensure that the transverse flow velocity is coupled to the magnetic and electric field vectors through relation (1) everywhere in this particular gasdynamic flow. The only way that solar wind plasma could penetrate into the magnetosphere in this extreme case is by diffusion through the magnetopause or by flow into the "one-dimensional" boundary neutral points that would exist in this closed-magnetosphere configuration. The efficiency of the entry process would depend on the particular diffusion mechanism envisaged, on the magnetosheath plasma distribution function in front of the magnetopause, on the microstructure of the boundary, and on the magnetic field inside.

Note that case (1) would correspond to a hypothetical situation in which $\underline{B}_i \to 0$, or to a model in which a magnetized, superalfvénic solar wind flows against a blunt object (the magnetopause) with superconducting properties (to insure $\underline{B}_\perp \equiv 0$). The picture of an unmagnetized solar plasma, though far remove from reality, has been used quite successfully in studies of the structure of the magnetopause (see review by Willis, 1975) and in numerical determinations of it shape (see review by Walker, 1976). The second model represents a condition under which the plasma equations decouple into a gasdynamic set (giving the flow configuration) and an electromagnetic set (describing the magnetic field) which can be used to draw up quantitative descriptions of the magnetosheath (see revie by Fairfield, 1976).

(2) The other extreme situation would be represented by a magnetopause that acts as a "one-way boundary," with the interplanetary magnetic field being allowed to penetrate undistorted into the magnetosphere [i.e., where the perpendicular magnetic field component on the magnetopause is equal to that of the unperturbed interplanetary field: $\underline{B}_\perp = (\underline{B}_i \cdot \underline{n}) \cdot \underline{n}$; $\underline{n}$: normal to the magnetopaus This extreme situation would imply an undisturbed flow of magnetosheath plasma right onto the magnetopause (no bow shock!). The resulting field geometry insid the magnetospheric cavity would be given by the linear superposition of the magnetospheric field (of sources on and within the magnetopause) and the (uniform) solar wind field (Forbes and Speiser, 1971). Two model examples are shown in Figs. 3a and b (Saunders, 1976), for southward- and northward-directed inter-

planetary magnetic fields, respectively. The important point is that plasma tubes drifting into the magnetopause will now be "cut" at points whose position will depend on the direction of $\underline{B}_i$. For an interplanetary field directed due south, these points lie on the equatorial surface (N_1 in Fig. 3a). For a northward field there would be two cutting points N_i located at high latitudes on each meridian (Fig. 3b). For a southward-directed field, the incoming solar wind plasma will drift onto and through field lines of class II (Fig. 3a), which are connected to the polar cap. Note that here we have a case of plasma flow between regions of different field topology (I and II). Solar wind plasma now would be allowed to flow into the magnetosphere everywhere along the magnetopause in region II (the magnetopause would be a wave-like structure). This entry flow would be governed by the particular magnetic field geometry connecting regions B and C (Fig. 2), by the plasma distribution function prior to entry, and by the microstructure of the magnetopause (Section 4). A similar plasma tube breaking is bound to occur at point N_2 in Fig. 3 a, where the plasma is again transferred to different field-topological regions (I and III). In the case of a due northward $\underline{B}_i$ no region II arises (Fig. 3b). The incoming plasma could drift into the closed field line region III at low latitudes (continuity of the tangential component of the electric field across the boundary); at high latitudes, above the breaking points N_1, it would remain on class I field lines which, however, do cross the magnetopause to become part of the distant magnetospheric tail (region I-C in Fig. 2).

In this extreme case (2) all plasma tubes projected in the direction of the bulk velocity $\underline{V}$ onto the magnetopause will be "broken." The points at which the intercepted plasma tubes are cut lie on a curve called the "X-line." Since field lines are equipotentials both outside and inside the magnetosphere (we are implicitly assuming that they are occupied by zero resistivity plasma everywhere in the domain under consideration), whenever a region of class II arises (Figs. 2, 3a) the solar wind electric field $\underline{E}_i$ is mapped right down into the area of the iono-

sphere intercepted by these field lines (Stern, 1973).*) Hence, plasma convection over the polar cap would be directly controlled by the convection of the solar wind [$\underline{E}_i$ is the "cause," $\overline{V}$ the "effect" in relation (1)]. It is important to note that in these models, for field-topological reasons only, the convection over the polar caps turns out to be mainly tailward for nearly all directions of the IMF (Stern, 1973; Saunders, 1976).

Finally, yet another extreme configuration could, in principle, be envisaged in which a magnetopause simply does not exist. In this case the magnetic field is a linear superposition of the fields of the solar wind and the planetary body everywhere in space. Though representing an even more unrealistic situation than case (2) above, such a superposition also gives rise to field-topological regions of type I, II and III, depending on the relative orientation of the superposed fields, and has been used in quantitative analyses of the geometric features of the resulting field configuration (Stern, 1973; Yeh, 1976).

The real situation of a planetary magnetosphere in steady-state configuration lies somewhere between the extremes (1) and (2), depending on the orientation of the interplanetary magnetic field and on the plasma processes occurring on and near the magnetopause. Incoming solar wind plasma tubes apposing on the magnetospheric boundary will be broken; however, the efficiency of this process (total intercepted flux) and that of solar wind penetration into the magnetosphere will be controlled by the fine-structure of the boundary and that of the magnetosheath plasma. Whatever boundary current system results, the actual magnetic field topology inside the magnetosphere and its connection with the interplanetary field will be determined by the actual distribution of the normal component $\underline{B}_\perp$ on the magnetopause. In a steady-state situation this represents a conceptually simple

---

*) The possible breakdown of the MHD approximation (1) in the vicinity of the magnetopause would not invalidate field line equipotentiality, provided the breakdown region along the field line is very thin (Vasyliunas, 1976).

magnetostatic problem (Voigt, 1976). An obvious but often neglected fact is that the distribution of the normal component $B_\perp$ on the magnetopause--even a very weak one--will necessarily affect the configuration of the magnetic field in the tail and all its topological features such as neutral lines (see Section 4). It is important to point out that the actual position and shape of the boundary and the magnetic field configuration adjacent to it are the result of all currents in the magnetospheric system, proximate as well as distant.

The experimental determination and theoretical description of how the magnetic field in the magnetosheath and the structure and shape of the magnetopause influence each other might well be called today's "task number one" of magnetospheric plasma physics. It is necessary to identify what properties of the magnetosphere are generated, and what properties are only modulated, by the interplanetary magnetic field. In particular, it is necessary to determine whether a unique steady-state configuration of the system of Fig. 2 exists and what the magnetic field topology on and near the magnetopause is for a given IMF direction; whether the actual steady state depends on the history of the system (i.e., on how B_i was set up), and whether there are conditions for which instabilities make a steady-state situation outright impossible.

For instance, a conspicuous place where a disruptive instability might occur is at those points of the X-line on the boundary on which the local magnetic field vanishes. In the neighborhood of such points (X-type neutral points, N_1 in Figs. 2 and 3a) the MHD approximation and isotropic fluid description break down; a solar wind plasma tube drifting into such a region (which requires an appropriate local electric field) will not only be cut, but, for the portion of the plasma flowing into the breakdown region, the individuality as pertaining to a given plasma tube will be lost. The question arises whether under such circumstances a steady-state regime can exist at all, i.e., whether the general magnetic field configuration can be maintained without change, or whether the plasma flow into the neutral point region will entice a temporal change in boundary configuration between the field-topological regions I and II such that the total magnetic flux in region II is

changed (for instance, increased). Note carefully that, necessarily, region III would also become involved in such a flux transfer process: any total magnetic flux increase of region II must occur at the expense of a decrease of flux in region III (this has been called "erosion" of the closed field line region III on the dayside). Also the plasma (if any) in region III will necessarily be involved. Indeed, since there is a flow into the neutral point in medium I caused by the convective electric field $\underline{E}_i$, continuity of the tangential component of the electric field requires that the plasma of region III (where the magnetic field is reversed) also flow into the neutral point (and that plasma flow away from it in region II.

The terms "magnetic merging" and "reconnection" have been chosen to designate a plasma transfer across the "separatrix" surface defined by field lines passing through an X-line into a region of different field topology (Vasyliunas, 1976). Such a transfer process necessarily implies the existence of a macroscopic electric field in the region of the X-line, directed along the latter, responsible for the plasma flow into and out of the region. It also implies the breakdown of the MHD approximation in the vicinity of the X-line because of $B \to 0$. Reconnection is a plasma-dynamic process in which field energy is converted into particle energy. But it is more than that (any region in which $\underline{j} \cdot \underline{E} > 0$ has this property). What counts in a merging or reconnection process are the feedback effects of MHD breakdown and associated turbulence and shocks on the entire macroscopic plasma flow and electromagnetic field configuration. (For a discussion of the processes in the breakdown region and their local effects, see reviews by Vasyliunas, 1975; and Sonnerup, 1976). In the present article, the term field line "connection" or "interconnection" will be reserved to merely describe the topological feature of field lines crossing the magnetospheric boundary ($\underline{B}_\perp \neq 0$, Region II, Fig. 2) (Roederer, 1970). It does not necessarily imply the occurrence of a plasma-dynamical process as described above. For instance, in a vacuum field we may have interconnection but not reconnection; in a plasma, there are conditions under which we may create an X-line by manipulating external currents and regulate the plasma transfer through the separatrix by manipulating an electric field of external sources, without the appearance of this X-line and associated MHD breakdown in any way causing a transition into a new plasma-field configuration. Most unfortunately, in the literature

the terms reconnection and merging are frequently used to merely designate the topological feature of field line connection across the magnetopause (open magnetosphere). Note that the existence of an X-line on the boundary of an "open magnetosphere" interconnected with the interplanetary magnetic field, though necessary, is by no means a sufficient condition for the occurrence of a magnetic merging process as defined above.

One of the most serious hurdles in the approach to "task No. 1" lies in the difficulty of obtaining experimental information on the magnetic field configuration adjacent to and across the magnetopause. Very high sampling rates are necessary to provide enough data prior to, during, and after the few seconds of satellite traversal time through the relevant region. Simultaneous measurements of all major plasma parameters are required. Single satellite observations make it difficult to separate spatial from temporal effects and to determine the local orientation of the boundary, which must be known in order to be able to determine $\underline{B}_{\perp}$, i.e., the field line connection topology. Last but not least, global information on the integral state of the magnetosphere as well as on the parameters of the incident undisturbed solar wind is needed to distinguish between boundary features governed by local processes and features which represent an integral response to distant conditions.

In spite of these difficulties some concrete results have been achieved in recent years. Measurements indicate that the magnetic field in the magnetosheath near the magnetopause surface is preponderantly parallel to the latter e.g., Paschmann et al., 1976; review by Fairfield, 1976), indicating that the gasdynamic "extreme" (1) described above may not be too far removed from reality [which comes as a surprise when considering a collisionless plasma (Heikkila, 1973)]. These observations, however, do not preclude the existence of a small perpendicular component $\underline{B}_{\perp}$ across the magnetopause. Indeed, some magnetopause crossings can be interpreted in terms of a rotational discontinuity (e.g., Sonnerup and Ledley, 1974); these events, however, seem to be rare. Quite generally, the experimental evidence of field line interconnection between

the magnetosphere and the solar wind so far is only indirect, sometimes rather inconclusive, or based on the analysis of single events. It is indeed fair to say that evidence for an "open" magnetosphere is mainly based on observations for which such a model offers the simplest (but not always unique) explanation requiring a minimum number of assumptions. For instance, the principal features of solar particle access and distribution over the polar caps can be explained quite convincingly by assuming that regardless of IMF direction there is a direct connection between geomagnetic and interplanetary magnetic field lines, with the region of connection lying within a few hundred earth radii in the magnetospheric tail (e.g., review by Paulikas, 1974; Meng and Kroehl, 1977). Observations of lunar absorption effects on solar electrons in the tail (Anderson and Lin, 1969) point to the existence of field lines of class II (Fig. 2). Yet, although there is a clear correlation of the north-south asymmetry of the solar particle flux in the polar caps with the azimuthal direction of the interplanetary field, other predicted features such as a day-to-night development pattern of particle influx (Michel and Dessler, 1975) have not been observed. Even some features of solar proton entry can be adequately explained by particle orbit integration across the tangential discontinuity of a closed magnetosphere boundary (Morfill and Quenby, 1971; Durney et al., 1972). On the other hand, observed correlations between interplanetary field direction and geomagnetic variations in, and the size of, the polar caps (e.g., Svaalgard, 1973; Akasofu et al., 1973a), or the configuration of the polar cap electric field (e.g., Heppner, 1973; Mozer et al., 1974) have been invoked as evidence for a topological interconnection between magnetospheric and interplanetary field lines.

Turning to the plasma-dynamical process of merging or reconnection on the boundary, plasma observations near the magnetopause have so far failed to confirm the characteristic flow that should be expected if a reconnection process were to take place on the dayside magnetopause on occasions of "favorable" field configurations (Paschmann et al., 1976). The absence of such a flow seems to argue against a local merging process but not necessarily against the topological interconnection of magnetospheric and interplanetary fields.

There are, however, effects that have been interpreted in terms of a merging process on the dayside magnetopause. The existence of a layer of field-aligned, antisunward-streaming energetic electrons in the magnetosheath within about 3 R_e of the magnetopause (Meng and Anderson, 1970, 1975; Domingo et al, 1974; Baker and Stone, 1977a) has been considered to be evidence for a merging process at the nose or the cusp of the magnetosphere (Axford, 1976). Another effect is the gradual increase in magnetic field intensity in the tail lobes that occurs during periods of sustained southward-directed $\underline{B}_i$ (e.g., review by Burch, 1974). This effect may not be due to a compression of the tail lobes; indeed, the tail radius has been reported to increase (Maezawa, 1975). (The associated decrease in tail plasma pressure required by pressure balance considerations so far has not been detected.) Here we have a situation in which an essentially "static" input configuration (the southward interplanetary field) leads to a dynamic response in the magnetosphere ($\frac{\partial B}{\partial t} > 0$ in the tail). Another effect is represented by the observation of more earthward dayside magnetopause positions in association with southward-directed interplanetary fields (Fairfield, 1971) (this effect being strongly washed out by variations in solar wind pressure) and by the fact that geomagnetic substorms are more likely to be detected by the existing chain of geomagnetic observatories during such periods of time (Akasofu et al., 1973a) (because of an increased size of the polar cap region during times of southward-directed IMF). The fourth effect frequently quoted as an indication for merging on the dayside magnetopause is one example in which a large inward motion of the dayside boundary was observed during a time of constant solar wind kinetic energy flux (Aubry et al., 1970).

However, alternate descriptions of some of these effects can be given that do not require anything "special" happening on the dayside boundary except for the appearance of a particular distribution of $\underline{B}_\perp$, i.e., a particular interconnection topology, and/or that only invoke internal mechanisms operating inside the tail (the plasmasheet). In Section 5 we shall describe such an alternative to explain the second abovementioned effect of tail field intensity increase. The third and fourth effects mentioned above, too, need not be interpreted as originating in a plasma-dynamical merging process localized at the nose of the magnetopause.

They could represent an integral field reconfiguration due to the increase (and earthward displacement) of the cross-tail current sheet (e.g., Unti and Atkinson, 1968), caused by an enhanced plasma convection into the tail during times of southward IMF. [To explain the large inward motion of the boundary mentioned in the preceding paragraph, the required tail current increase seems to be rather high (Russell et al., 1974); however, there are enough uncertainties in this event (e.g., in the actual direction of the normal to the magnetopause) that a field-geometric explanation could not be ruled out]. Finally, certain features of the energetic electron layer in the magnetosheath, such as its permanent nature, its latitude- and longitude-independent structure and spectrum, and the rather weak correlation of electron flux with the direction of the IMF (Meng and Anderson, 1975), are rather difficult to reconcile with the assumption that this layer originates in a merging process at the front of the magnetopause (see also p. 397).

4. The Mechanisms for the Entry of Solar Wind Plasma into the Magnetosphere

So far we have dealt mostly with magnetic field aspects of the solar wind interaction with the magnetosphere. This interaction, however, also controls the intrinsic, microscopic structure of the magnetospheric boundary, and it regulates the motion and energy dissipation of magnetosheath plasma during the process of its entry into the magnetosphere proper. The plasma structures under consideration here are the magnetopause, from now on to be considered a layer of small but finite thickness, and the plasma layers known as the entry layer, the "throat," the cleft or cusp, the mantle, and the magnetotail boundary layer, sketched in Fig. 4. A study of these boundary layers is of particular importance because they involve dynamical phenomena that are unique to plasma flow interfaces and do not occur in the more uniform portions of the solar wind sectors and inside the magnetospheric plasma "reservoirs" such as the plasmasheet and plasmasphere (Fig. 4).

The magnetopause layer can be defined as the region where the currents flow that cause a more or less abrupt change in the magnetic field and plasma configuration, separating magnetosheath from magnetosphere (see reviews by Willis, 1975, 1977; and Sonnerup, 1976). The predicted thickness of this layer lies anywhere between the average solar wind proton gyroradius in the boundary's magnetic field down to the plasma skin depth (geometric mean of average proton and electron gyroradii). As magnetosheath particles impinge on the confined magnetic field, they are deflected transversally to the B vector in opposite senses; this transverse motion represents the Chapman-Ferraro current (Ferraro, 1952). The Lorentz forces acting on this current system furnish the force system needed to equilibrate the dynamic plasma pressure of the impinging solar wind. The actual structure of this current layer depends on whether the electric polarization field created by the ensuing electron and ion charge separation (difference in turning points) is neutralized totally or partially by the ambient plasma. If this electric field is completely neutralized, the impinging magnetosheath ion and electron streams move independently of each other and every particle penetrates into the geomagnetic field a distance approximately equal to its gyroradius in the average ma

netic field within the boundary layer (~100 km for protons). If it is not neutralized at all, the average thickness of the magnetopause would be reduced to the plasma skin depth (~ 1 km). Neutralization should be possible if thermal particles are drawn up along magnetic field lines from the ionosphere to the boundary. The time-scale for this process (hours), however, is considerably longer than that of usual time-variations of solar wind parameters. Rapid diffusion of solar wind particles across magnetic field lines in the magnetopause layer would be another mechanism to neutralize the electrostatic field.

The actual microstructure of the magnetopause and its equilibrium are expected to depend on the angle between the magnetosheath bulk flow velocity $\underline{V}$ adjacent to the boundary and the magnetospheric field $\underline{B}$ immediately behind the magnetopause (Fig. 5). In one view (Parker, 1967) no static equilibrium should be possible if $\underline{V}$ has a component parallel to the confined magnetospheric field. In such case, two field-aligned ion and electron current sheets would appear in the magnetopause layer, generating an extra magnetic field transverse to the magnetospheric field. The Lorentz force due to this extra field acting on the ion current sheet would oppose the solar wind pressure-balancing Lorentz force on the main Chapman-Ferraro ion current in the confined magnetospheric field. The resulting lack of equilibrium should be a small-scale effect, leading to enhanced mixing between magnetosheath plasma and magnetospheric plasma and associated momentum transfer to the latter. However, other studies (e.g., Davies, 1969) indicate that the effect of this extra magnetic field should depend on the degree of electric field neutralization in the boundary and that equilibrium would be upheld in any case. None of the theoretical studies of intrinsic stability of the magnetopause takes into account the effects of a possible perpendicular component of the magnetic field $\underline{B}_\perp$ (interconnection topology, Section 3).

Even a steady-state boundary layer should be susceptible to micro-instabilities. For instance, streaming of magnetosheath plasma through the ambient plasma in the boundary layer would generate a two-stream ion-

cyclotron instability (Eviatar and Wolf, 1968), with the result of strong proton scattering and associated momentum and particle transfer to the magnetosphere. An electron-cyclotron instability would be responsible for electron scattering (Alpers, 1971). Recently attention has been called (Haerendel, 1977) to the possible effects on the magnetopause and particle transfer through it of an eddy turbulent flow in the vicinity of the cusp indentations (demarcation lines, Fig. 5).

On a larger scale-size, shock waves impinging on the magnetopause from the magnetosheath should cause local deformations and surface waves on the boundary. More significantly, attention was called recently (Lemaire and Roth, 1976) to the fact that even a steady-state solar wind flow consists of intertwined filamentary plasma elements (e.g., Siscoe et al., 1968; Turner et al., 1976), and that the excess momentum of these field-aligned inhomogeneities (of transverse scale size of 1 R_e or less) should cause dents and ripples on the magnetopause. Moreover, it is conceivable that in view of this filamentary structure of the solar wind, the normal component $B_\perp$, the associated field interconnection topology, the stability of the boundary, and the particle and momentum transfer may all be non-uniformly distributed over the magnetopause, which even for a quiet solar wind condition might have a "patchy" structure, with elongated "pockmarks" and "blisters." This patchy structure would map right down onto the polar caps along the interconnected flux tubes, and there would be no single separation boundary between "open" and "closed" field lines. In such a situation it would be impossible to predict which tail field lines will be "open" (interconnected) and which will be closed. Finally, in view of the tilt of the earth's geomagnetic axis with respect to the rotation axis, the diurnal rotation of the internal field sources is expected to cause a seasonally modulated diurnal shift of the magnetopause current system around the demarcation lines (Fig. 5) and, to a small extent, a diurnal variation of the shape of the boundary surface (e.g., Olson, 1969).

For a closed magnetosphere in a steady state ($B_\perp \equiv 0$) it is difficult to ascertain whether or not the magnetopause should be an electrostatic equipotential surface. Indeed, this would depend on whether it is made up of a bundle of field lines converging into a single neutral point on each "hemisphere" (Fig. 6a) as most numerical models predict, or whether the bound-

ary field lines converge into a demarcation line and intersect the ionosphere along a line of finite length (Fig. 6 b). If the boundary were an equipotential, there could be no dissipation or generation of electromagnetic energy by the magnetopause currents. In a steady state, transfer of energy, momentum and particles from the magnetosheath plasma to the magnetosphere would be possible only via diffusion mechanisms or instabilities in the boundary layer (see below).

This situation changes dramatically, however, if field line interconnection through the boundary is allowed. First, in such a case the Lorentz force on the boundary currents will have a component parallel to the boundary serving to accelerate (deflect) the plasma that is penetrating into the magnetosphere. Second, the impressed interplanetary electric field, as observed in a system fixed to the magnetosphere, is mapped onto the boundary along the equipotential magnetic field lines (p. 385). For a southward interplanetary magnetic field, for instance, the situation of Fig. 6c would arise. In a region where $\underline{j} \cdot \underline{E} > 0$ (nose and dayside magnetopause equatorward of the demarcation line), dissipation of electromagnetic energy takes place (the magnetopause acts as a "load"); magnetopause regions where $\underline{j} \cdot \underline{E} < 0$ (tailward of the cusp or demarcation line) act as a generator. The magnetopause current system becomes "active": in order to maintain it in steady state, kinetic energy (ordered or thermal) has to be withdrawn from the dayside magnetopause, whereas kinetic energy has to be supplied to the tail magnetopause. In the consideration of Fig. 6c it is necessary to include the cross-tail current sheet (sometimes inappropriately called "neutral sheet"), because it merges into the boundary current system at the flanks (the surface divergence is ± 0 there). An electric field as shown in Fig. 6c thus also leads to $\underline{j} \cdot \underline{E} > 0$ in the cross-tail current sheet.

It is important to point out here that, in view of the fact that the magnetopause does not seem to suffer any "zeroth-order" changes as a result of a change in the IMF, the electric field component tangent to the boundary must

be totally incidental to the mechanism that maintains the boundary current in operation (Heikkila and Pellinen, 1977). Thus, the (kinetic) energy generated in $\underline{j} \cdot \underline{E} > 0$ regions must ultimately be provided by the generator which maintains the electric field (in the distant solar wind); likewise, the (electromagnetic) energy generated in $\underline{j} \cdot \underline{E} < 0$ regions must be provided by the local flow (kinetic energy of the magnetosheath).

On a patch of boundary on which $\underline{B}_\perp \neq 0$, two alternatives are possible, depending on the field topology. Fig. 7a corresponds to the case of dayside magnetopause equatorward of the demarcation line with (interconnected) southward-directed IMF (steady state assumed). Note that $\underline{j} \cdot \underline{E} > 0$, the Poynting vector (parallel to $\underline{V}_\perp$) pointing toward the current sheet from both sides, energy being delivered to the current carriers, and plasma flowing from the magnetosheath into the magnetosphere along field lines (in principle, also a reverse flow would be possible). Whether the generated kinetic energy appears in random form and/or as an organized flow enhancement will depend on the fine-structure of the boundary current layer and on the microinstabilities therein; these factors will also control the plasma entry process and the associated change in particle distribution function. It has been pointed out (Heikkila, 1975) that if the total dayside magnetopause current ($\sim 9 \times 10^6$ A) flows through the average magnetospheric dawn-to-dusk potential difference (~ 60 kV), the total power dissipation would be about 5×10^{11} W. Any lack of experimental confirmation of this power dissipation would necessarily imply that $\underline{B}_\perp \simeq 0$ on the boundary [or $\underline{E} = 0$ --although this latter condition would mean zero transverse flow $\underline{V}_\perp$ in the magnetosheath near the magnetopause (Fig. 7), a most unrealistic situation when $\underline{B}_\perp \neq 0$]. The energetic electron layer observed in the magnetosheath adjacent to the magnetopause (p. 391) could well carry an important part of this power (Baker and Stone, 1977). Note that the electromagnetic energy dissipation on the boundary in the case of Fig. 7a does not require the existence of a neutral point in the immediate neighborhood, nor does it imply the operation of a plasma-dynamical merging process as described on p. 385.) On the other hand, it has been suggested (Paschmann et al., 1976) that on the higher latitude dayside magnetosphere this kind of boundary could represent

a standing Alfvén wave (rotational discontinuity) that originates in a merging process at an X-line (Levy et al., 1964).

Fig. 7b portrays the other alternative, as it would apply to the magnetopause for an interconnected southward IMF, tailward of the demarcation line. This represents a source of electromagnetic energy ($\underline{j} \cdot \underline{E} < 0$), with the Poynting vector directed away from the magnetopause on both sides, and field lines "seen" to emerge from it. The generated field energy must be provided by the mechanism that maintains the boundary current system (the magnetosheath flow).

In both cases of Fig. 7, a diversion of the boundary current along field lines into the ionosphere will irreversibly disturb the plasma equilibrium across the boundary. A macroscopic instability would set in, leading to macroscopic changes in the shape of the boundary that would depend on the plasma properties on both sides of the magnetopause (Coroniti and Kennel, 1973). At present, no theory exists for boundaries with $\underline{B}_\perp \neq 0$ of width comparable to the ion gyroradius (Sonnerup, 1976). The proper inclusion of the IMF requires that a realistic quantitative theory of the microstructure of the magnetopause would have to be based on the kinetic theory of anisotropic plasmas (Willis, 1977).

---

*) Of course, for field-topological reasons an X-line must exist somewhere on the boundary for a situation like that in Fig. 7a. But its existence is not at all necessary for the conversion of magnetic field energy into kinetic energy, even in a steady-state case: just note that in Fig. 7a the zeroth order drift velocity $\underline{V}_\perp = \underline{E} \times \underline{B}/\underline{B}^2$ is always parallel to the Poynting vector and directed into the current sheet. Those fond of the moving field line picture should thus look at these lines as "merging" or "collapsing" into the current sheet from both sides of the boundary with velocity $\underline{V}_\perp$ --well away from any X-line [of course, the plasma also has a parallel velocity $\underline{V}_{||}$ which completely escapes the "frozen field" description, but which is the one to be affected (with the temperature) during the entry process by microscopic dynamic processes in the magnetopause layer; to consider that each kinked field line shown in Fig. 7 is moving "rigidly" to the upper right, parallel to the boundary, physically does not make any sense, for such a statement would imply a non-existent constraint on $\underline{V}_{||}$].

Returning to the case of a closed magnetosphere, or, more generally, to the low-latitude region of the magnetopause where the magnetosheath flow is nearly perpendicular to the confined magnetic field behind the boundary (Fig. 5), yet another mode of particle penetration has been proposed. Under certain conditions of field gradient inside the magnetosphere (Cole, 1974), impinging solar wind particles could be drift-captured, i.e., would drift away from the boundary before they have completed the first cyclotron turn inside the magnetosphere. This process would work preferentially for particles whose cyclotron radii are considerably larger than the magnetopause thickness (i.e., particles belonging to the upper end of the thermal spectrum in the magnetosheath).

In general, whenever there is a bulk flow of boundary plasma perpendicular to the confined magnetospheric field impressed by some momentum transfer or viscous interaction mechanism, electric polarization will occur and a dynamo electric field will build up in the flow layer (Cole, 1976; see also Section 6). Due to ionospheric conductivity, this polarization will lead to an electric field inside of the boundary layer that on the equatorial plane is directed from dawn to dusk, if the magnetopause is an equipotential surface and no electric fields parallel to B exist (Mendillo and Papagiannis, 1971). In other words, a dawn-dusk electric field can exist even in the absence of field line interconnection. Note that cancellation of this permanent dawn-dusk electric field would require an impressed field of external (e.g., solar wind) origin directed from dusk to dawn. A polarized boundary layer represents a momentum transfer region (Piddington, 1960; Eastman et al., 1976) in which the efficiency of the transfer mechanism is controlled by the degree of leakage of the polarization charges out of the layer (see also Section 6).

The existence of plasma layers beneath the magnetopause proper, representing "freshly injected" magnetosheath particles, has been postulated since the inception of magnetospheric research. But theory has been unable to make many quantitative predictions--for instance, the distinct variety of

circumboundary regions (Fig. 4) had not even been suspected until they were discovered experimentally. We have chosen as "task number two" of magnetospheric plasma physics the experimental determination and the achievement of a quantitative theoretical understanding of the microstructure of the magnetopause, of the entry mechanism of solar wind plasma, and of the dynamic behavior of this plasma immediately after its entry. Evidently there is a great degree of overlap with "task number one" (Section 3), and the associated experimental difficulties are identical to the ones described on p. 389; for better clarity, however, we preferred to keep the field-topological aspects separated from plasma-dynamic aspects. A major theoretical difficulty is the fact that none of the three problems--the microstructure of the magnetopause, the plasma entry mechanism, or the dynamic behavior of the plasma after entry--can be treated in isolation.

Nevertheless, some concrete results have been achieved in recent years. The magnetopause reveals itself as a complicated boundary, exhibiting many different forms at different encounters (e.g., Neugebauer et al., 1974; review by Willis, 1975). The thickness of the boundary often depends on whether a change in magnetic field magnitude, field direction, field fluctuations, or ion flux is considered as the relevant signature. Generally, the observed value is of the order of an average ion cyclotron radius (but sometimes appreciably greater), indicating that effective neutralization of the polarization electric field takes place (p. 393). Magnetic field fluctuations in the frequency range around 0.5 Hz were observed in some cases, confirming the predicted ion-cyclotron instability (p. 395). In general, field and particle observations are consistent with the continuity of total pressure across the magnetopause. More recent observations in the high-latitude dayside magnetopause region (Paschmann et al., 1976) have revealed strong diamagnetic effects in the magnetosheath plasma near the boundary leading to strong depressions of the field intensity, which, however, did not bear any other neutral point signatures. They might be an indication of the incidence upon the boundary of solar wind flux tube inhomogeneities as mentioned on p. 395.

The entry layer (Fig. 4) is thought to be a consequence of the entry of magnetosheath plasma through the dayside magnetopause and, partly, of the adiabatic reflection of this plasma in the low-altitude cleft (Paschmann et al., 1976). The field lines in this layer seem to be closed, as evidenced by the existence of trapped energetic particles throughout. The entry layer consists of field-aligned streaming of plasma of density and temperature nearly the same as in the magnetosheath, but with reduced flow speed. Both the thickness of this layer and the plasma content increase gradually from zero at the subsolar point to the cusp latitude (about 78°) and appear to be independent of the IMF (Sckopke et al., 1976a). Streaming in the entry layer is irregular, at time turbulent, and can be directed away from or toward the sun. The field discontinuity which separates the entry layer from the magnetosheath is the seat of mechanisms which severely alter the plasma distribution function in velocity space. In other words, the magnetosheath plasma has easy but not free access to the entry layer. The density profile of this layer, which exhibits a rather well-defined inner boundary, suggests an entry mechanism based on coherent flow rather than overall diffusion. This, however, should not rule out diffusive transfer through the magnetopause proper at the initial stage of entry. Probably two kinds of mechanisms are operative (Reiff et al., 1977). The occurrence of sunward flows has been explained on the basis of magnetic mirroring of entry layer particles as they spiral into the cleft (Fig. 8).

The cusp or cleft is a longitudinally elongated region of intense low-energy charged particle fluxes, composed of entry layer plasma that is approaching the earth's ionosphere; of return streaming of these particles after they have mirrored or have been backscattered; and of upward streaming of particles of ionospheric origin. Since its discovery, (Heikkila and Winningham, 1971; Frank and Ackerson, 1971), the cusp has been considered a fascinating "plasma laboratory" where a great variety of phenomena such as plasma instabilities, emissions, wave-particle interactions, turbulence, and field-aligned currents and electric fields can be studied in situ, almost in isolation from the rest of the magnetosphere-ionosphere system (e.g., review by Vasyliunas, 1974). Near the magnetospheric boundary, the region under consideration seems to bear an oval cross-section (marked "throat" in Fig. 8), more restricted in local time extension than the plasma "cleft" observed at lower altitudes, where it intersects the ionosphere (e.g., review by Haerendel, 1976). The outer boundary of the "throat" is the magnetopause, which exhibits a clear indentation in this area (Fig. 8) (Sckopke et al., 1976a) with interesting vortex signatures in the magnetosheath flow. There are indications, mainly stemming from trapped energetic particle observations (e.g., McDiarmid et al., 1976), that on the sunward side the field lines of the cusp are closed and project into the entry layer, whereas tailward they are open and define the plasma mantle (Fig. 8). The broadening in local time or longitude as the cusp or cleft reaches down into the ionosphere may be due to plasma drifts away from the noon meridian caused by the particular configuration of the large-scale electric field in that region (Heelis et al., 1976). These observations also point to an essentially equipotential ($E_{||} = 0$) dayside magnetopause. In general, it is believed that the cusps or clefts are plasma features rather than magnetic field line features of the magnetosphere. A cusp signature has also been identified in laboratory plasma simulations of the magnetosphere (Podgorny and Dubinin, 1974).

The high-latitude large-scale electric field seems to be the principal organizing and modulating agent of the otherwise highly variable plasma behavior found in the cleft. This field, generally directed from dawn-to-dusk in the vicinity of the noon meridian, imposes a tailward drift on the down-flowing entry layer particles. Although an independent particle description may seem rather unrealistic under cleft conditions, it does explain qualitatively many observed features (Rosenbauer et al., 1975): the softening of proton spectra when the cleft is traversed in poleward direction; the flow and temperature profile of incoming particles that mirror and then "expand" along the open field lines into the mantle (Fig. 8); and the observed correlation of mantle thickness with the southward component of the IMF (see below).

Another most relevant characteristic of the cleft is the detection, at low altitudes, of impulsive plasma injections with a well-defined velocity dispersion (Carlson et al., 1976). The source locations were estimated at 10-12 R_e, indeed most presumably on the dayside magnetopause. Impulsive entry of magnetosheath plasma may point again to a non-uniform impact of solar wind inhomogeneities on the dayside boundary or to the effects of eddy turbulent flows (p. 395).

Finally, the role of the ionosphere as a source of cleft plasma is now well established with O^+ ions inferred to flow from the cleft into the mantle (Shelley et al., 1976). Strong field-aligned acceleration must be postulated to explain the high velocities of these ions, probably caused by parallel electric fields in regions of anomalous resistivity (see also Section 6).

The plasma mantle (Fig. 4) is a persistent layer of field-aligned tailward flow of magnetosheath-like plasma inside and adjacent to the magnetopause, tailward of the cusp (Rosenbauer et al., 1975). Its thickness at the high-latitude "top" of the magnetosphere varies between zero and more than 4 R_e, in positive correlation with the southward component of the IMF (Sckopke et al., 1976b). It tapers off from the tail's "top" toward lower latitudes, where it becomes what was originally called the boundary layer (Hones et al., 1972). The flow speed in the mantle is less than the concurrent flow speed in the magnetosheath, and is positively correlated with the latter. The particle density, temperature and bulk speed decrease gradually with depth from the magnetopause to the inner boundary of the mantle.

These latter features, and the occasional appearance of a plasma "gap" between the mantle and the magnetopause point against the possibility that the mantle consists of magnetosheath plasma locally diffused through the boundary. A more plausible mechanism is the outward expansion of cleft plasma that has been convected onto open field lines by a dawn-dusk electric field (Rosenbauer et al., 1975). Indeed, according to this picture (see also Fig. 8), the limited size of the "source" (the cleft) will automatically limit the thickness of the mantle, which thus will be controlled by the convection speed, i.e., by the convection electric field. Since the latter is correlated to the southward component of the IMF (e.g., Mozer et al., 1974), this field will exert a control on mantle thickness. Slower particles will spend a longer time in the cleft during reflection and thus be convected farther poleward; consequently, bulk speed and temperature will decrease toward the inner edge of the mantle threaded by these more poleward-rooted field lines (Fig. 8). Likewise, particles which spiral the largest distance down a cleft field line, i.e., which have the smallest pitch angles in the entry layer, will be convected farther poleward; consequently also particle density will decrease toward the inner boundary of the mantle.

An additional important consequence of this proposed mechanism is that a dawn-dusk convection electric field will also cause a gradual drift of mantle particles into the tail lobes toward the center of the tail (Fig. 8). This drift may play an important role in the transfer of mantle plasma to the plasmasheet (see Section 5).

The boundary layer consists of a flow of magnetosheath-like plasma behind the magnetopause at low latitudes (e.g., Akasofu et al., 1973b). This flow is expected to be mainly transverse to the local magnetic field, seat of the dynamo mechanism discussed on p. 399 (see Section 5 and Eastman et al., 1976 Laboratory experiments (Podgorny, 1976) also reveal the formation of a layer of viscous interaction flow in the closed field line region of an artificial plasmatail.

5. Plasma Storage, Acceleration and Release Mechanisms in the Magnetospheric Tail

The plasmasheet (Fig. 4) is a reservoir of warm plasma particles in the magnetospheric tail with an inner edge located at about 7-10 R_e in the geomagnetic equator and a pair of "horns" extending along magnetic field lines down into the ionosphere. It stretches along the tail past the moon orbit. The plasmasheet has been predicted theoretically (Parker, 1958; Piddington, 1960) and seems to be an intrinsic feature of the interaction of a plasma flow against a magnetized obstacle (Fig. 2); characteristic signatures of a plasmasheet have also been observed in laboratory experiments (Podgorny, 1976). The plasmasheet sustains the current sheet which divides the tail into two lobes of nearly opposite magnetic fields (Fig. 2). It is the seat of fundamental processes that control the dynamic response of the magnetosphere to certain changes in solar wind conditions.

Three facts make the theoretical and experimental study of the plasmasheet particularly difficult. One is that the actual configuration of the plasmasheet, in particular its thickness and inner edge position, depend significantly on the class and energy range of particles that are being considered. The second complicating factor is that the plasmasheet cannot be studied in isolation: its dynamic behavior is regulated by coupling mechanisms to the resistive ionosphere (Section 6) on one hand, and to the solar wind (Section 4) on the other. Third, a steady state of the plasmasheet of the terrestrial magnetosphere is never achieved in practice because of the particular time-scale of solar wind perturbations which trigger instabilities in the magnetospheric tail.

Broadly speaking, the plasmasheet consists of charged particles whose residence time in the magnetospheric tail is controlled by their motion in the peculiar magnetic field geometry of stretched field lines. This peculiar geometry is caused by the drift-current of the particles themselves; hence the whole problem of the plasmasheet demands a self-consistent approach from the theoretical point of view (see reviews by Hill, 1974; Schindler, 1975; and Cowley, 1976). In particular, the boundary and self-consistency conditions to be satisfied by any steady-

state plasmasheet theory must interrelate the particle injection mechanisms, the plasma and cross-tail current densities and the particle loss mechanisms.

Three mutually non-exclusive particle injection mechanisms have been postulated. One represents the entry of magnetosheath particles into the boundary layer (pp. 399 and 404) and magnetic drift from there through the plasmasheet. The other mechanism requires the existence throughout the magnetospheric tail of a large-scale electric field directed from dawn to dusk, responsible for the drift of mantle particles into the tail lobes toward the center of the tail (p. 404 and Fig. 8), where they are drift-captured in the stretched magnetic field line region. Finally, the existence of the polar wind (e.g., Lemaire and Scherer, 1973) and the observations of helium and oxygen ions flowing upwards from the high-latitude ionosphere along field lines (e.g., Hoffman et al., 1974) indicate that the ionosphere is a potential source of plasmasheet particles.

The total solar wind flux striking the magnetosphere cross-section is typically of the order of 10^{29} particles/sec (Brandt, 1970). Allowing for the fact that the incident flow is deflected in the magnetosheath (see Fig. 5c), the actual flux of solar wind particles impinging on the boundary may be smaller by perhaps two orders of magnitude. And, of course, only a certain fraction of these particles will actually penetrate into the magnetosphere. This leaves the estimated upper limit of total particle entry available for the plasmasheet between $10^{26} - 10^{27}$ sec^{-1}. On the other hand, the total escape rate of ions from the ionosphere has been estimated at 3×10^{25} sec^{-1} (Hill, 1974). No quantitative estimate exists for possible direct entry rates through the flanks of the magnetopause into the plasmasheet. It is quite conceivable that all three abovementioned entry mechanisms are operative simultaneously, with a relative importance that depends on position along the tail and on solar wind parameters (the IMF).

The cross-tail current intensity is sustained by the plasmasheet particles. In absence of an electric field, individual particle motion in a stretched field line geometry depends on the energy of the particle and on its pitch angle (e.g., Fejer, 1965; Speiser, 1965; Bird and Beard, 1972). Particles with small enough energy so that their cyclotron radius in the minimum-B region (where $B \simeq B_z$) is at

all times much smaller than the minimum radius of curvature R_c of the field line (Fig. 9a) will behave adiabatically, and curvature-drift in the current sheet region with velocity $V_c = \frac{m v_{\parallel}^2}{e R_c B_z}$ (Roederer, 1970) (the gradient-B drift is negligible in comparison). If the above condition is not met, or if V_c turns out to be of the order of, or greater than, $v_{\parallel}$, the motion in the current sheet region is non-adiabatic. Under certain conditions, the particle can be temporarily trapped in the current sheet in a "meandering" mode with the time-scales of "bounce" and "cyclotron" motion reversed (Fig. 9b). The effect of a large-scale dawn-dusk electric field throughout the tail lobes is to cause an electric drift with velocity $\underline{V}_E = \underline{E} \times \underline{B}/B^2$ toward the current sheet region, and, if the particle is captured therein, an earthward drift with velocity $\underline{V}_e = \underline{E} \times \underline{B}_z/B_z^2$ (Fig. 9c; Eastwood, 1972). If electric field drift entry from the two tail lobes were the only injection mechanism into the plasmasheet, the cross-tail linear current density λ (A/m) would be directly related to the flux of particles drifting into the current (Alfvén, 1968). Indeed, if B is the field intensity in the tail lobe and n the number density of particles drifting toward the current sheet, one obtains the relation $B^2/\mu_o = n e \Delta V$ (rationalized SI units), where ΔV is the electric potential difference between the dawn and dusk flanks of the tail (Fig. 9c). Quite generally, since $e\Delta V$ is likely to be an order of magnitude larger than the average kinetic energy of a solar wind particle, the cross-tail electric field is bound to have considerable influence on the structure and the behavior of the plasmasheet (Cowley, 1976). A recent study of particle motion through a model cross-tail current sheet (Swift, 1977) has quantitatively shown that indeed, nonadiabatic encounters of mantle or lobe plasma particles with such a magnetic field structure (with an assumed electric field) are sufficient to create the characteristics of a plasmasheet population (see also Pudovkin and Tsyganenko, 197

On the other hand, since it is believed that (at least during quiet times) plasmasheet particles reside on closed field lines (absence of lunar shadowing, see further below), their behavior will be dynamically coupled to the portion of the ionosphere intercepted by these field lines. In particular, the electric fields in the plasmasheet and in the ionosphere will be interrelated through these field lines which are equipotentials in absence of anomalous resistivity (or on which the parallel electric field component is controlled by the field-aligned current if

this resistivity is non-zero). Taking into account that ionospheric conductivity is strongly influenced by particle precipitation (with or without anomalous resistivity), we have here a closed chain of cause-and-effect relationships (Fig. 10). that is most difficult to describe quantitatively (e.g., Vasyliunas, 1970; Gurevich et al., 1976). A self-consistent description of the plasmasheet must take these effects into account (Rostoker and Boström, 1976; see also Section 6).

There are two major possible particle loss mechanisms for the plasmasheet in a steady state, which most likely play a crucial role in determining its configuration during quiet times. One is direct particle loss through the magnetc pause into the magnetosheath; the other is particle convection toward the earth and precipitation into the ionosphere. The total loss rate associated with precipitation during quiet times has been estimated at 10^{25} - 10^{26} particles/sec (Hill, 1974), comfortably below the estimated maximum solar wind injection rate (p. 406) (but too high to have the plasmasheet accounted for entirely by a polar wind source). The earthward boundary of the plasmasheet probably corresponds to the region where pitch angle scattering into the ionosphere and convection into the magnetopause dominate over local particle replenishment.

So far we have focused our attention on a "steady-state" plasmasheet. This represents, however, a highly hypothetical situation. Indeed, as mentioned above, a steady state is really never achieved. Changes in the interplanetary magnetic field cause changes in the topology of magnetic field connection across the magnetopause (Section 3) which in turn affects the particle transfer from magnetosheath to magnetosphere (Section 4). Under certain circumstances this is followed by a large-scale instability in the tail, the magnetospheric substorm (e.g., Akasofu, 1976a). Even a steady solar wind flow with persistent southward IMF appears associated with a sequence of these instabilities (see below).

Broadly speaking, the "expansive phase" of a substorm represents the sudden transition of the tail plasma system toward a more stable state. This reconfiguration occurs in the direction of higher to lower cross-tail current intensity, and from lower to higher plasmasheet particle kinetic energy (ordered as well as random) (Hones, 1976). In other words, this transition consists of an implosive conversion of magnetic energy, accumulated prior to this implosion during a period called the "growth phase" by some investigators, into particle energ

After the expansive phase, tail and plasmasheet undergo a slower "recovery phase" toward a state more similar to one that existed during pre-substorm conditions. There are indications (e.g., the poleward expansion of auroral effects) that the instability starts somewhere in the near-earth end of the plasmasheet and propagates down the tail, and that this instability is often triggered by a southward turning of the IMF. There is no general consensus regarding the actual size of the plasmasheet region primarily involved in this instability and no general agreement on the detailed time-sequence of events in the associated reconfiguration process (see further below).

The plasmaphysical process of magnetic merging or reconnection (p. 388) has been invoked as a plausible cause of the field, plasma and energy reconfiguration that is believed to take place in the tail during the so-called expansive phase of a magnetospheric substorm (e.g., reviews by Russell and McPherron, 1973; Schindler, 1975). Spontaneous merging is an attractive candidate because it appears as a rather basic and universal process of magnetic energy dissipation in astrophysical plasma systems (Vasyliunas, 1975), yielding a number of qualitative predictions about plasmasheet and magnetotail behavior during substorm conditions (see below) that seem to match the observations, especially concerning the control by the north-south component of the IMF. An often quoted (but by no means universally accepted) sequence of events is the following (Fig. 11): (i) A southward turning of the IMF increases the rate at which plasma flux tubes are transferred from the solar wind to the tail (p. 385); (ii) As a result, the cross-tail current intensity increases, tail field lines are increasingly stretched, and the intensity of the mutually opposing fields in the tail lobes increases; (iii) If the southward-directed IMF persists, the thickness of the plasmasheet decreases, an X-type neutral line (or several of them) is formed in the cross-tail current sheet, and a merging process is eventually triggered along the neutral line leading to a plasma flow as shown in Fig. 11; (iv) The plasma stream flowing toward the earth is accelerated by the effect of magnetic drift in an enhanced dawn-dusk electric field, feeding ring current and particle precipitation, while the plasma portion flowing down the tail (Fig. 11), is ejected into the solar wind; (v) As this process continues, the neutral line

migrates down the tail until the magnetic field relaxes back to a less stretched, more dipole-like configuration.

Assuming that the sequence of events indeed does take place as described above, it is not at all clear whether the existing quantitative theories of merging (e.g., review by Vasyliunas, 1975) can be applied to this process. First, these tend to focus mainly on the processes that take place in the region of MHD breakdown and in the immediate neighborhood of the X-line without treating the macroscopic system with all its distant boundary conditions as a whole. Second, they do not take into account the effects of $\partial B/\partial t$-induced electric fields that must be prominent during the rapid magnetic field reconfiguration of a substorm (Nishida and Obayashi, 1972; Heikkila and Pellinen, 1977).

The first abovementioned omission is mainly due to the extreme difficulty of devising a self-consistent quantitative theory of the macroscopic plasma system of the geomagnetic tail. However, it imposes serious limitations to the applicability of existing merging theories. For instance, just consider the question of the location of the neutral line. By definition, the neutral line is the locus of points where $\underline{B} \equiv 0$. The magnetic field in the cross-tail current sheet (essentially directed along the z-axis in solar-magnetospheric coordinates) has several partly independent constituents: the internal geomagnetic field $\underline{B}_D$; the field of the magnetopause currents $\underline{B}_P$; the field $\underline{B}_I$ determined by the IMF interconnection topology [i.e., given by the distribution of $\underline{B}_\perp$ on the boundary (p. 387)]; the field $\underline{B}_T$ determined by the cross-tail current sheet and magnetic-field-aligned currents in the plasmasheet; and the field $\underline{B}_L$ due to local current perturbations in the plasmasheet. A neutral line in the tail can thus appear because of "distant" causes such as an intense overall cross-tail current intensity (so that $\underline{B} = 0$, mainly because $\underline{B}_D + \underline{B}_P + \underline{B}_T = 0$); a southward interplanetary field partially penetrating into the tail (so that $\underline{B}_D + \underline{B}_P + \underline{B}_I = 0$)*); or because of "local" causes such as a strong current density gradient downstream from the neutral line (so that $\underline{B}_D + \underline{B}_P + \underline{B}_L = 0$). Occurrence, position and motion of neutral lines in the tail are thus controlled by local as well as distant current systems. None of them can be separately ignored in a quantitative study of the

*)The neutral point N_2 of Fig. 3a is determined by IMF penetration.

plasma system in question: the magnetospheric tail and its connection to the ionosphere must be considered as one integral system whose parts cannot be treated in isolation.

Neglect of the induced electric field caused by a magnetic field reconfiguration, too, may lead to an unrealistic description of the plasmasheet behavior during substorm conditions. For instance, consider Fig. 12 (Roederer, 1973). A southward-directed interplanetary field represents that configuration which is most efficient for plasma transfer to region II field lines in an open magnetosphere (Fig. 2). We shall assume that a sudden increase of plasma transfer into the tail leads to a gradual increase in cross-tail current sheet linear density λ (as a result of gradual increase in particle number density), causing the observed increase of the magnetic field intensity B_x in the tail lobes. An induced electric field E_i will appear, easily shown to be of the order of $\frac{1}{2}\mu_o \dot{\lambda}(R - |z|) = \dot{B}_x(R - |z|)$ [R: thickness of tail lobe (Fig. 12; z: distance to current sheet], directed from dusk to dawn.*) This induced electric field opposes the impressed solar-wind convection field $\underline{E}$, with the result that the plasma drift velocity in the tail lobes $(\underline{E} + \underline{E}_i) \times \underline{B}_x / B_x^2$, directed into the current sheet, will decrease as the latter is approached (Fig. 12). The plasma tubes will be seen to pile up and the field lines to gradually stretch out (plasmasheet thinning, see below). In other words, plasma will drift out of region II at a slower rate than it is drifting in through the dayside. In addition, the tail current increase will cause a shift of the neutral line N_2 toward the earth (a purely field-geometric effect), and a decrease of the magnetic flux in the closed field region III on both dayside and nightside (also a purely field-geometric effect). If the induced electric field happens to exactly neutralize the convection field, the flow of plasma into the neutral line N_2 would be exactly zero and there would be no energy dissipation or energy generation in the current sheet.

---

*) For $\dot{B}_x = 20\gamma$/hour (e.g., Russell et al., 1971) and $R = 25\,R_e$, $E_i = 0.9$mV/m in the cross-tail current sheet.

A sudden collapse of the cross-tail current density λ (e.g., by current flow diversion along field lines into the resistive ionosphere or by a sudden increase of local resistivity) would induce an electric field that now will be directed from dawn to dusk, i.e., in the same direction as the impressed convection field $\underline{E}$ (but much more intense), and the plasma flux tubes that previously were apposing onto the cross-tail current sheet would rush into the latter and break at the neutral line N_2, which, because of the decrease in λ, will be seen to move to the right in Fig. 12, down the tail. Everywhere along the current sheet (not just at the neutral line) will we have $\underline{j} \cdot (\underline{E} + \underline{E}_i) > 0$. The Poynting vector will be directed into the current sheet everywhere, and electromagnetic energy will be converted into particle energy all along the neutral sheet. Highly localized temporal changes in current density would produce particularly strong locally induced electric fields (Heikkila and Pellinen, 1977). This example shows that a merging process on a neutral line is not a necessary requirement to explain energy dissipation, field reconfiguration and particle acceleration during a magnetospheric substorm. The primary mechanism in the above example is the sudden collapse of cross-tail current with associated induced electric field effects. Of course, the neutral line may be instrumental in providing the region of enhanced resistivity that triggers the cross-tail current collapse.

To summarize our point in near-trivial fashion: whenever a current sheet collapses, elementary considerations (e.g., Lenz' rule) show that the local (induced) electric field $\underline{E}_i$ will be such that $\underline{j} \cdot \underline{E}_i > 0$ (trying to counteract the decrease of $|j|$). This necessarily implies that electromagnetic energy, tapped from the system's magnetic field energy reservoir, will flow into the collapsing current region, where it is being converted into mechanical energy. If the resistivity is strictly zero everywhere, the available mechanical energy will appear in the form of plasma bulk flow acceleration which, if there are strong magnetic gradients as in a "near-neutral" sheet, can be very large indeed. The actual configuration and direction of the $\underline{E} \times \underline{B}/B^2$ flow will of course depend on the total fields ($\underline{B}_{\text{current}} + \underline{B}_{\text{distant sources}}$; $\underline{E}_i + \underline{E}_{\text{electrostatic}}$). If the local resistivity is finite, part of the released energy will be converted into thermal energy and field-aligned streaming. If the resistivity along magnetic field lines is finite,

too, a field-aligned electrostatic-type electric field may build up and accelerate particles parallel to the magnetic field lines. Note that in the above picture there is no mention of neutral lines and field line merging or reconnection. The appearance of plasma acceleration and/or plasma jetting in the magnetotail can not be taken as an unambiguous test for merging--it could merely point to the occurrence of localized, short-term, perhaps turbulent time variations of the cross-tail current density. All this does not, of course, exclude the possibility that merging does take place as an additional plasmaphysical process in the plasmasheet. Finally, it should be noted that as there is no a priori restriction on the intensity of an induced electric field, particles can be accelerated to high energies (whereas acceleration in an electrostatic field is always bounded by the maximum potential difference that appears in the system).

The study of plasma storage and release mechanisms in the magnetospheric tail, chosen here as "task number three," has persistently remained a most fundamental problem since the very inception of magnetospheric physics. It also continues to feature most controversial "schools of opinion," perhaps because, almost paradoxically, it surpasses every other subject of magnetospheric physics in terms of wealth of available experimental information. Indeed, it involves many magnetospheric effects such as geomagnetic variations, optical auroras and particle precipitation which are accessible to observation from the ground or from balloons and rockets. What makes this study so difficult is the need to tie all observed manifestations causally together, both in space and time. Yet time-sequences and spatial locations of occurrence strongly depend not only on what particular effect is being observed, but also on the specific range of energies, frequencies or other parameter values to which a given instrument is sensitive.

Both in the experimental and theoretical study of the plasma storage and release mechanisms in the tail, it is necessary first of all to clearly separate quasi-steady-state situations from those involving large-scale instabilities. The understanding of particle injection, storage and release mechanisms in the plasmasheet during quiet conditions is indeed of special importance. Concerning injection, observations at lunar distance in the tail have provided most valuable information. Evidence is accumulating that the lobes of the magnetospheric tail are filled with cool plasma of characteristics similar to those of the mantle and

boundary layer, flowing antisunward along the magnetic field (e.g., Hardy et al., 1976), and drifting toward the cross-tail current sheet (McCoy et al., 1975). The ion temperature of the lobe plasma is of the order of 3 eV; number densities range between 0.1 and 3 cm^{-3}. The spatial distribution of this plasma throughout the tail cross-section is found to be correlated with the solar-magnetospheric y component of the IMF (Hardy et al., 1976) with characteristics similar to the correlation between the dawn dusk distribution of the polar cap electric field and B_{iy} (Heppner, 1972). On the other hand, the observations of particle acceleration in the vicinity of the boundary in the low-latitude flanks of the magnetosphere (Frank et al., 1976) point to the possibility of another, probably concurrent, continuous, and more direct injection mechanism into the plasmasheet. Finally, although the polar ionosphere cannot be ruled out as a particle source for the plasmasheet, the observed values of polar wind flux (p. 406) seem to be too low to account for a significant contribution. A similar conclusion is reached when the relative abundance of doubly charged helium among the precipitating ions is considered. However, it is clear the the O^+ ions observed in the distant tail (Frank et al., 1977) should mainly be of ionospheric origin, accelerated, thermalized and fed into the tail plasma by some as yet unidentified mechanism.

The quiet-time plasmasheet is considerably hotter (~ 0.5 keV ion temperature) than the inflowing lobe plasma, of a number density between 0.5-0.8 cm^{-3} (e.g., review by Hill, 1974). Electrons have average energies that are systematically 2-5 times lower than the proton energies. These facts indicate that capture in the plasmasheet after injection must be accompanied or preceded by substantial heating; the difference in ion and electron spectra suggests that this heating should be the result of a thermalization effect on an initially ordered accelerated particle flow (Frank, 1976). The considerable decrease in particle density from magnetosheath-lobe plasma to the plasmasheet (more specifically, the decrease in phase-space density) points to the operation of a highly selective or highly diffusive entry and acceleration mechanism (Hill, 1974). A physically most significant finding is the observation that the energy spectrum of plasmasheet particles in Mercury's "mini-magnetosphere" (Ogilvie et al., 1976) is nearly identical to that of the terrestrial plasmasheet particles. Taking into

account the different temporal and spatial scale-sizes of both magnetospheres (and the fact that Mercury does not have an atmosphere), this spectral similarity must be considered as an important piece of information in the theories of plasma-sheet generation and dynamics.

The absence of lunar shadowing effects on plasmasheet particles (Chase et al., 1973) has been interpreted as an indication that the main particle source lies on the earthward side of the moon and that the plasmasheet resides on closed field lines (class III, Fig. 2), at least out to 60 R_e. At the lunar distance the plasmasheet has a structure similar to that at the Vela orbits (18 R_e), but the energy density is down by a factor of 5. This could be explained by assuming a persistent adiabatic flow of plasmasheet particles toward the earth in a large-scale dawn-to-dusk electric field. Some observations, however, do not reveal any organized flow during quiet times (Stiles et al., 1977).

At this time it is difficult to ascertain the extent to which injection, acceleration and thermalization are continual processes, or whether their contribution is significant only sporadically, during the development of large-scale instabilities in the tail. The fact that parts of the plasmasheet have been seen to heat up to 1-3 keV during a substorm and thereafter gradually cool down (even to 100 eV or less) certainly reveals that the substorm instability does play a very important role as a kinetic energy source for plasmasheet particles. The question at heart here is: if all substorm activity were to cease for good--into what regime would the plasmasheet settle?

The behavior of the plasmasheet during substorms has been a subject of intensive studies in recent years, with in situ satellite measurements correlated with ground-based observations (e.g., reviews by Russell and McPherron, 1973; Akasofu, 1976a). The difficulties of reaching an unambiguous interpretation of the results are overwhelming because of the complexity of the phenomena under consideration, their huge spatial extent, and their apparent refusal to follow standard patterns. Since neither ground-based observatory networks nor satellites cover space and time in a near-continuous fashion, it is

extremely difficult to determine with a statistical study whether two types of correlated events are causally connected, or whether the occurrence of one simply caused the other, which took place anyway, to appear at the observational network used in the study (e.g., Feynman, 1976). For example, an important task is to determine whether the southward turning of the IMF is the primary cause of single substorm occurrence (e.g., McPherron et al., 1973), or whether it merely contributes to enhance the detectability of the ground-effects of a substorm that is occurring anyway (e.g., Akasofu et al., 1973a). Another factor that complicates statistical studies of the correlation between the IMF and substorm occurrence is the possibility that periods of unusually large southward component of the IMF can lead to a sequence of substorms (of decreasing intensity that subsists even after the IMF has turned northward (Akasofu, 1976b).

The detailed analysis of isolated substorm events, though of key importance in an initial "exploratory" phase of the study, has yet to yield the picture of a "typical sequence of events" in the magnetotail on which most experimenters can agree. Maybe there is no such thing as a "typical" sequence. For instance, while there are relatively undisputed indications that intense plasma cloud injections into the inner magnetosphere take place during or just after the expansive phase of a substorm (e.g., De Forest and McIlwain, 1971) and that a strong, transient, localized electric field in the near-earth tail must be involved (Roedere and Hones, 1974), observations of plasma flows, particle bursts and the magnetic field in the plasmasheet have yet to lead to a consistent picture. This is particularly true in regard to the scale size, location, and evolution of the initial instability region. Antisunward flows of plasma at ~ 18 R_e (e.g., Hones et al., 1974) and southward-directed magnetic field in the tail (e.g., Nishida and Nagayama, 1975) have been interpreted as being evidence for the formation of an X-line in the near-earth plasmasheet (Fig. 11) and subsequent down-tail migration. But this interpretation has recently been challenged (Lui et al., 1976). On the other hand, there are observations of solar particle fluxes (Lin et al., 1976) and of energetic tron bursts (Baker and Stone, 1976) whose anisotropy is characteristic of class I lines in the magnetotail Fig. 2), while a detailed analysis of antisunward plasma flow during one particular substorm has led to the suggestion that a plasma struc-

ture with class IV field lines (Fig. 2), termed "plasmoid," is formed earthward of the observing spacecraft and then ejected down-tail (Hones, 1976). Strong ($\gtrsim$ 1000 km/sec) streaming of plasma has been reported to occur in the magnetotail (Frank et al., 1976) on certain occasions (which happened to correspond to substorms), directed earthward if the local $\underline{B}$ vector (normally parallel to the cross-tail current sheet) is tipped northward, and away from the earth if tipped southward. This in turn has been interpreted as evidence for a localized merging region (called "fireball") situated near the observing spacecraft.

At higher particle energies, the question of the scale-size and evolution of the acceleration region is not decided either. High intensity 50-200 keV proton bursts (Keath et al., 1976) have been observed at ~ 35 R_e predominantly in the dusk side of the plasmasheet in correlation with intensifications of the westward auroral electrojet during substorms, directed tailward during the expansive phase and earthward during recovery. These observations again seem to point to an extended source and acceleration region that first appears in the near-earth region and then migrates down the tail. On the other hand, the analysis of simultaneous measurements of 200-500 keV proton anisotropies from two spacecraft with fine time resolution points to the existence of acceleration regions that are small (compared to the average proton gyroradius), mobile (sometimes with earthward motion), intrinsically time-varying (with a characteristic time scale of ~ 3 min) and probably multiple (Sarris et al., 1976b). Quite generally, the acceleration of particles to hundreds of keV in a few seconds in substorm-related events indicates the action of a localized, non-thermal mechanism, probably related to field-aligned electric fields and/or to strong induction fields (p. 412); magnetic merging does not seem to be a likely candidate (Sarris et al., 1976b). However, the formation of a neutral X-line may play an important role in providing an adequate field topology for (i) "linear" non-adiabatic particle acceleration in an induced electric field parallel to that line; (ii) transfer into a second stage of adiabatic (betatron) acceleration with high magnetic moment (because of a low B-value at injection) (Heikkila and Pellinen, 1977).

An "unbiased survey" of the recent literature reveals that the various investigators seem to agree only on the following points: (i) Substorms tend to appear after a persistent southward-turning of the IMF; (ii) There is a thinning of the plasmasheet during some early stage of the substorm development; (iii) There is plasma flowing and/or streaming toward the earth as a result of the expansive phase, with associated betatron and Fermi particle acceleration; (iv) Strong antisunward particle flows are frequently observed and there is spora non-thermal particle acceleration to high energies; (v) During the substorm there is a transition of a markedly stretched to a more dipole-like magnetic field configuration in the tail.

In general, a hierarchy of questions emerges in connection with the magnetospheric substorm mechanism. (1) Is a neutral X-line formed in the near-earth tail? (2) If it is formed, when does this happen, and in what proportion is its formation controlled by distant currents or by local currents (p. 410)? (3) If a neutral line is formed, does a merging process take place? (4) If a merging process does take place, is it the main cause of all other substorm man ifestations, or is it just a "circumstantial" effect of <u>local</u> energy dissipation in the plasmasheet? (5) Is there more than one neutral line, merging, heating, or acceleration region? (6) Is the assumption of a neutral line necessary at all? (7) Is the electric field, responsible for particle acceleration during a substorm, of a field-aligned nature or of inductive origin due to a cross-tail current collapse? (8) If so, is this current collapse strongly localized, or does it occur over an extended region of the current sheet? --and here we are back at question (1), because the case of a strongly localized current collapse will indeed favor the creation of a neutral line (pp. 410, 412)!

6. Magnetic-Field-Aligned Currents and Magnetosphere-Ionosphere Interactions

In the previous chapters we have alluded several times to some physical mechanisms responsible for a causal connection between processes in the magnetosphere and the ionosphere. The study of magnetosphere-ionosphere interactions is of particular interest, for it comprises physical mechanisms that could be directly or indirectly responsible for possible magnetospheric effects on man's most immediate environment, the lower atmosphere. As looked upon from the point of view of an ionospheric or atmospheric physicist, or as a geophysicist dealing with time variations of the geomagnetic field on the surface of the earth, the subject of magnetosphere-ionosphere coupling deserves a separate, full-fledged review that would extend well beyond the scope of the present article. Hence, we shall deal only in generalities, and restrict the problem mainly to certain aspects related specifically to the influence of the ionosphere on the quiet-time global state of magnetospheric plasma. Transient processes such as the appearance of electric fields parallel to the magnetic field, the ionosphere as a source of magnetospheric particles, and effects of the magnetosphere on the ionosphere will not be discussed explicitly.

From the plasma-physical point of view, the study of magnetosphere-ionosphere interactions presents a most interesting opportunity to examine the behavior of a large-scale system in which the resistivity tensor $\underline{\underline{\eta}}$ varies from zero to some finite value along any given magnetic field line. Two domains thus arise (Fig. 13a): a region (P) in which the MHD approximation (1) is valid; and a region (R) in which relation (1) has to be replaced by

$$\underline{E} + \underline{V} \times \underline{B} = \underline{\underline{\eta}}\,\underline{j} \qquad (2)$$

($\underline{V}$ is the bulk velocity of the resistive plasma). Note that in earlier chapters we have mentioned possible MHD breakdown regions in the outer magnetosphere and solar wind (e.g., pp.380,388), but that these were all expected to be "two-dimensional" or "one-dimensional" entities, i.e., boundary layers or neutral lines of transverse dimensions of the same order or smaller than a typical ion

gyroradius (with the exclusion of transient regions of strong particle precipitation with parallel electric fields).

The dynamic behavior of the plasma in the MHD region P (Fig. 13a) will be influenced or controlled by the resistive region R. Both regions "communicate" with each other by means of field-aligned currents $\underline{j}_{\parallel}$, i. e., electric charge exchange. Strictly speaking, there is only one, unique, plasma bulk velocity configuration for which no such field-aligned currents flow between the two regions. It corresponds to the case in which $\underline{j} \equiv 0$ in the resistive medium R, i.e., a situation in which the bulk flow velocity $\underline{V}_{\perp}$ is magnetic-flux-preserving along the entire magnetic field line domain in both regions (note again that neither (1) nor (2) contains any information on the field-aligned streaming velocity $\underline{V}_{\parallel}$). In this configuration, the plasma in the MHD region "co-moves" with the resistive gas [for instance, corotates rigidly if the central body is rotating (Vasyliunas, 1974)]. The currents in the plasma region P must be fully closed inside that region--accumulation of free charges would not be allowed, with the only possible charge density being due to moving currents ($\epsilon_o \mu_o \underline{V} \cdot \underline{j}$), and, eventually, local vorticity ($-\frac{1}{\epsilon_o} \underline{B} \cdot \underline{\nabla} \times \underline{V}$). This condition is possible only if no external forces are acting on the MHD plasma in region P. The resulting electric field (which also may have a solenoidal component if $\frac{\partial B}{\partial t} \neq 0$; for instance, when the rotating magnetic field is asymmetric) is precisely the one that causes the plasma to drift in co-motion with the resistive medium. The Lorentz force density $\underline{j} \times \underline{B}$ on the plasma is equal to $\rho \dot{\underline{V}}$ (ρ = mass density); this force system turns out to be non-dissipative.

Any flow configuration different from co-motion will entice $\underline{j} \neq 0$ somewhere in the resistive region. Since in general $\underline{\nabla} \cdot \underline{j}_{\perp} \neq 0$ in that region ($\underline{j}_{\perp}$ = current density perpendicular to $\underline{B}$), there will be parallel currents $\underline{j}_{\parallel}$ linking both domains [called "driving currents" (Vasyliunas, 1974)]. In the MHD region P, the current $\underline{j}_{\parallel}$ will necessarily be closed by perpendicular currents $\underline{j}_{\perp}$; the cor-

responding Lorentz force density $\underline{j}_\perp \times \underline{B}$ now plays the role of a viscous-type force on the plasma, trying to force the latter into co-motion. In the resistive region R the plasma contained in one given magnetic flux tube at one instant of time will not be found in a common flux tube at a different time. There is general energy dissipation, with kinetic energy of the plasma and/or work done by external mechanical forces acting on the plasma being converted into Joule heating of the resistive medium. [Note that this particular process is of importance in astrophysics (e.g., slowdown of pulsar rotation), laboratory plasma physics (e.g., a certain class of dissipative effects in mirror machines), and atmospheric physics (e.g., upper atmosphere heating).] As a result of all this, a plasma in the MHD region free of external forces that initially is not co-moving with the resistive gas will end up doing so. On the other hand, consider a plasma disconnected from a resistive region, under the action of external forces of density $\underline{f}$. Under such conditions, the plasma will be polarized [divergence of the force-drift current (e.g., Longmire, 1963)] in such a way as to generate an electric field that imparts a drift $\underline{V}$ whose acceleration turns out to be exactly $\dot{\underline{V}} = \underline{f}/\rho$ (i.e., the plasma will follow the dictates of the external forces). If this plasma is now coupled to a resistive region, the polarization charges will be drained into (or draw neutralizing charges from) the resistive medium in the form of field-aligned currents $\underline{j}_\parallel$: the polarization of the plasma will be altered, and so will the electric field configuration and associated plasma drift (bulk motion). Again, the end effect of the coupling is that of the appearance of viscous-type stresses on the plasma.

In a stationary state, the field-aligned current density $\underline{j}_\parallel$ is related to the transverse density $\underline{j}_\perp$ by $\underline{\nabla} \cdot \underline{j}_\parallel = -\underline{\nabla} \cdot \underline{j}_\perp$ (i.e., $-\underline{\nabla} \cdot \underline{j}_\perp$ represents the "source" of field-aligned currents). Points where $\underline{\nabla} \cdot \underline{j}_\perp \neq 0$ are expected to lie in regions with particle density gradients such as plasma boundaries--thus the field-aligned currents $\underline{j}_\parallel$ connecting regions R and P of Fig. 13a will preferentially flow along the field lines that project inhomogeneities and plasma boundaries arising in P onto the domain of R. Fig. 13b shows schematically the boundary situa-

tion for an "open" magnetosphere-ionosphere system. Region II is that of interconnected field lines intercepting the ionosphere in the polar cap (see also Fig. 2). Region III is that of closed field lines which in Fig. 13b has been further divided into two subregions: IIIa corresponds to field lines carrying the plasmasheet; IIIb to the plasmasphere and trough (Fig. 4). From the above considerations one should expect the field-aligned magnetosphere-ionosphere currents, also called Birkeland currents, to flow along the field lines defining the various plasma boundary structures (e.g., Boström, 1964).

In region II (Fig. 13b) the plasma flow and associated electric field are impressed by the processes responsible for the solar wind flow at the "other end" (the base of the corona, p.382); the electric field is mapped into the ionospheric domain along the interconnected field lines (p. 386), thus driving an antisunward plasma flow over the polar caps. A field-aligned current system must be expected on the boundary of region II, with at least part of the closing currents $\underline{j}_\perp$ in the MHD region flowing in the magnetosheath or solar wind plasma (the tail lobe portion of region II field lines most probably could not sustain such currents). The direction of these closing currents will be such as to cause a breaking force $\underline{j}_\perp \times \underline{B}$ on the solar wind flow (e.g., Stern, 1976).*) This necessarily will lead to a $j_\parallel$ directed into the ionosphere at the dawn (post-midnight) side, and out of it at dusk (pre-midnight), as sketched in Fig. 14a.

In an open magnetosphere the general electric field configuration over the polar cap (region II-R in Fig. 13b) should thus be expected to be driven by a dynamo in the solar wind and modulated by the interconnection field topology (Section 3). In region III, on the other hand, the electric field should be driven by dynamos in the resistive ionosphere (forcing the magnetospheric plasma to co-move), plus possible MHD dynamos in the plasmasheet (controlled by external

---

*) In a closed magnetosphere there would be no region II in Fig. 13b. It would have to be replaced by a region of (closed) field lines threading the boundary layer where a viscous interaction with magnetosheath flow takes place (see p. 399)

stresses). We identify two main large-scale ionospheric dynamos: (1) closure in region III-R of the flow impressed onto the polar region II-R or, equivalently, closure of electric equipotentials in the closed field line region III (Yasuhara and Akasofu, 1977); (2) viscous forces acting on the ionospheric plasma as a result of collisions with the neutral gas. In (2) we in turn distinguish two main contributions: (i) corotation of the neutral atmosphere, and (ii) the global S_q flow system associated with the diurnal variation of solar-produced ionization (Matsushita, 1968). The plasmasheet dynamo would somehow be related to the injection mechanism and external stresses. Fig. 14b shows four hypothetical cases. The first represents that of a "plasma blob" (plasmasheet!) that is stationary with respect to the earth-sun system, and a rotating ionosphere. Field-aligned and closure currents are such as to provide a $\underline{j}_\perp \times \underline{B}$ force system that tries to compel the plasma into co-motion. The second case corresponds to a stationary ionosphere with a plasma blob that has an impressed tailward flow. In the third case, the impressed plasma motion is directed away from the tail center toward the flanks. In the second and third cases, the $\underline{j}_\perp \times \underline{B}$ forces are again such as to compel the plasma into co-motion (i.e., oppose the impressed flow $\underline{V}$). The fourth case represents a stationary plasma blob surrounded by "boundary layer"-type plasma flowing on closed field lines (p. 399).

In the real case of the magnetosphere, the actual configuration of the field-aligned current system will strongly depend on the topology of the magnetic field, e.g., the form of the boundary between open and closed field lines and its projection onto the ionosphere; magnetopause interconnection topology; antisunward bending of magnetic field lines. This bending is especially important in case 4 of Fig. 14b, where the field-aligned "return" currents along the magnetospheric boundary field lines are not shown at all, for their topology would depend entirely on the field model assumed (e.g., Eastman et al., 1976). It is important to note that the real field-aligned current system might well be a superposition of two or more of the elementary cases shown in Fig. 14. Note, for instance, how the solar wind dynamo of Fig. 14a reinforces the poleward $j_{\parallel}$ currents of the case of Fig. 14b-3, and how the full dusk side current system of the latter is rein-

forced (and the dawn side system attenuated) by the "non-corotation" case (Fig. 14b-1).

The above-mentioned ionospheric dynamo mechanisms (1) and (2) play a fundamental role in shaping the large-scale electric field in the closed field line region III (Figs. 2 and 13b). Figure 15 is a sketch (not in scale) of the "first approximation" quiet-time electric field configuration in the tailward portion of the magnetosphere. Marked on the equatorial surface are electric equipotentials, that is, electric drift lines of plasma particles (e.g., Brice, 1967; Chen, 1970; Volland, 1973). The detailed structure of the theoretically predicted electric field will of course depend strongly on how far the self-consistency picture shown in Fig. 10 is carried through (e.g., Gurevich et al., 1976), on the assumptions made on ionospheric conductivity (e.g., Yasuhara and Akasofu, 1977) and on the penetrability of the convection electric field into the corotation region (e.g., see reviews by Wolf, 1975; and Stern, 1976). The electric field configuration predicted for the dayside magnetosphere depends very critically on the assumptions made regarding the electric field on or near the magnetopause. A question of particular theoretical importance is whether or not part of the dayside magnetopause current system is diverted into the ionosphere via field-aligned currents. This has a strong bearing on the stability of the dayside boundary (p. 398).

Although not an explicit subject of this article (p. 419), a few words on magnetic-field-aligned electric fields are in order (e.g., reviews by Stern, 1976; Evans, 1976). Several classes of mechanisms for this transient phenomenon have been envisaged: (1) a temporary difference between the distribution functions of trapped electrons and protons (e.g., Block and Fälthammar, 1976); (2) turbulence (anomalous resistivity) caused by plasma instabilities in regions of strong field-aligned currents (e.g., Papadopoulos, 1977); and (3) current-driven electrostatic shocks (Swift, 1975).

It seems almost preposterous to relegate the study of magnetosphere-ionosphere interactions to "task number four" of magnetospheric plasma physics. As was pointed out earlier, the subject is so multifaceted that it should be given a ranking all its own. Indeed, it comprises the study of field-aligned currents;

the large-scale electric field in the closed field region; transient magnetic-field-aligned electric fields, associated ionospheric particle acceleration and auroral phenomena; cusp phenomena; the polar wind; formation of the plasmasphere; wave-particle interactions; ionospheric heating; propagation of polar disturbances to lower latitudes; etc., etc. We shall deal below mainly with the first item, field-aligned currents, as perhaps the most basic manifestation of steady-state magnetosphere-ionosphere interaction.

Low altitude satellite measurements of the magnetic field have revealed a pattern of field-aligned currents (e.g., Zmuda and Armstrong, 1974; Iijima and Potemra, 1976) that has the following characteristics. (1) A poleward zone of field-aligned currents encircling the polar cap; 2-4° wide in latitude; with currents $j_{\parallel}$ flowing into the ionosphere in the morning side (maximum current density between 0700-0800 magnetic LT) and out of the ionosphere in the afternoon side (maximum at 1500-1600 LT); positively correlated with magnetic activity (K_p), but persisting even during very low activity. (2) An equatorward zone adjacent to zone (1), of systematically lower current density except in the night sector (2100-0300 LT); flowing away from the ionosphere in the morning sector (maximum current density between 0100-0300 LT) and into the ionosphere in the afternoon sector (maximum at 2100-2300 LT); correlated with K_p and the polar electrojets. See Fig. 15 for the direction of this field-aligned current system in the tailward side of the magnetosphere. Note that it corresponds to the directions shown in Fig. 14b-3. A field-aligned current system has important effects on the surface magnetic field, which thus can be used as a quantitative diagnostic tool (e.g., Fukushima, 1976).

The poleward zone (1) appears to be a permanent feature of the field-aligned current system. Measurements at greater distances from earth (Sugiura, 1975) and comparisons with the trapping boundary (Sugiura and Potemra, 1976) indicate that this system flows near the poleward (lobeward) boundary of the plasmasheet (see Figs. 13 and 15). The permanent component of this system might be driven either by a solar wind dynamo in the case of an open magnetosphere (Fig. 14a) or by an antisunward-flowing boundary plasma in a closed magnetosphere (Fig. 14b-4; see also Eastman et al., 1976). The K_p-modulated component of system (1) is probably driven by a dynamo in the plasmasheet (e.g.,

the case of Fig. 14b-3). In the ionosphere, it is possible that the closure currents $\underline{j}_\perp$ merge poleward into the polar cap Sq^P system (e.g., Iijima, 1973; Yasuhara and Akasofu, 1977), and equatorwards into the zone (2) system.

The equatorward zone (2) of field-aligned currents seems to be intrinsically associated with the plasmasheet, especially its earthward boundary (Sugiura, 1975), and must be driven by a dynamo therein. Two different models have been proposed for the closure currents in the plasmasheet. One assumes $\underline{j}_\perp$ to flow perpendicularly to the tail lobe-plasmasheet boundary (Rostoker and Boström, 1976) (the $\underline{j} \times \underline{B}$ force system thus being directed toward the midnight meridian of the tail from both premidnight and postmidnight sides). The other (Sugiura, 1975) assumes that zone (2) currents close through the cross-tail current sheet ($\underline{j} \times \underline{B}$ force system directed toward the earth in the current sheet). Obviously both models would require quite different dynamo mechanisms [outflow of plasma from the center of the plasmasheet towards its flanks in the first model, (rather unlikely) tailward flow of plasma in the second one; see Fig. 14b-2 and -3, respectively]). In the ionosphere, the equatorward zone (2) current system closes with the zone (1) system; indeed, the correlation with the polar electrojets strongly indicates that the latter represent the Hall currents associated with the poleward/equatorward closure currents of system (2) in the morning/afternoon sector.

The principal problem with field-aligned currents is the driving mechanism (Stern, 1976). How much is due to solar wind flow, how much to convective motions in the tail? Are parallel electric fields involved, are they a consequence of magnetic-field-aligned current intensification, or the cause thereof? What is the configuration of the closure currents in the solar wind/magnetosheath/tail lobes, in the plasmasheet, and in the ionosphere?

7. Magnetospheric Research in Coming Years

In the previous sections we have analyzed four fundamental problems of magnetospheric plasma physics. Is there a chance that they will be solved in the near future? During the International Magnetospheric Study 1976-79, (e.g., International Magnetospheric Study: Guidelines for United States Participation, Natl. Acad. of Sci., Washington, D.C., 1973; summary by Roederer, 1976), the International Sun-Earth Explorer mission (ISEE) will carry out detailed plasma and field measurements conducted simultaneously at nearby points by means of a "mother-daughter" pair of spacecraft (to be) launched in October 1977. Another spacecraft of this mission, to be launched in 1978, will be positioned near a Lagrangian point upstream in the solar wind to monitor the plasma input parameters. Observations of the state of the inner magnetosphere involve another IMS-dedicated spacecraft, the satellite GEOS, launched in April 1977. Intensive ground-based, balloon and rocket observations, coordinated over large regions of the globe, especially at high geomagnetic latitudes, many of them coordinated with GEOS, provide additional input on the global state of the magnetosphere, on magnetospheric perturbations and magnetosphere-ionosphere interactions.

Of the four major problems listed in this article, the ones on plasma storage and release mechanisms (Section 5) and on field-aligned currents and magnetosphere-ionosphere interactions (Section 6) have the best chances of being solved to a significant extent during the IMS and post-IMS years. The IMS-dedicated satellite missions GEOS and ISEE, the post-IMS Dynamic Explorer program, the IMS chains of magnetometers and auroral cameras, IMS rocket and balloon campaigns, and continued data acquisition from operational satellites already in orbit will provide key information on the structure and the dynamics of the near-earth portion of the plasmasheet and field-aligned current effects at high latitudes and low altitudes.

There are, however, some conditions attached to the tapping of this extraordinary data base if real progress is to be made. (1) The analysis of simultaneous multiple spacecraft observations, coordinated with ground-based, balloon and rocket measurements is necessary to make the required distinction between spatial and temporal effects. (2) A deliberate effort must be made to spell out and discuss a limited number of basic questions whose answers can realistically be expected to be obtained with existing and planned programs. (3) Only a deliberately coordinated, collective effort of data acquisition and interpretation will make it more likely that some of the difficulties involved (e.g., pp. 415, 416, 418 and 416) can be resolved. (4) Only a deliberately organized team effort by experimentalists and theoreticians can lead to credible, quantitative answers to the many questions posed.

More specifically, when it comes to substorm studies (Section 5), it is of particular importance that experimentalists and theoreticians give up subjective biases and join in an effort to seek the truth rather than the confirmation of pet ideas. Both experimentalists and theoreticians (including the author of this article) should eradicate from their brains the "classical" mental image of a due-southward interplanetary field "merging" with the terrestrial field (Dungey, 1961), give up overintuitive, overqualitative mental exercises with moving field lines, and start building a mental representation of the magnetospheric plasma system in which the relevant physical magnitudes are macroscopic distributions of electric charges and currents, bound together by the electromagnetic field. Both experimentalists and theoreticians should give up the habit of devising elaborate but only qualitative models based on the analysis of one single event or on the analysis of several events using data from only one spacecraft. In general, the event-oriented mode of data analysis and paper publication should be transformed into more systematic, synoptic and statistically oriented studies. Such a mode does not allow frequent publications; it is therefore urged that sponsoring agencies turn away from their entrenched "publish-or-perish" policy and allow for a transition from short grant periods to at least 3-year funding.

Other procedures that need to be reformed are the following. Too many scientific papers are published prematurely and hence go unread by a large percentage of scientists. Too many data taken by one experimenter are misinterpreted by another, too many data are stored in World Data Centers without ever having been used by the original experimenters, and too many data are deposited there without enough specifications to be deciphered by other users. Finally, individual scientists, institutions and funding agencies are beginning to be skeptical of the present structure of international scientific meetings and information exchange on research results. There are too many meetings on broad, vaguely defined subjects, and too many symposia prematurely arranged on the discussion of individual events.

Some of the problems discussed in this chapter require observations in the high-latitude, high-altitude magnetosphere. Satellites and magnetospheric multiprobes in highly eccentric, high-inclination orbits are the only means to gather the necessary detailed information in the critical regions; hence, the IMS will not lead to all the answers on these topics. However, this program can make substantial contributions to some aspects of the problems mentioned in Sections 3 and 4, involving the study of the low-latitude region of the boundary and underlying layers with the ISEE mother-daughter spacecraft, and of the low-altitude cleft using existing high-inclination satellites, an expanded sounding rocket program and appropriate ground-based, balloon and aircraft observations. Important questions can be answered by such methods. They pertain to the mantle and boundary layer near the equatorial plane and to possible local entry processes
which might not be operational at higher latitudes, i.e., to the possible existence of a sequence magnetosheath → boundary layer → plasmasheet. On the dayside, a systematic study of the low-latitude magnetopause structure will help clarify many questions related to its thickness, stability, and possible

effects of the filamentary structure of the solar wind, and will permit a further search for a possible merging process on the magnetospheric boundary. A systematic study of the low-altitude cleft, in particular of convection patterns, impulsive injections, field-aligned currents and wave-particle interactions, may shed light on the complicated dynamical processes that are believed to occur higher up in the "throat" and in the entry layer.

Quantitative theoretical research must be expanded, starting from "first principles," trying to first quantitatively understand basic, elementary plasma paradigms (such as a Vlasov theory of the boundaries shown in Fig. 7 and the dynamo mechanisms of Fig. 14), and only after this is accomplished tying them together to build a quantitative model of the global magnetospheric system in a self-consistent way.

7. Acknowledgments

The author acknowledges useful comments and criticism from J. L. Burch and G. Rostoker who have reviewed the manuscript for publication, and from many other colleagues, including S.-I. Akasofu, K. D. Cole, W. J. Heikkila, E. W. Hones, Jr., A. Nishida, I. Podgorny, J. J. Quenby, E. C. Roelof, K. Schindler, M. Schulz, and D. P. Stern.

The author is supported by grants from the National Science Foundation (Atmospheric Sciences Program) and the National Aeronautics and Space Administration (Office of University Affairs).

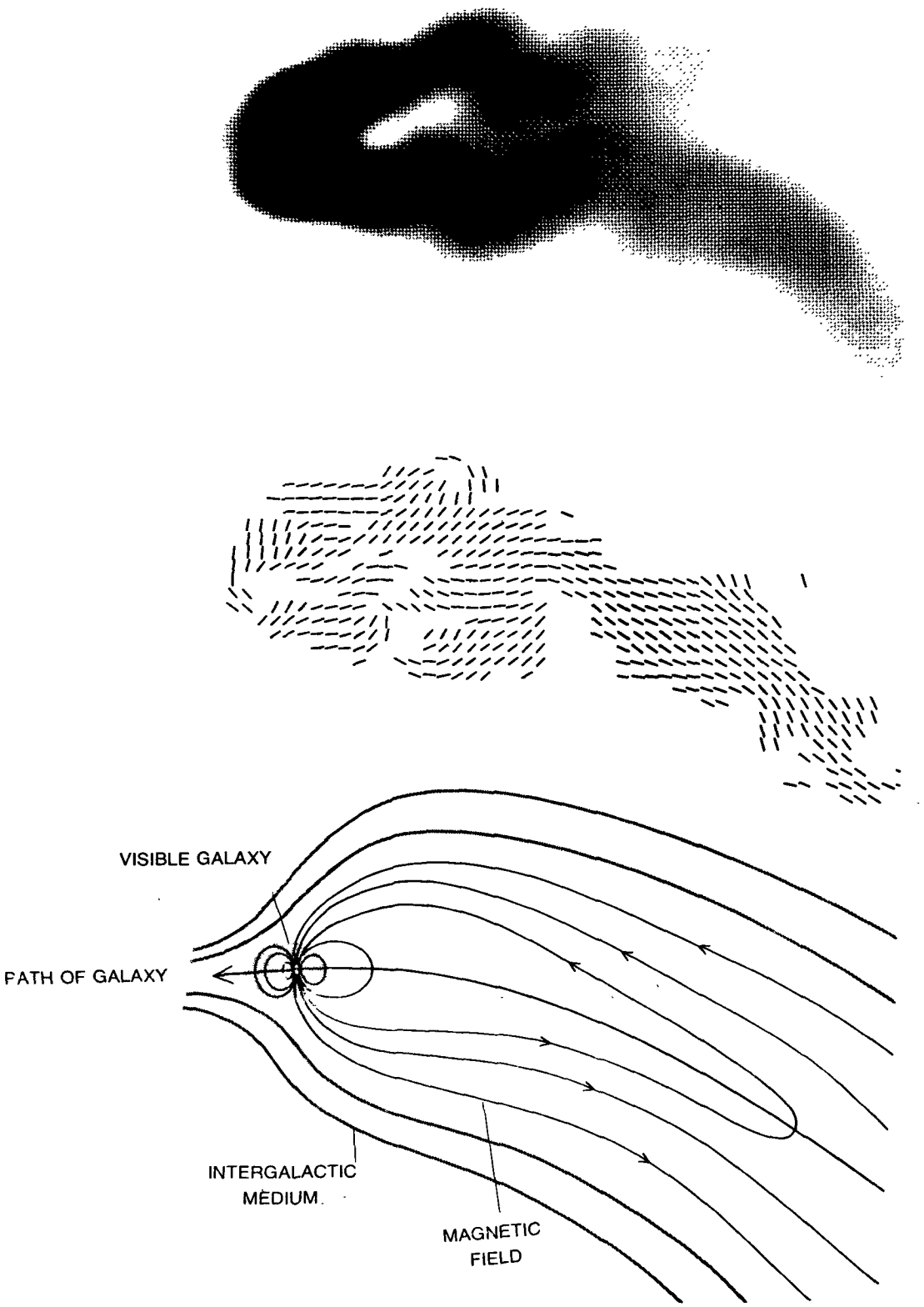

FIGURE 1 Top: 21-cm-wavelength radio photograph of radiogalaxy NGC 1265 (Strom *et al.*, 1975). Middle: direction of the magnetic field in the gas. Bottom: magnetospheric model of the galaxy.

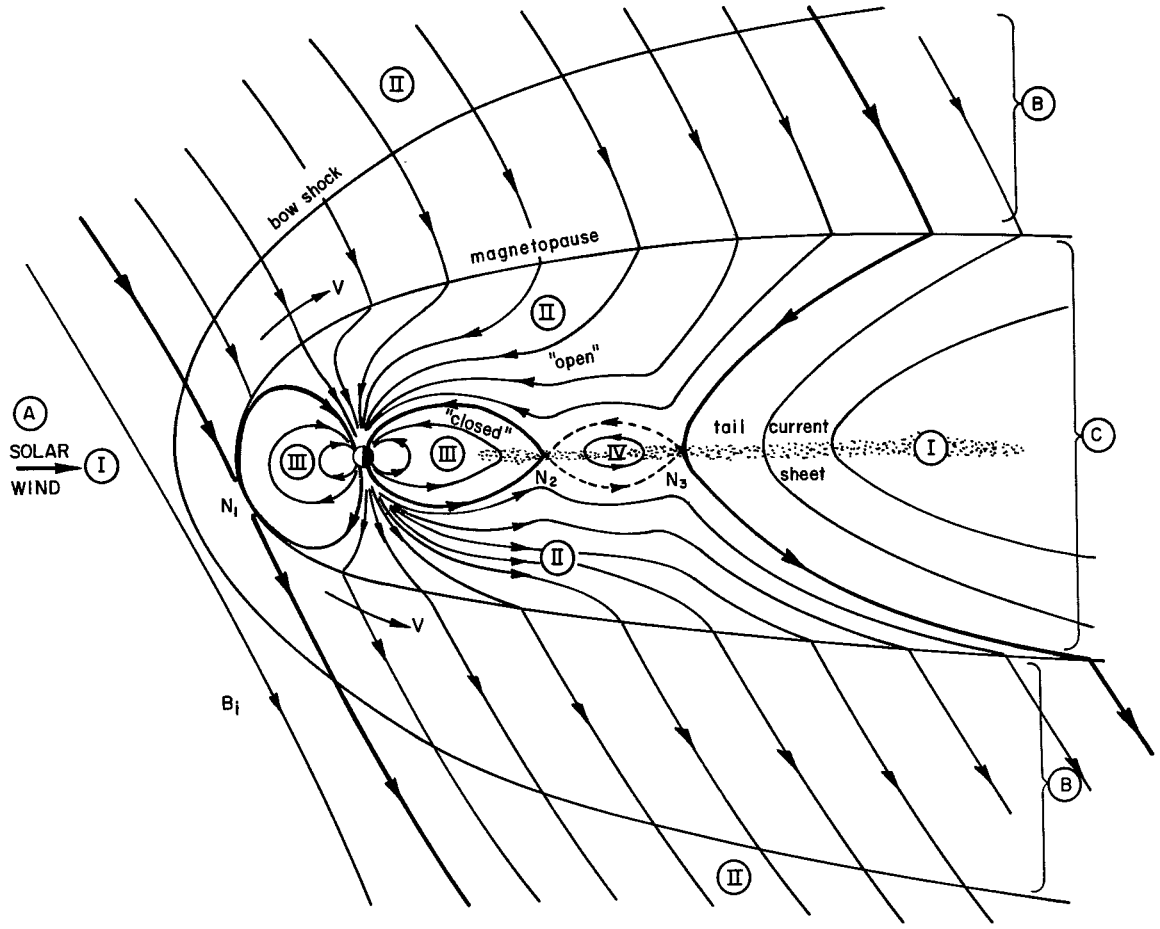

FIGURE 2 Sketch of a possible steady-state magnetic field topology of a planetary magnetosphere, drawn in the plane defined by the magnetic axis of the planet and the bulk velocity vector of the solar wind. See text for an explanation of the regions marked.

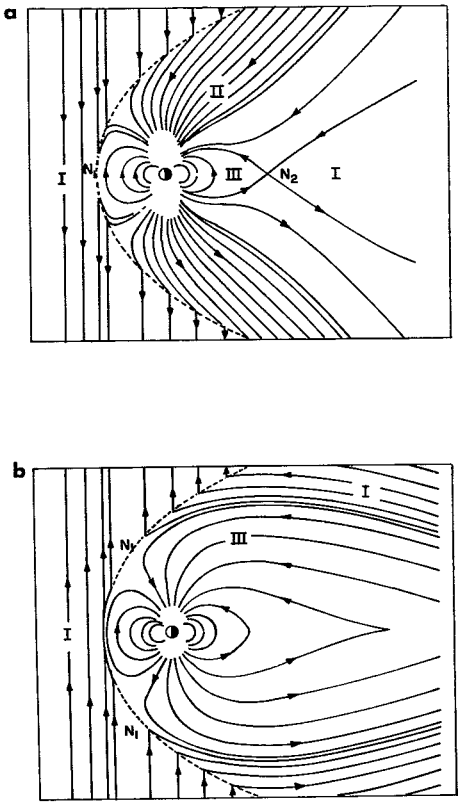

FIGURE 3 Two models of magnetic field topology, with the interplanetary magnetic field penetrating undistorted into the magnetosphere (Saunders, 1976). a): southward interplanetary field; b): northward field. (Note: field lines selected arbitrarily; field line "density" does not represent flux density.)

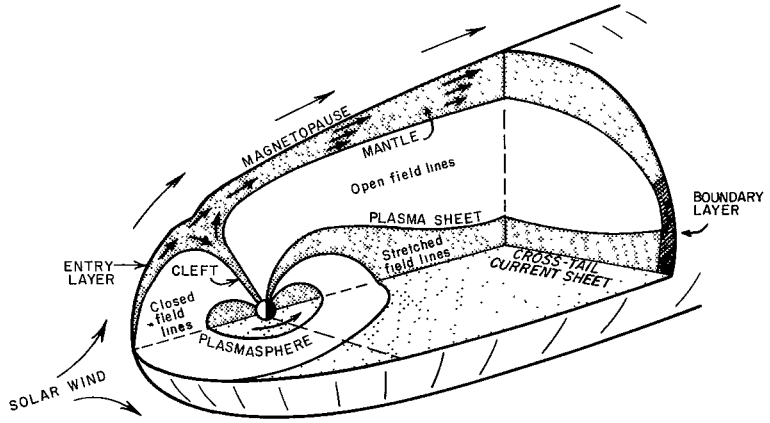

FIGURE 4 Sketch of fundamental plasma regions in the magnetosphere.

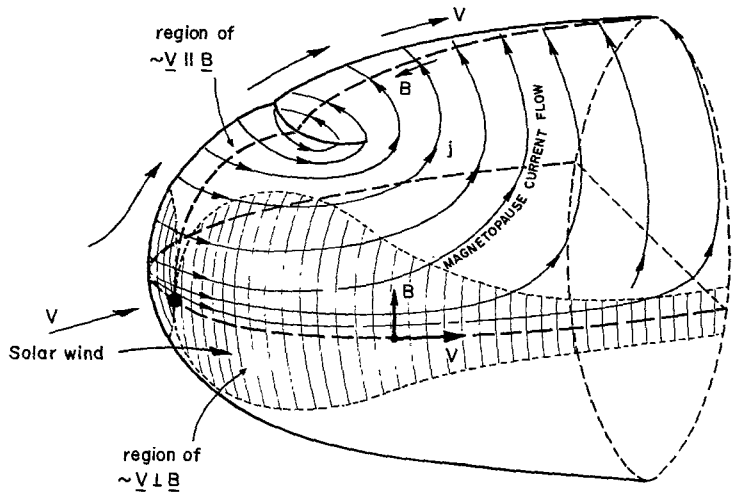

FIGURE 5 Sketch of magnetopause currents j in relation to magnetosheath plasma flow V and confined magnetic field direction B.

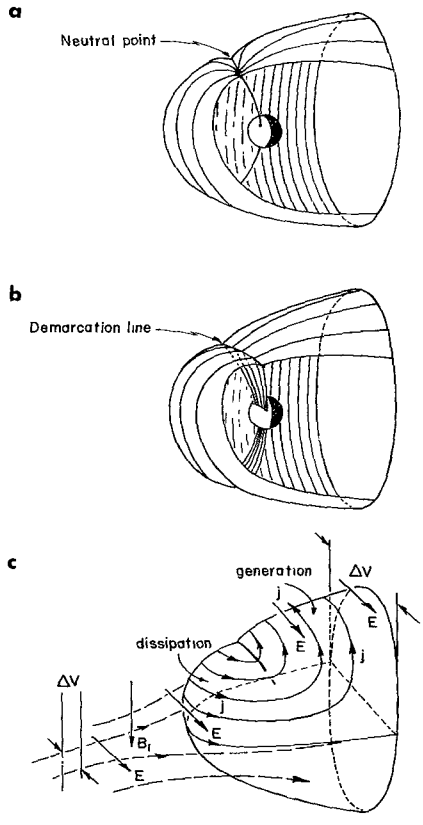

FIGURE 6 a) and b): possible magnetopause field line geometries in a closed magnetosphere model. c): open magnetosphere with southward IMF; the convection electric field E in relation to magnetopause currents j is shown. ΔV: potential difference across the magnetosphere (and polar cap).

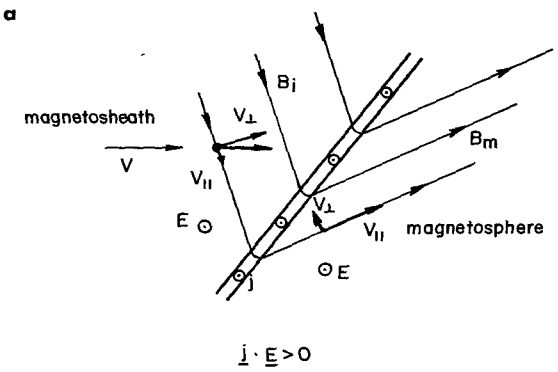

FIGURE 7 Alternatives for field topology on magnetopause with $B_\perp \neq 0$ (southward IMF assumed). a): dayside magnetopause equatorward of cleft; b): tailward of cleft. Anyone fond of the "moving field line picture" would "see" the field lines collapse from both sides into the boundary with velocity $V_\perp$ in case *a*, generating mechanical power at the rate $j \cdot E$ (>0); or emerge out of the boundary toward both sides in case *b*, generating electromagnetic power at the rate $j \cdot E$ (<0).

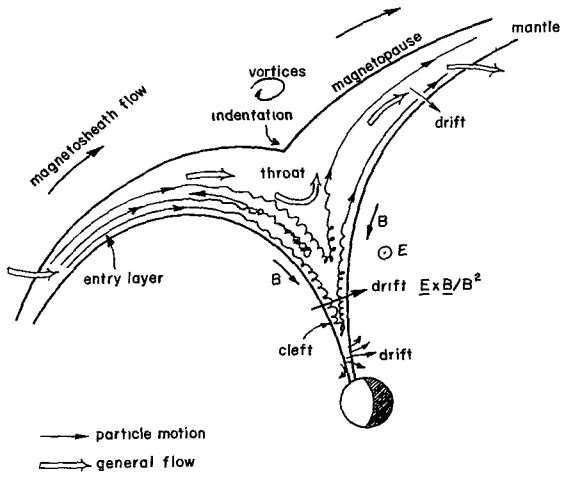

FIGURE 8 Sketch of particle motion and plasma flow into and out from the cleft region (not in scale!).

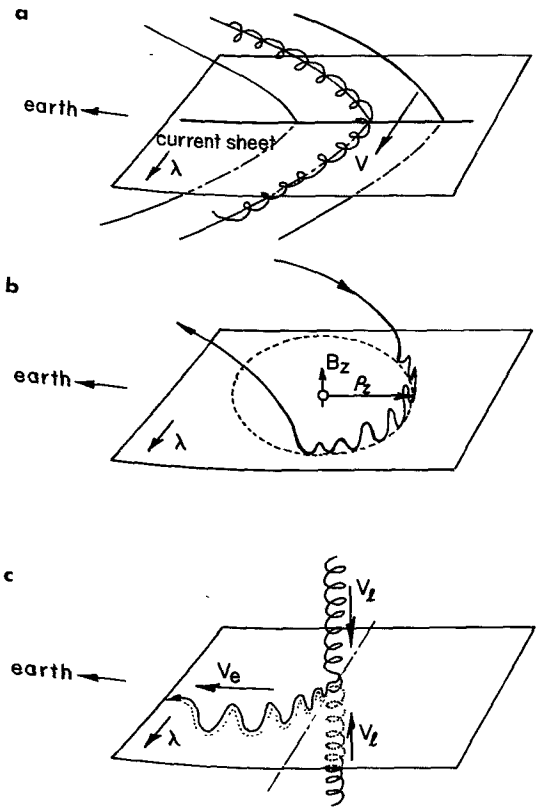

FIGURE 9 Sketch of possible particle trajectories in the plasmasheet (see text).

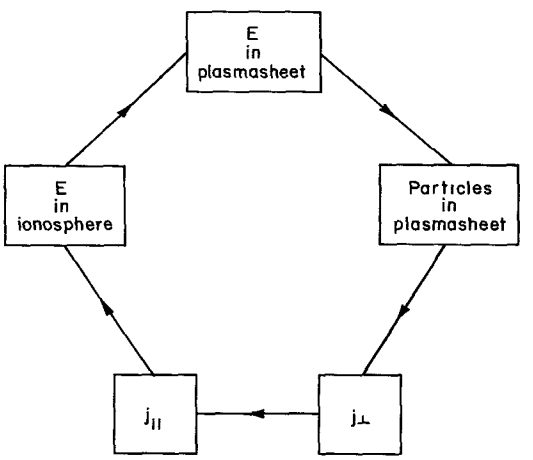

FIGURE 10 Closed chain of cause-and-effect relationships regulating the electric field in the plasmasheet-ionosphere system.

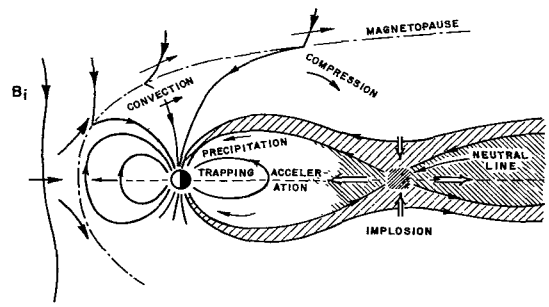

FIGURE 11 Sketch of plasma flows in a substorm model based on a magnetic merging process occurring in the magnetospheric tail.

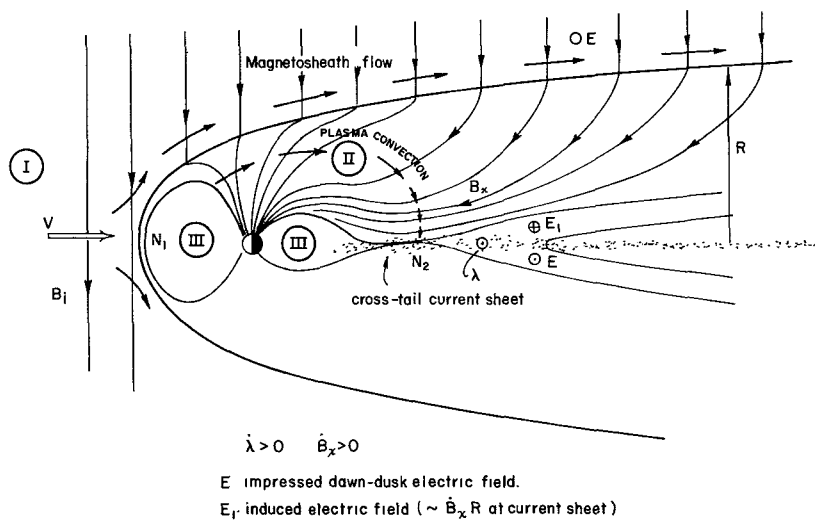

FIGURE 12 Sketch of plasma convection in a model in which the cross-tail current density increases with time so as to prevent energy dissipation in the plasmasheet.

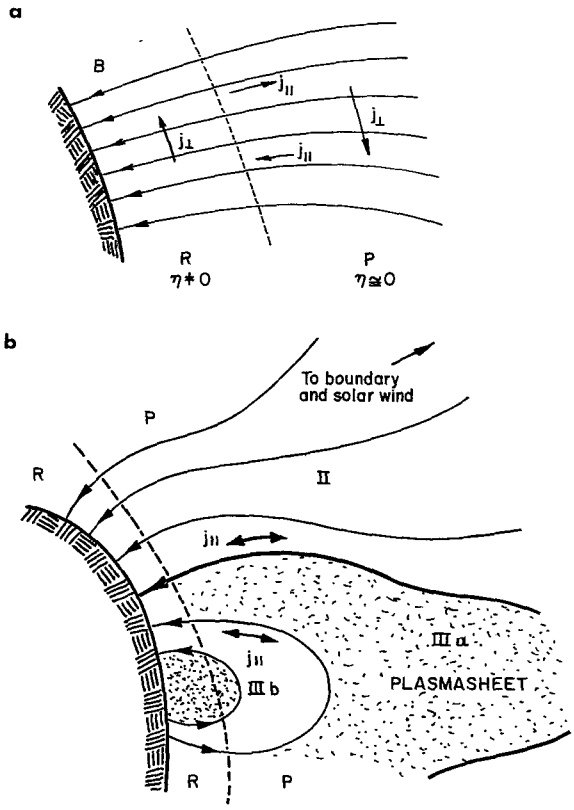

FIGURE 13 An MHD region P coupled to a resistive region R (see text).

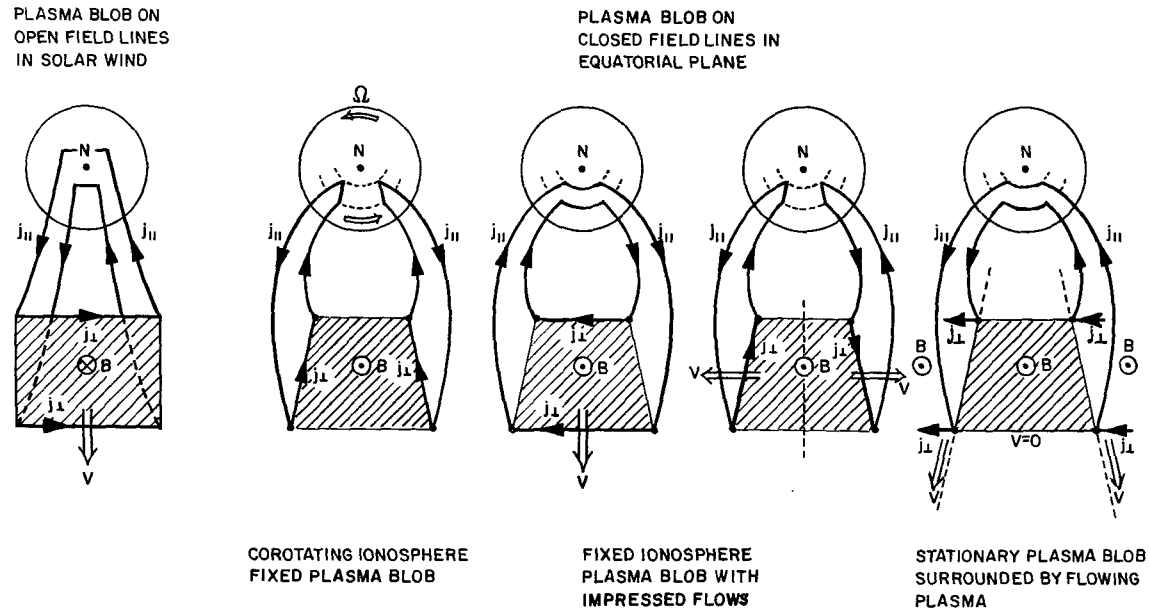

FIGURE 14 Hypothetical cases of an MHD plasma region in the solar wind (a) or the plasmasheet (b) coupled to the earth's resistive ionosphere. *V*: impressed plasma flow; $j_\parallel$: field aligned current; $j_\perp$: closing current in plasma (see text).

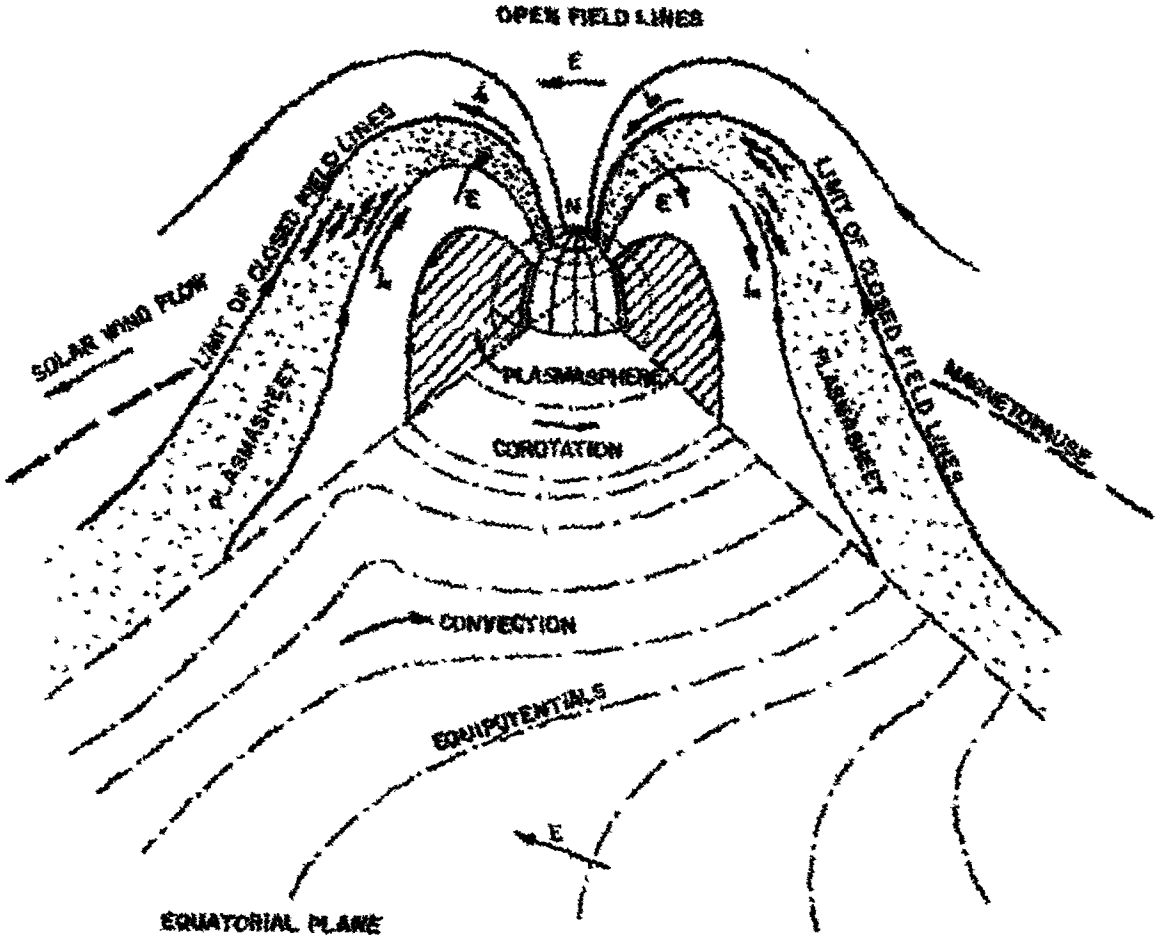

FIGURE 15 Sketch (not in scale) of the quiet-time electric field configuration in the inward portion of the magnetosphere. Marked on the equatorial surface are electric equipotentials (or plasma drift lines).

REFERENCES

Akasofu, S.-I., Physics of Magnetospheric Substorms, D. Reidel Publ. Co., Dordrecht, Holland, 1976a.

Akasofu, S.-I., Magnetospheric substorms, preprint, Univ. of Alaska, 1976b.

Akasofu, S.-I., P. D. Perreault, and F. Yasuhara, Auroral substorms and the interplanetary magnetic field, J. Geophys. Res., 78, 7490, 1973a.

Akasofu, S.-I., E. W. Hones, Jr., S. J. Bame, J. R. Asbridge, and A. T. Y. Lui, Magnetotail boundary layer plasmas at geocentric distance of ~18 R_e: Vela 5 and 6 observations, J. Geophys. Res., 78, 7257, 1973b.

Alfvén, H., Some properties of magnetospheric neutral surfaces, J. Geophys. Res., 73, 4379, 1968.

Alfvén, H., On frozen-in field lines and field-line reconnection, J. Geophys. Res., 81, 4019, 1976a.

Alfvén, H., Electric currents in cosmic plasmas, Lecture, AGU Fall Annual Meeting (preprint), 1976b.

Alpers, W., On the equilibrium of an exact charge-neutral magnetopause, Astrophys. Space Sci., 11, 471, 1971.

Anderson, K. A., and R. P. Lin, Observation of interplanetary field lines in the magnetotail, J. Geophys. Res., 74, 3953, 1969.

Aubry, M. P., C. T. Russell, and M. G. Kivelson, On inward motion of the magnetopause preceding a substorm, J. Geophys. Res., 75, 7018, 1970

Axford, W. I., Flow of mass and energy in the solar system, in Physics of Solar Planetary Environments, D. J. Williams, ed., Amer. Geophys. Union, p. 270, 1976.

Baker, D. N., and E. C. Stone, Observations of energetic electrons ($E \geq 200$ keV) in the earth's magnetotail: plasmasheet and fireball observations, J. Geophys. Res., 82, 1532, 1977.

Baker, D. N., and E. C. Stone, The magnetopause electron layer along the distant magnetotail, Geophys. Res. Letters, 4, 133, 1977a.

Bird, M. K., and D. B. Beard, The self-consistent geomagnetic tail under static conditions, Planet. Space Sci., 20, 2057, 1972.

Block, L. P., and C.-G. Fälthammar, Mechanisms that may support magnetic field-aligned electric fields in the magnetosphere, Ann. Geophys., 32, 161, 1976.

Boström, R., A model of auroral electrojets, J. Geophys. Res., 69, 4983, 1964.

Brandt, J. C., Introduction to the Solar Wind, W. H. Freeman, San Francisco, 1970.

Brice, N. M., Bulk motion of the magnetosphere, J. Geophys. Res., 72, 5193, 1967.

Burch, J. L., Observations of interactions between interplanetary and geomagnetic fields, Rev. Geophys. Space Phys., 12, 363, 1974.

Carlson, C. W., B. Parady, M. Temerin, R. Torbert, and M. C. Kelley, Impulsive plasma injections into the polar cusp, presented at the Second Magnetospheric Cleft Symposium, St. Jovite, Quebec, October 5-8, 1976.

Chase, L. M., R. E. McGuire, J. E. McCoy, R. P. Lin, K. A. Anderson and E. W. Hones, Plasma and energetic particles in the magnetotail at 60 R_E, Univ. of California, Berkeley, Space Sci. Lab. Ser., No. 14, 1973.

Chen, A. J., Penetration of low-energy protons deep into the magnetosphere, J. Geophys. Res., 75, 2458, 1970.

Cladis, J. B., G. T. Davidson, and L. L. Newkirk, editors, The Trapped Radiation Handbook, DASIAC General Electric Company--TEMPO, Santa Barbara, Calif. 93102, 1974.

Cole, K. D., Outline of a theory of solar wind interaction with the magnetosphere, Planet. Space Sci., 22, 1075, 1974.

Cole, K. D., The magnetospheric dynamo for geomagnetic disturbance, preprint, presented at the AGU Chapman Symposium, Yosemite, February 1976.

Coroniti, F. V., and C. F. Kennel, Can the ionosphere regulate magnetospheric convection?, J. Geophys. Res., 78, 2837, 1973.

Cowley, S. W. H., Energy transport and diffusion, in Physics of Solar-Planetary Environments, D. J. Williams, ed., American Geophysical Union, p. 582, 1976.

Davies, C. M., The structure of the magnetopause, Planet. Space Sci., 17, 333, 1969.

De Forest, S. E., and C. E. McIlwain, Plasma clouds in the magnetosphere, J. Geophys. Res., 76, 3587, 1971.

Domingo, V., D. E. Page, and K.-P. Wenzel, Energetic electrons at the magnetopause, in Correlated Interplanetary and Magnetospheric Observations, D. E. Page, ed., D. Reidel Publ. Co., Dordrecht, Holland, p. 159, 1974.

Dungey, J. W., Interplanetary magnetic field and auroral zones, Phys. Rev. Letters, 6, 47, 1961.

Durney, A. C., G. E. Morfill, and J. J. Quenby, Entry of high-energy solar protons into the distant geomagnetic tail, J. Geophys. Res., 77, 3345, 1972.

Dyer, E. R., editor, Critical Problems of Magnetospheric Physics, IUCSTP, Secretariat, c/o National Academy of Sciences, Washington, D.C., 1972.

Eastman, T. E., E. W. Hones, Jr., S. J. Bame, and J. R. Asbridge, The magnetospheric boundary layer: site of plasma, momentum and energy transfer from the magnetosheath into the magnetosphere, Geophys. Res. Letters, 3, 685, 1976.

Eastwood, J. W., Consistency of fields and particle motion in the "Speiser" model of the current sheet, Planet. Space Sci., 20, 1555, 1972.

Evans, D. S., Evidence for the low altitude acceleration of auroral particles, in Physics of the Hot Plasma in the Magnetosphere, B. Hultqvist and L. Stenflo, eds., p. 319, Plenum Publ. Co., New York, 1976.

Eviatar, A. and R. A. Wolf, Transfer processes in the magnetopause, J. Geophys. Res., 73, 5561, 1968.

Fairfield, D. H., Average and unusual locations of the earth's magnetopause and bow shock, J. Geophys. Res., 76, 6700, 1971.

Fairfield, D. H., Magnetic fields of the magnetosheath, Rev. Geophys. Space Phys., 14, 117, 1976.

Fejer, J. A., Geometry of the magnetospheric tail and auroral current systems, J. Geophys. Res., 70, 4972, 1965.

Ferraro, V. C. A., On the theory of the first phase of a geomagnetic storm:

a new illustrative calculation based on an idealized (plane not cylindrical) model field distribution, J. Geophys. Res., 57, 15, 1952.

Feynman, J., Substorms and the interplanetary magnetic field, J. Geophys. Res., 81, 5551, 1976.

Forbes, T. G., and T. W. Speiser, Mathematical models of the open magnetosphere, J. Geophys. Res., 76, 7542, 1971.

Frank, L. A., Hot plasmas in the earth's magnetosphere, in Physics of Solar-Planetary Environments, D. J. Williams, ed., American Geophysical Union, p. 685, 1976.

Frank, L. A., and K. L. Ackerson, Observations of charged particle precipitation into the auroral zone, J. Geophys. Res., 76, 3612, 1971.

Frank, L. A., and K. L. Ackerson, Acceleration of ionospheric ions into the earth's magnetotail, Univ. of Iowa preprint, 1976.

Frank, L. A., K. L. Ackerson, and R. P. Lepping, On hot tenuous plasmas, fireballs, and boundary layers in the earth's magnetotail, J. Geophys. Res. 81, 5859, 1976.

Frank, L. A., K. L. Ackerson, and D. M. Yeager, Observations of atomic oxygen (O^+) in the earth's magnetotail, J. Geophys. Res., 82, 129, 1977.

Fukushima, N., Ground magnetic effect of field-aligned currents connected with ionospheric currents, preprint, University of Tokyo, May, 1976.

Gurevich, A. V., A. L. Krylov, and E. E. Tsedilina, Electric fields in the earth's magnetosphere and ionosphere, Space Sci. Rev., 19, 59, 1976

Haerendel, G., Cleft plasma, presented at the Second Magnetospheric Cleft Symposium, St. Jovite, Quebec, October 5-8, 1976.

Haerendel, G., Microscopic plasma processes related to reconnection, J. Atm. Terr. Physics, 40, 343, 1978.

Hardy, D. A., J. W. Freeman, and H. K. Hills, Plasma observations in the magnetotail, in Magnetospheric Particles and Fields, B. M. McCormac, ed., D. Reidel Publ. Co., Dordrecht, Holland, 1976.

Heelis, R. A., W. B. Hanson, and J. L. Burch, Ion convection velocity reversals in the dayside cleft, J. Geophys. Res., 81, 3803, 1976.

Heikkila, W. J., Critique of fluid theory of magnetospheric phenomena, Astrophys. Space Sci., 23, 261, 1973.

Heikkila, W. J., Is there an electrostatic field tangential to the magnetopause and neutral line?, Geophys. Res. Letters, 2, 154, 1975.

Heikkila, W. J., and J. D. Winningham, Penetration of magnetosheath plasma to low altitudes through the dayside magnetospheric cusps, J. Geophys. Res., 76, 883, 1971.

Heikkila, W. J., and R. J. Pellinen, Localized induced electric field within the magnetotail, J. Geophys. Res., 82, 1610, 1977.

Heppner, J. P., Polar cap electric field distributions related to the interplanetary magnetic field direction, J. Geophys. Res., 77, 4877, 1972.

Heppner, J. P., High latitude electric fields and the modulations related to interplanetary magnetic field parameters, Radio Science, 8, 933, 1973.

Hess, W. N., The Radiation Belt and Magnetosphere, Blaisdell Publ. Co., Waltham, Mass., 1968.

Hill, T. W., Origin of the plasma sheet, Rev. Geophys. Space Phys., 12, 379, 1974.

Hoffman, J. H., W. H. Dodson, C. R. Lippincott, and H. D. Hammack, Initial ion composition results from the Isis 2 satellite, J. Geophys. Res., 79, 4246, 1974.

Hones, E. W., Jr., The magnetotail: its generation and dissipation, in Physics of Solar-Planetary Environments, D. J. Williams, ed., American Geophysical Union, p. 558, 1976.

Hones, E. W., Jr., A. T. Y. Lui, S. J. Bame, and S. Singer, Prolonged tailward flow of plasma in the thinned plasma sheet observed at r = 18 R_E during substorms, J. Geophys. Res., 79, 1385, 1974.

Hones, E. W., Jr., J. R. Asbridge, S. J. Bame, M. D. Montgomery, S. Singer, and S.-I. Akasofu, Measurements of magnetotail plasma flow made with Vela 4B, J. Geophys. Res., 77, 5503, 1972.

Iijima, T., Enhancement of the Sq^P field as the basic component of polar magnetic disturbance, Rep. Ionos. Res. Space Res. Jap., 27, 199, 1973.

Iijima, T., and T. A. Potemra, The amplitude distribution of field-aligned currents in the northern high latitudes observed by Triad, J. Geophys. Res., 81, 2165, 1976.

Keath, E. P., E. C. Roelof, C. O. Bostrom, and D. J. Williams, Fluxes

of ≥ 50-keV protons and ≥ 30-keV electrons at ~ 35 R_E. 2. Morphology and flow patterns in the magnetotail, J. Geophys. Res., 81, 2315, 1976.

Lemaire, J., and M. Scherer, Kinetic models of the solar and polar winds, Rev. Geophys. Space Phys., 11, 427, 1973.

Lemaire, J., and M. Roth, Penetration of solar wind plasma elements into the magnetosphere, Aeronomica Acta, A-166, 1976.

Levy, R. H., H. E. Petschek, and G. L. Siscoe, Aerodynamic aspects of the magnetospheric flow, AIAA J., 2065, 1964.

Lin, R. P., K. A. Anderson, J. E. McCoy, and C. T. Russell, Observations of magnetic merging and the formation of the plasma sheet in the earth's magnetotail, Univ. of California, Berkeley, preprint, 1976.

Longmire, C. L., Elementary Plasma Physics, John Wiley & Sons, Inc., New York, London, 1963.

Lui, A. T. Y., C.-I. Meng, and S.-I. Akasofu, Search for the magnetic neutral line in the near-earth plasma sheet: 1. Critical reexamination of earlier studies on magnetic field observations, J. Geophys. Res., 81, 5934, 1976.

Maezawa, K., Magnetotail boundary motion associated with geomagnetic substorms, J. Geophys. Res., 80, 3543, 1975.

Matsushita, S., S_q and L current systems in the ionosphere, Geophys. J. Roy. Astr. Soc., 15, 109, 1968.

McCormac, B. M., editor, Proceedings of the Summer Advanced Study School (on Magnetospheric Particles and Fields), D. Reidel Publ. Co., Dordrecht, Holland, 1968, 1970, 1972, 1974, 1976.

McCoy, J. E., R. P. Lin, R. E. McGuire, L. M. Chase, and K. A. Anderson, Magnetotail electric fields observed from lunar orbit, J. Geophys. Res., 80, 3217, 1975.

McDiarmid, I. B., J. R. Burrows, and E. E. Budzinski, Particle properties in the day side cleft, J. Geophys. Res., 81, 221, 1976.

McPherron, R. L., C. T. Russell, and M. P. Aubry, Satellite studies of magnetospheric substorms, 9, Phenomenological model for substorms, J. Geophys. Res., 78, 3131, 1973.

Mendillo, M., and M. D. Papagiannis, Estimate of the dependence of the

magnetospheric electric field on the velocity of the solar wind, J. Geophys. Res., 76, 6939, 1971.

Meng, C.-I., and K. A. Anderson, A layer of energetic electrons (E > 40 keV) near the magnetopause, J. Geophys. Res., 75, 1827, 1970.

Meng, C.-I., and K. A. Anderson, Characteristics of the magnetopause energetic electron layer, J. Geophys. Res., 80, 4237, 1975.

Meng, C.-I., and H. W. Kroehl, Enhanced uniform precipitation of low energy electrons over the polar cap, J. Geophys. Res., 82 (in press), 1977.

Michel, F. C., and A. J. Dessler, On the interpretation of low-energy particle access to polar caps, J. Geophys. Res., 80, 2309, 1975.

Morfill, G., and J. J. Quenby, Entry of solar protons over the polar cap, Planet. Space Sci., 19, 1541, 1971.

Mozer, F. S., W. D. Gonzalez, F. Bogott, M. C. Kelley, and S. Schutz, High-latitude electric fields and the three-dimensional interaction between interplanetary and terrestrial magnetic fields, J. Geophys. Res., 79, 56, 1974.

Neugebauer, M., C. T. Russell, and E. J. Smith, Observations of the internal structure of the magnetopause, J. Geophys. Res., 79, 499, 1974.

Newcomb, W. A., Motion of magnetic lines of force, Ann. Phys., 3, 347, 1958.

Nishida, A., and T. Obayashi, Magnetosphere convection, in Critical Problems of Magnetospheric Physics, E. R. Dyer, ed., IUCSTP Secretariat, Washington, D. C., 1972.

Nishida, A., and N. Nagayama, Magnetic field observations in the low-latitude magnetotail during substorms, Planet. Space Sci., 23, 1119, 1975.

Ogilvie, K. W., J. D. Scudder, V. M. Vasyliunas, R. E. Hartle, and G. L. Siscoe, Observations at the planet Mercury by the plasma electron experiment - Mariner 10, NASA Goddard Space Flight Center preprint X-692-76-223, 1976.

Olson, W. P., The shape of the tilted magnetopause, J. Geophys. Res., 74, 5642, 1969.

Papadopoulos, K., A review of anomalous resistivity for the ionosphere, Rev. Geophys. Space Phys., 15, 113, 1977.

Parker, E. N., Interaction of the solar wind and the geomagnetic field, Phys. Fluids, 1, 171, 1958.

Parker, E. N., Small-scale nonequilibrium of the magnetopause and its consequences, J. Geophys. Res., 72, 4365, 1967.

Paschmann, G., G. Haerendel, N. Sckopke, H. Rosenbauer, and P. C. Hedgecock, Plasma and magnetic field characteristics of the distant polar cusp near local noon: the entry layer, J. Geophys. Res., 81, 2883, 1976.

Paulikas, G. A., Tracing of high latitude magnetic field lines by solar particles, Rev. Geophys. Space Phys., 12, 117, 1974.

Piddington, J. H., A theory of polar geomagnetic storms, Geophys. J., 3, 314, 1960.

Podgorny, I. M., Laboratory experiments (plasma intrusion into the magnetic field), in Physics of Solar-Planetary Environments, D. J. Williams, ed., American Geophysical Union, p. 241, 1976.

Podgorny, I. M., and E. M. Dubinin, Laboratory experiments directed toward the investigation of magnetospheric phenomena, Space Sci. Rev., 15, 827, 1974.

Pudovkin, I., and N. A. Tsyganenko, Movement of particles and currents in the neutral layer of the magnetospheric tail (in Russian), Geomagnetic Researches, No. 14, Publ. House Nauka, Moscow, p. 39, 1975.

Reiff, P. H., T. W. Hill, and J. L. Burch, Solar wind plasma injection at the dayside magnetospheric cusp, J. Geophys. Res., 82, 479, 1977.

Roederer, J. G., Geomagnetically Trapped Radiation, Springer-Verlag, Heidelberg, New York, 1970.

Roederer, J. G., A kindergarten model of the substorm, Univ. of Denver preprint, 1973.

Roederer, J. G., IMS 1976-1979: new concepts in international scientific cooperation, E⊕S, 57, 6, 1976.

Roederer, J. G., and E. W. Hones, Jr., Motion of magnetospheric plasma clouds in a time-dependent electric field model, J. Geophys. Res., 79, 1432, 1974.

Rosenbauer, H., H. Grünwaldt, M. D. Montgomery, G. Paschmann, and

N. Sckopke, Heos 2 plasma observations in the distant polar magnetosphere: the plasma mantle, J. Geophys. Res., 80, 2723, 1975.

Rostoker, G., and R. Boström, A mechanism for driving the gross Birkeland current configuration in the auroral oval, J. Geophys. Res., 81, 235, 1976.

Russell, C. T., and R. L. McPherron, the magnetotail and substorms, Space Sci. Rev., 15, 205, 1973.

Russell, C. T., R. L. McPherron, and P. J. Coleman, Jr., Magnetic field variations in the near geomagnetic tail associated with weak substorm activity, J. Geophys. Res., 76, 1823, 1971.

Russell, C. T., M. Neugebauer, and M. G. Kivelson, ØGO-5 observations of the magnetopause, in Proc. Eslab Symp. on Correlated Interplanetary Magnetospheric Observations, D. E. Page, ed., D. Reidel Publ. Co., Dordrecht, Holland, 1974.

Sarris, E. T., S. M. Krimigis, C. O. Bostrom, and T. P. Armstrong, Simultaneous multispacecraft observations of energetic proton and electron bursts inside and outside the magnetosphere, preprint, Johns Hopkins University, Applied Physics Laboratory, JHU/APL 76-06, 1976a.

Sarris, E. T., S. M. Krimigis, T. Iijima, C. O. Bostrom, and T. P. Armstrong, Location of the source of magnetospheric energetic particle bursts by multispacecraft observations, Geophys. Res. Letters, 3, 437, 1976b.

Saunders, R. S., The characteristics of magnetospheric convection electric fields as mapped onto the polar caps, Dissertation, University of Denver, 1976.

Schindler, K., Plasmas and fields in the magnetospheric tail, Space Sci. Rev., 17, 589, 1975.

Schulz, M., and L. J. Lanzerotti, Particle Diffusion in the Radiation Belts, Springer-Verlag, Heidelberg, New York, 1974.

Sckopke, N., G. Haerendel, G. Paschmann, H. Rosenbauer, and P. C. Hedgecock, Mapping of the magnetospheric entry layer, paper presented at the Second Magnetospheric Cleft Symposium, St. Jovite, Quebec, October 5-8, 1976a.

Sckopke, N., G. Paschmann, H. Rosenbauer, and D. H. Fairfield, Influence of the interplanetary magnetic field on the occurrence and thickness of the plasma mantle, J. Geophys. Res., 81, 2687, 1976b.

Shelley, E. G., R. D. Sharp, and R. G. Johnson, Satellite observations of an ionospheric acceleration mechanism, Geophys. Res. Letters, 3, 654, 1976.

Siscoe, G. L., L. Davis, Jr., P. J. Coleman, Jr., E. J. Smith, and D. E. Jones, Power spectra and discontinuities of the interplanetary magnetic field: Mariner 4, J. Geophys. Res., 73, 61, 1968.

Sonnerup, B. U. O., Magnetopause and boundary layer, in Physics of Solar-Planetary Environments, D. J. Williams, ed., American Geophysical Union, p. 541, 1976.

Sonnerup, B. U. O., Magnetic field reconnection, preprint, Radiophysics Laboratory, Dartmouth College, 1976.

Sonnerup, B. U. O., and B. G. Ledley, Magnetopause rotational forms, J. Geophys. Res., 79, 4309, 1974.

Speiser, T. W., Particle trajectories in model current sheets; 1: Analytical solutions, J. Geophys. Res., 70, 4219, 1965.

Stern, D. P., A study of the electric field in an open magnetospheric model, J. Geophys. Res., 78, 7292, 1973.

Stern, D. P., Large-scale electric fields in the earth's magnetosphere, submitted to Rev. Geophys. Space Phys., NASA-GSFC preprint X-602-76-178, 1976.

Stiles, G. S., E. W. Hones, Jr., S. J. Bame, and J. R. Asbridge, The quiet-time plasmasheet, submitted to J. Geophys. Res., 1977.

Strom, R. G., G. K. Miley, and J. Oort, Giant radio galaxies, Sci. Am., 233, No. 9, 26, 1975.

Sugiura, M., Identifications of polar cap boundary and the auroral belt in the high-altitude magnetosphere: a model for field-aligned currents, J. Geophys. Res., 80, 2057, 1975.

Sugiura, M., and T. A. Potemra, Net field-aligned currents observed by Triad, J. Geophys. Res., 81, 2155, 1976.

Svalgaard, L., Polar cap magnetic variations and their relationship with the interplanetary magnetic sector structure, J. Geophys. Res., 78, 2064, 1973.

Swift, D. W., On the formation of auroral arcs and acceleration of auroral electrons, J. Geophys. Res., 80, 2096, 1975

Swift, D. W., The effect of the neutral sheet on magnetospheric plasma, J. Geophys. Res., 82, 1288, 1977

Turner, J. M., L. F. Burlaga, N. F. Ness, and J. F. Lemaire, Magnetic holes in the solar wind, GSFC preprint X-692-76-90, 1976.

Unti, T., and G. Atkinson, Two-dimensional Chapman-Ferraro problem with neutral sheet: 1. The boundary, J. Geophys. Res., 73, 7319, 1968.

Vasyliunas, V. M., Mathematical models of magnetospheric convection and its coupling to the ionosphere, in Particles and Fields in the Magnetosphere, B. M. McCormac, ed., D. Reidel Publ. Co., Dordrecht, Holland, p. 60, 1970.

Vasyliunas, V. M., Nonuniqueness of magnetic field line motion, J. Geophys. Res., 77, 6271, 1972.

Vasyliunas, V. M., Magnetospheric cleft symposium, E⊕S, 55, 60, 1974.

Vasyliunas, V. M., Theoretical models of magnetic field line merging, Rev. Geophys. Space Phys., 13, 303, 1975.

Vasyliunas, V. M., An overview of magnetospheric dynamics, in Magnetospheric Particles and Fields, B. McCormac, ed., in press, 1976.

Voigt, G.-H., A static-state field-line reconnection model for the earth's magnetosphere, paper presented at the Third European Geophysical Society Meeting, Amsterdam, September 7-10, 1976.

Volland, H., A semiempirical model of large-scale magnetospheric electric fields, J. Geophys. Res., 78, 171, 1973.

Walker, R. J., An evaluation of recent quantitative magnetospheric magnetic field models, Rev. Geophys. Space Phys., 14, 411, 1976.

Williams, D. J., editor, Physics of Solar Planetary Environments, American Geophysical Union, Washington, D.C., 1976.

Willis, D. M., The microstructure of the magnetopause, Geophys. J. Roy. Astr. Soc., 41, 355, 1975

Willis, D. M., The magnetopause: microstructure and interaction with magnetospheric plasma, J. of Atm. and Terr. Phys., in press (1977).

Wolf, R. A., Ionosphere-magnetosphere coupling, Space Sci. Rev., 17, 537, 1975.

Yasuhara, F., and S.-I. Akasofu, Field-aligned currents and ionospheric electric fields, J. Geophys. Res., 82, 1279, 1977

Yeh, T., Dayside reconnection between a dipolar geomagnetic field and a uniform interplanetary field, J. Geophys. Res., 81, 2140, 1976.

Zmuda, A. J., and J. C. Armstrong, The diurnal flow pattern of field-aligned currents, J. Geophys. Res., 79, 4611, 1974.

JUPITER'S MAGNETOSPHERE AND RADIATION BELTS

C. F. Kennel[1,3] and F. V. Coroniti[1,2]

University of California

Los Angeles, California 90024

(1) Department of Physics, University of California, Los Angeles, Calif. USA

(2) Department of Astronomy, University of California, Los Angeles, Calif. USA

(3) Institute of Geophysics and Planetary Physics, University of California, Los Angeles, Calif. USA

1. INTRODUCTION

Jupiter's magnetosphere, discovered twenty years ago by radio astronomers, has recently been traversed by the Pioneers 10 and 11 spacecraft. It is presently the only object in the cosmos for which inferences drawn from remote astronomical observation can be compared with direct *in situ* measurement of its neutral atom, plasma, and magnetic field environment.* Because Jupiter's magnetosphere is a rotating magnetized source of radio emissions and relativistic particles, it may resemble astrophysical cosmic ray and radio sources such as pulsars.

Pioneers 10 and 11 reached three important, unanticipated conclusions concerning Jupiter's magnetosphere. First, the magnetic field in its outer magnetosphere is radially extended into a highly time variable disk-like configuration which differs fundamentally from earth's outer magnetosphere. Jupiter's outer disk region, and the energetic particles confined within it, are modulated at Jupiter's 10 hour rotation period. Moreover, the entire outer magnetosphere appears to change drastically on time scales of a few days to a week, perhaps in response to variable solar wind conditions. Secondly, in addition to its known modulation of the Jovian decametric radio bursts, Jupiter's satellite Io was found by Pioneers 10 and 11 to have two other extremely important effects on its magnetosphere. Io absorbs some radiation belt particles and accelerates others, and most importantly, Io is a source of neutral atoms, and by inference, a heavy ion plasma which may significantly affect, and perhaps dominate, the hydromagnetic flow in Jupiter's magnetosphere. Thirdly, Jupiter's outer magnetosphere generates, or permits to escape, such intense fluxes of relativistic electrons that Jupiter is the dominant source of 1-30 MeV cosmic ray electrons in the heliosphere.

* We expect the magnetospheres of Saturn and Uranus to join Jupiter in this class in the next decade. Radio emissions, similar to Jovian decametric emissions, have been recently detected from Saturn and, with less certainty, from Uranus.

More than twenty years ago, Burke and Franklin[28] detected bursts of radiation from Jupiter in the decametric wavelength band. In 1956, Mayer et al.[97,98] detected 3.15 cm radiation from Jupiter, corresponding to a blackbody disk temperature of about 150°K. In 1958, 10.3 cm measurements indicated a temperature of 650° K 146, [99] suggesting the decimetric radiation was non-thermal. Subsequent measurements at longer wavelengths confirmed this trend. The Earth's radiation belts were also discovered in 1958 [165]. In 1959, Field[48] discussed several possible decimetric radiation mechanisms, one of which was synchrotron emission from a Jovian radiation belt. Drake and Hvatum[41] and Roberts and Stanley[129] also considered the synchrotron mechanism. In 1960, Radhakrishnan and Roberts[126] found that the Jovian decimetric radiation was linearly polarized, confirming the synchrotron hypothesis. Thus, by 1960, our understanding of the terrestrial and Jovian radiation belts was comparable: both contained fluxes of energetic electrons trapped in the dipolar regions of their magnetic fields.

During the 1960's, plasma measurements in the Earth's magnetosphere were extended to low energies, its magnetic field was completely mapped, its basic turbulent dissipation processes delineated, and its response to changes in solar wind boundary conditions understood phenomenologically. By 1970, a fairly complete understanding of the processes controlling the terrestrial radiation belts had emerged. The Earth's radiation belt particles, numerically and energetically a minor constituent of its magnetosphere, derive their energy from radially diffusing inward towards stronger magnetic fields, subject to losses caused by pitch angle scattering due to plasma turbulence. The radial diffusion is driven by fluctuations in solar wind dynamic pressure and electric field. Throughout the 1960's, refined measurements of the Jovian synchrotron source were also made.

Terrestrial radiation belt theory and Jovian source measurements were combined and examined together at a 1971 workshop sponsored by the Jet Propulsion Laboratory to evaluate the radiation hazard to the Pioneer spacecraft. The JPL workshop[15] stimulated the production of several quantitative radiation belt models based on physical principles. The strategy was to predict the intensity and spatial distribution of the synchrotron emission, using radial diffusion to energize and transport electrons from Jupiter's outer magnetosphere to its synchrotron region near 2 Jovian radii (2 R_J), accounting for foreseeable losses due to sweep-up by Jupiter's satellites and turbulent scattering from known instabilities. Prior to the first Pioneer 10 encounter, as much theory as could reasonably be done with remote data had been done. These pre-encounter radiation belt models stood the test of in situ measurements well[37], the first success in comparative magnetosphere studies. The outlines of Jovian radiation belt theory are now relatively clear. Energetic ions and electrons diffuse radially inward, gaining energy thereby, subject to losses from absorption by Jupiter's satellites and probably from scattering by microscopic plasma turbulence. Those electrons that diffuse as far inwards as two Jovian radii from Jupiter's center, and reach relativistic energies thereby, then lose energy by the synchrotron process to the Jovian decimetric radio emissions. The radial diffusion is driven by fluctuating hydromagnetic electric fields coupled to turbulent upper atmospheric winds whereas at earth, the radial diffusion is driven by fluctuating hydromagnetic electric fields coupled to variations in the solar wind. In retrospect, our success in this area is due to the fact that the Jovian radiation belts are in the inner dipolar region of the magnetosphere, where it is most like earth's.

Radio astronomical methods were unable to detect most of the plasma and most of the energy in the Jovian magnetosphere. Since the properties of the solar wind at Jupiter could be estimated theoretically, and since the 40 MHz cutoff of decametric bursts suggested a 10 Gauss surface magnetic field (assuming 40 MHz is the surface cyclotron frequency), one could attempt to scale the interaction of the solar wind with Jupiter's magnetosphere. Brice and Ioannidis [24], in a landmark paper, estimated that Jupiter's magnetopause would stand 50 R_J upstream from Jupiter in a shocked solar wind, making evident how much of Jupiter's magnet sphere had been missed. However, Jupiter's rapid rotation made it doubtful that scaling of Earth magnetospheric physics would do. Several authors[44, 110, 59, 124, 24, 81], observed that centrifugal forces should create an outer magnetospher radically different from Earth's. Just how different became clear when Pioneer 1 encountered the magnetosphere four days ahead of the schedule set by the 50 R_J magnetopause estimate.

Our modern understanding of the Jovian magnetosphere begins with Pioneers 10 and 11. It is not surprising that there is an extensive primary literature on their results. However, this literature is surprisingly well organized, with papers from each experimental group discussed in special issues of Science (Vols. 183, 188) and Journal of Geophysical Research (Vol. 79) devoted to Pioneers 10 and 11. Since this information will not be augmented until the Mariner-Jupiter-Saturn mission encounters Jupiter in 1979, it is not surprising that review articles have begun to appear. However, this literature is strikingly complete and unified. A symposium on the magnetospheres of Earth and Jupiter held at Frascati in May, 1974, led to a review volume[54] and a special issue of Space Science Reviews (Vol. 17). In May, 1975, a symposium covering all aspects of the planet Jupiter, its satellites, and its magnetosphere post Pioneer 11 was held at Tucson. The magnetospheric papers contributed to this meeting were published in special issue of the Journal of Geophysical Research (Vol. 81).

The forty-four remarkably detailed and complete review articles were published together in a single volume[57].

We present a selective review of the Jovian magnetosphere. In section 2 we briefly review the general features of the Jovian magnetosphere revealed by Pioneers 10 and 11. In section 3, we discuss Jupiter's radiation belts, concentrating upon the theoretical understanding achieved thus far. In section 4, we discuss Pioneer 10 measurements of Jupiter's outer magnetosphere, emphasizing their time dependent nature. In section 5, we discuss various theories of Jupiter's outer magnetosphere. Since theory has not in our opinion been as well reviewed as experiment, we will emphasize theoretical issues and those experimental results which appear to have theoretical significance at this time. We can only apologize in advance for whatever subjectivity has been introduced into our review by our choice of subjects and methods.

2. THE PIONEER 10 AND 11 MAGNETOSPHERIC EXPERIMENTS: AN OVERVIEW

2.1 On Board Experiments

Pioneer 10 carried six experiment packages of interest to magnetospheric physics, and Pioneer 11, seven. The dominant emphasis was on energetic particles, as it had been in the infancy of Earth magnetospheric studies. Each spacecraft contained four separate energetic particle detectors from the universities of Iowa, Chicago, and California (San Diego), and the University of New Hampshire—Goddard Space Flight Center. These measured fluxes, energy, and angular spectra of electrons and ions with energies exceeding 60 KeV. Both spacecraft carried a helium vector magnetometer, from the Jet Propulsion Laboratory, capable of measuring fields < 1.4 Gauss with an accuracy of $10^{-2}\ \gamma = 10^{-7}$ G. Pioneer 11 carried an additional Goddard flux gate magnetometer devoted to measuring strong magnetic fields up to 10 G. Measurements of low energy (0—60 KeV) plasma were not made, though some useful information has been derived from an Ames Research Center plasma detector designed for solar wind studies. Low frequency (1-100 KHz) electrostatic and electromagnetic plasma wave turbulence, essential to understanding the terrestrial radiation belts, was not investigated. Despite Jupiter's honorable history as a radio source, radioastronomy packages were not flown on Pioneers 10 and 11.

2.2 Trajectories

A flyby of the Jovian magnetosphere, from first to last encounter of the bowshock standing upstream of it, lasts several weeks. The encounter trajectories of Pioneers 10 and 11 are shown in Figures 1a and 1b, which have been taken from Simpson and McKibben[143]. It is convenient to break the two encounters down into four "passes"-- inbound and outbound for Pioneers 10 and 11. Each one has proven different. They may be categorized Jovigraphically as follows:

P-10 Inbound: Low southerly Jovigraphic latitudes, near 1000 hours local time (1000 LT)

P-10 Outbound: Low northerly Jovigraphic latitudes, near the dawn meridian (0600 LT)

P-11 Inbound: Low southerly Jovigraphic latitudes near 1000 hours local time

P-11 Outbound: Middle Jovigraphic latitudes, nearly local noon (1200 LT).

The Pioneer 10 and 11 inbound passes traversed the same regions of space, relative to Jupiter, albeit a year apart. Only Pioneer 11 outbound traversed reasonably high latitudes. There have been no passages into the all-important magnetic tail (2400 LT) or the local dusk (1800 LT) sectors. Comparison of local dawn and local dusk passages might reveal east-west asymmetries induced by Jupiter's rotation.

2.3 A General View of Jupiter's Magnetosphere.

At earth, the magnetopause is the boundary between the shocked solar wind (the "magnetosheath") and the earth's magnetic field. To first approximation, the solar wind does not penetrate the magnetopause. Because the magnetosphere is a blunt obstacle standing in the hypersonic, hyper-Alfvenic solar wind, a collisionless bowshock stands upstream of the magnetopause. In Figures 1a and 1b, the positions of the analogous crossings of the Jovian bowshock and magnetopause are marked by crosses and triangles respectively. For Pioneer 10, these crossings were identified using the solar wind plasma probe[173]. Upon crossing the bowshock, the plasma probe detected thermalized ion fluxes, and upon crossing the magnetopause, a complete dropout in ion flux. For Pioneer 11, the crossings were detected by characteristic signatures in the magnetic field data. There were multiple shock and magnetopause crossings on each of the passes.

Figure 2, taken from Smith et al.[150] shows the magnetic field magnitude, plotted against radial distance for the four passes. The portions within the magnetosphere are drawn in blackline, and in the magnetosheath or solar wind in grayline. Smith et al.[150] have argued that the field latitude δ best characterized the structure of the Jovian magnetic field. Figure 3 shows plots of δ versus distance for the four passes; $\delta < 0$ denotes a magnetic field pointed in a southerly direction, $\delta > 0$ northerly, and $\delta \approx 0$, radial field. Figure 4 shows a typical survey plot from one of the energetic particle detectors--the University of Chicago 6-30 MeV energetic electron detector[106]. Both inbound and outbound Pioneer 10 passes are shown; magnetopause and bowshock crossings are indicated by MP and BS respectively.

The dominant first impression from the Pioneer 10 and 11 data is of high time variability. On its inbound pass, Pioneer 10 first passed from the shocked magnetosheath into the magnetosphere at 98 R_J distance and then passed back into the magnetosheath at 55 R_J, re-entering the magnetosphere finally at 48 R_J. This behavior is typical. Pioneer 11 encountered three magnetopause crossings within 100 R_J on its inbound pass, and three on its outbound pass. Only on Pioneer 10 outbound did Jupiter's magnetosphere remain in the same state for a significant fraction of the pass. For this reason, Pioneer 10 outbound has attracted disproportionate attention. Yet even here, P-10 outbound re-encountered the magnetosphere between roughly 130-150 R_J. These facts alone make it evident that flyby data on Jupiter's magnetosphere is severely time-aliassed. Despite the inordinate long duration of the encounters; the time scale for changes of magnetospheric state is comparable to the duration of each pass. Separation of spatial from temporal variations in the data requires the extended coverage provided by an orbiter.

The second important aspect of Jupiter's magnetosphere is its surprisingly great scale and the great spatial scale of its temporal variations. Balancing solar wind dynamic pressure with the magnetic pressure of Jupiter's vacuum dipole field places its magnetopause at about 40 R_J at the subsolar point, yet magnetopause crossings beyond 80 R_J were encountered on each pass. Since, in the vacuum dipole model, the magnetopause distance depends only upon the sixth root of the dynamic pressure, this discrepancy cannot be completely explained an inordinately low dynamic pressure, and is not consistent with the measured dynamic pressure. Moreover, the temporal variations in size of the magnetosphere are a factor two--whereas ten per cent variations are typical for earth, and a factor two rare.

Thirdly, the magnetopause has never been encountered within the 40 - 50 R_J classical magnetopause position, though on Pioneer 10 and 11 outbound, the innermost magnetopause crossings lie near the classical position. Thus, the total pressure within Jupiter's magnetosphere typically exceeds that of the vacuum dipole. Figure 2 makes this obvious; at the most distant magnetopause crossing on each of the passes, the magnetic field amplitude is roughly $10\ \gamma = 10^{-4}$ G whereas the dipole field would be less than 1 γ. The magnetic pressure exceeds the dipole pressure by a factor one hundred. Moreover, on P-10 outbound at 95 R_J, the magnetosheath magnetic pressure exceeded that in the magnetosphere, suggesting that the internal particle and magnetic pressures were comparable within the magnetosphere at that time.

Energetic particles serve as useful tracers of magnetospheric structure. Even casual inspection of Figure 4 reveals a marked difference between the smooth behavior of the energetic electron fluxes within 20 R_J and the marked 10 hour variations in intensity in the outer magnetosphere. All the energetic particle

experimental groups have remarked that the magnetopause is a true boundary, since the particle fluxes drop rapidly by at least an order of magnitude. This indicates that the particles do not freely penetrate the magnetopause. However, Jovian energetic particles do find their way out of its magnetosphere somewhere, somehow, since Jupiter is probably the source of most of the few MeV electrons in the heliosphere.

How should we proceed with a more detailed study of the Pioneer data? If the magnetosphere were steady, we could divide Jupiter's magnetosphere into several physically different spatial regions and study them separately. But given that Jupiter's magnetosphere might switch in time between several distinct states, we should consider each pass unique. In fact, we will combine the two strategies. Despite the difficulties of separating space from time variations, the various experimental groups have all separated Jupiter's magnetosphere into three regions. One of the regions, the innermost one, is immediately obvious in Figure 4. Here the magnetic field is approximately dipolar, the energetic particle fluxes increase monotonically approaching Jupiter, and the magnetosphere is the most independent of time. This region was theoretically anticipated and subsequently confirmed by the Pioneers to closely resemble a more energetic version of the terrestrial radiation belts. Our understanding of the radiation belts is more secure than that of the rest of the magnetosphere. We discuss the radiation belts in section 3.

The outer magnetosphere is clearly distinct from the radiation belts; it is also natural to have a transition region--or "middle magnetosphere" separating the two. Since the magnetopause is time variable, the boundary separating the middle and outer magnetosphere should be fuzzy and time variable as well. It is typically placed between 20 and 40 R_J. In section 4, we review in greater

detail the observations of the middle and outer magnetosphere. Out understanding of the basic hydromagnetic processes occurring in the middle and outer magnetosphere is sufficiently weak that in our opinion the physics of the energetic particles there, however interesting, must take second position in our review. There, we will use energetic particles primarily as tracers of magnetospheric structure. In section 5, we consider various theories pertinent to Jupiter's outer magnetosphere.

3. RADIATION BELTS

The Jovian decimetric radiation has a temporally steady, flat frequency spectrum from 200-3000 MHz with a flux density of 7×10^{-26} watts/m^2-Hz [33, 17]. The decametric radiation[31] is bursty, Io modulated, and has a power law spectrum which extends up to a sharp cutoff frequency of 39.5 MHz which Warwick[171] interpreted as being equal to the electron cyclotron frequency at the foot of the Io flux tube; this interpretation implied a high latitude surface equatorial dipole magnetic field strength of $\approx 10^8/cm^2$-sec. A spatial deconvolution of the decimeter radiation by Roberts and Komesaroff [127] and Thorne[159] further indicated that the relativistic electron pitch angle distribution was strongly peaked at 90^o to the magnetic field, and the electrons therefore confined near the magnetic equator.

In anticipation of the Pioneer 10 encounter, a concerted theoretical effort was made to elaborate the above deductions into a comprehensive model of the radiation belts which could explain the origin and transport of the synchrotron electrons. Since the physics of this model forms the basis of our current, post-Pioneer understanding, we will first present a brief historical review of the central theoretical ideas. Pioneers 10 and 11 radiation belt data have been extensively reviewed by Fillius[49], McDonald and Trainor[100], Simpson and McKibben[143] and Van Allen[166]. Therefore, we will only briefly review data and compare it with theory.

Radioastronomical evidence had suggested that Jupiter's intrinsic magnetic field was not a perfect, centered dipole, but resembled more an off-center dipole whose axis is inclined to Jupiter's rotation axis[169, 170, 171, 33, 17]. Pioneers 10 and 11 confirmed this general impression and greatly refined the quantitative models of Jupiter's intrinsic field. Jupiter's magnetic dipole moment is approximately 4.2 Gauss R_J^3, is tilted about 10^o with respect to Jupiter's rotation axis,

and is offset by about 0.1 R_J from Jupiter's center. An alternative description in terms centered multipoles yields quadrupole and octopole moments of about 20% and 15% of the dipole moments[1, 147, 148, 149]. Detailed knowledge of the earth's magnetic field's structure had proven essential to detailed understanding of the terrestrial radiation belts[131], and is proving essential to detailed understanding of the Jovian radiation belts[132]. The longitudinal asymmetry provided by Jupiter's off-centered misaligned rotating dipole may prove important to understanding Jupiter's outer magnetic field [40, 88].

While it is difficult to underestimate the importance to many subjects of these detailed studies of Jupiter's intrinsic magnetic field, we will henceforth concentrate on elucidating the general physics of the Jovian radiation belts.

3.1 Pre-Pioneer 10 Theoretical Models

At L = 2 relativistic electrons have a synchrotron lifetime of about one year; L is the equatorial crossing distance of dipole field line in units of R_J. Since the decimeter radiation is essentially constant even over solar cycle time scales, electrons must either undergo *in situ* acceleration or newly energized electrons must continuously be transported to low L-shells. Since steady, localized acceleration mechanisms are difficult to envision, theorists opted for cross magnetic field transport, which is a familiar process in the terrestrial magnetosphere. At Earth particles are injected into the radiation belts by this process. The merging of solar wind and geomagnetic field lines drives an internal convection flow which injects hot plasma from the geomagnetic tail into the nightside radiation zone[7]. However, corotation prevents the convecting plasma from penetrating inside of about L = 4, the terrestrial plasmapause. Further inward transport requires radial diffusion, which results from violation of the third adiabatic invariant

due to electric and magnetic field fluctuations with periods comparable to the particle drift around the Earth[20, 130]. At Earth low frequency fluctuations arise from temporal variations in the solar wind dynamic pressure, which produces magnetic compressions, and the reconnection rate, which induces variations in the convection electric field.

At Jupiter, the corotation electric field greatly exceeds the solar wind-induced convection electric field throughout the inner magnetosphere ($L < 40$)[77] so that radial diffusion transport should dominate convection. Furthermore, since radial diffusion conserves the first adiabatic invariant $\mu = p_{\perp}^2/2mB$, in diffusing to low L-shells electrons increase their energy in proportion to the change in field strength B (if nonrelativistic) or $\sqrt{B}$ (if relativistic). The energy increase comes at the expense of the electromagnetic fluctuation energy which drives the radial diffusion. Solar wind electrons should enter the Jovian magnetosphere with typical moments $\mu \sim 10$ MeV/Gauss. Hence at $L = 2$ ($B \sim 1$ Gauss) the radially diffused electrons would have energies of a few MeV, in pleasant agreement with the synchrotron energy requirements.

For the large spatial scale of the Jovian magnetosphere, solar wind-driven radial diffusion is too weak to diffuse electrons into $L = 2$ in less than the synchrotron lifetime. Brice and McDonough[25] suggested that turbulent neutral winds in the Jovian ionosphere could generate fluctuating dynamo electric fields at the planet's spin period; dynamo electric fields occur when neutral winds drag ions, but not electrons, across the magnetic field. Since at low frequencies field lines are equipotentials, the dynamo electric fields map into the magnetosphere and produce a turbulent $E \times B$ velocity which results in radial diffusion. Brice and McDonough[25] and Coroniti[36] showed that reasonable neutral wind speeds could diffuse electrons into $L = 2$ in less than a year. If this diffusion hypothesis is correct, the ultimate energy source for the decimeter

radiation is the ionospheric wind systems.

A critical test of the radial diffusion model is whether it can account for the spatial distribution, intensity, and frequency spectrum of the decimeter radiation. Employing a variety of different assumptions, Birmingham et al.[21], Coroniti[36], and Stansberry and White[155] solved the radial diffusion transport equation including synchrotron energy losses to determine the spatial dependence of the electron distribution function. This distribution function was combined with the synchrotron radiation relations to calculate the decimeter radiation spectrum. Although the calculations differed in detail, two general conclusions can be extracted. The spatial distribution of Berge's[16] 10.4 cm and Branson's[22] 21 cm data can be fit by the radial diffusion model provided that the diffusion coefficient in L-space varies as $D_{LL} = D_o L^n$ with $n \approx 2\text{-}3$ and $D_o \sim 2 \times 10^{-9}$ to 2×10^{-10} sec^{-1}. The index n and D_o are consistent with Brice and McDonough's[25] neutral wind dynamo electric field model. Second, in diffusing from L = 4 to L = 2, electrons lose energy by synchrotron radiation faster than they gain energy by transport into the stronger magnetic field. Hence, in order to generate radiation up to 3000 MHz at L = 2, electrons at L = 4 must have magnetic moments in the range $\mu \approx 100\text{-}2000$ MeV/Gauss, i.e., far higher than typical solar wind values. Coroniti [36] suggested that such high μ electrons come from the neutral sheet in a Jovian magnetic tail and injected into the outer radiation zone ($4 < L < 20$) by magnetospheric convection.

Although the decimeter radiation constrains models of the inner zone, the electron flux levels outside L = 4 could be determined only by theoretical arguments. As electrons diffuse inward their flux increases due to the phase space compression associated with the decrease in flux tube volume. Even a pessimistic estimate of the fraction of solar wind electrons which are injected into the magnetosphere indicated that by L = 20 the electron flux would have increased

to levels above those required by the decimeter data. This estimate suggested that a large fraction of electron flux was lost before reaching the inner zone. At Earth electrons are precipitated out of the radiation belts by a variety of turbulent plasma waves which scatter the electrons to small pitch angles, causing them to mirror in the atmosphere. If the turbulence is strong, the length of time an electron resides in the radiation belt depends only on the solid angle of the atmospheric pitch angle loss cone[80]. For a dipole field, this minimum lifetime is

$$T_{min} = \frac{2L^4 R_J \gamma}{c(\gamma^2 - 1)^{1/2}}$$

where γ is the relativistic Lorentz factor. For large L, T_{min} exceeds the radial diffusion time scale D_{LL}^{-1} so that precipitation is unable to limit the radial diffusion compression of the electron flux. However, inside the point where $D_{LL}T_{min} \approx 1$, which occurs at $L \approx 20$ for Jupiter, precipitation should rapidly reduce the electron flux. Since the location where $D_{LL}T_{min} \approx 1$ depends on the 1/7 power of D_o, uncertainties in D_o do not greatly change the estimate of $L \approx 20$. Precipitation cannot decrease the flux to zero, since a finite flux is required to sustain the pitch angle scattering wave turbulence. Hence precipitation will reduce the flux to a minimum or stably trapped level [86] for which the wave turbulence is marginally stable. As electrons diffuse inward from L = 20, precipitation will maintain the flux at or below the stably trapped limit despite radial diffusion compression.

The stably trapped flux depends on the type of plasma turbulence excited. Since whistler mode turbulence theory has been extensively and successfully applied to the Earth's Van Allen belts[86, 95], its extension to Jupiter seemed reasonable. In order for whistlers to have unstable cyclotron resonant interactions with energetic electrons, the whistler phase must be less than the speed of light, which requires a modest density of cold plasma. Ioannidis and Brice[77] had developed a cold plasma model by assuming that photoelectrons would escape

from the Jovian ionosphere and become trapped near the magnetic equator by the large centrifugal force. They predicted a low density out to L = 6 and a rapid increase to $10^2 cm^{-3}$ at L = 7, which decreased outward as L^{-4}. Using this model, Coroniti[36] computed the whistler stably trapped limit to be about $10^8 cm^{-2} sec^{-1}$ between $7 < L < 10$, gradually decreasing to $6 \times 10^7 cm^{-2} sec^{-1}$ by L = 20. Inside L = 7 the low cold plasma density stabilizes the whistler mode, so the stably trapped limit concept becomes meaningless.

In order to reach the inner zone, electrons must diffuse safely past the Galilean satellites. Mead and Hess[107] and Hess et al.[70] suggested that satellite absorption could drastically reduce the radiation belt fluxes. Using the above estimates of the radial diffusion coefficient, the diffusion time across Io's orbit is comparable to Io's synodic period. However, the decimetric data had shown that Jupiter's magnetic dipole was tilted by about 10^o to the Jovian equator[33]. Hence electrons with flat pitch angles would only infrequently intersect Io's orbital plane and would diffuse past Io unattenuated.

Coroniti[36] showed that if the stably trapped electron flux at L = 7 were reduced by Io absorption and then allowed to diffuse inward with synchrotron energy losses, the predicted electron flux levels in the synchrotron emitting region were consistent with decimeter frequency spectrum and flux density. Aside from rough numerical consistency, the stably trapped limit-radial diffusion model naturally accounts for the long term stability of the decimeter radiation. Whistler mode precipitation should maintain the electron flux near the stably trapped limit inside L = 20 even if the fluxes in the distant magnetopshere are highly variable. In the inner zone the radial diffusion scale time is years, so that it would take several years to change the electron flux profiles and the synchrotron spectrum.

Decametric emission theories also predicted that at least Io would be a source of low to medium energy electrons[65, 68, 140]. In Gurnett's Io sheath model, the conductivity of the Jovian ionosphere is assumed sufficient to force the magnetosphere and Io's flux tube to corotate. In the Jovian corotation frame, Io moves in retrograde orbit at 54 Km/sec. If the conductivity of Io's surface and/or ionosphere is very high, then, in Io's rest frame, the electric field just cancels the Lorentz $\frac{1}{c}\,\underline{v} \times \underline{D}$ force. In the Jovian corotating frame, the electric field is directed toward Jupiter and corresponds to an approximately 500 Kv potential across Io since the potential across the foot of Io's flux tube in the Jovian ionosphere is zero, the 500 Kv must be dropped across two plasma sheaths on the inner and outer edges of Io. At the inner or Debye sheath, Shawhan et al.[140] estimate that 10^9 electrons/cm^2-sec from Io's ionosphere could be accelerated to hundreds of KeV producing a beam carrying 10^{13} watts toward the Jovian ionosphere. Presumably, this beam radiates, by an ill-defined process[153], 10^9 watts as Io-modulated decametric radiation. Shawhan et al.[140] speculate that some fraction of the strongly field-aligned electron beam may become trapped, probably by wave-particle scattering, and contribute to the radiation belt fluxes. The Debye sheath also accelerates 2×10^8 protons/cm^2-sec into Io's surface, which may contribute to the sputtering of heavy ions and neutrals[96].

3.2 Pioneer 10 and 11 Radiation Belt Data

Even though the analysis of the Pioneer 10 and 11 data is far from complete, a reasonably consistent picture of the radiation belts has emerged. We will present a brief synopsis of the observations and comment on their relation to the theoretical models.

Figure 5a,b shows the electron fluxes at various energies measured by Fillius and McIlwain[50] and Fillius et al.[51] on Pioneers 10 and 11. The general

increase of flux with decreasing L led all Pioneer particle experimenters[50, 167, 141, 142, 162, 163] to conclude that radial diffusion is the dominant transport and source process for the radiation belts. The Pioneer 11 flux minimum at 0100 December 3 is due to an increase in the magnetic latitude of the spacecraft coupled with a flat pitch angle distribution; the magnetic equatorial fluxes increase inward [167]. The inner zone fluxes, particularly the Pioneer 11 data at $L \sim 2$, are consistent with the synchrotron theory of the decimetric radiation[120, 37]. The Pioneer 10 and 11 fluxes are difficult to compare directly, since Pioneer 10's orbit was nearly equatorial, while Pioneer 11 was at higher magnetic latitudes. However, the two trajectories did come close together in the inner zone, and the Pioneer 10 and 11 fluxes there were nearly identified[50]. Hence the measurements support the decimeter observations and the radial diffusion model in that the inner zone radiation belt is stable over year time scales.

Pioneer 10 and 11 confirmed the expectation that the Galilean satellites interact strongly with the radiation belt. Europa strongly absorbs electrons in the energy range 0.16 to several MeV (see Fig. 5a; [141, 142, 167]), while Io absorbs $\sim$ 8 MeV electrons but has no effect at > 21 MeV energies. The pitch angle distribution of > 9 MeV electrons flattens toward 90° just inside Io's L-shell, indicating that Io preferentially absorbs electrons with pitch angles small enough to have mirror points above Io's orbital plane. At 20-30 MeV, the electron magnetic gradient plus corotation drift velocity nearly equals Io's orbital velocity, so that Io absorbs virtually none of these electrons. The large flux increases at 0.16 MeV (Fig. 5a) and 0.46 MeV (Fig. 5b) clearly demonstrate that Io is a source of low energy electrons, as predicted by the plasma sheath model of Gurnett[68] and Hubbard et al.[75]. The observations are somewhat at variance with the sheath model, since the injected electrons have a flat, rather than field-aligned pitch angle distribution[52] and energies

which exceed the maximum corotation potential across Io. A further mystery is that Pioneer 10 observed the flux increase just outside Io's L-shell while Pioneer 11 detected it just inside. However, the exact L-shell location depends on the field model used so that this apparent discrepancy may disappear when more accurate field models become available. Finally, the flux variations detected near 2 R_J (Fig. 5b) may be absorption signatures from Amalthea, but are probably complicated by magnetic field anomalies.

Figure 6a presents radiation belt energy spectra at different L-shells[10]. With decreasing L the differential energy spectrum above 1 MeV hardens from $dJ/dE \propto E^{-(3-4)}$ at $L \sim 9$ to $dJ/dE \propto E^{-(1-2)}$ near $L = 3$. The spectral hardening is consistent with inward radial diffusion and weak synchrotron energy losses outside $L = 3$. If the spectrum continued to harden to $L \sim 2$, it would approach the E^{-1} spectrum, which is required by optically thin synchrotron radiation theory [58] to explain the flat decimeter frequency spectrum.

A partially measured, partially analytically modeled six-dimensional phase space density which was constructed by McIlwain and Fillius [105] is shown in Figure 6b; Baker and Van Allen[10] have constructed a similar plot. In the absence of sources and sinks, steady state radial diffusion conserves the phase space density. The general decrease of the phase space density, which varies as L^4 for $10 > L > 3$, implies that energetic electrons are continuously lost from the radiation belts; note, however, the slight increase at low μ near Io, which in indicative of a local source. Fillius et al.[52] have analyzed possible loss terms and concluded that only pitch angle scattering is consistent with the observed phase space density increases.

Figure 7 shows how the flux of > 21 MeV electrons at a fixed L-shell varies with magnetic latitude[167]. Both Van Allen[166] and Scarf and Sanders [135] argue that the observed pitch angle distributions are consistent with whistler mode pitch angle scattering. The latter authors point out the strong similarity

between the L = 3 and 4 distributions and those found in the inner zone of the terrestrial radiation belts, which have been explained by a whistler turbulence theory including multiple cyclotron harmonic and Landau interactions[95]. Finally, Fillius et al.[52] noted that the flattened > 9 MeV electron pitch angle distribution due to Io absorption quickly relaxes to a more isotropic distribution just inside Io's orbit, which again suggests pitch angle scattering.

The sharp holes in the particle fluxes, which are produced by satellite absorption, are smoothed out by radial diffusion. Hence the radial flux gradients observed near the satellite's L-shells can be combined with simple absorption models to estimate the radial diffusion coefficient. Both Simpson et al.[141, 142] and Mogro-Campero et al.[116] have obtained values of $D_{LL} = (0.2 - 2.0) \times 10^{-10} L^4$ sec^{-1}, which are consistent with the theoretical estimates of Brice and McDonough[25], Birmingham et al.[21], and Coroniti[36]. In addition, Barbosa and Coroniti[11] reanalyzed the coupled radial diffusion-synchrotron energy loss equations using the observed electron energy spectra and 4 Gauss dipole magnetic field strength[147, 148]. They found that the L = 1.6 cutoff of the decimeter radiation placed sharp bounds on the diffusion coefficient which agree with the satellite-deduced values.

Unfortunately, neither Pioneers 10 nor 11 were instrumented to measure low energy plasma. However, after subtracting off the contributions from penetrating radiation, Frank et al.[55] obtained some information on the density of 0.1 - 2.0 keV protons from the plasma probe data. In the inner zone the proton density is 50 - 100 cm^{-3} with a temperature of $\tilde{\sim}$ 100 eV. Around Io the density drops to 1 - 10 cm^{-3} and is sporadic. At L $\sim$ 8 the density is steady at 10 - 15 cm^{-3} and gradually decreases to $\sim$ 1 cm^{-3} for

L >15; the temperature in this region is 400 eV. Neugebauer and Eviatar[118] have criticized the analysis of these measures. A radial density profile does not resemble the predictions of Ioannidis and Brice[77] with the largest discrepancy being the high inner zone densities. Göertz[61] has suggested that plasma flowing out of the ionosphere may be two-stream unstable; pitch angle scattering from the unstable waves might trap a reasonably high density of cold plasma on inner zone field lines. However, the high observed temperatures (100 - 400 eV) are difficult to explain if the source is the ionospher (photoelectrons have 10 - 30 eV) even with plasma turbulent heating. An alternative cold plasma source may be Io's ionosphere[90], the neutral hydrogen torus around Io[79], or the heavy neutrals and ions which form a disk from $6 < L < 10$ [161, 109]. Siscoe and Chen[144] have shown that cold plasma from an Io-related source would radially diffuse into inner zone and establish a cold density consistent with Frank et al's.[55] observations.

3.3 Whistler Stably Trapped Limit

Using Frank et al's.[55] cold plasma density, the 4 Gauss dipole field, and composite energy spectra and pitch angle distributions obtained from Pioneer data[50,105,167], Baker and Van Allen[10] and Barbosa and Coroniti[11,12] recomputed the stably trapped limit set by parallel propagating whistler waves. In Fig. 8, the stably trapped flux $J^*(>t_R)$, which is the integral flux above the minimum momentum $t_R mc$ which interacts with whistlers, is plotted against L and compared with the integral flux above 5 MeV obtained by McIlwain and Fillius[105] and Baker and Van Allen[10]; J^* varies as L^{-4} if the cold plasma density is uniformly distributed along the field line and as L^{-3} if the centrifugal forve confines the cold plasma density near the magnetic equator, as indicated by Frank et al.[55] for $L > 7$. If whistler turbulence limits the electron flux, the observed > 5 MeV electron flux should not exceed J^*. The reasonable agreement between the observed > 5 MeV flux and J^* over the range $4 < L < 12$ strongly suggests that

whistlers regulate the energetic electron fluxes, thus contributing to the long temporal stability of the radiation belts.

Inside L $\sim$ 4 whistlers cease to interact strongly with energetic electrons since Frank et al.'s [55] cold plasma densities are insufficient to give a low whistler phase speed. The whistlers are very weakly unstable so that the stably trapped flux becomes very large. However, the phase space density[105, 10] continues to decrease to at least L = 2.8. In order to explain the continued loss of electrons inside L = 4, either the cold plasma density is higher than observed, or unstable whistlers from L > 4 would have to propagate inward across the magnetic field, as they do in the earth's radiation belts[95]. Alternatively, another plasma instability, possibly a mixed electrostatic-electromagnetic mode, limits the fluxes inside L = 4.

3.4 Discussion

For the inner Jovian radiation belts, theory and observations are broadly in agreement. In the region L < 12, radiation belt electrons have the flat pitch angle distribution and spatial flux profile expected from radial diffusion transport, obey a whistler stable trapping limit into L $\tilde{<}$ 4, and for L < 3 have fluxes and energy spectra consistent with synchrotron radiation theory. The radial diffusion coefficient has a low power law index and value, which indicates, but does not prove, that ionospheric neutral wind turbulence exits with planetary scale wavelengths and periods. The magnitude of the diffusion coefficient is still uncertain by, perhaps, a factor of 10 to 100 [116]. Thomsen et al.[158] have pointed out that the neglect of non-Io associated particle losses can affect the estimates of the diffusion coefficient by changing the radial flux profile. In addition, the analyses which use satellite sweep-out to estimate D_{LL} assume that the flux profile is time stationary; however, satellite sweep-out introduces an inherent time dependence in the radial structure of the fluxes.

After the Pioneer encounters, the origin of the Jovian decametric radiation and its relation to Io are still mysteries surrounded by theories (see Smith[153] for a comprehensive review of theory). Io is both an absorber of particles and an emitter of low energy (∿ 0.5 MeV) electrons. The apparent sweep-out of energetic and 0.1-4.0 KeV protons[55] suggest that drift waves might be locally unstable on or near the Io flux tube[152, 174]. Drift wave turbulence would alter the radial diffusion rate near Io, thus making estimates of the global radial diffusion coefficient from spatial flux profiles at Io problematical. In addition, Smith[153] suggests that high frequency drift waves near the upper hybrid frequency may be responsible for the non-Io associated decametric radiation.

Although the observed pitch-angle distribution of the Io-accelerated electrons is somewhat at variance with the predictions of the Io sheath model, the observations strengthen the basic concept that the electromagnetic interaction of Io with the Jovian magnetosphere and ionosphere produces an electron beam which radiates near the ionosphere at decametric frequencies. The specific radiation mechanism remains obscure, but the observed broad pitch-angle distribution of the accelerated electrons casts some doubt on the direct electromagnetic instability[111] which requires a sharply peaked perpendicular thermal anisotropy. As an alternative, Scarf[134] has suggested that the electron beam excites electrostatic waves near 3/2 of the ionospheric electron cyclotron frequency which then mode couple into escaping electromagnetic waves. In any case, the recent discoveries of terrestrial kilometric[69] and Saturnian hectometric[26] radiation strongly suggests that radio emissions are an inherent feature of planetary magnetospheres, and probably possess a common origin in the instabilities of field-aligned electron currents[85].

The next phase of Jovian radiation belt research should concentrate on four issues. The distribution function of low energy plasma and its atomic composition should be measured to establish accurate densities and to determine whether the source is the ionosphere or the Galilean satellites. Plasma wave measurements should be made to either confirm or refute the whistler flux limitation model and to reveal other possible wave modes. Observations and theories of Io's interaction with the magnetosphere should be advanced, in order to complete our understanding of decametric radiation. Finally, the origin of the very high magnetic moment electrons which are observed and required for the decimeter radiation should be resolved. Are these electrons accelerated in a Jovian magnetic tail and transported to low L-shells by convection and radial diffusion, are they produced in the thin magnetic disks of the outer magnetosphere, or is the source the streaming, field-aligned fluxes of 40 - 500 KeV electrons detected in the middle magnetosphere[138]?

With Pioneers 10 and 11, space plasma physics met and passed a crucial test. After years of intensive observational and theoretical study, terrestrial radiation belt physics was successfully applied to another more energetic object. With increased confidence in its basic concepts, radiation belt theory should enhance our ability to comprehend astrophysical magnetospheres for which we have only the informational analogues of Jovian decimeter and decametric radiation.

4. PIONEER OBSERVATIONS OF JUPITER'S MIDDLE AND OUTER MAGNETOSPHERE

We now turn to the Pioneer 10 and 11 observations of the middle ($12\ R_J \lesssim R \lesssim 40\ R_J$) and outer ($R > 40\ R_J$) magnetospheres. We will review first the quasi-steady P-10 outbound pass and then P-11 outbound high latitude passes, constructing the conceptual models which could emerge from these passes alone. We will then consider together the P-10 and P-11 inbound passes which had very similar trajectories.

4.1 Pioneer 10 Outbound

Figure 9 is a different plot of the JPL magnetometer data[147, 148]. Each point in the bottom inset represents a one hour average value of the latitude δ. The top insert represents δ_D, the latitude had the field been a vacuum field. A ten-hour periodicity in δ_D due to the rotation of Jupiter's oblique dipole is apparent. In fact, about two cycles of this periodicity are apparent in the data, when Pioneer 10 was within 20 R_J. Thereafter, the field became nearly radial somewhat past 20 R_J. The solar wind plasma probe detected magnetosheath flowing plasma for the first time at 98 R_J. The magnitude of the magnetic field (Figure 2) varied approximately as $1/R^3$ within 20 R_J and as $1/R^{1.7}$ beyond, so that the magnetic pressure exceeded the dipole pressure by several hundred at the magnetopause crossing 98 R_J. Quantitative calculations[130] would place the classical magnetopause near 75 R_J on the dawn meridian. Smith et al.[147, 148] also plotted the longitude towards which the field points. In the region between 20 - 90 R_J the field, while remaining very nearly in a meridian plane, was gradually swept back so that by 90 R_J it pointed 30° out of the meridian plane, lagging precise co-rotation. A theoretically more meaningful display of the same data is shown in Figure 10, taken from Goertz et al[64]. Plotted is the ratio

of the azimuthal (B_ϕ) to radial (B_ρ) magnetic field components, divided by radial distance, denoted by ρ, against radial distance between 0 - 80 R_J. B_ϕ is nearly everywhere negative (the few positive points being questionable), and $B\phi/\rho B_\rho$ is weakly dependent on distance. Thus, the gardenhose angle increased almost linearly with distance.

The magnetopause at 98 R_J identified by the solar wind plasma probe is not evident in the one hour averages of field latitude, magnitude, or longitude. (It is identifiable, with higher time resolution magnetic data.) However, at roughly 90 R_J, a transition to a strongly southward, much more unsteady field occurs. An apparently related change in behavior is noticeable in the 6 - 30 MeV electron fluxes (Figure 4) where the amplitude of the ten hour flux modulations is sharply diminished beginning at 90 R_J. A similar change is even more apparent in the energetic electron data of Van Allen et al.[167] Thus, there is evidence of a separate layer near the magnetopause where the magnetic field is southward and highly time variable.

Figure 4 reveals that the 6 - 30 MeV electrons are modulated by a factor 100 between 20 and 90 R_J during the P-10 outbound pass. Ten hour modulations of the energetic particle fluxes were common on all the P-10 and 11 passes, but they were most pronounced on P-10 outbound. Figure 11 shows similar data for the 1.1 - 2.15 MeV (upper curve) and 14.8 - 21.2 MeV (lower curve) proton fluxes[163]. The proton and electron modulations are in phase. According to Trainor et al.[162, 163], the peak 0.41 - 2 MeV electron fluxes were roughly $10^5/cm^2$-sec, and the peak 1.1 - 2.14 MeV proton fluxes were $10^4/cm^2$-sec, so that the peak energy densities of MeV electrons and protons were comparable. The peaks in electron and proton fluxes are associated with partial or complete traversals of a current sheet-field reversal layer. Figure 12 [150] shows a current sheet traversal at about 75 R_J. While there is evidently considerable structure,

the field magnitude generally diminishes and changes from radial outside to more southward inside. Of particular significance is the 180° jump in field longitude near 22 GMT; evidently the spacecraft passed between lobes of the magnetosphere and the magnetic field reversed direction. The peak energetic particle fluxes coincide with sheet crossings; moreover, the electron energy spectra are consistently harder at the magnetic field minima. Figure 13 shows one minute resolution 0.5 - 1.8 MeV proton and 6 - 30 MeV electron fluxes for a P-10 outbound sheet crossing at 40 R_J [141]. The fluxes exhibit considerable fine structure on the minute time scale within the sheet but are much more slowing varying outside. Of particular significance is the fact that electron and proton fluxes jump simultaneously in minutes. The proton flux exhibits strong fluctuating field aligned anisotropies; the electrons do not. Simpson and McKibben[143] make two important suggestions: first, the simultaneous electron and proton increases are evidence of local acceleration; second, the acceleration may be due to magnetic field reconnection in the sheet. Sakurai[133] has estimated the reconnection rate to be sufficient to accelerate particles to MeV energies rapidly; however, a detailed theory of reconnection in the Jovian current sheet is still lacking. Kivelson (private communication, 1977) has examined the magnetic field data during some of the energetic particle events observed by Simpson and McKibben[143]. She finds no striking magnetic signatures reminiscent of reconnection; however since the precise instantaneous orientation of the current sheet may be uncertain, this conclusion must be regarded as tentative.

Since the energetic particle fluxes tend to be isotropic at the current sheet crossings, the particles may be contained on closed field lines within the sheet. This is consistent with the tendency for the magnetic field to be southward within the sheet. On P-10 outbound, the particles fluxes were modulated by a factor 100 at sheet crossings - much more than on the other passes -

suggesting that the field lines bounding the current sheet may be open[64]. Goertz et al.[64] emphasize that this reasoning is only applicable to P-10 outbound.

The global properties of the current sheet are difficult to ascertain with single spacecraft measurements. To know its thickness, for example, we must construct a model for its motions. Figure 14, taken from Goertz[62] sketches two possible models, which according to Goertz, cannot be resolved by present experimental data. The top, "hinged current sheet" model is due to Smith et al.[147]. Since the perturbation magnetic field (actual minus dipole) proved to be relatively invariant with respect to Jupiter's dipole axis, they argued that the current sheet is parallel to the rotation equator. They fix the hinge point between dipole and sheet at $\simeq 20\ R_J$ consistent with P-10 outbound observations. Goertz[62] argues that the current sheet should remain almost precisely in the magnetic equatorial plane. We defer further discussion of these models until Section 5.

In summary, from Pioneer 10 outbound alone, one would be tempted to construct the following phenomenological model of Jupiter's magnetosphere. The magnetosphere is divided into two lobes, northern and southern, separated by a thin current sheet which moves up and down as Jupiter rotates. The magnetic field is nearly radial near but outside the sheet, and is weakly swept back out of meridian planes into a garden hose configuration, slightly lagging co-rotation. The magnetic field is on the average southward in the sheet, indicating that energetic particles are contained in it. However, field reconnection may occur there, accelerating particles to high energy and temporarily reversing the dominant southward direction of the sheet magnetic field. The plasma whose pressure is needed to balance the magnetic pressure on either side of the current sheet has not yet been detected, although the intense

fluxes of MeV protons suggest that 10-100 KeV ions may be responsible. Next to the magnetopause, there is a thin (8 R_J radial thickness) layer where the current sheet is less prominent and the magnetic field is southward and irregular.

4.2 Pioneer 11 Outbound

P-11 outbound remained close to the local noon merdian plane, passing through the magnetosphere at Jovigraphic latitudes of 30-35°. We begin our examination of the magnetic field magnitude, Figure 2, and longitude, Figure 3, at a radial distance near 20 R_J where $X_{SJ} \simeq Z_{SJ} \simeq 15\ R_J$. As Pioneer 11 proceeded outward, the magnitude diminished smoothly, following an R^{-3} law much more closely than R^{-2}, until just before the first magnetopause crossing at 55 R_J, $X_{SJ} \simeq 45\ R_J$, $Z_{SJ} \simeq 30\ R_J$. (On Pioneer 10 outbound, the magnitude deviated from an R^{-3} law beginning at 20 R_J radial distance.) The P-11 outbound magnetic latitude, Figure 3, manifests weak 10 hour modulations between 10 and 50 R_J, similar to those in the top inset of Figure 9 for the undistorted dipolar field. The magnetic longitude data, not shown here, show that the field was not swept back but remained in a meridian plane. Thus within 55 R_J Pioneer 11 outbound found a weakly distorted dipole field; the distance of its first magnetopause crossing was consistent with this fact. However, the magnetosphere was evidently not stationary, for Pioneer 11's passage into the magnetosheath at 55 R_J was transient, and it found itself back inside the magnetosphere again at 63 R_J. This time the magnetic field strength exceeded the dipolar field, pointed strongly southward, and was irregular. Pioneer 11 exited a final time into the magnetosheath at $R \simeq 80\ R_J$, $X_{SJ} \simeq 65\ R_J$, $Z_{SJ} \simeq 42\ R_J$.

Figure 15 has been adapted by Kivelson[87] from Trainor et al.[164]. The bottom curve shows the fluxes of 0.1 - 2 MeV electrons, the middle curve 1.2 - 2 MeV protons, and the top curve, 0.5 - 2.1 MeV protons, for both inbound and outbound P-11 passes; the outbound portion of the flyby begins December 3, 1974. Bowshock and magnetopause crossings are denoted by B and M, respectively. Following Smith et al.[149], Kivelson[87] studied the time variability of the magnetic field in the internal boundary layer next to the magnetopause. Within this layer, the field is highly turbulent, down to time scales as short as tends of seconds. These turbulent regions, shaded in Figure 15, lie near but within the magnetopause, and, just as for P-10 outbound, the particle fluxes show little or no periodicity. A transition to the internal boundary layer is therefore marked by three characteristics: the hourly average field shifts to southward and becomes more variable; magnetic turbulence is present; and the energetic particle fluxes are smoother and less distinctly modulated.

Two facts concerning the P-11 energetic particle fluxes, Figure 15, stand out. The outbound high latitude fluxes are comparable in magnitude with the inbound low latitude fluxes. While the 10 hour modulations inbound might suggest disk confinement, 4 days later, there were copious fluxes at latitudes above thsoe expected from a disk model. Secondly, the electron flux exceeded the proton flux by somewhat more than an order of magnitude, again suggesting that the number densities of MeV electrons and protons were comparable.

In summary, if only the P-11 outbound data within 55 R_J were available, one would say that Jupiter's magnetosphere was Earthlike along the Jupiter-Sun line, with magnetopause position fixed approximately by the balance of solar wind dynamic and undistorted dipole magnetic pressure, and with the entire magnetosphere filled with energetic particles out to the magnetopause, as at

Earth. Why, then, a day after first passing the magnetopause, Pioneer 11 re-encountered something resembling a high latitude version of the turbulent internal boundary layer found next to the magnetopause on P-10 outbound remains mysterious.

4.3 Pioneer 10 and 11 Inbound

Looking at the magnetic field data alone, Figures 2 and 3, a case could be made that Pioneer 10 inbound encountered an approximately Earthlike magnetosphere from its last magnetopause crossing at $R \simeq 45\ R_J$ inward. The magnetic latitude δ showed periodic modulations approximately compatible with those of the spinning oblique vacuum dipole, the magnetic field magnitude exceeded dipolar by about a factor 2, consistent with the dipolar pressure balance model, and followed the dipolar spatial variation closely. Since the field near the Jovigraphic equator pointed dominantly southward during this portion of the pass, Smith et al.[147, 148] felt that there was little evidence for current sheet crossing within 45 R_J. Certainly, the 10 hour variations in particle flux were much less pronounced than on P-10 outbound.

Trainor et al.[162, 163] have published the proton flux energy spectra, shown in Figure 16, for this quiet portion of the Pioneer 10 inbound pass. Near the magnetopause, the proton energy spectrum is quite steep, varying as E^{-3}, and there is no evidence of a turnover. However, if the E^{-3} spectrum were to prevail below several tens of KeV, the plasma $\beta = 8\pi NT/B^2$ would exceed unity, which is contradicted by the magnetic field measurements. Very likely, the plasma β is near unity at the magnetopause, a common occurrence at Earth.

The relatively small velocities of $\sim$ MeV protons, together with a knowledge of the proton energy spectrum, permit a test of whether or not the protons co-rotate wtih Jupiter. Trainor et al.[162, 163] fit their angular distributions with a function of the form $J(\theta) = A_0 + A_1 \sin(\theta-\theta_1) + A_2 \sin 2(\theta-\theta_2)$, where θ_1

is the angle between their detector look direction and the normal to the ecliptic plane. Their results for A_1/A_0 and θ_1 are shown in Figures 17a and b, respectively. While A_1/A_0 varies significantly from the value expected on the basis of corotation beyond about 25 R_J, it appears that within 25 R_J, the particles co-rotate, coming from $\theta_1 = 90°$ as expected. The region 25-45 R_J is evidently a transition region, with a hint that co-rotation may be preserved. Interpretation of such plots becomes ambiguous if the particle fluxes have significant spatial gradients.

Despite the fact that they passed through approximately the same region of space relative to Jupiter, Pioneers 10 and 11 inbound encountered significantly different magnetospheres. Pioneer 11 inbound encountered the bowshock at 110 R_J, crossed the magnetopause twice at 97 and 92 R_J suggested its position was oscillatory, then the shock aagain at 92 R_J to remain in the solar wind, until the shock was again encountered at 78 R_J. The final durable crossing of the magnetopause occurred at 65 R_J. According to Figure 15, the spacecraft remained in the turbulent internal boundary layer until roughly the classical magnetopause position of 45 R_J. Within 45 R_J the behavior was much more like P-10 outbound than P-10 inbound. Strong modulations of the energetic particles associated with a current sheet were found. Rapid variations in intensity that were simultaneous for both electrons and protons, albeit less pronounced than on Pioneer 10 outbound, were again found, again suggesting local particle acceleration [143]. Within about 50 R_J, the field was swept back slightly out of meridian planes, again reminiscent of P-10 outbound.

The evidence (Figures 17a,b) for co-rotation found by Trainor et al.[162,163] on P-10 inbound corresponds to a time when the magnetosphere was dipolar within 45 R_J. Sentman and Van Allen[139] performed a similar analysis for their 0.6 - 3.4 MeV proton data on P-11 inbound, and found that co-rotation prevails within the last durable magnetopause crossing at 65 R_J to at least 30 R_J. Thus co-rotation seems to occur when the current sheet is present and also within the turbulent internal boundary layer. A striking confirmation of this fact is shown in Figure 18[143]. The data correspond to the brief interval of time when P-11 inbound was within the magnetosphere near 95 R_J; during this brief interval, the angular distribution of 0.5 - 1.8 protons was consistent with co-rotation.

On the three passes, P-10 in, P-11 in and outbound, for which the magnetosphere was evidently nonstationary, the current sheet was encountered on two of the three, and then only before the first or after the last "durable" magnetopause crossing. In all three cases, within the magnetosphere between magnetopause crossings, the field pointed southward and was irregular. At these times, the spacecraft were in the turbulent interval boundary layer. Since this signifies proximity to the magnetopause, neither the temporal duration nor the derived spatial extent of this layer indicates its geometry, since the magnetopause is evidently in motion.

It seems particularly striking to us that Pioneer 10 inbound encountered a dipolar magnetic field and Pioneer 11 inbound encountered a disk structure when both spacecraft were on approximately the same trajectories at low latitudes within 45 R_J, the classical magnetopause radius. This fact illustrates how changeable Jupiter's magnetosphere really is.

4.4 Possible Cause of Time Variability in Jupiter's Magnetosphere

Figure 19 is taken from Smith, Fillius, and Wolfe[151]. The top two inserts show a compressed display of the UCSD energetic electron fluxes and the magnitude of the magnetic field for the entire Pioneer 10 enounter. When P-10 was within the magnetosphere, the magnetic field plot is shaded. The bottom two insets show the Pioneer 11 solar wind magnetic field magnitude and solar wind dynamic pressure during the Pioneer 10 encounter, adjusted for solar wind travel time between P-11 and Jupiter. The solar wind magnetic field and dynamic pressure peaks every seven to ten days in association with solar wind sector boundaries. The dynamic pressure at P-11 varies by a factor 10-30. When P-10 first encountered the magnetopause at 98 R_J, the P-11 dynamic pressure was low; the second inbound magnetopause crossing was associated with a pressure peak, as was the first outbound crossing. The distant magnetosphere encounter between 130-150 R_J on P-10 outbound was associated with an anomalously low solar wind pressure. Thus, the available evidence suggests that when the solar wind dynamic pressure is low, Jupiter's magnetopause is found well beyond its classical position; when the solar wind dynamic pressure is high, Jupiter's magnetosphere is compressed and its magnetopause may approach its classical position. The solar wind dynamic pressure may therefore induce changes between a disk-like and more dipolar outer magnetosphere.

4.5 Signature of Middle Magnetosphere

While the spatial region between the dipolar radiation belts and the true outer magnetosphere is ill-defined because of time variations, it possesses a characteristic signature in the electron pitch angle distributions relative to the magnetic field. In the radiation belts, the pitch angle distributions are peaked perpendicular to the magnetic field, consistent with a distribution

which is stably trapped in the magnetic mirror field. In the middle magnetosphere (12 - 25 R_J) the low latitude P-10 in and out and P-11 outbound passes revealed electron fluxes peaked along the magnetic field in both directions; the ions were isotropic[50, 167, 139, 162, 163]. Sentman et al.[138], using P-11 outbound data, found that both proton and electrons stream along the magnetic field away from Jupiter. When these fluxes reach the magnetic equator they would form bi-directional field-aligned distributions as observed; they invoke (ad hoc) pitch angle scattering to account for isotropic proton distributions. Thus, either Jupiter, or the inner radiation belts, is a source of energetic particles for the middle magnetosphere. Sentman et al. al.[138] suggest, following Nishida[119], that inner radiation belt particles, which mirror at low altitudes, undergo poleward diffusion due to ionosphere electric field turbulence which violates the second adiabatic invariant. Upon reaching high latitudes, the particles would possess a strongly field-aligned pitch-angle distribution. A difficulty with this interpretation is that diffusion transport should produce a spatially smooth and temporally steady pitch-angle distribution, whereas the observations indicate high temporal and spatial variability.

4.6 Jupiter as a Cosmic Ray Source

Energetic particles generated in the Earth's magnetosphere can escape to the solar wind. They are detectable, for example, upstream of the Earth's bowshock[46, 56, 4]. It was natural, therefore, to search for energetic particles as the Pioneers approached Jupiter. More than 1 AU from Jupiter, both Chenette et al.[34] and Teegarden et al.[157] observed sporadic increases of electron fluxes in the few hundred KeV to a few MeV energy range, which became more frequent as Jupiter was approached, and quasi-continuous near Jupiter. Teegarden et al.[157] then showed that similar electron events observed at Earth's orbit, which had been found not to correlate with solar events, were of Jovian origin,

since they have a 13 month periodicity, Jupiter's synodic period. In Figure 20 [123] the time of year that the Earth crosses the solar wind field line that intersect Jupiter's magnetosphere is plotted for the period 1968-1974. The vertical bars indicate when quiet time electron bursts were present, again suggesting that Jovian electrons were detected at Earth[157]. McDonald and Trainor[100] have found simultaneous bursts of electrons on Pioneer 11 at 3-4.25 AU and IMP-7 at 1 AU, allowing for propagation delay. Pioneer 11, in the solar wind, apparently detected a flux increase observed when Pionner 10 was outbound in the Jovian magnetosphere. Thus, there is little doubt that Jupiter is a significant source of MeV electrons in the heliosphere.

Given that Jupiter, at times, strongly modulates its energetic electron fluxes at its rotation period, it is natural to ask whether similar modulations are found in the Jovian interplanetary electron bursts. Chenette et al.[34] reported that within each burst, the electron fluxes are modulated at a ten hour period and, moreover, the spectral index tracked the ten hour periodicity even more clearly. Even more remarkably, they claim that the phase of the interplanetary modulations is the same as that found inside the magnetosphere. Figure 21 plots the time intensity profiles of the 6 - 30 MeV fluxes (bottom curve) and the ratio of the 3 - 6 MeV to 6 - 30 MeV electron fluxes during an interplanetary event measured on Pioneer 10. The vertical dashed lines represent times of spectral index maximum for a period of 9 hours, 55 minutes, 30 seconds reference to a spectral index maximum measured when Pioneer 10 was subsequently within the magnetosphere. When a new burst commences after an old one dies away, the spectral index maxima have the same phas as in the previous burst. These observations have not been clearly confirmed by the other experiments on board the spacecraft.

The hypothesis that MeV electrons are contained in a flapping sheet in Jupiter's outer magnetosphere, attractive for P-10 outbound and P-11 inbound, has difficulty explaining the continuity in phase of interplanetary electron spectral modulations with those in the magnetosphere. Chenette et al.[24] argue that these facts can best be explained if Jupiter generates energetic electrons periodically in time throughout a significant part of its magnetosphere. No matter how they escape, they would then show phase continuity between the solar wind and magnetosphere.

It appears that a necessary but not sufficient condition for detection of an electron burst upstream of Jupiter is that the interplanetary magnetic field connect the spacecraft and Jupiter's magnetosphere[150], just as it must connect Jupiter and Earth if they are to be detectable at Earth. The electron intensity maxima are also associated with bursts of hydromagnetic waves in the solar wind[150]. Vasyliunas[168] has shown that Jovian cosmic ray electrons have minimum intensity and softest spectrum when the subsolar point on Jupiter is near the longitude of the most frequenct non-Io related decametric radio emissions.

The Jovian cosmic ray electrons immediately pose three questions. When and where are those MeV electrons destined to escape generated? How and where are they modulated? And how do they escape? In Figure 20 most of the Jovian cosmic ray events observed at Earth occur 1-3 months after Jupiter's nominal field line sweeps over Earth. Krimigis et al.[92], Pesses and Goertz[123], and Mewaldt et al.[114] propose that this delay can be explained if one assumes the electrons come when the Earth interplanetary field line intersects an extended Jovian magnetic tail. Krimigis et al.[92] estimate a tail length of 4.6 AU; Pesses and Goertz [123] argue there is an active region between 1 and 2 AU. Recently, Barnes et al.[14] have argued that Jovian cosmic ray electrons are present at flux levels lower than during the above 3 month window through the

full 13 month synodic period. Thus, electrons may diffuse out of Jupiter's magnetosphere and in the solar wind. A long tail may not be absolutely necessary to explain the observations[78]. However, the Pioneer 10 solar wind plasma detector may have detected the Jovian tail 4 AU downstream from Jupiter. At about the expected location, it detected on two occasions a complete dropout in plasma flux[76]. However, the P-10 magnetometer was unfortunately not functional, and the energetic particles experiments have not reported any significant perturbations.

4.7 Summary

Jupiter's outer magnetosphere is so time variable that flybys are unable to separate spatial from temporal variations. Eight days has the longest period Jupiter's magnetosphere remained in the same state (P-10 outbound). Spatially separated multiple magnetopause crossings were observed on all four Pioneer passes. The magnetopause encounters were found between roughly the classical magnetopause radius (about 40 R_J at the nose) and more than a factor two beyond the classical radius. When the magnetopause was in motion, Pioneers 10 and 11 often found themselves within a turbulent boundary layer, characterized by southward irregular magnetic fields. The evidence for periodic current sheet crossings is less compelling in the turbulent boundary layer than further within the magnetosphere.

In the region between 30-60 R_J, where the classical magnetopause should be found, Jupiter's magnetic field seems to change back and forth between dipolar and disk-like. A well developed current sheet was found between 20 and 80 R_J on Pioneer 10 outbound. Pioneer 10 inbound found a dipolar and Pioneer 11 a disk-like configuration near the equator in this region. While Pioneer 11 outbound's was at sufficiently high latitudes that it should not have encountered a current sheet, it is surprising to us that its field and particle data looked so dipolar within its first magnetopause crossing.

The challenge posed to the theoretician by the Pioneer 10 and 11 data is a severe one. He must develop a theoretical structure which can encompass time dependent changes between the dipolar and disk limits which at the same time accounts for the 10 hour modulations of energetic particles and magnetic fields when the current sheet is well developed. At present, there is some preliminary evidence which suggests that variations in solar wind dynamic pressure are associated with magnetopause motions, and possibly, changes in magnetospheric structure.

5. MODELS OF JUPITER'S OUTER MAGNETOSPHERE

Theoretical models of the Jovian magnetosphere can be divided into three general classes: Earth-like convection models, quasi-static disk models, and radial outflow models. We discuss Earth-like convection models first because they provide a reasonable historical introduction and a context in which the differences between the Jovian and terrestrial magnetospheres are illuminated. We then discuss static disk models in which magnetic tension just balances the corotation centrifugal force and plasma is quasi-permanently trapped. However, Jupiter has at least two internal sources of plasma--the ionosphere, and the Galilean satellites. If continuously supplied, this plasma must escape into the solar wind by flowing through the outer magnetosphere, thereby motivating radial outflow models.

5.1 Earthlike Models of Jupiter's Magnetosphere

The late Neil Brice was the pioneer who first systematically scaled out knowledge of Earth's magnetosphere to Jupiter[23, 24, 77, 25]. This work was reviewed and extended to then hypothetical magnetospheres of Saturn and the still hypothetical magnetospheres of Uranus and Neptune[81]. One starts with the theoretical scaling of steady state solar wind parameters from standard theory[122]:

$$U_r = 400 \text{ km/sec}, \quad U_\phi \simeq 0 \tag{5.1a}$$

$$N \; 5\text{-}7/r^2 \text{ cm}^{-3} \simeq 0.2 - 0.3 \text{ cm}^{-3} \tag{5.1b}$$

$$B_r = 5\gamma/r^2 \simeq 0.2\,\gamma \tag{5.1c}$$

$$B = 5\gamma/r \simeq 1\,\gamma \tag{5.1d}$$

$$B\,(B_r^2+B_\phi^2)^{1/2} = 5\gamma[(1+r^2)/r^4]^{1/2} \simeq 5\gamma/r \simeq 1\,\gamma \tag{5.1e}$$

$$NMU_r^2 = 1.25 \times 10^{-8}/r^2 = 5 \times 10^{-10} \text{ dynes/cm}^2 \tag{5.1f}$$

In (5.1a-f) above, U_r and U_ϕ are the radial and azimuthal components of the solar wind flow velocity, N is the ion or electron number density, B_r and and B_ϕ are the radial and azimuthal magnetic field components, and r is the heliocentric distance in AU. The first expressions in (1a-e) above give the scalings normalized to typical parameters at 1 AU, and the second expressions give approximate nominal values at the orbit of Jupiter $r \simeq 5$ AU. As noted earlier (Figure 19), the solar wind is highly time variable beyond the orbit of Earth, so that the above "nominal" parameters are only indicative

If the plasma pressure inside the magnetosphere were small or zero, the solar wind dynamic pressure would compress the dipole field until it is finally balanced by magnetic pressure. Since the current sheet at the interface between the solar wind and dipole region doubles the internal field, pressure balance at the nose stagnation point occurs at a distance

$$D = R_J[B_o^2/2\pi\rho u^2]^{1/6} = \text{classical magnetopause nose radiua} \qquad (5.2)$$

where B_o is the surface equatorial field strength. For the above "nominal" solar wind parameters, $D \tilde{\simeq} 41\ R_J$ and the magnetic field just inside the magnetopause is 11 γ. For the magnetopause to be at 80 - 100 R_J, this model requires a factor 30-50 reduction in ρu^2. Away from the stagnation point the super-Alfvenic, supersonic solar wind exerts a pressure normal to the magnetopause, which is well approximated by $\rho u^2 \cos^2\chi + P$ where χ is the angle of attack and P is the solar wind thermal pressure. Hydrodynamic calculations indicate that at dawn and dusk the magnetopause is located at 3/2 D [154].

The above model accounts quite well for the static, zeroth order configuration of the Earth's magnetosphere. However, it assumes that the solar wind is unmagnetized and that the magnetopause is dissipation-free. Even though the energy density of the solar wind magnetic field is only a few percent

of the flow energy density, magnetic field line reconnection between the solar wind and dipole fields, which creates a dissipative magnetopause, couples solar wind energy into the magnetosphere. Directional changes in the solar wind field vary the reconnection and energy input rates, and are thus ultimately responsible for many time varying, energetic phenomena within the earth's magnetosphere[42].

After merging on the dayside magnetopause, polar cap field lines now connected to the solar wind are dragged by the solar wind over and around the magnetosphere, and are stretched out into a long magnetic tail. In the ionosphere, the open field lines flow from the day to nightside corresonding to a dawn-dusk electric field. In the tail, the open field lines flow toward the equatorial plane where they again reconnect with their partners across a magnetic neutral sheet; in steady state the nose and tail reconnection rates must be equal. The newly closed flux must then flow from the tail reconnection region towards the nose to repeat the cycle. Thus, reconnection has the following general consequences for the Earth's magnetosphere: there is a region of open flux connecting to the polar caps in which cosmic rays have direct access to the earth's polar cap atmosphere; there is a long magnetic tail containing a magnetic neutral sheet where stored magnetic energy is dissipated and plasma is heated and accelerated towards the Earth; there is a connection flow of plasma and magnetic flux throughout the interior of the magnetosphere. Figure 22 shows an original sketch[42, 94] of the flow driven by reconnection in the noon-midnight magnetic meridian plane.

We now construct a convection model based on reconnection for Jupiter. We may estimate the energy dissipation rate due to reconnection as follows. The full solar wind emf Φ across the width 3D of Jupiter's classical magnetopause is given by

$$\Phi \simeq 5 \text{ MV} \simeq \frac{3 \text{ Ur BD}}{C} \qquad (5\text{-}3)$$

A fraction $\beta < 1$ of the solar wind flux impinging upon the magnetospheric cross section is reconnected; the rest flows around the magnetosphere Levy et al.[94]. Consequently the emf corresponding to the internal convective flow is $\beta\Phi$. Phenomenological studies indicate that $\beta \simeq 0.1\text{-}0.2$ at Earth. Thus, $\Phi \gtrsim 1$ MV at Jupiter. $e\beta\Phi$ is the largest energy a charged particle can acquire from a betatron accleration in a steady flow.

The energy dissipation rate W is given by computing the total current in the reconnection region of the dayside magnetopause and multiplying by $\beta\Phi$. The current per unit length in the magnetopause is $C\Delta B/4\pi$, where $\Delta \simeq 14\alpha$ is the jump in magnetic field strength at the magnetopause. The total current I is then approximately $\frac{C\Delta B}{4\pi}\,\ell$, where ℓ is the effective length of the reconnection region normal to the ecliptic plane, hence

$$W \simeq \frac{C\Delta B}{4\pi}\,\ell\,\beta\Phi \simeq 4 \times 10^{21}\,\beta \text{ ergs/sec} \quad . \tag{5.4}$$

At Earth, $W_E \simeq 10^{19}\,\beta$ ergs/sec. Thus, Jupiter's magnetosphere would be at least two orders of magnitude more energetic than Earth's in this model.

At Earth, much of the dissipated solar wind is deposited by energetic particle precipitation and Joule dissipation into the auroral zone atmosphere. The auroral zone is just equatorward of the polar cap open field region, and has an area comparable to that of the polar cap. The radius of the polar cap r_{pc} can be estimated by assuming that the open flux in the polar cap approximately equals the dipolar flux which closes beyond the radius D. Then, $r_{pc} \simeq R_J^{3/2}/D^{1/2} \simeq R_J/7 \sim 10^9$ km, corresponding to a co-latitude of $\simeq 8°$. At Earth, $r_{pc} \simeq R_E/3$, corresponding to a co-latitude of $\simeq 20°$. Assuming the auroral zone area is πr_{pc}^2, approximately $10^3\,\beta \simeq 10^2$ ergs/cm^2-sec of solar wind energy might be dissipated into the Jovian auroral atmosphere. This considerably exceeds the solar flux of UV photon energy deposited in Jupiter's atmosphere

and should be the dominant energy source for Jupiter's upper atmosphere and ionosphere in the auroral zone.

Given the polar cap radius, we may compute, following Dungey[43], the length of Jupiter's magnetic tail L_T. The convection electric field in Jupiter's polar cap ionosphere is of order $\beta\Phi/2r_{pc}$ in magnitude, directed dusk to dawn corresponding to a transport of flux from the day side to the night side. The convection speed is therefore $\beta C\Phi/2r_{pc}B_I$, where B_I is the ionospheric magnetic field strength. The ionospheric foot of a magnetic field line crosses the polar cap in a time $\tau = 4r_{pc}^2 B_I/C\Phi\beta$. During the time τ, the field line passes from the nose to the tail reconnection region. The entire flow cycle lasts approximately 2τ. The length of the tail is $L_T = U_r\tau$. Inserting our previous estimates, we find that $\tau \simeq 15/\beta$ hours and $L_T = \frac{400}{\beta} R_J$. If we assume that the reconnection efficiency $\beta = 0.1$ as at Earth, then τ is roughly one week. τ, the time required to change the convection state of the magnetosphere, is comparable with the duration of a given flyby pass, and with observed time scales on which Jupiter's magnetosphere does change. With $\tau \simeq 1$ week, $L_T \simeq 4000\ R_J \simeq 2$ AU, in order of magnitude agreement with that estimated from the propagation of Jovian cosmic ray electrons. We sketch this convection model of Jupiter's magnetosphere in Figure 23.

Since the length of Jupiter's magnetic tail and Jupiter's distance from the sun are comparable, Jupiter's magnetosphere and the solar wind have approximately the same scale. This suggests that Jupiter's magnetosphere varies in time in response to an entirely different set of solar wind inputs than earth, whose magnetospheric tail is only 0.04 AU long. For example, the solar wind is divided up into a number of sectors, typically four, in which the gardenhose field is directed towards or away from the sun and reverses as the sector boundary is crossed. Jupiter remains in one sector for one quarter

of a solar rotation, or about a week. Thus, the nose of Jupiter's magnetosphere could be in one sector, its distant tail in another, suggesting that Jupiter's magnetosphere rarely achieves a steady connective flow pattern. Magnetic storms, due to a solar flare enhanced solar wind, last typically only one or two days at Earth; storms might not last long enough to create a steady flow at Jupiter.

Finally, for later purposes, we need an estimate of the number flux of solar wind ions which circulate in the internal convection flow. The total number of solar wind ions per second traversing the cross-sectional area of Jupiter's magnetosphere $2.25\ \pi NUD^2 \simeq 7 \times 10^{30}$ per second. It is not known precisely how many of the particles circulating in the terrestrial magnetosphere originate in the solar wind and how many in the ionosphere, probably because the ratio varies strongly with solar wind activity. However, the typical number, 10^{26}/sec, corresponds to roughly 10^{-3} of the solar wind flux impinging upon the Earth's magnetospheric cross section. If this scaling applies to Jupiter, 10^{28} particles per second circulate through its magnetosphere.

5.2 Corotation and Plasmapause

For a dipole field with aligned magnetic moment and rotation axes, the radially outward co-rotation electric field is

$$E_{CR} = \frac{\Omega R_J B_o}{C} (R_J/r)^2 \quad . \tag{5-5}$$

If we assume that reconnection imposes a uniform dusk-dawn electric field E_C across the magnetosphere, there is a stagnation point ($E_{CR} = E_C$) in the combined co-rotation-convection flow at local dusk at a radial distance

$$r_p/R_J = [\Omega R_J B_o/CE_C]^{1/2} = [\Omega R_J B_o/\beta U_r B]^{1/2} \quad . \tag{5-6}$$

By adding co-rotation and convection electric potentials, the flow streamlines can be determined. The streamline passing through $r = r_p$ forms a closed curve in spin-magnetic equator, the plasmapause. Inside the plasmapause low energy particles co-rotate around Jupiter and cannot escape to the solar wind; if internal plasma sources exist, the plasmasphere should be a high density region. The minimum plasmapause radius is $0.4\ r_p$ and occurs at local dawn.

If we compare the mean plasmapause radius, $0.7\ r_p$, with the classical nose radius, we find

$$\frac{0.7\ r_p}{D} = 0.7 \left(\frac{\Omega R_J}{\beta B}\right)^{1/2} \left(\frac{2D\ B_{o\rho}}{U_r}\right)^{1/6} = 1/\sqrt{\beta} \quad . \qquad (5.7)$$

Thus Brice and Ioannidis [24] concluded that the Jovian plasmapause extends beyond the magnetopause; for Earth $0.7\ r_p/D \doteq 0.4$. This is one of the senses in which Jupiter is a fast, and Earth a slow, rotator. Brice and Ioannidis[24] argued that near the magnetopause there would be a thin region where all the magnetic flux involved in convection would return to the nose magnetopause. Their sketch of the flow streamlines is shown in Figure 24.

5.3 Interaction of the Magnetosphere with the Ionosphere and Atmosphere of Jupiter

Field aligned currents are a natural feaure of the coupling of an external hydromagnetic flow to a conducting central body[82]. While field aligned currents exert no stresses themselves, they communicate stresses between the magnetosphere and atmosphere-ionosphere, by forming part of a circuit whose current closes by flowing perpendicular to the magnetic field in the ionosphere, where the conductivity perpendicular to the magnetic field is finite, and in the magnetosphere, where significant plasma pressure gradients support perpendicular currents.

Neglecting convection for the moment, the current system necessary to enforce corotation is shown in Figure 25. The current is in over the poles, out at lower latitudes, and closes in the magnetosheath. Neglecting rotation, the topology of the currents threading Jupiter's polar cap ionosphere, which are demanded by convection, would be that given in Figure 25, which shows a slice through the dawn-evening meridian plane. The dusk-dawn convection electric field drives a dissipative Pderesen current, which must be fed by the field-aligned currents into (out of) the ionosphere at dusk (dawn); the current closes in the magnetosheath. The energy required to sustain these currents against ionospheric dissipation comes from decelerating the solar wind. The correct topology, which combines convection and corotation systems, has not yet been drawn, but is probably a nonlinear addition of the two.

As the nightside convective flow approaches Jupiter, co-rotation forces more flux and plasma around local morning than evening (Figure 24), thus investing angular momentum in a flow that, in the distant tail, possessed none by symmetry. Since the flow encounters the magnetopause before it can symmetrize on the dayside, a net angular momentum is lost from the system to the solar wind. Kennel and Coroniti[83] estimated the torque T, which Jupiter must exert on the flow to be $T \approx \Omega D^2 \dot{M}$ where $\dot{M}$ is the mass flux entrained in the convection flow. Estimating $\dot{M}$ by 10^{28} hydrogen ions per second, we find $T \approx 10^{23}$ dyne-cm, and the rotational energy dissipation rate $T\Omega \approx 10^{19}$ ergs/sec.

The $\underline{J} \times \underline{B}$ stress due to ion Pedersen currents is exerted against the neutral atmosphere. In a time $\tau_c = \nu_{in}^{-1} \rho_n/\rho_i$, where ν_{in} is the ion-neutral collision frequency and ρ is the respective mass density, the neutrals are accelerated to the $\underline{E} \times \underline{B}$ velocity, and, since $\underline{E} + 1/c\underline{V}\times\underline{B} = 0$ in the co-moving plasma-neutral frame, all currents cease[47]. Present solar UV production models[5] indicate that the Jovian ionosphere is similar to the Earth's F-region in that

ν_{in} is small compared to the ion cyclotron grequency and that the neutral gas at ionospheric altitudes has little inertia. For these models Coroniti[36] found $\tau_c \gtrsim 40$ minutes so that convection electric fields might rapidly stimulate ionospheric neutral wind systems. Kennel and Coroniti[83] pointed out that since $\Omega\tau_c << 1$, the ionospheric neutral atmosphere may possess insufficient inertia to enforce ionospheric neutral atmosphere may possess insufficient inertia to enforce co-rotation on magnetospheric field lines. Assuming an eddy diffusion coefficient of 10^8 cm^{-2} sec^{-1}, the upper limit in ionospheric models, they found that the upward diffusion of angular momentum from deeper layers in the atmosphere could only exert a torque of 10^{21} dyne-cm, a factor 10^2 less than the estimated torque that a convecting magnetosphere would exert on the polar ionosphere. Hence magnetospherically imposed torques may despin the polar ionosphere.

The observations of corotating protons in the outer magnetosphere suggest that present models of the polar Jovian ionosphere need revision. There seem to be three possibilities for enforcing corotation. First, unstable strong shears in the neutral wind spped induced by convection might lead to a large eddy viscosity and enhanced upward angular momentum transport. Second, since particle precipitation is expected to deposit 100 ergs/cm^2-sec in the polar region, the ionopshere could extend much deeper into the neutral atmosphere than predicted by solar UV models, thus increasing the ionopsheric inertia. Third, the neutral wind systems postulated by Brice and McDonough[25] to account for the radial diffusion in the radiation belts could transport angular momentum from low to high latitudes at rate sufficient to balance magnetospheric torques. Siscoe and Chen (private communication) point out that the existence of a H_3^+ ionospheric layer below the H^+ layer may create a region of large specific Pederson conductivity sufficiently deep into the atmosphere to increase τ_c well above 40 minutes. In any case the coupling between the magnetosphere, ionosphere, and neutral atmosphere is undoubtedly energetically significant, highly nonlinear, and a controlling influence on Jovian plasma dynamics.

Kivelson and Winge[89] found that the helium vector magnetometer on Pioneer 11 inbound recorded a structured transient perturbation with the characteristic

signature of a field aligned current near the L-shell of Ganymeade. They find it interpretation ambiguous; it could have been caused by turbulence in the wake of Ganymeade, or by coupling of ionospheric and magnetospheric flows. To date, this is the only report of a field-aligned current in the Jovian magnetosphere.

An indirect theoretical argument suggests that field-aligned currents may exist at Jupiter. Terrestrial kilometric radiation, which resembles Jovian decametric radiation, as associated with intense auroral displays[69], which are in turn associated with field-aligned currents. Thus kilometric and decametric radiation may be produced by similar processes involving field aligned currents[85]. A theory of the Io-modulation of Jovian decametric radiation directly invokes field aligned currents flowing between Io and ionosphere (not shown in Figure 25)[65].

5.4 Quasi-Static Disk Model of the Jovian Magnetosphere

As presently construed, the convection model has dipolar geometry and co-rotation flow out to the distant plasmapause, which occurs just inside the magnetopause. However, even a low density cold plasma in the distant magnetosphere would have a co-rotation dynamic pressure which exceeds the containing magnetic pressure. Hence the magnetic field, even inside the plasmapause, would be distorted away from dipolar. There have been three attempts to calculate a quasi-static magnetic disk supported by centrifugal forces motivated by the Pioneer observations of thin current sheets. Before turning to the calculations of disk structure, we discuss briefly the parameters deduced from observations of the "hinged current sheet" model of Smith et al.[147]. If the sheet's hinge is at 20 R_J and if it moves rigidly beyond 20 R_J, the rotation of Jupiter's oblique dipole causes the sheet to move through the spin equatorial plane at a speed of approximately 30 km/sec, larger than the spacecraft speed. Combined with the 1-2 hour duration of a typical sheet crossing, this leads to a sheet thickness of 2 R_J. The observed magnitudes of the magnetic field reversals

then imply a linear current density of 10^{-2} amps/m, which extended over 60 R_J, as for P-10 outbound, gives 10^8 amps total current, leading to quasi-uniform north-ward perturbation field of about 10γ in the inner magnetosphere. Regardless of the ultimate correctness of this model, it probably gives a reasonable rough estimate of the physical magnitudes involved.

A number of authors[44, 59, 110, 112] pointed out the importance of centrifugal forces to Jupiter's outer magnetosphere. Gleeson and Axford[60] attempted a partially self-consistent model of the disk for an aligned dipole. They considered the disk to be sufficiently thin that the magnetic field outside is due to a thin sheet of azimuthal current. The plasma within the sheet is contained by balancing centrifugal forces with magnetic tension, which requires a component of the magnetic field normal to the sheet. Radial pressure gradients are neglected. They then model, ad hoc, the radial distribution of the azimuthal sheet current, calculate the resulting magnetic field, and the cold plasma density profiles it would contain. They sketch a number of sample magnetic field configurations. Since several of their configurations contain non-closed field lines, they suggest that magnetic connection would occur, rendering their disks unsteady.

Goertz[62] has produced a calculation similar to Gleeson and Axford's, but allows the dipole and spin axes to be misaligned and considers a plasma pressure comparable with the co-rotational energy density. Goertz et al.[64] had argued that the hinged disk model of Smith et al.[147, 148] is less consistent with the observations than a current sheet confined to Jupiter's magnetic equatorial plane. Recall that they required field lines to be closed within the disk and open outside to account for the strong 10 hour energetic particle modulations on this pass. Goertz[62] writes the magnetic field as the sum of a dipole plus disk perturbation, parameterizes the pressure by $P = k(r,z)\ \rho\Omega r^2/z$,

and solves the hydromagnetic force-balance equations in the thin disk approximation. He then fits his model according to Pioneer 10 outbound data and finds that even with finite pressure, the disk remains thin (1 - 2 R_J). The plasma density consistent with this fitting is roughly 6 x 10^7 $(R/R_J)^{-5.4}$ which disagrees with the cold plasma density of $\simeq$ 80 cm^3 measured by Frank et al.[55] by an amount possibly reconcilable with theoretical and observational inaccuracy.

Barish and Smith[13] pursued another tack in quasi-static current sheet modeling. They did not solve hydromagnetic equations, but sought an analytic representation of the magnetic field, which is consistent with a partial cut through the Pioneer 10 data, namely a field in the magnetic equator that falls off as r^{-3} within 20 R_J and as r^{-2} beyond with a confined current "sheet" near the equator. Figure 26 shows a drawing of their derived configuration. It seems to accord with observation in two ways. First, the field is southward at the magnetopause (taken here to be at 100 R_J). Secondly, the above computation, performed before the P-11 encounter, was compatible with the P-11 outbound pass, which showed a weakly distorted dipole at 30-35° latitude.

Several comments are now in order. The above models require that co-rotation extend to the magnetopause. At 100 R_J the co-rotation speed is 1100 km/sec corresponding to an ion energy of 7.5 μ KeV, where μ is the mass in units of the hydrogen mass. The co-rotation speed exceeds the solar wind speed, is oppositely directed to the solar wind velocity at local daw, and adds to it at local evening.

None of the above models have an azimuthal field component B_ϕ, which is consistent with portions of the P-10 inbound and P-11 outbound passes. However, as in standard solar wind theory, an azimuthal field--which

requires a radial current--is a signature of outward angular momentum transport. This in turn requires that there be a net outward flow of plasma supplied by Jupiter or its inner magnetosphere. If the radial flow velocity is sub-Alfvenic and subsonic, the flow dynamic pressure is negligible and the quasi-static disk models may be approximately valid.

Finally, none of the above models explicity include a finite time delay for the information that Jupiter is rotating to propagate from the inner to the outer magnetosphere. The fact that a current sheet rigidly flapping beyond its hing would not produce sheet crossings on P-10 outbound led Smith et al.[147, 148] to suggest that radially propagating Alfven waves might ripple the sheet sufficiently to permit crossings at large distances. Eviatar and Ershkovich[45] estimate a wave speed from the observed magnetic variations and the ten hour periodicity; assuming the wave is an Alfven wave which is not convected by a radial outflow, they estimate a mean plasma density of 4 cm^{-3} in the sheet, roughly the same as that estimated by Wolfe et al.[173] using pressure balance arguements.

Kivelson et al.[88] argue that the near equatorial current sheet is a surface whose shape is determined by the velocity at which the perturbations produced by a rotating tilted dipole propagate to large radial distances. They fit the P-10 outbound data to a surface modeled by the equation $\cos|\phi + \Omega(r - ro)/v_r| + \cot\lambda \cot\theta = 0$ where $\underline{\Omega}$ is Jupiter's angular rotational velocity, $\phi = -\Omega(t-to)$, t the time, λ is the angle between $\underset{\sim}{\Omega}$ and the dipole moment, and ϕ and θ the Jovigraphic longitude and latitude respectively. They find $r_o \simeq 14\ R_J$ and $v_r \simeq 800$ km/sec. They find this model fits the data better than either the hinged current sheet or the rigid equatorially localized current sheet.

5.5.1 Jovian Plasma Sources - Solar Wind

Where does the plasma in Jupiter's magnetosphere come from? Earth has two possible plasma sources, the ionosphere and the solar wind, and Jupiter three--solar wind, ionosphere, and satellites, particularly Io. An experimental determination of plasma origin throughout the magnetosphere would resolve many theoretical difficulties. Surprisingly enough, even at earth, estimates of the solar wind source strength are difficult, primarily because diffusion and/or transport across the magnetopause and in the magnetic tail are not well understood. If Earth-like scaling prevailed, 10^{28} solar wind particles might cycle through Jupiter's magnetosphere each second.

5.5.2 Jovian Plasma Sources - Ionosphere

At Earth, the proton gravitational escape energy is about 1 eV, and the ion temperature at the top of the ionosphere is 0.1 - 0.5 eV. Within Earth's plasmasphere, subsonic motions adjust the plasma pressure in space to the ionospheric boundary conditions. Beyond the plasmapause, and particularly on open field lines, where the plasma pressure is low, ionospheric plasma expands supersonically into space in a miniature version of the solar wind--the polar wind. By contrast, at Jupiter, the proton energy to escape to infinity is about 19 eV, and the Jovian ionosphere is thought to be cold. Straightforward thermal ionospheric expansion seems difficult at Jupiter. However, Ioannidis and Brice [77] and Michel and Sturrock [115] observed that photoelectrons from solar-UV ionization of the Jovian upper atmosphere would have energies in the 5-20 eV range. If, as these electrons expand along field lines, they are scattered either by Coulomb collisions or plasma turbulence onto magnetically trapped orbits, they would pull protons along with them by electrostatic ambipolar couplings. The photoelectron energies are certainly sufficient to bring ions to the equatorial plane in the inner

magnetosphere; for instance to escape to L = 2 R_J, about 7 eV is required. If the escaping photoelectrons are in strong diffusion[80], so that they are scattered across their loss cone in less than their transit time between conjugate ionospheres, the ion injection flux approaches its upper limit, which equals the photoelectron flux leaving the ionosphere. At Earth, this photoelectron flux F ≃ 7 × $10^8/cm^2$-sec. Since the solar UV flux is reduced by ∿ 25 at Jupiter, the photo electron flux there is ≃ 2.5 × $10^7/cm^2$-sec [77, 115]. Recognizing that photoelectrons are produced on Jupiter's dayside only, the maximum number of protons $\dot{N}$ delivered to Jupiter's magnetosphere by photoelectrons is $\dot{N} \simeq 2\pi R_J^2 F \simeq 10^{28}$/sec, approximately equal to the much less well founded estimate of the solar wind source.

Ioannidis and Brice [77] and Michel and Sturrock [115] calculated the equilibrium plasma density in the equatorial plane, taking into account one significant difference between Earth's and Jupiter's magnetospheres. The terrestrial synchronous orbit is at 6.6 R_E, beyond the usual position of Earth's plasmapause, whereas Jovian synchronous orbit is at 2.2 R_J. Thus centrifugal forces play no role within Earth's plasmasphere, and an important one throughout Jupiter's magnetosphere. The component of centrifugal force parallel to the magnetic field is directed towards the equator, which flattens the plasma equilibrium distribution into a disk, concentrating the density near the equator. Ioannidis and Brice's [77] model of the equatorial plasma density produced densities of < 1 cm^{-3} in the inner radiation belts within the orbit of Io (L = 6); beyond Io the equatorial density increased rapidly until it reached ≃ $10^2/cm^3$ at L = 8, whereupon the co-rotational energy approaches the equatorial magnetic energy density. They then invoked the centrifugally driven interchange instability to[7] radially diffuse plasma outward, whereupon the density profile follows at L^{-4} law. Thus arose the idea that plasma expanding onto field lines connecting to Jupiter's inner magnetosphere would be a source for Jupiter's outer magnetosphere.

The wisdom of hindsight permits a more modern view of this idea. The observations of the Jovian radiation belts are compatible with a radial diffusion mechanism that derives its energy not only from magnetospheric plasma but also from atmospheric winds. Thus, ionospheric plasma will be injected onto flux tubes that are always executing flux tube interchange motions driven by winds.

Using the Jovian photoelectron flux calculated by Swartz et al.[156]. McDonough et al.[104] updated the diffusive equilibrium calculations of Ioannidis and Brice[77]. Due to differences in atmospheric composition, the Jovian photoelectron flux above 10 eV energy is an order of magnitude smaller than the scaled terrestrial flux, though the flux below 10 eV energy is larger. Thus, the above calculation produced smaller equilibrium densities than that of Ioannidis and Brice[77]. The effect of this revision upon disk and radial outflow models is discussed by Prakash and Brice[125].

Dessler and Hill[40] have pointed out a possible rotational asymmetry in the Jovian ionospheric plasma source due to the large multipole moments in Jupiter's intrinsic magnetic field. Flux tubes of the same equatorial area connect to different ionospheric areas; those connecting to the largest area (smallest surface field) would fill most rapidly. Thus, the density, and consequently the distant magnetic field would be modulated in space at Jupiter's rotation frequency. Roederer et al.[132] have examined this suggestion using the magnetic field model of Acuna and Ness[2, 3]. They assume the ionospheric plasma source is proportional to $|B_N^{-1}\cos T_N + B_S^{-1} \cos T_S|$ where B_N, B_S, T_N, T_S, are the surface magnetic field and Jovigraphic latitude of the North (N), and South (S) field line intersects. The cos T dependence is consistent with the plasma source being escaping photoelectrons. The source function has a roughly $\pm$ 25% variation with local time for the L = 10 field line.

Precipitation of energetic electrons into Earth's atmosphere produces copious fluxes of backscattered secondaries of several eV energy. If the outward secondary flux exceeds the inward primary flux, ionospheric plasma could again expand into the magnetosphere. Evaluation of this mechanism requires a detailed calculation of secondary production in a hydrogen atmosphere which is at present difficult to do because the peak in the electron precipitation energy flux has not been determined experimentally. The convection model of the magnetosphere predicts that $\sim$ 100 ergs/cm^2-sec will be deposited into the high latitude auroral zones, moreover, at mid-latitudes, L $\lesssim$ 10, Coroniti[37] has estimated the precipitation energy fluxes from electrons with E > 1 MeV could be a few tenths of an erg/cm^2-sec. The energy flux at lower energies is likely to exceed this value. Thus, there is good reason to consider the effects of energetic electron precipitation upon the Jovian ionosphere in general, and upon secondary electron production in particular.

Frank et al.[55] have derived some information on the plasma density in the inner magnetosphere (L < 6) from the solar wind plasma detector. Their measured ion energies (> 100 eV) do not fit the picture of cold ions expanding from the ionosphere. Moreover, the measured densities exceed the Ioannidis-Brice densities by a large factor in the inner magnetosphere. Goertz[61] has re-examined the flux tube filling arguments, maintaining that instabilities from colliding streams of the equator may be able to produce the required densities. Nonetheless, it seems to us that there is presently no decisive proof that the cold plasma in Jupiter's magnetosphere comes predominantly from the ionosphere.

5.5.3 Jovian Plasma Sources - Io

Siscoe and Chen[144] propose that Io's neutral hydrogen ring may be a source for plasma within Io's orbit. Judge and Carson[79] observed a torus of neutral hydrogen centered radially on Io's orbit and extending a significant portion of the way around it. Frank et al.'s[55] measured plasma densities are

sufficient to account for the neutral hydrogen losses by charge exchange needed to explain the azimuthal extent of the ring. However, charge exchange is not a plasma source since it leaves the proton density constant. Photo-ionization, though slower than charge exchange, produces about 10^{25} new hydrogen ions per second. If the electron temperature exceeds about 10 eV, collisional ionization could exceed the photo-ionization rate. They point out that the measured flux tube content η, which is proportional to nL^4, peaks at Io, consistent with an Io source and radial diffusion losses. Atmospherically driven radial diffusion at the rate demanded by radiation belt observations, yields plasma densities within L = 6 in reasonable accord with observations. However, the true test of radial diffusion transport in this case, is not the spatial dependence of the flux tube content, but the spatial dependence of the phase space density (Goertz, private communication 1977). The Siscoe-Chen model predicts that the plasma at L = 3 would have 800 eV energy, if it has 100 eV energy at Io.

In addition to hydrogen, Io emits heavy atoms such as sodium and potassium and perhaps others[27, 161, 108, 160, 30, 18, 93, 19]. Since the main loss mechanisms for neutral atoms is probably electron impact ionization[30] (Eviatar, private communication 1976) the Jovian magnetosphere must contain a heavy ion plasma. Eviatar and Ershkovich[45] suggested that the Jovian sodium plasma should have 3 separate energy components--cold, thermal, and energetic plasma, depending upon whether ionization takes place near Io, in the outer magnetosphere, or in the solar wind. Hill and Michel[74] have suggested that these heavy ions are a significant source of plasma for Jupiter's outer magnetosphere. They point out that ions of Io origin are confined to a disk of about 1 R_J thickness about the Jovian equator and are probably more confined than ionospheric ions. They did not estimate the heavy ion fluxes delivered to the outer magnetosphere.

The first direct observation of a heavy ion in Jupiter's magnetosphere was reported by Kupo et al. [93] The forbidden doublet of singly ionized sulfur was observed on a large number of plates over several months. The line intensities are consistent with a sulfur ion density of about $10^2/cm^3$ and require electron densities of $5 \times 10^2/cm^3$ in the sulfur cloud, which extends out to 8 R_J. Neutral sodium has been also observed [93]. Its cloud extends from 4 - 10 R_J near Io, but cuts off sharply at about 7 R_J on the other side of Io's orbit. The total ion and neutral populations are about 7×10^{33} and 10^{30} respectively. If the sulfur ions radially diffuse on the radiation belt determined time scale of about a year, then about 2×10^{26} sulfur ions/sec are delivered to the outer magnetosphere, a mass flux roughly equal to the upper limit mass flux of ionospheric hydrogen. For Te $\simeq$ 10 eV, the impact ionization time for sulfur is $\sim 5 \times 10^4$ sec, so the neutral to ion ratio in the cloud should be less than 10^{-3}.

In summary, both Jupiter's ionosphere and Io are possible sources of cold plasmas. Both sources are concentrated within L < 10; since 90% of Jupiter's surface area lies on field lines connecting to L $\ll$ 10. The ionosphere produces an upper limit of 10^{28} hydrogen ions per second from photo-ionization, Io produces at least 10^{25} H ions/sec, 10^{26} sulfur ions/sec, and probably other heavy ions. A fraction of this plasma radially diffuses into Jupiter's outer magnetosphere on time scales, determined by energetic particle measurements, of months to a year. As far as the outer magnetosphere is concerned, its inner magnetosphere sources, however intrinsically variable in time, will appear constant on scales shorter than the radial diffusion time scale. Therefore, variations in these sources probably cannot account for the gross changes in Jupiter's outer magnetosphere observed to take place in a week.

5.6 Radial Outflow Models

Since the centrifugal force confines the cold plasma to near the magnetic equator, thus inhibiting its precipitation loss to the atmosphere, the most likely cold plasma sinks possible are radial diffusion inward to Jupiter and outward into the middle and outer magnetosphere. In diffusing outward, conservation of the first two adiabatic invariants implies that the plasma thermally cools while it gains co-rotational kinetic energy. In the theory of stellar winds [113], a cold plasma can break out into radially outflowing wind if the co-rotational energy density approximately equals the magnetic energy density of the flow critical point. This "magnetic sling" stellar wind solution led Michel and Sturrock [115] to propose that the Jovian internal plasma sources would centrifugally drive a planetary wind similar to stellar and pulsar winds. This model has been elaborated in a series of papers by the Rice group [72, 40, 74, 29].

In this section we present the physical content of this model. We first discuss a cold, centrifugal wind, computing the critical Alfven point. We tie the critical Alfven radius to the now measured plasma density Io. We then compare the dynamic pressure at the Alfven point with the dynamic pressure in the solar wind, to decide whether a sub-Alfvenic or super-Alfvenic flow is expected beyond the critical point. Then we consider the confinement of Jupiter's planetary wind by the solar wind.

5.6.1 Centrifugally Driven Winds

Equation co-rotational and dipolar equatorial magnetic energy densities leads to the following expression for the Alfven radius $r_A = L_A R_J$.

$$n_A L_A^8 = B_I^2/4\pi\mu M_H \Omega^2 R_J^2 \qquad (5\text{-}8)$$

where n_A is the density at the Alfven point, and μ is the mean molecular weight

of the diffusing plasma. If the outward radial diffusion is loss free, the flux tube content is preserved so that nL^4 is constant. Then $n_A L_A^4 = g n_o L_o^4$, where $n_o \simeq 10^2/cm^3$ is the number density at Io, $L_o = 6$, and $g < 1$ takes into account the possibility that some ions are lost in diffusing to the Alfven point. Therefore

$$L_A = [B_I^2/4\pi\mu M_H \Omega^2 R_J^2 n_o L_o^4]^{1/4} = 41\ \Delta_o^{-1/4} \qquad (5.9)$$

where $\Delta_o = \mu g n_o/100$. The above probably underestimates L_A because $g \leq 1$ and the measured magnetic field usually exceeds dipolar. Increasing μ by 16 decreases L_A by a factor 2. The uncertainties therefore compensate. Dessler and Hill[40] suggest that the Alfven critical point L_A can vary about $\pm 10\%$ due to longitudinal asymmetries in the ionospheric plasma source.

Hill and Michel[74] and Siscoe[145] have analyzed the centrifugal confinement of plasma emitted by Io to the magnetic equator. They find that Io plasma would be confined to a sheet beyond Io of a virtually uniform thickness of several R_J. In this case, the mean density should vary as L^{-3}, and then

$$L_A = |B_I^2/4\pi\mu M_H \Omega^2 R_J^2 n_o L_o^3|^{1/5} \Delta^{-1/5} \simeq 30\Delta^{-1/5} \qquad (5.10)$$

Beyond the critical point L_A, radially diffusing plasma cannot be contained by the magnetic field; we therefore expect it to break out into a hydromagnetic outflow. The outflow may either be a super-Alfvenic wind or a sub-Alfvenic breeze, depending upon the confining pressure of the solar wind. In this section, we discuss the nature of the flow along the Jupiter-sun line, and in the next, its nature at other local times.

We have shown that the critical radius r_A and the classical nose radius D may be comparable. D is determined by balancing the stagnation pressure of the shocked solar wind flow with the dipolar magnetic pressure; r_A, by balancing rotational energy density with dipolar magnetic pressure. If $r_A \simeq D$ the ro-

tational energy density is comparable with the solar wind stagnation pressure. In a super-Alfvenic wind, the radial and azimuthal velocities are comparable to one another and to the Alfven speed at critical Alfven point[172]. Therefore, the rough equality of r_A and D implies that the dynamic pressure of a potential planetary wind and the dynamic pressure of the nominal solar wind are comparable. As Figure 19 indicated, the dynamic pressure of the solar wind is highly variable in the outer solar system. If the dynamic pressure is low, so that $D > r_A$, we expect a super-Alfvenic outflow along the subsolar line. When the solar wind dynamic pressure is high, so that $D < r_A$, we do not expect a super-Alfvenic wind along the subsolar line. However, since the inner magnetosphere is a source, there must be a sub-Alfvenic wind to transport away the plasma diffusing across r_A. Thus, variations in solar wind dynamic pressure may induce transitions between a super-Alfvenic Jovian wind and a sub-Alfvenic breeze[39].

The two-dimensional structure of the radial outflow in the local noon meridian plane containing the sun-Jupiter line is uncertain. However, it seems reasonable to expect that a super-Alfvenic wind would stretch out its magnetic field into a disk-like configuration, whereas the sub-Alfvenic breeze would not, because good communication with the ionosphere is maintained. If so, variations in solar wind dynamic pressure might also induce changes between disk-like and more dipolar outer magnetospheres.

Figure 19, and the discussion leading up to it, offers some support for this hypothesis, which cannot be definitively tested until the flows in Jupiter's outer magnetosphere are measured. Pioneer 10 inbound entered the Jovian magnetosphere about 45° from the Jupiter-sun line. Just before it entered, it measured a solar wind dynamic pressure a factor 6 below nominal, suggesting that a super-Alfvenic wind was possible at that time. If so, the planetary wind dynamic pressure would have scaled as $(r_A/r)^2$ so that pressure equality

with the solar wind at the subsolar point would have been achieved at $r = \sqrt{6}\ R_A \simeq 100\ R_J$, roughly the distance of which Pioneer 10 first briefly entered the magnetosphere. Since the azimuthal structure of a planetary wind confined by the solar wind is not known quantitatively, and since the magnetosphere was varying when P-10 first encountered it (P-10 later re-encountered a dipolar magnetosphere within 45 R_J), the above estimates are only suggestive of a possible agreement.

The structure of the magnetopause depends upon whether the planetary outflow is a super-Alfvenic wind or a sub-Alfvenic breeze. In the wind case, an internal fast shock must occur near the pressure equality radius. The shock decelerates the flow below the Alfven speed; along the subsolar line, the post shock sub-Alfvenic wind should be decelerated to a stagnation point. The flows of solar and planetary wind origin would be separated by a tangential discontinuity which is the magnetopause. The structure of the internal shock is not understood; however the planetary wind flow between the internal shock and magnetopause should contain both large scale hydromagnetic and small scale plasma turbulence. The distance between the magnetopause and internal shock could be about 10% of the radius of curvature of the shock, in perhaps a few R_J, in steady state. The internal shock is not needed for the sub-Alfvenic breeze, and Jupiter's magnetopause might then more nearly resemble earth's.

5.6.2 Heliospheric Models of Radial Outflow.

For a hypersonic, hyper-Alfvenic solar wind, the pressure normal to the magnetopause is approximately $\rho u^2 \cos^2\psi + P$ where P is the solar wind static pressure at Jupiter. In the magnetic tail, $\cos^2\psi \to 0$ so the pressure within the magnetosphere asymptotes to P. Since $P/\rho u^2 << 1$, a centrifugal super-Alfvenic flow would be expected in the tail nearly always, and only for weak solar winds at the nose[72, 73].

The planetary wind outflow pattern in the two dimensions of the equatorial plane might be similar to the solar wind's heliosphere moving supersonically thorugh the interstellar medium[8]. The closet analogy would be with the low solar wind dynamic pressure case, where a super-Alfvenic planetary wind is expected at all local times. This outflow is sketched in the accompanying Figure 27, which shows schematic flow boundaries in the equatorial plane. The bow shock decelerates the solar wind. The magnetopause is the boundary between shocked solar and planetary winds. In the absence of turbulent mixing, there could be a sharp composition gradient across the magnetopause. The internal shock decelerates the planetary wind at the nose and deflects the planetary wind in the tail, so that eventually all the material emitted by Jupiter's inner magnetosphere escapes tailward. The Alfven surface is the boundary between co-rotation dominated diffusion and wind regimes. Because the mathematical solution for this magnetosphere involves calculating four free boundaries self-consistently, the above sketch is necessarily schematic.

The case of high solar wind pressure, where the outflow on Jupiter's day-side may be sub-Alfvenic, has no analog in heliosphere physics. A sketch of a possible configuration is shown in Figure 28. In this sketch, the subsonic region extends directly to the magnetopause on the day side. In this region, the plasma should still dominantly co-rotate, and so we would expect most of it to exit on the local evening side, bulging the magnetopause somewhat. The internal shock has moved back into the tail and now only deflects the radial outflow into the anti-solar direction.

Both Figures 27 and 28 have a small "dimple" in the Alfven surface, to represent an important idea of Hill et al.[73] and Carbary et al.[29]. They proposed that the longitude at which Jupiter's ionospheric source is strongest corresponds to the strongest planetary wind. Thus the planetary wind strength should be modulated with a ten hour period. When the solar wind pressure is

low, this fast stream could penetrate the day side.

Carbary et al.[29] suggest that since the fast stream is first generated on closed field lines, as its source rotates past local dusk reconnection will occur near the Alfven point permitting a bubble of plasma to flow downstream with the planetary wind. Since reconnection can generate copious fluxes of energetic particles, they suggest that

(1) Reconnection will be modulated with a 10 hour period.

(2) The particles generated beyond the Alfven point by reconnection will reach the solar wind. Thus, the particle fluxes escaping to the solar wind will have a 10 hour modulation. Roederer et al.[32] find that the time when the peak ionospheric source longitude faces Jupiter's magnetic tail does in fact correspond to the time of peak escape of 1-30 MeV electrons to the heliosphere.

(3) The particles generated within the Alfven point by reconnection will radially diffuse inward. Since the co-rotation speed exceeds the gradient and curvature drift speeds, the 10 hour modulated pulse of energetic particles diffusing inward will be only slowly dispersed by differential drifts. They suggest these pulses are responsible for the observed modulations of energetic particles in the outer magnetosphere.

(4) Same the energetic particles escaping to the solar wind and diffusing inward are generated by the same reconnection event, they should have the same modulation phase. In this way, they explain the results of Chenette et al.[34].

We have used the liberty provided by a review format to discuss the Rice model of Jupiter's magnetosphere taking advantage of hindsight. We have added several features; first, we have tied the estimate of the Alfven radius to

the measured plasma density at Io; we have discussed the models in a heliospheric context; finally, we have suggested that variations in solar wind dynamic pressure (magnetic storms) may turn on and off a super-Alfvenic wind on the day side.

6. SUMMARY AND DISCUSSION

We present below our personal summary of the current state of Jupiter magnetospheric modeling. We have discussed three classes of Jupiter models: first, Earth-like reconnection models, including Ioannidis and Brice's[77] picture of the ensuing internal convection pattern for an inertia and pressure free plasma; second, static rotating disk models; and third, radial outflow models--either super-Alfvenic, sub-Alfvenic, or mixed. In addition, we discussed the extent to which Jupiter and Io can feed the outer magnetosphere with plasma. All models agree on two points: first, Jupiter's large dipole field can enforce co-rotation to radial distances the order of 40 R_J, provided the atmosphere can enforce co-rotation at ionospheric levels. Co-rotation to such large distances seems to be observed experimentally. Second, all the models predict a transition layer within the magnetopause on the day side. In Ioannidis and Brice's model, it is the convection layer beyond the co-rotation region; in radial outflows, it is the region between the critical point and the magnetopause for sub-Alfvenic flows, and the region between the internal shock and the magnetopause for super-Alfvenic flows. Static disk models also imply a transition near the magnetopause where solar wind stresses perturb the static force balance.

As stated, Earth-like models can only apply to those times when Jupiter's magnetosphere was essentially dipolar within the classical magnetopause radius D, such as P-10 inbound with $\simeq$ 50 R_J and perhaps P-11 outbound. The reconnection model is consistent with the length of the Jovian magnetic tail inferred from Jovian energetic particle propagation arguments and also with the time scales ($\simeq$ 1 week) associated with changes in state of the Jovian magnetopause.

The Earth-like models do not account for magnetopause encounters beyond, say, 60 R_J, or for the radially extended fields.* The disk models do account for radially extended fields and aid us in visualizing the magnetic configuration within the critical point; however, they require that there are no sources and sinks of plasma, which seems unlikely. If plasma and angular momentum radially diffuse outward, the magnetic field will be swept back out of meridian planes, an effect not considered in static disk models.

It appears that Jupiter's inner magnetosphere and Io supply about 10^{28} hydrogen masses per second, motivating models of radial outflows which commence beyond the critical point. Super-Alfvenic winds, because they extend the magnetic field, are appropriate to such passes as P-10 outbound and P-11 inbound, at least conceptually. However, there exist no accurate solutions for winds carrying an entrained magnetic flux, and so no quantitative statements about vertical disk structure are possible. If our current estimates are correct, strong solar wind dynamic pressure could suppress, at times, a super-Alfvenic wind on the day side, converting the flow to sub-Alfvenic. Something like this is needed to account for the difference between P-10 and P-11 inbound, both of which traversed Jupiter's magnetosphere near 1000 LT, yet P-10 inbound found little, and P-11 inbound considerable, evidence for a disk.

Future progress in understanding Jupiter's outer magnetosphere may come in part from a unification of the above models, paying attention to encompassing the gross time dependences observed. In our opinion, unified models should

* However, Kennel and Coroniti[83] did suggest that convection driven by strong tail reconnection could drive a super-Alfvenic flow, which would extend the field lines on the day side. They pointed out that radially extended magnetopauses have been observed at Earth during magnetic storms.

take into account the following general principles:

(1) Jupiter's ionosphere and satellite Io probably inject dynamically significant quantities of plasma into the outer magnetosphere. If radial diffusion is the transport mechanism, these internal plasma sources are constant over a few months to year time scale and so variations in the source cannot account for the observed magnetospheric variability. While the winds so produced could be azimuthally asymmetric, producing a 10 hour modulation, it is difficult to account for the 1 week time scales observed.

(2) The nature of the wind produced at the critical point depends on exterior solar wind boundary conditions. Changes in solar wind dynamic pressure may change the day side flow from sub- to super-Alfvenic, with concomitant changes in magnetic field from quasi-dipolar to radially extended.

(3) Experience with the Earth's magnetosphere suggests that it would be perilous to neglect reconnection of solar wind and Jovian field lines, the resulting formation of the magnetic tail, and the internal convection pattern demanded by solar wind reconnection. Kennel and Coroniti[84] have discussed a combined planetary wind and reconnection model for Jupiter's magnetosphere.

(4) The scale of Jupiter's convection magnetosphere suggests that rarely, if ever, will it be steady.

In our opinion, the primary goal of future experimental research in Jupiter's outer magnetosphere should be to determine the nature and causes of the time dependent changes of Jupiter's magnetosphere. To understand this question, several subsidiary questions need to be addressed. How does the solar wind couple to the Jovian magnetosphere? What are the sources of plasma and how

do they couple to the Jovian magnetosphere? What is the nature of the Jovian magnetic tail? How do the Jovian atmosphere, ionosphere, and magnetosphere couple to one another? From the point of view of the above questions, several experimental investigations appear to have high priority:

(1) It is important to measure the properties of the hydromagnetic flow within Jupiter's magnetosphere, which was not done on Pioneer 10 and 11.

(2) It is important to discriminate between ions of different mass to elucidate the Jovian plasma sources.

(3) It is important to search for reconnection events, at the Jovian magnetopause, in its magnetodisk when it exists, and in the tail.

(4) It is important that the state of the solar wind upstream of Jupiter be known at times when spacecraft are in the Jovian magnetosphere.

(5) It is important that plasma turbulence be measured in the magnetosphere, in order to test radiation belt theories, and to estimate energetic particle fluxes into the Jovian ionosphere and therefrom to revise ionospheric models.

The forthcoming Mariner-Jupiter-Saturn Voyager mission will address some of these questions for both Jupiter and Saturn. The existence of hectometric radio emissions strongly suggest that Saturn has a magnetosphere[26]. The properties of Saturn's magnetosphere have been estimated using an earth-like model by Kennel[81]. Given the success of this procedure with the Jovian radiation belts, a detailed a priori model of Saturn's radiation belts may well be worth the effort. However, since Saturn is a rapid rotator like Jupiter, its outer magnetosphere may resemble Jupiter's more than Earth's. There could be a significant difference, however. All things being equal, Saturn's

photoelectron ionospheric plasma source should be roughly a factor 4 smaller than Jupiter's. On the other hand, its potentially interesting satellite source, Titan, may lie in a region corresponding to Jupiter's time dependent outer magnetospehre. Since the interaction and steepening of fast streams leads to increasingly larger dynamic pressure variations in the outer solar system, Saturn's outer magnetosphere could be as or more time variable than Jupiter's. Thus, it is possible that the Voyager may not successfully address the over-riding problem of time dependence at either Jupiter or Saturn. Since the time scale for gross changes in Jupiter's outer magnetosphere - and possibly Saturn's - is comparable with a flyby duration, a flyby may not be able to resolve the causes of the time dependences. Hence, we may need to wait for orbiters to sort out the various possibilities.

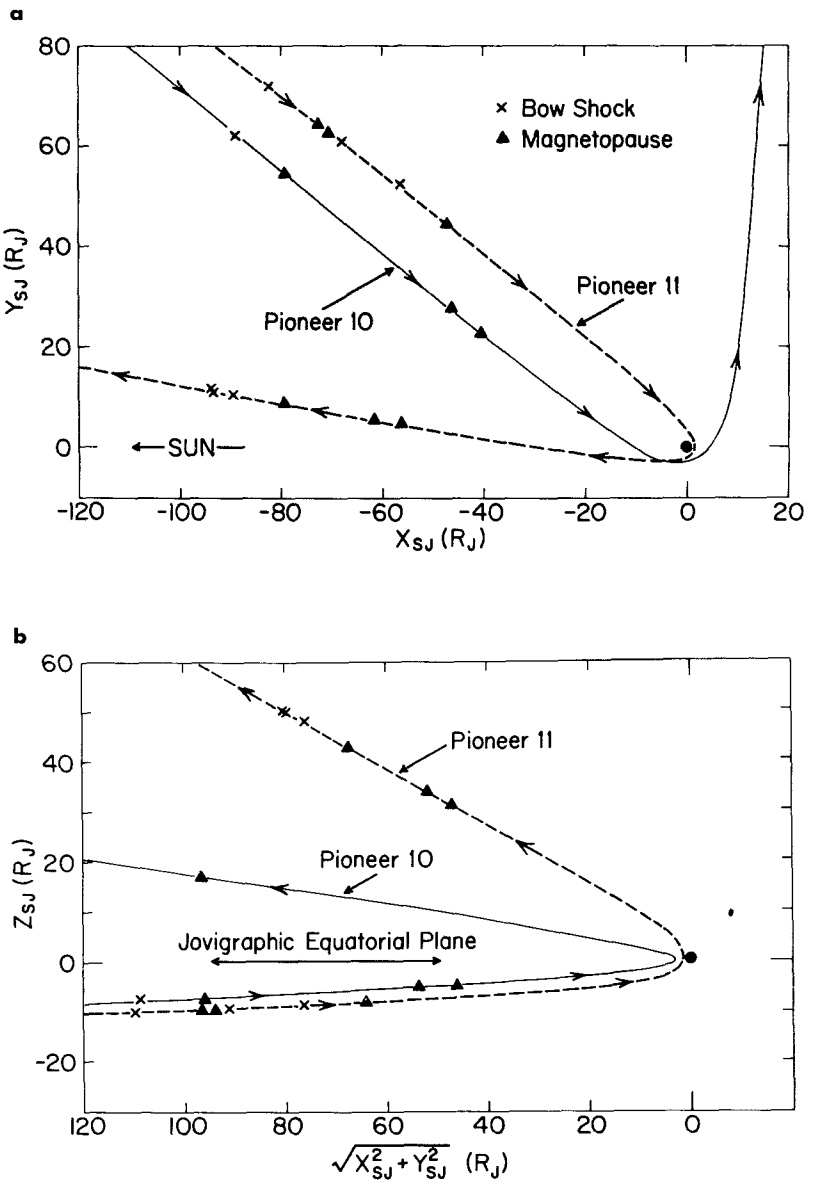

FIGURE 1 Pioneer 10 and 11 Trajectories. X_{SJ} is in the ecliptic plane, positive radially away from the sun along the sun-Jupiter line; Z_{SJ} is positive toward the north pole and perpendicular to the ecliptic; Y_{SJ} completes the righthanded coordinate system. 1 Jovian radius = 1 R_J = 71,372 km.[143]

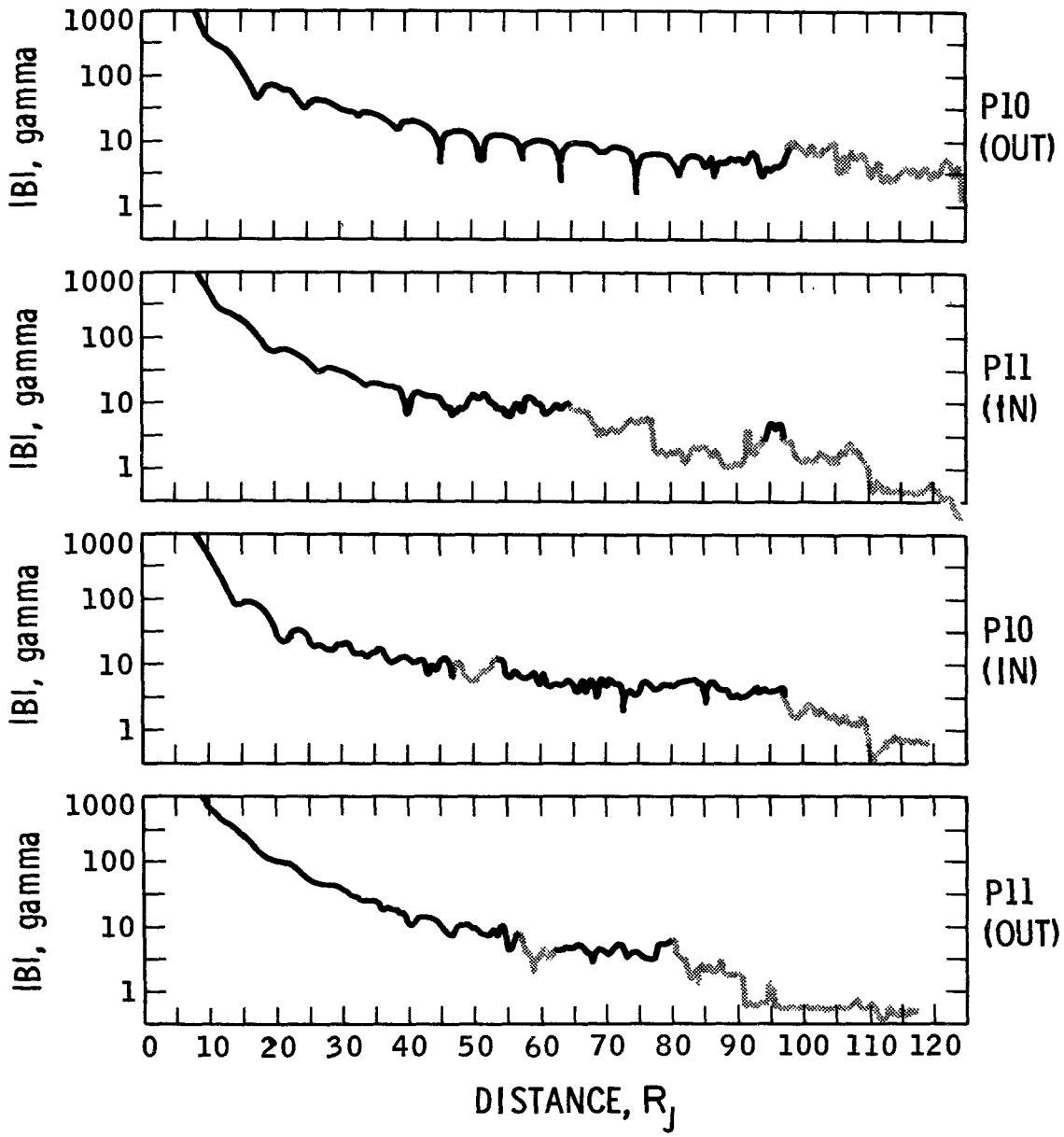

FIGURE 2 Pioneer 10 and 11 Magnetic Field Magnitude. The magnetic field magnitude measured by the JPL magnetometer is plotted against radial distance from Jupiter's center in R_J. 1 gamma = $1\gamma = 10^{-5}$ Gauss. When the spacecraft were within (outside) magnetosphere, the data are plotted as a solid (gray) line. P-11 (in) P-10 (in) and P-11 (out) all encountered a magnetosheath region inside a magnetospheric region, indicating the magnetosphere was unsteady. P-10 (out) encountered the magnetosphere again between 130-150 R_J. The dips in the P-10 (out) pass correspond to current sheet crossings. The data have been ordered in local time, with pre-dawn data in the top panel and pre-noon data in the bottom panel.[150]

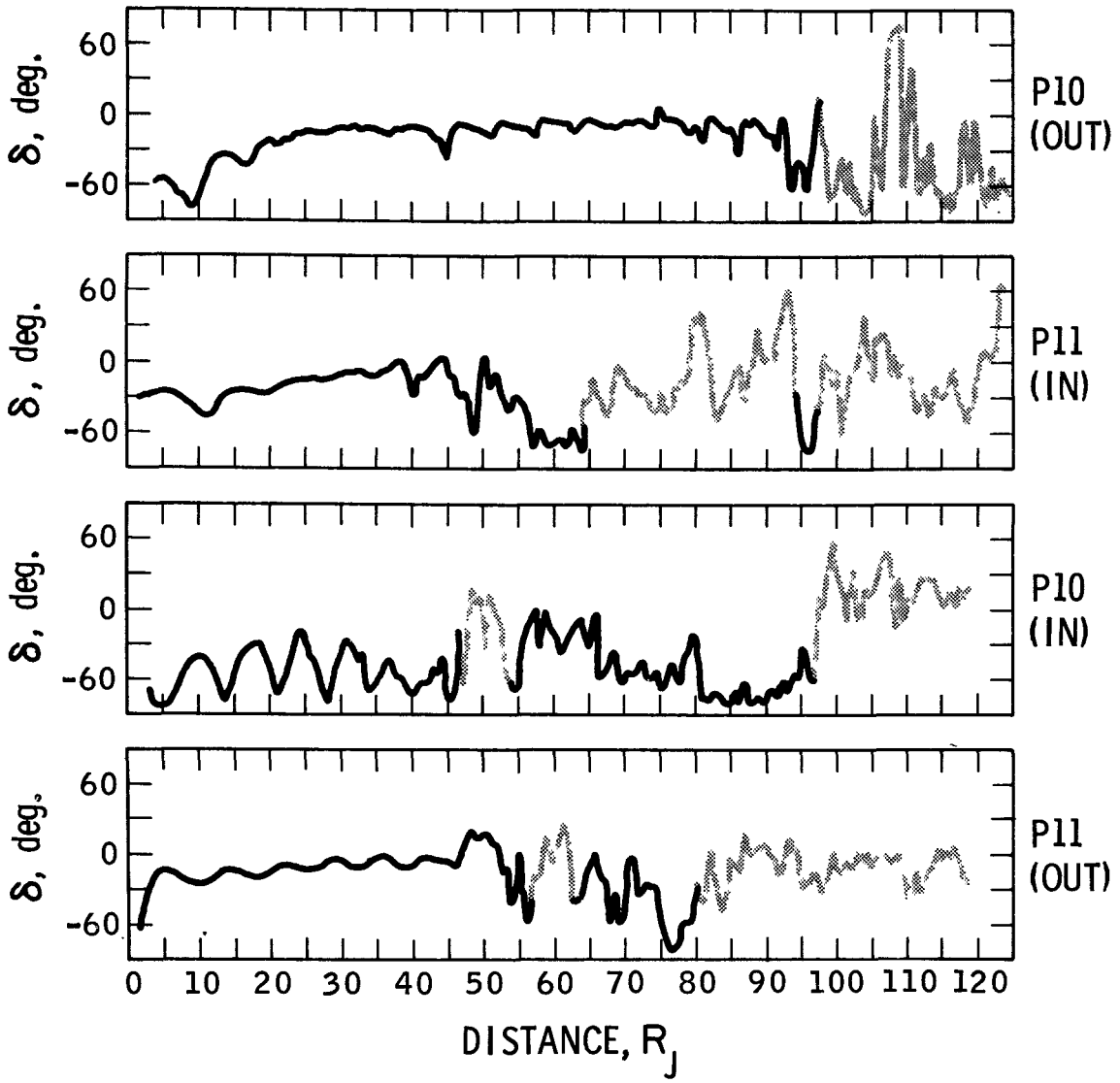

FIGURE 3 Pioneer 10 and 11 Magnetic Field Longitude. δ is the Jovigraphic latitude towards which the magnetic field points, $\delta < 0$ implies a southward directed field. These data are derived from hourly averages. Features to be discussed in the text include the following: On P-10 (out), the field was directed radially outward between 20-95 R_J. The smooth oscillations with a 10 hour period within 40 R_J (P-10 in) 45 R_J (P-11 out), and the one cycle visible within 20 R_J on P-10 (out) resemble those expected from Jupiter's rotating misaligned dipole field. Within but near the magnetopause, the field turns sharply southward at 95 R_J (P-10 out), 55 R_J (P-11 in), 80 R_J (P-10 in), and at 48 and 75 R_J on P-11 out.[150]

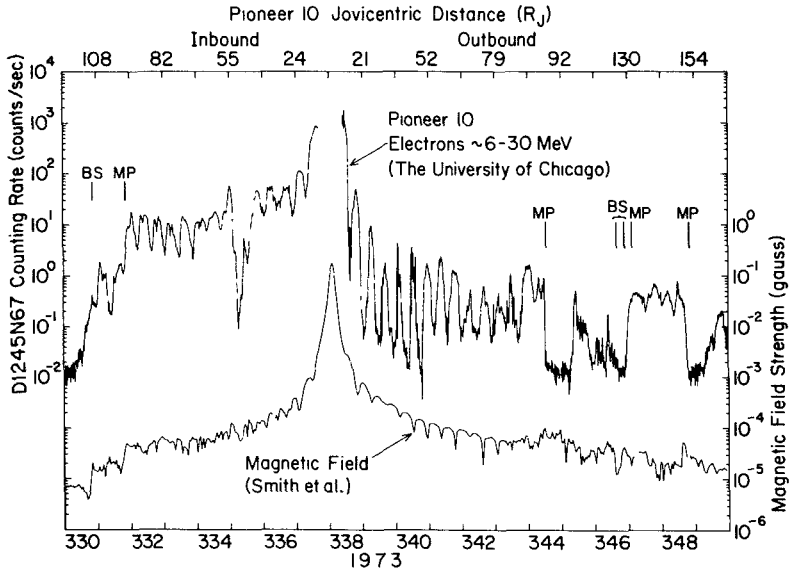

FIGURE 4 Pioneer 10 6-30 MeV Electron Fluxes and Magnetic Field. 6-30 MeV electron fluxes in counts/sec and the magnetic field magnitude are plotted against day of year 1973 (bottom) and radial distance (top). Features to be discussed include: (1) the steady increase of 6-30 MeV electron flux prior to the first magnetopause crossing (MP), indicating that Jupiter is a source of cosmic ray electrons to the solar wind; (2) the smooth increase in electron flux with decreasing radial distance within 20 R_J defining the radiation belt region; (3) the pronounced sawtooth modulation with 10 hour period on the outbound pass associated with current sheet crossings. Note that when P-10 outbound re-entered the magnetosphere between 130-150 R_J, the 6-30 MeV electron fluxes were comparable to the peaks found further in. Bow shock crossings are indicated by BS.[106]

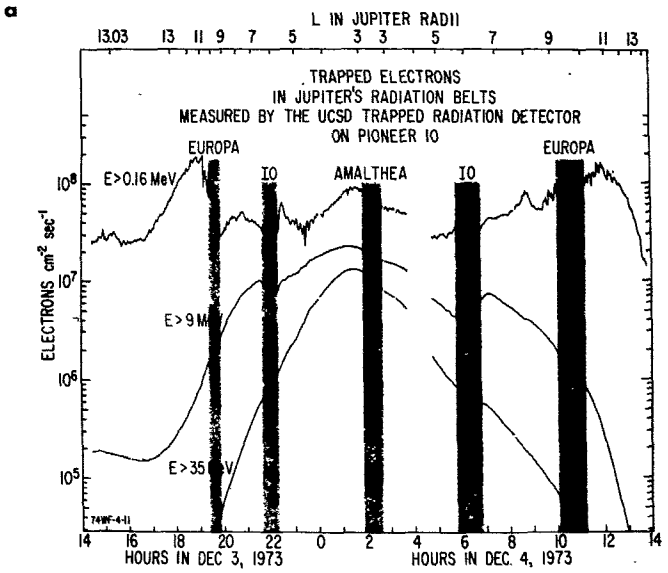

FIGURE 5a Inner Zone Electron Fluxes—Pioneer 10. Electron fluxes with $E > 0.16$ MeV, $E > 9$ MeV, and $E > 35$ MeV plotted against time and L-shell. The shaded regions indicate the L-shell width intercepted by the inner satellites. Note the decrease in the $E > 0.16$ MeV flux at Europe and the increase just inside Io's orbit.[50]

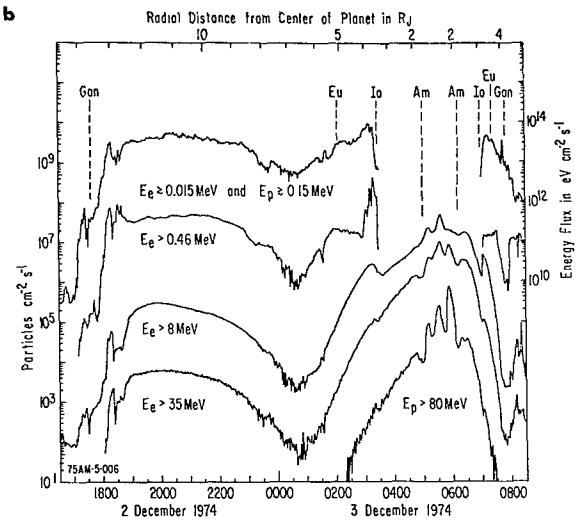

FIGURE 5b Inner Zone Fluxes—Pioneer 11. Note the sharp increase in the $E > 0.46$ MeV flux at Io. The drop-out of the 0.015 and 0.46 MeV channels inside Io is consistent with zero flux, but the data are contaminated by penetrating radiation from energetic electrons.[51]

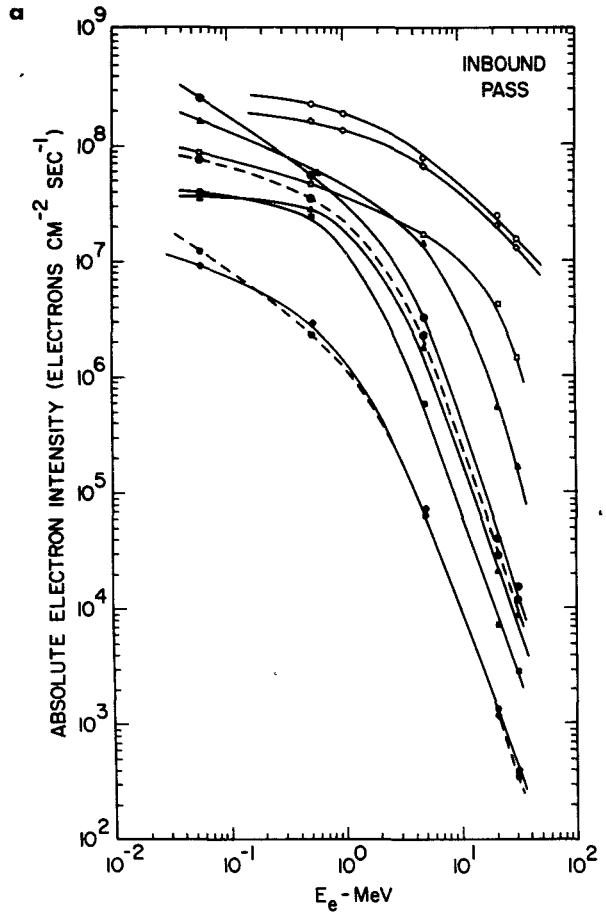

FIGURE 6a Electron Energy Spectra. The electron energy spectrum at different radial distances. Note the hardening of the spectrum above 5 MeV as the satellite moves to lower L-shells.[10]

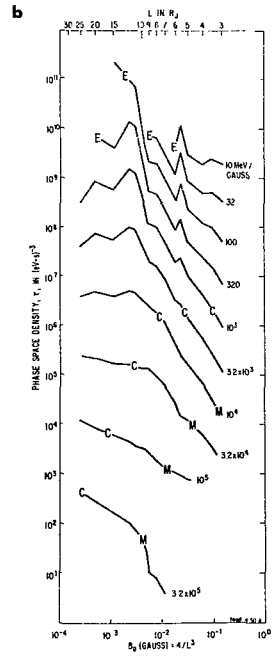

FIGURE 6b Electron Phase Space Density. The electron phase space density constructed by passing an analytic fit through the data at fixed first adiabatic invariant. In the absence of sources and sinks, the phase space density is constant. Inside L = 10, the phase space density decreases roughly as L^4 indicating that particles are lost from the radiation belts. Note, however, the increase at low first invariant near Io which indicates that Io is an electron source at low energy.[105]

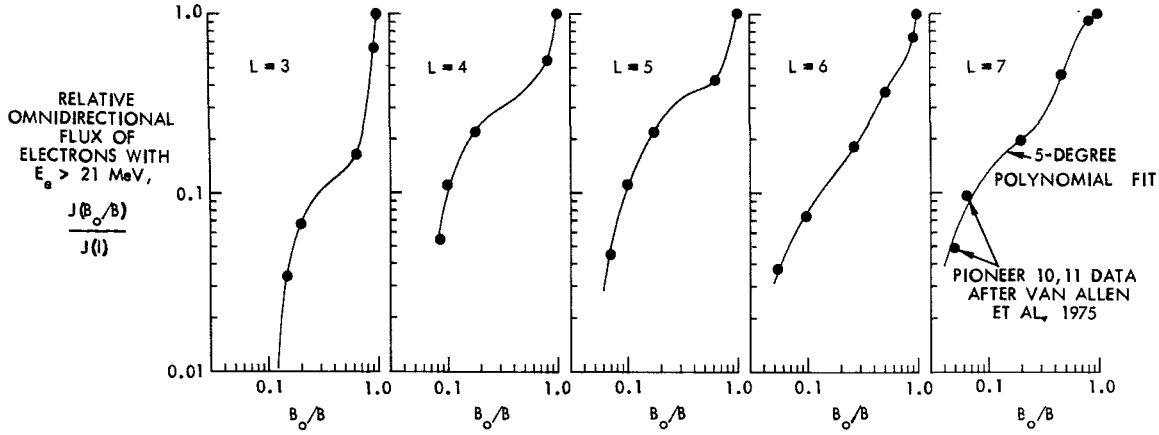

FIGURE 7 Electron Pitch-Angle Distribution. The ratio of the omni-direction flux of E > 21 MeV electrons at a magnetic field strength B to the equatorial flux at field strength B_o is plotted against B_o/B for various L-shells. The sharp peak at $B_o/B = 1$ (the equator) and the fall-off with decreasing B_o/B indicates that the pitch-angle distribution is peaked at 90°. In going from L = 7 to L = 3 the pitch-angle distribution becomes flatter, a trend which is consistent with inward radical diffusion (from Scarf and Sanders,[135] who adapted a similar figure from Van Allen, et al.[167]).

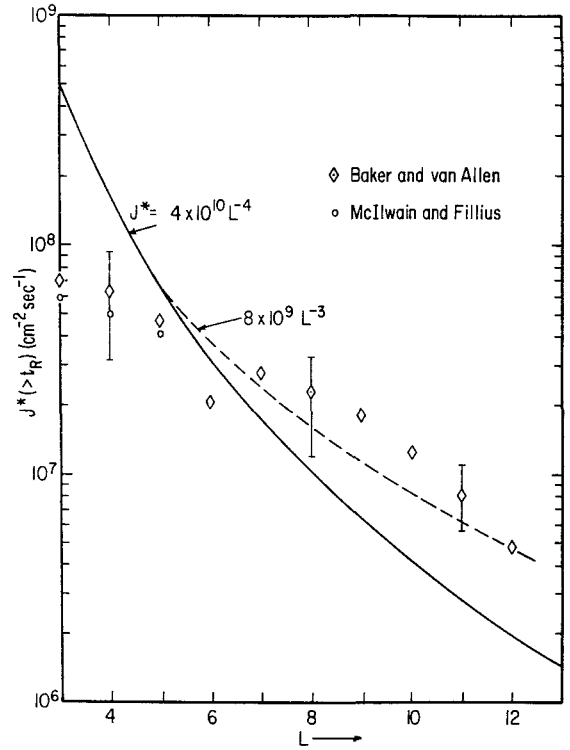

FIGURE 8 Electron Stably Trapped Limit Flux. The theoretically computed stably trapped flux using the observed electron energy and pitch-angle distributions. The solid curve assumes that the cold plasma density extends along the entire flux tube; the dashed curve assumes that the cold density is centrifugally confined to ± 1 R_J of the magnetic equator. The data points are E > 5 MeV fluxes measured by McIlwain and Fillius[105] and Baker and Van Allen[10] (from Barbosa and Coroniti[11,12]).

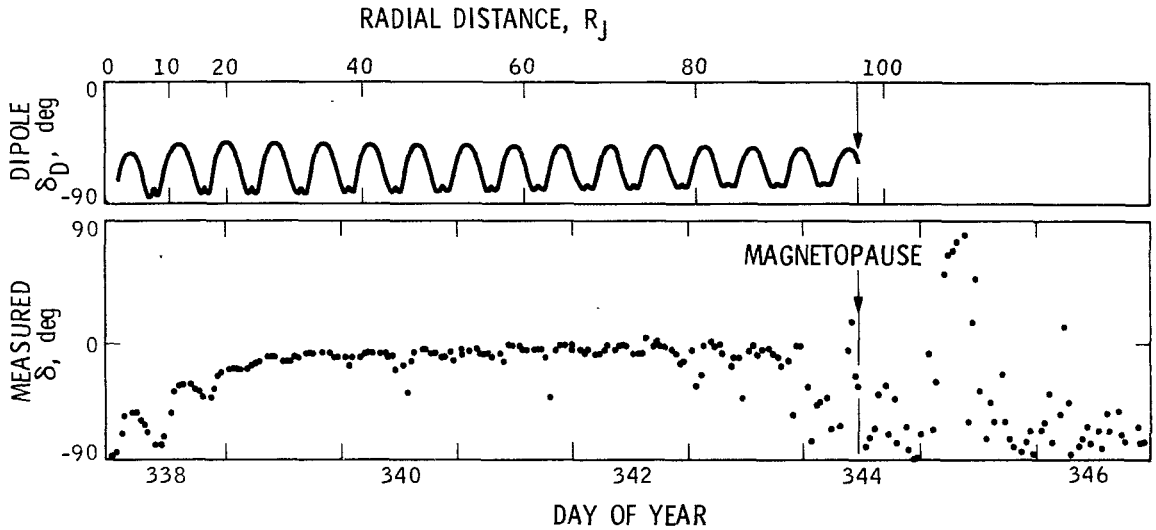

FIGURE 9 Pioneer 10 Outbound Magnetic Longitudes. Shown in the bottom panel, point by point, is the hourly average magnetic longitude δ; δ_D, in the top panel, is the longitude for Jupiter's rotating misaligned dipole field. One cycle of the ten-hour modulation of δ_D appears within 20 R_J. Beyond 20 R_J, δ is very small, indicating a predominantly radial field. Hourly averages do not clearly reveal current sheet crossing; however, these appear as southward excursions represented by a few data points (e.g., near 45 R_J). Before the magnetopause was crossed, the field turned southward, and the hourly averages reveal a highly irregular behavior.[147,148]

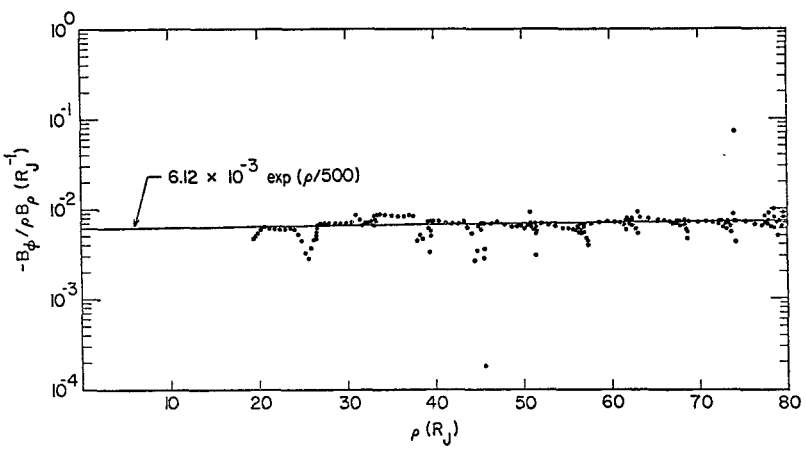

FIGURE 10 Pioneer 10 Outbound Gardenhose Angle. The azimuthal field B_ϕ divided by the radial distance ρ and the radial field B_ρ is plotted versus distance in units of R_J^{-1}. The solid line is an empirical best fit. Deviations from the theoretical line occur at current sheet crossings. In a radially expanding super-Alfvenic wind, the radial flow speed $v_\rho \simeq | \Omega\rho B_\rho/B_\phi |$, where Ω is Jupiter's rotation frequency, 1.75×10^{-4} rad/sec. The above data imply v_r exceeds 10^3 km/sec; however, the data may not be usable in a velocity determination.[64]

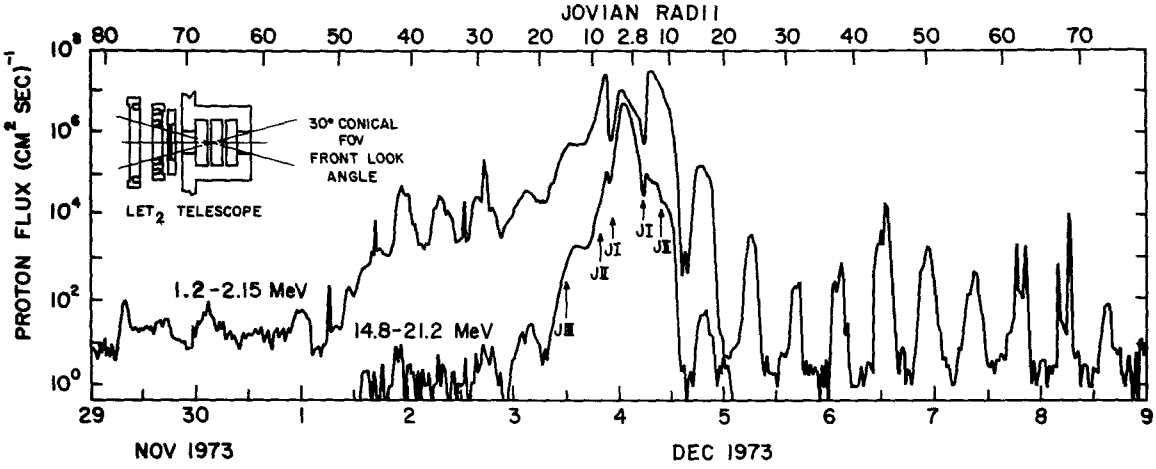

FIGURE 11 Pioneer 10 Energetic Proton Fluxes. The fluxes of 1.2 - 2.15 MeV and 14.8 - 21.2 MeV protons are plotted against time below and radial distance above. Crossings of the orbits of Jupiter's satellites are indicated by JI, JII, etc. Within 15-20 R_J in the radiation belt region, the proton fluxes increase smoothly with decreasing distance. Ten hour sawtooth modulations of the 1.2 - 2.15 MeV proton fluxes are evident between 20 - 80 R_J. They are in phase with the electron modulations.[163]

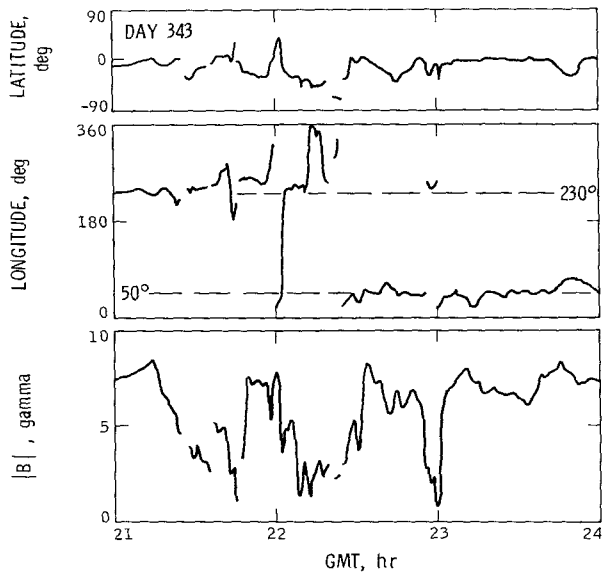

FIGURE 12 Pioneer 10 Outbound Current Sheet Crossing. Shown here is 4 hours of high time resolution magnetic field data for a current sheet crossing near 90 R_J at 5^h 30^m local time. The most important feature is the 180° reversal of the longitude towards which the magnetic field points near 22 GMT, indicating Pioneer 10 passed between lobes of the magnetosphere. While the magnitude fluctuates it diminishes to roughly 1γ during the crossing. There is a tendency for the field to point more southward within the sheet than outside.[150]

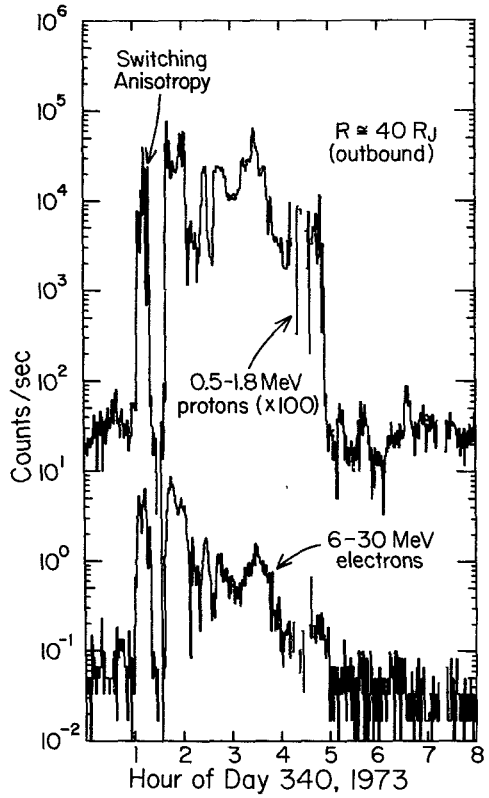

FIGURE 13 Rapid Temporal Particle Fluctuations in a Current Sheet Model. Shown here is high time resolution 6-30 MeV and 0.5 - 1.8 MeV proton flux data for a current sheet crossing near 40 R_J on Pioneer 10 outbound. Note that electrons and protons are accelerated *simultaneously* on minute time scales. Simpson and McKibben[143] suggest that magnetic field reconnection within the sheet accelerates these particles.[141]

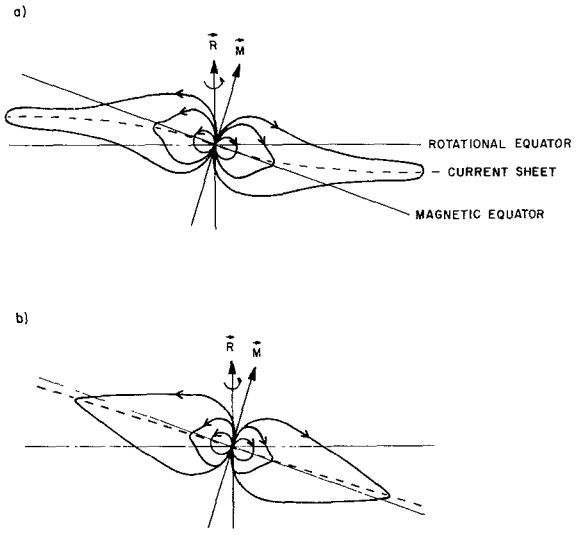

FIGURE 14 Two Possible Disk Models. At the top is shown the "hinged current sheet" model of Smith et al.[147,148] At the bottom is Goertz'[62] model of a sheet localized to the magnetic equatorial plane.

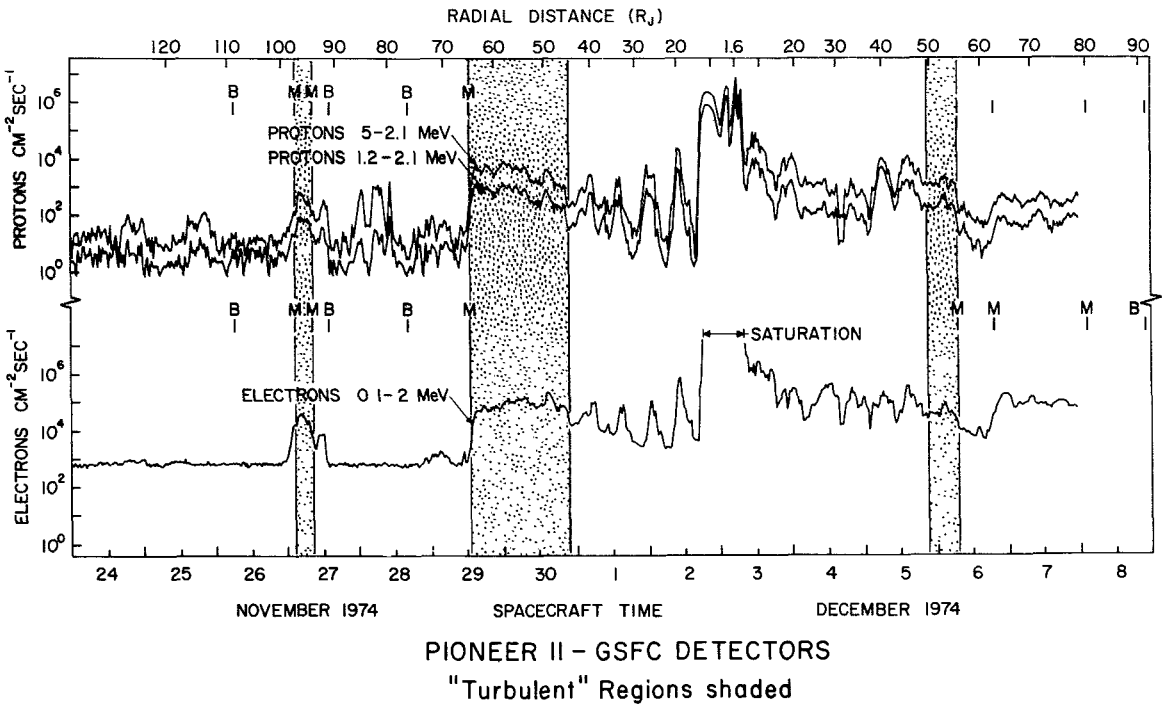

FIGURE 15 Pioneer 11 Energetic Electrons, Protons, and Turbulent Regions. The fluxes of 0.1 - 2 MeV electrons, 1.2 - 2.1 MeV protons, and 0.5 - 2.1 MeV protons are plotted against time (lower) and radial distance (upper scale). Magnetopause and bowshock crossings are denoted by M and B, respectively. The shaded regions indicate where Kivelson[87] has found magnetic turbulence in the JPL magnetometer data. Note the turbulent region within the magnetopause between 45-65 R_J on P-11 inbound; the energetic particles showed little or no 10 hour modulation in this turbulent boundary layer. Within the classical magnetopause radius at 45 R_J, electrons and protons showed pronounced 10 hour in phase modulations reminiscent of P-10 outbound. P-11 outbound was at high latitudes, and the particle fluxes were weakly modulated at best; however, turbulence was encountered at high latitudes next to the magnetopause at 55 R_J. Note that the particle fluxes on P-11 outbound were comparable with the peak fluxes observed inbound; this seems inconsistent with particle confinement to a thin disk.[87]

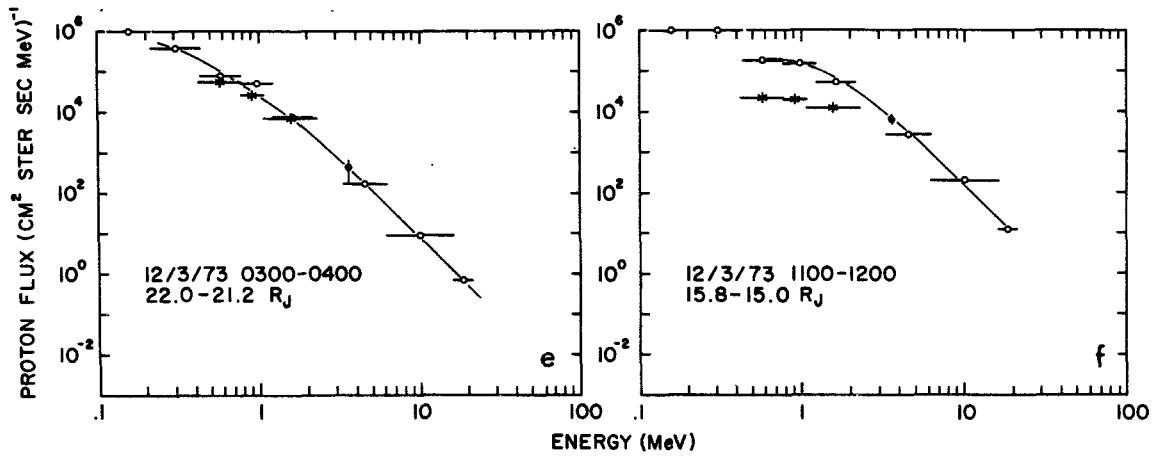

FIGURE 16 Pioneer 10 Outbound Proton Energy Spectra. Shown here are proton energy spectra between 100 KeV and 20 MeV. The spectra fall off as $1/E.^3$ The spectra are quite similar at larger radial distances. If the $1/E^3$ spectrum extends down to, say, 10 KeV at larger radial distances, the proton pressure could be comparable to the magnetic pressure.[162]

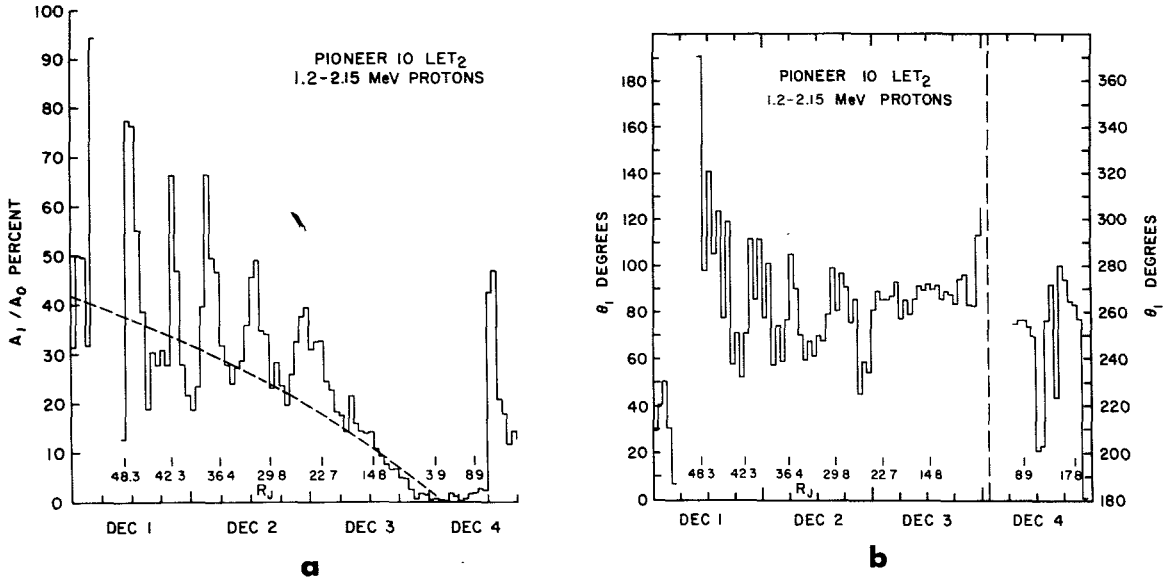

FIGURE 17 Pioneer 10 Inbound Proton Anisotropies. Knowing the proton energy spectrum, one can estimate the directional anisotropy of the proton fluxes, assuming the protons co-rotate rigidly with Jupiter. The amplitude is plotted in the left panel, with the theoretically expected curve dashed, and the phase at the right. On the inbound pass, a phase of 90° corresponds to that expected from co-rotation. Various radial disturbances are indicated at the bottom. The protons appear definitely to co-rotate within 20 R_J inbound, and there is a hint that co-rotation is preserved out to 40 R_J. The magnetic field on this portion of the pass was not strongly radially extended.[147,148]

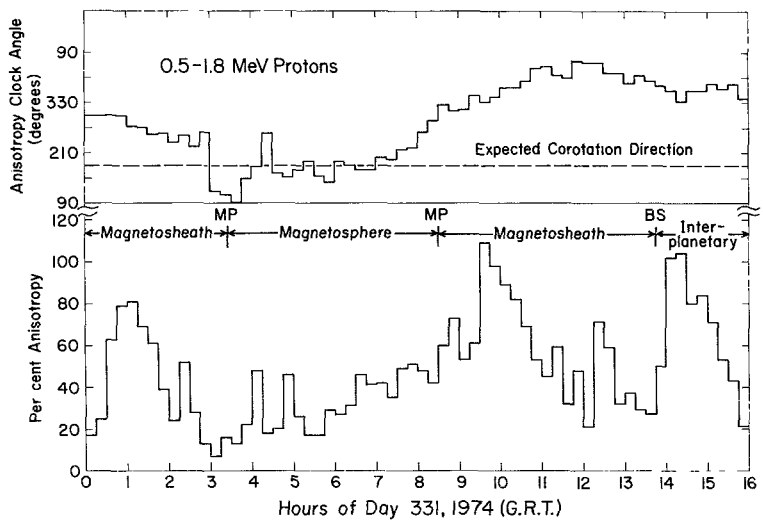

FIGURE 18 Co-Rotation in the Distant Magnetosphere. Figures 2 and 3 indicate that Pioneer 11 inbound found itself within the magnetosphere for a brief interval of time near 95 R_J. During this interval, the clock angle or phase of the proton angular distribution was consistent with co-rotation at 95 R_J.[143]

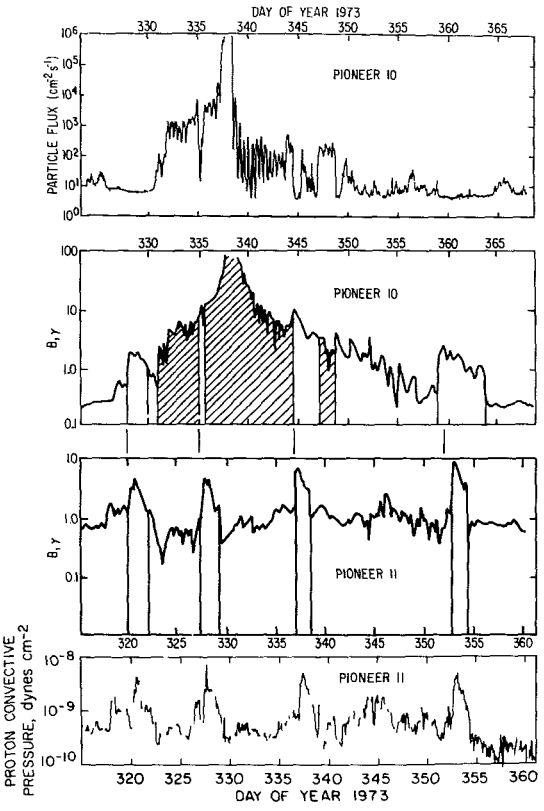

FIGURE 19 Solar Wind Dynamic Pressure Modulation of Jupiter's Outer Magnetosphere. The top two panels show the UCSD energetic electron fluxes and the JPL magnetic field magnitude for Pioneer 10 inbound; Pioneer 10 was within the magnetosphere in the shaded portions of the diagrams. The bottom two panels show simultaneous Pioneer 11 solar wind data, adjusted for travel time between P-10 and P-11; the magnetic field magnitude and dynamic pressure are shown. Each 7-10 days there is a strong peak in dynamic pressure and magnetic field associated with solar wind fast streams; the dynamic pressure increases by a factor 10-30 over its "nominal value" of 5×10^{-10} dynes/cm.^{2} When the pressure is nominal, Jupiter's magnetosphere is radially extended; the high pressure pulses compress the magnetosphere.[151]

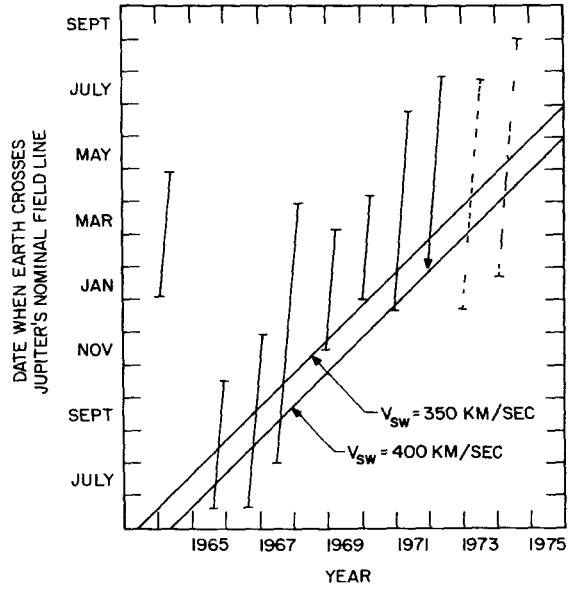

FIGURE 20 Arrival of Jovian Cosmic Ray Electrons at Earth. Shown here are the times when MeV electrons of nonsolar origin attributed to Jupiter arrive at Earth, for the years 1964-1975. The oblique lines indicate when the solar wind field line threading Earth also threads Jupiter for solar wind spreads of 350 and 400 km/sec. The fact that Jovian electrons are seen as much as 3 months after the Earth line threads the nose of Jupiter's magnetosphere suggests that many Jovian electrons come from a tail several A.U. long. The geometry is sketched in Figure 13.[123]

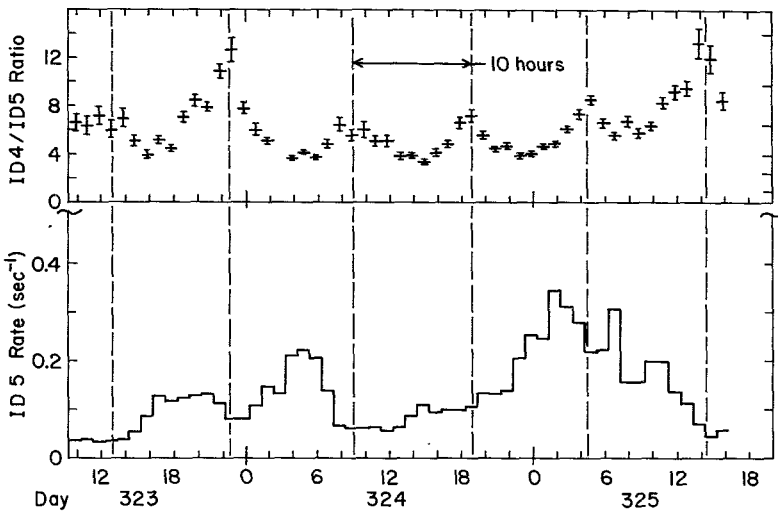

FIGURE 21 10 Hour Modulations of Jovian Electrons in the Solar Wind. According to Chenette et al.[34] the spectral index (as indicated here by the ratio of count rates in two energetic electron detectors) is modulated with a 10-hour period—a proof of their Jovian origin. In addition, their phase is identical with the phase encountered within the magnetosphere. The vertical lines indicate predicted phase maxima based on Jupiter's rotation period established when Pioneer 10 eventually entered the magnetosphere and extrapolated backwards in time to these solar wind observations.[34]

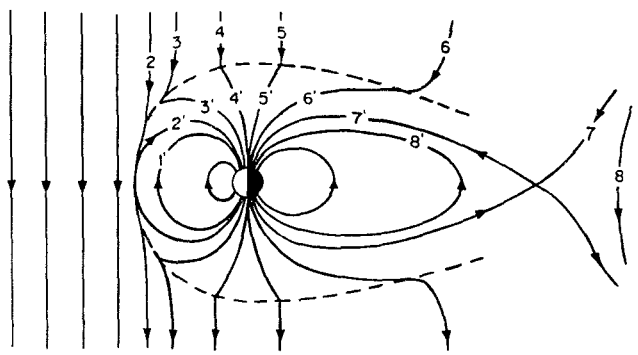

FIGURE 22 Convection Model of a Dipolar Magnetosphere. This figure, originally drawn for Earth, shows successive stages in the life cycle of a convecting magnetic flux tube. At 1′ it is closed and flowing towards the nose magnetopause, where it is reconnected with a solar wind field line (2-2′) and opened. (Cosmic ray electrons can leave or enter the magnetosphere on open field lines.) It is then dragged by the solar wind (3, 4, 5, 6) over the polar caps (3′, 4′, 5′, 6′) to form a long magnetic tail. At 7 it re-reconnects with its southern hemisphere partner; at 8 it is closed again and flowing towards the nose. This diagram shows a slice through the noon midnight meridian plane perpendicular to the ecliptic. Since Jupiter's dipole is oppositely directed to Earth's, a *northward* solar wind field is optimum for nose reconnection.

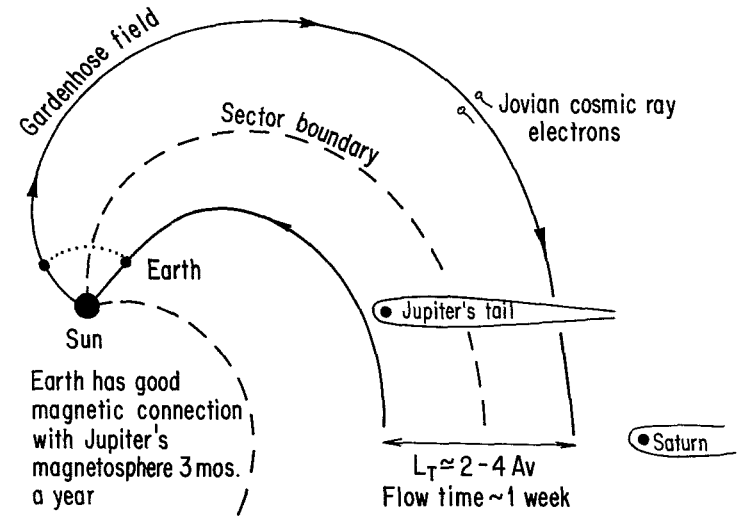

FIGURE 23 Global Geometry of Jupiter's Reconnection Magnetosphere. According to Earthlike theory, Jupiter's magnetic tail should be several A.U. long, and the convection time the order of a week. Solar wind field lines connecting Earth and Jupiter's tail contain bursts of Jovian cosmic ray electrons. Earth connects to Jupiter's tail for ¼ of a revolution, about 3 months. The solar wind is typically divided into 4 magnetic sectors, about ¼ solar rotation period, or 7 days apart Jupiter's nose can be in one sector, its tail in another, with correspondingly different reconnection boundary conditions. In addition, large dynamic pressures are associated with sector boundary crossings; Figure 21 indicates these compress at least the nose region. Since all these changes take place on the convection flow time, we expect Jupiter's magnetosphere to be steady only for an exceptionally quiet solar wind.

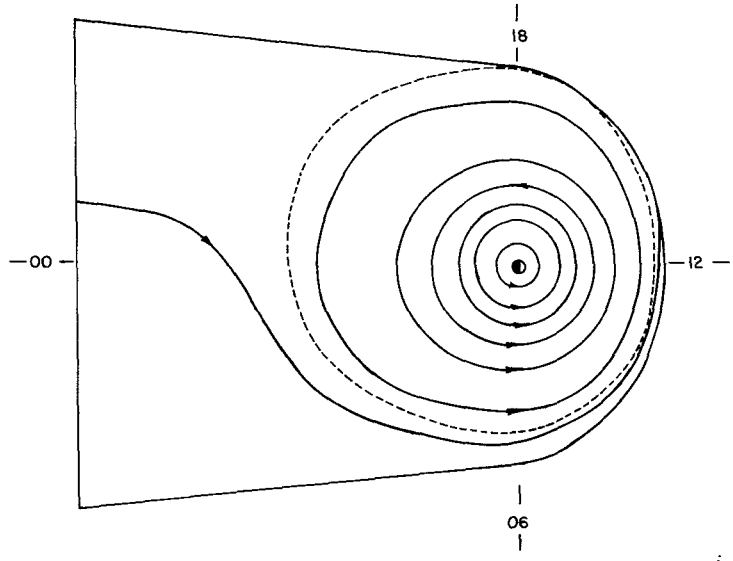

FIGURE 24 Jupiter's Plasmasphere and Co-Rotation Region. Shown here is a cut through Jupiter's equatorial plane; the outer line represents the classical magnetopause. Adding a uniform convection electric field to Jupiter's co-rotation electric field permits the flow streamlines to be drawn. They are closed co-rotating around the planet within the plasmapause-dashed line. All the flux and plasma transported by convection—symbolized by the single flow streamline entering from the magnetic tail—reaches the nose reconnection region in a twin layer between the plasmapause and magnetopause. If there are plasma sources within it, the plasmasphere should be a high density region; radial transport therein must be diffusive.[24]

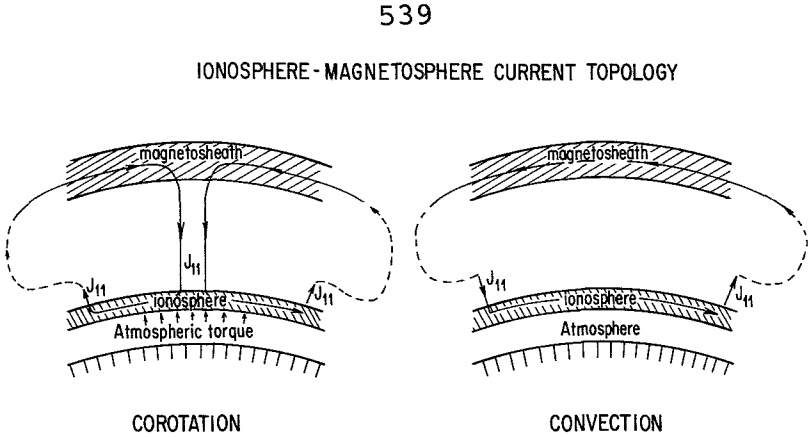

FIGURE 25 Polar Cap Current Systems. The left panel suggests the topology of the polar cap ionospheric current systems required to despin Jupiter's atmosphere and enforce co-rotation on the magnetosphere; the right panel shows the current system corresponding to the convection of field lines antisunward over the polar cap (see Figure 22). The combined co-rotation convection system is some nonlinear addition of the two.

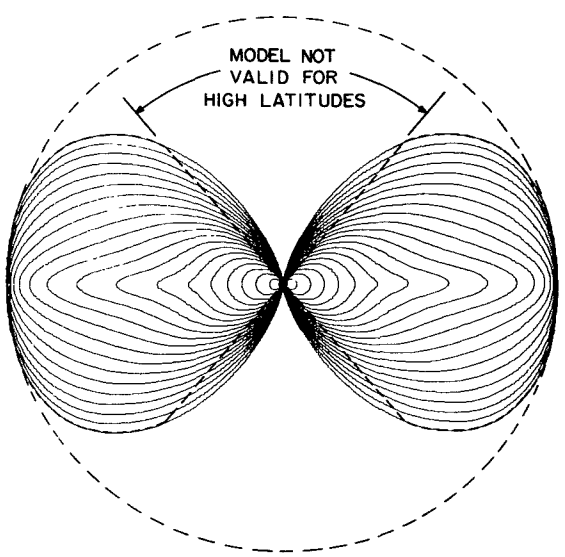

FIGURE 26 Model of Jupiter's Magnetic Disk and Magnetosphere. Shown here is a static magnetic field model fit analytically by Barish and Smith[13] to the general behavior of the Pioneer 10 outbound data. This model is in rough accord with observation both of a southward field near the magnetosphere and of a dipolar structure at high latitudes, and therefore helps us to visualize the magnetosphere; however, it neglects all dynamics.[13]

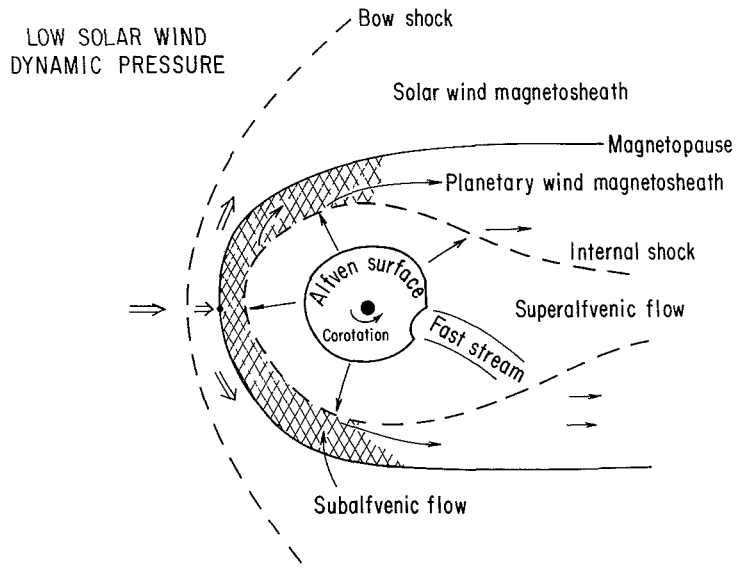

FIGURE 27 Heliospheric Model of Super-Alfvenic Jovian Wind. Shown here is a cut through the equatorial plane. The Alfven surface is at approximately 40 R_J. For low solar wind dynamic pressure, a super-Alfvenic wind is generated at all local times; it is terminated by an internal shock, which decelerates the planetary wind and deflects it into the tail. The whole planetary wind flow is confined by the solar wind; shocked planetary and solar wind are separated in ideal MHD by a tangential discontinuity, the magnetopause. This whole picture neglects magnetic field line reconnection.

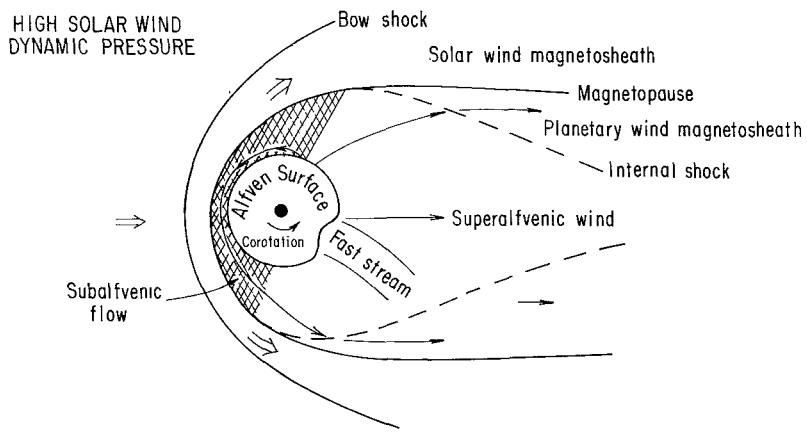

FIGURE 28 Heliospheric Model of Sub-Alfvenic Jovian Breeze. When the solar wind dynamic pressure is high, it is possible that only a sub-Alfvenic breeze, which would not radially extend the field lines, develops on the dayside. However, the planetary wind should still be super-Alfvenic in the tail. The large observed dynamic pressure variations could induce wind-breeze changes on Jupiter's dayside.

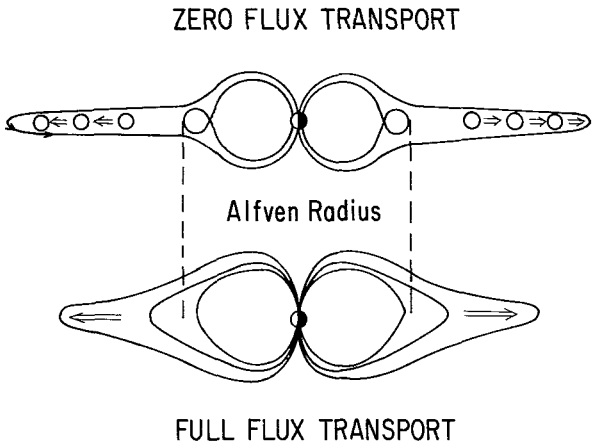

FIGURE 29 Flux Transport in the Jovian Super-Alfvenic Wind. No flux is transported to the Alfven radius from within by radial diffusion. We can visualize two extreme limits for flux transport beyond the Alfven radius. First, that no flux is transported by the wind; this would require that reconnection disconnect bubbles of magnetic flux which are convected with the wind. At the opposite limit, flux is transported by the wind without slippage. No good models for wind transport of magnetic flux exist at present.

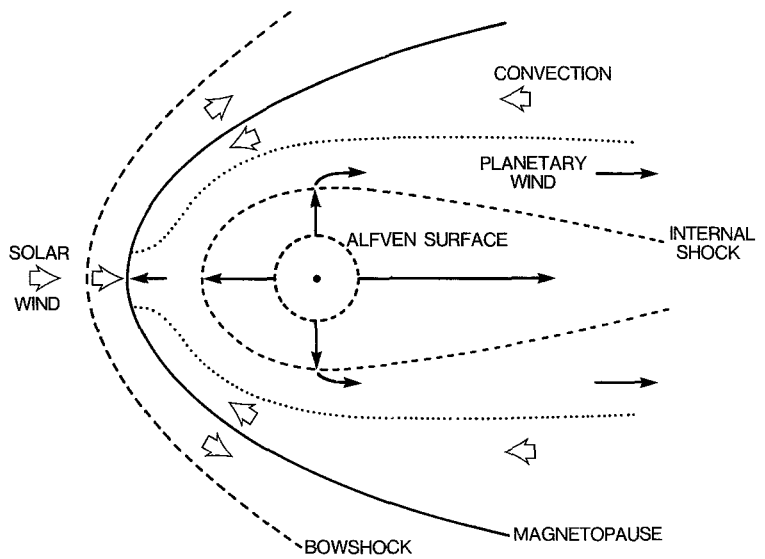

FIGURE 30 Combined Convection-Planetary Wind Magnetosphere. When the planetary wind transports no magnetic flux, and the flux lines bounding the wind region reconnect with the solar wind magnetic field, the planetary wind and convection flow could be essentially separate systems, with convection taking place outside the wind region as shown. When the planetary wind transports magnetic flux into Jupiter's tail, it is difficult to see how to construct a steady flow which transports flux back to the Alfven point.

1. Acuña, M. H., and N. F. Ness, Jupiter's main magnetic field measured by Pioneer 11, Nature, 253, 327, 1975.

2. Acuña, M. H., and N. F. Ness, The main magnetic field of Jupiter, J. Geophys. Res., 81, 2917, 1976a.

3. Acuña, M. H., and N. F. Ness, Results from the GSFC fluxgate magnetometer on Pioneer 11, in Jupiter, T. Gehrels (ed.), U. Ariz. Press, 830-847, 1976b.

4. Anderson, K. A., Energetic electrons of terrestrial origin upstream in the solar wind, J. Geophys. Res., 73, 2387-2398, 1968.

5. Atreya, S. K., Donahue, T. M., McElroy, M. B., Jupiter's ionosphere prospects for Pioneer 10, Science, 184, 154-56, 1974.

6. Axford, W. I., Hines, C. O., A unifying theory of high-latitutde geophysical phenomena and geomagnetic storms, Can. J. Phys, 39, 1433-1464, 1961.

7. Axford, W. I., Magnetospheric convection, Rev. Geophys, 7, 421-459, 1969.

8. Axford, W. I., in Solar Wind, Scnett, C. P., Coleman, P. J., Wilcox, J. M. (eds.), NASA, 609, 1972.

9. Axford, W. I., Mendis, D. A., Satellites and magnetospheres of the outer planets, Ann. Rev. Earth and Planet. Sci., 2, 419-474, 1974.

10. Baker, D. N., Van Allen, J. A., Energetic electrons in the Jovian magnetosphere, J. Geophys. Res., 81, 617-632, 1976.

11. Barbosa, D. D., Coroniti, F. V., Relativstic electrons and whistlers in Jupiter's magnetosphere, J. Geophys. Res., 81, 4531-6, 1976a.

12. Barbosa, D. D., Coroniti, F. V., Lossy radial diffusion of relativistic Jovian electrons, J. Geophys. Res., 81, 4553-60, 1976b.

13. Barish, F. D., and R. A. Smith, An analytical model of the Jovian magnetosphere, Geophys. Res. Lett., 2, 269-272, 1975.

14. Barnes, C. W., D. L. Chenette, T. F. Conlon, K. R. Pyle, and J. A. Simpson, Interplanetary acceleration of nucleons and modulation of Jovian electrons between 1 and 10 Au by corotating regions of solar origin, accepted for publication, Ap. J. Letters, 1977.

15. Beck, A. J. (ed.), Conclusion. Proceedings of the Jupier Radiation Belt Workshop, NASA Technical memorandum 33-543, 473-485, Washington, D. C., 1972.

16. Berge, G. L., An interferometric study of Jupiter's decimeter radio emission, Ap. J., 146, 767-798, 1966.

17. Berge, G. L., and S. Gulkis, Earth-based radio observations of Jupiter: Millimeter to meter wavelengths, in Jupiter, T. Gehrels ed., Univ. Arizona Press, Tucson, 621-692, 1976.

18. Bergstralh, J. T., Matson, D. L., Johnson, T. V., Sodium D-live emission from Io: Synoptic observations from Table Mountain Observatory, Ap. J., 195, L131-L135, 1975.

19. Bergstralh, J. T., J. W. Young, D. L. Matson, and T. V. Johnson, Sodium D-line emission from Io: A second year of synoptic observation from Table Mountain Observatory, Ap. J., 211, L51-L56, 1977.

20. Birmingham, T. J., Convection electric fields and the diffusion of trapped magnetospheric radiation, J. Geophys. Res., 74, 2169-2181, 1969.

21. Birmingham, T., Hess, W., Northrup, T., Baxter, R., Lujko, J., The electric diffusion coefficient in Jupiter's magnetosphere, J. Geophys. Res., 79, 87, 1974.

22. Branson, N. J. B. A., High resolution radio observation of the planet Jupiter, Mon. Not. R. Astr. Soc., 139, 155-162, 1968.

23. Brice, N. M., Jupiter's outer atmosphere, Cornell-Sydney University Astronomy Center unpublished preprint CSUAC 124, 1968.

24. Brice, N. M., Ioannidis, G. A., The magnetospheres of Jupier and Earth, Icarus, 13, 173, 1970.

25. Brice, N. M., McDonough, T. R., Jupiter's Radiation belts, Icarus, 18, 206-219, 1973.

26. Brown, L. W., Saturn emission near 1 Mhz, Astrophys. J. Letters, 198, L89, 1975.

27. Brown, R. A., R. M. Goody, F. J. Murcray, F. H. Chaffee, Jr., Further studies of line emission from Io, Ap. J., 200, L49, 1975.

28. Burke, B. F., and K. L. Franklin, Observations of a variable radio source associated with the planet Jupiter, J. Geophys. Res., 60, 213, 1955.

29. Carbary, J. F., T. W. Hill, A. J. Dessler, Planetary spin period acceleration of particles in the Jovian magnetosphere, J. Geophys. Res., 28, 5189, 1976.

30. Carlson, R. W., Matson, D. L., Johnson, T. V., Electron input ionization of Io's sodium emission cloud, Geophys. Res. Lett., 2, 469-472, 1975.

31. Carr, T. D., Desch, M. D., Recent decametric and hectometric observations of Jupiter, in Jupiter, T. Gehsels (ed.), U. Ariz. Press, 693-737, 1976.

32. Carr, T. D., and S. Gulkis, The magnetosphere of Jupiter, Ann. Rev. Astron. and Astrophys., 7, 577-610, 1967.

33. Carr, T. D., Gulkis, S., The magnetosphere of Jupiter, Ann. Rev. Astron. and Astrophys. (L. Goldberg, ed.), Vol. 7, p. 477-618, Palo Alto, Calif., Annual Reviews, Inc., 1969.

34. Chenette, D. L., Conlon, T. F., Simpson, J. A., Bursts of relativistic electrons from Jupiter observed in interplanetary space with the time variation of the planetary rotation period, J. Geophys. Res, 79, 3551-3558, 1974.

35. Conlon, T. F., and J. A. Simpson, Modulation of Jovian electron intensity in interplanetary space of co-rotating interaction regions, Ap. J., 211, L45-L50, 1977.

36. Coroniti, F. V., Energetic electrons in Jupiter's magnetosphere, Ap. J., Suppl. series, 27, 261, 1974.

37. Coroniti, F. V., Denouement of Jovian radiation belt theory, Space Sci. Rev., 17, 837, 1975.

38. Coroniti, F. V., C. F. Kennel , Can the ionosphere regulate magnetospheric convection ?, J. Geophys. Res., 78, 2837-2851, 1973.

39. Coroniti, F. V., and C. F. Kennel, Possible origins of time variability in Jupiter's outer magnetosphere; 1. Variations in solar wind dynamic pressure, submitted, Geophysical Research Letters, 1977.

40. Dessler, A. J., Hill, T. W., High-order magnetic multipoles as a source of gross asymmetry in the distant Jovian magnetosphere, Geophys. Res. Lett., 2, 567-570, 1975.

41. Drake, F. P., Hvatum, H., Non-thermal microwave radiation from Jupiter, Astron. J., 64, 329-330, 1959.

42. Dungey, J. W., Interplanetary magnetic field and the auroral zones, Phys. Rev. Lett., 6, 47, 1961.

43. Dungey, J. W., The length of the magnetospheric tail, J. Geophys. Res., 70, 1753, 1965.

44. Ellis, G. R. A., The decametric radio emission of Jupiter, Radio Sci., 65d, 1513-1530, 1965.

45. Eviatar, A., and A. I. Ershkovich, Plasma density in the outer Jovian magnetosphere, J. Geophys. Res., 81, 4027-4028, 1976.

46. Fan, C. Y., G. Gloeckler, and J. A. Simpson, Evidence for > 30 KeV electrons accelerated in the shock transition region beyond earth's magnetospheric boundary, Phys. Rev. Lett., 13, 149-153, 1964.

47. Fedder, J. A., Banks, P. M., Convection electric fields and polar thermospheric winds, J. Geophys. Res., 77, 2328-2340, 1972.

48. Field, G. B., The source of radiation from Jupiter at decimeter wavelengths, J. Geophys. Res., 64, 1169-1177, 1959.

49. Fillius, W., The trapped radiation belts of Jupiter, in Jupiter, T. Gehrels (ed.), U. Ariz. Press, 896, 1976.

50. Fillius, R. W., McIlwain, C. E., Measurements of the Jovian radiation belts, J. Geophys. Res., 79, 3589-3599, 1974.

51. Fillius, R. W., C. R. McIlwain, and A. Mogro-Campero, Radiation belts and Jupiter: a second look, Science, 188, 465-467, 1975.

52. Fillius, R. W., McIlwain, C., Mogro-Compero, A., Steinberg, G., Evidence that pitch angle scattering is an important loss mechanism for energetic electrons in the inner radiation belt of Jupiter, Geophys. Res. Lett., 3, 33-36, 1976.

53. Flagg, R. S., D. S. Krausche, and G. R. Lebo, High resolution spectral analysis of the Jovian decametric radiation. II. The bank-like emissions, Icarus, 29, 477-482, 1976.

54. Formisano, V. (ed.), The Magnetospheres of Earth and Jupiter, D. Reidel, Dordrecht, Holland, 1975.

55. Frank, L. A., Ackerson, K. L., Wolfe, J. H., Mihalov, J. D., Observations of plasmas in the Jovian magnetosphere, J. Geophys. Res., 81, 457-468, 1976.

56. Frank, L. A., Van Allen, J. A., Measurements of energetic electrons in the vicinity of the sunward magnetospheric boundary with Explorer 14, J. Geophys. Res., 69, 4923-4932, 1964.

57. Gehrels, T., Jupiter, U. Ariz. Press, 1976.

58. Ginzburg, V. L., Syrovatskii, S. I., Cosmic magnetobremsstrahlung (synchrotron radiation), Ann. Rev. Astron. Astrophys., 3, 297-350, 1965.

59. Gledhill, J. A., Magnetosphere of Jupiter, Nature, 214, 155-156, 1967.

60. Gleeson, L. J., Axford, W. I., An analytic model illustrating the effects of rotation on a magnetosphere containing low-energy plasma, J. Geophys. Res., 81, 3403-06, 1976.

61. Goertz, C. K., Plasma in the Jovian magnetosphere, J. Geophys. Res., 81, 2007-2014, 1976a.

62. Goertz, C. K., The current sheet in Jupiter's magnetosphere, J. Geophys. Res., 81, 3368-3372, 1976b.

63. Goertz, C. K., Jupiter's magnetosphere: Particles and fields, in Jupiter, T. Gehrels (ed.), U. Ariz. Press, 32-58, 1976c.

64. Goertz, C. K., Jones, D. E., Randall, B. A., Smith, E. J., Thomsen, M. F., Evidence for open field lines in Jupiter's magnetosphere, J. Geophys. Res., 81, 3393, 1976.

65. Goldreich, P., Lynden-Bell, D., Io, a Jovian unipolar inductor, Ap. J., 156, 59-78, 1969.

66. Gross, S. H., and G. V. Ramanathan, The atmosphere of Io, Icarus, 29, 493-508, 1976.

67. Gubbins, D., Speculations on the origin of the magnetic field of Mercury, Icarus, 30, 186-191, 1977.

68. Gurnett, D. A., Sheath effects and related charged-particle acceleration by Jupiter's satellite Io, Ap. J., 175, 525-533, 1972.

69. Gurnett, D. A., The earth as a radio source: Terrestrial kilometric radiation, J. Geophys. Res., 79, 4227, 1974.

70. Hess, W. N., Birmingham, T. J., Mead, G. D., Absorption of trapped particles by Jupiter's moons, J. Geophys. Res., 79, 2877-2880, 1974.

71. Hill, T. W., Interchange stability of a rapidly rotating magnetosphere, Planet. Space Sci., 24, 1151-1154, 1976.

72. Hill, T. W., Dessler, A. J., Michel, F. C., Configuration of the Jovian magnetosphere, Geophys. Res. Lett., 1, 3-6, 1974a.

73. Hill, T. W., Carbary, J. F., Dessler, A. J., Periodic escape of relativistic electrons from the Jovian magnetosphere, Geophys. Res. Lett., 1, 333-336, 1974b.

74. Hill, T. W., Michel, F. C., Heavy ions from the Galilean satellites and the centrifugal distortion of the Jov magnetosphere, J. Geophys. Res., 81, 4561, 1976.

75. Hubbard, R. F., Shawhan, S. D., Joyce, G., Io as an emitter of 100-keV electrons, J. Geophys. Res., 79, 920-928, 1974.

76. Intriligator, D. S., and J. Wolfe, private communication concerning Jupiter's magnetic tail, 1976.

77. Ioannidis, G. A., Brice, N. M., Plasma densities in the Jovian magnetosphere: Plasma slingshort or Maxwell demon?, Icarus, 14, 360, 1971.

78. Jokipii, J. R., The interplanetary magnetic field and energetic electrons from Jupiter, Geophys. Res. Letters, 3, 281, 1976; Correction, Geophys. Res. Letters, 3, 363, 1976.

79. Judge, D. L., Carlson, R. W., Pioneer 10 ultraviolet photometer observations in the vicinity of Jupiter, Science, 183, 317-318, 1974.

80. Kennel, C. F., Consequences of a magnetospheric plasma, Rev. Geophys., 7, 379, 1969.

81. Kennel, C. F., Magnetospheres of the planets, Space Sci. Rev., 14, 511, 1973.

82. Kennel, C. F., What we have learned from the magnetosphere, Comments on Astrophysics and Space Physics, 6, 3, 71-81, 1975.

83. Kennel, C. F., Coroniti, F. V., Is Jupiter's magnetosphere like a pulsar's or Earth's?, Space Sci. Rev., 17, 857, 1975.

84. Kennel, C. F., and F. V. Coroniti, Possible origins of time variability in Jupiter's outer magnetosphere. 2, Variations in solar wind magnetic field, submitted, Geophys. Res. Letters, 1977.

85. Kennel, C. F., and J. E. Maggs, On the detection of magnetospheric radio bursts from Uranus and Neptune, Nature, 267, 299, 1976.

86. Kennel, C. F., Petschek, H. E., Limit on stably trapped particle fluxes, J. Geophys. Res., 71, 1-28, 1966.

87. Kivelson, M. G., in Physics of Solar Planetary Environments, edited by D. J. Williams, American Geophysical Union, Washington D. C., 1976.

88. Kivelson, M. G., P. J. Coleman, Jr., L. Froidevaux, and R. L. Rosenberg, A time dependent model of the Jovian current sheet, submitted to J. Geophys. Res., 1977.

89. Kivelson, M. G., and C. R. Winge, Field-aligned currents in the Jovian magnetosphere: Pioneer 10 and 11, J. Geophys. Res., 81, 5853-5858, 1976.

90. Kliore, A., Cain, D. L., Fjeldbo, G., Seidel, B. L., Rasool, S. I., Preliminary results of the atmospheres of Io and Jupiter from Pioneer 10 S-band occulation experiment, Science, 183, 323-324, 1974.

91. Krausche, D. S., R. S. Flagg, G. R. Lebo, and A. G. Smith, High resolution spectral analyses of the Jovian decametric radiation. I. Burst morphology and drift rates, Icarus, 29, 463-476, 1976.

92. Krimigis, S. M., E. T. Sarris, and T. P. Armstrong, Observations of Jovian electron events in the vicinity of Earth, Geophys. Res. Letters, 2, 561, 1975.

93. Kupo, I., Y. Mekler, and A. Eviatar, Detection of ionized sulfur in the Jovian magnetosphere, Astrophys. J., 205, L51, 1976.

94. Levy, R. H. Petschek, H. E., Siscoe, G. L., Aerodynamic aspects of magnetospheric flow, AIAA J, 2, 2065, 1964.

95. Lyons, L. R., Thorne, R. M., Kennel, C. F., Pitch-angle diffusion of radiation belt elections within the plasmasphere, J. Geophys. Res., 77, 3455-3474, 1972.

96. Matson, D. L., Johnson, T. V. Fanale, F. P., Sodium D-line emission from Io: Sputtering and resonant scattering hypothesis, Ap. J., 192, L43-L46, 1974.

97. Mayer, C. H., McCullough, T. R., Sloanaker, R. M., Observation of Mars and Jupiter at a wave length of 3.15 cm, Ap. J., 127, 11-16, 1958a.

98. Mayer, C. H., McCullough, T. R., Sloanaker, R. M., Measurements of planetary radiation at centimeter wavelengths, Proc. IRE, 46, 260-266, 1958b.

99. McClain, E. F. Sloanaker, R. M., Preliminary observations at 10 cm wavelength using the NRL 84-foot radio telescope. Proceedings IAU Symposium No. 9 - URSI Symposium No. 1 (R. N. Bracewell, ed.), Stanford Univ. Press, 61-68, 1959.

100. McDonald, F. B., Trainor, J. H., Observations of energetic Jovian electrons and protons, in Jupiter, T. Gehrels (ed.), U. Ariz. Press, 961-987, 1976.

101. McDonough, T. R., Jupiter after Pioneer: a progress report, Nature, 251, 17, 1974.

102. McDonough, T. R., A theory of the Jovian hydrogen torus, Icarus, 24, 400, 1975.

103. McDonough, T. R., Meeting Review, II. Fields and particles, Icarus, 27, 171-179, 1976.

104. McDonough, T. R., A. Prakash, and W. E. Swartz, On Jupiter's inner magnetospheric thermal plasma density, EOS Trans. AGU, 56, 428, 1975.

105. McIlwain, C. E., Fillius, R. W., Differential spectra and phase space densities of trapped electrons at Jupiter, J. Geophys. Res., 80, 1341-5, 1975.

106. McKibben, R. B., Simpson, J. A., Evidence from charged particle studies for the distortion of the Jovian magnetosphere, J. Geophys. Res., 79, 3545, 1974.

107. Mead, G. D., Hess, W. N., Jupiter's radiation belts and the sweeping effect of its satellites, J. Geophys. Res., 78, 2793-2811, 1973.

108. Mekler, Y., Eviatar, A., Spectroscopic observations of Io, Ap. J., 193, L151-L152, 1974.

109. Mekler, Y., A. Eviatar, and I. Kupo, submitted to J. Geophys. Res., 1976.

110. Melrose, D. B., Rotational effects on the distribution of thermal plasma in the magnetosphere of Jupiter, Planet. Space Sci., 15, 381-393, 1967.

111. Melrose, D. B., An interpretation of Jupiter's decametric radiation and the terrestrial kilometric radiation as direct amplified gyro-emission, preprint, University of Colorado, 1975.

112. Mendis, D. A., and W. I. Axford, Satellites and magnetospheres of the outer planets, Ann. Rev. of Earth and Planet. Sci., (F. A. Donath, ed.), 419-474, 1974, Ann. Rev. Inc., Palo Alto.

113. Mestel, L., Magnetic braking by a stellar wind, I, Monthly Notices of the Royal Astronomical Society, 138, 359, 1968.

114. Mewaldt, R. A., Stone, E. C., Vogt, R. E., Observations of Jovian electrons at 1 AU, J. Geophys. Res., 81, 2397-2400, 1976.

115. Michel, F. C., Sturrock, P. A., Centrifugal instability of the Jovian magnetosphere and its interaction with the solar wind, Planet. Space Sci., 22, 1501-1510, 1974.

116. Mogro-Campero, A., R. W. Fillius, and C. E. McIlwain, Electrons and protons in Jupiter's radiation belts, Space Research, Vol. XV, Berlin, Academie Verlag, 1975.

117. Mogro-Campero, A., and W. Fillius, The absorption of trapped particles by the inner satellites of Jupiter and the radial diffusion coefficient of particle transport, J. Geophys. Res., 81, 1289-1295, 1976.

118. Neugebauer, M., and A. Eviatar, An alternative interpretation of Jupiter's plasmapause, Geophys. Res. Lett., 3, 708, 1976.

119. Nishida, A., Outward diffusion of energetic particles from the Jovian radiation belt, J. Geophys. Res., 81, 1771-1773, 1976.

120. Northrup, T.G., Birmingham, T. J., The magnetosphere of Jupiter as observed with Pioneer 10. 3. Jovian synchrotron radiation at 10.4 cm as deduced from observed electron fluxes, J. Geophys. Res., 79, 3583-3587, 1974.

121. Northrup, T. G., C. K. Goertz, M. F. Thomsen, The magnetosphere of Jupiter as observed with Pioneer 10, 2. Nonrigid rotation of the magnetodisc, J. Geophys. Res., 79, 3579-3582, 1974.

122. Parker, E., Interplanetary Dynamical Processes (New York: InterScience Publishers), 1963.

123. Pesses, M. E., Goertz, C. K., Jupiter's magnetail as the source of interplanetary Jovian MeV electrons observed at Earth, Geophys. Res. Lett., 3, 228-230, 1976.

124. Piddington, J. H., Jupiter's magnetosphere, U. Iowa Tech. Report 67-63, 1967.

125. Prakash, A., and N. Brice, Magnetospheres of Earth and Jupiter after Pioneer 10, in The Magnetospheres of Earth and Jupiter (V. Formisono, ed.), D. Reidel, Dordrecht-Holland, pp. 411-423, 1975.

126. Radhakrishnan, V., Roberts, J. A., Polarization and angular extent of the 960 Mc/sec radiation from Jupiter, Phys. Rev. Lett., 4, 493-494, 1960.

127. Roberts, J. A., Komesaroff, M. M., Observations of Jupiter's radio spectrum and polarization in the range from 6 cm to 100 cm, Icarus, 4, 127-156, 1965.

128. Roberts, J. A., and M. M. Komesaroff, Circular polarization of the 1.4 GHz emission from Jupiter's radiation belts, Icarus, 29, 455-462, 1976.

129. Roberts, J. A., Stanley, G. J., Radio emission from Jupiter at a wavelength of 31 centimeters, Publ. Astron. Soc. Pacific, 71, 485-496, 1959.

130. Roederer, J. G., Dynamics of Geomagnetically Trapped Radiation, Springer-Verlag, Berlin, New York, 1970.

131. Roederer, J. G., Geomagnetic field distortions and their effects on radiation belt particles, Rev. Geophys. Space Phys., 10, 599, 1972.

132. Roederer, J. G., M. H. Acuña, and N. F. Ness, Jupiter's internal magnetic geometry relevant to particle trapping, preprint, Univ. of Denver, Denver Research Institute, Denver, Colo.; submitted to J. Geophys. Res., 1977.

133. Sakurai, K., A possible method of accelerating relativistic electrons in the neutral sheet in the Jovian outer magnetosphere, Planet. Space Sci., 24, 1207-1208, 1976.

134. Scarf, F. L., A new model for the high frequency decametric radiation from Jupiter, J. Geophys. Res., 79, 3835, 1974.

135. Scarf, F. L., Sanders, N. L., Some comments on the whistler mode instability at Jupiter, J. Geophys. Res., 81, 1787-1790, 1976.

136. Schulz, M. and A. Eviatar, Charged particle absorption by Io, Ap. J., 211, L149, 1977.

137. Seidelmann, P. K., and Neil Divine,Evaluation of Jupiter longitudes in System III (1965), Geophys. Res. Lett., 4, 65, 1977.

138. Sentman, D. D., Van Allen, J. A., Goertz, C. K., Recirculation of energetic particles in Jupiter's magnetosphere , Geophys. Res. Lett., 2, 465-468, 1975.

139. Sentman, D. D., Van Allen, J. A., Angular distributions of electrons of energy $E_e > 0.06$ MeV in the Jovian magnetosphere, J. Geophys. Res., 81, 1350-1360, 1976.

140. Shawhan, S. D., Goertz, C. K., Hubbard, R. F., Gurnett, D. A., Joyce, G., Io - accelerated electrons and ions, in The Magnetospheres of Earth and Jupiter, V. Formisano (ed.), D. Reidel Publ. Co., Dordrecht, Holland, pp. 375-389, 1975.

141. Simpson, J. A., Hamilton, D., Lentz, G., McKibben, R. B., Mogro-Campero, A., Perkins, M., Pyle, E. D., Tuzzolino, A. J., and J. J. O'Gallagher, Science, 183, 306, 1974a.

142. Simpson, J. A., Hamilton, D. C., McKibben, R. B., Mogro-Campero, A., Pyle, K. R., Tuzzolino, A. J., The protons and electrons trapped in the Jovian dipole magnetic field region and their interaction with Io, J. Geophys. Res., 79, 3522-3544, 1974b.

143. Simpson, J. A., McKibben, R. B., Dynamics of the Jovian magnetosphere and energetic particle radiation, in Jupiter, T. Gehrels (ed.), U. Ariz. Press, 738, 1976.

144. Siscoe, G. L., Chen, C.-K., Io, a source for Jupiter's inner plasmasphere, UCLA department of Atmospheric Sciences preprint 1976.

145. Siscoe, G. L., On the equatorial confinement and velocity space distribution of Satellite ions in Jupiter's magnetosphere, J. Geophys. Res., 82, 1641, 1977.

146. Sloanaker, R. M., and J. W. Boland, Observations of Jupiter at a wave length of 10 cm, Ap. J., 133, 649-656, 1959.

147. Smith, E. J., Davis, L., Jones, D. E., Colburn, D. S., Coleman, P. J., Dyal, P., Sonett, C. P., Magnetic field of Jupiter and its interaction with the solar wind, Science, 183, 305-306, 1974a.

148. Smith, E. J., Davis, L., Jr., Jones, D. E., Coleman, P. J., Colburn, D. S., Dyal, P., Sonett, C. P., Frandsen, A. M. A., The planetary magnetic field and magnetosphere of Jupiter: Pioneer 10, J. Geophys., 79, 3501-3513, 1974b.

149. Smith, E. J., Davis, L., Jones, D. E., Coleman, R. J., Colburn, D. S., Dyal, P., Sonett, C. P., Jupiter's magnetic field magnetosphere and interaction with the solar wind: Pioneer 11, Science, 188, 451-454, 1975.

150. Smith, E. J., Davis, L. R., Jr., Jones, R. E., Jupiter's magnetic field and magnetosphere, in Jupiter, T. Gehrels (ed.), U. Ariz. Press, 788-829, 1976.

151. Smith, E. J., R. W. Fillius, and J. Wolfe, Compression of the Jovian magnetosphere by the solar wind, submitted to JGR, 1977.

152. Smith, R. A., On the Io-modulated Jovian decametric radiation, Ph.D. dissertation, Department of Physics and Astronomy, University of Maryland, College Park, Maryland, 1973.

153. Smith, R. A., Models of Jovian decametric radiation, in Jupiter, T. Gehrels (ed.), U. Ariz. Press, Tucson, 1976, p. 1146-1189.

154. Spreiter, J. R., Alksne, A. Y., , Plasma flow around the magnetosphere, in Magnetospheric Physics, D. J. Williams and G. D. Mead (eds.), Vol. 7, pp. 11-50, Washington, D.C., Amer. Geophys. Union, 1969; Rev. Geophys., 7, 11,

155. Stansberry, K. G., White, R. S., Jupiter's radiation belts, J. Geophys. Res., 79, 2331-2342, 1974.

156. Swartz, W. E., R. W. Read, and T. R. McDonough, Photoelectron escape from the ionosphere of Jupiter, J. Geophys. Res., 80, 495, 1975.

157. Teegarden, B. J., McDonald, F. B., Trainor, J. H., Webber, W. R., Ruelof, E. C., Interplanetary MeV electrons of Jovian origin, J. Geophys. Res., 79, 3615, 1974.

158. Thomsen, M. F., C. K. Goertz, and J. A. Van Allen, On determining a diffusion coefficient from the observed effects of Jupiter's satellite Io, EOS, 57, 991, 1976.

159. Thorne, K. S., Dependence of Jupiter's decimeter radiation on the electron distribution in its Van Allen belts, Radio Sci., 69D, 1557-1560, 1965.

160. Trafton, L., Detection of a potassium cloud near Io, Nature, 258, 690-692, 1975.

161. Trafton, L., Parkinson, T., Macy, W., Jr., The spatial extent of sodium emission around Io, Ap. J., 190, L85-L89, 1974.

162. Trainor, J. H., McDonald, F. B., Teegarden, B. J., Webber, W. R., Roelof, E. C, Energetic particles in the Jovian magnetosphere, J. Geophys. Res., 79, 3600-3613, 1974a.

163. Trainor, J. H., Teegarden, B. J., Stilwell, D. E., McDonald, F. B., Roelof, E. C., Webber, W. R., Energetic particl population in the Jovian magnetosphere: A preliminary note, Science, 183, 311-313, 1974b.

164. Trainor, J. H., McDonald, F. B., Stilwell, D. F., Teegarden, B. J., Webber, W. R., Jovian protons and electrons: Pioneer 11, Science, 188, 462-465, 1975.

165. Van Allen, J. A., The geomagnetically trapped corpuscular radiation, J. Geophys. Res., 64, 1683-9, 1959.

166. Van Allen, J. A., High-energy particles in the Jovian magnetosphere, in Jupiter, T. Gehrels (ed.), U. Ariz. Press, 928-960, 1976.

167. Van Allen, J. A., Baker, D. N., Randall, B. A., Sentman, D. D., The magnetosphere of Jupiter as observed with Pioneer 10. 1. Instrument and principal findings, J. Geophys. Res., 79, 3559-3577, 1974.

168. Vasyliunas, V. M., Modulation of Jovian interplanetary electrons and the longitude variation of decametric emissions, Geophys. Res. Letters, 2, 87-8, 1975.

169. Warwick, J.W., The position and sign of Jupiter's magnetic moment, Astrophys. J., 137, 1317, 1963.

170/ Warwick, J. W., Radio emission from Jupiter, Ann. Rev. Astron. Astrophys., 2, 1-22, 1964.

171. Warwick, J. W., Radiphysics of Jupiter, Space Science Rev., 6, 841-891, 1967.

172. Weber, E. J., Davis, L., Jr., The angular momentum of the solar wind, Astrophys. J., 148, 217, 1967.

173. Wolfe, J. H., Mihalov, J. D., Collard, H. R., McKibbin, D.D. Frank, L. A., Intrilligator, D. S., Pioneer 10 observations of the solar wind interaction with Jupiter, J. Geophys. Res., 79, 3489-3500, 1974.

174. Wu, C. S., Modulation of the Jovian decametric radio emissions by Io, Astrophys. J., 186, 313, 1973.

TOWARDS A COMPARATIVE THEORY OF MAGNETOSPHERES*

by

G. L. Siscoe**

Department of Atmospheric Sciences
University of California
Los Angeles, CA 90024

May 1977

Chapter 1

The Contemporary Basis for a Comparative Theory of Magnetospheres

A magnetosphere is an astrophysical entity that arises whenever a self gravitating system posesses a magnetic field that interacts with one or more populations of charged particles. The magnetosphere is the region of space in which the magnetic field dominates in determining the characteristics of the particles. That a definition this general can be useful is due to a recognition, acquired gradually over two decades, that fundamental physical attributes are shared by such systems.

There is growing evidence that magnetic organization is common in the universe. To obtain a definite perspective, it is useful to compare magnetic organizations of matter, that is magnetospheres, with gravitational organizations of matter in the universe. The observations suggest that the two classes are roughly equivalent in terms of the volume of space that each organizes, at least in the size range from individual gravitating bodies to galaxies.

Of course, gravitationally organized matter tends to be more visible and is a richer source of information than the other. Because of this, greater importance attaches to it. But even here the situation is changing in the direction of equality. Intrusive probing of solar system magnetospheres by instrumented spacecraft provide in situ observations of their interiors from which their three dimensional structure and behavior can be obtained directly. Except for atmospheres

the interior properties of gravitationally organized matter are revealed by indirect or theoretical means. Magnetically organized matter tends to radiate at wavelengths between microwave and radio - with some well known and exciting exceptions. Large ground-based and satellite-born instruments are required to see at these wavelengths. The potential for increasing the sensitivity and expanding the capabilities of these types of instruments in the future is very great, and it will most likely happen. It is entirely possible that when it does, we will be presented with a flood of data on magnetospheres of stars, nebulae, galaxies, and planets of other stars. Even with existing instruments, galactic magnetospheres can be seen.

The exceptions alluded to above are pulsars which have magnetospheres that radiate from x-ray to radio wavelengths. Since the only information on the physical conditions at these exotic objects comes from interpretations of their magnetospheric radiations, it is important to explore the possible kinships between them and the more accessible solar system examples where the same types of interpretations can be checked. It is the possibility of finding a common framework uniting objects as disparate as planets, pulsars and galaxies that provides the scientific interest in a comparative study of magnetospheres.

The solar system, an accessible mesocosm of diverse magnetospheres, is a natural place to begin such a study. The focus of this review is restricted to planetary magnetospheres, where direct comparisons between theories and observations are now possible, and where there is a high probability that opportunities for significant comparisoms will continue to occur in the futuer. Only in this way can a solid, i.e. observationally tested, theory of comparative magnetospheres be achieved.

Chapter 2

An Overview of the Present State of Knowledge of Planetary Magnetosphere

Our purpose here is to consider the magnetospheres of the planets as a family of related objects, as planetary examples of the magnetic organization matter. We will bias the discussion in terms of the viewpoint to be developed quantitatively in the next section, that planetary magnetospheres are specific realizations of a continuous evolutionary sequence or hierarchy of possible magnetospheres. The variables defining the ordinates of the continuum are the independent solar wind and planetary variables affecting magnetospheric structure and processes. The existent planetary examples of magnetospheres can be thought of as windows through which the evolutionary sequence can be viewed. In some instances the windows lie close together and the evolutionary progression can be seen in relatively small changes in homologous features. In other cases they are widely separated. Then homologous features tend to lose their resemblance and new emergent features and processes can appear. It is necessary also to introduce another category of magnetospheric phenomena which we will label accidental. These consist of all items that can not be thought of as being specific realizations of an evolutionary sequence defined by the continuous variation of a governing parameter. Examples

are all of the satellite effects in the magnetospheres of the outer planets that are contingent upon the accidental positions and idiosyncracies of the satellites themselves. Thus in this scheme,a magnetospheric feature or process is either evolutionary or accidental. One of our problems will be to identify the evolutionary links between the planetary magnetospheres and to recognize emergent and accidental features and processes.

A major cause of the variety that we observe is a dynamic range of 30 million in the magnetic dipole moments of the planets. It is illustrated by the comparison of sizes shown in Figure 2.1. If we examine the figure in terms of the usual grouping of four inner terrestrial planets and four outer giant planets, we see that the magnetospheres of the outer planets are typically one and a half orders of magnitude larger than the planets themselves and each one completely engulfs the orbit of at least one major satellite. The magnetospheres of the inner planets are comparable in size to the planets - with the interesting exception of Earth. In terms of the relative sizes of magnetosphere and planet, Earth resembles the outer planets.

Figure 2.2 shows a typical representation of the structure of Earth's magnetosphere and identifies its main features. The sizes of the other inner planets relative to their magnetospheres is indicated by the superimposed circles. The magnetospheres of Mercury, Venus and Mars are characterized by the dominating presence of the planet itself.

Mercury with a subsolar stagnation point half a planetary radius above its surface nearly fills a scaled down replica of Earth's magnetosphere almost precisely as suggested by the figure (1,2). Its small size implies a quick response to solar wind changes. A characteristic

time for magnetospheric processes at Mercury is minutes compared to hours at Earth (3). Particle acceleration events with a time scale of the order of minutes have been observed in Mercury's magnetosphere (4). Because the regions homologous to the radiation belts and the plasmasphere of Earth lie inside the planet's surface, these features are absent. The lunar-like surface and the lack of an appreciable ionosphere make it likely that the contact conductivity between Mercury and its magnetosphere is small (5). Magnetospheric coupling to the planet is therefore very different at Mercury than at Earth where field-aligned currents can close in the conducting ionosphere to provide strong electrodynamic coupling.

Venus presents an example of a planetary magnetosphere in which the dominant interaction occurs between the solar wind and the planet's ionosphere. The interior features of such a magnetosphere are largely unknown, a condition the Pioneer-Venus-Orbiter mission in 1978 is intended to remedy (but see Ref. 11). Atmospheric origins have been inferred for exterior features observed by Mariner and Venera spacecraft, such as regions of depleted superthermal electrons in the magnetosheath and a thick trailing viscous boundary layer (6-9). The possibility of a significant absorption of the solar wind by the atmosphere has also been suggested to account for bow shock positions that appear to be anomalously close to the planet (10).

However, the exact status of Venus in the hierarchy of planetary magnetospheres is uncertain at present because ambiguities in the existing data on the planetary magnetic field have resulted in very different estimates for the value of the intrinsic dipole moment (12). They range from a value so low that the interior field makes essentially no contribution to the plasma and magnetic structure around the planet to a value large enough that the interior field is comparable to the field

induced by the interaction. If the first case is correct, Venus represents perhaps the only example of a planet experiencing a pure atmospheric interaction with the solar wind. In the second case, it represents the extreme limit of a continuum of magnetic interactions in which the field becomes so weak that the force of the solar wind is opposed mainly by contact with the physical material of the planet, in this instance the planet's ionosphere. In either case the atmosphere exerts an overwhelming control over plasma and magnetic structures. This is a special and perhaps unique condition in the solar system.

There is also at present an uncertainty concerning the actual field strength at Mars. Data interpretations support both the position that it is large enough to stand off the solar wind well above the atmosphere (13) (the case illustrated in Figure 2.2) and the position that the solar wind interacts directly with the atmosphere (11). In the second case the Venus and Mars situations are very similar. However, if the finite magnetic field interpretations are correct in both cases, then the position of Mars in the hierarchy of planetary magnetospheres is located between Venus and Mercury. (For the sake of the present comparison we have implicitly assumed that the hierarchy of planetary magnetospheres is one dimensional. As we shall see later, it is not.) To keep the example of a finite magnetosphere for comparative purposes, we adopt the finite field position, without implying a judgement of validity. Mars apparently possesses a plasma feature analogous to the plasma sheet of Mercury and Earth (14). However, more like Venus, a large contact conductivity and consequent strong coupling between Mars and its magnetosphere provided by the presence of an ionosphere, combined with the relatively dominating size of the planet imply a higher degree of planetary control over the magnetosphere at Mars than at either Mercury or Earth. Theoretical considerations of this condition suggest important modifications to an Earth-type magnetosphere are needed to describe the situation at Mars (5, 136).

The jump from Mercury, Venus and Mars to Earth is a big one. The size of the magnetosphere relative to the planet increases by an order of magnitude. There is an associated emergence of major new magnetospheric features: the radiation belts and the plasmasphere. The second of these is the first manifestation of planetary rotation that we have encountered in our progression toward more fully evolved magnetospheres. Earth is also the first planet in this progression for which strong radio emissions of magnetospheric origin have been detected (17). Another jump, comparable to the last in terms of magnetosphere to planet size ratio, takes us to the outer planets.

The magnetosphere of Jupiter is enormous, and the spin rate of the planet is rapid. Thus, at Jupiter the rotational influence first noted at Earth has increased to dominating importance. We have here the possibility of feeding important amounts of rotational energy into magnetospheric motions and ultimately into dissipation. The energy can be transferred either through the action of centrifugal force on magnetospheric matter (18-22) or by frictional coupling to the solar wind (23). By contrast the sole source of energy for the major magnetospheric processes of the inner planets is the sun through the action of the solar wind or through the action of atmospheric motions. The suggestion of a significant Jupiter source of energy for magnetospheric motions has an interesting correspondence to Jupiter's internal source of energy for atmospheric motions.

The presence of important centrifugal force effects at Jupiter has been inferred from the magnetometer and energetic particle data returned by the Pioneer 10 and 11 spacecraft (24). The rotational characteristics of equatorial distension and flattening result in a centrifugal distortion of the shape of magnetosphere, perhaps similar to the illustration in Figure 2.3.

The blow-up of the interior region in the figure shows the existence of two low energy plasma features. The outer one is perhaps extended into a plasma disc by the centrifugal force. At present the origin of these features is uncertain. The ionosphere of Jupiter and the satellites Io and Europa are possible sources of ions for these regions. A plasmasphere with ions originating from the ionosphere of the planet has been theoretically predicted for Jupiter (27,28). (To restate this in the present context, Earth's plasmasphere has been projected theoretically up the hierarchy of planetary magnetospheres to Jupiter.) The predicted plasmasphere has properties similar to those ascribed to the outer plasmasphere, but the presence of Europa in this feature raises the question of an alternate source. However, the main point for the subject of comparative magnetospheres is that the theoretically projected plasmasphere becomes detached from the planet when centrifugal force becomes important. Thus the topology of the plasmasphere changes radically from Earth to Jupiter.

The suggested outward, disc-like extension of the outer plasmasphere is consistent with a rotationally driven outward radial transport of the material in this region, perhaps by flux tube interchange diffusion giving way to a radial wind further out. This is a possible specific form that emergent rotational processes can take in the jump between Earth and Jupiter.

If the inner plasmasphere is due to a Jovian ionsophere source, existing theory suggest that it does not arise out of an Earth-type plasmasphere by a direct line of magnetospheric evolution. Some sort of new emergent physical process is required (29). If it originates with Io, it is an accidental, non-evolutionary feature (30).

In either case Jupiter's inner plasmasphere represents the appearance of a new phenomenon in the progression of magnetospheric evolution.

The aspect of significant satellite effects is peculiar to the magnetospheres of the outer planets. The well-known modulation by Io of the decametric radio emission of Jupiter is the earliest evidence of this. More recently the co-orbiting gas clouds of Io and Titan and perhaps other satellites have been realized to be the source of magnetospheric ions through photoionization (30-32,72). The location of Io in the inner magnetosphere of Jupiter and of Titan in the outer magnetosphere of Saturn (according to the present estimate) point up possibilities for qualitatively different magnetospheric phenomena resulting from these ions. For example, a difference can be expected due to the change from magnetic to centrifugal domination between the inner and outer magnetosphere. Another satellite effect, predicted in advance and confirmed by the Pioneer 10 and 11 spacecraft, is that satellites can be both sources and sinks of energetic particles in the magnetosphere (24). These few examples serve to illustrate that the presence of satellites which are the size of terrestrial planets within the magnetospheres of the outer planets greatly enriches the possible varieties of magnetospheric phenomena to be expected there.

The magnetosphere of Jupiter is also distinguished by the presence of intense trapped particle radiation belts. It seems clear that Jupiter's radiation belts are linked to those of Earth in a way that we are here calling evolutionary. But in this case the jump is a big one and important differences may have emerged in the gap. The Pioneer 10 energetic particle data have been interpreted with some success in terms of the physics of radial diffusion and stable trapping, as

developed in connection with the radiation belts of Earth, but satellite collisional losses, peculiar to the outer planets, need to be included (33). Other important differences have also already been suggested. In the case of Earth the energy to drive the radial diffusion comes from the solar wind in the form of impulsive pressure changes and impulsive convection. These processes do not appear to be effective enough at Jupiter to account for the rate of radial diffusion there. Instead, winds in Jupiter's ionosphere seem to be responsible (33-35). The detection by the Pioneer spacecraft of significant numbers of electrons with energies well above the upper limit imposed by a solar wind source and subsequent diffusion under constant first adiabatic invarient is another indication of an emergent evolutionary process (33). An ionospheric source and internal recycling have been invoked to account for these particles (36,37). The spin synchronous release of energetic particles into the interplanetary medium is an emergent process, which might have its origin in the relatively larger strength of the non-dipolar components of the planetary magnetic field at Jupiter (37-39).

The synchrotron radio emission from Jupiter's radiation belts is automatically contained in the magnetospheric hierarchy once the magnetic field and the radiation belts themselves are specified. The hierarchial status of the sporadic magnetospheric radio bursts is not as clear. Such bursts have been detected from Earth (17), Jupiter (40), Saturn (41), and, possibly from Uranus (42). It is very plausible that they are due to a common type of magnetospheric process whose evolution between the stated planets involves no emergent aspects. Specific scaling relations based on this assumption have been proposed to relate characteristics of these emissions to the strength of the planetary magnetic field (43,44).

They will meet their test in the coming spacecraft encounters with Saturn and Uranus.

Saturn is subjected periodically to an accidental experience that is probably unique among the planets. For an interval of about one month centered around the inferior conjunction of Jupiter with respect to Saturn, the tail of Jupiter's magnetosphere is most likely extended by the solar wind far enough to completely engulf Saturn. A similar thing happens at Earth each month when the moon passes through the Earth's magnetic tail. But Saturn has a strong magnetic field (as inferred from the observed radio emissions) and therefore also a large magnetosphere. The consequences of this unique type of interaction have only begun to be considered.

If Uranus has a magnetic field, this planet has an especially important role to play in the subject of comparative magnetospheres. Its spin axis lies nearly in the ecliptic plane, and twice each Uranian year it points to within 8 degrees of the sun. If like all known examples its magnetic field is a near-spin-aligned dipole, for a few years out of every forty, Uranus would possess the only example of a 'pole-on' magnetosphere in the solar system (45). (It is not actually necessary that the dipole be spin-aligned for a pole-on magnetosphere to occur because the special spin orientation of Uranus causes every point on its surface to face the sun twice each orbital revolution (46). However, it is <u>a priori</u> most likely that the dipole would be spin-aligned.) The existence of this possibility needs to be stressed because of the central role played by the planetary dipole moment in the comparative

study of magnetospheres. A magnetic dipole is a vector quantity, possessing both a magnitude and a direction. The effect of magnitude variations on magnetospheric structure and processes is well illustrated by planetary examples covering a dynamic range of 30 million. However, the effects of variations in the orientation of the dipole are poorly known due to the restricted range of this variable in the sampled planets. Earth exhibits a typical range of dipole orientations, having a combined diurnal and annual oscillation of 35 degrees. With Uranus we can explore the full range. A simple extension of an Earth-type magnetosphere to a pole-on orientation is shown in Figure 2.4. A stringent test for an evolutionary theory of planetary magnetospheres would be to account for actual observations made in a pole-on magnetosphere.

The outer planets are far enough from the sun for solar wind characteristics to be significantly altered compared to 1 AU. It is now clear that because of the presence of the large scale structures called streams, the simple extrapolation of solar wind parameters from 1 AU to the outer solar system assuming time independence and spherical symmetry gives wrong results (48). By Jupiter and beyond nearly all streams have produced a pair of shock waves, one traveling out and one in relative to the center of the stream (48,49). The shock waves greatly amplify the range of the density and temperature variations associated with the stream structure. This results in a greater range in the external boundary conditions on the magnetospheres of the outer planets compared to the inner planets.

At the outer planets there are possibly magnetospheric effects from the interaction of the solar wind with the interstellar medium, and at Uranus and Neptune, from the presence of the interstellar medium itself.

Beyond Jupiter the solar wind should be modified by the interaction either by being heated or by acquiring a super-thermal ion component.(50,51). The magnetospheric consequences of these modifications have yet to be considered. In the direction of the sun's motion through the local medium, the interstellar neutral hydrogen penetrates into the solar system essentially undiminished to the orbit of Uranus (52). When Uranus and Neptune are in the portions of their orbits that are exposed to the interstellar wind, photoionization of the neutral hydrogen could be an important source of ions in their magnetospheres.

Table 2.1 summarizes qualitatively the evolutionary and accidental aspects of planetary magnetospheres. In the next section we will attempt to make these qualitative characterizations more quantitative. For this we need to identify explicitly the controlling independent variables. These will include planetary, satellite, solar wind, and interstellar parameters. Magnetospheric features and processes then need to be described in terms of dependent variables that can be derived from the independent ones. The possible superficially distinct regimes that can be occupied by planetary magnetospheres (for example, magnetospheres with strong dissipative planetary control, like those of Venus and Mars; small planetary control - Mercury and Earth; strong rotational planetary control - Jupiter; etc.) can then be classified in terms of the largeness or smallness of appropriate dimensionless ratios formed from the dependent and independent variables. The number of independent dimensionless ratios needed to separate superficially distinct regimes (a subjective judgement) determines the dimensionality of the hierarchy of planetary magnetospheres.

PLANET	MAGNETOSPHERIC FEATURES AND PROCESSES
Venus	Bow Shock Magnetosheath Atmospheric Control Dominant Marked atmospheric features
Mars	Emergent Magnetopause Atmospheric Control Strong Plasma Sheet Present
Mercury	Planetary Control Weak Time Dependent Processes and Energetic Particle Events
Earth	Plasmasphere Emergent rotational feature Trapped Particle Radiation Belts Magnetospheric Radio Bursts
Jupiter	Strong Rotational Effects Detached plasmasphere Centrifugal distortion Centrifugally driven mass transport(?) Emergent Trapped Radiation Processes Radial diffusion due to winds Super-energetic electrons atmospheric source(?) recycling(?) Spin-synchronous Ejection non-dipole field components(?) Emergent Inner Plasmasphere(?) Satellite Effects Accidental inner plasmasphere(?) Source and sink for energetic particles Modulation of radio bursts Source for centrifugally driven wind(?)
Saturn	Periodic Immersion in Jupiter's Magnetospheric Tail
Uranus Neptune	Example of Pole-on Magnetosphere(?)

Magnetosphere much larger than planet

Change in solar wind characterized by corotating shocks and large density and temperature variations

Detectable effects of the solar wind interaction with the interstellar medium

Direct effects of the interstellar medium

Table 2.1 A summary of known and suspected evolutionary and accidental features and processes of planetary magnetospheres. Emergent items are mentioned only for the first known example. Thus, most of the items listed for Jupiter apply to the outer planets generally. The dashed extension of the right hand column is to indicate that although the interstellar hydrogen density is somewhat reduced at Saturn and Jupiter, it might never-the-less be large enough to have an effect.

TYPE	VARIABLE
Planetary	Magnetic Parameters Strength and orientation of the dipole moment Relative importance of nondipolar components Radius Magnitude and Orientation of Spin Vector Contact Conductivity (surface or atmosphere) Ion flux from Ionosphere to Magnetosphere
Satellite	Orbital Parameters Intrinsic Magnetic Parameters Contact Conductivity Neutral Atmosphere Parameters
Interplanetary	Solar Wind Velocity (speed and direction) Solar Wind Mach Number Solar Wind Density Interplanetary Magnetic Field Vector Solar Cosmic Rays
Interstellar	Galactic Cosmic Rays Neutral Particle Density Interstellar Wind (speed and direction) Ions of Interstellar Origin Magnetic Field Vector

Table 3.1 A list of spatially distinct sources, sinks and boundary conditions for magnetospheric features and processes.

Chapter 3

Independent Variables Affecting Planetary Magnetospheres:

The previous section identified four spatially separate categories of physical parameters that act as sources, sinks and boundary conditions for magnetospheric phenomena. They are listed again in Table 3.1 along with some of the specific parameters belonging to each one. The large qualitative range of magnetospheric behavior is, of course, due to the actual range of numerical values that exists for these parameters. The known and estimated values for the planetary parameters are summarized in Table 3.2

It is primarily because of the existence of measured values and reasonable estimates in the column marked 'Dipole Moment' that the subject of comparative magnetospheres is possible. This prerequisite has existed only recently due to the in situ measurements at Mercury, Venus, Mars and Jupiter, and the observed radio emissions from Saturn characteristic of a magnetosphere. Although characteristic radio emissions may also have been received from Uranus, the values of the dipole moments given in the Table for this planet and for Neptune are based on an empirical relation that seems to organize the relative strengths of the known dipole moments remarkably well. This so-called 'magnetic Bode's law expresses the observed approximate linearity between the dipole moment and the spin angular momentum of a planet (64). It is illustrated in Figure 3.1 (65). The sun is also encompassed in its extension. The low angular momentum examples in the figure show the largest scatter from the linear trend, but the trend is still evident if they are taken as a group. It is perhaps significant that the organization present in the figure is more closely attuned to the Earth-Moon system than to Earth alone. The values of the dipole moments for Uranus

	SOLAR DISTANCE (AU)	RADIUS R_p (10^3 km.)	ANGLE (a) ($\overline{\Omega}$, NEP)	SPIN PERIOD	SYNCH. (b) R_p	CONTACT CONDUCTIVITY Σ (c) (mhos)	ION FLUX (g) IONOSPHERE to MAGNETOSPHERE
Mercury	0.4	2.49	< 7	58.6d	100	$\lesssim$ 0.1 (5)	~ 0
Venus	0.7	6.10	~ 179	243d	254	> 1000 (d)	?
Earth	1.0	6.37	23.5	24h	6.6	10 (55)	6×10^{26} (56)
Paleo-Earth	"	"	22 to 24	$\lesssim$ 24h	$\lesssim$ 6.6	3 - 100 (e)	6×10^{26}
Mars	1.5	3.38	25	24.5h	6.0	3000 (5)	8×10^{25}
Jupiter	5.2	71.4	3.1	10h	2.3	0.4 (28)	3×10^{27} (18, 57)
Saturn	9.5	60.4	26.7	10h	1.9	0.2 (f)	6×10^{26}
Uranus	19.2	23.8	97.9	~24h(h)	4.5	0.1 (f)	2×10^{25}
Neptune	30.0	22.2	28.8	~24h(h)	4.5	0.07 (f)	9×10^{24}

Table 3.2a Measured and estimated values for planetary parameters affecting magnetospheres. (A) Non-magnetic parameters: Solid planet and astronomical parameters from Refs. 53 and 54. (a) Angle between spin axis and north ecliptic pole. (b) Ratio of synchronous orbit radius to the planetary radius. (c) Estimated height integrated Pederson conductivity. (d) Assumed to be probably greater than the value for Mars. (e) Based on the range of variation of the strength of the dipole moment. (f) Based on the value of Jupiter reduced by the ratio of heliocentric distances (28). (g) Dayside hemispheric flux based on a value of 2.5×10^8 cm^{-2} sec^{-1} at Earth (56) and reduced by the square of heliocentric distance ratio for the other planets, except for Mercury where there is a negligable ionosphere, and Venus where there is no dayside magnetosphere. (h) Most recent determinations - M. Belton, private communication.

	DIPOLE MOMENT Mp ($G - cm^3$)	EQUATORIAL SURFACE FIELD	POLARITY (c)	ANGLE (d) ($\bar{\Omega}$, M) (deg.)	RATIO (e) NONDIPOLE DIPOLE n = 2 n = 3	$\frac{Rm}{Rp}$ (f)
Mercury	5×10^{22}(1)(h)	350γ	N R	~ 10 <<90		1.6
Venus	6.5×10^{22}(R) (12) (a) < 8×10^{21}(D)(58)	30γ 4γ				1.1
Earth	8.05×10^{25}	.31G	N	11.5	0.14 0.09(62)	11
Paleo-Earth	≲ 8×10^{24} to 3×10^{26} (59)	.03 to 1G	N&R	~ 11	~ 0.1 to ~ 1.0(63)	3 - 16
Mars	2.5×10^{22}(13) (g)	65γ	R	< 20		1.4
Jupiter	1.5×10^{30}(60, 61)	4.1G	R	10	0.24 0.21(61)	50
Saturn	2.2×10^{29}(43) (b)	1.0G				40
Uranus	1.9×10^{28}(b)	1.4G				50
Neptune	1.4×10^{28}(b)	1.3G				50

Table 3.2b Magnetic parameters: (a) The two values for Venus result from different interpretations of existing magnetic data at Venus, one giving a definite estimate for the value, the other an upper limit. (b) Obtained by the "magnetic Bodes law" -- see text. (c) Polarity designations are based on paleomagnetic usage of normal (N) and reverse (R), the first applies when the north magnetic pole lies in the same hemisphere as the south rotational pole. (d) The angle between the magnetic and rotational axes. (e) The ratio of the surface strengths of the non-dipole to dipole components of the planetary magnetic field, n = 2 is the quadrupole and n = 3 the octupole component. The numbers for Paleo-Earth refer to the total nondipolar field. (f) Ratio of the distance between the solar wind stagnation point and the planet's center (R_m) to the planetary radius. (g) The finite magnetic field interpretation of the Russian Mars data (see Ref. 11). (h) Initial estimate. Recent studies suggest a factor of 2 reduction (118, 194).

and Neptune adopted from this figure are to be taken in a special way. They are values suggested by the best available empirical sense of the way in which dipole strengths vary between planets.

The factor of 2 range around the central value of the dipole moment given for Earth in the figure is the characteristic variation (or standard deviation) of the paleomagnetic dipole field over the last 8 million years as inferred by geologists (59). Paleo-Earth is listed as a separate planet in Table 3.2 because the magnetosphere of Earth at times in the past was very different than at present. Knowledge of the paleomagnetic field is good enough to enable such paleomagnetospheres to be constructed with the tools provided by the evolutionary approach to the theory of planetary magnetospheres.

The presence of many missing entries in the table point up the need both for more extensive in situ measurements and for extended theoretical work.

The properties of the natural satellites in the solar system have been well reviewed elsewhere (28,66). To illustrate the primary satellite effects on magnetospheres, we will restrict attention to the major companions of the outer planets. Their orbits all lie entirely inside the estimated nominal magnetospheres. The main parameters of interest here are listed in Table 3.3. Because of their accidental nature, satellite effects will be de-emphasized in the discussion of evolutionary aspects given below. So we shall discuss them more fully here before going on to the next category in Table 3.1

The simplest effect to appreciate is absorption of magnetospheric particles by the satellites. The Pioneer missions revealed absorption signatures in energetic particle fluxes at Io, Europa and Ganymede (and

	Distance in Units of Rp	Distance in Units of Rm	λm (deg) (a)	Orbital Speed (km/sec)	Corotational Speed (km/sec)	Δv (km/sec) (b)	Max Proton Rot. K.E. (eV) (c)	Radius (km)	Rot. Elct. Potential (kV) (d)	Atmosphere	Torus (e)
Jupiter											
Io	6.0	0.12	66	17.3	76.4	59.1	96	1820	408	Yes	Yes
Europa	9.6	0.19	71	13.8	122	108	278	1550	155	?	?
Ganymede	16	0.32	75.5	10.9	201	190	803	2635	100	Yes (?)	?
Callisto	27	0.54	79	8.2	348	340	2485	2500	35	?	?
Saturn											
Titan	20	0.54	77	5.6	209	203	891	2500	13	Yes	Probably
Neptune											
Tritan	14.3	0.33	74.5	(-4.4)	40.2	44.6	38	2000	8	?	?

Table 4

Table 3.3 Magnetospherically important physical properties of the major satellites of the outer planets. (a) The dipole latitude on the planet of the field line linking the satellite. (b) The corotational speed in the satellite's frame of reference. (c) The maximum corotational energy picked up by a proton that starts from rest in the satellite's frame of reference. (d) The potential across the satellites diameter of the motional electric field based on the corotation speed in the satellites frame of reference. (e) A corotating neutral gas cloud derived from the satellite's atmosphere. (Based on a table in Ref. 28).

also Amalthea) (24). The absorption phenomena were highly structured in energy, pitch angle, space and/or time and also were very dependent on particle species. The signatures are most pronounced for Io, but they are also distinct for Ganymede and Europa. Effects associated with Io include energy dependent depletions of protons and electrons and modification of the proton pitch angle distribution across its orbit. The signatures of Europa and Ganymede were more position dependent. On separate crossings of Ganymede's orbit, electron fluxes exhibited both huge decreases in all energies sampled and then almost no change at all but high frequency structure in the lowest energy channel. Bursts of 1 MeV protons were also observed near Ganymede's orbit and possibly indicate a local acceleration process in some way controlled by the presence of the satellite. The inbound intersection of Pioneer 10 and Europa's orbit coincided with a small decrease in proton fluxes ($E \sim 1$MeV) and a larger decrease in low energy electron fluxes ($E \sim 0.1$ to 5MeV). The outbound intersection and also the Pioneer 11 intersections exhibited either no signature or high frequency structure. The different satellites at different times and/or locations appear to be capable of removing protons and electrons in specific energy and pitch angle ranges. The resulting modified particle distributions in phase space have been used as tags for following diffusion processes (67). They might also initiate instabilities leading to particle accelerations, the high frequency structure that was observed, and possibly radio emissions.

This brief summary serves to show that the satellites can significantly modify energetic particle characteristics, although in some respects the modifications at Jupiter were less severe than anticipated (33). In comparing radiation belt features between planets, caution will be needed to separate emergent and accidental differences.

We turn next to the lower energy particles. The outer boundary of the inner plasmasphere is slightly beyond the orbit of Io. It has been suggested that Io produces the boundary by absorbing the particles (26). But at the orbit of Io itself, there is a local peak in the radial profile of density, suggestive more of a source there. Also Europa does not seem to have a similar effect upon the outer plasmasphere. There is direct evidence that Io is a source of some magnetospheric particles. A spike of low energy (E>160KeV) electrons was observed just inside its orbital radius (68), and also a large spike of medium energy electrons (E>460KeV), apparently associated with the Io flux tube (69). A cloud of ionized sulfur (SII) has been detected in Jupiter's magnetosphere by means of ground based optical measurements (70,71). The cloud is related to the orbit of Io in a way that is consistent with a source at Io and subsequent co-rotational transport in Jupiter's magnetosphere. The well known co-orbiting clouds of neutral hydrogen and sodium must also be sources of magnetospheric ions through photoionization and electron impact ionization. These undoubtedly make important contributions to magnetospheric features and processes (72,30,31).

A satellite will necessarily be a source of low energy magnetospheric charged particles if it has an atmosphere. The efficiency of the source is greatly increased by the existence of a co-orbiting gas torus, which is probably also a necessary consequence of an atmosphere (73). The columns labelled "Atmosphere" and "Torus" in Table 3.3 are therefore especially important, and they have been expanded into Table 3.4. Io is known to have an atmosphere both from the emissions of the associated gas clouds and from the radio occultation data obtained by Pioneer 10 (31,74). The derived atmospheric parameters for Io are model

	Neutral Parameters	Ionosphere Parameters	Torus Parameters
Io	Surface Density 10^9 to 10^{12} cm^{-3} Primary Component NH_3 or Ne Surface Pressure 10^{-8} to 10^{-10} bar (Refs. 74 - 76)	Dayside Peak 6×10^4 el cm^{-3} at 100 km altitude Nightside Peak 9×10^3 el cm^{-3} at 50 km (Refs. 74, 75) Integrated Ionospheric Conductivity (est.) 260 mhos (77)	Neutral Hydrogen total number $\sim 2 \times 10^{33}$ Angular extent $\sim 120^o$ centered on Io Thickness ~ 2 R_J Lifetime $\sim 2 \times 10^5$ sec Required flux $\sim 10^{28}$ sec^{-1} (Refs. 31, 78, 79) Loss process-charge exchange with inner plasmasphere (26, 31, 72, 78 - 80) Proton source strength $\sim 10^{25}$ sec^{-1} (30) Neutral Sodium total number $\sim 5 \times 10^{29}$ to 5×10^{30}, angular extent $\sim$ 1/5 orbit for bright part, faint part extends 23 R_J from Jupiter in thin disc, Lifetime $\sim 10^5$ sec, required flux $\sim 4 \times 10^{24}$ to 4×10^{25} sec^{-1}, loss process-electron impaction-ization (Refs. 81 - 84, 91). Neutral Potassium detected (85) Ionized Sulfur (SII) detected, possibly time dependent, co-rotates with Jupiter, loss process-recombination (70, 71).
Gany-mede	Surface pressure $> 10^{-6}$ bar (85)	?	?
Titan	> 1.6 km amagats of CH_4 5 ± 3 km amagats of H_2 Presence of others (87)	?	Hydrogen torus predicted (73, 88) Flux (est.) $\sim 2 \times 10^8$ sec (?) Total number $\sim 5 \times 10^{35}$ (?) } (90) Proton source strength $\sim 5 \times 10^{26}$ sec^{-1} (?) Loss process - charge exchange (?)

Table 3.4 Measured and estimated atmospheric parameters of the satellites.

dependent which accounts for the large indicated range. The hydrogen torus is a source for protons through photoionization. The strength of this source is about 7×10^{24} sec^{-1}. (Charge exchange, which is the dominant loss mechanism for the neutral hydrogen, is not a source for protons because a fast proton and slow neutral are merely interchanged resulting in a fast neutral that leaves the system and a slow proton that is subsequently accelerated but remains within the system.) In the case of neutral sodium the loss mechanism is most likely electron impact ionization, and so all of the sodium becomes magnetospheric ions. The sodium ion source strength is then the total sodium flux given in the table, which is comparable to the proton source strength. The source strengths for the potassium and sulfur ions are still unknown.

The meager information on the possible atmosphere of Ganymede is based on the interpretation of data from a stellar occultation by the satellite. The inferred surface pressure is several orders of magnitude larger than that of Io. If the interpretation is correct, Ganymede should also have an appreciable neutral particle torus, which could have substantial magnetospheric effects. However, the measurement is difficult, and caution has been urged in accepting the interpretation (66).

The data on Titan's atmosphere result from the interpretation of absorpiton features in its spectrum which suggest a rather massive atmosphere, comparable to that of Earth, composed mainly of methane and hydrogen. The existence of an associated massive hydrogen torus seems a necessity. The prediction of its properties rests on poorly known boundary conditions, and the resulting numerical estimates have large uncertainties. The values given for it in the table are representative order of magnitude estimates. Based on the total number given there,

the proton source strength by photoionization is about 5×10^{26} sec^{-1}, or approximately 100 times that of Io and comparable to the total flux of ions from Saturn's ionosphere. There is likely to be an important, accidental plasma feature in Saturn's magnetosphere from such a source.

A final but very important satellite effect is the electro-dynamic coupling to the planet if the electrical conductivities are high enough. Here again the primary example is Io (42). It is known to have an ionosphere with an estimated height integrated conductivity of 260 mhos (compared to 10 mhos for Earth). The motion of Io relative to the co-rotating magnetic field of Jupiter creates an electromotive (unipolar) potential of about 400 kilovolts, and this increases to about 580 kilovolts when the vertical extent of the ionosphere is included. The strong interaction that is implied by this combination of circumstances has excited a great deal of theoretical interest. The most elaborate model of the interaction produced so far incorporates a plasma sheath around the satellite with a carefully tailored spatial structure (93). Some of the magnetospheric consequences that have been suggested for such an interaction are the acceleration of electrons to a significant fraction of the unipolar potential and a local distortion of the magnetospheric field with an associated production of Alfven waves. The electrons accelerated in this way are field aligned and can precipitate into the Jupiter ionosphere to produce optical and x-ray emissions that should be observable from a spacecraft and radio bursts that may be part of the Io related radio emissions from Jupiter.

The unipolar potentials for the other Jovian satellites decrease with distance away from the planet but remain fairly large. For comparison, we note that the typical potential across the ionosphere of Earth

due to magnetospheric motions is 50 kilovolts. Thus, if any of them possesses a conducting surface or an atmosphere and hence an ionosphere, there could be important magnetospheric consequences. The suggestion of an atmosphere and the bursts of 1 MeV protons near Ganymede give added interest to this possibility. In the case of Titan, although it must be a good conductor because of its atmosphere, the estimated unipolar potential is only 13 kilovolts. The implication is clear that the electrodynamic effects of satellites will be most strongly manifested by Io.

We return now to the next category listed in Table 3.1. The solar wind presents a variable boundary condition to planetary magnetospheres. Variations between the planets result from their different heliocentric distances. At a given planet they result from spatial and temporal variations in the solar wind itself. Average values of solar wind parameters have been derived with data from a number of different spacecraft covering various time periods since 1961. The differences between the averages so derived is small compared to the differences between the planets. Thus, to illustrate the latter we may choose a particular set of averages. The averages for 1969 from the Heos 1 spacecraft have been compiled in a convenient form for our purpose (94). These are the baseline values for Earth boxed off in Table 3.5. To obtain the values at the other planets, we use what might be called a pure radial extrapolation. The solar wind expansion is assumed to be spherically symmetric, time independent, and adiabatic; and the expansion speed is assumed to be constant throughout. In view of the well known violations of these conditions, the entries in the table should be considered order of magnitude estimates. They are quite adequate to

	Radial Speed (km/sec)	Density (cm^{-3})	Proton Temperature (10^{5}°K)	Magnetic Field		Stagnation Field Strength $B_s(\gamma)$	Corotation Speed at Rm (km/sec^{-1})	Intercepted Particle Flux		Intercepted Momentum Flux Total (10^{10} dyne)	Intercepted Energy Flux	
				B(γ)	ψ(°)			Total (10^{26} sec^{-1})	Normalized (cm^{-3} sec^{-1})		Total (10^{17} erg sec^{-1})	Normalized (ev-cm^{-3}sec^{-1})
Mercury	409	26	25	29	22	135	.01	5.4	1.9	3.7	7.4	1.6×10^{5}
Venus	409	8.6	12	11	35	77	2×10^{-3}	4.8	0.38	3.3	6.6	3.2×10^{4}
Earth	409	4.2	7.4	6.0	45	54	5.1	260	1.8×10^{-2}	180	350	1.5×10^{3}
Mars	409	1.9	4.3	3.4	56	36	0.34	0.52	0.12	0.35	0.70	1.0×10^{4}
Jupiter	409	0.16	0.82	0.83	79	10	623	2.5×10^{4}	1.3×10^{-5}	1.7×10^{4}	3.4×10^{4}	1.1
Saturn	409	4.7×10^{-2}	0.45	0.45	84	5.7	422	3.4×10^{3}	5.7×10^{-6}	2.3×10^{3}	4.6×10^{3}	0.48
Uranus	409	1.1×10^{-2}	0.22	0.22	87	2.8	155	135	3.5×10^{-6}	92	180	0.30
Neptune	409	4.7×10^{-3}	0.14	0.14	88	1.8	112	53	1.5×10^{-6}	36	72	0.13

Table 6

Table 3.5 Selected solar wind parameters extrapolated to the various planets from average values at 1 AU (taken from Ref. 94) by the assumption of a constant speed, spherically symmetric, time independent, and adiabatic expansion. (Tables with larger ranges of parameters and with different averages at 1 AU can be found in Refs. 47, 95-98).

illustrate the effect of distance variations, and we will take up separately the question of the distance variation of solar wind structure below.

We see in the table the actual extent of the density and temperature reductions due to the expansion from Mercury to Neptune - factors of 5000 and 300. The field strength over this distance is reduced a factor of 200, and the field spiral tightens from nearly radial to nearly circular. The magnetic field strength needed to stop the solar wind drops from 135γ at Mercury to 1.8γ at Neptune. The other items in the table take account of the estimated sizes of the magnetospheres. Co-rotational speeds at the stagnation points are very small for the terrestrial planets but comparable to the solar wind speed for the giant ones. The total flux of solar wind particles, momentum and energy through circles with radii equal to the stagnation point distances (R_M) - a characteristic magnetosphere cross-section - have their largest values at Jupiter and Saturn, as would be expected. It is interesting that the fluxes intercepted at Earth are larger than at Uranus or Neptune. If these fluxes are normalized by dividing by a characteristic volume for a magnetosphere - a sphere of radius R_M - the flux per unit volume is seen to be much larger for the terrestrial planets.

To convert intercepted fluxes into magnetospheric densities we need to know characteristic magnetospheric time scales and capture efficiencies for the various quantities. These are known approximately for Earth. The capture efficiency for momentum flux (the drag coefficient in aerodynamic parlance) is about 100 per cent for the cross section used in the table (99,100). To say this differently, the solar wind ram force on the magnetosphere is about the same as the solar wind dynamic

pressure acting on a circle of radius R_M. Capture efficiencies for energy and particles based on this cross-section are about 1 per cent and $\lesssim 0.1$ per cent respectively (101-103). The characteristic time scale for Earth's magnetosphere is on the order of one hour. These can be scaled to the other planets by the use of some naive scaling relations to be described below, but the modifications that are bound to be necessary to take account of strong atmospheric or rotational effects have yet to be considered.

As is described in some detail in the companion article on the solar wind, the non-linear evolution of the stream structure seen at 1 AU increases the relative range of variability in the solar wind at distances beyond 1 AU. What was not generally appreciated until fairly recently is that the growth of the relative range (or the increase in the stream-induced contrast) of the density, temperature and field strength is quite remarkable at the distance of the outer planets. The magnetospheric consequences of the resultant condition of persistent extreme variability of the solar wind in the outer solar system have not yet been fully explored. The situation is illustrated by the change in the histogram of solar wind dynamic pressure (which is also essentially the stagnation pressure in the hypersonic solar wind) between the orbits of Earth and Uranus shown in Figure 3.2.At 1 AU, the modal value is not very far from the average value. At 20 AU, it is strongly displaced toward low values. Higher resolution histograms show that the modal value is less the 0.2 of the average. Thus the situation in the outer solar system is characterized by long intervals of very low dynamic pressure punctuated by brief intervals of very high dynamic pressure. The large variation in the location of Jupiter's magnetopause that was observed by Pioneer 10 is probably accounted for by this type of behavior, as was suggested by the experimenters (24).

The last in our list of boundary conditions and sources for planetary magnetospheres is the interstellar medium. It can act both indirectly through modifying the solar wind and directly as a source for magnetospheric ions. Several distinct ways in which it can modify the solar wind have been discussed, such as creating substantial heating, or a superthermal ion component or a shock transition to subsonic flow. To determine the actual situation existing at the planets a more definitive theory or in situ measurements will be required.

Estimates for the numerical values of some of the physical properties of the local interstellar medium are given in Table 3.6. The shape of the cavity around the sun formed by ionization of the interstellar neutrals is shown by the contours in Figure 3.3. Both photoionization and charge exchange with the solar wind are involved in determining the shape of the contours. It also depends upon the ratio of solar light pressure to the force of gravity. This ratio is of the order of unity for hydrogen because of the strong solar Lyman α emission, but it is not precisely known and it can vary over a solar cycle. The contours in the figure are for a ratio of unity. The interstellar hydrogen densities derived from it at the outer planets in the apex direction are representative of the farily narrow spread of values one finds by letting this ratio vary over its expected range.

The estimates of the interstellar neutral hydrogen densities at the outer planets given in Table 3.7 are based on the figure and Table 3.6. With these and the photoionization life times at various planets, we find the associated source strengths for protons in the magnetospheres given in the last column of the table. They are seen to be small by comparison with the solar wind source as given in Table 3.5. However the capture efficiency for solar wind protons must also be considered, and in this is a big uncertainty. For example at Neptune, where the comparison most favors the interstellar source,

Properties of the Local Interstellar Medium at the Outer Planets	
Neutral hydrogen density	0.1 cm^{-3}
Neutral helium density	0.008 cm^{-3}
Electron density	0.03 - 0.12 cm^{-3}
Temperature	100 - 10,000 K
Relative velocity	20 km sec^{-1}
Interstellar H flux	2×10^5 cm^{-2} sec^{-1}
Solar wind change exchange flux	$\sim 10^4$ cm^{-2} sec^{-1}

Table 3.6 Properties of the local interstellar medium. (Adapted from Refs. 47 and 104).

	Neutral H Photoionization Lifetime (sec)	Neutral H Charge Exchange Lifetime in Solar Wind Flux (sec)	Interstellar Neutral H Density (cm^{-3})	Ion Production Rate	
				Total (sec^{-1})	Normalized (cm^{-3} sec^{-1})
Mercury	1.1×10^{6}	5.0×10^{5}			
Venus	3.3×10^{6}	1.5×10^{6}			
Earth	6.7×10^{6}	3.1×10^{6}			
Mars	1.5×10^{7}	7.0×10^{6}			
Jupiter	1.8×10^{8}	8.5×10^{7}	.05	5.3×10^{25}	2.8×10^{-10}
Saturn	6.0×10^{8}	2.8×10^{8}	.07	7.1×10^{24}	1.2×10^{-10}
Uranus	2.5×10^{9}	1.2×10^{9}	.08	1.3×10^{23}	3.2×10^{-11}
Neptune	6.0×10^{9}	2.8×10^{9}	.09	5.5×10^{22}	1.5×10^{-11}

Table 3.7 Neutral hydrogen parameters at the various planets. The ion production rates are based on photoionization of the interstellar density inside a sphere of radius R_m for each planet.

with a particle capture efficiency of 0.1 per cent, the solar wind source is larger by two orders of magnitude. The interstellar source strength at Jupiter is comparable to that of Io's neutral hydrogen ring. But the disparity in spatial scale of these sources must imply very different consequences for the associated plasma features. At Saturn the interstellar source is considerably weaker than the estimate for Titan's torus. However as will be seen later, the exact nature of the radial transport of ions inside a magnetosphere can greatly affect the densities resulting from the various sources.

During many previous epochs in the history of the solar system, the interstellar source has been more important. The local value for the interstellar neutral hydrogen density given in Table 3.6 is an order of magnitude less than the average value within 1 kpc of the sun as determined by measurements from the OAO-2 satellite (105). Also over the life time of the solar system it is statistically probably that 50 or so encounters have occurred with interstellar gas clouds in which the neutral hydrogen density can exceed 100 cm^{-3} (106). Encounters with gas clouds with intermediate densities are, of course, even more common. The magnetospheric consequences of such encounters will be considered in later sections.

The entry "Galactic Cosmic Rays" under the "Interstellar" category in Table 3.1 is another source of particles for planetary magnetospheres. In the case of Earth, it is now known that the decay of cosmic ray albedo neutrons produces the high energy trapped protons in the inner radiation belt (121, 132). In the same way, this mechanism must be a source of high energy protons at other planets, but a systematic, comparative evaluation has yet to be done.

Dependent Magnetospheric Variables - External: That region of space around a planet, lying wholly in the solar wind, in which the bulk flow properties of the solar wind are modified by the presence of the magnetosphere defines the external domain of the magnetosphere. External features include a bow shock with associated upstream disturbances, the region filled by the post-shock flow (the magnetosheath), boundary layers, and wakes. As the terminology indicates, the external domain is usually treated within the framework of continuum fluid mechanics, and especially that part of aerodynamics dealing with supersonic flows past blunt bodies. The aerodynamic approach to providing quantitative models for comparison with observations has been one of the most successful theoretical efforts in magnetospheric physics. (For a recent review of this subject see Ref. 107).

Numerical computer codes exist that calculate the location and shape of the bow shock and the post-shock flow parameters for a given shape of blunt body and for given upstream solar wind conditions. These codes are limited by the assumptions that the magnetic pressure can be neglected, the gas pressure is isotropic, that there is no dissipation except in the shock, and that the body is axisymmetric with its axis parallel to the flow direction. For the special case in which the field and the flow are everywhere parallel, the magnetic pressure can be included, and thus a full MHD solution obtained. Such calculations have been made for the shapes appropriate to magnetic dipole or atmospheric interactions for all of the planets (96,97,107,108). A recently completed full MHD calculation for the flow in the vicinity of the stagnation streamline for the case in which the magnetic field in the solar wind is

perpendicular to the flow direction shows significant departures from the aerodynamic solutions in a narrow region near the stagnation point (109). Another effect of the magnetic field, which is not included in the aerodynamic codes, is to produce large particle pressure anisotropies in the subsonic region of the post-shock flow (110,111). However, such complications have small effects on the gross features and properties usually observed by spacecraft. Hence, in spite of the stated assumptions, the aerodynamic calculations have greatly assisted the interpretation and correlation of spacecraft encounter data obtained at Mercury, Venus, Mars, and Jupiter.

The bow shock and magnetosheath flow aspects fit well into the evolutionary perspective of comparative magnetospheres. The controlling variables are the continua of solar wind parameters and magnetosphere sizes. Over the planetary range of these parameters, there are apparently no emergent differences predicted by the codes in the qualitative nature of the bow shock or magnetosheath flow that could be used as a basis for making taxonomic distinctions. However, emergent features do characterize other aspects of the external domain. The structure of the bow shock itself, which is treated as a mathematical discontinuity in the aerodynamic calculations, can change significantly across the planetary hierarchy because of its dependence on the ambient solar wind conditions (64). Shock character is very sensitive to the angle between the upstream magnetic field and the shock normal (112), and this changes from planet to planet for corresponding portions of the shock (113). There might also be a change in structure associated with a transition from the subsonic flow relative to the electrons in the solar wind that prevails in the inner solar system to supersonic flow farther out (98).

The importance to plasma physics of the ability to study the dependence of collisionless shock structure on the ambient flow parameters by making in situ measurements in Earth's bow shock has been stressed elsewhere (114). It should be repeated here with the emphasis changed to measurements at planetary bow shocks because of the large increase in ambient parameters that this would provide.

A qualitative change in the geometry of the bow shock and magnetosheath will occur as a function of the size of the magnetosphere when the size becomes comparable to that of solar wind streams, about 1 AU. Then different portions of the shock surface would be responding to the full range of solar wind variation at that planet at the same time. The scale size of the largest existent magnetosphere, Jupiter, is about 1/40 AU, and so there is no example of this condition at present among the planets. At the other extreme, there will be a change in character when the size becomes comparable to that of the shock structure or of characteristic plasma lengths in the magnetosheath, such as the proton gyroradius (97). Examples of this condition exist on the Moon (139) and possibly at asteroids if they have surface magnetic fields comparable to or larger than the stagnation field at their distance, about 20γ (115).

If there is a significant transfer of the rotational energy of the outer planets to the solar wind by viscous or magnetic contact at the magnetopause as has been suggested (23), it should be observable as a systematic departure from bilateral symmetry of the flow in the magnetosheath. The observable signature of this hypothesis is well defined, and a measurement of it offers a very direct method for studying the nature of the coupling between the solar wind and the magnetosphere. In view of this unusually fortunate aspect of the hypothesis, a careful

theoretical treatment of the problem and a deliberate effort to determine the optimum observational strategy would be very desirable.

Some of the external features of the planet Venus and possibly also Mars are qualitatively different from the other planets because of the dominant influence of the atmosphere on the interaction. A major difference would occur if a portion of the solar wind flows directly into the atmosphere and is lost. One consequence would be to bring the bow shock closer to the planet than predicted by aerodynamic calculations. Viewed as a function of the fraction of flow absorbed, as that fraction increases continuously from zero, the shock distance would decrease until it touched the atmosphere at which point it becomes an attached shock wave. Further increase in absorption would slide the contact point leeward until it reaches the terminator after which the shock disappears, the Moon being an example of that ultimate stage. The fraction of the flow that is absorbed at Venus is at present unknown. The bow shock signatures in the Mariner 5 and 10 encounter data are very diffuse leading to uncertainty as to where to place the shock for matching with the aerodynamic models (116). A comparison of the data from the two Mariner encounters and from three Venera missions has resulted in the interesting conclusion that the data are most consistent with the existence of an attached bow shock, in which case flow absorption of the order of 30 per cent would be required (10). A similar interpretation has been made of the Russian Mars data (117).

Although it might be the case that an appreciable fraction of the solar wind is lost to Venus' atmosphere, there is a consensus among theorists that some of its atmosphere is also lost to the solar wind (15, 116,119). These are not mutually inconsistent processes because they

take place in different regions of the flow field. Mass and energy exchange between the solar wind and atmosphere will result in characteristic boundary layer and wake features in the flow (120) and such features have been observed at Venus (7,9,116). Some theoretical effort has already been directed at describing these features (6,8), but not yet in terms of specific mass and energy transfer mechanisms (see, however, 120).

Summary: Although improvements are possible, the aerodynamic theory describing the bow shock and magnetosheath flow is in very useable form. It predicts the absence of significant taxonomic divisions over the planetary range of parameters. Its predictions give the evolutionary description of the system. The theory of external features arising out of mass, momentum and energy exchange interactions is in poorer condition in spite of some good initial efforts, due in part to its greater intrinsic difficulty and also to the need for it being more recent. But the need will soon be critical. The future Venus and Jupiter orbiting spacecraft will make in situ measurements in the boundary layers and wakes due to such interactions. A theory is needed to interpret these data in terms of the specific nature of the interaction.

Figure 4.1 illustrates in a schematic way the taxonomic divisions in parameter spaces governing the external features. In Figure 4.1a, the planets all lie in a single domain. The Moon, asteroids and heliosphere are shown in different domains, and because the Moon has magnetically organized features on both planetary and local scales, it also appears

in the domain with the planets. (For a discussion of the heliosphere see the companion article on the solar wind.) In Figure 4.1b, the vertical ordinate is the 0.1 percent solar wind absorption line, where Earth is approximatel located. The other "non-atmospheric magnetospheres" are also placed on this line, although it seems likely that they should be displaced from it in the directions of the arrows. For example, if the absorption is simply proportional to the relative surface area, then the displacements are proportional to $(R_p/R_m)^2$. The planets with "atmospheric magnetospheres", Venus and Mars, are displaced along the axis parametrizing the pick-up of atmospheric ions. The actual locations of these planets in the horizontal plane of the space are very uncertain, and this is suggested by the shading. The inadequacy of the present theory to treat the external interactions shows up in the figure in the unreduced labels on the axes in the horizontal plane. These axes should be functions of the independent variables listed in the previous section.

Chapter 5

Dependent Magnetospheric Variables - Boundary and Internal

5.1 Introduction

The large numbers of items under this heading makes it desirable to look for natural subdivisions. The list of spatially separate independent variables given in Table 3.1 are the boundary conditions and the sources and sinks that, in principle, completely determine the features and processes of all planetary magnetospheres. The entries in that table are also suited to the evolutionary or hierarchial approach adopted here, since the phenomenological divisions between the planets can be bridged by a continuous variation of the appropriate independent variables or by a consideration of the accidental satellite variables. However the "Type" categories in Table 3.1 do not have equal status as can be seen by referring to the definition of a magnetosphere given at the beginning.

In the present context the gravitating system is the planet under consideration, and the populations of charged particles either are or originate from the solar wind, the ionosphere of the planet, the atmospheres and ionospheres of the satellites, and the interstellar medium. The planetary variables are therefore common to each of the populations and they enter into the description of all magnetospheric features and processes. In this sense, the planetary variables are primary, and the other categories of independent variables and also the ionosphere of the planet viewed as a source of particles are secondary. The present discussion is therefore organized into sections that treat the secondary categories separately, that is the features and processes due to the different populations of charged particles. This turns out to be not wholly adequate because of interactions between categories, but these can be dealt with as they arise.

5.2 Solar Wind Features and Processes:

A. Orientational Types:

Before we can consider how solar wind features and processes evolve and emerge within the planetary system, a preliminary, purely geometrical classification of magnetospheres is necessitated by the vector nature of both primary and secondary variables in this case. The vector quantities are the solar wind velocity and the representations of the planetary magnetic field and rotation. Although there is a usual set of relative orientations of these vectors for the planets, other sets exist within the solar system at various times. Other sets doubtless also exist within different astrophysical systems. A consideration of the physical nature of these quantities shows that all possible orientations can be represented by four limiting cases (122). If we denote the vectors by

$\underset{\sim}{V}$, $\underset{\sim}{M}$ and $\underset{\sim}{\Omega}$, the four cases are $\underset{\sim}{M}||\underset{\sim}{\Omega}\perp\underset{\sim}{V}$, the usual one for the planets, $\underset{\sim}{M}||\underset{\sim}{\Omega}||\underset{\sim}{V}$, Uranus at solstice (?), $\underset{\sim}{M}\perp\underset{\sim}{\Omega}\perp\underset{\sim}{V}$, Paleo-Earth during field reversals (?), $\underset{\sim}{M}\perp\underset{\sim}{\Omega}||\underset{\sim}{V}$, Uranus at solstice during field reversals (??). We will discuss magnetic field reversals more fully later. Their use here to illustrate magnetospheric types III and IV is based on the assumption that as the dipole is in the process of reversing directions, it spends some time in a near-equatorial orientation. However, in the case of Earth the strength of the dipole is known to decrease at these times, and the paleomagnetic data at least for some reversals allow the possibility that the non-dipolar components dominate, at least at Earth's surface. We therefore need to add a fifth type of magnetosphere to cover the cases when the planetary field is non-dipolar or "indefinite" (122). The orientational classes are summarized in Table 5.1.

B. Boundary shapes:

If the solar wind reaches out to beyond the orbit of Pluto, as we are assuming it does in the contemporary solar system, then it forms the outer boundary of all planetary magnetospheres - perhaps their most characteristic feature. The size and shape of each boundary is controlled by the requirements for transferring the momentum flux of the solar wind to the planet by means of magnetic stresses. In addition to momentum, each magnetosphere captures some of the solar wind particles at its boundary. The particles then become organized into interior features. To use the example of Earth, the features include the polar cleft (the three dimensional extension of the polar cusp region shown in Figure 2.2), the plasma sheet, the ring current, and the trapped radiation belts. There are particles from other sources mixed in with the features, such as the high energy inner proton belt formed by the decay of cosmic ray albedo neutrons, and some energetic ions of atmospheric origin; but we consider here only

Orientational Type	Defining Characteristic	Examples
I	$\underset{\sim}{M}\,\|\,\|\,\underset{\sim}{\Omega}\,\|\,\underset{\sim}{V}$	Mercury, Venus (R), Earth, Mars, Jupiter
II	$\underset{\sim}{M}\,\|\,\|\,\underset{\sim}{\Omega}\,\|\,\|\,\underset{\sim}{V}$	Uranus at solstice (assuming spin aligned dipole)
III	$\underset{\sim}{M}\,\dagger\,\underset{\sim}{\Omega}\,\|\,\underset{\sim}{V}$	Earth (or any Type I planet) during magnetic reversals
IV	$\underset{\sim}{M}\,\|\,\underset{\sim}{\Omega}\,\|\,\|\,\underset{\sim}{V}$	Uranus at solstice during magnetic reversal
V	$\underset{\sim}{M}$ non-dipolar or "indefinite"	Weak field intervals: magnetic reversals and excursions
	(a) $\underset{\sim}{\Omega}\,\|\,\underset{\sim}{V}$, (b) $\underset{\sim}{\Omega}\,\|\,\|\,\underset{\sim}{V}$	(a) Earth, (b) Uranus at solstice

Table 9

Table 5.1 The classes of magnetospheres determined by the possible relative orientations of the vectors: the solar wind velocity, $\underset{\sim}{V}$, the magnetic dipole movement of the planet, $\underset{\sim}{M}$, and the angular velocity of the planet, Ω. The examples listed for types II through V are hypothetical, although some or all of them might be actual. They function here merely as concrete examples to fix ideas. (Modified from Ref. 122).

the pure solar wind component. Each feature maps along field lines down to the atmosphere to define an associated precipitation region where it causes atmospheric effects, for example, the auroral zones. Magnetosphere boundaries also capture some of the solar wind energy by at least two separate mechanisms and in highly variable amounts. Again in the case of Earth, the energy drives the radial diffusion of radiation belt particles, the internal convection of plasma sheet and ring current particles, and in general, all of the activity associated with geomagnetic storms and substorms.

Thus, the boundary is perhaps the most essential solar wind feature because it governs the transfer of solar wind quantities to the magnetosphere. The simplest aspect of the boundary to consider is its shape. The shape of the boundary clearly depends upon the orientation type. We can see that there are only two basic shapes, equator-on and pole-on, for types I through IV, although these can be distorted and modified by the various kinds of planetary control. There are, of course, a continuum of intermediate forms, corresponding to all latitudes between the equator and pole. The two basic shapes are merely the extreme limits of the continuum. They are also stationary shapes for orientational types I and II respectively. The rotation in type III causes the magnetosphere to alternate between the two basic shapes twice each rotation, passing through all intermediate forms in the process, and in type IV it causes an equator-on shape to rotate about its long axis (always parallel to the solar wind), which in this case is an axis through the equator.

The equator-on shape and intermediate forms in its neighborhood (so-called tilted magnetospheres) have received extensive and almost exclusive attention of theorists (see review Ref. 123). Only one study has been made to determine theoretically the pole-on shape (described in Ref. 64). The problem has only been attempted for cases in which the

interplanetary magnetic field is ignored and the magnetospheric field is totally confined within the boundary. Then the boundary shape can be calculated by means of computer codes derived from first principles if the external pressure is specified as a function of the spatial parameters of the boundary and the only sources of magnetic field are the currents on the boundary and the planetary dipole. The dipole tilt angle can be varied in these codes which allows the investigation of intermediate shapes. However, the specification of the external pressure is not done self-consistently but by means of the Newtonian or hypersonic assumption, which is the continuum mechanics analog of specular reflection. It is acknowledged that the assumption is a good approximation where the boundary is not too close to being parallel to the ambient solar wind direction. This condition is violated in the neighborhood of the boundary expression of a polar cusp. The standard aerodynamic resoltuion of the difficulty is to postulate the existence of a relatively stagnant, separated flow region over the polar cusp (124). Circulating eddys induced by the external flow might exist within the separated gas region. The theory of the separated region, even in its static form, has not yet been applied to predict the corresponding boundary shape of the polar cusp and its neighborhood. In the equator-on case, these poorly determined regions lie appreciably away from the stagnation point and in a confined meridian sector. Thus, the codes that predict the shape can be applied and tested over a fairly large portion of the boundary away from the known areas of inaccuracy. In the pole-on case, the polar cusp is centered on the stagnation point, and the inaccuracy can be expected to propagate from there and to affect the entire boundary. The pole-on case thus presents the biggest challenge to the theorists to predict the boundary shape.

C. The Fundamental Problem of Magnetospherics:

The problem of calculating the boundary shape at a polar cusp from first principles exposes a fundamental level of difficulty in our understanding of magnetospheric physics. Derivations from first principles have only been achieved for idealized magnetospheres. The idealization consists of the following: 1) magnetic field totally confined by the boundary - no leakage out of field lines, 2) solar wind force strictly perpendicular to the boundary - no tangential component, 3) no transfer of mass across the boundary, 4) no transfer of energy across the boundary, and 5) no internal sources of magnetic field except the planetary dipole. All of the idealizations are violated to some extent, and all of them modify the calculated boundary shape to some extent. But more importantly, they are responsible for all interior solar-wind features and processes. The first four have to do directly with - and the fifth one indirectly with - the transfer of physical quantities across the boundary. The phenomenology of the transfer processes is poorly understood, even in the case of Earth; and the theory is in a similar condition. It is clearly necessary to understand the precise physical nature of the transfer mechanisms before deductive, quantitative models can be derived to predict boundary shapes and solar-wind interior features and processes. This crucial problem, especially as it applies to Earth, is now the subject of intensive experimental and theoretical study (see the companion article on Earth's magnetosphere).

As a concrete illustration of the importance of the problem, we note that in an idealized magnetosphere, one for which a complete deductive theory exists (given the external boundary conditions), there would be no magnetospheric tail. A tail results from some form of tangential stress on the boundary. The stress acting against the solar wind flow can

transport power through the boundary to supply the energy that is needed to stretch and fill the tail with magnetic flux from the planet. There must be a concomitant entry of particles to populate the tail plasma structures. These carry the electric currents associated with the stretched field lines and contribute in an essential way to the maintenance of pressure equilibrium in the tail. In the case of Earth, the tail is generally acknowledged to be the main portal of entry for the particles and the energy that make up the ring current and the radiation belts of the magnetosphere proper and that excite the atmosphere into visible auroral displays.

D. Magnetospheric Scaling Relations:

Because of the uncertainties and disagreements over the boundary transfer mechanisms, a complete, deductive, comparative theory of solar wind-magnetospheric features and processes is not possible at this time. Nevertheless, partial, semi-empirical theories based on specific assumptions about the boundary processes have been advanced. They at least open the theoretical discussion of comparative magnetospheres. They are based primarily on induction from the single example of Earth. Where comparisons have been possible, at Mercury and Jupiter, the data allow the interpretation that predictions of these interim theories have been reasonable confirmed.

The present comparative theories of solar wind-magnetospheric features and processes are concerned with: 1) the shapes and sizes of the features, 2) the transfer of energy - here the sole mechanism that has been considered is dayside field line reconnection, 3) the trapped radiation parameters, and 4) magnetospheric radio bursts. There is at present no comparative theory for the mass transfer rate, due in part to the quantity being inherently more subtle to measure than the others.

However, to keep the topic visible in the table of relations given below, we use the hypothesis described in connection with Figure 4.1, which is based on the obvious and very superficial dimensional argument that the capture efficiency is proportional to the ratio of the cross-sectional areas of the planet and its magnetosphere. The theories provide specific formulas relating certain dependent variables of the types just mentioned in terms of planetary and solar wind variables. The relations can be used to form appropriate dimensionless ratios the largeness or smallness of which determine the taxonomic divisions between magnetospheric types. However, since the method of approach is induction from Earth, the divisions encountered are the borders in parameter space of Earth-type magnetospheres. The formulas describe the intra-divisional evolution of such magnetospheres. The modifications required to extend their validity across divisions have not been attempted as yet. Nevertheless the relations in the table below describe the existing situation quite fully, and at the same time they illustrate what is required of a more complete and inter-divisional theory.

Since the formulas are clearly interim, at least in principle, we give to their collection into a single table an interim label: "The 1976 Solar Wind - Pure Dipole Magnetospheric Scaling Relations". The qualifier "Pure" is added here to denote the absence of appreciable active control by other planetary parameters, for example, the atmosphere and rotation. The effects of these parameters can, nevertheless, be deduced from the formulas, which allows the boundaries of the pure dipole scaling relations to be determined. The relations are given in Table 5.2.

The independent variables in the table consist of three solar wind parameters, particle flux, stagnation pressure and merging electric field, and three planetary parameters, dipole strength, radius, and angular

1976 Solar Wind - Pure Dipole Magnetospheric Scaling Relations		
	Scaling Relations	Fiducial Values
Independent Variables	$d = D/D^*$ $\Phi = F/F^* d^2$ $\alpha = p_{st}/p_{st}^* d^2$ $E_m(mV/m) = \{V_{sw}\|(B_{sw})_z\| \times 10^{-3}/d$ (0) $\mu_p = M_p/M_E^*$ $r_p = R_p/R_E^*$ $\omega_p = \Omega_p/\Omega_t^*$	$D^* = 1$ AU $F^* = 1.6 \times 10^8 cm^{-2} sec^{-1}$ $p_{st}^* = 1.2 \times 10^{-8}$ dyne cm^{-2} $\vec{B}_{sw} \cdot \vec{M}_p > 0$ $\vec{B}_{sw} \cdot \vec{M}_p < 0$ $M_E^* = 8.0 \times 10^{25}$ Ga s cm^3 $R_E^* = 6.37 \times 10^3$ km $\Omega_E^* = 7.3 \times 10^{-5}$ rad sec^{-1}
Solar Wind Pressure Relations	$B_{st}(\gamma) = B_{st}^* \alpha^{1/2}$ $R_m(R_p) = R_m^* \mu_p^{1/3} \alpha^{-1/6} r_p^{-1}$ $R_T(R_p) = \begin{cases} R_T^* \mu_p^{1/3} \alpha^{-1/6} r_p^{-1} \\ (R_T^*/R_m^*) R_m \end{cases}$ $B_T(\gamma) = \begin{cases} B_T^* \alpha^{1/2} \\ (B_T^*/B_{st}^*) B_{st} \end{cases}$ $F_T(m) = F_T^* \mu_p^{2/3} \alpha^{1/6}$ $\cos \lambda_p = (\cos \lambda_p^*) \mu_p^{-1/6} \alpha^{1/12} r_p^{1/2}$	$B_{st}^* = 54$ $R_m^* = 11$ $R_T^* = 20$ $R_T^*/R_m^* = 1.8$ $B_T^* = 30$ $B_T^*/B_{st}^* = 0.56$ $F_T^* = 7.5 \times 10^{16}$ $\lambda_p^* = 72°$
Solar Wind Electric Field Relations	$E_c(mV/m) = \eta E_m$ $R_\Omega(R_p) = R_\Omega^* E_m^{-1/2} \mu_p^{1/2} \omega_p^{1/2} r_p^{-1}$ $R_\mu(R_p) = R_\mu^* E_m^{-1/4} \mu_p^{1/4} \alpha^{-1/8} r_p^{-1}$ $\Phi_c(kV) = \Phi_c^* E_m \mu_p^{1/3} \alpha^{-1/6}$ $T_c(hr) = T_c^* E_m^{-1} \mu^{1/3} \alpha^{1/3}$ $P_c(watts) = P_c^* E_m \mu_p^{2/3} \alpha^{1/6}$ $d\,Dst/dt\ (\gamma/hr) = (d\,Dst/dt)^* \times E_m \mu_p^{-1/3} \alpha^{1/6}$	$\eta = 0.2$ $R_\Omega^* = 8.5$ $R_\mu^* = 7.5$ $\Phi_c^* = 42$ $T_c^* = 5$ $P_c^* = 2.8 \times 10^{11}$ $(d\,Dst/dt)^* = 5.4$

(table continued with "Trapped Radiation Relations" on next page)

Table 5.2(continued)

The intercepted flux variables based on a circular cross section of radius R_m are: the total particle flux, F_p, the momentum flux, F_M, and energy flux, F_E; and based on a sphere of radius Rm, the normalized particle flux, f_p, and energy flux, f_E.

These relations have been abstracted with some extensions from References 2, 3, 43, 44, 47, 64, 130, 131, and 134.

Trapped Radiation Relations	(Max E_p) (MeV) = (Max E_p)*μ_p $T_D(hr) = T_D^*$ $J_p(cm^{-2}\ sec^{-1}) = J_p^* \mu_p$ $D_{\Phi\Phi} = D_{\Phi\Phi}^* \mu_p^{\nu}$	(Max E_p)* = 5.0 $T_D^* = 0.091\ L^2\ \mu^*/\mu$ $\mu^* = 16$ MeV/Gauss $J_p^* = 5 \quad 10^{10}/L^4$ $5 < \nu < 6$
Radio Burst Relations	$f_c(Mhz) = f_c^* \mu_p\ r_p^{-3}$ $f_p(Mhz) = f_p^* \mu_p\ r_p^{-3}$ $P_R\ (watts) = P_R^* \mu_p^{2/3}\ \alpha^{2/3}$	$f_c^* = 1.7$ $f_p^* = 0.3$ $P_B^* = (1 \text{ to } 10) \times 10^9$
Intercepted Flux Relations	$F_p(sec^{-1}) = F_p^* \mu_p^{2/3} \phi^{2/3}$ $F_M(dyne) = F_n^* \mu_p^{2/3}\ \phi^{2/3}$ $F_E(erg\ sec^{-1}) = F_E^* \mu_p^{2/3}\ \phi^{2/3}$ $f_p(cm^{-3} sec^{-1}) = f_p^* \mu_p^{-1/3}\ \phi^{7/6}$ $f_E(ev\ cm^{-3} se^{-1}) = f_E^* \mu_p^{-1/3}\ \phi^{7/6}$	$F_p^* = 2.6 \times 10^{28}$ $F_n^* = 1.8 \times 10^{12}$ $F_E^* = 3.5 \times 10^{19}$ $f_p^* = 1.8 \times 10^{-2}$ $f_E^* = 1.5 \times 10^3$
Solar Wind Particle Relations	$F_{pc}(sec^{-1}) = F_{pc}^*\ \phi\ r_p^2$ $P_{pc}(Watts) = P_{pc}^*\ \phi\ r_p^2$	$F_{pc}^* = 3 \times 10^{25}$ $P_{pc}^* = 4 \times 10^9$

Table 5.2 The independent variables are: the heliocentric distance of the planetary orbit, d; the particle flux, ϕ; the stagnation pressure, α; the (merging) component of the solar wind electric field, E_m, with B_{sw} and V_{sw} in cgs units; the planetary dipole moment, μ_p; the planetary radius, r_p; and the planetary angular velocity, ω_p. All are normalized to typical or actual values at Earth - the starred quantities.

The dependent variables are: the stagnation magnetic field strength, $B_{st} \equiv \sqrt{8\pi p_{st}}$; the planetocentric distance to the stagnation point, R_m, in units of planetary radii, R_p; the radius of the tail, R_T; the field strength in the tail, B_T; the magnitude flux is the tail from one polar cap , F_T, in units of maxwells; the latitude of edge of the polar cap that supplies the flux in the tail, λ_p; the convection electric field in the dawn-dusk meridian plane, Ec, based on an empirical merging efficiency η; the planetocentric distance to the stagnation point for convecting zero energy plasma, R_Ω; the same for 1 keV convecting plasmasheath electrons assuming no planetary rotation, R_μ; the convection potential, Φ_c; the convection time through the tail, T_c; the power into the magnetosphere from field line reconnection, P_c; the rate of change of the world-averaged disturbance field, d Dst/dt; the maximum energy of trapped radiation particles that radially diffuse under constant first invariant from a solar wind source, Max Ep; drift time (assuming no rotation), T_D; stably trapped particle flux, Jp; radial diffusion coefficient for violations of the third invariant, $D_{\Phi\Phi}$ (applicable to Paleo-Earth only); high frequency cut-off of radio burst, fc; frequency of peak power of radio bursts, fp; typical power in intense bursts assuming isotropic radiation over a hemisphere, P_R; the capture rate of the solar wind particle flux, F_{pc}; the concomitant capture rate of energy assuming conserved energy per particle, P_{pc}.

velocity. The heliocentric distance is also an independent variable, but it enters only into the independent solar wind quantities. It has been included directly into the definitions of the flux, pressure and electric field variables. The functional forms given in the table assume the model of pure radial expansion of the solar wind. Thus, in this 1976 compilation, the magnetospheric dependences on seven independent variables are encorporated. In the construction below of the division-defining demensionless ratios, the ionospheric conductivity, which is another function of heliocentric distance, is also included.

The stagnation pressure, p_{st}, is calculated under the hypersonic approximation, $p_{st} = K\rho V^2$, where K is a constant, ρ is mass density, and V is velocity of the solar wind. If ρ is based on the solar wind proton number density, then $K \cong 1$ (107, 125). The explicit formula for evaluating the merging component of the electric field is based on the semi-empirical rectifier model of merging (126), but other models can be used as well (e.g. 127-129). The majority of the dependent variable relations have been discussed in detail elsewhere (see table caption for references).

The table allows us to make a preliminary exploration of the boundaries of pure dipole magnetospheres and to classify the planets accordingly. Also as a practical use, one can construct "evolutionary profiles" for a given planet by varying the dipole parameter, μ_p (or any other independent quantity), and tracing the consequent evolution of the dependent variables. This will be illustrated for Uranus, where mission planning in the absence of a known value for the dipole strength necessitates consideration of a range of values, and for Paleo-Earth, where the dipole strength is known to vary over a certain range. In a critical role, the table allows us

to identify in a concrete way the empirical elements in the formulation that need to be replaced with derivations from a theoretical foundation. Establishing such a foundation is a prerequisite to achieving an inter-divisional theory.

E. Practical Applications:

Consider first the boundaries due to planetary control. We can distinguish three types of control due to planetary size, rotation and contact conductivity. The dimensionless ratios defining the divisions for planetary size are simply the R_m, R_Ω and R_μ in the table, since they are already normalized to the planetary radius. For example, the magnetopause either stands off from or is attached to the atmosphere or surface of the planet depending on whether $R_m > 1$ or $R_m < 1$. The division which occurs at $R_m = 1$ has already been discussed in connection with the exterior features.

The meaning of R_Ω and R_μ now needs to be explained. The larger of the two is approximately the planetocentric distance to the inner edge of the plasma sheet in the equatorial plane. Which one is larger depends on the angular velocity and will be discussed under rotational control. The point here is that, if we denote the larger value by R_{ps}, then when $R_{ps} > 1$, the plasma sheet stands off from the planet at the equator, and when $R_{ps} < 1$, it touches the planet at the equator. Since the equatorial edge of the plasma sheet maps along field lines to the equatorward edge of the auroral zones, the first case results in separate auroral zones in both hemispheres, whereas in the second case, there is one continuous auroral zone spanning the latitude range $\pm \lambda_p$, the poleward edge of the auroral zone.

The inner edge of the plasma sheet is determined by locating where the convection velocity, associated with the convection electric field,

is canceled by the combined action of rotation and gradient drift. The division between drift dominance and rotational dominance occurs at $R_\Omega/\sqrt{2}R_\mu = 1$. Rotation dominates when the ratio is greater than one. This is probably not a very important division in magnetospheric types. Earth is typically near 1 and takes on values on both sides over the normal range of merging electric fields.

A more important division occurs at $R_{ps}/R_m = 1$, which in practice usually occurs when $R_{ps} = R_\Omega$, and hence is another rotational division. It separates Earth-type magnetospheres, for which the ratio is less than one, from magnetospheres in which convection is essentially excluded from the magnetosphere proper by rotation (see, however, 21).

Rotation begins to affect the boundary shape when the centrifugal force makes an appreciable contribution to the pressure balance at the boundary. The division here is marked by the approximate equality of the solar wind speed and the corotation speed at the boundary. A strict balance between the solar wind and rotational dynamic pressures would require also equality of the mass densities of the solar wind and the plasma just inside the boundary. In the case of Earth, the density inside is typically a factor of 10 less than in the solar wind (e.g. 135). If this condition is general, the suggested criterion marks only the onset of rotational effects rather than the transition to rotational dominance in determining the boundary shape. The ambiguity in the criterion is due to the lack of a theory for determining the interior mass density. The failure can be traced back to the fundamental problem of magnetospherics, which must be solved to provide the boundary conditions that determine the mass distribution.

A mostly unknown but probably very important type of planetary control concerns the electrical reaction of the ionosphere or surface to magnetospheric convection (5, 136). The motional electric field associated with

the convection is mapped to the ionosphere or surface along highly conducting field lines, where it drives an electric current of an amount determined by the contact conductivity. The current closes by out-and-back paths along field lines to the source of the stress producing the convection, where it then completes its loop in the sense to oppose the stress. The reaction is a magnetospheric example of Lenz's law. The effects of this current are not contained in the relations given in the table. It seems clear that a division has been reached when the magnetic field produced by the current equals that present in the absence of the current (5, 136). This criterion expressed in terms of the contact conductivity, Σ, and the field line reconnection formulas in the table is $\Sigma/\Sigma_0 = 1$, where $\Sigma_0 = \Sigma_0^* E_m^{-1}\alpha^{1/2}$ and $\Sigma_0^* = 72$ mho. In the combination $E_m^{-1}\alpha^{1/2}$, the d dependence cancels exactly; thus Σ_0 is the same for all planets (5). For typical values, $E_m = 1$ and $\alpha = 1$, we have $\Sigma_0 = 72$ mho. All planets with $\Sigma > \Sigma_0$ must have significantly altered magnetospheres with regard to their convection and boundary properties compared to the magnetospheres described by the table.

As a final example we note that the table includes two expressions for power into the magnetosphere from the solar wind. The one (Pc) due to field line merging on the dayside, can be thought of as arising in work done by the solar wind flow as it stretches and thus energizes Earth field lines prior to their reconnection in the tail. The loss of energy by the solar wind in this case results merely in slowing it down. The second mode of power transfer (Ppc) involves direct entry of energy along with the captured particles, since each particle brings with it approximately its original kinetic energy. In the case of Earth the two modes can be distinguished in polar cusp auroral precipitation (Ppc) and in substorm auroral precipitation (Pc). For Earth the latter dominates. But for the other terrestrial planets, which have larger relative surface ratios, more energy might enter

by the direct mode.

Table 5.3 roughly locates the planets relative to the magnetospheric divisions defined by the dimensionless ratios. Planets for which the ratio in question is of the order of unity are grouped separately. Members of these groups might have characteristics of one or both of the types separated, or characteristics that alternate between the two types because of solar wind variations, or characteristics of a truly intermediate nature. The large number of entries in the order-of-unity groups points up the need for a trans-divisional theory as well as an inter-divisional one.

The first entry in the table, Rm, again shows that Mercury, Venus, and Mars nearly or completely fill their magnetospheres. The second ratio shows that the near-planet dynamics of plasma sheet convection is dominated by particle drift for the inner planets, except for Earth and Paleo-Earth, and by rotation for the outer planets. The ratio for Earth is 0.8. The inner edge of the plasma sheet stands off the equatorial surface for all of the planets, but it is close for Mercury, Venus, and Mars. Rotation excludes the plasma sheet from the magnetospheres proper of the outer planets, but the situation for the inner planets is transitional or ambiguous. The value of R_{pS}/Rm for Earth is 0.7. The onset of rotational distortion of the boundary can be expected for the outer planets, but not the inner ones. Power into the magnetosphere is dominated by field line merging at most of the planets, but at Mercury, Venus and Mars, the power from direct entry is comparable.

Contact conductivity, the final ratio in the table, dominates the convection process at Venus and Mars, but not at the other planets. However, the low dipole strength portion of the range for Paleo-Earth extends into the intermediate region. For $\mu(P\text{-}E) = 0.1$, $\Sigma/\Sigma_0^* = 1.4$. This suggests that the magnetosphere of Mars, which in contrast to Venus might have both $Rm > 1$ and $\Sigma/\Sigma_0^* > 1$, might have characteristics that are now unique in the solar system, but that were acquired by the paleomagnetosphere of Earth during low field

Ratio	≤ 0.3	Order of Unity 0.3 to 3	≥ 3
Rm		My, V, Ms	P-E, E, J, S, U, N
$R_r/\sqrt{2}\ R_\mu$	My, V, Ms	E, P-E	J, S, U, N
Rps		My, V, Ms	E, P-E, J, S, U, N
Rps/Rm		My, V, E, P-E, Ms	J, S, U, N
ΩRm Rp/Vs	My, V, E, P-E, Ms	J, S, U, N	
P_{pc}/P_c	E, P-E, J, S, U, N	My, V, Ms	
Σ/Σ_0^*	My, E, J, S, U, N, P-E	P-E	V, Ms

Table 5.3 Selected dimensionless ratios for the dependent variables of solar wind - magnetospheric features and processes. Rm, R_Ω, R_μ, P_{pc} and P_c are defined in Table 10. $R_{ps} = R_\Omega$ if $R_\Omega/\sqrt{2}\ R_\mu > 1$ and $R_{ps} \cong R_\mu$ otherwise. Other parameters are independent planetary and solar wind variables defined in Section IIB, and $\Sigma_0^* = 72$ mho.

The numerical values assume $E_m = 1$, and $\alpha = 1$ at $d = 1$. For the table the dipole moment V(R) has been used.

intervals. The dramatic change in magnetospheric character that is expected to accompany the onset of control by contact conductivity implies that in situ measurements at Mars could be very important for the study of long term solar-terrestrial relations.

The examples in Table 5.3 illustrate the use of the scaling relations for finding taxonomic divisions and for locating the planets relative to them. Other examples could be found, especially among the trapped particle relations. However, the studies of the trapped particles of Jupiter suggest that the table is too incomplete to find many useful divisions (33). Radial diffusion at Earth is dominated by the solar wind and at Jupiter by the atmosphere. Relations are needed to bridge this division in a continuous way to generalize the diffusion process for comparative purposes. In view of the likely presence of intense trapped radiation features at Saturn, Uranus and Neptune, a comparative parametric description of trapped radiation phenomena is very desirable.

Mangetospheric profiles for individual planets can be constructed from the relations in Table 10 by varying one or more of the independent variables. A magnetospheric profile for Uranus has been constructed by varying the unknown strength of its magnetic moment, and the results are shown in Figure 5.1. It shows the emergence of magnetospheric features including the detachment of the magnetosphere from the atmosphere (by extrapolation at $\mu_p = 2 \times 10^{-3}$), the appearance of a plasmasphere, the engulfing of the satellites, the onset of rotational distortion, and the detachment of the plasmasphere and its growth until it fills the magnetosphere - the subject of subheading B below. Other items can, of course, be included in such a profile, such as the rotation-drift and conductivity effects on convection and radiation belt parameters.

Profiles have also been constructed for Paleo-Earth where the range of dipole strength variation is fairly well defined. In this case the effects of solar wind variations have also been included. The results are shown in Figures 5.2 and 5.3. The first of these gives the dependence of scale sizes of magnetosphere and plasmasphere (to be discussed below) on dipole strength. The effects of solar wind fluctuations is indicated by the range in the scale sizes at each value of μ. The second figure illustrates the electric field relations. The figure is general and can be used for dipole strength variations around a central value for any planet. The indicated range is appropriate to Paleo-Earth. It reveals the interesting result that although the total power decreases as μ_p decreases, the power per unit volume increases. This implies that small magnetospheres are relatively more "noisy" than large ones.

F. Critical Application:

The relations in Table 5.2 are semi-empirical, and it is the purpose of this section to identify the empirical elements. Their derivations are quite heterogeneous and consequently so are their reliances on experimentally determined factors. Dimensional arguments, scaling hypotheses, and derivations from first principles are all employed. The first two types of derivations always require fixing of dimensionless constants or scaling parameters by observations.

The relations for B_{st} and R_m are purely theoretical (100). The associated fiducial values depend only upon the experimental determination of the typical solar wind stagnation pressure (p_{st}^*), which is an independent variable. Thus, the relations for these quantities are fully reduced. The tail radius, R_T, is obtained from a scaling hypothesis: under a variation of dipole strength or solar wind pressure, magnetospheres change their size but not their shape. This is justified under the assumption that the only factors determining shape are the solar wind and the dipole

geometry of the planetary field. Then, except for plasma dynamical scale lengths which are small and can be ignored (in the steady aerodynamic domain), the only scale length that can be formed from the available parameters is R_m. In a single scale length situation, there can be no changes in shape, only changes in size determined by R_m. Thus, all other scale lengths characterizing shape must be proportional to R_m. The proportionality factors should be determined theoretically for fully reduced relations, but they can also be found by measurement. In this case the required factor is R_T^*/R_m^*, and it is only known experimentally. As mentioned previously the existence of the tail requires transfer of energy across the boundary. Thus, the problem of finding R_T^*/R_m^* theoretically is tied to the fundamental problem of magnetospherics. Given the relation for R_T and the prerequisite scaling hypothesis, the other pressure relations follow directly.

The initial and primary electric field relation is merely a dimensional statement defining the electric field leakage efficiency, η. The content of the relation is the statement that η is a constant, that is, not a function of any of the independent variables. This is a pure assumption with controvertible observational support (e.g. 126, 130). The justification is that it is the simplest assumption possible in lieu of a determining theory and there is no incontrovertible observational evidence against it. The value for η is an estimate extracted indirectly from observations (137, 138). The theoretical situation here is clearly in need of improvement, and some good starts have been made in this direction (127-129). The present difficulty centers around the three dimensional aspects of the problem and the coupling to the external flow. Since the process involves "leakage" across the boundary, it also falls under the fundamental problem of magnetospherics. Its solution can be expressed

by giving η as a function of the independent variables, then the other electric field relations in the table remain formally unchanged. The R_Ω and R_μ relations assume a pure dipole geometry for the magnetic field. This is merely a practical assumption, that can be removed by using a realistic field model. However, such field models, which must include the tail field and magnetospheric particle fields, are all empirical and therefore are justified only for Earth. Also in the R_μ relation, the value of μ for the electrons is based on an assumed energy of 1 Kev in the plasma sheet in the tail. This is another observational value awaiting a theoretical prediction. The value appears to be the same at Earth, Mercury and perhaps also at Mars, and thus it is probably related to the solar wind post shock particle spectrum. As such it should be approximately the same for all planets, as was assumed to universalize the relation for inclusion in the table. The quantities Φ_c and T_c follow directly from the above together with the size scaling relations. The power, P_c, is based on the Poynting flux into the tail associated with the electric field. It requires the specification of the length of the tail that communicates power to the magnetosphere. Since there is no theory yet capable of predicting the length, it is estimated from observations. Once the length is known, by theory or observation, it should scale as R_m under the size scaling assumption, and the relation for P_c then follows.

Substorms in Earth's magnetosphere are contiguous sequences of temporally similar events characterized by impulsive injections of particles and energy from the tail to the magnetosphere and atmosphere. The phenomenon suggests that the circulation of magnetic flux between the dayside and nightside is intrinsically non-steady. This is not a unique interpretation of the phenomenon because the solar wind itself fluctuates with significant amplitude at the characteristic time scale of substorms.

Mercury appears to exhibit a similar phenomenon with a characteristic time that scales like T_c compared to the substorms of Earth, thus supporting the first interpretation. Except for the time scale, T_c, the non-steady aspects of magnetospheric phenomena are not included in the table. The presence or absence of non-steadyness is itself an important characterizing quality, which might vary between magnetospheric types. It has been suggested that the condition of non-steadyness in the sense of substorms might not characterize magnetospheres for which $\Sigma/\Sigma_0 > 1$ (5). The physical process that gives rise to the phenomenon of substorms at Earth is at present unknown, and there are several lines of thought about where the solution lies (see companion article on Earth's magnetosphere). Thus there is no theory of intrinsic non-steady behavior that can be used for comparative purposes. This subject is one of the oldest and most unyielding of the topics that fall under the fundamental problem of magnetospherics.

5.3 Planetary Ionosphere Source - Features and Processes:

Magnetosphere-ionosphere coupling at Earth is the sole topic of a companion article. To illustrate its role in comparative magnetospherics, we extract only aspects related to the ionosphere as a particle source. Comparative estimates of ionosphere source strengths are given in Table 3.2.

On open field lines, the ionosphere source constitutes a planetary wind, known as the polar wind in the case of Earth. Where field lines are closed, it is the source of the primary plasmasphere, to be distinguished from secondary plasmaspheres of interstellar origin and accidental plasmaspheres of satellite origin. The primary plasmasphere is a large feature at Earth and possibly also at the outer planets. Theoretical models of these features are fairly well developed because the associated sources and sinks are reasonably well specified.

A. The Static, Diffusive Equilibrium State:

The primary plasmasphere is merely the outward extension of that part of a planetary ionosphere that is magnetically restrained from blowing away. The characteristics of the confined plasma are governed by balances between the ionosphere source and various loss processes. To begin the discussion of these characteristics, consider a model of the diffusive equilibrium state that would be reached if there were no time dependent processes, no loss processes, and if the forces exerted by the plasma on the field could be ignored. Then since by assumption time is unlimited, even the low collision rates of magnetospheric plasmas would bring about a diffusive equilibrium between the ionosphere and the plasmasphere with hydrostatic balance between the thermal, gravitational and centrifugal forces (18, 140-143). Also since by assumption plasma transport is confined to rigidly corotating flux tubes, only components of forces parallel to the magnetic field are relevant, and the equilibrium is one dimensional. At this most elementary level of description, we imagine the hydrostatic diffusive equilibrium to extend in association with dipole field lines out to a definite distance beyond which is the open field line, low density planetary wind domain. Aside from the geometrical inconsistency of dipole field lines boardering open field lines, this hypothetical type of plasmasphere termination is a priori unlikely because the conditions for its existence occupy a narrow range in the parameter space of independent variables. In general some form of transport process dominates in the remote portions of the plasmasphere, radically changing the nature of the plasmasphere termination. Nevertheless, the evolutionary profile of the static, diffusive equilibrium state is a useful basis for comparing primary plasmaspheres because the nature of the departure from this state characterizes magnetosphere types.

The spatial extent of the closed field line dipolar region in this picture can be found from Table 10 as the maximum distance reached by a field line leaving the surface of the planet at the latitude λp. That distance turns out to be simply 0.9 R_m. Thus, the hypothetical pure-diffusive plasmasphere always terminates within the magnetosphere boundary.

In static, isothermal, ambipolar diffusion, the number density is distributed in space according to

$$n_d(r, \theta) = n_o \exp [\Delta\Phi(r, \theta)/2kT] \qquad (5.1)$$

where n_o is the density on the equipotential surface defining the ionospheric source, and $\Delta\Phi(r, \theta)$ is the potential difference between the point (r, θ) and the source equipotential. An approximation to the above expression, in a dimensionless form useful for comparison purposes, is

$$\frac{n_d}{n_o} = e^{-\beta\phi} \qquad (5.2)$$

where

$$\phi = \frac{L-1}{L} - \frac{L^2-1}{2L_s^3} \sin^2\theta \qquad (5.3)$$

and where $L = r/R_p$, $L_s = R_s/R_p$ with R_s the distance of synchronous orbit ($R_s^3 = GM/\Omega^2$), and $\beta = GMm/2R_pkT$. The approximation consists in taking the source equipotential surface to be a sphere of radius R_p. Thus $n = n_o$ when $L = 1$. The expression shows that the normalized density distribution depends on two independent parameters, β and L_s, which measure the ratios of the escape speed to the thermal speed and the escape speed to the surface corotation speed respectively. However, the spatial structure is determined by ϕ, which is parameterized by L_s only. Figure 5.4 shows contours of constant ϕ for the case of Jupiter, for which $L_s \cong 2.26$.

In the equatorial plane, the local maximum in ϕ at $L = L_s$ corresponds to a local minimum in the density. Beyond L_s the density increases, and

at $L \cong 4.3$, where ϕ returns to zero, it reaches the value it has at the ionospheric source surface. This is obviously non-physical in the full context of the problem, but here we are exploring merely the logical consequences of diffusive equilibrium in isolation. For the case of Earth, the equatorial distance to the point where ϕ returns to zero is about $L = 23.6$ (18), and in general it is $L(\phi = 0) = (\sqrt{1+8L_S^3} - 1)/2$.

Off of the equatorial plane, it is usual to speak in terms of the density distribution along a field line. Then it is useful to refine the definition of L to make it a field line lable with a numerical value equal to the equatorial crossing distance of the field line, again normalized to planetary radii (i.e., the usual MacIllwain L parameter for a dipole field). Inside the $L_F \equiv (2/3)^{1/3} L_S$, the local minimum of density along a field line is at the equator. But beyond this distance it separates into a pair of density minima that move off the equator symmetrically. The density minima are at the local maxima in ϕ illustrated in Figure 5.5 for the 60° latitude field line of Jupiter (L=4). The figure shows that beyond $L = L_F$ there will be a local density maximum along the field line at the equator.

As one moves out from $L = L_F$, the movement away from the equatorial plane of the field line density minima describes an axially symmetric surface, $r^3 \sin^2\theta = (2/3)R_S^3$, illustrated for Jupiter in Figure 5.6. The expression for the surface shows that if distance is normalized to R_S, the surface is the same for all planets. That is, the figure applies universally if the size of the planet is appropriately adjusted. The surface divides the pure-diffusive plasmasphere into high-density inner and high-density outer regions.

Table 5.4 summarizes for each of the planets the characgeristic sizes relevant to a pure-diffusive plasmasphere. The termination of this hypothetical plasmasphere is geometrically determined by the maximum extent of the closed field line, dipolar region, namely at $L = L(\lambda_p)$. The location

(a)	L_s	L_F	$L(\phi=0)$	$L(\lambda_p)$	L_Ω	$\frac{M_p}{m_i}T(10^{3\circ}K)\beta$	ϕ_{eq}(max)	(-) Product	$-2\ \phi(\lambda_p)$
Mercury	100	87.4	1414	1.4	.062	0.58	0.985	-0.571	-
Venus	254	222	5724	1.0	.019	3.30	0.994	-3.28	-
Earth	6.6	5.8	23.6	1.0	12	3.73	0.774	-2.84	-
Paleo-Earth	"	"	"	2.7 to 15	3.8 to 21	"	"	"	-
Mars	6.0	5.2	20.3	1.3	0.48	0.79	0.752	-0.594	-
Jupiter	2.3	2.0	4.3	45	531	114	0.389	-44.3	164
Saturn	1.9	1.7	3.2	36	319	46.1	0.283	-13.0	187
Uranus	4.5	3.9	13.0	45	220	16.5	0.672	-11.1	20.3
Neptune	4.5	3.9	13.0	45	252	14.4	0.672	-9.68	20.3

(b) Extent of Pure-Diffusive Plasmasphere	No Inner Region	Partial Inner Region	Full Inner Region and Partial Outer Region	Full Outer Region
	V	My, Ms, P-E	E, P-E	J, S, U, N

Table 5.4 (a) Characteristic sizes of pure-diffusive plasmaspheres, and exponential factors. The factor β is normalized to hydrogen ions at $10^{3\circ}$K.
(b) The plasmasphere extents based on the termination of the closed field line region, $L=L(\lambda_p)$. No inner region, $L(\lambda_p)<1$; partial inner region, $1<L(\lambda_p)<L_F$; partial outer region, $L_F<L(\lambda_p)<L(\phi=0)$; full outer region $L(\phi=0)<L(\lambda_p)$.

of this termination relative to the inner and outer plasma regions varies between the planets, as is explicitly shown in the second part of the table. Only Earth and the giant planets have the potential for a high-density outer region.

It is instructive to evaluate the density characteristic of the minimum that separates the inner and outer regions. We know that the density at $L(\phi = 0)$, which is a function of L_s only, should be the same as at the source surface, but the depth of the intervening valley is determined mainly by the value of β, the other independent parameter. The particles in the high-density outer region came from the source surface through the density minimum, which therefore acts as a nozzle regulating the flow to the outer region, the maximum flux being roughly the minimum density times the thermal speed.

The exponential factors by which the minimum density is reduced from the source density, $\beta\phi_{eq}(\max)$, are given in the table. For hydrogen ions at $10^{3\circ}$K, the factor is about 20 for Earth. This corresponds to a minimum density of about 5×10^3 cm^{-3} compared to a source density of 10^5 cm^{-3} (40). For the giant planets, the reduction ranges from 20 orders of magnitude for Jupiter to 4 orders of magnitude for Neptune, again for hydrogen ions at $10^{3\circ}$K. It seems clear then that for Jupiter the minimum density nozzle is effectively closed, and that thermal diffusive equilibrium between the inner and outer regions can not be attained on realistic time scales (27). This same conclusion seems likely to hold also for the other giant planets, but the question should be considered more carefully by estimating the range of possible temperatures and the competing time scales associated with the possible loss mechanisms which will be discussed below.

In cases where a significant thermal flux from the inner to the outer region is prevented by a large value of β, a significant non-thermal flux

of photoelectrons is still possible (27). The resulting charge imbalance creates an electric field which assists ions across that potential maximum to maintain quasi charge balance, as in ordinary ambipolar diffusion, but in this case the temperature is appropriate to the photoelectrons, namely about 10 ev or 10^{5}°K. Thus the outer region may be filled with a photoelectron-temperature gas in equilibrium with the photoelectron flux from the source surface. A better approximation is obtained by noting that the lowest energy ions produce the largest densities. The appropriate temperature to use to determine β is then that corresponding to the minimum energy necessary to pass from the source region over the potential maximum into the outer region. This gives for β the value of approximately 2 for all of the giant planets. Thus in each case at the distance $L(\phi = 0)$, the density is the same as the photoelectron density at the source surface, which varies over the order of magnitude range 0.01 cm^{-3} to 0.1 cm^{-3}. Beyond that distance, the density rises very rapidly as the L^2 dependence controls the behavior of the exponent, such that the density becomes impossibly large at the distance of the last closed field line, as is shown in the last column of the table and in Figure 5.7 The question is now, what limits the density in the outer region? This is a question of loss mechanisms.

The above outline is a generalization of the original and more detailed application of the method to Jupiter (27). A similar calculation in which the isothermal assumption is replaced by adiabatic behavior in the outer region gives essentially the same conclusions regarding mass distribution, and it supplies the additional information on increasing temperature with increasing distance (28). An alternative approach that invokes selective wave-particle interactions to trap ions in the potential well of the outer region predicts densities much greater than photoelectron-diffusive equilibrium values inside of the $L(\phi = 0)$ distance (29). However the difficulty

that this fact presents is not addressed in the model. What prevents the excess counter current of electrons from the outer region which would continue until the outer region density is reduced to a point where the counter current is in balance with the source current? This balance is achieved at the photoelectron-diffusive equilibrium density.

The assumption of thermodynamic equilibrium of the photoelectron component implies that collisions or interactions have isotropied the photoelectron beams from the source regions. The references cited note that in the equatorial region interactions between the oppositely directed beams from the two hemispheres should be strong and serve to populate the outer region quickly. Although Coulomb scattering will also serve, its efficiency depends on density, and at the low initial densities it could be negligible (29). The importance of two-beam processes might be tested by comparing observations at Jupiter, Saturn and Neptune where they are expected to operate with those at Uranus at solstices when only one beam from the sunlit hemisphere exists, although, as will be seen, the actual densities there are expected to be small.

B. Loss Processes: In-place removal, i.e. neutralization, and removal by radial transport, inward or outward, characterize the static and dynamic forms of possible loss processes. Neutralization entails only recombination since in charge exchange there is no net loss of ions. Radial transport can take the forms of organized convection, flux tube interchange diffusion, and a centrifugally driven radial wind blowing along outer region field lines that have been extended to disruption by the centrifugal force. If radial transport is not efficient enough, the density will be self-limited by recombination. We therefore look first at the transport loss processes.

Convection is normally associated with the magnetospheric circulation driven by the solar wind, and which is paramaterized in Table 5.2. by the

convection electric field. In the sense that convection means organized magnetospheric circulation, other forms are possible. Organized atmospheric winds can couple through ion-neutral collisions in the ionosphere to drive magnetospheric convection, as for example, in the case of Earth tidal winds drive Sq convection (144). The centrifugal force acting on a fixed azimuthal density inhomogeniety in the plasmasphere can give rise to an autogenic convection system (145). However the importance as loss mechanisms of these non-solar-wind forms of convection has not been demonstrated, and we will consider only the solar wind form.

Convection essentially sweeps away all plasmasphere particles beyond the distance R_Ω given in Table 10. Thus if R_Ω is less than $L(\lambda_p)$, the plasmasphere is terminated by convection rather than by the tail. However a practical matter prevents a straight-forward comparison. Table 5.2 shows the dependence of R_Ω on the solar wind merging electric field, E_m, which is essentially a stochastic variable. Thus R_Ω is also essentially a stochastic variable. The question then arises, what value of R_Ω should be used for the intended comparison? To find the answer involves combining the steady ionospheric source with the stochastic removal to obtain statistics on the now variable extent of the plasmasphere. Such a program has been carried out only for Earth (146). This case illustrates the nature of the problem. The average value of E_m at Earth is about 0.5mV/m, which corresponds to R_Ω equal to about 12 R_E. But the median distance to the plasmapause is only about 5 R_E. The large difference results from the fact that the characteristic time for refill from the ionospheric source is long compared to the time interval between large positive excursions of E_m which drive the convection close to Earth sweeping away the accumulated ionospheric flux.

These results for Earth can not be simply transformed, by scaling laws for example, to obtain comparable results for other planets. The nonlinear

evolution of solar wind structure should radically change electric field statistics between 1 AU and the outer solar system. Thus we leave for future effort the stochastic treatment needed to find the appropriate value of R_Ω for comparison with $L(\lambda_p)$.

It is nevertheless useful for the purposes of discussion to compare the values of R_Ω obtained with the average of E_m for each planet with the characteristic diffusive-plasmasphere dimensions listed in Table 5.4. These values labeled L_Ω are also listed in the table. The above comments indicate that L_Ω greatly overestimates the convection limit of the plasmasphere. For present Earth it is about a factor of two too large; and for Paleo-Earth with $\mu_p = 3$, it is a factor of three too large (cf. Figure 5.2). The interesting results pertain to the giant planets, since Mercury has no ionosphere to act as a plasmasphere source, and as noted in the previous section, the ionospheric conductivities at Venus and Mars dominate the dynamics and invalidate the electric field scaling relations of Table 5.2.

The values of L_Ω are larger than the corresponding values of $L(\lambda_p)$ by factors of about 10 for Jupiter and Saturn and about 5 for Uranus and Neptune. This comparison has frequently been used to conclude that solar wind convection can be ignored at the giant planets. In light of the above discussion, however, these factors do not seem so convincingly large. For example, an electric field 100 times larger than average at Jupiter would bring convection into the outer region of the diffusive plasmasphere. Such an electric field was easily exceeded during the solar wind storm of August, 1972 (147). The recurrence period for such storms is probably less than 100 years, since the storms of September, 1859, and February, 1872, were probably even larger (148). However about 600 years are needed by the ionosphere source to fill the flux tubes at L=45 to an average density of 1 cm^{-3}. Infrequent, extreme values of E_m can therefore hold the density in the outer

most plasmaspheres of Jupiter and Saturn to values less than 1 cm^{-3}, many orders of magnitude less than the predicted pure-diffusive equilibrium value.

In the cases of Uranus and Neptune, a hundred-fold increase in E_m would sweep out plasmasphere ions beyond roughly L=20. Thus, it appears likely that the densities beyond that distance are kept low by convection. The ionospheric flux would fill a L=20 flux tube to an average density near 1 cm^{-3} in a period of 100 years -- which we take to represent the recurrence period of extreme convection events. But for these planets, one particle per cubic centimeter exceeds the diffusive equilibrium density at that distance. Convection and diffusive equilibrium appear to be sufficient to keep the outer region densities below 1 cm^{-3} throughout.

The primary plasmaspheres of Uranus, Neptune and Earth are very similar in this description, in the sense that convection and diffusive equilibrium alone can control the density distribution. In the cases of Jupiter and Saturn, additional loss processes seem to be required, because diffusive equilibrium values become excessively large inside of the distance where even the extreme convection events are likely to penetrate (see Figure 5.7.

We note that the customary exclusion of convection from the magnetospheres of the giant planets has also been questioned in a different context (21). Convective flows at these objects, in contrast to at Earth, are predicted to be super-Alfvenic. The flow kinetic energy can therefore distort the dipole field and result in deeper penetration of the flow. Also it is questionable whether the ion-neutral coupling in the ionosphere can enforce corotation in the outer magnetospheres of the giant planets. A reduced effective corotation speed also permits deeper convection. The quantitative aspects of these possibilities have yet to be determined,

but the qualitative effect will be to aid in eliminating the high-density catastrophy predicted for diffusive equilibrium acting alone.

The non-convective loss processes for the Jupiter and Saturn situations are illustrated in Figure 5.8, following the physical conceptualization first developed for Jupiter (27). The density is expected to be equal to the lowest limit at any given distance, L. The figure shows the density to be bounded by diffusive equilibrium values inside of L≈7 to 8 and by interchange diffusion values at greater distances. However, some discussion of each of the mechanisms is in order.

The static loss process, recombination, limits the density to the value where the recombination rate in a flux tube balances the ionospheric flux into the tube. For L>1, this limit is given approximately by $\sqrt{f_o/\alpha R_p}\ L^{-9/4}$, where f_o is the maximum ionospheric flux (taken to be $2.5 \times 10^8\ d^{-2}\ cm^{-2}\ sec^{-1}$, where d is the heliocentric distance to the planet in units of AU), and α is the recombination coefficient (taken to be $5\times10^{-12}\ cm^3 sec^{-1}$).

Considerable attention has been given to the Alfvenic limit (18, 141, 149), which occurs where the corotation speed is equal to the Alfven speed, or equivalently, where the corotation kinetic energy density is equal to the magnetic energy density. The limit is given by $n_A = n_A^* L^{-8}$, where $n_A^* = B_p^2/(4\pi m_i \Omega^2 R_p^2)$. Beyond this limit the centrifugal force is envisioned to dominate, stretching the field to disruption and thereby allowing the plasma to escape by flowing along field lines. The aspect of a centrifugally driven planetary wind gives this process special interest. If it occurs, the stellar characteristics of Jupiter and Saturn would be augmented by the addition of a stellar-like wind: material from the atmosphere blown off with energy derived internally. The analogy is not perfect. The intermediate step of transporting ions from the source surface to the outer region uses external energy. Nevertheless, the interaction with the solar wind would acquire some new aspects compared to Earth-like inter-

actions. Because of the solar wind dynamic pressure on the dayside, the planetary outflow would most likely be confined to the nightside (19). The interesting question of how tailward outflow and planetward inflow from convection can both occur has yet to be resolved. The figure suggests that the resolution might not be necessary. Interchange diffusion as presently calculated keeps the density below the Alfvenic limit. But as is discussed below, the calculation is not free from uncertainty, and a density exceeding the Alfvenic limit can not definitely be excluded.

The discussion of the interchange diffusion limit centers around the appropriate diffusion coefficient, D_{LL}, to use in the associated diffusion equation.

$$\frac{d}{dL}\left[\frac{D_{LL}}{L^2}\frac{d}{dL}(nL^4)\right] = -S/2\pi R_p^3 \qquad (5.4)$$

(See for example 150. - In the usual application to energetic particle diffusion, n is the phase space density. But since for low energy particles D_{LL} does not depend on particle velocity (34), we integrate over velocity space, so that n here is number density. More precisely n is the average number density in a flux tube, but for simplicity we are ignoring density variations along the flux tube). The source term S is the number of new ions per second added to the magnetic shell between L and L+dL. For the ionospheric source, we find the approximate expression (for L > 1)

$$S = \left(1-\frac{n}{n_d}\right) 2\pi R_p^2 f_o L^{-5/2} \qquad (5.5)$$

The ionospheric source strength is the part outside of parenthesis. The part in parenthesis takes account of ambipolar diffusive connection between the ionosphere and the magnetosphere, which tends to drive the solution to the diffusive equilibrium limit. If $n<n_d$ there is a net flux

out of the ionosphere, and a positive source for the magnetosphere; if $n>n_d$, the reverse obtains.

Two separate mechanisms for producing interchange diffusion are described in the literature: centrifugally driven interchange instability (27, 28, 141-145, 152-154) and interchange motions driven by ion-neutral coupling to atmospheric winds in the ionosphere (33-35, 155). However as yet only the first has been invoked to estimate density limits at Jupiter (27, 28) and Saturn (98). Such estimates have been made only in the strong diffusion limit in which D_{LL} is assumed to be so large that the condition nL^4 = constant must hold as an approximation in order to balance the diffusive and source terms in equation (5.4). An explicit expression for the diffusion coefficient associated with the mechanism is therefore not required and none has been determined. There is a logical difficulty with the procedure. The balance could also be achieved by the condition that $(D_{LL}/L^2)(d/dL)(nL^4)$ be approximately constant. The first choice, which has been made in practice, amounts to replacing a second order differential equation with a first order one, which has just one integration constant. This has the consequence of restricting the ability of the solution to fit boundary conditions. The expectation that the plasmasphere density at the outer boundary should be comparable to the solar wind density leads to density profiles similar to those in Figure 5.8. The maximum density occurs around L=10 with a value between 10 and 100 cm^{-3} (27, 28).

However, in the context of a diffusive process, the outer boundary represents a sink to plasmasphere particles, either through escape onto open field lines in the tail or through convective sweep-up. Thus plasmasphere particles that reach the boundary are lost and none return. The outer boundary condition should therefore be, n=0. An explicit expression

for the diffusion coefficient and two integration constants are needed to accommodate arbitrary inner and outer boundary conditions.

The second mechanism, atmospherically driven interchange motions, has been investigation in connection with the inward diffusion of relativistic electrons needed to supply the energy to maintain Jupiter's decimetric synchrotron emission. Its operation at least at Jupiter seems necessary to account for the observations (e.g. 33). The diffusion coefficient derived for this process has the form $D_{LL} = \kappa L^3$, where κ for Jupiter lies in the range 2×10^{-10} to 2×10^{-9} sec^{-1}. How κ varies between the planets depends on whether the motions arise internally by the dynamical instability of the atmosphere, or as has been suggested (35), if they are induced externally by the magnetospheric convection.

Estimates of the Richardson number, which characterizes the overall dynamical stability of a planetary atmosphere, are shown in Figure 5.9 for the giant planets and Earth (156). The larger the Richardson number, the more stable the atmosphere. Jupiter and Saturn are more than an order of magnitude more unstable than Earth; and Uranus and Neptune are more than three orders of magnitude more stable than Jupiter and Saturn. If atmospheric instability is the origin of interchange motions, then on the basis of this comparison, the diffusion coefficient for Saturn should be similar to but a little smaller than that for Jupiter. The diffusion coefficients for Uranus and Neptune should be very much less than for Jupiter.

To obtain rough, illustrative values in the case that the motions are induced by magnetospheric convection, we use a scaling relation based on the calculation of the atmospheric interchange diffusion coefficient (34), $D_{LL} \sim \Omega\phi_c^2/B_p^2$, where the convection potential ϕ_c scales according to Table 5.2, and B_p is the surface field strength. The

diffusion coefficients are then found to be in the ratios J:S:U:N::1:2:0.06:0.03.

The diffusive equilibrium limits shown in Figure 5.8 are based on the values 2×10^{-10} for Jupiter and 1×10^{-10} for Saturn. These are at the low ends of the ranges just discussed. The calculated density values are then upper limits within the given ranges. Also, it should be mentioned that the existing contact between theory and experiment is confined to the inner magnetosphere of Jupiter, to distances less than approximately 6 R_J. Estimates of the diffusion coefficient at greater distances is based on uniform extrapolation. Thus, calculations serve more the purpose of illustrating the behavior of the system than the purpose of providing quantitatively accurate predictions.

The inner boundary condition must be given to completely specify the solution. The natural boundary condition is $n=n_d$ at L=1. However, an approximate analytic solution is obtained by noting that in the region of inward diffusion, the density will remain close to the diffusive equilibrium profile. This is because the ionospheric source strength increases rapidly inward, whereas the interchange diffusion coefficient decreases rapidly inward. Thus, if we start at a point where diffusive equilibrium dominates and move outward until interchange effects appear, keeping in mind that diffusion must always act to decrease the gradient that would be present in the absence of diffusion, we see that the motion away from the diffusive equilibrium profile must be a rapid outward downturning into the outward diffusion portion of the curve. The diffusive equilibrium process can therefore be treated as a fully absorbing wall at some as yet unspecified inner distance. In this approximation, all particles brought to the fictitious wall by interchange diffusion are immediately lost to the atmosphere along field lines. With the interchange diffusion

term now replaced by an inner boundary condition, equations (5.4) and (5.5) can be integrated directly with the integration constants fixed by the conditions n=0 at the inner and outer boundaries. The resulting density profile has a maximum with the approximate value $n_m = f_o/(6\kappa R_p L^{11/2})$, where the value of L is determined by the condition $n_m(L) = n_d(L)$. The profiles in Figure 5.8 were obtained by this method.

The expression for n_m illustrates the sensitivity of the calculation to the uncertainties in the parameters characterizing the physical processes involved. It is directly proportional to the photoelectron flux, inversely proportional to the interchange diffusion coefficient, and through its dependence on L, it is also controlled by the exponential factor β. Nevertheless, the similarity between the peak in the calculated density profile for Jupiter and the feature labeled the ring current in the report of the Pioneer 10 plasma observations (26) suggests that the primary plasmasphere of Jupiter may have been detected, although future in situ measurements are needed to make such an identification definite.

5.4 Satellite Sources -- Features and Processes:

Satellite effects on energetic particles have been mentioned in the earlier sections on magnetospheric phenomenology, and they are more fully discussed in the companion article on Jupiter's magnetosphere. In this section we will concentrate on the satellites and their neutral particle rings as sources of low energy plasma for planetary magnetospheres. Interest in this topic is generated by the many observations of Io-related magnetospheric neutrals and ions, and the high probability of similar phenomena associated with other satellites, as have been summarized in Table 3.4.

The approach to be taken is the same as in the previous section. Atmospheric interchange diffusion will be used to disperse the ions

radially inward and outward from each source. The source in each case is taken to be a torus of neutral particles, spatially confined to radial and latitudinal dimensions that are small compared to the distance from the planet's center to the satellite's orbit. The aspects of the problem to be considered are the spatial distribution of the ions, the radial profile of density, and the contribution satellite ions make to the possible generation of a centrifugally driven magnetospheric wind.

A. Spatial Distribution of Satellite Ions:

In the context of particle drift theory, interchange diffusion violates the third adiabatic invariant but preserves the first two (150). The first invariant is determined by the condition that the corotating planetary magnetic field accelerates a newly created ion such that in the satellite's frame of reference it acquires a guiding center velocity equal to the corotation velocity and a gyro speed also equal to the corotation speed (157). The second invariant is determined by the fact that the gyro speed acquired in this way is much larger than the particle's pre-ionization speed, so that the ion is in effect created at its mirror point (30). These determinations are sufficient to specify the particle's velocity characteristics, which include its mirror point location, at any subsequent radial distance to which it is carried by interchange diffusion. By tracing the radial trajectories of the mirror points of ions created near the latitudinal extremes of the neutral ring, one obtains an envelope roughly enclosing the radially dispersed ion cloud.

This procedure carried out for the Jovian system predicts the spatial distribution shown in Figure 5.10 (158). It is a meridional cross section through an axially symmetric (with respect to Jupiter's dipole axis) geometry giving the latitudinal extents of the ion clouds originating from each of the satellites. The distribution in each case is seen to be

described by a constant thickness disc outside the satellite's orbit (which was also predicted by a different approach, 20) and an approximately constant angle conical disc inside the orbit. The conical angle, which characterizes the latitudinal extents of the neutral particle rings relative to the magnetic equator, is determined in this case primarily by the 10° tilt between magnetic and rotational axes. The circular arcs at the distances of each of the satellites indicate the diurnal oscillation of the rings relative to the magnetic equator.

Interchange diffusion is seen to produce strong equatorial confinement of satellite ions. Confinement in the constant thickness region is the result of centrifugal force acting against the field aligned motion that would carry a particle to higher latitudes (20, 158). The usual diamagnetic or mirror force confines the particles in the conical region. As the figure indicates, the transition between the regions in which each force dominates occurs rapidly and at approximately the distance of the parent satellite.

The discussion so far only describes where satellite ions are allowed to be -- under stated assumptions. However, if a satellite is not a source of ions, it will not contribute to the density in its allowed confinement disc. If a satellite is an ion source, the density at any distance in its confinement disc must be determined by a radial transport equation.

B. The Radial Density Profile of Satellite Ions:

Under interchange diffusion the radial density profile of satellite ions will be governed by an equation similar to (5.4), but with modifications to take account of the latitudinal confinement geometry. With regard to the ions from a particular satellite, the satellite's orbit approximately separates the constant thickness and conical disc regions, and it also

separates the regions of inward and outward diffusion. Different forms of the diffusion equation apply to each region. Since the satellite is a point source in this one dimensional problem, the flux in each region is constant, and the equations can be integrated once immediately. The boundary conditions are 1) absorption of the ions at the inner and outer boundaries which are at L=1 and $L_b=L(\lambda_p)$, ignoring convection, 2) the inward and outward region densities must be equal at the satellite orbit, and 3) the sum of the inward and outward fluxes must be equal to the total ion production rate of the satellite, assumed constant. The relevant equations are

$$\frac{d}{dL}(n_i L^4) = \frac{F_i L^2}{4\pi\theta_c R_p^3 D_{LL}} \qquad \text{(inward)} \qquad (5.6)$$

$$\frac{d}{dL}(n_o L^3) = -\frac{F_o L^2}{4\pi\theta_c R_p^3 L_r} \qquad \text{(outward)} \qquad (5.7)$$

where θ_c (assumed small) is equal to the half-cone angle, L_r is the location of the satellite, F_i and F_o are the inward and outward fluxes, and the different powers of L on the left hand sides reflect the different geometries of the two regions.

As discussed in the previous section, atmospherically driven interchange diffusion is most likely the dominant process at Jupiter, at least in the inner magnetosphere, and possibly also at Saturn. Integration of the equations with the diffusion coefficient appropriate to this mechanism (κL^3) and application of the first boundary condition results in

$$n_i = \frac{F_i}{4\pi\theta_c R_p^3 \kappa} \frac{\ln L}{L^4} \qquad (5.8)$$

$$n_o = \frac{F_o}{4\pi\theta_c R_p^3 L_r \kappa} \frac{\ln(L_b/L)}{L^3} \qquad (5.9)$$

The second boundary condition gives the interesting result that the ratio of inward to outward fluxes depends only on the locations of satellite ($L = L_r$) and the outer boundary ($L = L_b$)

$$F_i/F_o = \frac{\ln(L_b/L_r)}{\ln L_r} \tag{5.10}$$

The ratios thus obtained for the major satellites are given in Table 5.5. Except for Io, the outward flux is larger than the inward flux in all cases.

Satellites	L_r	L_b	F_i/F_o
Jupiter			
Io	6	45	1.1
Europa	9.6	45	0.7
Ganymede	16	45	0.4
Callisto	27	45	0.2
Saturn			
Titan	20	36	0.2
Neptune			
Tritan	14.3	45	0.4

Table 5.5 Ratios of inward to outward fluxes of satellite ions calculated on the basis of atmospherically driven interchange diffusion and the stated boundary locations.

This marked asymmetry in the fluxes is not reflected in the behavior of the density. Application of the final boundary condition gives the complete solution, which is shown in Figure 5.11. The normalized density profile is seen to be remarkably insensitive to satellite and boundary positions. The density maximum occurs at L=1.28 for all satellites. The profiles begin to separate in the outer half of the radial range as a result of different satellite and boundary positions. Nevertheless,

all of the Galilean satellites and Tritan are contained between the curves labeled Io and Callisto.

The density for the "universal" profile is normalized to the value $(F_T/4\pi\theta_c R_p^3 \kappa)$ where F_T is the total ion production rate of the satellite. The absolute density on the right hand margin is based on Jovian parameters with $\kappa = 2\times10^{-10}$ sec^{-1} and $F_T = 10^{25}$ ions sec^{-1}, corresponding to the estimated Io source strengths for H^+ and Na^+ (Table 3.4).

Inside of about L = 8, the Io source dominates the ionospheric source in this calculation. The predicted densities can easily account for the inner plasmasphere detected by Pioneer 10 (30, 157). For example at L = 4 the predicted density exceeds 100 cm^{-3} and the density inferred from the data is roughly 60 cm^{-3}. Recombination must act to reduce the very large densities predicted close to the planet. For example, in a spherical volume with radius $6R_J$, the average density needed to cause recombination at the rate of 10^{25} sec^{-1} (the Io source strength) is n = 56 cm^{-3}. However, this is not an absolute upper limit, because radial diffusive transport makes the density nonuniform. This effect will be demonstrated explicitly in the following section on the interstellar medium.

C. Satellite Ion Contribution to Centrifugal Winds:

The Alfvenic limits associated with the absolute density scale and Jovian parameters are shown in Figure 5.11 for both hydrogen and sodium ions. For the chosen set of parameters, which represent present best estimates, the density of the sodium ion cloud from the Io source exceeds the Alfvenic limit beyond about L = 30. This result is consistent with the suggestion that heavy satellite ions might have a dominant effect on magnetospheric dynamics at Jupiter (20) and that the observed change from a dipolar to a disc-like magnetic field configuration at L = 30

might be an effect of the centrifugal force acting to eject low energy ions from the magnetosphere (19).

A rough Alfvenic limit for a source strength of 5×10^{26} H^+ ions in Saturn's magnetosphere is also indicated, but the associated absolute density scale is omitted. (The parameters $\theta_c = 20°$ and $\kappa = 1 \times 10^{-10}$ sec^{-1} were used to make the estimate.) As Table 3.4 shows such a source strength is not unreasonable for Titan. The density from such a source exceeds the Alfvenic limit near L = 14, well inside the distance of Titan, L = 20. This result predicts that if the parameters choosen are representative of the actual condition, nearly all of the ions from Titan are centrifugally ejected in the form of a magnetospheric wind. In this case the density inside of Titan's orbit should be based on the outer boundary condition $n = n_A$ at L = 20, where n_A is the Aflenic density limit.

5.5 Interstellar Medium Source -- Features and Processes:

The solar system appears to be presently in a hole in the interstellar medium. The local interstellar density is only about 10 percent of the average density within 1 kpc of the sun (105). There must be times when the sense of the anomaly is reversed. It is estimated that the solar system has traversed clouds with H_2 densities exceeding 10^2 cm^{-3} and 10^3 cm^{-3} on at least 45 and 5 occasions, respectively (106, 159).

Such high density clouds can profoundly effect the solar wind, as is described in the companion article on that topic. They can result in a condition in which the orbits of the outer planets lie wholly outside of the heliosphere, or in which they intersect it only in a restricted portion. For substantial periods of time, outer-planets magnetospheres would then not be confined by the solar wind, and the associated features and processes would not exist. The outer boundary conditions used in the previous sections to obtain solutions for primary and accidental plasma-

spheres must also be respecified accordingly. This section will be restricted to a discussion of 1) contemporary secondary plasmaspheres of the outer planets, that is, plasmaspheres for which the source is the ionization of the interstellar neutrals that are inside of the magnetosphere, and 2) the modifications of the various kinds of plasmaspheres that occur in the high density interstellar cloud situation described above.

A. Specification of the Source:

The ionization mechanisms are photoionization, charge exchange, and electron-impact ionization. Although the last mentioned is very important in some contexts (e.g. 83) in the present problem it does not change the formalism or general conclusions obtained without it; and we consider only the first two.

Magnetospheres are "optically thin" with respect to the passage of the interstellar medium through them. That this is so is not obvious a priori since although charge exchange does not cause a net change in the ion density, it can act to deplete the neutrals if the characteristic speed of the ion population is larger than that of the neutrals. Each reaction then results in a neutral that leaves the system faster than it otherwise would have done. By acting to deplete the neutrals, this mechanism reduces the source strength for magnetospheric ions. For a given interstellar density, the charge exchange rate is proportional to the product of ion density and corotation speed. Thus, the depletion effect will be important only for ion densities larger than a certain value. Assuming a north-south component of flow of the neutrals across the magnetosphere of 10 km sec^{-1} (this is the shortest path through it), we find that value to be roughly $10^5/L^2$ cm^{-3}. As will be seen, it exceeds the den-

sities actually achieved by secondary plasmaspheres, even in high density clouds.

The interstellar source strength is therefore uniform throughout each magnetosphere and has the value N_o/τ_{ph} ions cm^{-3} sec^{-1}, where N_o is the interstellar neutral particle density at the planet in question and τ_{ph} is the associated life-time against photoionization.

B. Loss Processes in Static Magnetospheres:

We take the magnetospheres of Uranus and Neptune to be examples of cases in which non-centrifugally driven interchange diffusion can be ignored. This is very likely to be the case in the high density cloud situation when any possible interchange diffusion derived from the coupling to the solar wind is eliminated. The modification of the static density limits caused by interchange diffusion is estimated in the following section.

In a static situation the steady accumulation of ions by photoionization of the interstellar medium is limited by recombination according to the relation familiar from ionospheric physics $\alpha n_i^2 = N_o/\tau_{ph}$. Static equilibrium densities for contemporary values of N_o (Table 3.7) and for $N_o = 10^2$ are given in Table 5.6.

Of course the recombination limit can not apply to indefinite distances. Centrifugal interchange diffusion can transport ions radially outward in the region beyond roughly $L = L_s$. Without taking up the question of the form of the diffusion coefficient for this process a rough conservative estimate can be made under the assumption of strong diffusion, which results in a L^{-4} profile for density.

The results of the procedure applied to contemporary values of the parameters for Uranus and Neptune are shown in Figure 5.12. (The time required to accumulate the equilibrium densities is longer than the

orbital periods in both cases. The effective source strengths are then about half of the values in the apex direction of Figure 3.3, which were used here. However, the uncertainty in the values are larger than a factor of two, and the numbers in the figure are at the low end of the empirical range, so we have ignored the complication of integrating around the orbits.) The secondary plasmasphere densities of these planets exceed those of their primary plasmaspheres inside of about L = 15 (cf. Fig. 15). In the case of Uranus the interstellar source therefore dominates in forming low energy plasma features inside of the solar wind convection limit. The same will be true for Neptune if Tritan is not a significant ion source, or if it is a source but interchange diffusion is controlled by the centrifugal force. Then the secondary and accidental plasmaspheres will dominate separately in the regions divided by Tritans orbit at L ≈ 14.

C. Loss Processes in Dynamic Magnetospheres:

In the cases where ions are transported radially by interchange diffusion, equation (5.4) applies. In the present case the source function is

$$S = 2\pi R_p^3 L^2 \frac{N_o}{\tau_{ph}} \qquad (5.11)$$

and solutions using the atmospheric form of the diffusion coefficient with absorption boundary conditions and contemporary parameters are shown in Figure 5.12 for the cases of Jupiter and Saturn. Even with the contemporary values of N_o = .05 cm^{-3} at Jupiter and .07 at Saturn, the predicted density of the secondary plasmaspheres is appreciable. At Jupiter, it exceeds that of the primary plasmasphere inside of L = 7, and it is about a factor of 50 less than the density of the accidental plasmasphere of Io.

The static density limit, which is proportional to $N_o^{1/2}$, increases faster than the dynamic limit as N_o increases. This corresponds to the fact that L_{rec} approaches L_d as N_o increases. When they merge, radial transport does not augment the source strength, and the two limits are the same.

D. Plasmaspheres in High Density Clouds.

Consider first dynamic magnetospheres. The inner boundary condition to the diffusion equation is still $n(L=1) = 0$, but the solar wind absorption boundary condition does not exist in this case. What to replace it with is not immediately obvious. Without an external constraint, the system must determine its own outer boundary condition. It seems apparent that the boundary to the diffusion region will be an Alfvenic transition to a centrifugally driven magnetospheric wind. But even when this constraint is imposed, there remains one more unknown than there are equations. Some extra condition is needed to fix the solution. A consideration of the internal stability of the solutions with respect to small changes in time (in the source, say), leads us to conclude that the stable solution is the one in which the Alfvenic point is as close to the planet as possible, consistent with its being in the region of outward directed diffusive flux. Actually, as close to the planet as possible means that it be at the separation between the inward and outward diffusive flux regions.

In the present proposal the plasmasphere sits at the point of marginal stability with the density adjusted such that any additional accumulation of ions inside the Alfvenic point are transported towards the planet by diffusion, and ions accumulated outside that point are carried away in the centrifugal wind.

This condition applies formally to all three types of plasmaspheres.

(In the case of satellite ion plasmaspheres, it is possible for the Alfvenic point to lie outside the satellite orbit and still be at a point of zero outward flux by requiring the density profile to be strictly L^{-3} in the separation.) In the case of more than one source, the one that predicts the closest Alfvenic point determines its location. The other density profiles are then determined by the condition that the density vanishes at the now fixed Alfvenic point.

The Alfvenic distances for the case $N_o = 10^2$ cm^{-3} for the various plasmaspheres of Jupiter and Saturn are given in Table 5.7. We find that the interstellar source dominates in determining the distance at both planets. Within the diffusion region, the secondary plasmasphere also dominates the density profile in both cases, with densities rising to the dynamic recombination limit given by equation (5.12), namely, 400 cm^{-3} (J) and 200 cm^{-3} (S).

	Primary		Accidental		Secondary	
	$L(R_p)$	$n(cm^{-3})$	$L(R_p)$	$n(cm^{-3})$	$L(R_p)$	$n(cm^{-3})$
Jupiter	55	.01	23	12	17	130
Saturn	33	.05	20	3	17	10
Uranus	-	-	-	-	109	3×10^{-4}
Neptune	-	-	-	-	122	3×10^{-4}

Table 5.7 Alfvenic distances separating diffusive inward flow from centrifugally driven outward flow (a magnetospheric wind) for isolated plasmaspheres. (The accidental plasmasphere of Jupiter is the Na^+ cloud of Io). Based on self-determined outer boundary condition and $N_o = 10^2$ cm^{-3}. Dynamic cases -- Jupiter and Saturn, static cases -- Uranus and Neptune.

The determination of the outer boundary condition for static magnetospheres is straight-forward since the centrifugally driven diffusion is outwards only and its value at every point is fixed by its inner boundary condition namely n = static recombination limit at $L = L_s$ (Table 5.6). Then it is only a matter of finding where the L^{-4} profile of diffusion crosses the L^{-8} dependence of the Alfvenic limit. The results, given in the Table show

that the diffusive plasmaspheres extend to very large limits in these cases.

Chapter 6
Long-Term Aspects

6.1 Introduction

One theme implicit in the preceding sections is that the subject of comparative magnetospheres can be unified by representing each magnetosphere by its determining set of independent variables. The various qualitative types of magnetospheres are separated by divisions in the parameter space defined by these variables. If the project of mapping the divisions could be completed and the phenomenology characterizing all magnetospheric types identified, specification of the independent parameters of a particular magnetosphere would immediately classify it and give its relation to all other magnetospheres. The project was illustrated with the contemporary examples of planetary magnetospheres. In this section we note that the principle of the project can be used to discuss the long term aspects of planetary magnetospheres in terms of the time variations of their determining independent parameters.

6.2 Time Variations of the Independent Variables:

Of the four types of variables, solar, planetary, galactic, and satellite, all but the last have well defined and characteristic time variations. These affect planetary magnetospheres on time scales ranging from seconds in the case of solar wind shock waves to several hundred million years which separate encounters with dense interstellar clouds and characterize the long term modulation in the rate of geomagnetic reversals. There are even longer term variations associated with the stellar evolution of the sun. With regard to the more poorly documented time changes in satellite parameters, one could mention the suspected rapid appearance of the suflur ion cloud of Io (70). Under this heading one could also include the change in the rotation period of Earth with perhaps an associated change in its dipole moment that has taken

Approximate Periods and Characteristic Times	Types of Variations in Solar, Planetary and Galactic Parameters
7 sec to 3 hours	Passage of Solar Wind Shock Wave over the Magnetosphere of Each Planet
5 to 10 days	Solar Wind Streams and Magnetic Sectors
25 days	Solar Rotation Period -- Disturbance Recurrences
.1 to 100 years	Semiannual and Annual Variations at Each Planet
11 years	Sunspot Cycle
22	Solar Magnetic Cycle
80	Gleissberg Solar Cycle
Several Hundred	Long Term Solar Activity Cycle
1 to 10 Thousand	Geomagnetic Drift Period, Geomagnetic Excursion and Reversal Durations
200 to 300 Thousand	Characteristic Interval Between Geomagnetic Reversals
100 Million	Characteristic Interval Between Dense Interstellar Cloud Encounters
300 Million	Characteristic Interval Between Changes in the Rate of Geomagnetic Reversals
>1 Billion	Evolutionary Changes in the Sun

Table 6.1 Abreviated list of characteristic times and periods associated with different types of variations in solar, planetary and galactic parameters. (Abstracted from 164-166).

place as a result of the dynamic interaction of the Earth-Moon system (e.g. 167). A short list of non-satellite variations is given in Table 6.1. These topics have been well reviewed recently (160-166), and the comments on them here can be correspondingly selective and brief. The magnetospheric effects of variations in galactic parameters have already been considered in the previous section.

A. Solar Wind Variations:

Direct monitoring of the solar wind with instrumented spacecraft has occurred since 1962, but with some gaps in coverage. A little more than one solar cycle has been observed. The data indicate that solar wind variations fall roughly into two groups, those associated with long lived streams more-or-less localized to quasi-permanent solar longitude sectors, and those associated with solar transient events. Both types are related to the structure and activity of the solar magnetic field. There is a subtle solar cycle variation of solar wind parameters, which involves changes in the dominance of the two types of variations, and which reflects a corresponding solar cycle variation in the determining solar magnetic field. The full subject is described in the companion article on the solar wind. Its relevance here is that the measured variations which are restricted in time to essentially one particular solar cycle (number 20) make up the entire data base from which the averages and deviations of solar wind parameters can be calculated. The values so obtained have been used to derive long term statistics on the magnetospheric parameters at Mercury (168) and Paleo-Earth (131- see Figure 5.2. The results are instructive and illustrative, but it now appears that they need to be qualified by the statement that they are representative of a solar condition that is transient, although most likely recurrent.

There are several indications that the unsteadyness of the sun extends to periods beyond the 11 and 22 year sunspot and magnetic cycles. The well known Gleissberg 80 year cycle is evident in the variation of sunspot cycle amplitudes (169, 170) and in power spectra of the sunspot waveform (172). It seems to be present also in the shorter record of geomagnetic disturbance indices (173, 174). In

particular the series of yearly averaged aa indices taken at consecutive solar minima shows such a variation. An empirical calibration between the aa index and solar wind parameters has been used to suggest that during the solar minimum around 1900, the average solar wind speed was of the order of 200 km sec^{-1}, or the average strength of the interplanetary magnetic field was correspondingly reduced (175). These are significantly below the normal range of yearly averages based on direct measurements (176).

The Maunder Minimum, the period from 1645 to 1715 during which sunspots were essentially absent from the face of the sun, is now a well documented instance of long term solar variability (165, 177). Solar wind conditions were affected as evidenced by a sympathetic absence of aurora during that period. The associated solar wind effect is revealed also in anomalous values of the ^{14}C content of contempoaneous tree rings. The sense of the anomaly implies a reduction in the efficiency with which solar wind opposes the entry into the solar system of galactic cosmic rays, which produce the ^{14}C in the upper atmosphere. The tree ring record of ^{14}C extends back about 9000 years. It gives evidence for the existence of many positive and negative anomalies, of which the Maunder Minimum is the most recent example (Figure 6.1) (164). The implication is that either the intensity of the galactic cosmic rays itself has changed to produce the anomalies, or the solar wind modulation of galactic cosmic ray intensity has changed. The additional information pertaining to the Maunder Minimum supports the second interpretation.

The very long term record of solar wind and solar cosmic ray behavior that is contained in the lunar surface is now beginning to be deciphered in the samples returned to Earth (e.g. 171). Preliminary

indications are that the average solar wind speed for the last approximately one billion (10^9) years is close to the directly measured, contemporary (~10 year) average. The ~500 lunar sample values, on which the long term average is based, are themselves approximate 2000 year averages, because of the way the speed is recorded. Individual values show appreciable departures from the average, with a rather high frequency of low values (around 200 km sec^{-1}), and a high value tail reaching to around 1000 km sec^{-1}. Similarly, the average energy distribution of solar flare cosmic rays has apparently not changed significantly over the last several billion years. Although they have not been discussed in detail, the deviations from average in this case have a direct application to terrestrial effects during magnetic reversals (see below).

The last comment leads to another important aspect of long term solar variability, the topic of extreme solar events, such as the solar flare sequence of August 1972. As is well known in many geophysical and astrophysical contexts, a single extreme event or the cumulative effects of more than one can cause changes in the environment that are quasi-permanent. In order to investigate such possibilities in the present context, it is desirable to have a quantitative measure of the extreme events the sun is capable of producing. Two efforts in this direction have been made.

The occurrence frequency of extreme solar wind compression events can be inferred from a statistical study of extreme inward displacements of the magnetopause of Earth (178, 179). For example, the subsolar magnetopause was found to be inside the distance to synchronous orbit (6.6 R_E) about 0.3 percent of the time in a two year interval of observation. Compared to its average value, an increase of about a factor

of 20 in the dynamic solar wind pressure is needed to produce such a compression. However, the short span of observation necessarily restricts the usefulness of the result to the general subject of long term solar variability.

In a somewhat less restrictive study the theory of extreme value statistics was applied to the 100 year record of geomagnetic aa indices and the 200 year record of sunspot numbers (180, 181). The technique gives the expected range of the largest value the index achieves in a solar cycle as a function of the number of cycles considered. It is illustrated in Figure 6.2 for the case of the first, second and third largest storms per solar cycle as measured by twelve hour averages of the aa index. The result shows that the largest value per solar cycle increases slowly with the number of cycles considered. In a set of 100 cycles, the range of the largest value is expected to be only 39 percent larger than the range for the 9 cycles that were used to do the study. However, some of these cycles will be very active, with the aa index of the third largest storm exceeding the largest value presently on record.

The technique of extreme value statistics has yet to be applied to solar cosmic ray events, for which the record might be too short. The records used in the above studies do not include the Maunder Minimum, or more specifically, a representative set of solar anomalies, and so the results must be qualified as applying to intervals in which the mode of solar activity is the same as at present. However, the lunar sample analyses suggest that the "statistical weight" of the present mode might be large. It would nevertheless appear at the present time that the best hope of quantifying extreme solar events for the purposes of long term studies lies in further lunar sample analyses, especially of the solar cosmic ray component.

B. Planetary Magnetic Field Variations and Non-Dipolar Magnetospheres:

The only planet for which there is a record of magnetic field variation is Earth. That the magnetic dynamo theory which appears to account for the field of Earth can be extended to other planets, as is described in the companion article on that topic, suggests that there might be similarities in the time dependent behavior of planetary magnetic fields. However, the theory is not developed to the point where it can either predict that behavior outright or transform the observations at Earth to predict the behavior at other planets. The comments here are therefore restricted to the case of Earth.

As we have seen, with regard to the plenatary variables, the subject of comparative magnetospheres focuses on the strength and orientation of the dipole moment. Paleomagnetic studies, which are quite reliable concerning field directions, show that the present 11° offset between the dipole and rotational axes is typical of the paleofield, and that deviations from this value are not large (182) (except during reversals and excursions which are considered below). On the other hand, the strength of the paleofield, which is a more difficult measurement, appears to vary by a factor of roughly two around approximately the present value (183, 184). A cyclic oscillation in strength is evident in the results of paleomagnetic studies of archeological materials dating back to 9000 years before present (183). It is also revealed in the large, systematic variation of the ^{14}C data shown in Figure 21. The variation in strength of the magnetic field modulates the intensity of the galactic cosmic rays that enter the atmosphere, and hence the production rate of ^{14}C. The period of the revealed cycle is around 8000 years. The dipole was at a maximum (~1.5 × present value) ca. 1500 years ago, and at a minimum (~0.5 × present value) ca. 5500 years

ago. The strength of the field is presently decreasing at a rate that if extrapolated linearly would cause a reversal at 2230 AD (185). Over longer periods of time, the range of measured dipole strengths increases. The range characterizing the period back to about 10 million years ago is roughly 10 percent to 300 percent of the present value (184). This is the range chosen to illustrate the variability of magnetospheric parameters for Paleo-Earth in Figures 10 and 11.

Magnetic reversals recur irregularly but on average about every 200 thousand years (166, 186). The present polarity epoch, which began 700 thousand years ago, is unusually long. This average rate applies to roughly the last 100 million years. Over longer periods there is a modulation of the rate such that intervals with about the present recurrence rate alternate with intervals with a much smaller recurrence rate, so called quiet intervals (187).

An overly simplified model of a magnetic reversal, one which is violated in varying details in individual cases, is the following. The reversal onset is marked by a reduction in dipole strength to the order of 10 to 20 percent of the pre-reversal value. The time span over which the reduction occurs is short compared to the duration of the reversal itself, and so the onset appears to be sharp. The reduced dipole strength condition persists for the order of 10 thousand years and ends by a return to a pre-reversal strength in an abrupt manner, as it began. The reversal of the dipole orientation occurs somewhere in the middle of this period, and may require only 2 or 3 thousand years as evidenced by the actual motion of the field direction at a given site. The surface intensity of the reduced dipole field is of the order of that of non-dipolar components, based on 1) the historical ratio of non-dipolar to dipolar field strengths, 2) the assumption that that ratio is typical

of the paleo-field (for which there is supporting evidence, 188), and 3) the assumption that the non-dipolar field strength does not change significantly during reversals (see 189 for a discussion of this point). The reversal itself appears to be the result of an excursion of the dipole strength through zero rather than an excursion of the dipole direction through 180° (but see 186 for a fuller discussion). In this case and under the same assumptions, the non-dipolar terms would dominate the surface field during the reversal phase of the reversal event.

The historical non-dipolar field alone could stop the contemporary solar wind at a geocentric distance of about 3 R_E, although the distance would vary diurnally because of the longitudinal structure of the field (190). However, at 3 R_E and beyond a residual dipolar component with a surface strength of only 30 percent of the non-dipolar field would begin to dominate (122). The reversal process is not likely to cancel the planetary dipole field exactly, and many magnetospheric scenarios are therefore possible. For example, the solar wind might interact mainly with the residual dipole field, but the interior of the magnetospheric might be structured primarily by the higher order field.

The orientation of the residual dipole field is essentially indeterminate as far as present knowledge of it is concerned. Assuming that the orientation is equally likely to be in any direction, we see that it is more likely to be near the equator than near the poles, because of the larger solid angle per degree of latitude at the equator. Thus, it is a priori most likely that the solar wind would interact with a near equatorial, and therefore rotating dipole, as identified as a Type III interaction in Table 5.1 (122).

If we consider the aspects of a Type III interaction and a non-dipolar interior structure separately, we can see that the major mag-

netospheric consequences in each case are as illustrated in Figures 6.3 and 6.4. The rotating, equatorial dipole interacts with a constant polarity solar wind magnetic sector to cause an alternating sequence of open and closed magnetospheres (122). A non-dipolar field as exemplified by the historical quadupole component, results in globally distributed auroral precipitation in association with two great circles intersecting at right angles (191). The main points are that the major part of the solar wind electric field is in a merging orientation for an extended period each day, and that the region of the atmosphere accessible to magnetospheric and solar particle precipitation is greatly increased compared to the non-reversal situation.

The condition of increased vulnerability of the atmosphere to solar cosmic ray events and the ~10 thousand years duration of this condition suggests that events much larger than that of August, 1972, can cause major changes in stratospheric temperatures and ozone content on one or more occasions during reversals (192, 193). Such events might affect global weather and they might account for the observation of faunal extinctions that occur in coincidence with magnetic reversals. The causal mechanism in the latter case is the depletion of statospheric ozone and, hence, increased ultraviolet radiation at the ground (193).

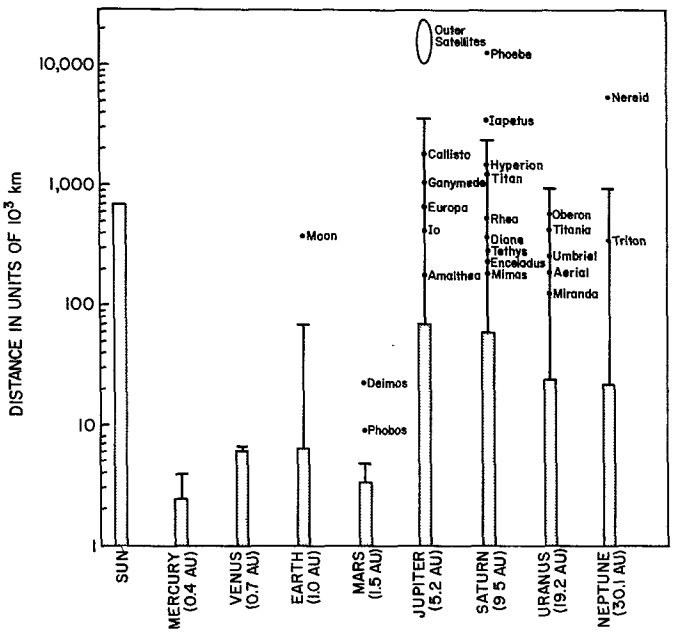

FIGURE 2.1 Dimensions of the radii of the sun and planets (cross-hatched), the radii of the orbits of their satellites (dots), and the characteristic dimensions of their magnetospheres (bars)—defined as the planetocentric distance to the subsolar stagnation point of the solar wind. The magnetospheric dimensions for Mercury, Venus, Earth, Mars, and Jupiter are based on spaceprobe data. Those for Saturn, Uranus, and Neptune are based on scaling relations for which there are some supporting radio emission data (see text for details). For Pluto there are insufficient planetary data to do the scaling procedure.

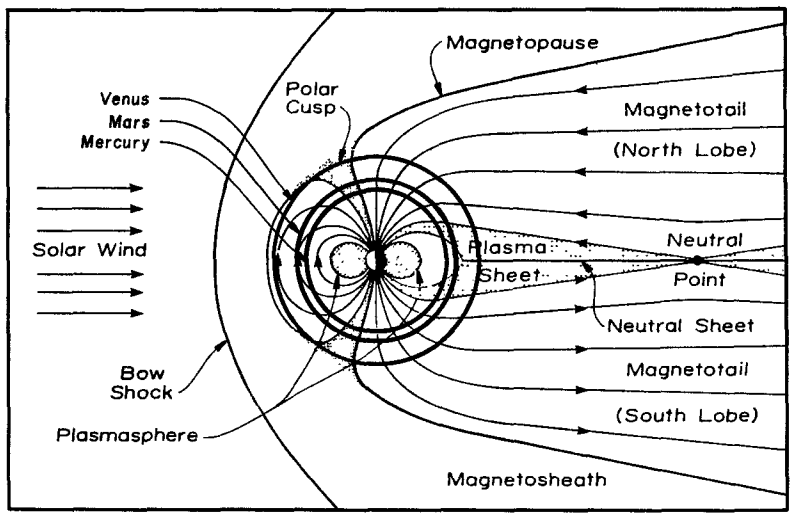

FIGURE 2.2 A typical representation of the structure of Earth's magnetosphere identifying most of the principle plasma and magnetic features (from Ref. 16). The sizes of the planets Mercury, Venus and Mars relative to their magnetospheres are indicated by the circles.

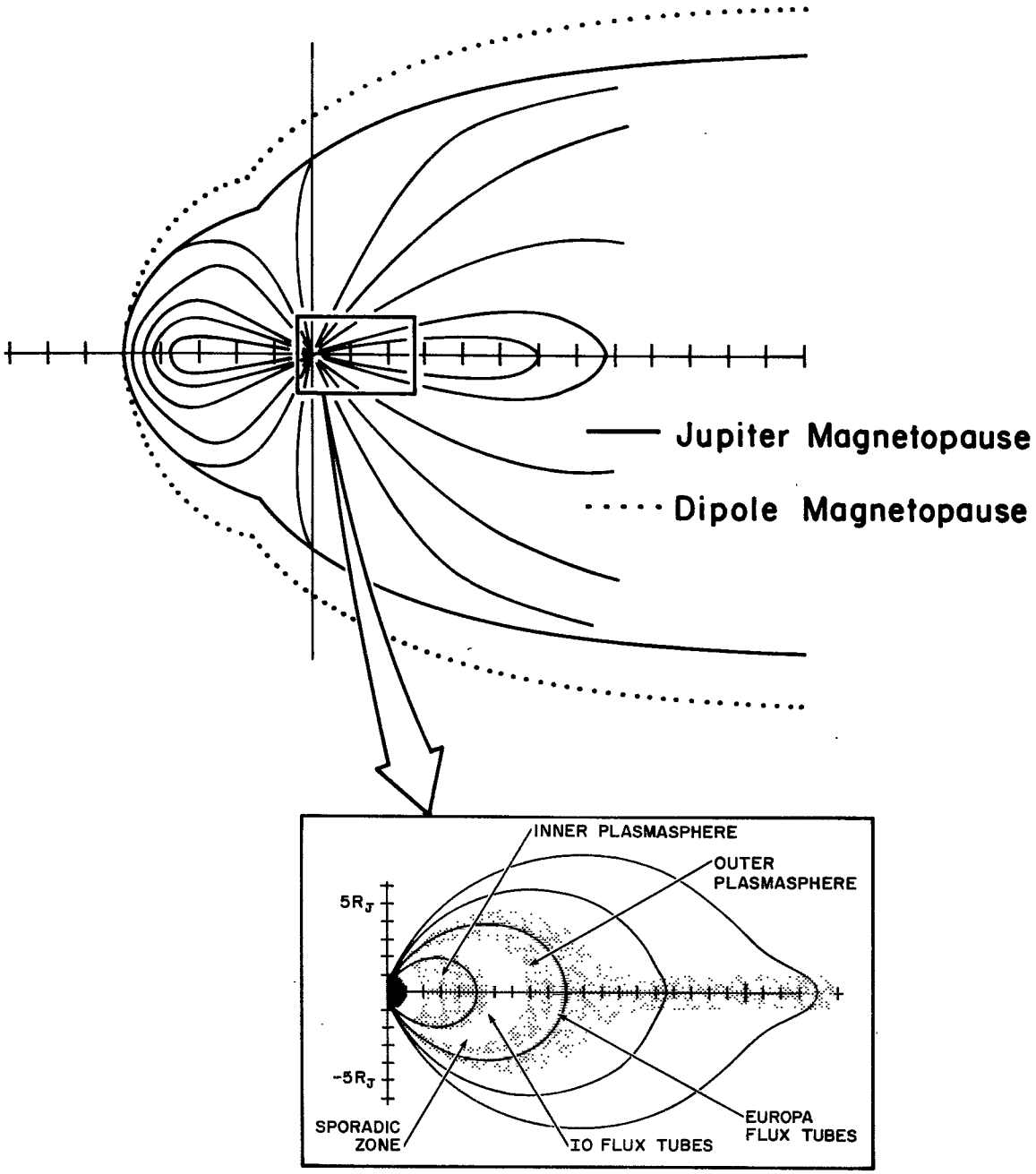

FIGURE 2.3 Calculated shapes for Jupiter's magnetopause and magnetic field lines based on Pioneer 10 magnetic field observation showing the effects of centrifugal distortion by comparison with a pure dipole distortion (modified from Ref. 25). The blow-up of the inner region shows the two low energy plasma regimes—the inner and outer plasmaspheres—observed by Pioneer 10 (modified from Ref. 26). The effects of the centrifugal force is also apparent in the suggested shape of the outer plasmasphere.

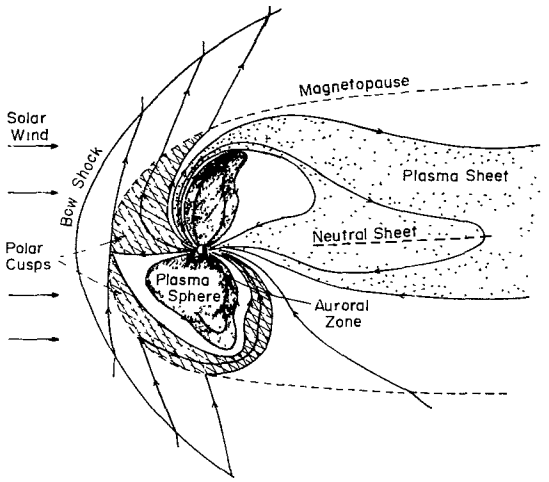

FIGURE 2.4 A sketch of a hypothetical 'pole-on' magnetosphere for Uranus based on a simple 90 degree rotation of an Earth-type magnetosphere such as is shown in Figure 2.2. (From Ref. 47.)

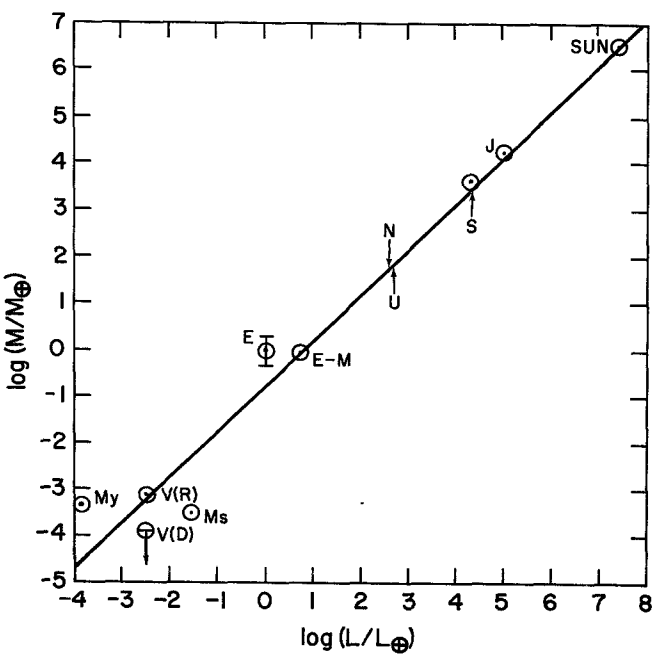

FIGURE 3.1 The magnetic Bode's law—an approximate empirical linear relationship between planetary angular momenta and magnetic moments. (Modified and extended from Ref. 46.)

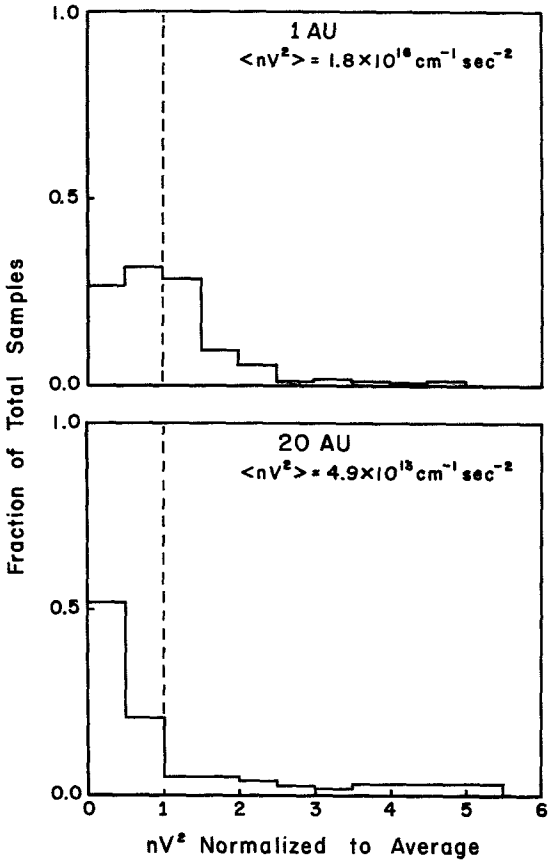

FIGURE 3.2 Histograms of the dynamic pressure of the solar wind (divided by the proton mass) based on equally spaced samples in time at 1 AU (measured) and at 20 AU (calculated from 1 AU data by a non-linear computer code—see comparison article on the solar wind for other examples) (133).

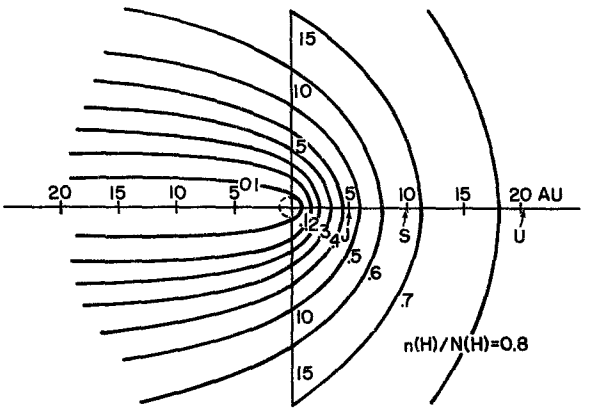

FIGURE 3.3 Isodensity contours of the interstellar neutral hydrogen in relation to the position of the outer planets. Contours are based on equal forces due to radiation pressure and gravity. (Adopted from 52.)

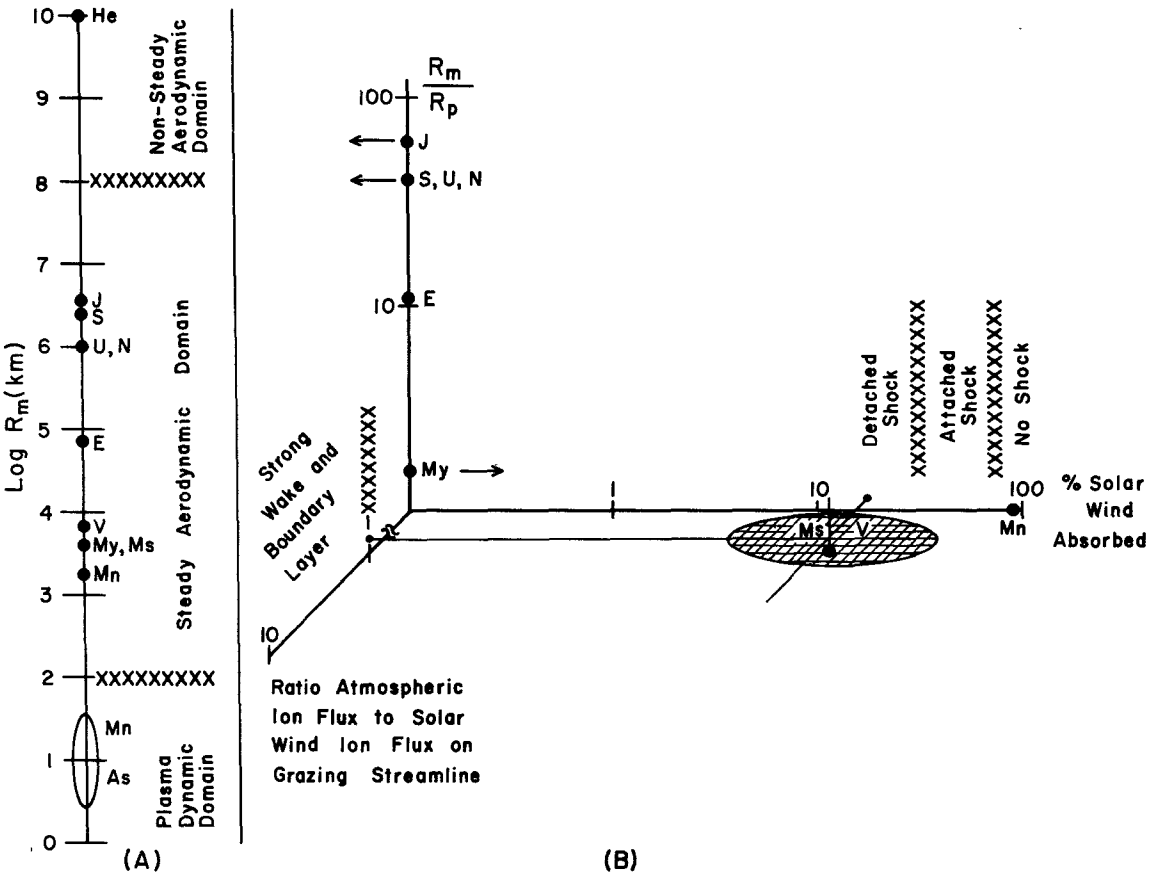

FIGURE 4.1 A schematic representation of the approximate locations of the planets in the continuous parameter space associated with external magnetospheric features. Their relationships to the divisions between several qualitatively distinct regimes is suggested. (A) A one-dimensional parametrization based on the absolute size of the magnetosphere. (B) A parametrization illustrating the effects of solar wind absorption and atmospheric ion pick-up when the magnetosphere and planet are about the same size.

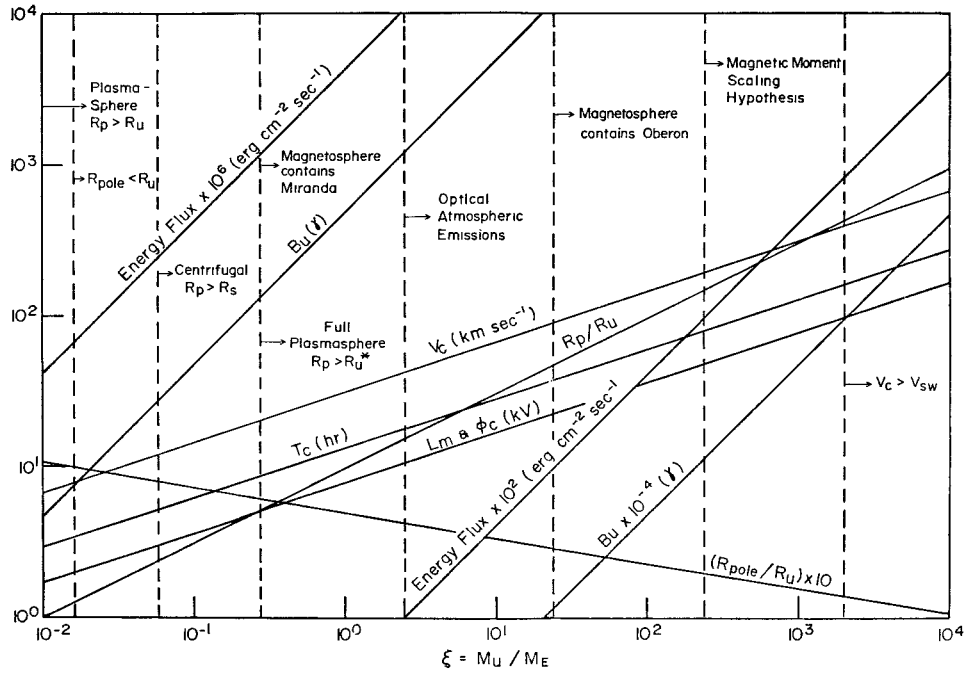

FIGURE 5.1 Magnetospheric profile for Uranus. The solid lines give the estimated variation as a function of the dipole strength ($\xi \equiv \mu_p$ present notation) of: the energy flux into the auroral zones; the surface, equatorial field strength (B_u); corotation speed at the stagnation point (V_c); convection time through the tail (T_c); the radius of the plasmasphere in units of planetary radii (Rp/Ru); the distance to the stagnation point ($L_m \equiv$ Rm present notation); the convection electric potential ($\phi_c = L_m$ in this case), and the radius of the polar cap of field lines that map into the tail, normalized to the planetary radius (R_p/R_u). The dashed lines identify the appearances of emergent features or processes or various milestones in the evolution of the magnetosphere. (From Ref. 47.)

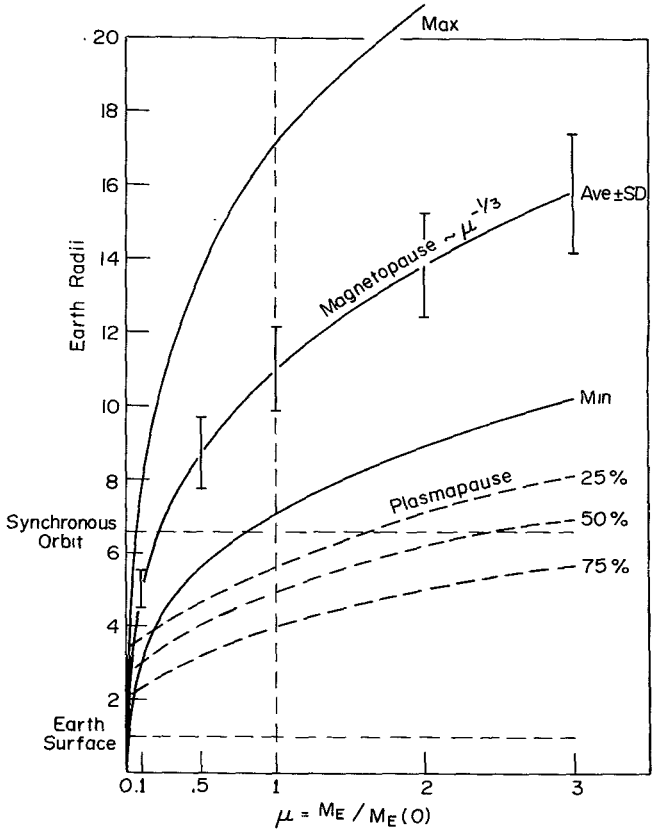

FIGURE 5.2 Plasmapause and stagnation point magnetopause distances as functions of μ. The variation of these distances for a given value of μ due to solar wind variations is also given. Solar wind statistics for calculating magnetopause distances were obtained from 12,254 hourly averages of stagnation pressures computed with data from the Explorer 33 and 35 spacecraft. The maximum and minimum curves correspond to the smallest and largest of these values. Solar wind electric field statistics used in calculating the plasmapause distances were obtained from 166 days of data from the Mariner 5 spacecraft. Percentage values on the plasmapause curves give the fraction of time that the plasmapause lies beyond the distance given by the curve. (From Ref. 131.)

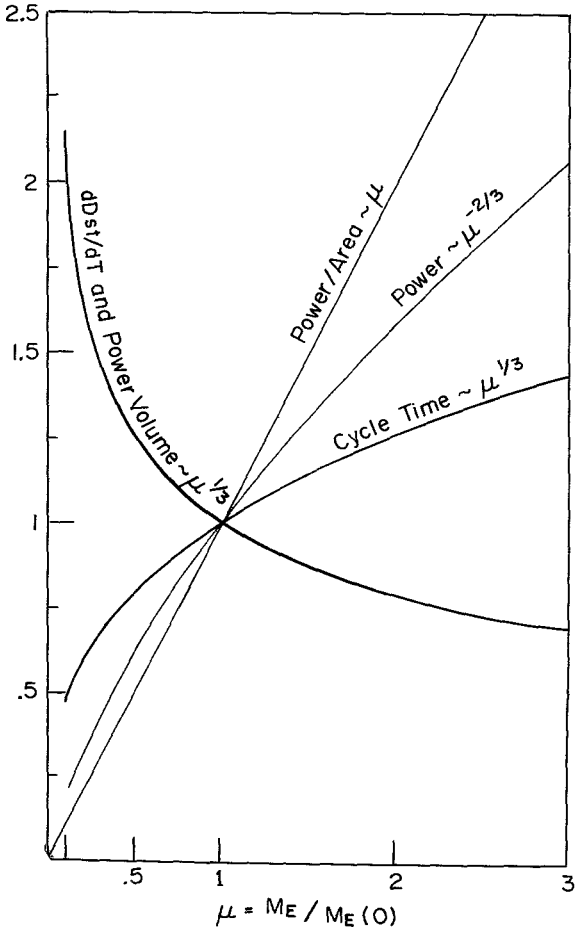

FIGURE 5.3 The five dynamical parameters, power (total power into the magnetosphere due to day side magnetic merging), power per unit polar cap area, power per unit magnetosphere volume, dDst/dt, and cycle time of magnetic flux through the geomagnetic tail, are given as a function of μ. All quantities are normalized to unity at $\mu = 1$. Thus the curves give the size of these quantities relative to their value for the present magnetic moment of the earth and for the same solar wind conditions. (From Ref. 131.)

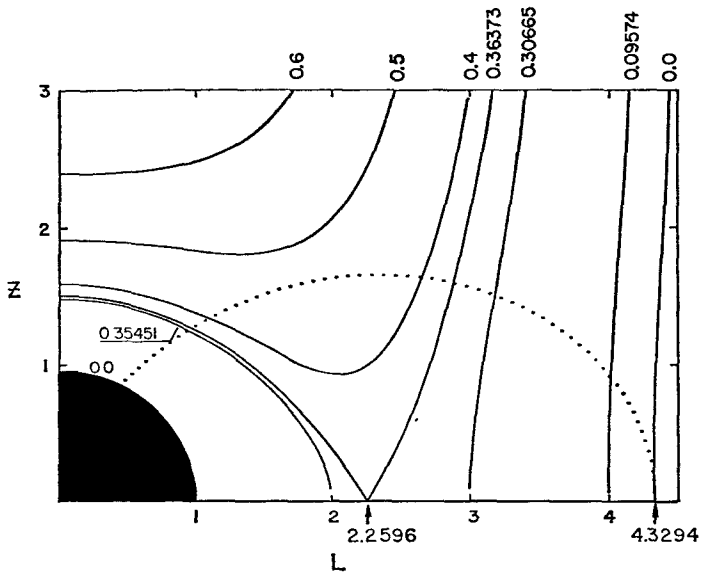

FIGURE 5.4 Lines of constant potential ϕ about Jupiter. (From 18)

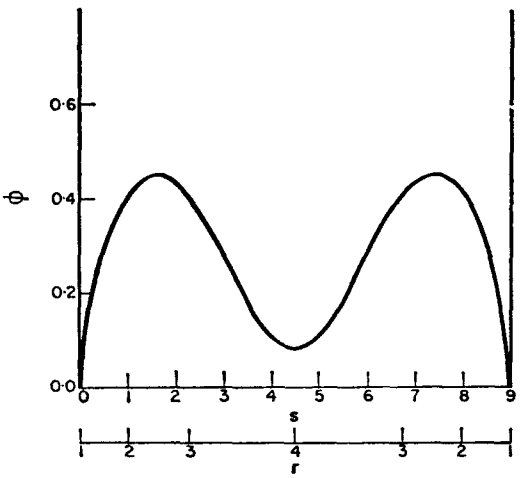

FIGURE 5.5 The potential ϕ along the 60° field line of Jupiter is plotted against distance s along the field line and radial distance r from the center of the planet, both in Jovian radii. The central minimum falls below zero for field lines originating at magnetic latitudes greater than 61° (L = 4.3). (From 141)

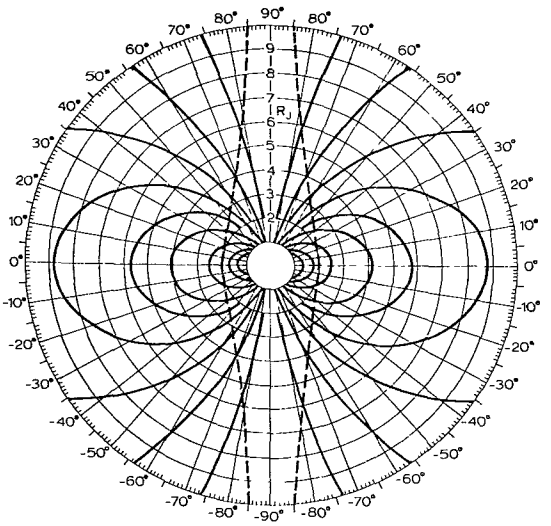

FIGURE 5.6 Meridional cross section of a rotating dipole field with radial units scaled to the Jovian situation. Dashed lines are intersections of the plane with the axisymmetric surface (cylinder) on which the potential ϕ along a field line is a maximum (e.g. as in Fig. 13). On this surface the components of gravitational and centrifugal force along a field line cancel. (From 195)

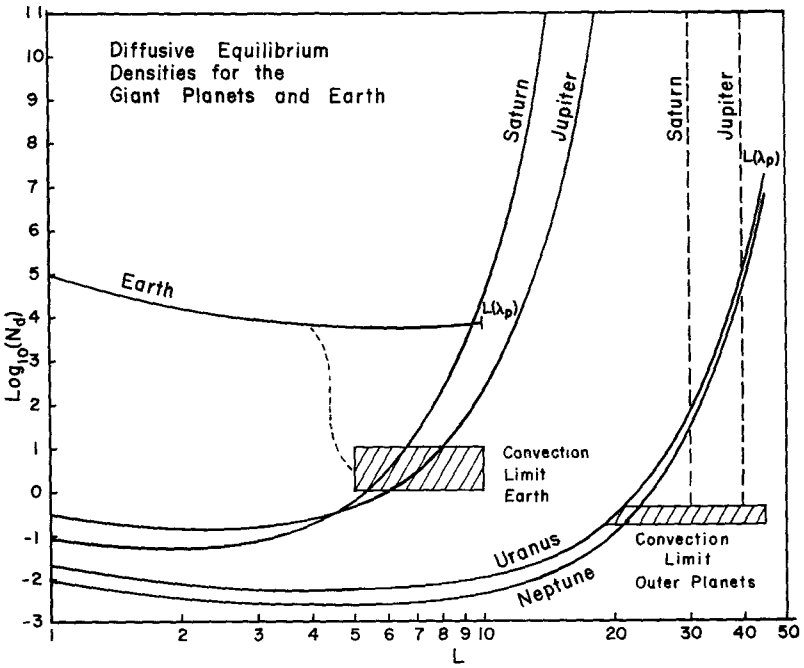

FIGURE 5.7 Diffusive equilibrium density profiles for the giant planets and Earth. In the case of the giant planets the equilibrium is between the plasmasphere and the photoelectron flux from the ionosphere. Solar wind convection limits to the outer boundaries are indicated.

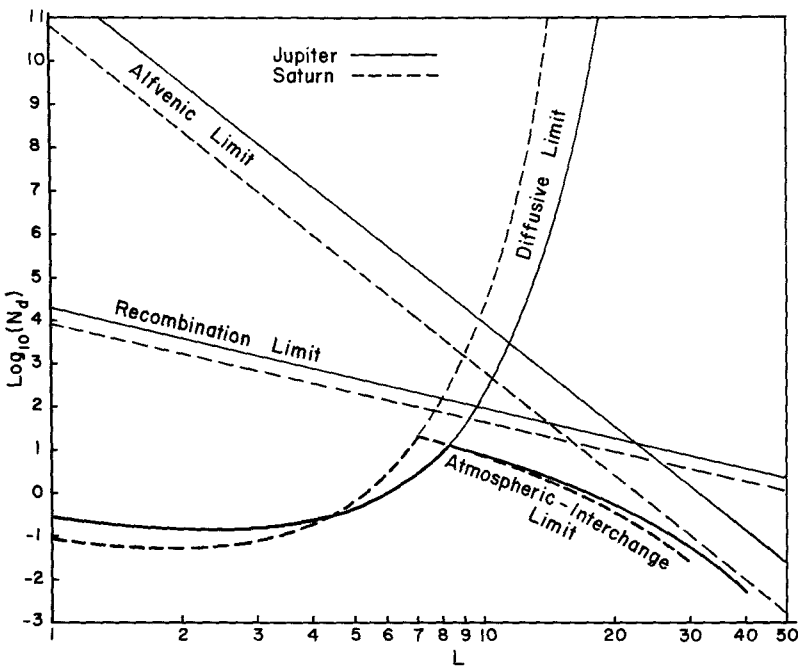

FIGURE 5.8 The limits imposed on the plasmasphere densities of Jupiter and Saturn by diffusive equilibrium with the ionosphere, radial transport by interchange diffusion and a centrifugal wind (Alfvenic limit), and the static recombination limit.

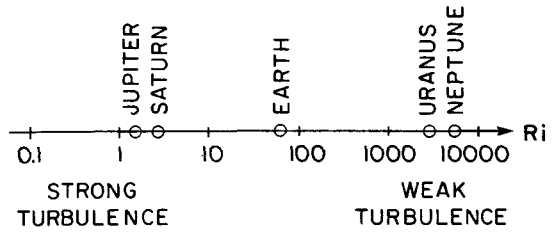

FIGURE 5.9 The dynamical states of the atmosphere of the giant planets and Earth as inferred from the planetary Richardson number (Ri). (From 156)

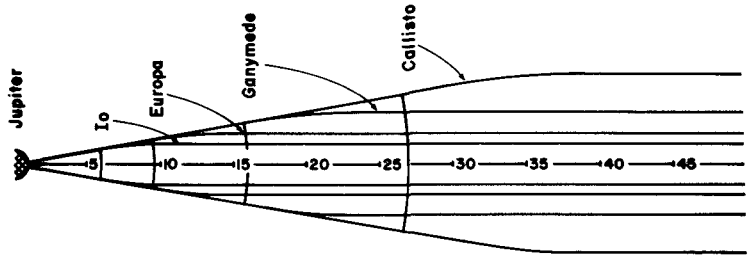

FIGURE 5.10 The ion confinement discs of each Galilean satellite. The horizontal axis is the magnetic equator. The common flaring angle is 10° corresponding to the diurnal excursion of each satellite relative to the magnetic equator as shown by the arcs. (From 158)

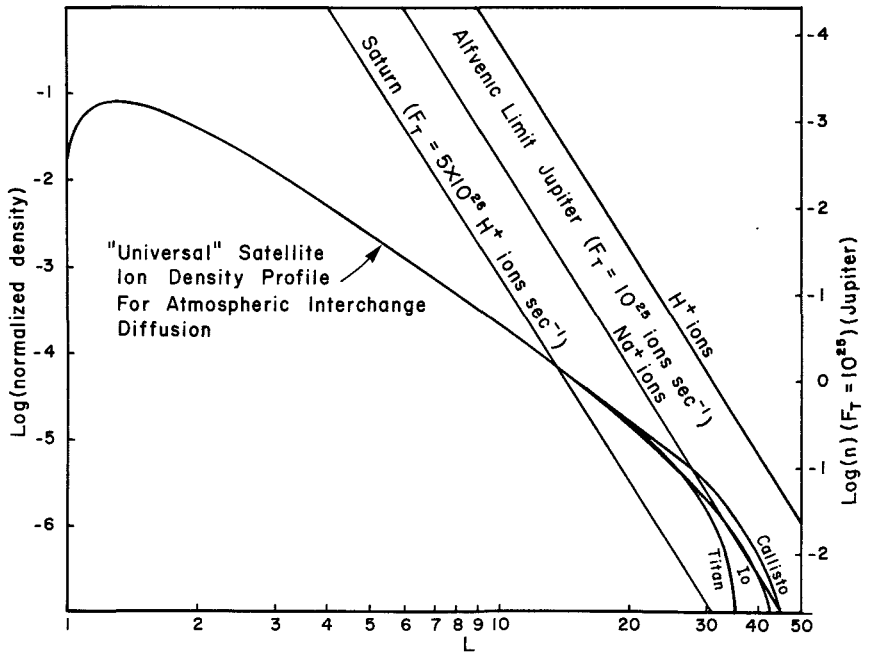

FIGURE 5.11 The satellite ion density profile obtained under the assumption of atmospheric interchange diffusion. Left margin density scale normalized to $(F_t/4\pi\theta_c R^3\kappa)$ right margin absolute density scale for Jovian parameters. Alfvenic limits appropriate to Io and Titan are indicated.

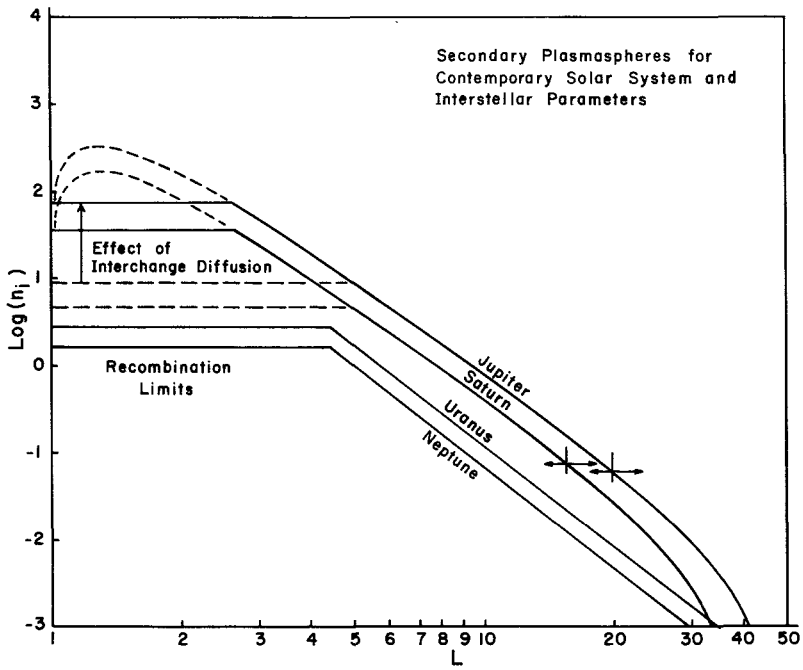

FIGURE 5.12 Secondary plasmasphere density profile based on contemporary parameters (Figure 7 and Table 8) and on static recombination limits and centrifugal interchange diffusion for Uranus and Neptune and dynamic recombination limits and atmospheric interchange diffusion for Jupiter and Saturn.

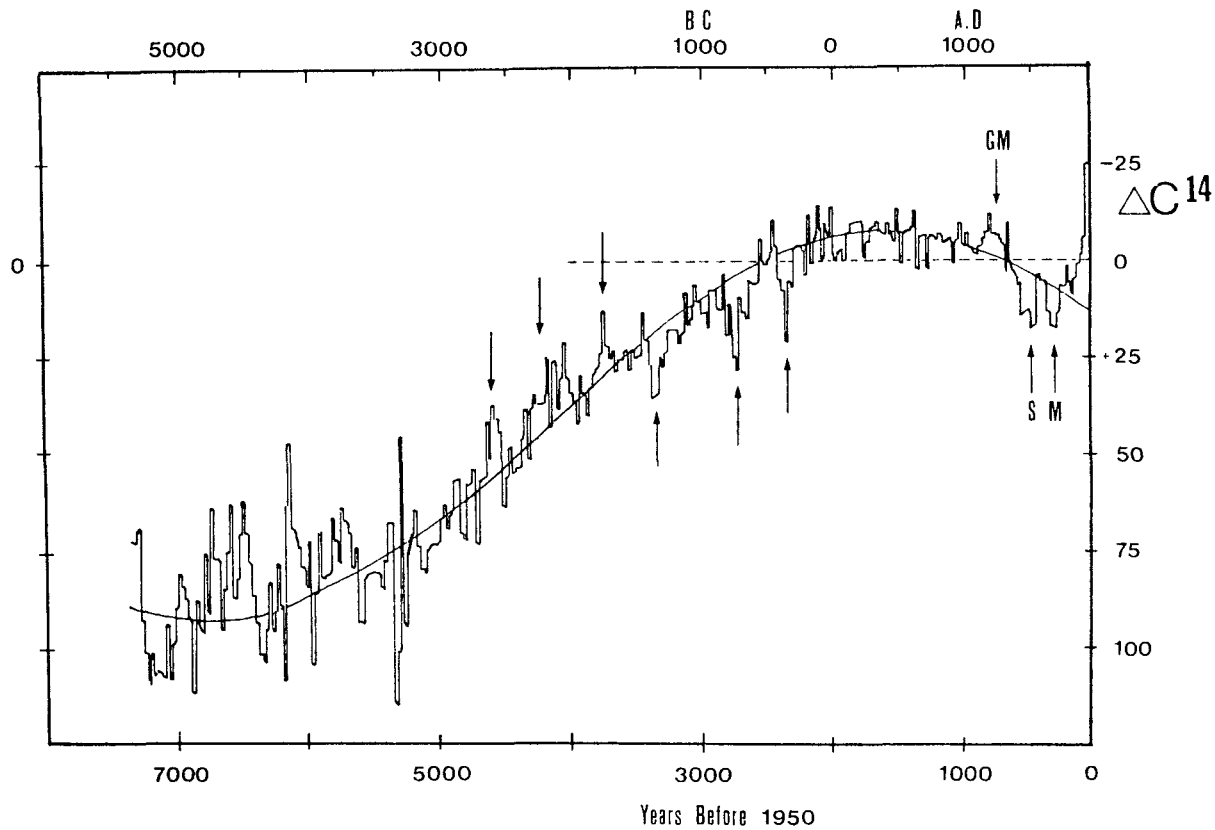

FIGURE 6.1 Record of deviations of relative atmospheric carbon-14 concentration for tree ring analyses, in parts per mil, for about 7000 years before the present (B.P.). Increased relative abundances (positive deviations) are plotted downward from the A.D. 1890 norm, which is shown as a dashed line. Solid curve is a sinusoidal fit which matches very closely the observed change in terrestrial magnetic field strength. Remaining significant features are of probable solar cause; some of the ones are marked with arrows. M = Maunder Minimum, S = Sporer Minimum, GM = Medieval Maximum. (From 164)

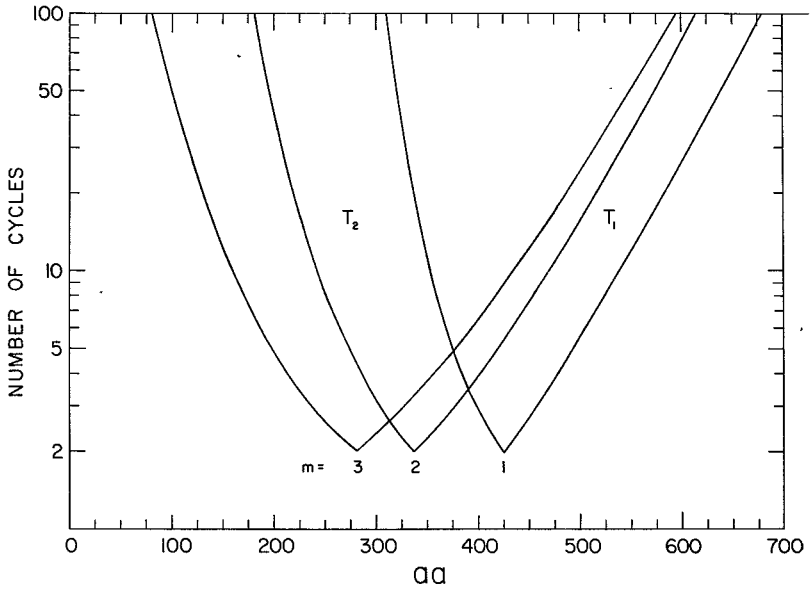

FIGURE 6.2 Plots of the expected number of sunspot cycles needed to find one with an aa extreme equal to or exceeding abscissa (T^1 branch) and to find one with aa extremes less than abscissa (T_2 branch). The labels m = 1, 2 and 3 correspond to the first, second and third largest geomagnetic storms per solar cycle as measured by the aa index. (From 180)

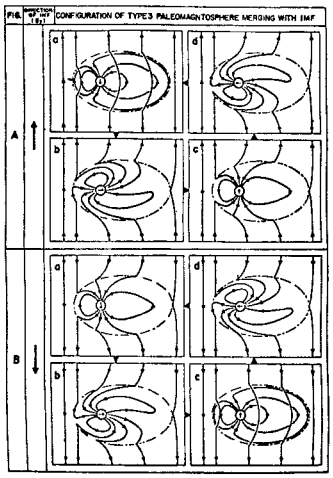

FIGURE 6.3 Hypothetical Type III paleomagnetosphere for Earth postulated for magnetic reversals. Earth rotation axis out of paper. Solar wind sectors indicated: (A) towards sector, (B) away sector. (From 122)

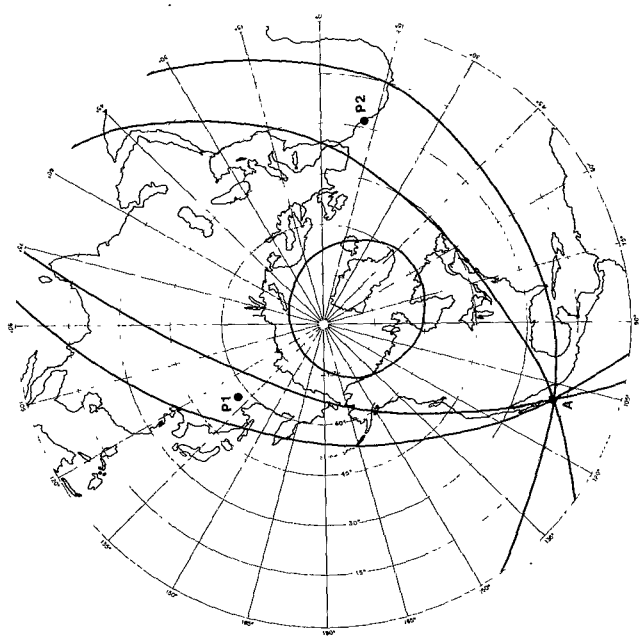

FIGURE 6.4 Polar view quadrupole auroral zones with present auroral zone for comparison. (From 165, 190)

REFERENCES

1. Ness, N. F., K. W. Behannon, R. P. Lepping, and Y. C. Whang: Interaction of solar wind with Mercury and its magnetic field, in Solar-Wind Interaction with the Planets Mercury, Venus, and Mars, edited by N. F. Ness, NASA SP-397, pp. 87 - 100, 1976.

2. Ogilvie, K. W., J. D. Scudder, R. E. Hartle, V. M. Vasyliunas, and G. L. Siscoe: Observations at the planet Mercury by the plasma electron experiment -- Mariner 10, submitted to J. Geophys. Res., 1976.

3. Siscoe, G. L., N. F. Ness, and C. M. Yeates: Substorms on Mercury?, J. Geophys. Res., 80, 4359, 1975.

4. Simpson, J. A., J. H. Eraker, J. E. Lamport, and P. H. Walpole: Electrons and protons accelerated in Mercury's magnetic field, Science, 185, 160, 1974.

5. Hill, T. W., A. J. Dessler, and R. A. Wolf: Mercury and Mars: The role of ionospheric conductivity in the acceleration of magnetospheric particles, Geophys. Res. Letter, 3, 429 - 432, 1976.

6. Rizzi, A. W.: "Solar Wind Flow Past the Planets Earth, Mars, and Venus," Ph.D. dissertation, Stanford University, Palo Alto, California, 1971.

7. Bridge, H. S., A. J. Lazarus, J. D. Scudder, K. W. Ogilvie, R. E. Hartle, J. R. Asbridge, S. J. Bame, W. C. Feldman, and G. L. Siscoe: "Observations at Venus Encounter by the Plasma Science Experiment on Mariner 10," Science, 183, pp. 1293 - 1296, 1974.

8. Pérez de Tejada, H., and M. Dryer: Viscous boundary layer for the Venusian ionopause, J. Geophys. Res., 81, 2023 - 2029, 1976.

9. Russell, C. T.: The magnetosphere of Venus: Evidence for

a boundary layer and a magnetotail, submitted to Geophys. Res. Lett., 1976.

10. Russell, C. T.: The Venus bow shock: Detached or Attached, submitted to J. Geophys. Res., 1976.

11. Solar Wind Interaction with the Planets Mercury, Venus, and Mars, edited by N. F. Ness, NASA SP-397, 1976.

12. Russell, C. T.: Venera - 9 magnetic field measurements in the Venus wake: Evidence for an Earth-like interaction, Geophys. Res. Lett., 413 - 416, 1976.

13. Dolginov, Sh., Sh., Ye. G. Yeroshenko, and L. N. Zhuzgov: The magnetic field of Mars according to the data from the Mars 3 and Mars 5, J. Geophys. Res., 81, 3353 - 3362, 1976.

14. Gringauz, K. I., V. V. Bezrukikh, M. I. Verigin, and A. P. Remizov: On electron and ion components of plasma in the antisolar part of near-Martian space, J. Geophys. Res., 81, 3349 - 3352, 1976.

15. Michel, F. C.: Solar-wind-induced mass loss from magnetic field-free planets, Planet Space Sci., 19, 1580, 1971a.

16. Russell, C. T.: The configuration of the magnetosphere, in Critical Probelms of Magnetospheric Physics, edited by E. R. Dryer, Published by the IUCSTP Secretariat c/o National Academy of Sciences, Washington, D.C., pp. 1 - 16, 1972.

17. Gurnett, D. A.: The earth as a radio source: Terrestrial kilometric radiation, J. Geophys. Res., 79, 4227 - 4238, 1974.

18. Michel, F. C., and P. A. Sturrock: Contrifugal instability of the Jovian magnetosphere and its interaction with the solar wind, Planet. Space Sci., 22, 1501 - 1510, 1974.

19. Hill, T. W., A. J. Dessler, and F. C. Michel: Configuration

of the Jovian magnetosphere, Geophys. Res. Lett., 1, 3-6, 1974.

20. Hill, T. W., and F. C. Michel: Heavy ions from the Galilean satellites and the centrifugal distortion of the Jovian magnetosphere, J. Geophys. Res., 81, 4561-4565, 1976.

21. Kennel, C. F., and F. V. Coroniti: Is Jupiter's magnetosphere like a pulsars on Earth's?, in The Magnetospheres of Earth and Jupiter, edited by V. Formisano, D. Reidel Publishing Co., pp. 451 - 477, 1975.

22. Gleeson, L. J., and W. I. Axford: An analytic model illustrating the effects of rotation on a magnetosphere containing low-energy plasma, J. Geophys. Res., 81, 3403 - 3406, 1976.

23. Gold, T.: The magnetosphere of Jupiter, J. Geophys. Res., 81, 3401 - 3402, 1976.

24. See the issues of Science devoted to the Pioneer 10 and 11 Jupiter encounters, Vol. 183, No. 4122, 1974 and Vol. 188, No. 4187, 1975 and the Jupiter dedicated issue of J. Geophys. Res., 79, No. 25, 1974.

25. Beard, D. B., and D. L. Jackson: The Jovian magnetic field and the magnetosphere shape, J. Geophys. Res., 81, 3399 - 3400, 1976.

26. Frank, L. A., K. L. Ackerson, J. H. Wolfe, and J. D. Mihalov: Observations of plasmas in the Jovian magnetosphere, J. Geophys. Res., 81, 457 - 468, 1976.

27. Ioannidis, G., and N. M. Brice: Plasma densities in the Jovian magnetosphere: Plasma slingshot or Maxwell demon?, Icarus, 14, 360 - 373, 1971.

28. Mendis, D. A., and W. I. Axford: Satellite and magnetospheres of the outer planets, Ann. Rev. Earth. Planet. Sci., 2, 419 - 474, 1974.

29. Goertz, C. K.: Plasma in the Jovian magnetosphere, J. Geophy Res., 81, 2007 - 2014, 1976.

30. Siscoe, G. L., and C.-K. Chen: Io: A source for Jupiter's inner plasmasphere, Icarus, in press, 1977.

31. Judge, D. L., and R. W. Carlson: Pioneer 10 observations of the ultraviolet glow in the vicinity of Jupiter, Science, 183, 317, 1974.

32. Scarf, F. L.: The magnetospheres of Jupiter and Saturn, in The Magnetospheres of the Earth and Jupiter, edited by V. Formisano, D. Reidel Publ. Co., pp. 433 - 449, 1975.

33. Coroniti, F. V.: Dénouement of Jovian radiation belt theory, in The Magnetospheres of the Earth and Jupiter, edited by V. Formisano, D. Reidel Publ. Co., pp. 391 - 410, 1975.

34. Brice, N., and T. R. McDonough: Jupiter's radiation belts, Icarus, 18, 206-219, 1973.

35. Coroniti, F. V.: Energetic electrons in Jupiter's magnetosphere, Astrophys. J. Suppl., 27, 261 - 281, 1974.

36. Nishida, A.: Outward diffusion of energetic particles from the Jovian radiation belt, J. Geophys. Res., 81, 1771 - 1773, 1976.

37. Carbary, J. F., T. W. Hill, and A. J. Dessler: Planetary-spin-period acceleration of particles in the Jovian magnetosphere, submitted to J. Geophys. Res., 1976.

38. Hill, T. W., J. F. Carbary, and A. J. Dessler: Periodic escape of relatioistic electrons from the Jovian magnetosphere, Geophys. Res. Lett., 1, 333 - 336, 1974.

39. Hill, T. W., and A. J. Dessler: Latitudinal symmetry of the Jovian magnetosphere and the periodic escape of energetic particles, J. Geophys. Res., 81, 3383 - 3386, 1976.

40. Burke, B. F., and K. L. Franklin: Observations of a variable radio source associated with the planet Jupiter, J. Geophys. Res., 60, 213 - 217, 1955.

41. Brown, L. W.: Saturn radio emission near 1 MHz, Astrophys. J., 198, L89 - L92, 1975.

42. Brown, L. W.: Possible radio emission from Uranus at 0.5 MHz, Astrophys. J., 207, L209 - L212, 1976.

43. Kaiser, M. L., and R. G. Stone: Earth as an intense planetary radio source: Similarities to Jupiter and Saturn, Science, 189, 285 - 287, 1975.

44. Kennel, C. F., and J. E. Maggs: Possibility of detecting magnetospheric radio bursts from Uranus and Neptune, Nature, 261, 299 - 301, 1976.

45. Siscoe, G. L.: Two magnetic tail models for Uranus, Planet. Space Sci., 19, 483, 1971.

46. Hill, T. W., and F. C. Michel: Planetary magnetospheres, Rev. Geophys. Space Phys., 13, 967 - 973, 1975.

47. Siscoe, G. L.: Particle and field environment of Uranus, Icarus, 24, 311 - 324, 1975.

48. Gosling, J. T., A. J. Hundhansen, and S. J. Bame: Solar wind stream evolution at large heliocentric distances: experimental demonstration and the test of a model, J. Geophys. Res., 81, 2111, 1976.

49. Smith, E. J., and J. H. Wolfe: Observations of interaction regions and corotating shocks between one and five AU: Pioneer 10 and 11, Geophys. Res. Lett., 3, 137, 1976.

50. Holzer, T. E.: Interaction of the solar wind with the neutral component of the interstellar gas, J. Geophys. Res., 77, 5407, 1972.

51. Vasyliunas, V. M., and G. L. Siscoe: On the flux and spectra of interstellar ions in the solar wind, J. Geophys. Res., 81, 1247, 1976.

52. Johnson, H. E.: Backscatter of solar resonance radiation-I., Planet. Space Sci., 20, 829 - 840, 1972.

53. Allen, C. W.: Astrophysical Quantities, The Athlone Press, Univ. of London, 1973.

54. Hartmann, W. K.: Moons and Planets, Bogdon and Quigley, Inc. Publishers, 1972.

55. Kennel, C. F., and M. H. Rees: Dayside auroral-oval plasma density and conductivity enhancements due to magnetosheath electron precipitation, J. Geophys. Res., 77, 2294, 1972.

56. Banks, P. M., A. F. Nagy, and W. I. Axford: Dynamical behavior of thermal protons in the mid-latitude ionosphere and magnetosphere, Planet. Space Sci., 19, 1053 - 1067, 1971.

57. Swartz, W. E., R. E. Reed, and T. R. McDonough: Photoelectron escape from the ionosphere of Jupiter, J. Geophys. Res., 80, 495 - 501, 1975.

58. Dolginov, Sh. Sh., Y. G. Yeroshenko, and L. Davis: On the nature of the magnetic field near Venus, Kosmich. Issled., 7, 747, 1969.

59. Kono, M.: Intensity of the earth's magnetic field during the Pliocene and Pleistocene in relation to the amplitude of mid-ocean magnetic anomaly, Earth Planet. Sci. Lett., 11, 10, 1971.

60. Smith, E. J., L. Davis, Jr., D. E. Jones, P. J. Coleman, Jr., D. S. Colburn, P. Dyal, C. P. Sonett, and A. M. A. Frandsen: The planetary magnetic field and magnetospheric of Jupiter: Pioneer 10, J. Geophys. Res., 79, 3501 - 3513, 1974.

61. Acuna, M. H., and N. F. Ness: The main magnetic field of Jupiter, J. Geophys. Res., 81, 2917 - 2922, 1976.

62. Roederer, J. G.: Planetary plasmas and fields, EOS, 57, 53 - 62, 1976.

63. Cox, A., J. Hillhouse, and M. Fuller: Paleomagnetic records of polarity transitions, excursions, and secular variation, Rev. Geophys. Space Phys., 13, 185 - 189, 1975.

64. Kennel, C. F.: Magnetospheres of the planets, Space Sci. Rev., 14, 511 - 533, 1973.

65. From a figure in Ref. 46 as extended by M. G. Kivelson.

66. Morrison, D., and D. P. Cruikshank: Physical properties of the natural satellites, Space Sci. Rev., 15, 641 - 739, 1974.

67. Thomsen, M. F., C. K. Goertz, and J. A. Van Allen: On determining a diffusion coefficient from the observed effects of Jupiter's satellite Io, University of Iowa preprint, August, 1976.

68. Fillius, R. W., and C. E. McIlwain: Measurements of the Jovian radiation belts, J. Geophys. Res., 79, 3589, 1974.

69. Fillius, R. W., C. E. McIlwain, and A. Mogro-Campero: Radiation belts of Jupiter: A second look, Science, 188, 465, 1975.

70. Kupo, I., Y. Mekler, and A. Eviator: Detection of ionized sulfur in the Jovian magnetosphere, Astrophys. J., 205, L51 - L53, 1976.

71. Brown, R. A.: A model of Jupiter's sulfur nebula, Astrophys. J., 206, L179 - L183, 1976.

72. McElroy, M. B., and Y.-L. Yung: The atmosphere and ionosphere of Io, Astrophys. J., 196, 227 - 250, 1975.

73. McDonough, T. R., and N. M. Brice: A Saturnian gas ring and the recycling of Titan's atmosphere, Icarus, 20, 136 - 145, 1973.

74. Kliore, A., D. L. Cain, G. Fjeldbo, B. L. Seidel, and S. I. Rasool: Preliminary results on the atmospheres of Io and Jupiter from the Pioneer 10 S-band occultation experiment, Science, 183, 323 - 324, 1974.

75. Kliore, A. J., G. Fjeldbo, B. L. Seidel, D. N. Sweetnam, T. T. Sesplankis, P. M. Woiceshyn, and S. I. Rasool: The atmosphere of Io from Pioneer 10 radio occultation measurements, Icarus, 24, 407 - 410, 1975.

76. Whitten, R. C., R. T. Reynolds, and P. F. Michelson: The ionosphere and atmosphere of Io, Geophys. Res. Lett., 2, 49 - 51, 1975.

77. Shawhan, S. D., C. K. Geortz, R. F. Hubbard, D. A. Gurnett, and G. Joyce: Io-accelerated electrons and ions, in The Magnetospheres of Earth and Jupiter, edited by V. Formisano, D. Reidel, Dordrecht, Netherlands, pp. 375 - 389, 1975.

78. Carlson, R. W., and D. L. Judge: Pioneer 10 ultraviolet photometer observations at Jupiter encounter, J. Geophys. Res., 79, 3623 - 3633, 1974.

79. Carlson, R. W., and D. L. Judge: Pioneer 10 ultraviolet photometer observations of the Jovian hydrogen torus: The angular distribution, Icarus, 24, 395 - 399, 1975.

80. McDonough, T. R.: A theory of the Jovian hydrogen torus, Icarus, 24, 400 - 406, 1975.

81. Brown, R. A., and F. H. Chaffee: High-revolution spectra of sodium emission from Io, Astrophys. J., 187, L125, 1974.

82. Macy, W. W., Jr., and L. M. Trafton: Io's sodium emission cloud, Icarus, 25, 432 - 438, 1975.

83. Carlson, R. W., D. L. Matson, and T. V. Johnson: Electron impact ionization of Io's sodium emission cloud, Geophys. Res. Lett., 2, 469 - 472, 1975.

84. Wehinger, P. A., S. Wyckoff, and A. Frohlich: Mapping of the sodium emission associated with Io and Jupiter, Icarus, 27, 425 - 428, 1976.

85. Trafton, L.: Detection of a potassium cloud near Io, Nature, 258, 690 - 692, 1975.

86. Carlson, R. W., J. C. Bhattacharyga, B. A. Smith, T. V. Johnson, B. Hidayat, S. A. Smith, G. E. Taylor, B. T. O'Leary, and R. T. Brinkmann: An atmosphere on Ganymede from its occulation of SAO 186800 on June 7, 1972, Science, 182, 53 - 55, 1973.

87. Trafton, L. M.: Near-infrared spectrophotometry of Titan, Icarus, 24, 443 - 453, 1975.

88. Hunten, D. M.: The escape of H_2 from Titan, J. Atmos. Sci., 30, 726 - 732, 1973.

89. Tabarié, N.: The Atmosphere of Titan, edited by D. M. Hunten, NASA SP-340, 1974.

90. Fang, T.-M., W. H. Smyth, and M. B. McElroy: The spatial distribution of long lived gas clouds emitted by satellites in the outer solar system: Planet. Space Sci., 24, 577 - 588, 1976.

91. Trafton, L., T. Parkinson, and W. Macy: The spatial extent of the sodium around Io: Astrophys. J., 190, L85, 1974.

92. Piddington, J. H., and J. F. Drake: Electrodynamic effects of Jupiter's satellite Io: Nature, 217, 935 - 937, 1968.

93. Shawhan, S. D.: Io sheath-accelerated electrons and ions, J. Geophys. Res., 81, 3373 - 3379, 1976.

94. Formisano, V., G. Moreno, and E. Amata: Relationships among

the interplanetary plasma parameters: Heos 1, December 1968 to December 1969, J. Geophys. Res., 79, 5109 - 5117, 1974.

95. Montgomery, M. P.: The solar wind in the outer solar system, Space Sci. Rev., 14, 559, 1973.

96. Dryer, M.: Solar wind interactions -- hypersonic analog, Cosmic Electrodynamics, 1, 115, 1970.

97. Dryer, M., Rizzi, A. W., and Shen, W.-W.: Interaction of the solar wind with the outer planets, Astrophys. Space Sci., 22, 329, 1973.

98. Scarf, F. L.: Some comments on the magnetosphere and plasma environment of Saturn, Cosmic Electrodynamics, 3, 437 - 447, 1973.

99. Schieldge, J. P., and G. L. Siscoe: An empirical determination of aerodynamic factors for the magnetosphere, Cosmic Electrodynamics, 2, 141, 1971.

100. Carovillano, R. L., and G. L. Siscoe: Energy and momentum theorems in magnetospheric dynamics, Rev. Geophys. Space Phys., 11, 289, 1973.

101. Axford, W. I.: Viscous interaction between the solar wind and the earth's magnetosphere, Planet. Space Sci., 12, 45, 1964.

102. Crooker, N. U.: A comparison between magnetospheric energy and solar wind kinetic energy, Rept. CSRTR-74-4, M.I.T., Cambridge, Mass., 1974.

103. Hill, T. W.: Origin of the plasma sheet, Rev. Geophys. Space Phys., 12, 379 - 388, 1974.

104. Axford, W. I.: Interaction of the interstellar medium with the solar wind, Space Sci. Rev., 14, 582 - 590, 1973.

105. Jenkins, E. B., and B. D. Savage: Ultraviolet photometry from the Orbiting Astronomical Observatory. XIV. An extension of the survey of Lyman -- α absorption from interstellar hydrogen, Astrophys. J., 187, 243 - 255, 1974.

106. McCrea, W. H.: Ice ages and the galaxy, Nature, 255, 607 - 609, 1975.

107. Spreiter, J. R.: Magnetohydrodynamic and gas dynamic aspects of solar-wind flow around terrestrial planets: A critical review, in Solar-Wind Interaction with the Planets Mercury, Venus, and Mars, edited by N. F. Ness, NASA SP-397, pp. 135 - 148, 1976.

108. Spreiter, J. R., and A. Y. Alksne: Solar-wind flow past objects in the solar system, in Annual Review of Fluid Mechanics, Vol. 2, 313 - 354, 1970.

109. Zwan, B. J., and R. A. Wolf: Depletion of solar wind plasma near a planetary boundary, J. Geophys. Res., 81, 1636 - 1648, 1976.

110. Crooker, N. U., G. L. Siscoe, and R. B. Geller: Persistent pressure anisotropy in the subsonic magnetosheath region, Geophys. Res. Lett., 3, 65 - 68, 1976.

111. Crooker, N. U., and G. L. Siscoe: A mechanism for pressure anisotropy and mirror instability in the dayside magnetosheath, J. Geophys. Res., 82, 185-186, 1977.

112. Greenstadt, E. W., I. M. Green, G. T. Inouye, D. S. Colburn, J. H. Binsack, and E. F. Lyon: Dual satellite observations of Earth's bow shock, Cosmic Electrodynamics, 1, 316 - 327, 1970.

113. Greenstadt, E. W.: Dependence of shock structure at Venus and Mars on the orientation of the interplanetary magnetic field, Cosmic Electrodynamics, 1, 380 - 388, 1970.

114. Kennel, C. F.: What we have learned from the magnetosphere, Comments Astrophys. Space Phys., 6, 71 - 80, 1975.

115. Greenstadt, E. W.: Conditions for magnetic interaction of asteroids with the solar wind, Icarus, 14, 374 - 381, 1971.

116. Bridge, H. S., R. E. Hartle, A. J. Lazarus, K. W. Ogilvie, J. D. Scudder, G. L. Siscoe, and C. M. Yeates: Interaction of the solar wind with Venus, in Solar Wind Interaction with the Planets Mercury, Venus, and Mars, ed. by N. F. Ness, NASA-SP-397, pp. 63 - 80, 1976.

117. Vaisberg, O. L., A. V. Bogdanov, V. N. Smirnov, and S. A. Romanov: On the nature of the solar-wind-Mars interaction, in Solar-Wind Interactions with the Planets Mercury, Venus and Mars, ed. by N. F. Ness, NASA SP-397, pp. 21 - 40, 1976.

118. Jackon, D. J., and D. B. Beard: The magnetic field of Mercury, University of Kansas, Department of Physics and Astronomy preprint, 1977.

119. Cloutier, P. A.: Solar-wind interaction with planetary ionospheres, in Solar-Wind Interaction with the Planets Mercury, Venus, and Mars, ed. by N. F. Ness, NASA SP-397,

120. Cloutier, P. A., R. E. Daniell, Jr., and D. M. Butler: Atmospheric ion wakes of Venus and Mars in the solar wind, Planet. Space Sci., 22, 967, 1974.

121. White, R. S.: High-energy proton radiation belt, Rev. Geophys. Space Phys., 11, 595 - 632, 1973.

122. Saito, T., T. Sakurai, and K. Yumoto: The Earth's paleomagnetosphere as the third type of planetary magnetosphere, Planet. Space Sci., in press, 1976.

123. Walker, R. J.: An evaluation of recent quantitative magnetospheric magnetic field models, Rev. Geophys. Space Phys., 14, 411 - 427, 1976.

124. Spreiter, J. R., and A. L. Summers: On conditions near the

neutral points on the magnetosphere boundary, Planet. Space Sci., 15, 787 - 798, 1967.

125. Siscoe, G. L., V. Formisano, and A. J. Lazarus: Relation between geomagnetic sudden impulses and solar wind pressure changes -- an experimental investigation, J. Geophys. Res., 73, 4869, 1968.

126. Burton, R. K., R. L. McPherron, and C. T. Russell: The terrestrial magnetosphere: a half-wave rectifier of the interplanetary electric field, Science, 189, 717 - 718, 1975.

127. Gonzalez, W. D., F. S. Mozer: A quantitative model for the potential resulting from reconnection with an arbitrary interplanetary magnetic field, J. Geophys. Res., 79, 4186, 1974.

128. Sonnerup, B. U. O.: Magnetopause reconnection rate, J. Geophys. Res., 79, 1546, 1974.

129. Sonnerup, B. U. O.: The reconnecting magnetosphere, Magnetospheric Physics, B. M. McCormac, ed., D. Reidel, Dordrecht, pp. 23 - 33, 1974.

130. Siscoe, G. L., and N. U. Crooker: A theoretical relation between Dst and the solar wind merging electric field, Geophys. Res. Lett., 1, 11, 1974.

131. Siscoe, G. L., and C.-K. Chen: The paleomagnetosphere, J. Geophys. Res., 80, 4675, 1975.

132. Walt, M., and T. A. Farley: The physical mechanisms of the inner Van Allen belt, Fund. Cosm. Phys., 2, 1 - 110, 1976.

133. Hundhausen, A. J., and V. J. Pizzo: private communication.

134. Schulz, M.: Paleomagnetospheric radial diffusion, Geophys. Res. Lett., 2, 173 - 175, 1975.

135. Eastman, T. E., E. W. Hones, Jr., S. J. Bame, and J. R. Asbridge: The magnetospheric boundary layer: site of plasma, momentum ar energy transfer from the magnetosheath into the magnetosphere, Geophys. Res. Lett., in press, 1976.

136. Rassbach, M. E., R. A. Wolf, and R. E. Daniell, Jr.: Convection in a Martian magnetosphere, J. Geophys. Res., 79, 1125 - 1127, 1974.

137. Burch, J. L.: Rate of erosion of dayside magnetic flux based on a quantitative study of the dependence of polar cusp latitude on the interplanetary magnetic field, Radio Sci., 8, 955 - 961, 1973.

138. Burch, J.L.: Observations of interactions between interplanetary and geomagnetic fields, Rev. Geophys. Space Phys., 12, 363 - 378, 1974.

139. Siscoe, G.L., and B Goldstein: Solar wind interaction with lunar magnetic fields, J. Geophys. Res., 78, 6741, 1973.

140. Angerami, J.J., and J.O. Thomas: Studies of planetary atmospheres 1. The distribution of electrons and ions in the Earth's exosphere, J. Geophys. Res.,69, 4537-4560, 1964.

141. Melrose, D.B.: Rotational effects on the distribution of thermal plasma in the magnetosphere of Jupiter, Planet. Space Sci., 15, 381-393, 1967.

142. Lemaire, J.: The "Roche-limit" of ionospheric plasma and the plasmapause formation, Planet. Space Sci., 22, 757-766, 1974.

143. Lemaire, J.: The mechanisms of formation of the plasmapause, Ann. Geophys., 31, 175-190, 1975.

144. Matsushita, S.: Dynamo currents, winds, and electric fields, Radio Sci., 4, 771-780, 1969.

145. Chen, C. - K.: Topics in Planetary Plasmaspheres, Ph.D Dissertation, Dept. Atmospheric Sciences, U.C.L.A., 1977.

146. Chen, C.-L., and G.L. Siscoe: A method for finding plasmasphere statistics from solar wind measurements, J. Geophys. Res., 82, 1158-1162, 1977.

147. Smith, E.J.: The August 1972 solar-terrestrial events: interplanetary magnetic field observations, Space Sci. Rev., in press, 1977.

148. Siscoe, G.L., Solar-terrestrial relations: stone age to space age. Technology Review, 78,26, 1976.

149. Gledhill, J.A.: Magnetosphere of Jupiter, Nature, 214, 155, 1967.

150. Falthammar, C.-G: Radial diffusion by violation of the third adiabatic invariant in Earth's Particles and Fields, edited by B.M. McCormac, Reinhold Book Corporation, New York, pgs. 157-169, 1968.

151. Birmingham, T., W. Hess, T. Northrup, R. Baxter, and M. Lojko: The electron diffusion coefficient in Jupiter's magnetorphere, J. Geophys. Res., 79, 87, 1974.

152. Gold, T.: Motions in the magnetosphere of the earth, J. Geophys. Res., 64, 1219-1224, 1959.

153. Sonnerup, B.U.Ö., and M.J. Laird: On magnetospheric interchange instability, J. Geophys. Res., 68, 131-139, 1963.

154. Hill, T.W.: Interchange stability of a rapidly rotating, magnetosphere, Planet. Space Sci., in press, 1977.

155. Cole, K.D.: On the depletion of ionization in the outer magnetosphere during magnetic disturbances, J. Geophys. Res., 69, 3595-3601, 1964.

156. Stone, P.H.: The atmosphere of Uranus, Icarus, 24, 292-298, 1975.

157. Neugebauer,M.,and A. Eviatar: An alternative interpretation of Jupiter "plasmapause", Geophys. Res. Lett.,3, 708-710, 1976.

158. Siscoe, G.L.: On the equational confinement and velocity space distribution of satellite ions in Jupiter's magnetosphere, J. Geophys. Res., 82, 1641-1645, 1977.

159. Talbot, R.J., Jr., D.M. Butler, and M.J. Newman, Climatic effects during passage of the solar system through interstellar clouds, Nature, 262, 561-563, 1976.

160. Neugebauer, M.: Large scale solar cycle variations of the solar wind, Space Sci. Rev., 17,221, 1975.

161. Akasofu, S.-I.: Solar cycle review (General aspects) in Physics of Solar Planetary Environments, edited by D.J. Williams, AGU publication, 1, 1-33, 1976.

162. Bridge, H.S.: Solar cycle manifestations in the interstellar medium in Physics of Solar Planetary Environments, edited by D.J. Williams, AGU publication, 1, 47-62, 1976.

163. Wilcox, J.M.: History of solar-terrestrial relations as deduced from spacecraft and geomagnetic data: Solar M regions in Physics of Solar Planetary Environments edited by D.J. Williams, AGU publication, 2, 947-957, 1976.

164. Eddy, J.A.: The sun since the Bronze Age in Physics of Solar Planetary Environments edited by D.J. Williams, AGU publication, 2, 958-972, 1976.

165. Siscoe, G.L.: Long-term aspects of magnetospheric variability in Physics of Solar Planetary Environments edited by D.J. Williams, AGU publication, 2, 973-1004, 1976.

166. Kane, R.P.: Geomagnetic field variations, Space Sci. Rev., 18, 413-540, 1976.

167. Kaula, W.M., and A.W. Harris: Dynamics of lunar origin and orbital evolution, Rev. Geophys. Space Phys., 13, 363, 1975.

168. Siscoe, G.L., and L. Christopher: Variations in the solar wind stand-off distance at Mercury, Geophys. Res. Lett., 2, 158, 1975.

169. Gleissberg, W.: The eighty-year cycle in auroral frequency numbers, J. Brit. Astron. Assc., 75, 227-231, 1965.

170. Gleissberg, W.: Ascent and descent in the eighty-year cycles of solar activity, J. Brit. Astron. Assc.,76, 265-268, 1966.

171. Maurette, M., and P.B. Price: Electron microscopy of irradiation effects in space, Science, 187, 121-129, 1975.

172. Cohen, T.J., and P.R. Lintz: Long term periodicities in the sunspot cycle, Nature, 250, 398, 1974.

173. Mayaud., P.N.: A Hundred Year Series of Geomagnetic Data 1868-1967, IAGA Bulletin No.33, 1973.

174. Currie, R.G.: Long period magnetic activity - 2 to 100 years, Astrophys. Space Sci., 39. 251-254, 1976.

175. Feynman, J.: Long term changes in geomagnetic activity and the solar wind (abs), Trans. Am. Geophys. Un.,57, 998, 1976.

176. Crooker, N.U.: On the high correlation between long-term averages of solar wind speed and geomagnetic activity (abs), Trans. Am. Geophys. Un., 57, 998, 1976.

177. Eddy, J.A.: The Maunder Minimum, Science, 192, 1189-1202,1976.

178. Fairfield, D.H.: Average and unusual locations of the earth's magnetopause and bow shock, J. Geophys. Res., 76, 6700, 1971.

179. Russell, C.T.: On the occurrence of magnetopause crossings at 6.6 R_e, Geophys. Res. Lett., 3, 593-595, 1976.

180. Siscoe, G.L.: On the statistics of the largest geomagnetic storms per solar cycle, J. Geophys. Res., 81, 4782-4784, 1976.

181. Siscoe, G.L.: On the statistics of the largest sunspot number per solar cycle, J. Geophys. Res., 81, 6224-6226, 1976.

182. Doell, R.R., and A. Cox, Pacific geomagnetic secular variation, Science, 171, 248-254, 1971.

183. Smith, P.J.: The intensity of the ancient geomagnetic field: A summary of conclusions, in Paleogeophysics, edited by S.K. Runcorn, Academic Press, New York, pp. 79-90, 1970.

184. Kono, M.: Intensity of the earth's magnetic field during the Pliocene and Pleistocene in relation to the amplitude of mid-ocean ridge magnetic anomalies, Earth Planet. Sci.Lett., 11, 10-17, 1971.

185. Harwood, J.M., and S.R.C. Malin: Present trends in the earth's magnetic field, Nature, 259, 469-471, 1976.

186. Cox, A.,J. Hillhouse, and M. Fuller: Paleomagnetic records of polarity transitions, excursions, and secular variation. Rev. Geophys. Space Phys., 13, 35, 1975.

187. Irving, E., and G. Pullaiah: Reversals of the geomagnetic field, magnetostratigraphy, and relative magnetude of paleosecular variation in the Phanerozoic, Earth-Sci.Rev., 12, 35-64, 1976.

188. Cox, A.: The frequency of geomagnetic reversals and the symmetry of the nondipole field, Rev. Geophys. Space Phys., 13, 35-51, 1975.

189. McElhinny, M.W., and R.T. Merrill: Geomagnetic secular variation over the past 5 million years, Rev. Geophys. Space Phys., 13, 687-708, 1975.

190. Siscoe, G.L., C.-K. Chen, and M. Harel: On the altitude of the magnetopause during geomagnetic reversals, J. Atmose. Terr. Phys., 38, 1327-1331, 1976.

191. Siscoe, G.L., and N.U. Crooker: Auroral zones in a quadrupole magnetosphere, J. Geomag, Geoelectr., 28, 1-9, 1976.

192. Crutzen, P.J., I.S.A. Isaksen, and G.C. Reid: Solar proton events: stratospheric sources of nitric oxide. Science, 189:457, 1975.

193. Reid, G.C., I.S.A. Isaksen, T.E. Holzer, and P.J. Crutzen: Influence of ancient solar-proton events on the evolution of life. Nature, 259:177, 1976.

194. Ogilvie, K.W., J.D. Scudder, V.M. Vasyliunas, R.E. Hartle, and G.L. Siscoe: Observations at the planet Mercury by the plasma electron experiment-Mariner 10, submitted to J. Geophys. Res., 1976.

195. Prakash, A., and N. Brice, Magnetospheres of Earth and Jupiter after Pioneer 10, in The Magnetospheres of Earth and Jupiter, edited by V. Formisano, D. Reidel Publishing Co., pp. 411-423, 1975.

MAGNETOSPHERE, IONOSPHERE AND ATMOSPHERE INTERACTIONS

P.M. Banks

Department of Physics
and
Center for Research in Aeronomy
Utah State University
Logan, Utah 84321

1. INTRODUCTION

In this review the general character of the earth's space environment is discussed with emphasis on the various physical processes which link the magnetosphere, the ionosphere and the upper atmosphere. The importance of these couplings has become increasingly appreciated during the past decade as experiment and theory, acting in tandem, have provided new information and insight about the interactive behavior of plasmas and neutral gases in the vicinity of the earth. Perhaps surprisingly, it has been found that subtle couplings exist which closely link the electrical and mass properties of these regions. Some of the couplings, such as the precipitation of energetic electrons into the upper atmosphere or the action of winds acting as a dynamo to create ionospheric plasma drifts, have been known for many years. Others, such as the formation of the plasmasphere through the mutual actions of convective electric fields and ionospheric plasma flow, are of more recent vintage.

As with many interdisciplinary topics, awareness of the full range of problems involving interactive processes in the magnetosphere, ionosphere and upper atmosphere has depended upon accurate experimental observations spanning vastly different environments. In the present case, even after 15 years of concentrated observation in space we lack adequate information to define accurately the basic processes associated with space plasma dynamics when cool, thermal plasma of ionospheric origin interacts with the neutral atmosphere, the energetic plasma of the magnetosphere, and the solar wind. The phenomena under consideration

are exceptionally complex, often grand in scale, and are frequently transient in time. Further, the measurements themselves are difficult to make in the tenuous space environment. These factors, when taken together, help to explain the slow development of experimental bases for many conjectured processes which are thought to relate phenomena in the three regions.

In this section, brief descriptions of the three regions are given as a prelude to discussions of the coupling processes. Extensive reviews probing far deeper with specific details can be found in companion papers and in the literature. The intent here is to provide a general introduction to the more challenging processes as they are now known.

1.2 Magnetosphere

The magnetosphere is a vast volume of space surrounding the atmosphere laced by magnetic field lines tied to the earth. Within the magnetosphere (see the campanion review by Roederer), the plasma is almost fully ionized with components of terrestrial and solar wind origin, each reflecting through its energy, pitch angle and spatial distribution the complexity of competing production and loss mechanisms, each component reacting in differeing ways to electric and magnetic fields. It is a characteristic of the magnetosphere that the density of the ionized gases greatly predominates over that of the neutral gases. Although the gross features of the magnetosphere have been probed at length, especially with regard to energetic particle fluxes and magnetic field topology, only a few of the most important physical processes have been adequately explained with quantitative models.

Schematic diagrams of magnetospheric structure as it related to MIA

coupling are given in Figures 1 and 2, taken from Heikkila[1] and Frank[2]. The two sectional views of Figure 1 indicates the spatial relationships between the magnetopause and the inner magnetosphere. The overall magnetic field structure results both from the earth's intrinsic field and the cintrobution of various currents in space. The outermost sheet current establishes the boundary between the solar wind plasma and magnetospheric plasma. As shown, on the front of the magnetosphere this current passes from dawn towards dusk with an increasing meridional component as one progresses to the tail of the magnetosphere. In the tail, this pattern is continued with the addition of a neutral sheet current across the equatorial plane. Closer to earth, currents along magnetic field lines serve to connect the ionosphere to the magnetopause, to the neutral sheet currents system and to an internal ring current.

With regard to plasma, the solar wind has direct access to the magnetosphere in the dayside regions only in the vicinity of the polar cusp. On the flanks of the magnetosphere, there is evidence for solar wind leakage leading to the formation of the plasma sheet, a hot plasma which, when convected by electric fields towards the nightside of the earth, leads to atmospheric excitation and a diffuse auroral glow.

Somewhat closer to earth, copious quantities of cool plasma of ionospheric origin are contained within the plasmasphere, a torus-like volume extending outwards to distances of 4 to 5 earth radii. In contrast to the plasma sheet, which moves within the non-rotating frame of the magnetosphere, the plasma of the plasmasphere generally shares the earth's rotational motion with dynamic fluctuations described later.

Figure 2 shows many of these same phenomena in a noon-midnight

meridional section. Extensions of the polar cusp, the ring current and the plasmasphere to the vicinity of the earth are indicated, together with projections of the auroral ovals where energetic electron and proton impact with the upper atmosphere takes place.

1.3 Ionosphere

The ionosphere lies beneath the magnetosphere, situated as a transition zone between the fully ionized gases of the more distant regions and the electrically neutral atmosphere lying below. Owing to its importance to radio communications, morphological and scientific studies of the ionosphere have been made for the past 50 years. Its origin, for the most part, lies in the absorption of solar ultraviolet radiation by neutral gases in the upper atmosphere. Reactions by the resulting photo-ions (often in excited states) and the atmosphere are complex, with specific reaction channels varying in importance in relation to atmospheric composition and temperature[3]. The resulting ion composition is found to depend upon a number of factors, including solar radiation spectral intensity, atmospheric composition, neutral gas temperature, ion diffusion, electron and ion temperatures, plasma flow to (or from) the magnetosphere, and the strength of the ionospheric electric field (which results in $\bar{E}x\bar{B}$ plasma drifts).

As a transition zone the ionosphere has a number of interesting features. For example, at its nominal upper boundary (1000-3000 km), the ionosphere merges smoothly with the magnetosphere as collisions between the charged particles of the ionospheric plasma and neutral particles of the atmosphere become increasingly rare owing to the general exponential decrease of atmospheric density with altitude (Figures 3

and 4 show altitude distributions of charged and neutral gas constituents of the ionospheric regions). At lower altitudes collisions become increasingly frequent such that the ionosphere becomes progressively partially, then only weakly ionized.

The altitude variation of the collision rate has several important physical consequences. Within the magnetosphere and much of the upper ionosphere, the ion-neutral collision frequency is much smaller than the ion gyrofrequency. As a result, in the absence of electric fields, ion motions perpendicular to the ambient geomagnetic field, $\bar{B}$, are very strongly inhibited. On the other hand, owing to the low ion collision frequency, ion drift motions parallel to $\bar{B}$ can proceed rapidly in response to ion pressure gradients, electric fields, gravity, etc.

In the altitude regime above 150 km, overall plasma drift motions can be broken into two components: Motions of plasma perpendicular to $\bar{B}$ caused by electric fields perpendicular to $\bar{B}$ ($\bar{v} = \bar{E} \times \bar{B}/B^2$) and motions parallel to $\bar{B}$ caused by plasma diffusion processes. (Electric fields parallel to $\bar{B}$ are, in most cases, very small. However, at high latitudes there is considerable evidence for parallel electric fields occuring in connection with auroras[4].) This separation of motions, in the absence of large parallel electric fields, leads naturally to the idea that plasma convection transverse to $\bar{B}$ (arising from perpendicular electric fields) can occur independently of plasma diffusion parallel to $\bar{B}$ (see Figure 5). Plasma motion transverse to $\bar{B}$ arising from $\bar{E}\times\bar{B}$ drift can also be shown to be incompressible for most cases of interest to MIA couplings since the influence of $\partial\bar{B}/\partial t$ e.m.f.'s are usually small[5]. On the other hand, the plasma is compressible in directions parallel to

$\overline{B}$, creating the possibility of inward and outward plasma flows of low and high speed, depending upon the particular geophysical situation[6]. As described later, most of the cool, background plasma found within the magnetosphere is of ionospheric origin.

In the lower regions of the ionosphere, between 85 and 150 km, there are different conditions which affect the electrical properties of the ionosphere[7]. At high altitudes, the lack of ion or electron collisions with neutral particles prevents, according to conventional theories for cool plasma, currents perpendicular to $\overline{B}$. Passing downward from 150 km altitude, however, the ratio of ion-neutral collision frequency to ion gyrofrequency becomes progressively larger, reaching values greater than one near 125 km. For ions in this region, an ionospheric electric field perpendicular to $\overline{B}$ will cause ion drift motion in two directions: in the $\overline{E} \times \overline{B}$ direction (Hall drift) and, as a consequence of the ion-neutral collisions, in the direction of $\overline{E}$ (Pedersen drift). This behavior is shown in Figure 6. With regard to the electron gas, the electron-neutral collision frequency remains much smaller than the electron gyrofrequency down to an altitude of 80 km. Hence, perpendicular electric fields will cause only a Hall drift for electrons in the altitude regime where ions have an appreciable Pedersen drift. As a consequence of these factors, the application of a perpendicular electric field will result in currents parallel to $\overline{E}$ (Pedersen) and in the $\overline{E}x\overline{B}$ (Hall) direction[8]. These currents have strengths which vary with altitude according to their electrical resistivities.

Currents from the magnetosphere pass horizontally through the ionosphere. Since the ionosphere is a resistive medium, horizontal

changes in electric potential occur in proportion to the Pedersen current and the Pedersen resistivity[9] (see Figure 7). In contrast, since Hall currents are perpendicular to $\bar{E}$, there is no change in electrical potential or energy dissipation associated with them. The net result of these processes is that magnetospheric field-aligned currents sustain ionospheric currents with subsequent establishment of ionospheric electric fields in the E-region.

In general, electric fields in the ionosphere and magnetosphere arise in a number of ways[93]. These include, among others,

1. Electric fields associated with the rotation of the earth and its magnetic field.
2. Electric fields resulting from flows of energetic plasma within the magnetosphere.
3. Electric fields resulting from differential motions of positive ions and electrons in the geomagnetic field.
4. Electric fields associated with differential motions of the neutral atmosphere and the ionospheric plasma.

As shown by Figures 1 and 9, magnetospheric field-aligned currents connect to the ionosphere in the auroral ovals. Thus, at high geomagnetic latitudes the ionosphere helps to complete a portion of the general system of magnetospheric currents[10]. At low latitudes, electric fields associated with the magnetospheric current system are considerably smaller than at high latitudes. Nevertheless, in these regions a lower level of electrodynamic activity is maintained as winds in the upper atmosphere act as a dynamo source to sustain a global system of currents, electric fields and associated high altitude plasma drifts[11].

1.4 Atmosphere

The neutral atmospheric regions participating most actively in MIA couplings lie above 100 km altitude. This region, called the thermosphere, is characterized by a heterogeneous composition as a consequence of a decline in the effectiveness of atmosphere mixing processes. (General discussions of the upper atmosphere can be found in references 3 and 8.) It is also a region of rapid temperature rise as a consequence of N_2 and O_2 absorption of solar ultraviolet radiation. Through photodissociation, as well as chemical and ion processes, atomic and molecular species absent at lower altitudes are present in substantial number. Further, owing to the low rate of quenching collisions, metastable states of various atoms (and also ions) are present in significant quantity. Concentration profiles of the major atmospheric species are given in Figure 3.

Winds in the thermosphere arise in several ways. First, as a result of the uneven distribution of solar heating over the globe and tidal effects, large scale wind patterns are established. The patterns of these winds are strongly modified in two separate ways. At high latitudes there is substantial additional atmospheric heating as a result of energy dissipation associated with the ionospheric current systems[12-14] and auroral particle precipitation[9,15,16]. Such heating eventually affects the entire thermosphere, causing local gas pressure gradients and consequent gas flows which act to alter the total atmospheric density at high altitudes as well as the overall gas composition[15,17,18].

A second influence on thermospheric winds is associated with plasma motion. Differing velocities of the ionospheric plasma and the neutral

atmosphere result in frictional drag, as a consequence of ion-neutral collisions. Above 150 km altitude however, the plasma is strongly tied to magnetic field lines. Thus, neutral gas moving through the ionosphere above 150 km altitude cannot appreciably accelerate the plasma in the direction of neutral gas motion. Instead, plasma is driven up or down $\overline{B}$, changing the altitude distribution of plasma density in accordance with the various processes acting in the ionosphere (ion production, ion loss, gravity, charge separation electric fields, and plasma diffusion). In addition, as a result of collisions with the ions, the neutral gas itself experiences a frictional drag force and heating which can substantially influence the global pattern of atmospheric winds[19].

A related momentum transfer phenomenon can occur when ionospheric electric fields are present with consequent $\overline{E} \times \overline{B}$ plasma drifts. In this case, the plasma accelerates and heats the neutral gases with a conversion of electrical energy to mechanical and thermal energy of the ion and neutral gases. Details of this coupling are discussed later.

2. ELECTRODYNAMIC COUPLING PHENOMENA

Various electrodynamic phenomena occur throughout the magnetosphere with varying scales of space and time. Of principal concern here are those electrical couplings which exhibit only slow temporal variation; i.e., the nearly d.c. component of electrodynamic activity.

From recent work[20-22] it is known that the earth's ionosphere is an integral circuit element in a widespread system of magnetospheric currents. It has long been known that the magnetopause incorporates an

extensive current system which acts to divert the solar wind around the magnetosphere. As shown in Figure 10, these currents also pass through the tail of the magnetosphere and, by way of paths leading along magnetic field lines, to and from the E-region of the ionosphere. In the high latitude ionosphere, Hall and Pedersen currents flow electrically connecting with field-aligned currents, and, consequently, to opposite sides of the magnetosphere. As mentioned before, with the ionosphere potential drops (perpendicular to $\bar{B}$) occur across Pedersen resistivity, leading to the establishment of electric fields in the ionosphere. By means of small polarization currents flowing parallel to $\bar{B}$, voltage drops and electric fields within the ionosphere can be communicated outward to the various regions of the magnetosphere at the plasma Alfven speed. On the other hand, magnetospheric processes can result in the imposition of an electric field upon the ionosphere with consequent currents in the E-region and along magnetic field lines. In such cases, the assessment of cause and effect may prove difficult to determine.

The magnetosphere field-aligned currents are found[25-27] to enter the ionosphere in the vicinity of the auroral oval, then spread horizontally in accordance with Hall and Pedersen conductivities and conductivity gradients.

The statistical results obtained for the global distribution of field-aligned currents are summarized in Figure 11 for weakly disturbed magnetospheric conditions. The currents seen at the highest latitudes apparently connect to the magnetopause and plasma sheet, as indicated by the diagram of Figure 10. The lower latitude sheets are located on closed, dipolar magnetic field-lines which lead to the region of the

ring current[28]. The amplitude distribution of these currents is not well known, but it seems that in the northern hemisphere the net current is inward on the morningside of Figure 11 and outward on the evening-side[27]. The situation is reversed in the southern hemisphere.

Using the equations of current continuity, calculations have been made of the ionospheric currents which result from the measured field-aligned currents[30]. The result confirm the important role played by auroral oval conductivity enhancements in concentrating the ionospheric currents to form auroral 'electrojets'. Another feature of interest arises because the classical electrical conductivity parallel to $\overline{B}$ is very high in the ionosphere and magnetosphere. Thus, electrical coupling between magnetically conjugate hemispheres is assumed to occur in the form of currents parallel to $\overline{B}$. Such parallel currents permit the magnetospheric electric circuit to include the regions of highest ionospheric conductivity, taking advantage of both general solar EUV produced ionization and that produced in the auroral oval by precipitating particles (see Figure 12).

The electric fields established within the ionospheric E-region are responsible for convective $\overline{E} \times \overline{B}$ plasma drift patterns of low energy thermal plasma within the high latitude ionosphere and magnetosphere. Maps of the electric field pattern are best represented in terms of contours of electric potential which are equivalent to the streamlines of thermal plasma motion perpendicular to $\overline{B}$. Owing to a lack of comprehensive experimental information and the inaccuracies associated with theoretical models, empirical models have recently been developed[23,24]. The results of one model are shown in Figure 13, projected onto the

north polar ionosphere using magnetic coordinates. A maximum potential difference of 77 kilovolts is present across the polar cap, giving an average dawn to dusk ionospheric electric field of 20 mv/m. Much stronger electric fields are present in the midnight sector and near dawn within the auroral oval (65^{o} - 70^{o} magnetic latitude).

The pattern of plasma convection shown in Figure 13 is two-celled with antisunward motion over the polar cap and sunward motion equatorward of the regions of entry and exit of the driving field-aligned currents. Recent observations[31] supplement the empirical model by showing the presence of the narrow throat (not present in Figure 13) near local noon through which a large portion of convecting ionospheric plasma passes in its global convection path. This throat, shown in Figure 14, occurs within a more general dayside region of particle precipitation called the polar cleft, a feature intimately linked to the structure of the dayside magnetopause. A local set of field-aligned currents is also present (see Figure 11) in this same region.

The electric fields arising from the driving magnetospheric field-aligned currents have an important subsidiary effect upon energetic plasma in the magnetospheric plasma sheet (see Figure 1). In the region of the plasma sheet lying behind the earth in the midnight sector, the onset of $\overline{E} \times \overline{B}$ drift moves plasma towards the Earth, increasing its density and energy. Gradient and curvature forces associated with the geomagnetic field act upon the plasma, establishing currents perpendicular to the magnetic field[21]. Consequently, in addition to the original sheet currents connecting the magnetopause and magnetospheric tail regions to

the ionosphere, the drift of energetic plasma within the magnetosphere appears to create both a magnetospheric ring current and a set of secondary sheet currents connected to the ionosphere which act to reduce the original electric field in the regions equatorward of the driving currents[22].

Another aspect of the global electrodynamic model described above relates to auroral particle precipitation. There is a close but poorly understood connection between the acceleration of plasma to produce auroras and the presence of field-aligned currents[10,32,33]. As a result of particle impact ionization, the auroral oval has substantially higher electrical conductivities (Hall and Pedersen) than surrounding regions. Thus, the gross global electric field tends to be smaller within the auroral oval than in the polar cap or the regions immediately equatorward of the oval. This factor affects the speed of ionospheric and magnetospheric plasma convection and influences the way the plasma sheet associated particle ring current establishes itself[32].

A further influence upon the overall behavior of the magnetospheric system relates to atmospheric dynamo effects in the ionospheric E-region. In the polar cap, ion drag and the normal day to night atmospheric pressure gradient act to establish an antisunward wind pattern[34]. Figure 15 shows the results of recent calculations of this coupling effect for high altitudes (200 km) while Figure 16 shows the results at 110 km.

In the absence of any magnetospheric driving currents, E-region winds tend to move ions antisunward (through ion-neutral collisions) while leaving electrons behind (no electron-ion collisions). The resulting space charge would establish an ionospheric electric field and ionospheric current system. This current could in the correct circumstances, result in a secondary polarization electric field which would $\overline{E} \times \overline{B}$ drift ionospheric plasma in the same direction as the original neutral wind; i.e., an ionospheric dynamo is created which can drive magnetospheric plasma motions[35]. It has been pointed out that with sufficient inertia, such a dynamo could modulate time variations in magnetospheric plasma convection[36].

With the foregoing information as a brief conceptual background, more specific problems of electrodynamic coupling can be presented to indicate the complexity of the geophysical environment. It must be realized, however, that much of the foregoing material is based upon models of how plasma should behave according to simple theories rather than how it actually behaves in nature. The differences, when properly documented, will guide future development in the field.

2.1 Discussion of the Basic Model

Most of the present ideas of large scale magnetosphere-ionosphere electrical coupling are based upon plasma hydrodynamical models which neglect the possibility of anomalous behaviors described in a companion review by Falthämmer. In particular, electrical conductivities derived

from consideration of particle-particle collision effects are assumed to be valid, with the result that the parallel electrical conductivity is assumed to be much greater than the perpendicular conductivities in all regions except the lower ionosphere. As a consequence, in this model magnetic field lines have constant electrical potential along their length with ionospheric potential drops occurring perpendicular to $\overline{B}$ and potentials propagating upward into the magnetosphere according to the geometrical properties of the earth's magnetic field[35].

Unfortunately, it is difficult to obtain direct evidence pertaining to the validity of these concepts. Within narrow regions of auroral precipitation there have been a number of measurements which indicate the presence of substantial electric potential drops parallel to $\overline{B}$[4, 37, 38]. Whether such features result from anomalous conductivities or dynamical plasma relationships is not known although there exists an extensive literature describing the growth of instabilities which limit the current-carrying capacity of the plasma[39,40].

Most of our present factual information about magnetospheric electrodynamics has been gathered in the ionosphere. Balloons, with electric potential probes, incoherent scatter radars, rockets with potential probes and plasma drift detectors, barium cloud releases, as well as spacecraft potential probes and plasma drift detectors have all been used with substantial success[7,41-43,94]. Through observations of energetic particles and plasma boundaries at geosynchronous orbit, it has also been possible to deduce the outer magnetospheric electric field. Figure 17, for example, shows electric field potentials deduced from geosynchronous satellite energetic particle data[44]. Such models, when projected back

into the ionosphere along magnetic field lines, do not appear to reproduce the strong ionospheric electric fields obtained from models such as shown in Figure 11 or obtained from experiments[45]. The reason for this discrepancy remains to be determined.

An example of high latitude plasma drift caused by ionospheric electric fields, taken from the Atmospheric Explorer C satellite while over the south polar region, is shown in Figure 18. Zones of rapid plasma convection are seen above 60° invariant latitude consistent in magnitude and direction with the predictions of the qualitative model results previously shown in Figure 13.

With regard to field-aligned currents, results from the TRIAD[26,27,29] and ISIS[47] spacecraft show the presence of latitudinally narrow, longitudinally extended sheet currents in the vicinity of the auroral oval. Figure 11, has shown the statistical spatial distribution of the incoming and outgoing currents. The poleward sheet currents seem to be associated with the magnetopause and magnetospheric tail regions, while the counter-direction currents equatorwards connect the regions occupied by plasma sheet particles. Further, there seems to be a statistical tendency for the poleward current sheets to be larger in magnitude than the equatorward sheets, a condition which would be consistent with the latter being established through secondary processes involving the plasma sheet particles and a partial ring current.

The existence of high latitude field-aligned currents and electric fields provides direct evidence for one aspect of magnetosphere-ionosphere electrical coupling. Still to be explored, however, is the way energetic plasma of the inner magnetosphere influences the general distribution of

currents and electric field. As mentioned before, electric fields resulting from ionospheric potential drops, when communicated upward to trapped energetic plasma in the magnetosphere, cause charged particle drifts and consequent formation of a partial ring current which is thought to connect to the ionosphere via field-aligned currents. Theoretical models based on these ideas have been developed[21,22], but remain largely untested owing to the difficulty in gathering simultaneous data from the magnetosphere and ionosphere. In fact, several middle latitude ionospheric plasma drift experiments appear to contradict the theoretically deduced time response of the plasma sheet to electric field onset[48].

In summary, there exists ample evidence for strong quasi-static electrical coupling between the magnetosphere and ionosphere. In the absence of adequate experimental information, the extent to which present models accurately represent the gross pattern of electric field, current and plasma dynamics cannot be evaluated. Further, the basic model does not incorporate any direct relationship to dynamical phenomena such as auroras, substorms or general magnetospheric storms. Such uncertainty leaves the topic of magnetospheric electrodynamic coupling as one of the most challenging within the context of solar system plasma physics.

2.2 Electrodynamic Phenomena

The last section emphasized the quasistatic electrical couplings between the magnetosphere and ionosphere. Observations of currents and electric fields, however, reveal continual fluctuation, implying the need for considering the time scales implicit in the coupling processes.

Very little is presently known of the characteristics of the

magnetopause and magnetotail processes which give rise to the field-aligned currents feeding the ionosphere. Changes in interplanetary magnetic field, the solar wind and the magnetospheric reconnection rate, can reasonably be expected to alter the location and intensity of the primary current system. Furthermore, such changes are related to the auroral oval itself. Magnetospheric substorms also play an important, but very poorly understood, role in the dynamical coupling, both through changes in the ionospheric conductivity and through injection of energetic plasma within the magnetosphere which, through pressure gradients, can act to drive currents and establish electric fields.

With such dynamical events commonplace, it is reasonable to ask whether electric coupling between the ionosphere and magnetosphere is adequately described by static models? Unfortunately, experimental observations of global electric fields and currents are too sparse to provide an answer. The state of the art is such that while the presence of fields and currents has been demonstrated, a consistent pattern of variation in response to changes in the solar wind, magnetospheric plasma, or ionospheric parameters cannot be determined.

In the absence of observations, there have been recent advances in developing time dependent models of electrical coupling. One approach has been to simulate time changes through a model which incorporates a series of steady state solutions to the coupling equations[22]. This model has been very useful in predicting the way the plasma sheet advances towards the earth while establishing the ring current and global scale current patterns.

A second approach has been to treat the magnetosphere-ionosphere system as an electrical circuit composed of spatially distributed

reactive elements arranged much like an electrical transmission line. Such a model has been used, for example, to explore the effects of magnetic field reconnection at the dayside magnetopause on the polar cap electric field[49]. From this model, it is found that abrupt changes in reconnection at the magnetopause create oscillatory systems of current and electric field which eventually act to increase (or decrease) the size of the polar cap region encircled by the driving field-aligned currents. The relationship between such electrodynamic changes and corresponding changes in the regions of auroral particle precipitation (the auroral oval) is clear observationally but still lacks theoretical explanation. A similar model has been used to describe the electrodynamic coupling between the ionosphere and magnetosphere associated with an auroral arc[50,51].

At lower latitudes in the ionosphere and overlying magnetosphere, field-aligned currents associated with the dynamics of the plasma sheet strongly influence of global electric field pattern, tending to limit the equatorward extension of the electric field. At the present time the time scale associated with such shielding remains uncertain, especially when the theoretical predictions are evaluated in terms of possible anomalous plasma behavior which may limit the currents extending into the ionosphere.

Another aspect of ionospheric electrical coupling has been revealed by recent measurements of electric field driven plasma drifts at the geomagnetic equator. It has been found that sudden changes in plasma drift speed in the equatorial electrojet region occur at the same time that substorms occur in the auroral oval[52,53]. This result implies a

reasonably strong electrical coupling between the two zones such that currents established through magnetospheric processes at high latitudes can cause, within minutes, abrupt changes in equatorial electric fields, plasma drift and, presumably, the generation of ionospheric irregularities. At the present time, models explaining this global coupling have not been developed.

2.3 Dynamo Couplings

As described earlier, winds in the E-region selectively impart momentum to ambient ions, thereby establishing a small polarization electric field (since electrons are tied to magnetic field lines) which creates a Hall current in the ionosphere through $\bar{E}x\bar{B}$ drift of electrons. This process is equivalent to an atmospheric dynamo and the resulting currents establish a global pattern of ionospheric electric field. Above the ionosphere, Hall drifts of plasma (electrons and ions) are present, thus providing a strong coupling between the pattern of E-region winds, the global distribution of ionospheric conductivity, and the high altitude pattern of plasma drift.

At the geomagnetic equator, winds blowing from the heated dayside atmosphere towards the cooler nightside create, through a process of electrical polarization, a narrow belt of strong electron drift[8]. This belt, termed the equatorial electrojet, has been intensely studied as a consequence of plasma irregularities associated with the currents.

At middle latitudes, a more complex situation arises owing to the global pattern of E-region winds, the possibility of electrical coupling to magnetically conjugate hemispheres, and the intrusion of currents associated with high latitude current systems. Extensive calculations

of dynamo currents and electric fields have been made including these factors[11,12]. It is found that the results agree reasonably well with ground based magnetic observations and high altitude plasma drifts.

At high latitudes separate influences are felt in the form of auroral oval ionization and an almost verticle magnetic field. Intense winds are present in these regions as a consequence of atmospheric heating by particles and currents and momentum transfer from the convecting ionospheric plasma. In the polar cap, E-region winds are sufficiently strong to create a substantial dynamo action. However, fundamental information about the way polarization currents can close in this region is lacking. Hence, the importance of the polar dynamo to high latitude plasma convection must remain uncertain.

2.4 Auroral Couplings

There presently exists no generally accepted theory describing the electrical couplings between the ionosphere and magnetosphere in the vicinity of an auroral arc. (Individual arcs are imbedded within the auroral oval. For further details, consult the campanion review by Fälthammer.) Within arcs, intense horizontal currents flow, Hall and Pedersen conductivities are greatly enhanced over those of surrounding regions, and there are often intense field-aligned currents in the vicinity.

From such information, many theoretical models have evolved[39,51,54], some based upon electric circuit analogies, others based on anomalous properties of plasma. The latter models include both wave-particle interaction processes[55] and the formation of electrostatic "double-layers"[56]. In both cases, substantial electric potential along auroral

magnetic field lines is assumed to exist. This situation results in electric fields which are "oblique" to magnetic field lines, a situation in disagreement with classical models of plasma behavior. Auroral observations of particle fluxes and electric fields in the vicinity of "inverted Vee" structures[57-59] are best explained by theoretical models which discard conventional plasma electrical conductivities, using instead transport coefficients derived for plasmas characterized by current driven instabilities. Recent AC and DC vector electric field measurements have detected anomalous regions of very large electric fields ($\sim$ 500 mV/m) in the vicinity of the auroral oval at altitudes between 2000 and 8000 km[95]. These electric fields are oriented largely perpendicular to the magnetic field and are much larger than would be obtained if magnetic field lines were equipotentials tied to observed ionospheric auroral electric fields. Since the results also indicate the presence of intense ion cyclotron waves, one is led to the conclusion that the observed magnetic field lines are not equipotentials and that electric field acceleration of electrons and positive ions occurs in these same regions.

While the electrical structure of auroras remains as an outstanding current problem of magnetosphere-atmosphere coupling, other related couplings are also present with regard to the neutral atmosphere. Auroral precipitation, for example, results in substantial atmospheric heating above 100 km. In addition, heating in the same region also arises from Joule dissipation of currents. The energy released in the neutral atmosphere by these two processes is sufficiently intense to create local vertical circulation cells[60] as well as large scale alterations to global wind patterns[17,18]. Since such energy input is associated with the auroral oval, there is a daily "sweeping" action as the oval

moves relative to the geographical axis under the influence of magnetospheric processes. The resulting wind system also introduces a dynamo effect, influencing the high latitude pattern of electric field and current. As mentioned before, the importance of this effect within the general set of magnetospheric processes is not established.

3. THERMAL PLASMA COUPLINGS

The ionosphere is a cool, weekly ionized plasma having electron and ion temperatures from 300^{o} to $10,000^{o}$ K and electron densities from 10^{3} to $10^{6} cm^{-3}$. Figure 19 illustrates the ionospheric regions as characterized by early radio experiments and the differing ion composition arising from competing ion-neutral gas reaction channels. Above 200 km altitude, plasma diffusion (parallel to $\bar{B}$) becomes increasingly important in determining the vertical profile of ion concentration. In fact, the formation of the F_2-region ion and electron density peak is a direct consequence of competition between ion production and loss and plasma diffusion. Below the peak, ionic reactions are most important in determining the altitude profile of ion density while above the F_2-peak, the profile is determined by a balance between the plasma pressure gradient and gravity.

The presence of protons in the ionosphere is an accident of nature. O^+, when mixed with neutral atomic hydrogen, (an important atmospheric constituent at high altitudes) undergoes an accidentally resonant charge exchange reaction[6]

$$O^+ + H \rightleftarrows O + H^+ \qquad (3.1)$$

which creates protons with temperatures characteristic of atomic hydrogen in the upper atmosphere (750^o to 1500^oK). Above 600 km altitude, plasma is largely free of collisions with neutral particles and the distribution of H^+ along a magnetic flux tube is determined by the distribution of plasma pressure and gravity. Below 600 km altitude the reverse reaction converting H^+ to O^+ becomes increasingly important as the atomic oxygen concentration rises. Below 500 km H^+ and O^+ are largely in balance according to the density and statistical weight factors implicit in (3.1).

The distribution of thermal plasma within the magnetosphere is indicated by Figure 1,2 and 20. Below about 60^o magnetic latitude ob-

servations show a torus-like volume (which extends outward to 4-5 Earth radii in the magnetic equatorial plane), the plasmasphere, filled with thermal plasma of ionospheric origin. Above 60^{o}, the thermal plasma has a very low density and moves away from the Earth with a bulk flow velocity parallel to $\bar{B}$ which may reach 10 km sec^{-1}. The boundary of the plasmasphere, called the plasmapause, is thought to be aligned along magnetic field lines, although confirming observations are absent. Spacecraft and ground based radio experiments have obtained radial profiles of plasma density variation in the geomagnetic equatorial plane (Figures 21 and 22) as well as the local time dependence of the boundary (Figure 20). Many additional features of this region have been discussed recently[61,62].

As described in the following sections, the peculiar spatial distribution of thermal plasma in the magnetosphere results from two forms of ionosphere-magnetosphere coupling: (1) electric fields which act to convect plasma in patterns related to the structure of the ionospheric electric field and the geomagnetic field, and (2) the ability of the ionosphere to supply H^{+} to the magnetosphere at a finite rate along magnetic field lines to regions of low plasma pressure.

The basic hydrodynamical equations used to obtain plasma densities, temperatures and flow speeds have been given elsewhere[6]. Models based on these equations give a variety of results depending upon the boundary conditions. At low altitudes, chemical equilibrium exists while at high altitudes it is convenient to categorize the results in terms of the plasma pressure (see Figure 23). For high pressure models, typical of the low latitude plasmasphere, the upward flux of H^{+} is very small unless a pressure assymmetry exists between conjugate regions. In the middle latitude regions,

a reduced plasma pressure is appropriate, giving the center profile of Figure 23, while for very low plasma pressure the lower profile results as a consequence of a large outward flow of H^+.

Interestingly, it has been found that the H^+ escape flux is subject to a saturation effect as a result of H^+-O^+ collisions. For progressively lower plasma pressures, the H^+ flux rises rapidly to a saturation value near 2×10^8 ions cm^{-2} sec^{-1}. Further decreases in pressure cannot increase the flux[6].

With this information as background, attention can be given to specific examples of thermal plasma coupling.

3.1 The Plasmasphere

Below 60^o magnetic latitude, electric fields associated with the magnetospheric current system are small and, within the limits prescribed by dynamo electric fields, the ionosphere and related magnetospheric plasma tends to co-rotate with the earth. In this same region, magnetic field lines connect to conjugate hemispheres so that plasma created in the ionosphere can diffuse upwards along $\bar{B}$ until equilibrium is reached. The external factors influencing this equilibrium include gravity, the density of O^+ in the two underlying ionospheres, atmospheric composition, and plasma temperatures. In practice, these factors vary with time and, as a result, there is thought to be a continual ebb and flow of thermal plasma along magnetic flux tubes with both inward and outward plasma flow, as described in Figure 23. During the daytime, for example, there is a general rise in plasma density along a given field tube as the ionospheric density rises. At night, O^+ in the ionosphere decays by ionic recombination processes and H^+ flows downward from the magnetosphere in response to the resulting plasma pressure gradient.

As one progresses to high latitudes, the volume laced by magnetic field lines extending into the magnetosphere rises rapidly[62]. Consequently, the time needed for plasma to fill flux tubes to a given density also rises to the point where diurnal variations in the ionosphere are important. In these regions the plasma density in the equatorial region of a magnetic flux tube cannot rise to the near-equilibrium values found along lower latitude flux tubes. This region of dynamic flows, called the outer plasmasphere, undergoes continual fluctuation in response to the frequent intrusion of convective electric fields which remove thermal plasma from the closed magnetic field lines, thereby restarting the plasma filling process. In essence, the magnetic flux tubes of the plasmasphere act as thermal plasma reservoirs which interact with the ionosphere lying below[64].

Ions other than H^+ also populate the magnetosphere. He^+, for example, arises from photoinization of He and has a diffusive character similar to H^+. NO^+ has been seen on occasion, being linked mainly to geomagnetic activity. Similarly, O^{++} and N^+ have also been detected on a regular basis. Minor constituent ions such as these do not play an important part in the general plasma coupling process. Nevertheless, they do act as tracers useful for defining different physical processes acting upon the thermal plasma

3.2 The Polar Wind Regions

Above 60^o magnetic latitude, ionspheric electric fields are present in association with field-aligned currents and the auroral oval. The general convective pattern (see Figure 13) is found to carry thermal plasma through two distinctive regimes: (1) regions of open magnetic

field lines which connect to the magnetopause and/or magnetotail, and (2) closed field regions. Along open magnetic field lines, thermal plasma is thought to be free to escape to some unknown destination (possibly interplanetary space), leading to a gross upward flow of thermal plasma at speeds which may exceed the random ion thermal speed. As plasma convects onto closed field lines in the midnight sector of the polar regions, the upward flux attempts to fill the field tubes. The time constant for filling, however, is 5 to 8 days so that the upward flow continues unabated during the convective cycle, which may be as short as several hours[64].

Observations in the topside ionosphere (see Figure 24) show low plasma densities in these high latitude regions, consistent with the observation of rapid H^+ outflow. Thus, one finds a steep latitudinal density variation associated with the transition from rapid flow (polar wind) to low flow (inside the plasmasphere). In a steady state, the density boundary (the plasmapause), represents a transition from outward plasma flow to no flow. However, since there are continual changes in the latitudinal extent of the ionospheric convective electric field, the plasmapause itself must move poleward with a response time determined by the time needed to fill a flux tube with plasma. Erosion of the plasmasphere, on the other hand, can progress as rapidly as plasma can be convected from middle latitudes to the open field lines of the polar caps or destroyed through ionic reactions sensitive to rapid plasma motions. Thus, during the onset of enhanced plasma convection the plasmapause is closely related to the lower latitude boundary of convection but during periods of recovery (5 to 8 days) no simple relationship is present.

Notions such as these have led to the concept of "inner" and "outer" plasmasphere. The inner region remains isolated from high latitude plasma convective processes and the daily ebb and flow is determined by ionospheric processes along particular flux tubes. The outer plasmasphere, in contrast, is subject to frequent emptying as a consequence of changes in the equatorward extent of convective electronic fields. Upward flow in the topside ionosphere exists throughout much of this region with equilibrium high densities being reached in the magnetosphere only after periods of extended calm. This behavior is well shown by radio whistler measurements of flux tube equatorial electron density[66] as a function of time. Figure 25, obtained by Park[66] shows the recovery of the electron content as a function of time (day number) and geocentric distance (L). Data from low latitudes show a rapid rise in density following a period of ionization removal, while near 60^{o} (L≃4) magnetic latitude the approach to equilibrium is far more gradual.

3.3 Plasma Flow Theory

Generally speaking, the theoretical foundations of the polar wind are much more complicated than that for the analogous solar wind[6]. In the polar wind, H^{+} escape is accomplished with the aid of a polarization electric field associated with the presence of O^{+}. Further, H^{+}-O^{+} Coulomb collisions play an important part in limiting the H^{+} escape flux to values near 2×10^{8} ions $cm^{-2}sec^{-1}$. In the solar wind, H^{+} is a dominant species and collisions do not have a direct part in determining the escape flux.

The original polar wind theory [67] was based on simple hydrodynamic models. More complex treatments based upon a 13 moment approach have

features of ionospheric density associated with a steady plasma convection pattern and the presence of auroral precipitation. A large tongue of enhanced plasma density is seen entering the dayside polar cap, while deep troughs form in slow convection regions equatorward of the auroral oval.

3.5 Plasmapause Structure

Observations of the radial plasma density near the magnetosphere equatorial plane frequently show the presence of ionization "islands" beyond the main body of the plasmasphere. These "detached" plasma regions were originally interpreted as discrete regions separated from the plasmasphere by an enhancement of the convection electric field[71]. Examples of the detached regions taken from OGO-5 data are shown in Figure 28.

As described in the next section, these regions of relatively high electron density may have an important effect upon the trapping stability of energetic particles normally present outside the plasmasphere[72]. The presence of ELF radio noise, long period magnetic field oscillations, as well as discrete patches of particle precipitation may all be associated with the high density, cold plasma region[73].

The spatial structure of detached regions has been studied to see whether the density enhancements are "islands" or longitudinally extended "tails" which lead back to the plasmasphere. Theoretical models of a temporally changing electric field pattern, together with a simplified model of the plasma density distribution along magnetic field lines, have been used to simulate the dynamic conditions characteristic of a convection enhancement[74]. Such a model tends to produce "plasma tails"

wrapped about the earth[75]. However, the actual onset of enhanced convection may not proceed in the manner predicted by the models which use spatially continuous electric fields. In fact, the temporal fluctuation of electric fields in the vicinity of the auroral zone where spatial gradients of conductivity are present may lead directly to the detachment of plasma rather than the formation of plasma tails. Hence, the question of the spatial structure of these anomalous regions, as well as their effect upon energetic trapped particles, remains to be clarified.

Studies of the general structure of the plasmapause, as seen in the equatorial plane, give local time plots similar to that shown in Figure 20. The shape is thought to relate to the magnetospheric plasma convection. Whether or not this relates directly to ionospheric convection depends upon the extent to which electric fields map between the two regions. Recent study has revealed a number of inconsistencies with the theoretical models, especially with regard to the plasma flux required from the ionosphere[76].

Pronounced variations also occur in plasmapause location in response to changes in the size of the auroral oval[77]. Such changes, normally reported in terms of a magnetic activity index gathered from many high latitude magnetometers, can greatly alter the shape of the plasmasphere by removing plasma to latitudes as low as 40° magnetic[78-80]. The recovery during subsequent quiet conditions depends upon the rate at which the ionosphere can refill the plasma depleted flux tubes, a quantity which depends strongly upon a number of factors, including ionospheric density, plasma temperature and atomic hydrogen abundance[81,82].

4. HOT PLASMA COUPLINGS

4.1 The Ring Current

The magnetosphere is populated with substantial fluxes of trapped energetic protons and electrons which, if destabilized, can produce

substantial atmospheric ionization and excitation[82]. A major feature of this trapped particle population is the ring current, composed of medium energy (5 to 100 keV) protons and electrons which drift in the geomagnetic field following nearly circular paths (clockwise and counterclockwise, respectively, looking down on the north pole) around the earth. These particles are thought to originate in the midnight sector of the magnetosphere where they are impulsively injected, in association with magnetospheric substorms, from the plasma sheet[84].

The ring current is important for magnetosphere-ionosphere couplings in several ways[85]. First, the plasma pressure gradients associated with the advance of the midnight sector plasma sheet towards the earth creates a current system which involves the earth's ionosphere. Second, the total energy contained in the ring current particles is of the order of 10^{23} ergs, an amount sufficiently large to cause appreciable atmosphere ionization or heating if released in a short time[84].

The initial injection of ring current particles during a magnetic storm is not well understood owing to the chaotic character of the substorms which act as the driving mechanism and the large number of possible plasma instabilities which can act to scatter the particles in pitch angle[86]. During the initial phase of geomagnetic storms, the ring current is assymetric but as time passes it becomes symmetric about the earth and processes affecting the pitch angle distribution of the particles become important in determining the loss of particles to the atmosphere[83].

Of particular importance to the lifetime of trapped ring current protons is the presence or absence of thermal electrons. According to theory[72,84], such plasma, if present in sufficient density ($\sim$100 cm^{-3}),

can help establish ion-cyclotron turbulence which causes strong pitch angle scattering of the energetic ions and consequent precipitation into the atmosphere. In addition, through a Landau-resonant interaction, it is also thought that substantial energy is transferred to ambient electrons, heating them to high temperatures with consequent heat conduction to the ionosphere below[86].

Within the geophysical context, energetic plasma moving towards the earth in the midnight sector of the magnetosphere lies outside the plasmapause (see Figure 29). As the energetic protons and other positive ions reach the plasmapause, turbulence is established and just inside the plasmasphere ion cyclotron waves result in subsequent proton precipitation. At the same time, heat is conducted through the thermal electron gas to the ionosphere where the enhanced electron temperatures result in 6300A emission from atomic oxygen.[96] This last feature is thought to explain Stable Auroral Arcs (SAR-arcs), frequently seen during periods of geomagnetic disturbance[84].

Further information about the processes described above can be found in reviews and the literature. The theory has not been universally accepted. Recent measurements from Explorer 45, however, provide direct evidence for pitch angle scattering of protons located just inside the plasmasphere[87]. Further, simultaneous occurrences of hydrogen arcs and SAR-arcs have been seen by groundbased observations with the SAR-arc 6300A emission being present at the plasmapause and the hydrogen arc (proton precipitation) slightly poleward[88].

4.2 Energetic Ions

One of the most intriguing recent discoveries is that of intense fluxes of energetic O^+ and He^+ in the high latitude topside ionosphere

during magnetic storms[89-91]. The O^+ ions, discovered in 1972, appear to have an energy spectrum extending from 1 to 12 keV with integrated fluxes on the order of 10^7 ions cm^{-2} $sterad^{-1}$. He^+, on the other hand, seems to have a softer energy spectrum with a peak energy near 1 keV and a flux as great as 2×10^7 ions cm^{-2} sec^{-1} $sterad^{-1}$. Energy spectrums for one particular event are plotted in Figure 30.

Consideration of various sources for these energetic ions leads to the surprising conclusion that they are of ionospheric origin. The process by which they are energized remains uncertain although one theory[92] ascribes the acceleration to a resonance effect with ion cyclotron waves. In any case, their presence in the ionosphere points to the existence of a transient acceleration process giving particles energy far above that of the background plasma. Further, the role these particles play in the ring current remains to be determined, one idea being that they contribute substantially to the overall energy budget.

5. CONCLUSIONS

The problems inherent in magnetosphere, ionosphere and atmosphere interactions span a broad range of diverse physical mechanisms. Much of our present knowledge is based upon incomplete models more appropriate for laboratory plasmas than the environment of space. The problems of electrical coupling, for example, are far more complex than would be expected for quiescent plasmas and indicate the way that plasma waves can profoundly influence the usual electrical behavior. In addition, the need to obtain quantitative agreement between theory and observation has pushed the frontiers of knowledge with respect to the way hot and cold plasmas can be electrically coupled.

With regard to thermal plasma, there is now appreciation of the dynamical influence played by thermal particle fluxes linking the magnetosphere and ionosphere. Unfortunately, many of the current ideas are strongly influenced by simple theory without corroborative observational evidence. Thus, one is left without confirmation of the adequacy of the physical processes affecting the flows as well as a lack of information concerning their geophysical context.

The recent observations of energetic O^+ and He^+ emerging from the auroral ionosphere provide new evidence for non-thermal particle acceleration mechanisms. Clarification of the processes involved in such acceleration will undoubtedly lead to a better appreciation of plasma energization in a variety of astrophysical environments.

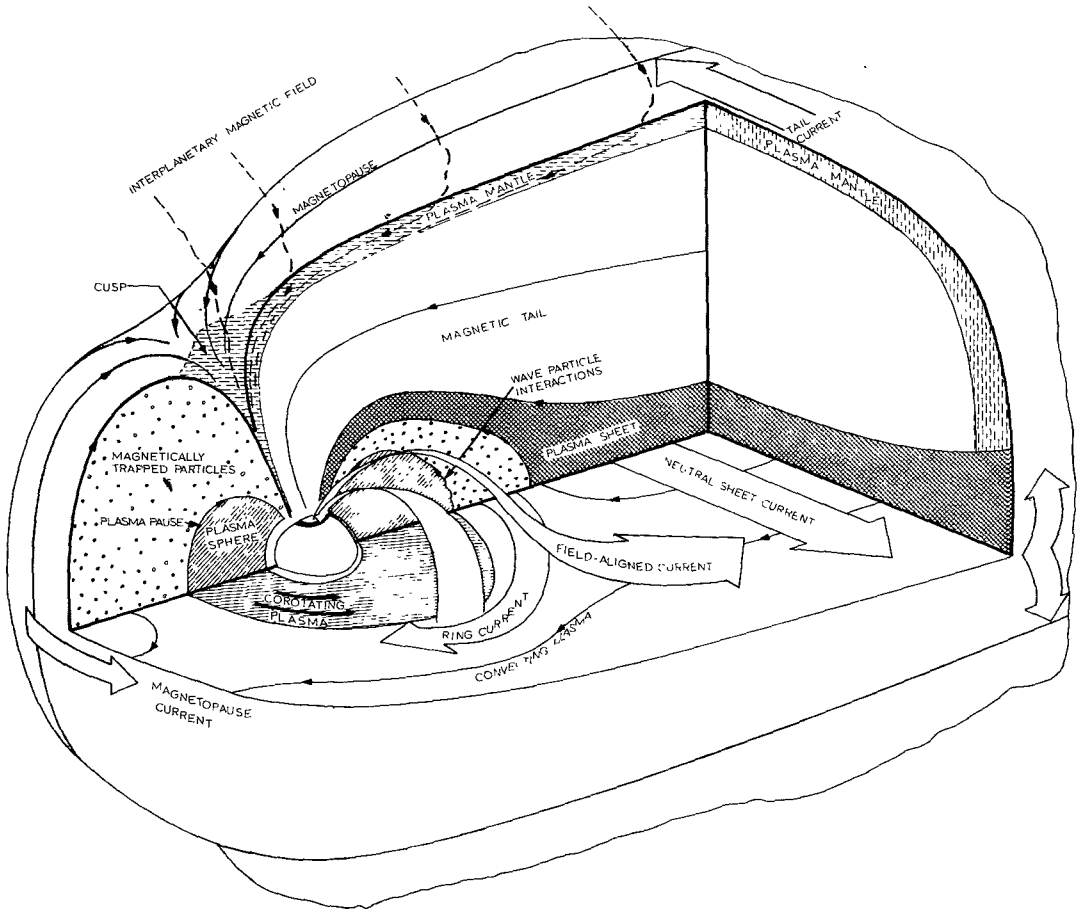

FIGURE 1 A schematic view of the magnetosphere showing the interior and exterior regions, thermal plasma, and currents of importance to atmosphere-ionosphere-magnetosphere coupling processes. From Heikkila.[1]

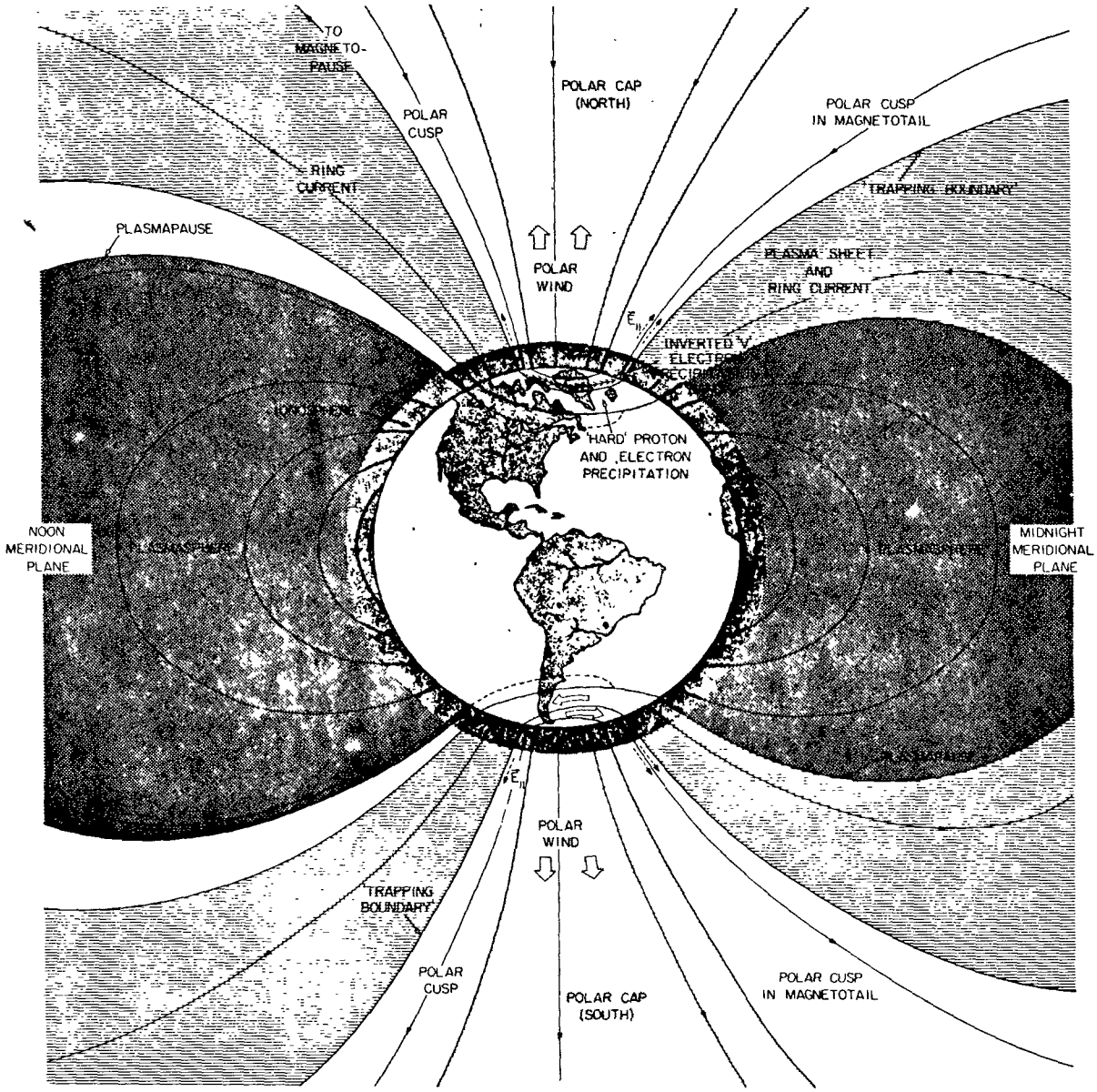

FIGURE 2 Meridional cross section of the magnetosphere in the vicinity of Earth, showing the major plasma regimes encountered at local noon and midnight. From Frank.[2]

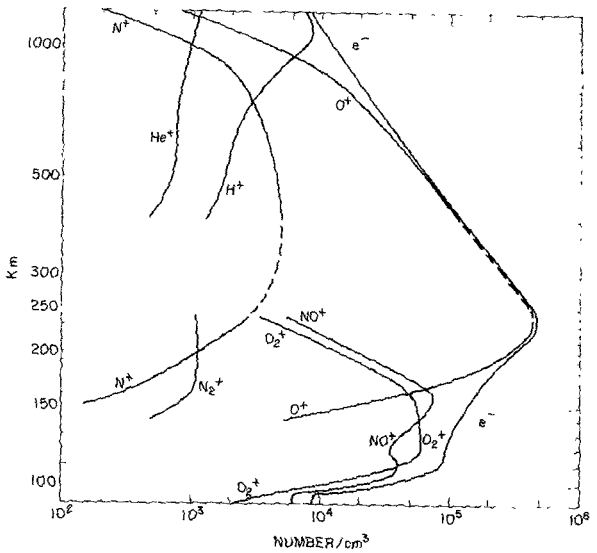

FIGURE 3 Ion composition of the ionosphere. The positive ions O^+, NO^+, O_2^+, N_2^+, He^+ result from photoionization in the upper atmosphere. H^+ and N^+ result from secondary ion reactions. Below 240 km, chemical processes determine the ionic structure. Above this altitude, diffusive processes act to reduce the overall plasma density with increasing altitude. From Banks and Kockarts.[3]

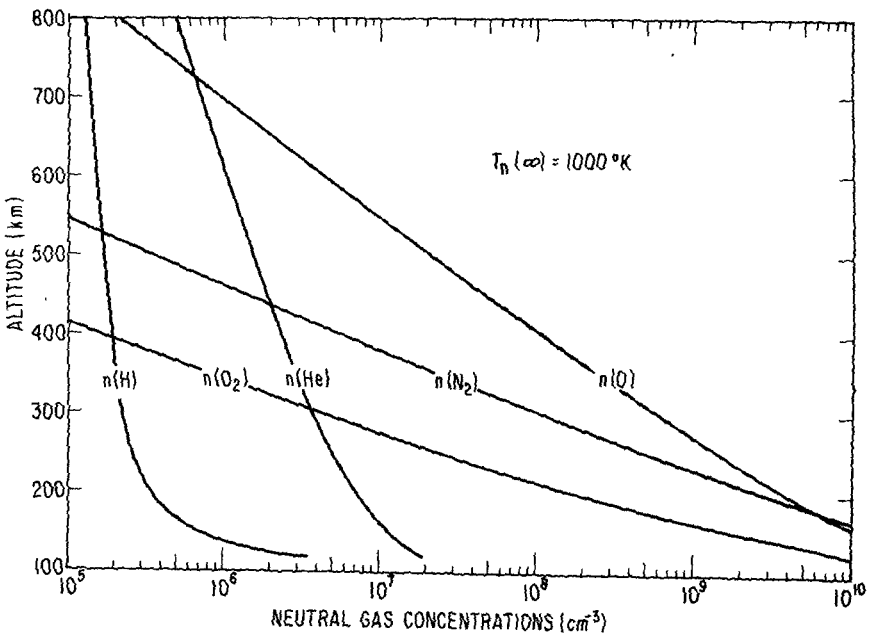

FIGURE 4 Neutral gas concentration profiles as a function of altitude in the upper atmosphere. Diffusive separation of the constituents above 120 km leads to an increasing fraction of light particles in the atmosphere. From Banks and Kockarts.[3]

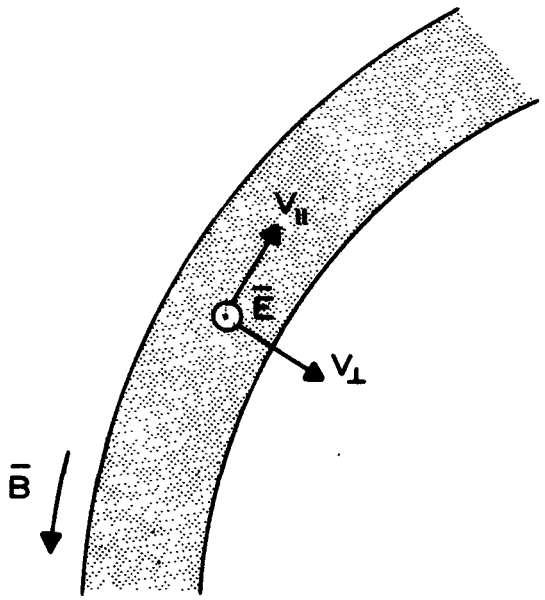

FIGURE 5 Ionospheric plasma motion can be separated into components of motion parallel and perpendicular to the magnetic field. Drifts of plasma perpendicular to the magnetic field result from applied electric fields, while parallel motions are a result of the effects of gravity, pressure gradients, and frictional drag between the plasma and the neutral gases in the atmosphere.

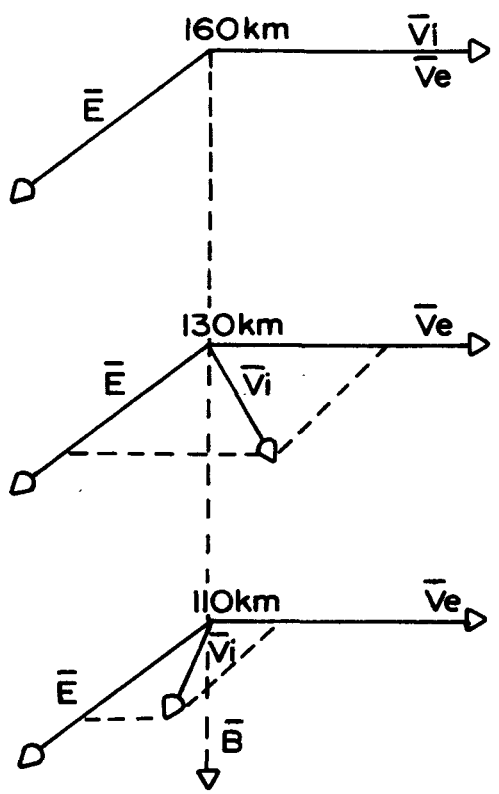

FIGURE 6 Ion and electron drift motions perpendicular to a magnetic field through the action of an applied electric field. At 160 km altitude, electrons and ions drift in the same direction. At 130 km, however, the ion motion is affected by the neutral gas and the magnitude of the ion drift velocity is reduced and rotated in the direction of the electric field, $\bar{E}$. The electron drift velocity remains unchanged. At 110 km, the ion drift velocity is greatly reduced and rotated almost parallel to the electric field.

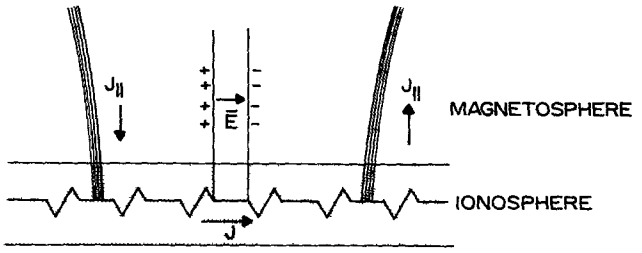

FIGURE 7 A schematic diagram of the way field aligned magnetospheric currents connect to the ionosphere producing electric fields as a consequence of electric potential drops through the distributed resistance of the ionosphere. Through polarization currents, the consequent gradients of potential map upwards to the magnetosphere above the ionospheric current path.

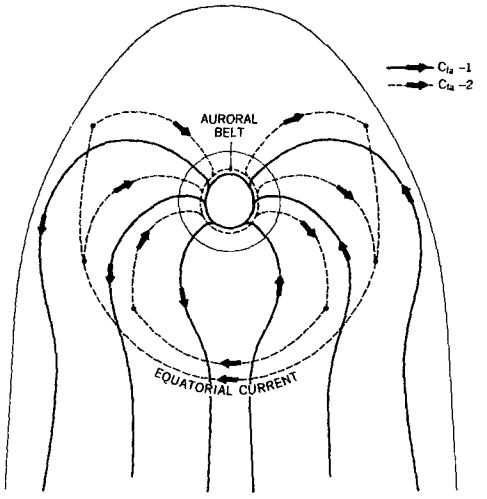

FIGURE 8 Showing the relationship between high latitude, field-aligned currents, thought to connect to the magnetopause and magnetospheric tail region, and the equatorial ring current. From Sugiura.

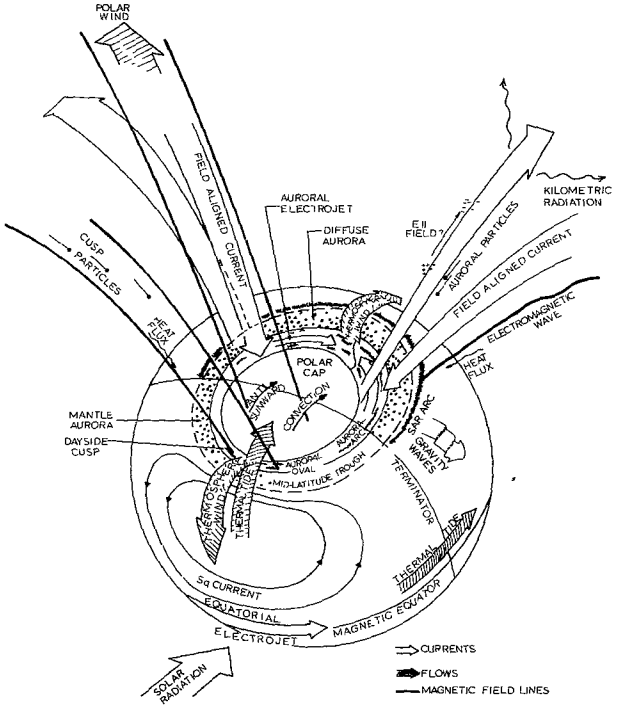

FIGURE 9 A schematic illustration of the relationship between field-aligned currents at high latitudes and the ionospheric currents connecting them through the northern auroral oval. From Heikkila.

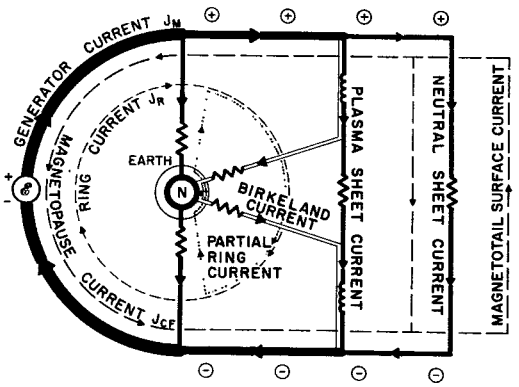

FIGURE 10 A schematic diagram of the geometrical and circuit aspects of important magnetospheric currents. The source current is driven by generator at the magnetopause and derives its power from the solar wind plasma as it flows around the dayside magnetosphere. Many auroral phenomena are associated with the different return paths for the current from the generator. From Heikkila.[20]

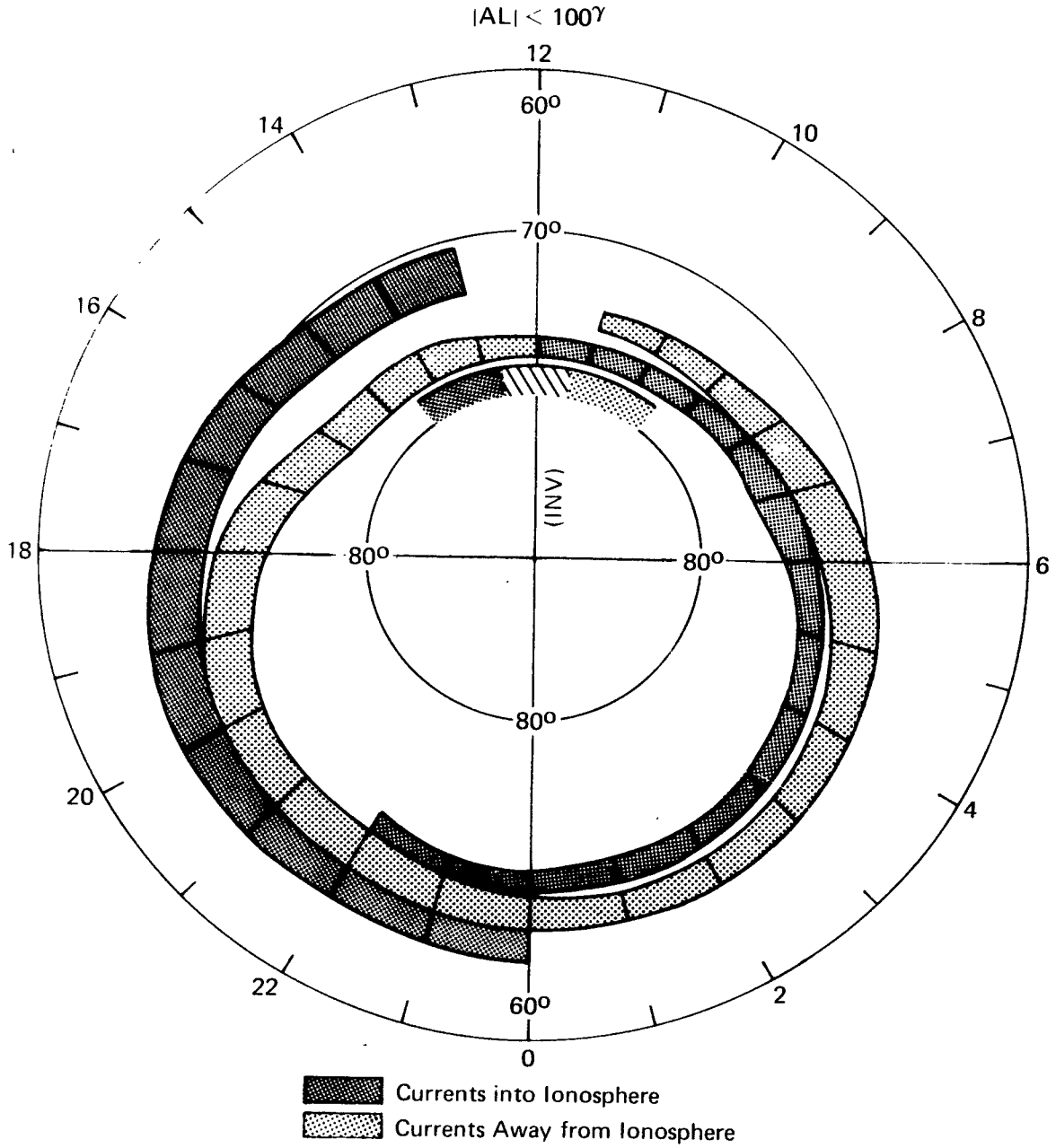

FIGURE 11 Summary of the distribution and flow directions of large scale field-aligned currents determined from the Triad spacecraft during weakly disturbed conditions. A region of confused currents exist near magnetic noon. From Iijima and Potemra.[27]

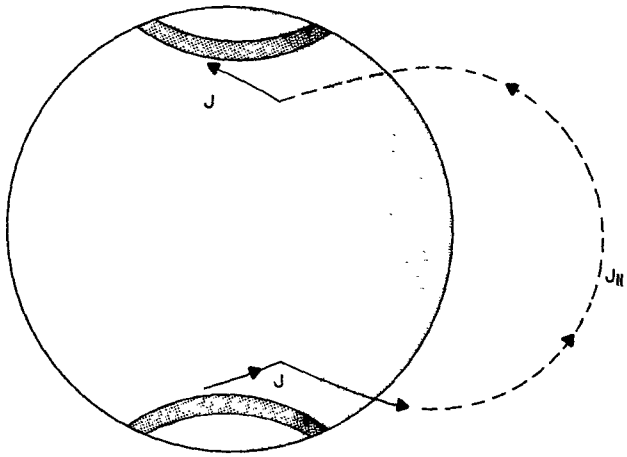

FIGURE 12 Showing the way in which horizontal ionospheric currents can take advantage of low resistance currents paths along magnetic field lines in the magnetosphere to electrically connect conjugate hemispheres.

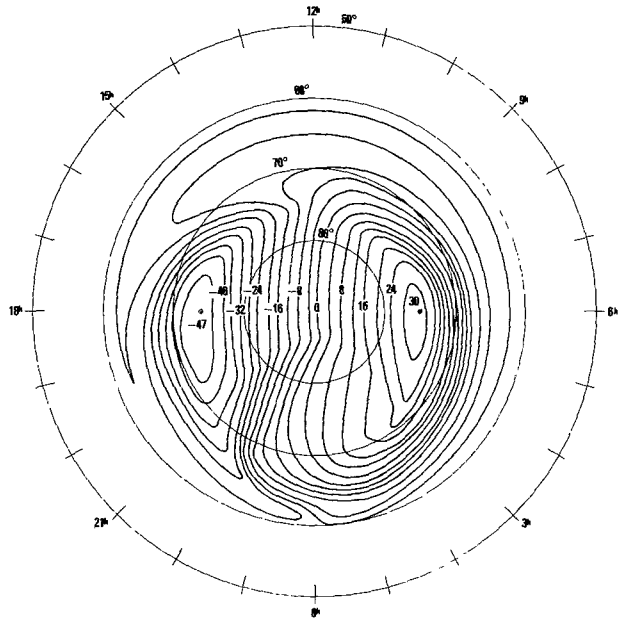

FIGURE 13 Northern hemisphere electric potential patterns designed to fit nightside electric field observations with the effect of co-rotation added. From Heppner.[24]

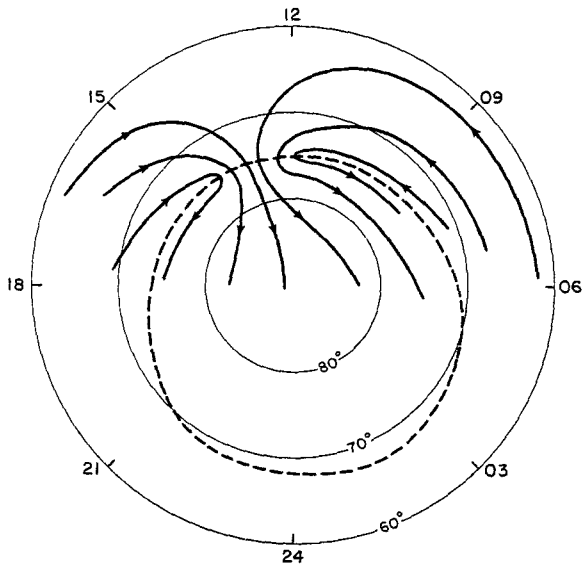

FIGURE 14 A north polar view of the dayside high latitude, plasma flow pattern deduced from Atmospheric Explorer ion velocity data. Co-rotation effects have been removed from the data. From Heelis, et al.[31]

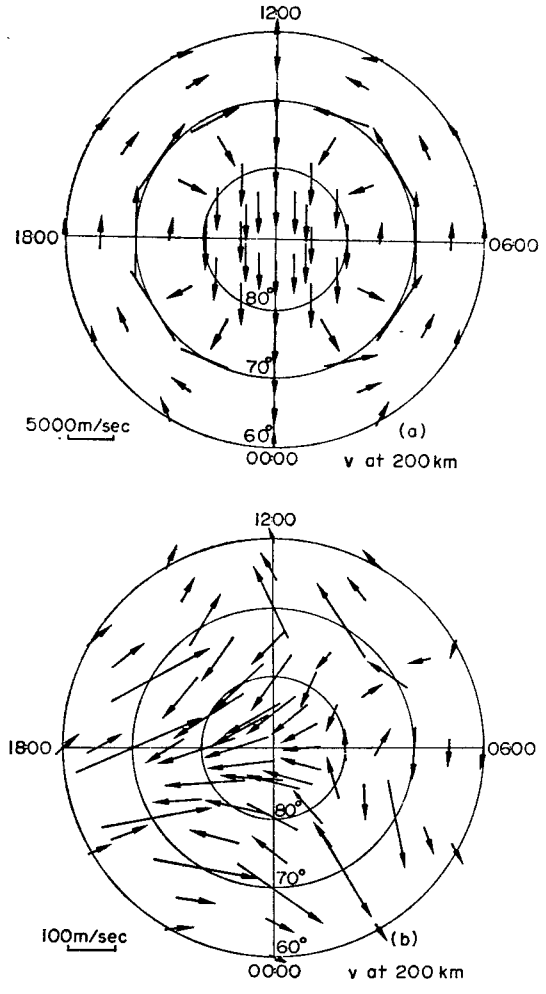

FIGURE 15 Distribution of ion drifts (upper diagram) and neutral winds (lower diagram) at 200 km altitude calculated using the equations of motion for the neutral atmosphere.[34]

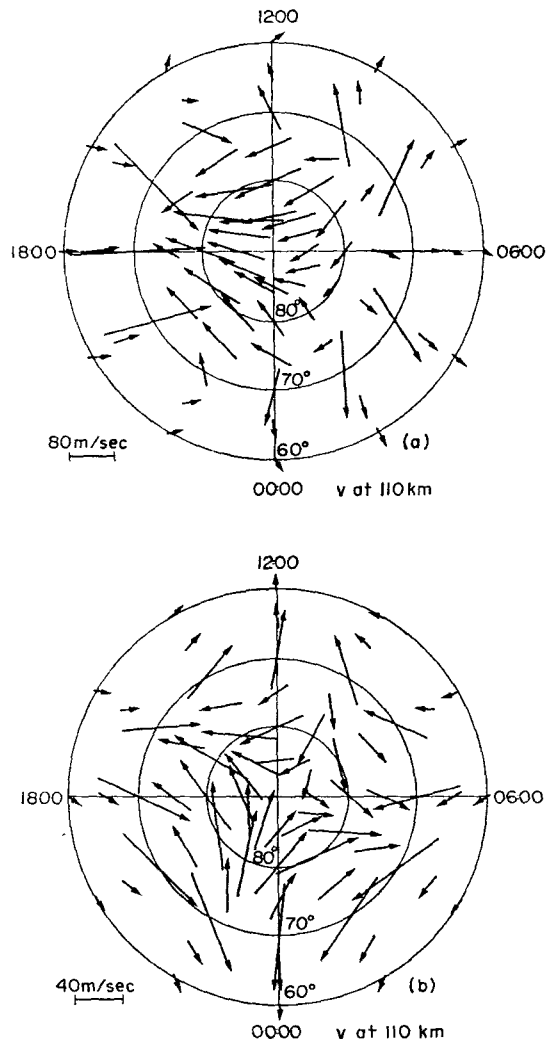

FIGURE 16 Distribution of ion drifts (upper diagram) and neutral winds (lower diagram) at 110 km altitude calculated using the equations of motion for the neutral atmosphere. The rotation of ion motions apparent upon comparing Figures 15 and 16 is a result of ion collisions with the neutral atmosphere.

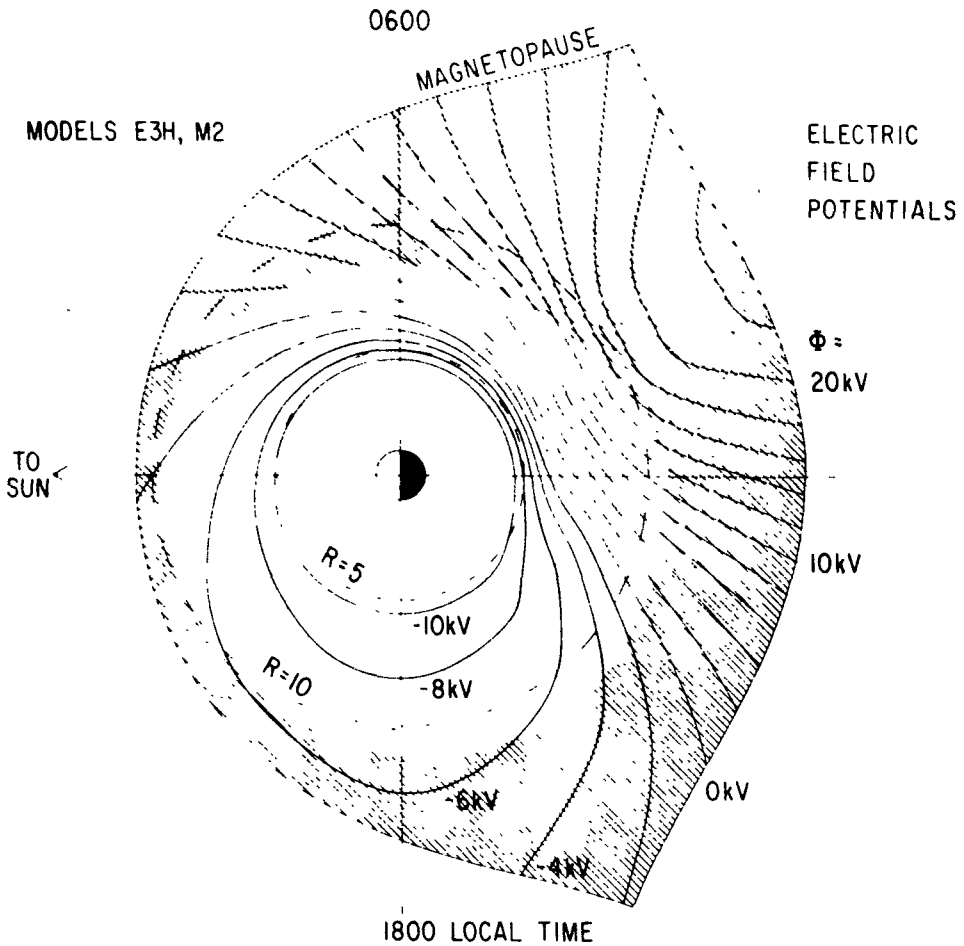

FIGURE 17 Contours of electric potential displayed in magnetospheric equatorial plane. These results are based upon energetic particle energy spectrums observed at geosynchronous orbit. From McIlwain.[44]

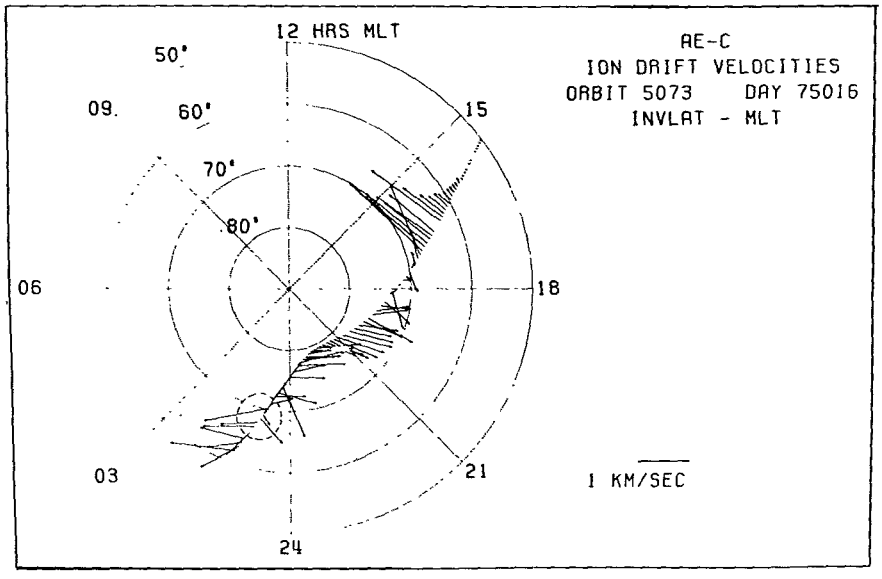

FIGURE 18 South polar ion drift velocities in the ionosphere as observed by Atmospheric Explorer-C. In agreement with theoretical models, in the afternoon sector large sunward drift of plasma is observed. Over the polar cap, however, the flow is not strictly anti-sunward, but shows a strong component towards the evening sector. The circled region indicates a shear flow reversal. From Burch, et al.[46]

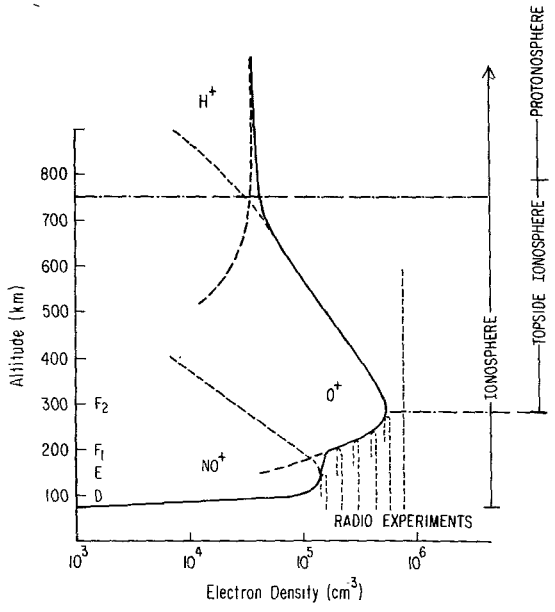

FIGURE 19 Schematic illustration of the ionosphere showing the various layers D, E, F_1, and F_2. From Banks, et al.[6]

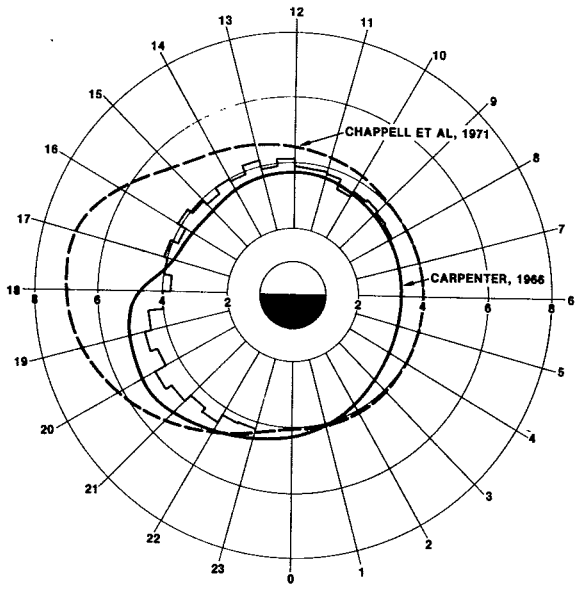

FIGURE 20 The average position of the plasmapause as a function of local time as determined from Whistler observations (Carpenter, 1966), the OGO-5 ion mass spectrometer data (Chappell, et al., 1971), and the Explorer 45 DC probe data.[61] The bulge region seen in the afternoon sector is believed to be caused by the general pattern of magnetospheric electric fields. From Maynard and Grebowsky.[61]

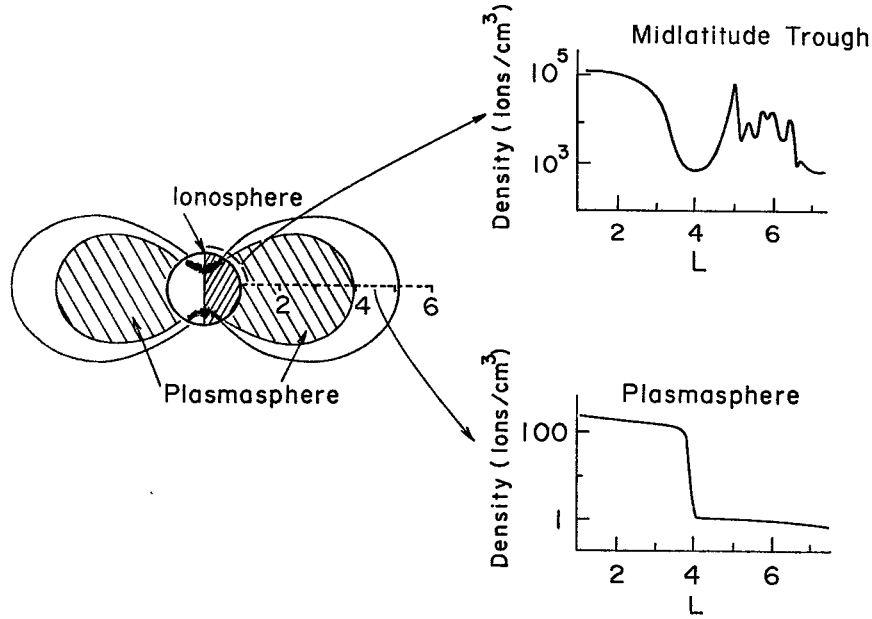

FIGURE 21 A meridional view of the plasmasphere showing both the radial density profile as a function of distance measured in earth radii (L) and the electron density profile over the same range.

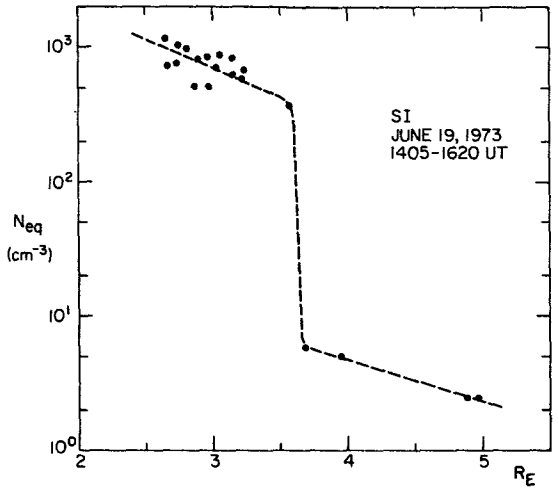

FIGURE 22 Equatorial electron density as a function of geocentric distance showing the plasmasphere and plasmapause as deduced from radial whistler observations. From Park and Seely.[63]

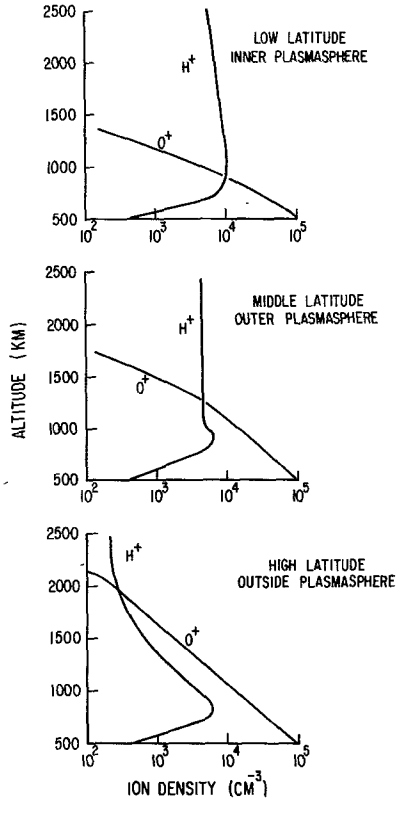

FIGURE 23 Illustration of the altitude profiles of cool plasma composition for motions parallel to the lines of magnetic force within the magnetosphere.

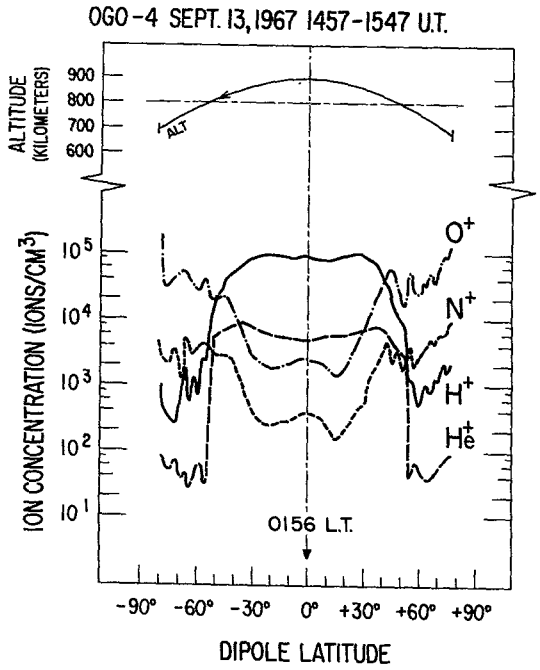

FIGURE 24 Latitudinal profiles of ion composition in the topside ionosphere obtained by satellite OGO-4. The plasmapause is seen in the abrupt decrease of hydrogen and helium ion concentrations near 55° dipole latitude. From Taylor and Walsh.[65]

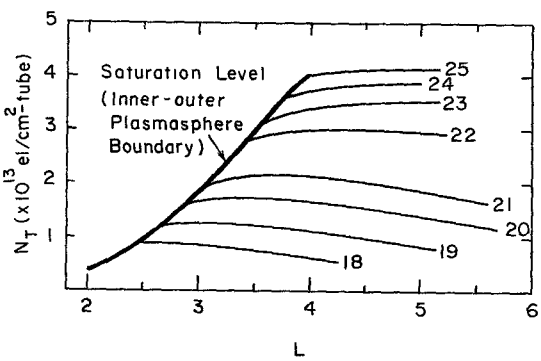

FIGURE 25 Experimental observations of the filling of magnetic flux tubes with thermal plasma from the ionosphere. The coordinate L is a measure of geocentric distance measured in earth radii. The filling of the flux tubes as a function of geocentric distance is measured in terms of day number. From Park.[66]

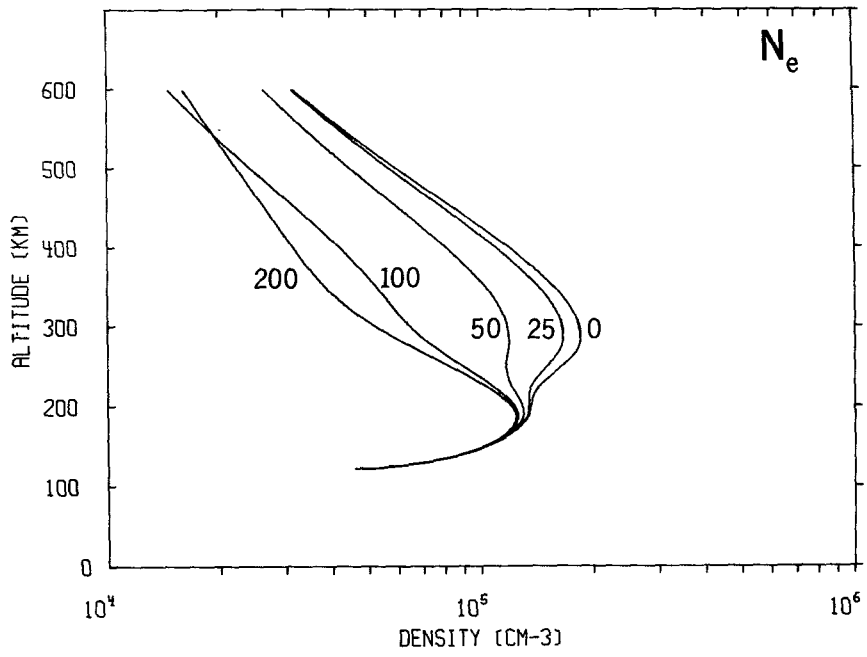

FIGURE 26 Profiles of electron density as a function of altitude for various values of perpendicular electric field, measured in millivolts per meter. From Schunk, et al.[69]

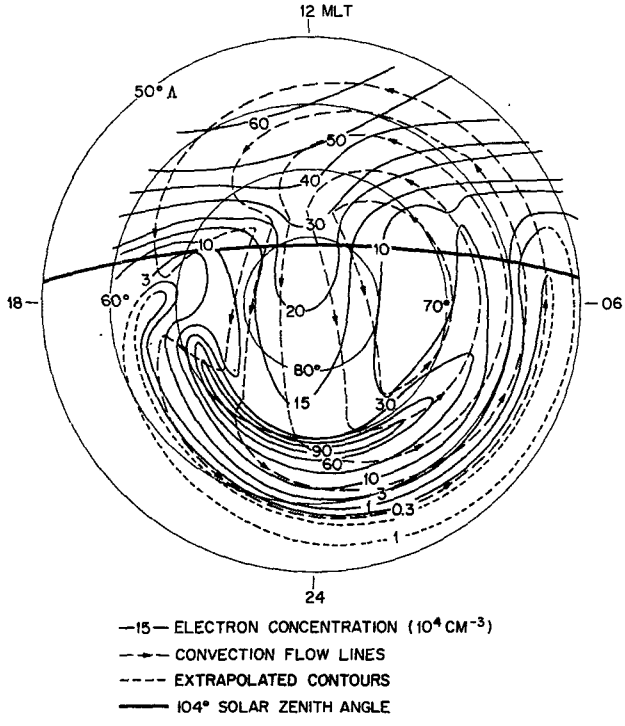

FIGURE 27 Contours of peak F_2 region electron density over the north polar cap under the influence of a general ionospheric convection electric field. Plasma convection brings a large tongue of ionization deep within the polar cap. In the vicinity of the auroral oval, deep ionization troughs are formed as a result of the slow plasma convection speed. From Knudsen, et al.[70]

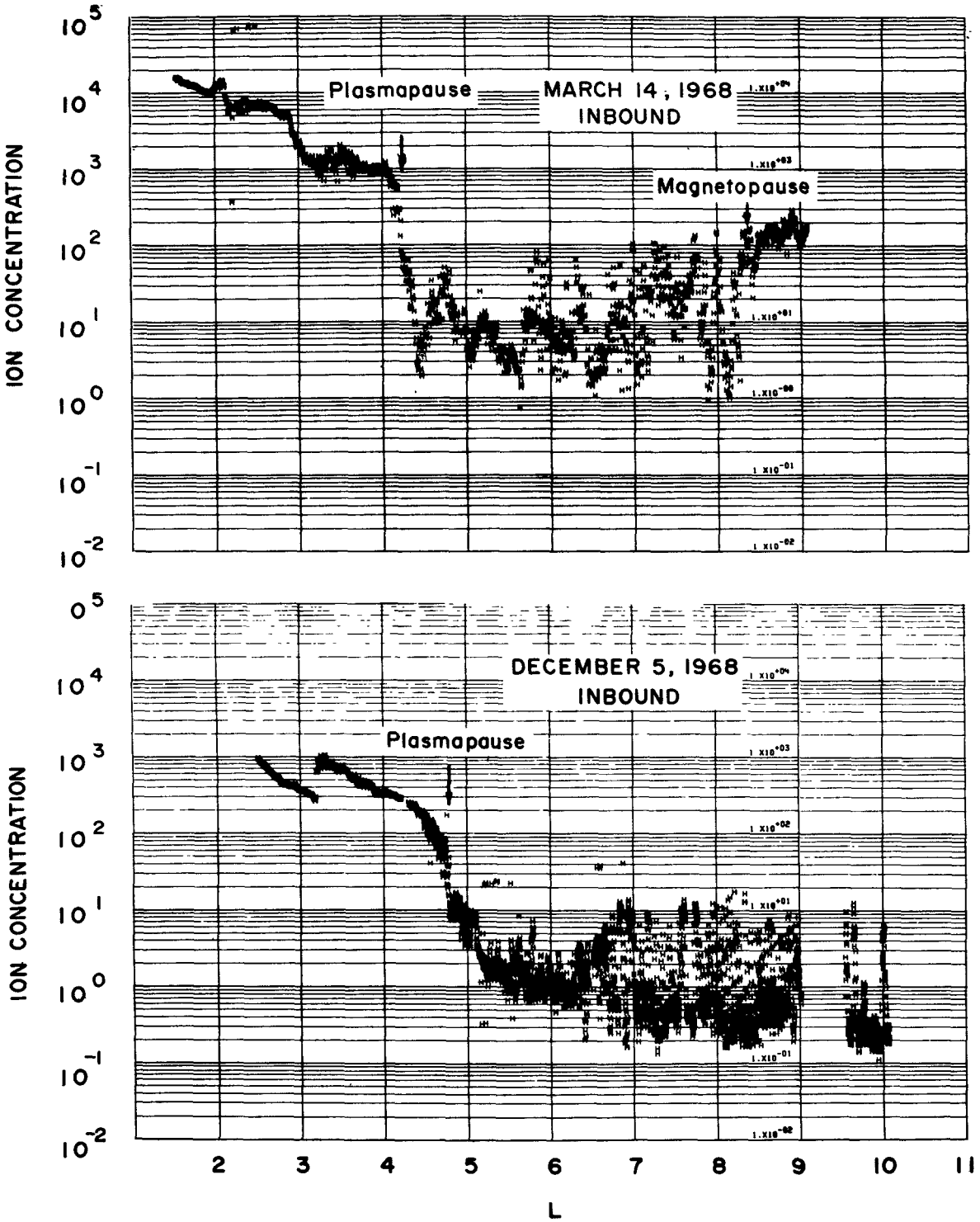

FIGURE 28 Ion concentration profiles obtained in the magnetosphere from the OGO-5 spacecraft showing H^+ ion density as a function of geocentric distance measured in earth radii. Regions of enhanced thermoplasma density are seen lying between the plasmapause near L approximately equal to 4 and the magnetopause L approximately equal to 8.5. These ion density enhancements indicate the presence of electrodynamic processes which remove plasma from the plasmasphere. From Chappell.[71]

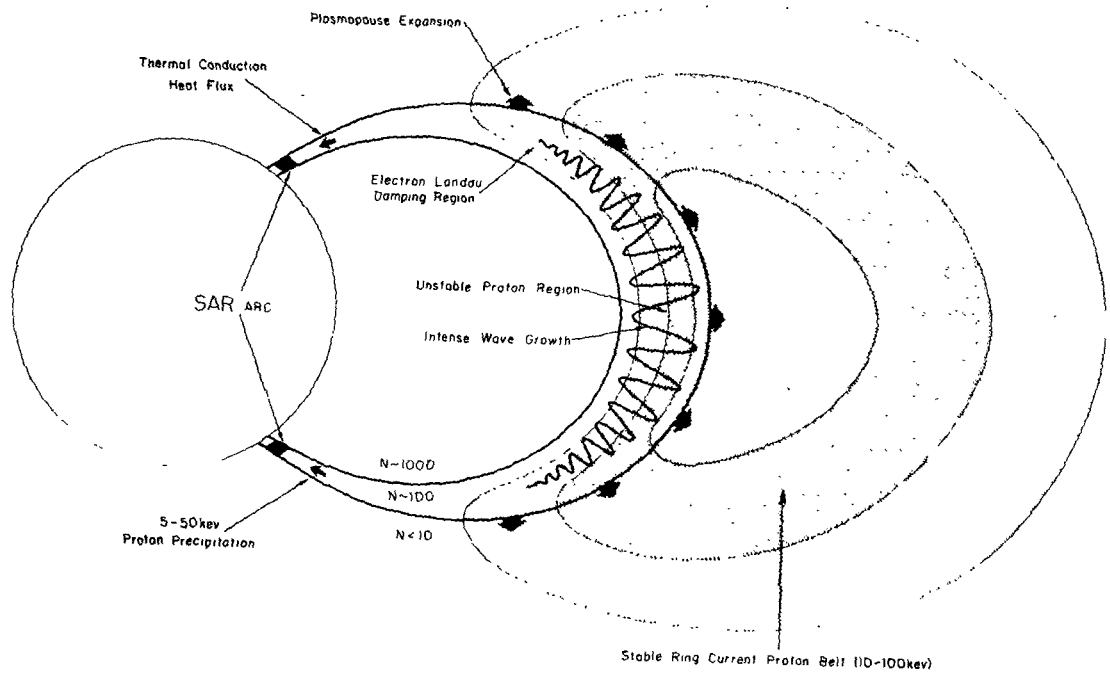

FIGURE 29 A schematic illustration of the interaction between ring current protons and the cool thermoplasma of the plasmasphere. From Cornwall.[84]

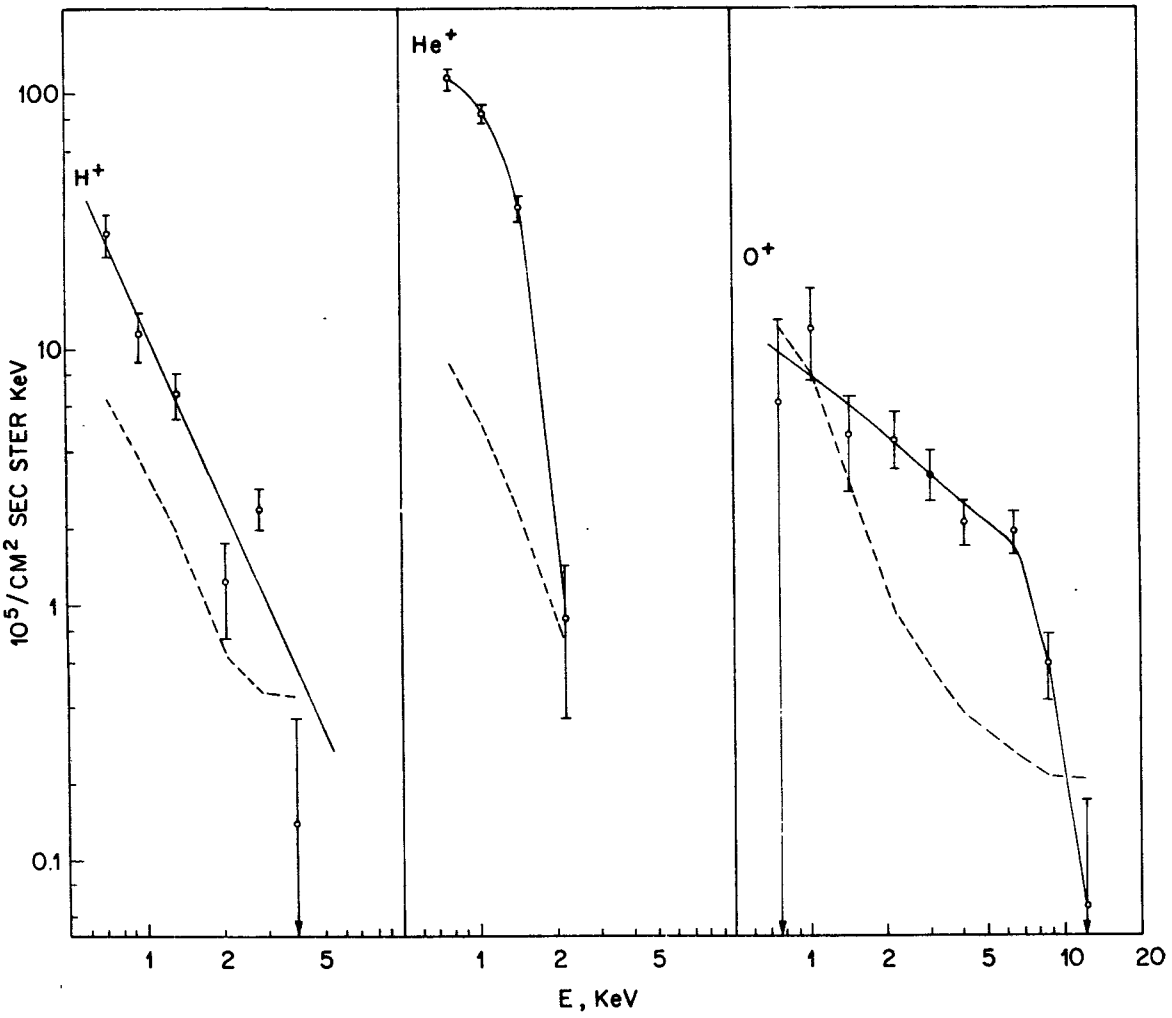

FIGURE 30 Energy spectrums of H^+, He^+, and O^+ obtained from spacecraft data. From Johnson, et al.[87]

ACKNOWLEDGEMENTS

This work has been supported, in part, through NASA Grant NSG-7289 at the Utah State University, Logan, Utah.

REFERENCES

1. Heikkila, W. J., Penetration of particles into the polar cap and auroral regions, in Critical Problems of Magnetospheric Physics, edited by E. R. Dyer, U. S. National Academy of Science, Washington, D. C. p. 67, 1972.

2. Frank, L. A., Magnetospheric and auroral plasmas: A short survey of progress, Rev. Geophys. and Space Physics, 13, 974, 1975.

3. Descriptions of ionospheric formation can be found, for example, in Banks, P. M. and G. Kockarts, Aeronomy, Academic Press, N.Y., Chapter 17, 1973; or Bauer, S. J., Physics of Planetary Atmospheres, Springer-Verlag, 1973.

4. Block, L. P. and C. G. Falthammer, Mechanisms that may support magnetic-field-aligned electric fields in the ionosphere, Ann. Geophys., 32, 1926, 1976.

5. H. Rishbeth and W. B. Hanson, A comment on plasma 'pile-up' in the F-region, J. Atmos. Terr. Phys, 36, 703, 1974.

6. Banks, P. M., R. W. Schunk, and W. J. Raitt, The Topside Ionosphere: A region of dynamic transition, in Annual Review of Earth and Planetary Sciences, 4, 381, 1976.

7. Gurevich, A. V., A. L. Krylor and E. Tsedilina, Electric fields in the earth's magnetosphere and ionosphere, Space Science Reviews, 19, 59, 1976.

8. For further details, see Rishbeth, H. and O. K. Garriott, Introduction to Ionospheric Physics, Academic Press, p. 126, 1969.

9. Cole, K. D., Energy deposition in the thermosphere caused by the solar wind, J. Atmos. Terr. Phys. 37, 939, 1975.

10. Anderson, H. R. and R. R. Vondrak, Observations of Birkeland currents at auroral latitudes, Reviews of Geophys. and Space Phys. 13, 243, 1975.

11. Richmond, A. D., S. Matsushita and J. D. Tarpley, On the production mechanism of electric currents and fields in the ionosphere, J. Geophys. Res. 81, 547, 1976.

12. Richmond, A. D., Electric field in the ionosphere and plasmasphere on quiet days, J. Geophys. Res. 81, 1447, 1976.

13. Walbridge, E., The limiting of magnetospheric convection by dissipation in the ionosphere, J. Geophys. Res. 5213, 1967.

14. Fedder, J. A. and P. M. Banks, Convection electric fields and polar thermospheric winds, J. Geophys. Res. 77, 2328, 1972.

15. Dickenson, R. E., E. C. Ridley and R. G. Roble, Meridional circulation in the thermosphere, I. Equinox conditions, J. Atmos. Sci. 32, 1737, 1975.

16. Banks, P. M., Observations of Joule and particle heating in the auroral zone, J. Atmos. Terr. Phys. 39, 1977.

17. Richmond, A. D. and S. Matsushita, Thermospheric response to a magnetic storm, J. Geophys. Res. 80, 2839, 1975.

18. Straus, J. M. and M. Schulz, Magnetospheric convection and upper atmospheric dynamics, J. Geophys Res. 81, 5822, 1976.

19. See Evans, J. V., Review of F-region dynamics, Rev. Geophys. Space Phys. 13, 887, 1975.

20. Heikkila, W. J., Outline of a magnetospheric theory, J. Geophys. Res. 79, 2496, 1974.

21. Vasyliunas, V. M., Mathematical models of magnetospheric convection and its coupling to the ionosphere, in Particles and Fields

in the Magnetosphere, ed. by B. M. McCormac, p. 60, D. Reidel, Dordrecht, Netherlands, 1970.

22. Jaggi, R. K., R. A. Wolf, Self-consistent calculation of the motion of a sheet of ions in the magnetosphere, J. Geophys. Res. 78, 2852, 1973.

23. Volland, H., Models of global electric fields within the magnetosphere, Ann. Geophys. 159, 1975.

24. Heppner, J. P., Empirical models of high latitude electric fields, Report X-625-76-219, Goddard Space Flight Center, Greenbelt, Md, September 1976.

25. Armstrong, J. C. and A. J. Zmuda, Three-axis magnetic measurements and field-aligned currents in the auroral region: Initial results, J. Geophys. Res. 78, 6802, 1973.

26. Zmuda, A. J., J. C. Armstrong, A Diurnal flow pattern of field aligned currents, J. Geophys. Res. 79, 4611, 1974.

27. Iijima, T. and T. A. Potemera, Field-aligned currents in the dayside cusp observed by Triad, J. Geophys. Res. 81, 5971, 1976.

28. Sugiura, M., Identifications of the polar cap boundary and the auroral belt in the high altitude magnetosphere: A model for field-aligned currents, J. Geophys. Res. 80, 2057, 1975.

29. Sugiura, M. and T. A. Potemera, Net field-aligned currents observed by Triad, J. Geophys. Res. 81, 2155, 1976.

30. Yasuhara, F., Y. Kamide, and S.-I. Akasofu, Field-aligned and ionospheric currents, Planet. Space Sci. 23, 1355, 1975.

31. Heelis, R. A., W. B. Hanson and J. L. Burch, Ion convection velocity reversals in the dayside cleft, J. Geophys. Res. 81, 3803, 1976.

32. Coroniti, F. V. and C. F. Kennel, Can the ionosphere regulate magnetospheric convection?, J. Geophys. Res. 78, 2837, 1973.

33. Arnoldy, R. L., Auroral particle precipitation and Birkeland currents, Rev. Geophys. Space Phys. 12, 217, 1974.

34. Maeda, H., Neutral winds and ion drifts in the polar ionosphere caused by convection electric fields-1, J. Atmos. Terr. Phys. 38, 197, 1976.

35. Volland, H., The atmospheric dynamo, J. Atmos. Terr. Phys. 38, 869, 1976.

36. Banks, P. M., Magnetospheric processes and the behavior of the neutral atmosphere, Space Res. 12, 1051, 1972.

37. Mozer, F. S., Anomalous resistivity and parallel electric fields, in Magnetospheric Particles and Fields, ed. by B. M. McCormac, D. Reidel, p. 125, 1976.

38. Wescott, E. M., H. C. Stenback-Nielsen, T. J. Halliman, T. N. Davis and H. M. Peck, The Skylab barium plasma injection experiments, 2, Evidence for a double layer, J. Geophys. Res. 81, 4495, 1976.

39. Kindel, J. M. and C. F. Kennel, Topside current instabilities, J. Geophys. Res. 76, 3055, 1971

40. Papadopoulos, K. and T. Coffey, Anomalous resistivity in the auroral plasma, J. Geophys. Res. 79, 1558, 1974.

41. Kivelson, M. G., Magnetospheric electric fields and their variation with geomagnetic activity, Rev. Geophys. Space Phys. 14, 189, 1976.

42. Banks, P. M., Ionosphere-magnetosphere coupling 2. Electric fields, Rev. Geophys. Space Phys. 13, 874, 1975.

43. Cauffman, D. P. and D. A. Gurnett, Satellite measurements of high latitude convection electric fields, Space Sci. Rev. 13, 369, 1972.

44. McIlwain, C. E., Substorm injection boundaries, in Magnetospheric Physics, edited by B. M. McCormac, D. Reidel, Dordrecht, Netherlands, 1974.

45. Banks, P. M. and J. R. Doupnik, A review of auroral zone electrodynamics deduced from incoherent scatter radar observations, J. Atmos. Terr. Phys. 37, 951, 1975.

46. Burch, J. L., W. Lennartsson, W. B. Hanson, R. A. Heelis, J. H. Hoffman and R. A. Hoffman, Properties of spikelike shear flow reversals observed in the auroral plasma by Atmosphere Explorer C, J. Geophys. Res. 81, 3886, 1976.

47. Burrows, J. R., M. D. Wilson and I. B. McDiarmid, Simultaneous field aligned current and charged particle measurements in the cleft, in Magnetospheric Particles and Fields, edited by B. M. McCormac, D. Reidel, Dordrecht, Netherlands, 1976.

48. Testud, J., P. Amayenc and M. Blanc, Middle and low latitude effects of auroral disturbances from incoherent scatter, J. Atmos. Terr. Phys. 37, 989, 1975.

49. Holzer, T. E. and G. C. Reid, The response of the dayside magnetosphere-ionosphere system to time-varying field-line reconnection at the magnetopause 1. Theoretical model, J. Geophys. Res. 80, 2041, 1975.

50. Sato, T., T. E. Holzer, Quiet auroral arcs and electrodynamic coupling between the ionosphere and the magnetosphere, 1, J. Geophys. Res., 78, 7314, 1973.

51. Holzer, T. E. and T. Sato, Quiet auroral arcs and electrodynamic coupling between the ionosphere and the magnetosphere, 2, J. Geophys. Res. 78, 7330, 1973.

52. Fejer, B. G., D. T. Farley, B. B. Balsley and R. F. Woodman, Radar studies of anomalous velocity reversals in the equatorial ionosphere, J. Geophys. Res. 81, 4621, 1976.

53. Onwumechili, A., K. Kawasaki and S.-I. Akasofu, Relationships between the auroral electrojet and polar magnetic variations Planet. Space Sci. 21, 1, 1973.

54. Coroniti, F. V. and C. F. Kennel, Polarization of the auroral electrojet, J. Geophys. Res. 77, 2835, 1972.

55. Swift, D. W., H. C. Stenback-Nielsen and T. J. Halliman, An equipotential model for auroral arcs, J. Geophys. Res. 81, 3931, 1976.

56. Block, L. P., Coupling between the outer magnetosphere and the high latitude ionosphere, Space Sci. Rev. 7, 198, 1967.

57. Gurnett, D. A. and L. A. Frank, Observed relationships between electric fields and auroral particle precipitation, J. Geophys. Res. 78, 145, 1973.

58. Frank, L. A. and D. A. Gurnett, Distributions of plasmas and electric fields over the auroral zones and polar caps, J. Geophys. Res. 76, 6829, 1971.

59. Burch, J. L., S. A. Fields, W. B. Hanson, R. A. Heelis, R. A. Hoffman and R. W. Janetzke, Characteristics of auroral electron acceleration regions observed Atmosphere Explorer C, J. Geophys. Res. 81, 2223, 1976.

60. Hays, P. B., R. A. Jones and M. H. Rees, Auroral heating and the composition of the neutral atmosphere, Planet. Space Sci. 21, 559, 1973.

61. Maynard, N. C. and J. M. Grebowsky, The plasmapause revisited, NASA Technical Report X-625-76-220, Goddard Space Flight Center, Greenbelt, Md., September 1976.

62. Carpenter, D. L. and C. G. Park, On what ionospheric workers should know about the plasmapause-plasmasphere, Rev. Geophys. Space Phys. 11, 133, 1973.

63. Park, C. G. and Seely, Whistler observations of the dynamical behavior of the plasmapause during June 17-22, 1973, Geophys. Res. Ltrs. 3, 301, 1976.

64. Banks, P. M., A. F. Nagy and W. I. Axford, Dynamical behavior of thermal protons in the mid-latitude ionosphere and magnetosphere, Planet. Space Sci. 19, 1053, 1971.

65. Taylor, H. A., Jr. and W. J. Walsh, The light ion trough, the main trough, and the plasmapause, J. Geophys. Res. 77, 6716, 1972.

66. Park, C. G., Whistler observations of the interchange of ionization between the ionosphere and the protonosphere, J. Geophys. Res. 75, 4249, 1970.

67. Banks, P. M. and T. E. Holzer, The polar wind, J. Geophys. Res. 73, 6846, 1968.

68. Lemaire, J. and M. Scherer, Kinetic models of the solar and polar winds, Rev. Geophys. Space Phys., 11, 427, 1973.

69. Schunk, R. W., W. J. Raitt and P. M. Banks, Effect of electric fields on the daytime high latitude E and F regions, J. Geophys. Res. 80, 3121, 1975.

70. Knudsen, W. C., P. M. Banks, J. D. Winningham and D. M. Klumpar, Numerical model of the convecting F_2 ionosphere at high altitudes, J. Geophys. Res. 82, 1977.

71. Chappell, C. R., Detached plasma regions in the magnetosphere, J. Geophys. Res. 79, 1861, 1974.

72. Brice, N. M., Artificial enhancement of energetic particle precipitation through cold plasma injection; A technique for seeding substorms[2], J. Geophys. Res. 75, 4890, 1970.

73. Cornwall, J. M., F. V. Coroniti, and R. M. Throne, Unified theory of SAR arc formation at the plasmapause, J. Geophys. Res. 76, 4428, 1971.

74. Chen, A. J., and R. A. Wolf, Effects on the plasmasphere of a time-varying convection electric field, Planet. Space Sci. 20, 483, 1972.

75. Taylor, H. A., J. M. Grebowsky and W. J. Walsh, Structured variations of the plasmapause: Evidence of a corotating plasma tail, J. Geophys. Res. 76, 6806, 1971.

76. Chen, A. J., J. M. Grebowsky and K. Manebashi, Diurnal variation of thermal plasma in the plasmasphere, Planet. Space Sci. 24, 765, 1976.

77. Chappell, C. R., Recent satellite measurements of the morphology and dynamics of the plasmasphere, Rev. Geophys. Space Phys. 10, 951, 1972.

78. L. H. Brace and R. F. Theis, The behavior of the plasmapause at mid-latitudes: ISIS 1 Langmuir probe measurements, 79, 1871, 1974.

79. Chappell, C. R., K. K. Harris, and G. W. Sharp, A study of the influence of magnetic activity on the location of the plasmapause as measured by Ogo 5, J. Geophys. Res. 75, 50, 1970.

80. Carpenter, D. L., Whistler studies of the plasmapause in the magnetosphere; Temporal variations in the position of the knee and some evidence of plasma motions near the knee, J. Geophys. Res. 71, 693, 1966.

81. Maribashi, K. and J. M. Grebowsky, A model study of diurnal behavior of the ionosphere and the protonosphere coupling, J. Geophys. Res. 81, 1700, 1976.

82. Murphey, J. A., G. J. Bailey and R. J. Moffett, Calculated daily variations of O^+ and H^+ at mid-latitudes-I. Protonospheric replenishment and F-region behavior at sunspot minimum, J. Atmos. Terr. Phys. 38, 351, 1976.

83. Thorne, R. M. and C. F. Kennel, Relativistic electron precipitation during magnetic storm main phase, J. Geophys. Res. 76, 4446, 1971.

84. Cornwall, J. M., F. V. Coroniti and R. M. Thorne, Turbulent loss of ring current protons, J. Geophys. Res. 75, 4699, 1970.

85. Kennel, C. F., Consequences of a magnetospheric plasma, Rev. Geophys. Space Phys. 7, 379, 1969.

86. Thorne, R. M., The importance of wave-particle interactions in the magnetosphere, in Critical Problems of Magnetospheric Physics, edited by E. R. Dyer, U. S. National Academy of Sciences, Washington, D. C., 1972.

87. Williams, D. L. and L. R. Lyons, The proton ring current and its interaction with the plasmapause; storm recovery phase, J. Geophys. Res. 79, 4195, 1974.

88. Kleckner, F. W. and R. J. Hoch, Simultaneous occurrences of hydrogen arcs and mid-latitude auroral red arcs, J. Geophys. Res. 78, 1187, 1973.

89. Johnson, R. G., R. D. Sharp and E. C. Shelley, The discovery of energetic He^+ ions in the magnetosphere, J. Geophys. Res. 79, 3135, 1974.

90. Sharp, R. D., R. G. Johnson, E. G. Shelley, and K. K. Harris, Energetic O^+ in the magnetosphere, J. Geophys. Res. 79, 1844, 1974.

91. Sharp, R. D., R. G. Johnson and E. G. Shelley, The morphology of energetic O^+ ions during two magnetic storms: Latitudinal variations, J. Geophys. Res. 81, 3292, 1976.

92. Cladis, J. B., Effect of magnetic field gradient on motion of ions resonating with ion cyclotron waves, J. Geophys. Res. 78, 8129, 1973.

93. Stern, D. P., Large scale electric fields in the earth's magnetosphere, Rev. Geophys. Space Phys., 15, 1977.

94. Mozer, F. S. and P. Lucht, The average auroral zone electric field, J. Geophys. Res., 79, 1001, 1974.

95. Mozer, F. S., C. W. Carlson, M. K. Hudson, R. B. Torbet, B. Parady, and J. Yatteau, Observations of paired electrostatic shocks in the polar magnetosphere, Phys. Rev. Ltrs., 1977.

96. Cole, K. D., Stable auroral red arcs, sinks for energy of D_{st} main phase, J. Geophys. Res., 70, 1689, 1965.

AUTHOR LIST

(10) Anderson, H. R. and R. R. Vondrak, Observations of Birkeland currents at auroral latitudes, Reviews of Geophys. and Space Phys., 13, 243, 1975.

(25) Armstrong, J. C. and A. J. Zmuda, Three-axis magnetic measurements and field-aligned currents in the auroral region: Initial results, J. Geophys. Res., 78, 6802, 1973.

(33) Arnoldy, R. L., Auroral particle precipitation and Birkeland currents, Rev. Geophys. Space Phys., 78, 6802, 1973.

(42) Banks, P. M., Ionosphere-magnetosphere coupling 2. Electric fields, Rev. Geophys. Space Phys., 13, 874, 1975.

(36) Banks, P. M., Magnetospheric processes and the behavior of the neutral atmosphere, Space Res., 12, 1051, 1972.

(16) Banks, P. M., Observations of Joule and particle heating in the auroral zone, J. Atmos. Terr. Phys., 39, 1977.

(45) Banks, P. M. and J. R. Doupnik, A review of auroral zone electrodynamics deduced from incoherent scatter radar observations, J. Atmos. Terr. Phys., 37, 951, 1975.

(67) Banks, P. M. and T. E. Holzer, The polar wind, J. Geophys. Res., 73, 6846, 1968.

(3) Banks, P. M. and G. Kockarts, Aeronomy, Academic Press, N.Y., Chapter 17, 1973.

(64) Banks, P. M., A. F. Nagy and W. I. Axford, Dynamical behavior of thermal protons in the mid-latitude ionosphere and magnetosphere, Planet. Space Sci., 19, 1053, 1971.

(6) Banks, P. M., R. W. Schunk and W. J. Raitt, The topside Ionosphere: A region of dynamic transition, in Annual Review of Earth and Planetary Sciences, 4, 381, 1976.

(3) Bauer, S. J., Physics of Planetary Atmospheres, Springer-Verlag, 1973.

(56) Block, L. P., Coupling between the outer magnetosphere and the high latitude ionosphere, Space Sci. Rev., 7, 198, 1967.

(4) Block, L. P. and C. G. Fälthammer, Mechanisms that may support magnetic-field-aligned electric fields in the ionosphere, Ann. Geophys., 32, 1926, 1976.

(78) Brace, L. H. and R. F. Theis, The behavior of the plasmapause at mid-latitudes: ISIS 1 Langmuir probe measurements, 79, 1871, 1974.

(72) Brice, N. M., Artificial enhancement of energetic particle precipitation through cold plasma injection; A technique for seeding substorms[2], J. Geophys. Res., 75, 4890, 1970.

(59) Burch, J. L., S. A. Fields, W. B. Hanson, R. A. Heelis, R. A. Hoffman and R. W. Janetzke, Characteristics of auroral electron acceleration regions observed Atmosphere Explorer C, J. Geophys. Res., 81, 2223, 1976.

(46) Burch, J. L., W. Lennartsson, W. B. Hanson, R. A. Heelis, J. H. Hoffman and R. A. Hoffman, Properties of spikelike shear flow reversals observed in the auroral plasma by Atmosphere Explorer C, J. Geophys. Res., 81, 3886, 1976.

(47) Burrows, J. R., M. D. Wilson and I. B. McDiarmid, Simultaneous field aligned current and charged particle measurements in the cleft, in Magnetospheric Particles and Fields, edited by B. M. McCormac, D. Reidel, Dordrecht, Netherlands, 1976.

(80) Carpenter, D. L., Whistler studies of the plasmapause in the magnetosphere; Temporal variations in the position of the knee and some evidence of plasma motions near the knee, J. Geophys. Res., 71, 693, 1966.

(62) Carpenter, D. L., and C. G. Park, On what ionospheric workers should know about the plasmapause-plasmasphere, Rev. Geophys. Space Phys., 11, 133, 1973.

(43) Cauffman, D. P. and D. A. Gurnett, Satellite measurements of high latitude convection electric fields, Space Sci. Rev., 13, 369, 1972.

(71) Chappell, C. R., Detached plasma regions in the magnetosphere, J. Geophys. Res., 79, 1861, 1974.

(77) Chappell, C. R., Recent satellite measurements of the morphology and dynamics of the plasmasphere, Rev. Geophys. Space Phys., 10, 951, 1972.

(79) Chappell, C. R., K. K. Harris, and G. W. Sharp, A study of the influence of magnetic activity on the location of the plasmapause as measured by Ogo 5, J. Geophys. Res., 75, 50, 1970.

(76) Chen, A. J., J. M. Grebowsky and K. Manebashi, Diurnal variation of thermal plasma in the plasmasphere, Planet. Space Sci., 24, 765, 1976.

(74) Chen, A. J., and R. A. Wolf, Effects on the plasmasphere of a time-varying convection electric field, Planet. Space Sci., 20, 483, 1972.

(92) Cladis, J. B., Effect of magnetic field gradient on motion of ions resonating with ion cyclotron waves, J. Geophys. Res., 78, 8129, 1973.

(9) Cole, K. D., Energy deposition in the thermosphere caused by the solar wind, J. Atmos. Terr. Phys., 37, 939, 1975.

(96) Cole, K. D., Stable auroral red arcs, sinks for energy of D_{st} main phase, J. Geophys. Res., 70, 1689, 1965.

(84) Cornwall, J. M., F. V. Coroniti and R. M. Thorne, Turbulent loss of ring current protons, J. Geophys. Res., 75, 4699, 1970.

(73) Cornwall, J. M., F. V. Coroniti, and R. M. Thorne, Unified theory of CAR arc formation at the plasmapause, J. Geophys. Res., 76, 4428, 1971.

(32) Coroniti, F. V. and C. F. Kennel, Can the ionosphere regulate magnetospheric convection?, J. Geophys. Res., 78, 2837, 1973.

(54) Coroniti, F. V. and C. F. Kennel, Polarization of the auroral electrojet, J. Geophys. Res., 77, 2835, 1972.

(15) Dickenson, R. E., E. C. Ridley and R. G. Roble, Meridional circulation in the thermosphere, I. Equinox conditions, J. Atmos. Sci., 32, 1737, 1975.

(19) Evans, J. V., Review of F-region dynamics, Rev. Geophys. Space Phys., 13, 887, 1975.

(14) Fedder, J. A., and P. M. Banks, Convection electric fields and polar thermospheric winds, J. Geophys. Res., 77, 2328, 1972.

(52) Fejer, B. G., D. T. Farley, B. B. Balsley and R. F. Woodman, Radar studies of anomalous velocity reversals in the equatorial ionosphere, J. Geophys. Res., 81, 4621, 1976.

(2) Frank, L. A., Magnetospheric and auroral plasmas: A short survey of progress, Rev. Geophys. and Space Physics, 13, 974, 1975.

(58) Frank, L. A., and D. A. Gurnett, Distributions of plasmas and electric fields over the auroral zones and polar caps, J. Geophys. Res., 76, 6829, 1971.

(7) Gurevich, A. V., A. L. Krylor and E. Tsedilina, Electric fields in the earth's magnetosphere and ionosphere, Space Science Reviews, 19, 59, 1976.

(57) Gurnett, D. A. and L. A. Frank, Observed relationships between electric fields and auroral particle precipitation, J. Geophys. Res., 78, 145, 1973.

(60) Hays, P. B., R. A. Jones and M. H. Rees, Auroral heating and the composition of the neutral atmosphere, Planet. Space Sci., 21, 559, 1973.

(31) Heelis, R. A., W. B. Hanson and J. L. Burch, Ion convection velocity reversals in the dayside cleft, J. Geophys. Res., 81, 3803, 1976.

(20) Heikkila, W. J., Outline of a magnetospheric theory, J. Geophys. Res., 79, 2496, 1974.

(1) Heikkila, W. J., Penetration of particles into the polar cap and auroral regions, in Critical Problems of Magnetospheric Physics, edited by E. R. Dyer, U. S. National Academy of Science, Washington, D.C., p. 67, 1972.

(24) Heppner, J. P., Empirical models of high latitude electric fields, Report X-625-76-219, Goddard Space Flight Center, Greenbelt, Maryland, September, 1976.

(49) Holzer, T. E. and G. C. Reid, The response of the dayside magnetosphere-ionosphere system to time-varying field-line reconnection at the magnetopause 1. Theoretical model, J. Geophys. Res., 80, 2041, 1975.

(51) Holzer, T. E., and T. Sato, Quiet auroral arcs and electrodynamic coupling between the ionosphere and the magnetosphere, 2, J. Geophys. Res., 78, 7330, 1973.

(27) Iijima, T. and T. A. Potemera, Field-aligned currents in the dayside cusp observed by Triad, J. Geophys. Res., 81, 5971, 1976.

(22) Jaggi, R. K., R. A. Wolf, Self-consistent calculation of the motion of a sheet of ions in the magnetosphere, J. Geophys. Res., 78, 2852, 1973.

(89) Johnson, R. G., R. D. Sharp and E. C. Shelley, The discovery of energetic He^+ ions in the magnetosphere, J. Geophys. Res., 79, 3135, 1974.

(85) Kennel, C. F., Consequences of a magnetospheric plasma, Rev. Geophys. Space Phys., 7, 379, 1969.

(39) Kindel, J. M. and C. F. Kennel, Topside current instabilities, J. Geophys. Res., 76, 3055, 1971.

(41) Kivelson, M. G., Magnetospheric electric fields and their variation with geomagnetic activity, Rev. Geophys. Space Phys., 14, 189, 1976.

(88) Kleckner, F. W. and R. J. Hoch, Simultaneous occurrences of hydrogen arcs and mid-latitude auroral red arcs, J. Geophys. Res., 78, 1187, 1973.

(70) Knudsen, W. C., P. M. Banks, J. D. Winningham and D. M. Klumpar, Numerical model of the convecting F_2 ionosphere at high altitudes, J. Geophys. Res., 82, 1977.

(68) Lemaire, J. and M. Scherer, Kinetic models of the solar and polar winds, Rev. Geophys. Space Phys., 11, 427, 1973.

(34) Maeda, H., Neutral winds and ion drifts in the polar ionosphere caused by convection electric fields-1, J. Atmos. Terr. Phys., 38, 197, 1976.

(81) Maribashi, K. and J. M. Grebowsky, A model study of diurnal behavior of the ionosphere and the protonosphere coupling, J. Geophys. Res., 81, 1700, 1976.

(61) Maynard, N. C. and J. M. Grebowsky, The plasmapause revisited, NASA Technical Report X-625-76-220, Goddard Space Flight Center, Greenbelt, Maryland, September 1976.

(44) McIlwain, C. E., Substorm injection boundaries in Magnetospheric Physics, edited by B. M. McCormac, D. Reidel, Dordrecht, Netherlands, 1974.

(37) Mozer, F. S., Anomalous resistivity and parallel electric fields, in Magnetospheric Particles and Fields, edited by B. M. McCormac, D. Reidel, p. 125, 1976.

(95) Mozer, F. S., C. W. Carlson, M. K. Hudson, R. B. Torbet, B. Parady, and J. Yatteau, Observations of paired electrostatic shocks in the polar magnetosphere, Phys. Rev. Ltrs., 1977.

(94) Mozer, F. S. and P. Lucht, The average auroral zone electric field, J. Geophys. Res., 79, 1001, 1974.

(82) Murphey, J. A., G. J. Bailey and R. J. Moffett, Calculated daily variations of O^+ and H^+ at mid-latitudes-I. Protonospheric replenishment and F-region behavior at sunspot minimum, J. Atmos. Terr. Phys., 38, 351, 1976.

(53) Onwumechili, A., K. Kawasaki and S. -I. Akasofu, Relationships between the auroral electrojet and polar magnetic variations, Planet. Space Sci., 21, 1, 1973.

(40) Papadopoulos, K. and T. Coffey, Anomalous resistivity in the auroral plasma, J. Geophys. Res., 79, 1558, 1974.

(66) Park, C. G., Whistler observations of the interchange of ionization between the ionosphere and the protonosphere, J. Geophys. Res., 75, 4249, 1970.

(63) Park, C. G., and Seeley, Whistler observations of the dynamical behavior of the plasmapause during June 17-22, 1973, Geophys. Space Phys., 11, 133, 1973.

(12) Richmond, A. D., Electric field in the ionosphere and plasmasphere on quiet days, J. Geophys. Res., 81, 547, 1976.

(17) Richmond. A. D., and S. Matsushita, Thermospheric response to a magnetic storm, J. Geophys. Res., 80, 2839, 1975.

(11) Richmond, A. D., S. Matsushita and J. D. Tarpley, On the production mechanism of electric currents and fields in the ionosphere, J. Geophys. Res., 81, 547, 1976.

(8) Rishbeth, H. and O. K. Garriott, Introduction to Ionospheric Physics, Academic Press, p. 126, 1969.

(5) Rishbeth, H. and W. B. Hanson, A comment on plasma 'pile-up' in the F-region, J. Atmos. Terr. Phys., 36, 703, 1974.

(50) Sato, T., T. E. Holzer, Quiet auroral arcs and electrodynamic coupling between the ionosphere and the magnetosphere, 1, J. Geophys. Res., 78, 7314, 1973.

(69) Schunk, R. W., W. J. Raitt and P. M. Banks, Effect of electric fields on the daytime high latitude E and F regions, J. Geophys. Res., 80, 3121, 1975.

(91) Sharp, R. D., R. G. Johnson and E. G. Shelley, The morphology of energetic O^+ ions during two magnetic storms: Latitudinal variations, J. Geophys. Res., 81, 3292, 1976.

(90) Sharp, R. D., R. G. Johnson, E. G. Shelley, and K. K. Harris, Energetic O^+ in the magnetosphere, J. Geophys. Res., 79, 1844, 1974.

(93) Stern, D. P., Large scale electric fields in the earth's magnetosphere, Rev. Geophys. Space Phys., 15, 1977.

(18) Straus, J. M. and M. Schulz, Magnetospheric convection and upper atmospheric dynamics, J. Geophys. Res., 81, 5822, 1976.

(28) Sugiura, M., Identifications of the polar cap boundary and the auroral belt in the high altitude magnetosphere: A model for field-aligned currents, J. Geophys. Res., 80, 2057, 1975.

(29) Sugiura, M. and T. A. Potemera, Net field-aligned currents observed by Triad, J. Geophys. Res., 81, 2155, 1976.

(55) Swift, D. W., H. C. Stenback-Nielsen and T. J. Halliman, An equipotential model for auroral arcs, J. Geophys. Res., 81, 3931, 1976.

(75) Taylor, H. A., J. M. Grebowsky and W. J. Walsh, Structured variations of the plasmapause: Evidence of a corotating plasma tail, J. Geophys. Res., 76, 6806, 1971.

(65) Taylor, H. A., Jr. and W. J. Walsh, The light ion trough, the main trough, and the plasmapause, J. Geophys. Res., 77, 6716, 1972.

(48) Testud, J., P. Amayenc and M. Blanc, Middle and low latitude effects of auroral disturbances from incoherent scatter, J. Atmos. Terr. Phys., 37, 989, 1975.

(86) Thorne, R. M., The importance of wave-particle interactions in the magnetosphere, in Critical Problems of Magnetospheric Physics, edited by E. R. Dyer, U. S. National Academy of Sciences, Washington, D.C., 1972.

(83) Thorne, R. M. and C. F. Kennel, Relativistic electron precipitation during magnetic storm main phase, J. Geophys. Res., 76, 4446, 1971.

(21) Vasyliunas, V. M., Mathematical models of magnetospheric convection and its coupling to the ionosphere, in Particles and Fields in the Magnetosphere, edited by B. M. McCormac, p. 60, D. Reidel, Dordrecht, Netherlands, 1970.

(23) Volland, H., Models of global electric fields within the magnetosphere, Ann. Geophys., 159, 1975.

(35) Volland, H., The atmospheric dynamo, J. Atmos. Terr. Phys., 38, 869, 1976.

(13) Walbridge, E., The limiting of magnetospheric convection by dissipation in the ionosphere, J. Geophys. Res., 5213, 1967.

(38) Wescott, E. M., H. C. Stenback-Nielsen, T. J. Halliman, T. N. Davis and H. M. Peck, The Skylab barium plasma injection experiments, 2, Evidence for a double layer, J. Geophys. Res., 81, 4495, 1976.

(87) Williams, D. L. and L. R. Lyons, The proton ring current and its interaction with the plasmapause; storm recovery phase, J. Geophys. Res., 79, 4195, 1974.

(30) Yasuhara, F., Y. Kamide, and S. -I. Akasofu, Field-aligned and ionospheric currents, Planet. Space Sci., 23, 1355, 1975.

(26) Zmuda, A. J., J. C. Armstrong, A diurnal flow pattern of field aligned currents, J. Geophys. Res., 79, 4611, 1974.